INVESTIGATION OF THE ANION BINDING PROPERTIES OF TRIPODAL AND ARYLETHYNYL-BASED RECEPTORS

by

MICHELLE MARIE WATT

A DISSERTATION

Presented to the Department of Chemistry and Biochemistry
and the Graduate School of the University of Oregon
in partial fulfillment of the requirements
for the degree of
Doctor of Philosophy

September 2014

DISSERTATION APPROVAL PAGE

Student: Michelle Marie Watt

Title: Investigation of the Anion Binding Properties of Tripodal and Arylethynyl-Based Receptors

This dissertation has been accepted and approved in partial fulfillment of the requirements for the Doctor of Philosophy degree in the Department of Chemistry and Biochemistry by:

Victoria DeRose	Chairperson
Darren Johnson	Advisor
Michael Haley	Core Member
Michael Pluth	Core Member
Bruce Bowerman	Institutional Representative

and

J. Andrew Berglund	Dean of the Graduate School

Original approval signatures are on file with the University of Oregon Graduate School.

Degree awarded September 2014

DISSERTATION ABSTRACT

Michelle Marie Watt

Doctor of Philosophy

Department of Chemistry and Biochemistry

September 2014

Title: Investigation of the Anion Binding Properties of Tripodal and Arylethynyl-Based Receptors

Anion sensing is important due to the roles anions play in biological systems and the environment. Given the complexity of these environments, selectivity in receptors is crucial. Research in the labs of Profs. Darren Johnson and Mike Haley focuses on developing novel receptors which use non-covalent interactions to reversibly bind anions – ideally for use in sensors. This dissertation presents novel tripodal-structured receptors, as well as systems based on a previously established arylethynyl scaffold – a conjugated backbone that often provides fluorescent properties to the receptor.

Chapter I is an introduction of the less commonly utilized non-colvalent interactions for anion binding – anion–π interactions and C_{aryl}–H hydrogen bonds. The design and synthesis of cryptand and tripodal receptors with electron-deficient arenes ideal for anion–π interactions is presented in Chapter II. Chapters III and IV discuss work on novel tripodal 1,3,5-tris(arylethynyl)benzene receptors which demonstrate either anion–π interactions and C_{aryl}–H···X^- hydrogen bonds. A chloride selective bis(urea) arylethynylpyridine receptor is presented in Chapter V. Lastly, Chapter VI introduces initial efforts on the synthesis of mono(urea) arylethynyl receptors which will be used to further explore the anion–π binding capabilities of these systems and may also demonstrate the preference of anion–π binding interactions over C_{aryl}–H hydrogen bonding when binding nitrate, as is demonstrated in Chapters III and IV.

This dissertation includes previously published and unpublished coauthored material.

CURRICULUM VITAE

NAME OF AUTHOR: Michelle Marie Watt

GRADUATE AND UNDERGRADUATE SCHOOLS ATTENDED:

University of Oregon, Eugene
Saint Louis University, St. Louis, Missouri

DEGREES AWARDED:

Doctor of Philosophy in Chemistry, 2014, University of Oregon
Master of Science (Research) in Chemistry, 2009, Saint Louis University
Bachelor of Science in Biochemistry, 2007, Saint Louis University

AREAS OF SPECIAL INTEREST:

Physical Organic Chemistry
Non-covalent Interactions

PROFESSIONAL EXPERIENCE:

Graduate Teaching Fellow, University of Oregon, 2009–2010, 2012

Graduate Research Assistant, University of Oregon, 2010–2014

GRANTS, AWARDS, AND HONORS:

GK-12 National Science Foundation Fellowship, University of Oregon, 2012–2014

Travel Award, Department of Energy, 2013

Graduate Teaching Fellowship, University of Oregon, 2009–2010

PUBLICATIONS:

Watt, M. M.; Zakharov, L. N.; Haley, M. M.; Johnson, D. W. *Angew. Chem., Int. Ed.* **2013**, *52*, 10275–10280.

Watt, M. M.; Collins, M. S.; Johnson, D. W. *Acc. Chem. Res.* **2013**, *46*, 955–966.

Hardebeck, L. K. E.; Johnson, C. A.; Hudson, G. A.; Ren, Y.; Watt, M.; Kirkpatrick, C. C.; Znosko, B. M.; Lewis, M. *J. Phys. Org. Chem.* **2013**, *26*, 879–884.

Watt, M.; Hardebeck, L. K. E.; Kirkpatrick, C. C.; Lewis, M. *J. Am. Chem. Soc.* **2011**, *113*, 3854–3862.

Cormier, K.; Watt, M.; Lewis, M. *J. Phys. Chem. A* **2010**, *114*, 11708–11713.

Watt, M.; Hwang, J.; Cormier, K.; Lewis, M. *J. Phys. Chem. A* **2009**, *113*, 6192–6196.

Beg, S.; Waggoner, K.; Ahmad, Y.; **Watt, M.**; Lewis, M. *Chem. Phys. Lett.* **2008**, *445*, 98–102.

Klotzbach, T.; Watt, M.; Ansari, Y. Minteer, S. *J. Mem. Sci.* **2008**, *311*, 81–88.

Jelliss, P.; Minteer, S.; Patel, M.; Siemiarczuk, A.; Watt, M.; Winter, R. E. K. *J. Mater. Chem.* **2008**, *18*, 2104–2111.

Klotzbach, T.; Watt, M.; Ansari, Y.; Minteer, S. *J. Mem. Sci.* **2006**, *282*, 276–283.

ACKNOWLEDGMENTS

Firstly, I would like to thank my family - no words can express my gratitude or their supportiveness. Most importantly I would like to thank my friends I have made during my time at the University of Oregon, as well as my friends back home in St. Louis. I can't imagine these past five years without their endless support and friendship. Kara Nell and Shana Tyler are my soul mates and partners in crime. Cindy and Rob Bardgett have been there for me throughout the years and I am blessed to have them in my life. Kristina Bradley is my spirit animal and can always brighten my day. My cohort, roommates, and friends Emma Downs, Bryan Nell, and Anna Oliveri have been a fantastic support system. I could not ask for a partner better than Aaron Docter, he is incredibly supportive and he means so much to me.

I would like to thank my advisors Professors Darren Johnson and Mike Haley for their continued support throughout my years at University of Oregon and their assistance in preparation of this dissertation. Special thanks to Chris Butler and Dean Livelybrooks for granting me the opportunity to participate in the NSF GK-12 program, which connected me further to my interest in teaching. Debbie and Chip Ambler are wonderful and inspirational teachers who I had the opportunity to work with and live with during my participation in this program. My Master's advisor is the sole reason I continued my graduate career and I could not appreciate his encouragement more.

My doctorate has been supported by the National Science Foundation GK-12 Fellowship, DGE-0742540, and the National Institutes of Health, GM087398-01A1.

This dissertation is dedicated to my Grandpa Joe. I miss him everyday and can only imagine how proud he would be.

TABLE OF CONTENTS

Chapter Page

Chapter Page

LIST OF FIGURES

Figure Page

Chapter I

Figure Page

Chapter II

Chapter III

Figure Page

Chapter IV

Chapter V

Figure Page

Chapter VI

LIST OF TABLES

LIST OF SCHEMES

CHAPTER I

AN INTRODUCTION TO ANION–ARENE INTERACTIONS

Part of the work in Chapter I was published as a review in volume 46 of the journal *Accounts of Chemical Research* in April 2013. Chapter I is composed of a portion of this original manuscript, prior to its final editing for publication, as well as an unpublished summary of other relevant studies. Mary Collins wrote the original version of the main group cation section of the manuscript – the edited final version is presented in Appendix A. My advisor and principle investigator Prof. Darren W. Johnson conceptualized the original research and provided editorial assistance for this publication. The remainder of Chapter I is an unpublished review or assessment of the current and past literature to supplement the previously published *Account*. Chapter II consists of entirely unpublished work of my own doing. Lev Zakharov collected and solved the crystallographic data. Advisors and principle investigators Profs. Darren W. Johnson and Michael M. Haley assisted in the editing of Chapter II. The work in Chapter III was published in volume 52 of the journal *Angewandte Chemie, International Edition* in September 2013. Dr. Lev Zakharov collected and solved the diffraction data for all of the crystal structures. Profs. Darren W. Johnson and Michael M. Haley conceptualized this research and provided editorial assistance for this publication. Chapter IV is composed of unpublished co-authored work, which will be submitted to the journal *Chemical Science* later this year. I wrote the document and performed many of

the spectroscopic titrations within. This work is supplemented by synthetic advances and further titrations performed by an undergraduate student I advised, John Houlihan. The crystal structure data were collected and solved by Dr. Lev Zakharov. Editing was performed by Profs. Darren W. Johnson and Michael M. Haley. The contents of Chapter V are a revised and unpublished manuscript originally written by previous graduate student, Jeff Engle. Jeff also performed the original experiments with the assistance of an undergraduate, Timothy Robitshek. I have reperformed many experiments, expanded on the data contained within, and rewrote the original manuscript. Editing was performed by Profs. Darren W. Johnson and Michael M. Haley.

I.1. General Introduction

Interactions between ions and aromatic rings are now a mainstay in the field of supramolecular chemistry.[1-3] The prototypical cation–π interaction, first characterized in the gas phase, is now well known as an important contributor to protein structure, enzyme function, and as a noncovalent force found in many synthetic systems.[4-7] The complementary "anion–π interaction" – defined as an electrostatic attraction between an anion positioned over the centroid of an aromatic ring – has recently emerged as another reversible ion–π interaction in supramolecular systems.[8,9] Such an interaction potentially offers new selectivity in binding poorly basic, strongly solvated anions, and may have implications in biological function, structure, and anion transport as well. Anion–π interactions fall under the more general "anion–arene interactions," which also includes the more recently highly investigated C_{aryl}–H hydrogen bond, in addition to the halogen bond and weak-σ interaction. This work focuses on anion–arene interactions with an emphasis in observing anion–π interactions in solution. Many molecules presented within also utilize other types of non-covalent interactions to

strengthen the overall binding as well as provide spectroscopic handles. The overall goal of this research is to further our knowledge on the design and synthesis of selective anion receptors for sensor applications.

I.2. Chapter Introduction

The *Account* included within Chapter 1 describes the Darren Johnson group's initial efforts in ion–π interactions in two contexts (Figure 1). A series of self-assembled Group 15 (pnictogen)–thiolate complexes is described, featuring prominent cation–π interactions between the trivalent pnictogen and an aromatic ring of the ligand (Appendix A). In every example, pnictogen–π interactions appear to provide additional stability to these surprisingly robust complexes. The latter half of this review highlights efforts to characterize the interaction between anions and electron-deficient aromatic rings in solution.

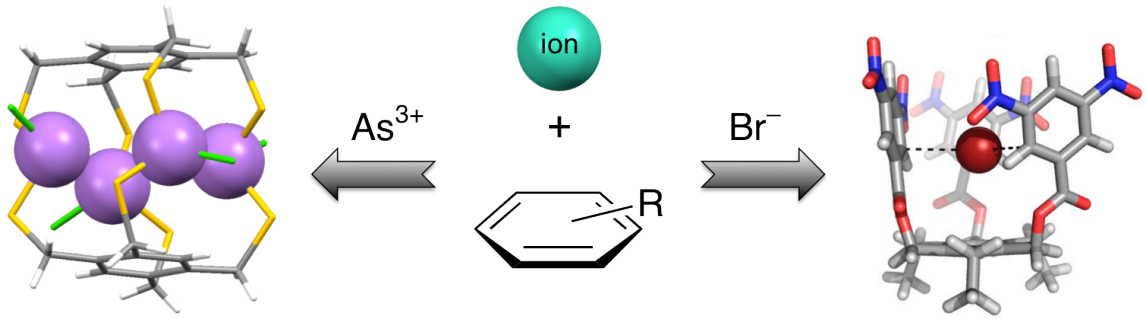

Figure 1. Cartoon illustration depicting the two main ion–π interactions focused on within the Johnson lab.

Complementary crystallographic and computational studies suggest off-center weak-σ interactions play the dominant role in stabilizing the anion–arene adducts unless an acidic C–H bond is present to participate in favorable C_{aryl}–H···anion hydrogen bonds. Initial solution studies suggest these reversible interactions are weak in organic solvents, but perhaps the Hofmeister bias in anion binding is mitigated, if not reversed, in the halides using anion–π type interactions. The *Account* seeks to

provide a thorough overview of our work in this field with references to leading reviews and related primary literature to guide the interested reader to other elegant work in these fields. Chapter 1 has been expanded beyond the *Account*, to provide a more recent and complete background relevant to the subsequent chapters.

I.3. Historical Overview of Anion–Arene Interactions

Multiple binding modes of anions with arenes have been demonstrated through experimental and theoretical studies. One such complex, known as the 'Meisenheimer' or a strong σ-complex, has been known since its isolation in 1902. The σ-complex results from the nucleophilic addition of an anion to an electron-deficient aromatic ring and is an intermediate in the S_NAr mechanism (Figure 2).[10,11]

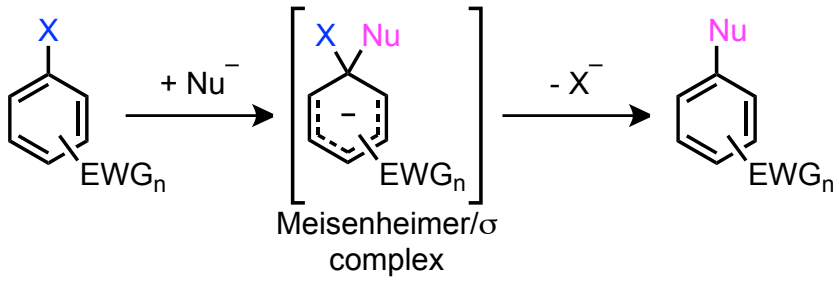

Figure 2. S_NAr reaction with the formation of a Meisenheimer complex intermediate.

Another type of anion–arene interaction occurs through hydrogen bonding (Figure 3a). Similar to the history of anion–π interactions, C_{aryl}–H hydrogen bonds have been the source of a large amount of controversy and debate in their lifetime.[12-14] The prevalence and discussion of C_{aryl}–H hydrogen bonds were limited before the 1960s. One convincing study presented IR data demonstrating changes in position and intensity of the OH absorption bands of methanol and water when dissolved in

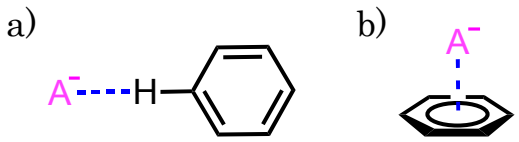

Figure 3. General representations of (a) C_{aryl}–H hydrogen bonding and (b) anion–π interactions.

solvents with good hydrogen bond acceptor atoms versus solvents without these atoms.[15] The first crystallographic analysis of C–H···O hydrogen bonding was published in 1962 and was quickly followed with additional structural details the following year.[16,17] Many arguments followed these publications, both in support of and against the C–H···O hydrogen bond, and thus the C_{aryl}–H hydrogen bond.[18-21] Ultimately, the C_{aryl}–H hydrogen bond was found not only to exist, but also to be of great importance in supramolecular and biological chemistry.[22,23]

In an early study of C_{aryl}–H hydrogen bonds, gas phase mass spectrometry was used to determine binding energies for a series of arenes hydrogen bonded to Cl^-.[24] Hexafluorobenzene was investigated in this same study and, despite the lack of aryl hydrogens, a binding energy was surprisingly still found. Follow up research showed similar results for Br^- and I^-. Initial theoretical calculations assigned this binding to an interaction of the halide anion over the center of the arene (Figure 3b).[25]

Further advances on these studies, at the time deemed "anion–π" interactions, were not made until 2002, when several papers inspired renewed interest in the interactions between anions and aromatic rings. These reports used theoretical calculations to show favorable interactions between anions and 1,3,5-triazine, -trinitrobenzene, -trifluorobenzene, hexafluorobenzene, and other perfluorinated arenes.[26-29] These four theoretical papers spawned new investigations probing anion–arene interactions, in particular anion–π interactions[8,9,30-32] and sparked a lively discussion on the nature and definition of the interaction.[29,33-35]

I.4. Anion–π Interactions

I.4.1. Initial Solution Studies

Enzymes are an excellent example of anion–π interactions being extremely relevant and important in nature – even if slightly unfavorable, or barely favorable.[36]

For this, and other, reasons a large effort has focused on observing anion–arene interactions in solution, particularly anion–π. The nature of the interaction itself, however, makes this a difficult task because binding of anions to the π-system is typically too weak for detection via NMR spectroscopy. As a result, systems have been investigated which allow observation of such interactions through other techniques.

An "enforced proximity" approach[37] was used to quantify anion–π interactions in calix[4]pyrroles (Figure 4).[38] A series of *p*-substituted tetraarylcalix[4]pyrroles were synthesized and chloride association constants were determined. A binding event observed to be slow on the NMR timescale was concluded to indicate a change in cone-conformation of the receptor induced by the addition of the anion. When quantified, only the R = NO_2 substitution showed a small attractive chloride–arene interaction.

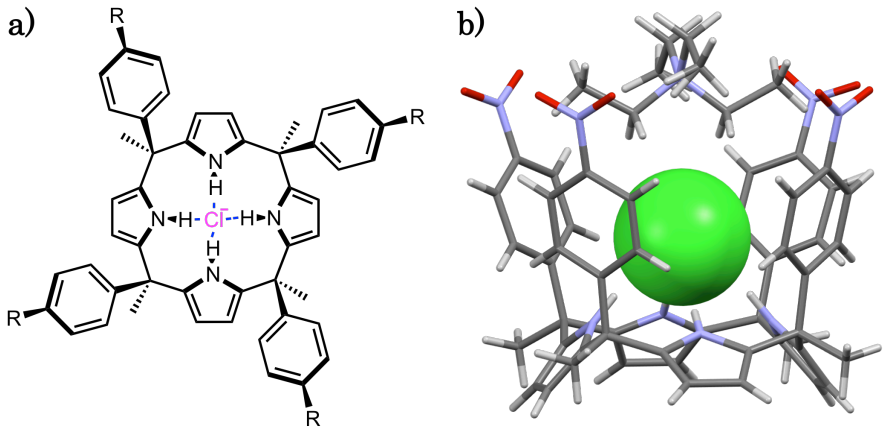

Figure 4. (a) Substituted tetraaryl calix[4]pyrroles used to quantify anion–π interactions in solution. (b) Crystal structure demonstrating anion–π interactions between the nitro-substituted receptor and a chloride–tetraethylammonium ion pair.

A dichloro-substituted tetraoxacalix[2]arene[2]triazine also showed Cl^- anion–π interactions in the solid state. A water molecule is found in the binding pocket in addition to the tetraethylammonium ion pair (Figure 5a). While no visible change was observed in solution via UV-Vis or ^{1}H NMR spectroscopy – indicating the lack of C_{aryl}–H hydrogen bonds – a binding constant was obtained by florescence

spectroscopy.[39] Highly π-acidic $HAT(CN)_6$ was shown to complex in a 3:2 stoichiometric ratio with Cl^-, Br^-, and I^- through charge transfer and anion–π interactions in the solid state (Figure 5b,c). The charge transfer complexes were further characterized in solution via UV-Vis, ^{13}C, and halogen NMR spectroscopy.[40] A naphthalenediimide chain with all anion interactions (other than those with the arene π-surface blocked by functionalization) showed a preference in solution for chloride and nitrate over other halides and oxyanions, respectively.[41] The cyano-substituted systems of the naphthalenediimide chains posses a highly electron-deficient π-surface and demonstrated the noted selectivity through transmembrane transport (Figure 5d). The

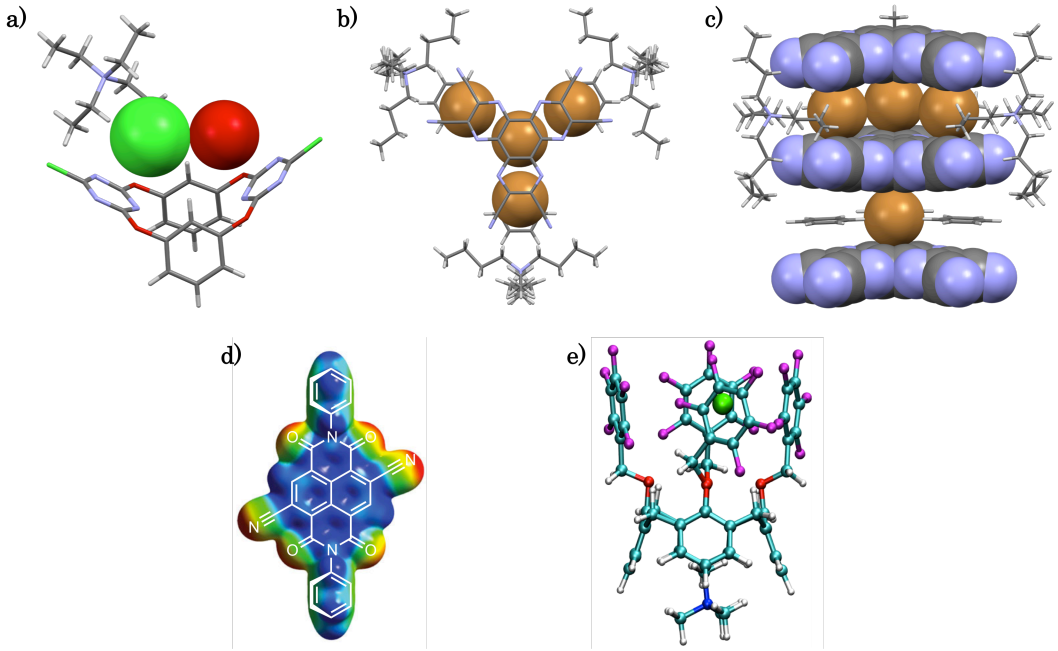

Figure 5. Receptors demonstrating anion–π interactions in solution: (a) Crystal structure of dichloro-substituted tetraoxacalix[2]arene[2]triazine binding ion-pair tetrabutylammonium chloride and a water molecule in its pocket (C: dark grey, H: light grey, N: blue, O: red, Cl: green). (b, c) Top and side views, respectively, of the crystal structure for $HAT(CN)_6$ indicating one anion–π interaction with Br^- for every three charge transfer interactions with Br^- (Br: brown). (e) Electrostatic potential surface of dicyano-substituted naphthalenediimide determined at MP2/6-311++G**// PBE1PBE/6-311G** indicating a favorable interaction between an anion and the π-surface (positive: blue, negative, red). (f) Density function theory (PBE1PBE/6-311G**) optimized structure of the perfluoroaryl-substituted calixarene binding tetramethylammonium chloride in a ditopic fashion (F: pink).

same group also used transmembrane transport to demonstrate Cl^- ion transport by a perfluorobenzene ditopic calixarene-based receptor (Figure 5e).[42] No detectable Cl^- binding was observed via ^{19}F NMR spectroscopy, indicating the weak nature of the interaction. Our studies probing anion–arene interactions were performed primarily with the goal of quantifying the strength and selectivity of anion–π interactions in solution and are highlighted in the following section.

I.4.2. Interactions Between Anions and Electron-Deficient Arenes: Our Investigations Using Combined Crystallographic, Computational, and Solution Phase Studies

Neutral electron-deficient sulfonamide receptor **1** and control receptor **2** were synthesized to investigate anion–π interactions in solution (Figure 6a).[43] ^1H NMR spectroscopic titrations were used to measure the association constants of receptors **1** and **2** with tetra-*n*-butylammonium salts of chloride, bromide, and iodide. The electron-deficient ring of **1** encourages a small, but measurable association constant for each of the halides. Association constants were determined by monitoring the change in chemical shift of the sulfonamide hydrogen. Receptor **2**, lacking an electron-deficient ring, shows no measurable binding with any of the halides. Receptor **1** binds Cl^-, Br^-, and I^- in a 1:1 fashion with binding constants of 30 ± 3, 20 ± 2, and 36 ± 6 M^{-1},

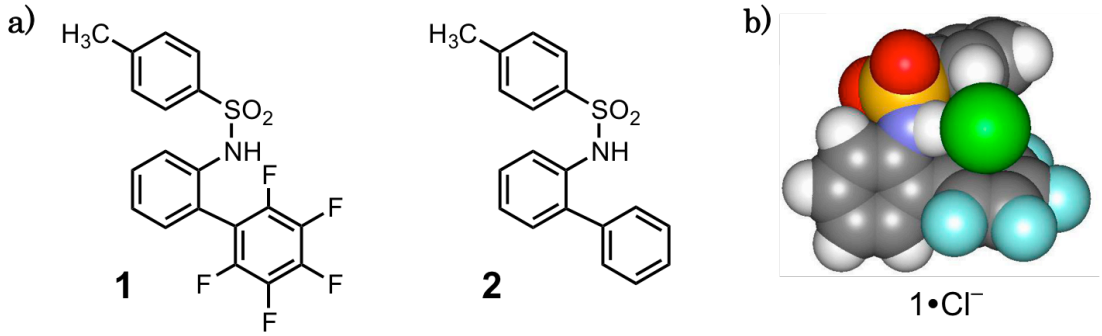

Figure 6. (a) Molecular structures of neutral sulfonamide receptors. (b) One of two minimum geometries of **1** with chloride optimized at HF/6-31+G*.

respectively. In comparison to receptor **2**, the electron-deficient arene clearly encourages or assists in the binding of the halides; therefore, the interaction between a halide and pentafluorobenzene is less repulsive than with benzene. While Hartree-Fock calculations found a centered anion–π interaction as one of two local minima (Figure 6b), no direct experimental evidence classifies the interaction as anion–π. Our future studies served as a reminder for the existence of other binding modes between anions and arene rings. Even with this in mind, neither charge transfer nor weak-σ complexes have been demonstrated for perfluoroarenes thus far. A more systematic change of the substituents may provide more insight on the nature of the anion–arene interaction present in this system.

Further investigation into anion–π interactions led to the study of 1,2,4,6-tetracyanobenzene (TCB) in the presence of halides.[44] Crystal structures of the halide salts KBr, KI, and NaI with 18-crown-6 binding TCB demonstrated three of the four binding modes possible between anions and electron-deficient arenes (Figure 7). Two charge transfer, or weak-σ, complexes were formed above the arene plane and along the periphery of the ring situated nearest to the C–CN bond (**3**) and the C–H bond (**4**). The third interaction was a C_{aryl}–H hydrogen bond within the plane of the arene (**5**). The local environment around the anion in the crystal structure for each of the halides was surprisingly similar. Interestingly, no centered anion–π interaction (**6**) was found as

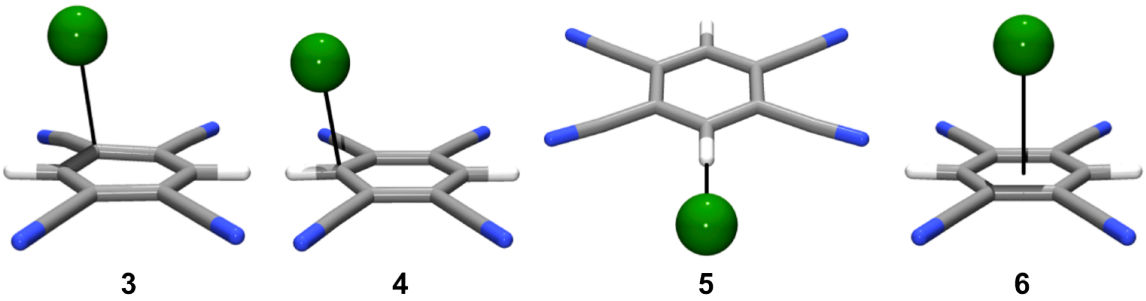

Figure 7. MP2/aug-cc-pVDZ optimized geometries for chloride complexes with TCB demonstrating the four modes of binding between anions and arenes.

part of the crystal structure. Calculations of 1:1 complexes between TCB and F^-, Cl^-, and Br^- at the MP2/aug-cc-pVDZ level of theory were used to evaluate the relative energy differences between the three geometries listed above in addition to the anion–π complex (Figure 7). Receptors **3**-**5** were found as minima for each of the halides, with the exception of **3** for Br^-. The centered anion–π configuration (**6**) was not found as a minimum on the potential energy surface for any of the three halides, but the binding energy of each halide for **6** was calculated by imposing C_{2v} symmetry. These results were the first example in which non-covalent anion–π complexes with Cl^- and Br^- were not found as minima on the potential energy surface. Global minima corresponded to complex **4** for each of the halides. Bond distances of less than 2 Å and a binding strength of -53.06 kcal mol^{-1} for F^- in complex **4** indicated a strong-σ or Meisenheimer complex. Cl^- binds more strongly than Br^- by 1.12 kcal mol^{-1} with binding energies of -29.80 and -28.68 kcal mol^{-1}, respectively. This study demonstrated the weak nature of anion–π interactions and their less favorable formation in comparison to other anion–arene modes of binding – at least for extremely electron-deficient arenes.

Equipped with this knowledge, our next studies sought to reduce the weak-σ interaction to practice in solution, in a designed synthetic receptor. Neutral tripodal receptors utilizing only electron-deficient aromatic rings were shown to bind halides in a 1:1 stoichiometry by ^1H NMR spectroscopic titrations and DFT calculations (Figure 8).[45] An unsubstituted receptor designed as a negative control failed to bind halides. These results demonstrate the binding of anions to receptors by interaction with only electron-deficient arenes in solution through either weak-σ or C_{aryl}–H···X^- hydrogen bonds, as well as provide a quantitative measure and comparison of the

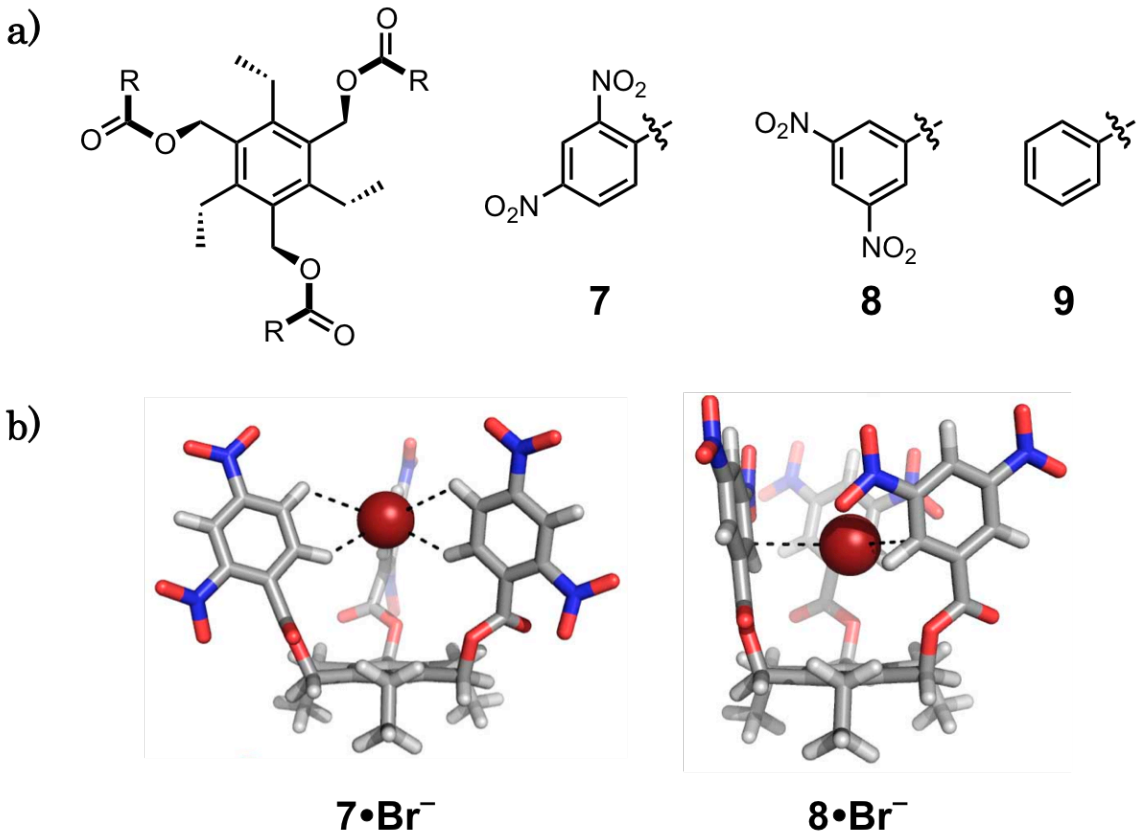

Figure 8. (a) Structures of tripodal anion receptors **7**-**9** and optimized geometries of **7** and **8** complexed with bromide at the B3LYP/DZVP level of theory.

relative stabilities for such interactions in solution. While **7** and **8** are structural isomers, the substitution pattern of **8** does not allow for C_{aryl}–H hydrogen bonding interactions due to the steric hindrance the nitro groups provide.

Titration experiments were performed with tetra-*n*-heptylammonium halide salts in C_6D_6 at 27 °C and the determined 1:1 association constants are shown in Table 1. Titration of **7** vs **8** with Cl^-, Br^-, and I^- yielded larger changes in chemical shifts (as well as color changes) for **7**, despite having association constants of the same magnitude as **8**. The difference in $\Delta\delta$ between receptors **7** and **8** is indicative of the modes by which each receptor binds the anion. Since **7** is able to bind anions through a stronger C_{aryl}–H hydrogen bond interaction, a larger overall chemical shift is observed. DFT

Table 1. Average[i] K_a (M^{-1}) values for receptors **7**-**9**[ii] binding halides[iii]

	Cl^- (M^{-1})	Br^- (M^{-1})	I^- (M^{-1})
7	26	18	11
8	53	35	26
9	<1[iv]	<1[iv]	<1[iv]

[i] Average K_a is reported from two or three titration experiments, except for receptor **9**. [ii] All titrations were performed in C_6D_6 with initial receptor concentrations at ~2 mM; errors are estimated at ± 10 %. [iii] Tetra-*n*-heptylammonium halide salts were used as halide sources and titrations were performed at 27 °C to account for the insolubility of $NHep_4^+I^-$ at room temperature. [iv] Changes in chemical shift for control receptor **9** were too small to determine K_a values.

calculations of the two receptors binding Br^- confirm this finding (Figure 8b). Control receptor **9** shows no measurable binding in C_6D_6, demonstrating the need for the electron deficient arene rings in this receptor series.

While in these studies we have been unable to quantify or definitively display purely centered (electrostatic) anion–π interactions, we have learned much about the interaction of anions with electron-deficient arenes. Our efforts have served as a reminder of the various types of anion–arene interactions possible, of which purely electrostatic anion–π seems to be the least favored with the arenes we have studied. Nevertheless, these remain an important component in ligand design for anions, and understanding the preferred geometry of the various interactions for receptor optimization is critical. Subsequent sections and chapters will take note of this expanding field and include more recent references regarding its development, including our work on the design of new receptors – utilizing hydrogen bonds to C_{aryl}–H groups or electrostatically favorable pyridinium moieties – to test the selectivity of these interactions in solution for a variety of anions.

I.4.3. Recent Advances in Solution Studies of Anion–π Interactions

The importance of anion–π interactions in biologically relevant systems was originally postulated with the crystal structure of a chloride-ion channel – arguing weak, nearly unfavorable interactions play critical roles in enzymes.[36] Recently, with the investigation of more examples, computational and experimental results further

demonstrated the importance of anion–π interactions in proteins and enzymes, including their inhibition mechanisms.[46-50] An anion–π interaction was found in urate oxidase with both an inhibitor and substrate.[46] The interaction is proposed to be crucial in the inhibition of the enzyme via either an aromatic inhibitor or by cyanide anions interacting with the π-face of the uric acid substrate (Figure 9).

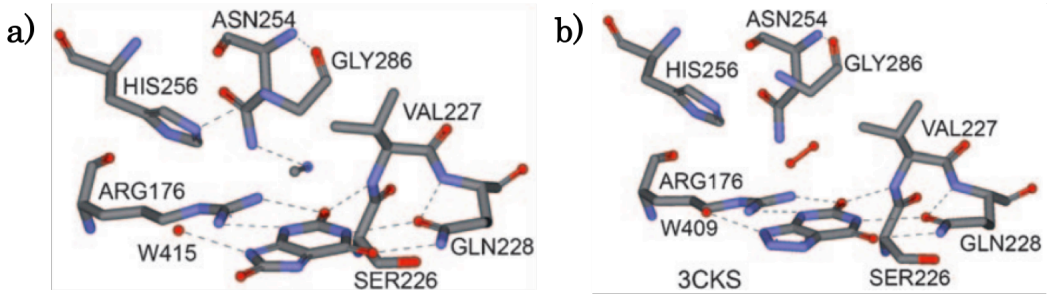

Figure 9. Representation of the active site of urate oxidase, crystalized with the (a) uric acid substrate and a cyanide inhibitor and (b) inhibitor 8-azaxantine and dioxygen.

The establishment of anion–π interactions as important and relevant supramolecular interactions has turned studies towards further utilization in synthetic ion transporters,[51,52] vesicles,[53] generation of radical anions and dianions on π-acidic surfaces,[54,55] catalysis,[56,57] and coordination chemistry.[58,59] Calixarene- and calixpyrrole-based anion receptors have continued to play a significant role in the establishment of anion–π interactions.[60,61] Two-walled calix[4]pyrroles were recently designed and synthesized to ideally bind nitrate.[52] The bis(3,5-dinitroaryl)calix[4]pyrrole (Figure 10a) demonstrated anion–π interactions while binding nitrate, evidenced by the observed changes in chemical shift during ^{1}H NMR spectroscopic titrations and energy comparisons to variously bis-substituted calix[4]pyrroles. The anion–π interactions were also supported through crystal structures – two binding conformations were found, perpendicular and pseudo-parallel (Figure 10b,c). The pseudo-parallel structure was

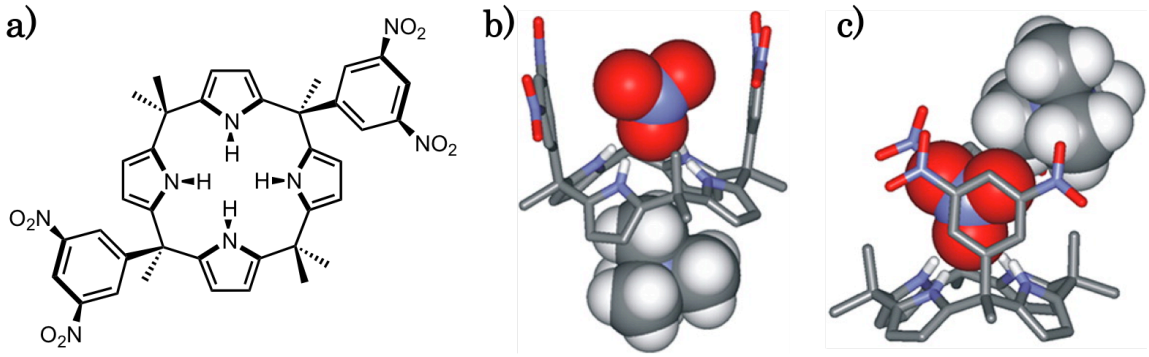

Figure 10. Dinitroaryl-substituted calix[4]pyrrole (a) molecular structure and solid-state binding structures of the receptor binding tetramethylammonium nitrate in a (b) perpendicular and (c) pseudo-parallel geometry.

concluded to be most similar to what is observed in solution. This system was then used to show selective transport of nitrate in vesicles.

Several papers have designed experiments to quantify anion–π interactions and compare them to previously calculated free energies of association. Gas phase and theoretical studies[26,29,32,44,62,63] have determined binding energies up to 20 kcal mol^{-1} while experimental solution results[38,52,64-67] have indicated energies of 0.1 – 2.1 kcal mol^{-1} for favorable interactions. Recent investigations have also focused on the thermodynamic contributions of some of these anion–π interactions.[65,67]

Tren-substituted nitroso-amino-pyrimidine compound (Figure 11a) previously shown to bind inorganic and adenosine phosphate anions,[64,68,69] demonstrated anion–π binding energies of approximately 2 kcal mol^{-1} for select inorganic anions, including sulfate, via pH-metric titrations and isothermal titration calorimetry (ITC) experiments

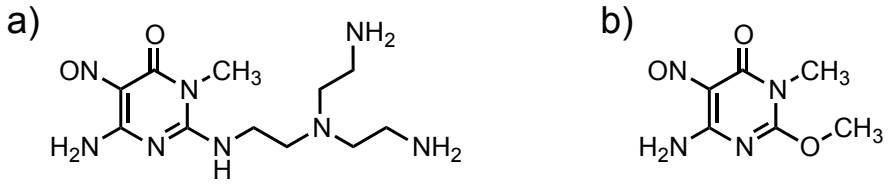

Figure 11. Molecular structure of the (a) tren-substituted nitroso-amino-pyrimidine compound and (b) non-tren-substituted analogue.

in water.[65] The ITC experiments also provided the thermodynamic breakdown of the contributions of enthalpy and entropy. To determine the values related to just an anion–π interaction, a non-tren-substituted system was also investigated (Figure 11b). This system found large entropic contributions attributed to "the reduced hydrophobic pyrimidine surface exposed to water after anion aggregation, and the consequent reduced disruptive effect on the dynamic water structure."[65]

A study released shortly following the pyrimidine investigation found the opposite result.[67] Once again, "two-walled" substituted-bis(aryl)calix[4]pyrroles were employed to quantify anion–π interaction energies and also their thermodynamics. In comparison, halide anions were more weakly associated than in the pyrimidine investigation; however, the enthalpic parameter was determined to be much more influential on the binding energies in chloroform and related to the increase in electrostatic surface potential value at the ring centroid.

I.4.4. Anion–π Interaction Section Conclusions

Ion–π interactions continue to play a prominent role in supramolecular chemistry. The *Accounts* article highlighted our group's efforts on the design of ligands and receptors featuring prominent ion–π interactions in their complexes. Early work in the Johnson lab, described within, focused on efforts to understand and to quantify anion–arene interactions in solution. Our work has revealed a variety of interactions between anions and electron-deficient arenes as favorable, including weak-σ and C_{aryl}–H···anion hydrogen bonds. Purely centered anion–π interactions remained elusive in the systems studied here, although they presumably comprise a portion of the attractive forces in these complexes. The projects have developed to other receptor syntheses which took advantage of ionic interactions with a pyridinium core. These systems have been further expanded to neutral based receptors allowing varied types of anion–arene interactions, which will be discussed in the following section.

I.5. Interactions of Anions and Arene Edges: N^+–H and C_{aryl}–H Hydrogen Bonds

I.5.1. Solution Studies of C_{aryl}–H Hydrogen Bond Interactions

Through the last decade, use of C_{aryl}–H hydrogen bond interactions has expanded into anion receptors. Computational work established the ability of C_{aryl}–H hydrogen bond interactions to match 50 – 100 % the strength of OH and NH hydrogen bonds depending on the substitution of the arene ring.[70,71] A benzene strapped calix[4]pyrrole (Figure 12) introduced in 2002 demonstrated strong binding of tetrabutylammonium chloride in DMSO via ITC experiments.[72] The solid state showed chloride resides within the cavity with a $C_{aryl}\cdots Cl^-$ distance of 3.793 Å, indicating a strong C_{aryl}–H$\cdots Cl^-$ hydrogen bond.[73] This class of compounds was expanded upon,[74,75] including receptors designed to specifically address the strength of a C_{aryl}–H$\cdots Cl^-$ vs. a N_{aryl}–H$\cdots Cl^-$ hydrogen bond.[75] Previously synthesized benzene-strapped calix[4]pyrrole was studied with newly introduced pyrrole- and furan-strapped calix[4]pyrroles as comparisons for an N–H donor and a negative control with no donor, respectively (Figure 12).[75] An order of magnitude difference in chloride 1:1 association constant was found in acetonitrile via ITC between the pyrrole and benzene systems as well as

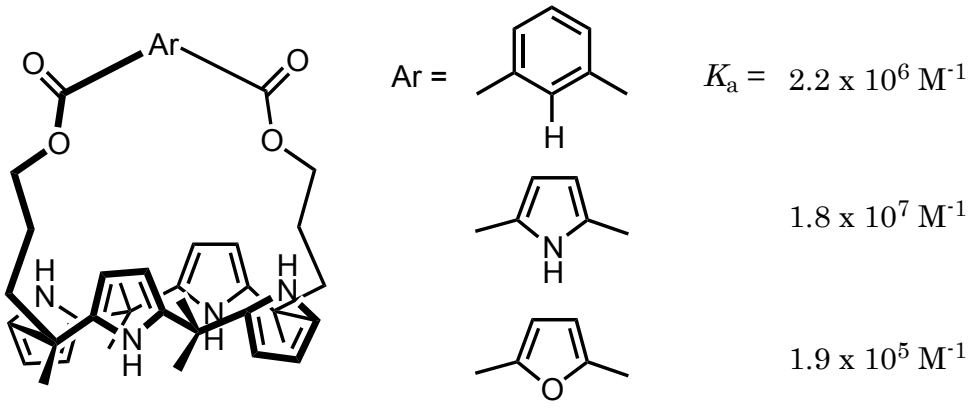

Figure 12. Molecular structure (left) and corresponding association constants (right) of the strapped calix[4]pyrrole receptors. Association constants were determined at 25 °C in acetonitrile through ITC experiments with tetrabutylammonium chloride.

between the benzene and furan control. In further support of the solution data, the crystal structure of the pyrrole-strapped receptor showed a 0.63 Å smaller interaction with chloride than the corresponding benzene system.

To further establish the strength and ability of C_{aryl}–H groups to hydrogen bond to anions, a purely C–H hydrogen bonding macrocyclic receptor was synthesized containing phenyl and triazole rings (Figure 13a).[76] Downfield shifts were observed during ^{1}H NMR titrations in CD_2Cl_2 with tetrabutylammonium chloride. A 1:1 association constant of 1.0 x 10^5 M^{-1} for chloride, the anion selected to best fit the proposed pocket of the macrocycle, was determined through UV-Vis titrations in CH_2Cl_2. Another all C–H hydrogen bonding macrocycle recently synthesized was shown to bind anions and form [3]rotaxanes with dialkylphosphates (Figure 13b).[77] This receptor, named "cyanostar", is well known predominately due to its high yielding, one pot synthesis but also its ability to strongly bind large, typically weakly associating anions. Based on UV-Vis titrations in 2:3 MeOH:CH_2Cl_2, BF_4^-, ClO_4^-, and PF_6^- bind cyanostar at association constants of $K_{1:1} > 10^5$ M^{-1} and $\beta_2 > 10^{11}$ M^{-2}. The cavity of the macrocycle is extremely electropositive due to the electron-withdrawing cyano groups

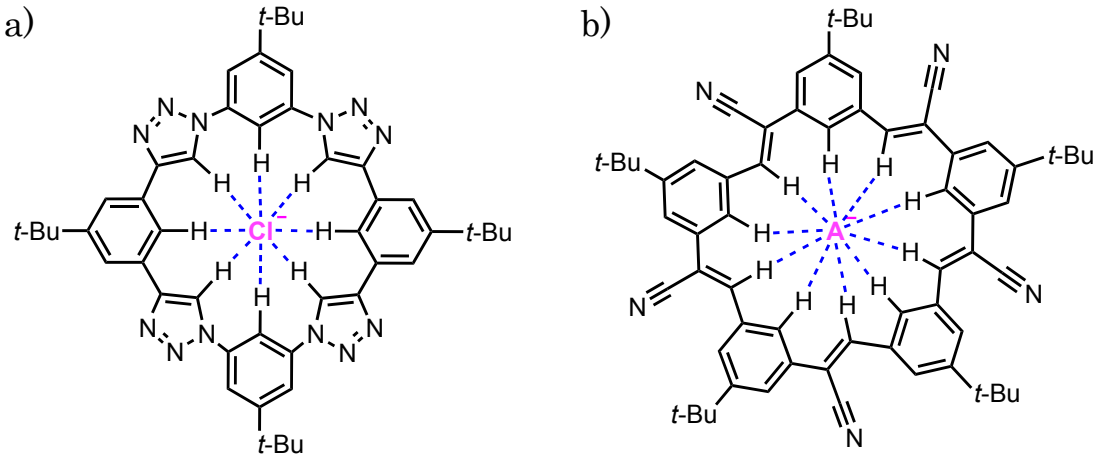

Figure 13. Molecular structure of (a) the phenyl and triazole-based macrocycle shown to bind chloride and (b) the cyanostilbene macrocycle shown to strongly bind typically non-coordinating anions, both through purely C_{aryl}–H hydrogen bonds.

on the periphery of the receptor. While the receptors presented within this dissertation do not solely use C_{aryl}–H hydrogen bonds to bind anions, some do utilize the interaction within the binding pocket.

I.5.2. Our Work Using Crystallographic and Solution Studies

Previously, the Haley and Johnson lab modified an arylethynyl scaffold for use in supramolecular assemblies. Molecules with a rigid arylethynylpyridine scaffold showed an electronic response when protonated upon coordination of a guest via interaction with a lone pair on the heterocycle or induced changes in geometry.[78,79] Sulfonamide and urea receptors (Figure 14) show interesting fluorescent properties. In $CHCl_3$, the bisurea methoxyphenyl and nitrophenyl compounds had opposite results, which was postulated to result from the switch between an electron-donating and electron-withdrawing substituent. While both systems went from essentially colorless to yellow upon the addition of HCl in chloroform, the methoxyphenyl bisurea switched from the "on" state to the "off" state, and the nitrophenyl switched from "off" to "on" with regards to fluorescence.[79] Both of these urea receptors were investigated *in vitro* for signaling ability using NIH3T3 murine embryo fibroblasts. The methoxy-substituted bisurea moiety showed fluorescence in cells when treated with a high [Cl^-] buffer (Figure 15).[80] To solubilize and transport the bisureas into cells, a 10 % aqueous DMSO

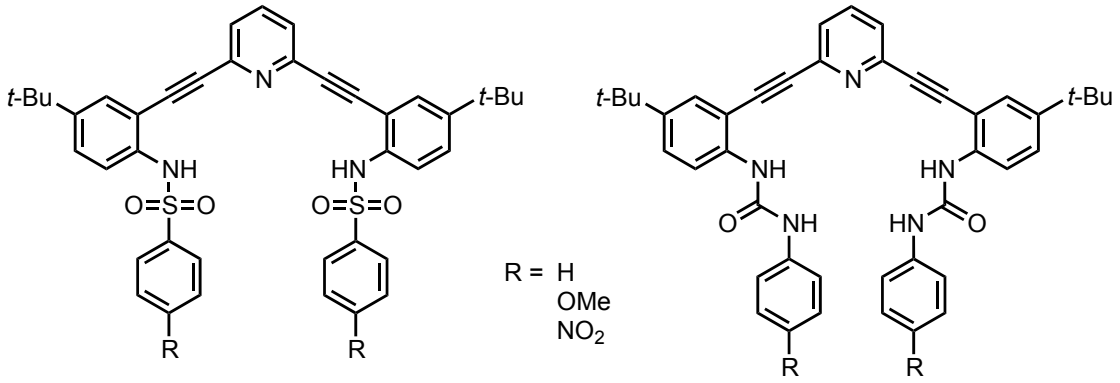

Figure 14. Arylethynylpryidine scaffolds investigated as anion receptors.

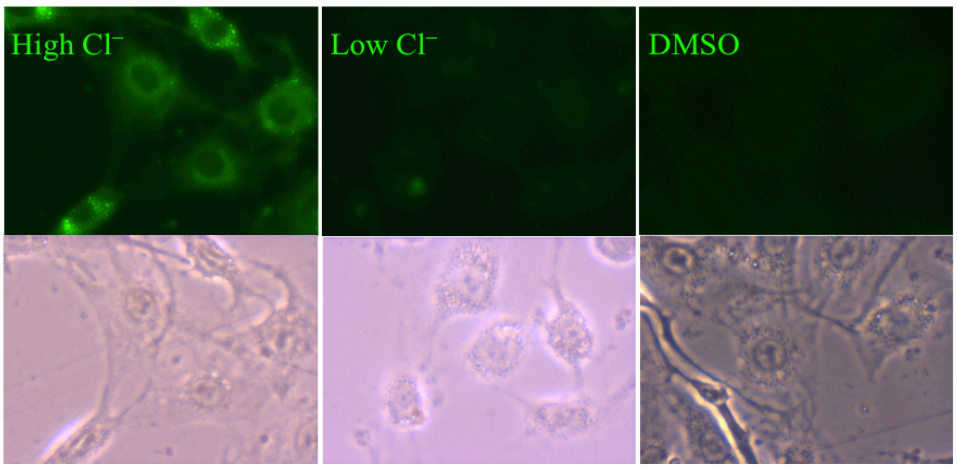

Figure 15. Images of NIH3T3 murine embryo fibroblasts with the methoxy-substituted phenylurea incubated in high chloride concentrated 10 % aqueous DMSO buffer (left), low chloride concentrated 10% aqueous DMSO buffer (middle), and with straight DMSO (right) as a control.

buffer was utilized, which ultimately results in apoptosis of cells. As a result, this project turned to focus on designing more water-soluble receptors.

Initial studies into water-soluble arylethynylpyridine receptors focused on polyethylene glycol (PEG) substitutions on the "arms" of the parent urea receptors. Compounds shown in Figure 16 were synthesized and investigated for their ability to bind anions, but more importantly, for their solubility in water.[81] Unfortunately, none of these systems were solubilized by water, and demonstrated simple PEG additions are not sufficient to transfer these receptors into aqueous environments. Focus has shifted to varying substitution on the pyridine core, as it allows for the addition of water solubilizing groups through simple S_NAr reactions, as well as tuning of the pyridine pKa. Protonation of the pyridine receptors has been a requirement of the strong fluorescent response to chloride throughout the development of this class of receptors.[79,82] However, neutral receptors have long been coveted for the application of sensors, particularly to remove the dependence of the receptor's properties on the pH of the solution or media used. Tuning the pyridinium to a higher pKa is ideal for

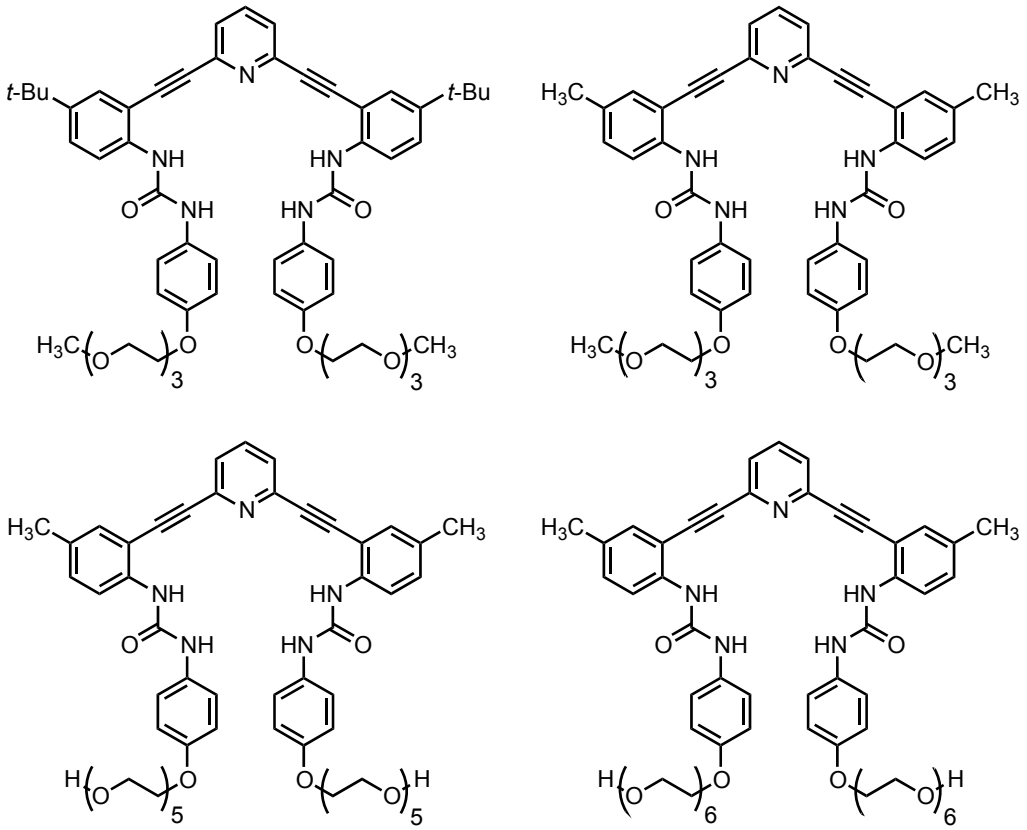

Figure 16. Molecular structures of four previously investigated PEG-substituted pyridine-based receptors.

applications in cells, particularly to a pKa greater than physiological or neutral pH – this would allow for the pre-protonation step of the receptors to be forgone as the receptors would protonate upon their addition to aqueous solutions. This will be discussed further in Chapter V.

Other efforts have focused on moving to neutral receptors to further expand upon this class of compounds as well as to assess the need for the pyridine in both strength of binding and fluorescent response. In addition to the neutral tripodal compounds discussed in Chapter III and IV, a phenyl analogue of the arylethynylpyridine bisurea has been synthesized (Figure 17a), which takes advantage of a C_{aryl}–H hydrogen bond in the binding pocket.[83] ^{1}H NMR titrations in water-saturated

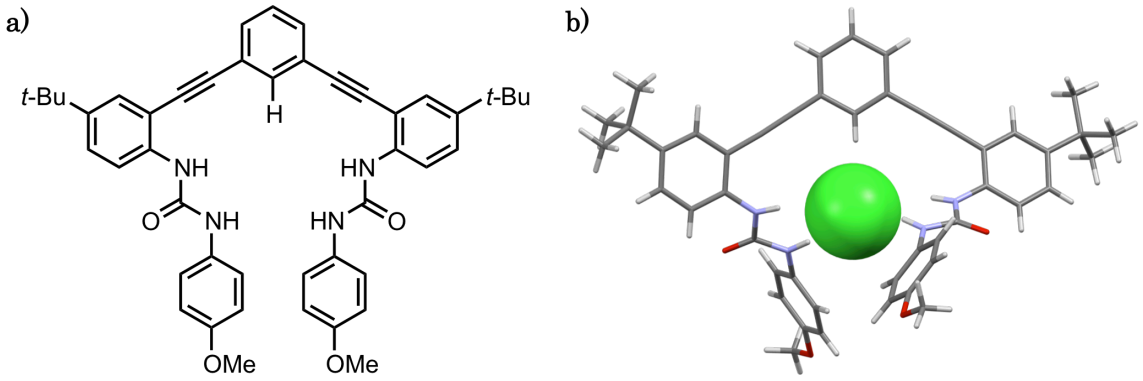

Figure 17. (a) Molecular structure of the phenyl analogue to the arylethynylpyridine bisurea receptor. (b) Crystal structure of the receptor binding chloride (green). Tetrabutylammonium cation and chloroform molecule were removed for clarity.

$CDCl_3$ indicated the phenyl-based receptor binds chloride with urea and C_{aryl}–H hydrogen bonds through large downfield shifts of the respective proton resonances. A solid state structure of the receptor binding tetrabutylammonium chloride in the pocket demonstrated a 3.579(3) Å and 169° C_{aryl}–H···Cl^- hydrogen bond (Figure 17b). Investigations into the fluorescent properties of this new compound class is underway as well as a study looking at the effects of *para*-subsitution on the phenyl ring on strength of binding and fluorescent response.

I.6. Conclusions

Both anion–π interactions and C_{aryl}–H hydrogen bonds have had controversial histories – as is quite common for emergent phenomena. Anion–π interactions still remain a somewhat debated topic to this day, however. After further studies better established these non-covalent interactions, many researchers moved on to take advantage of both within supramolecular chemistry. Anion receptor chemistry has benefited greatly through these systems, specifically with regards to ion transport, sensing, and catalysis.

I.7. Bridge to Chapter II

Chapter I represented a short synopsis of past and current work in the fields of anion–π interactions and C_{aryl}–H···anion hydrogen bonds, most specifically for the design of receptors for binding or transporting anions. The following chapters will touch on the topics discussed in Chapter I – if only briefly for some. Chapter II discusses early work of a new receptor class designed to bind anions solely through anion–π interactions.

CHAPTER II

EXPLORATION OF ARENE–II INTERACTIONS AS A MODE OF BINDING FOR PUTATIVE ANION SENSORS

Chapter II consists of work of my own doing which is unpublished. Lev Zakharov collected and solved the diffraction data of the crystal structure. Advisors and principle investigators Profs. Darren W. Johnson and Michael M. Haley assisted in the editing.

II.1. Chapter Introduction

The basic structures of most anion receptors are crown complexes, porphyrins, cryptands, calixarenes, and tripods. Typically these receptor classes contain arenes; thus, anions bind through the previously mentioned modes: anion–π, weak σ-bond, halogen bonding, and C_{aryl}–H hydrogen bond interactions, among other typical hydrogen bonds. To expand on our previous work and further elucidate anion–π interactions in solutions utilizing enforced proximity and/or electron-deficient arenes a new series of cryptands were envisioned (Figure 1). This system takes advantage of multiple arene rings, which would ideally implement anionic guest inclusion.

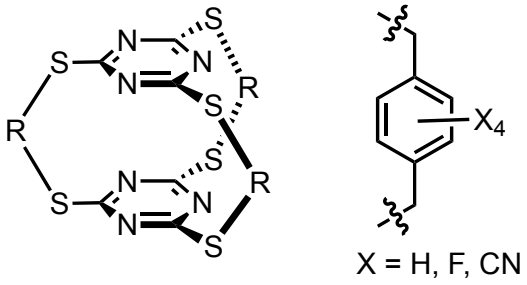

Figure 1. Proposed cryptand anion receptor comprised of triazine and substituted benzene rings.

Definitions of cryptand vary in source, however here we use the most general of definitions: bicyclic structures composed of two "caps" and three "bridges", as depicted in Figure 2a. Specifically, the resulting internal cavity must be capable of encapsulating guests such as anions in order to be deemed a cryptand. Most cryptands designed for anionic guests utilize multiple hydrogen-bonding functionalities.[1] Importantly, the limited conformational freedom of cryptands leads to predictable interactions with guests, yet still allows enough flexibility to permit their inclusion.

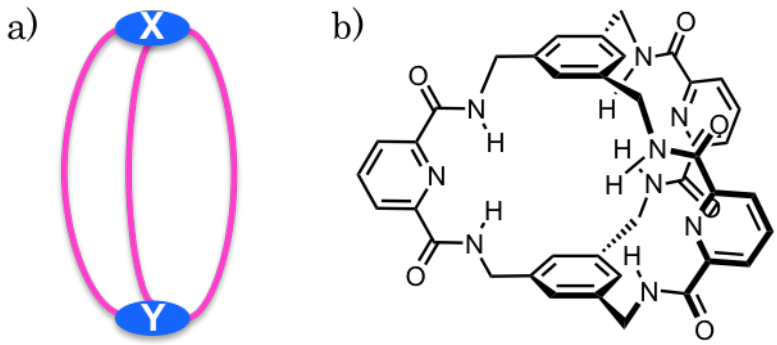

Figure 2. (a) Cartoon depicting the general molecular structure of cryptands consisting of three bridges (pink) and two caps (blue), where X = Y or X ≠ Y. (b) An example cryptand utilizing benzene caps and diamido-pyridine bridges.

Examples in which the cryptand has aryl bridges as well as caps are rare. However, one such compound with 1,3,5-triethylbenzene caps and 2,6-pyridine diamide bridges (Figure 2b), exhibits high binding with nitrate and acetate.[2] The bridging functionality binds anions through hydrogen bonding via the amide hydrogens.[2] No mention of anion–π interactions with regards to the benzene caps is made in the paper. A system utilizing more electron-deficient caps may have seen variation in binding strength or selectivity.

While anion receptors are typically equipped with hydrogen bonding motifs acting to bind the anion within the receptor cavity, proposed within is a series of receptors utilizing multiple electron-deficient π-systems instead of hydrogen bonding

motifs. An investigation into the association of anions to this cryptand would follow successful synthesis – providing a fundamental understanding of not only the anion binding capabilities, but also the selectivity of this class of host.

II.2. Results and Discussion

II.2.1. Cryptand

A series of cryptand receptors with bis(mercaptomethyl)benzene bridges and triazine caps were designed to serve as anion hosts utilizing anion–π interactions (Figure 1). As discussed, the preorganized structure provided by the cryptand makes them interesting targets for anion binding. Certain building blocks have continuously been implemented in receptors to investigate and promote anion–arene interactions. For example, 1,3,5-triazine is a versatile synthon well known for its participation in supramolecular interactions and is often a part of theoretical, solid state, and solution-based anion–π investigations.[3-12]

This proposed system utilizes thiol linkages to the triazine caps. Thiols were primarily chosen due to their ease of reactivity with halo-substituted functionalities and the familiarity of such systems in the Johnson lab. Electron density maps of trithiocyanuric acid and 1,3,5-triazine (Figure 3) demonstrate the presence of the sulfur atoms induces no significant change in the electron density of the π-cloud. Fluorinated arenes are also known to be highly electron-deficient and are commonly observed to partake in anion–π interactions in theoretical and solution studies.[5,13-15]

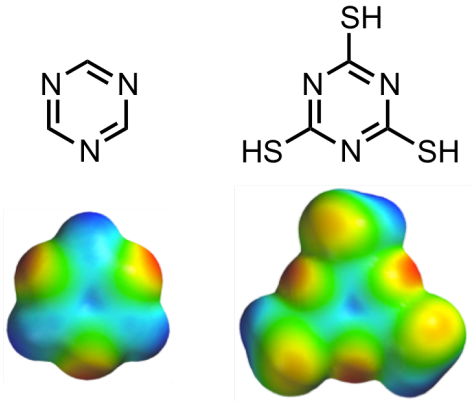

Figure 3. Electron density maps of 1,3,5-triazine (left) and trithiocyanuric acid (right) calculated at RHF/6-31G**. Color scheme: positive, blue and negative, red.

Molecular modeling of the unsubstituted receptor (RHF/6-311+G**) indicates the cryptand cavity can fit anions as large as bromide, while perchlorate is most likely too large to be favorably accommodated (Figure 4). Computational attempts to investigate the flexibility of the cage to allow an anion to enter proved unsuccessful due to structure distortion when holding distances constant. The results obtained are thus inconclusive as the distortion is likely due to the constraints imposed.

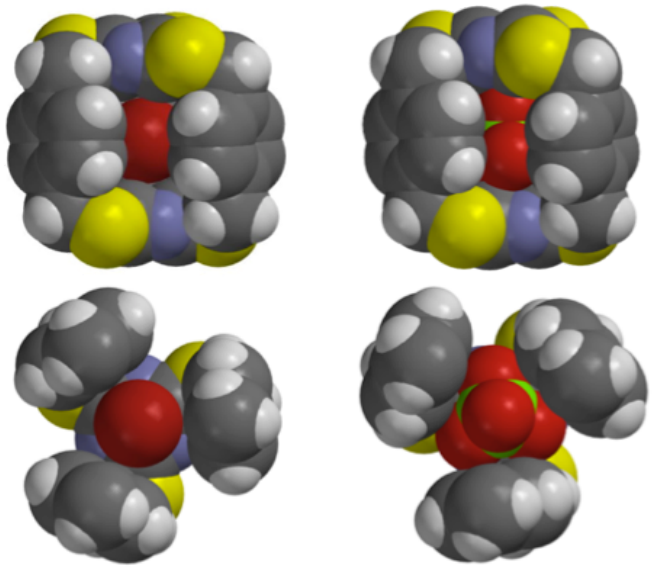

Figure 4. Modeling of the unsubstituted cryptand with bromide (left) and perchlorate (right) in the binding pocket. Top images: cryptand side-view. Bottom images: cryptand above-view with upper triazine removed. Atom colors: carbon, dark gray; hydrogen, light gray; sulfur, yellow; nitrogen, blue; bromine, dark red; chlorine, green; oxygen, red.

Synthesis of the unsubstituted parent cryptand was based on literature procedures (Scheme 1).[16,17] Simultaneous slow addition of trithiocyanuric acid and base (KOH or DIPEA) in THF and *p*-xylylene dibromide in THF with high dilution under N_2 will provide the parent, unsubstituted cryptand. Synthetic approaches using a syringe-pump system were made, and while ^{1}H NMR indicated the presence of a new compound, separation of the reaction products and starting material proved problematic. Insoluble polymer was also obtained from the reaction due to the

Scheme 1. General reaction for cryptand synthesis.

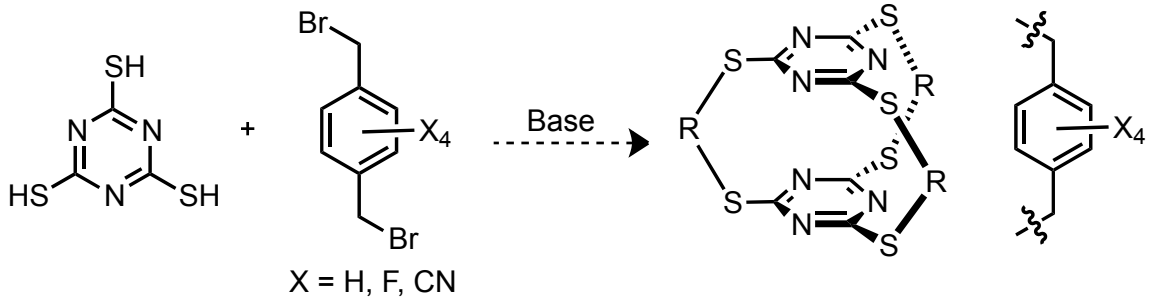

introduction of an air bubble in one of the syringes. A more precise, air-free set-up would be required for a more high yielding synthesis of the cryptand. Due to the known difficulties in synthesizing cryptands in general and their low yields, this project evolved to examine the simpler, uncapped or tripodal version of the proposed cryptand.

II.2.2. Tripod

Before continuing to hone-in on the synthesis of the cryptand, a proof of concept receptor was designed which utilized the same aryl rings but in a tripodal scaffold in order to determine if measurable or observable binding is feasible in this general receptor class. New tripodal receptor **1**, based on the original cryptand, was realized. The synthesis of **1**, based on literature procedure for a similar compound,[16] was performed in one step as shown in Scheme 2. Reflux of trithiocyanuric acid with an excess of pentafluorobenzyl bromide and DIPEA provided **1** in 77 % yield. The white solid product was fully characterized by ^{1}H, ^{19}F, and ^{13}C NMR as well as mass spectrometry (Appendix B).

Single crystals of **1** were obtained by slow evaporation from a concentrated solution in $CHCl_3$. The solid state structure shows the three arms of a single monomer orient away from each other with one nearly perpendicular to the triazine plane and the other two arms located above and below this plane (Figure 5a). Short S–S

Scheme 2. Synthesis of tripodal receptor **1.**

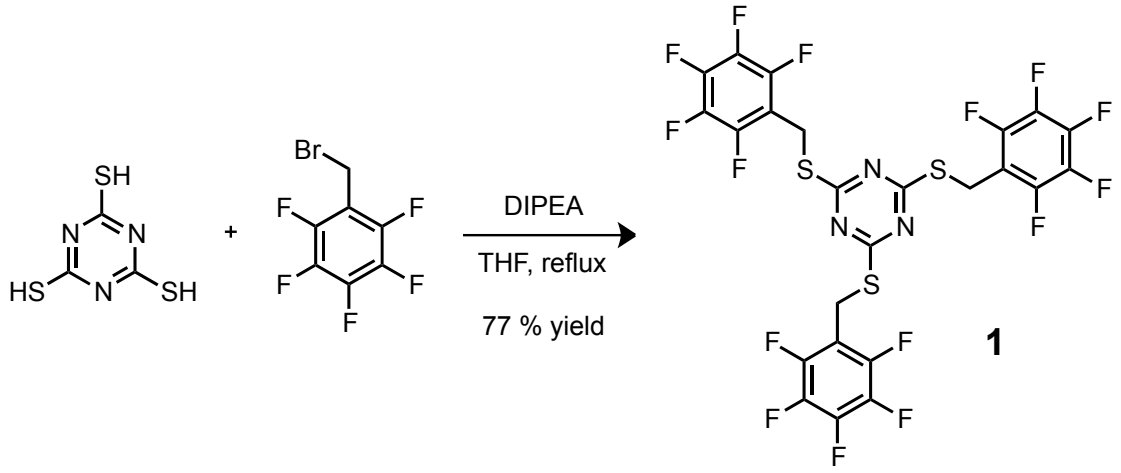

contacts of 3.38 Å exist between one monomer and another rotated 180° in conformation from the first. (Figure 5b). No solvent molecules are contained within the crystal packing (Figure 5c).

Originally we thought UV-Vis spectroscopic titrations might provide the best visualization of anion binding due to the density of aromatic rings in the structure and the corresponding lack of proton handles. Unfortunately, the λ_{max} of the peak showed no significant shift upon the addition of excess Cl^- or I^- as tetrabutylammonium salts (TBA) (Figure 6a). The change in intensity upon the addition of iodide proved to be an artifact of iodine itself and not a charge transfer complex with the arene rings. ^1H NMR spectroscopy was next investigated to monitor binding. In these studies Br^- and I^- were both added in excess upon a single addition, while Cl^- was titrated in a few increments. Minimal shifts of the single proton resonance were observed upon the addition of TBACl (Figure 6b). While this result is not surprising given the weak nature of anion–π interactions, the peak shifts are not necessarily attributable to binding as the change in ionic strength of the solution could also produce a shift. Since an endpoint was not reached with over 100 equivalents of chloride, the latter is most

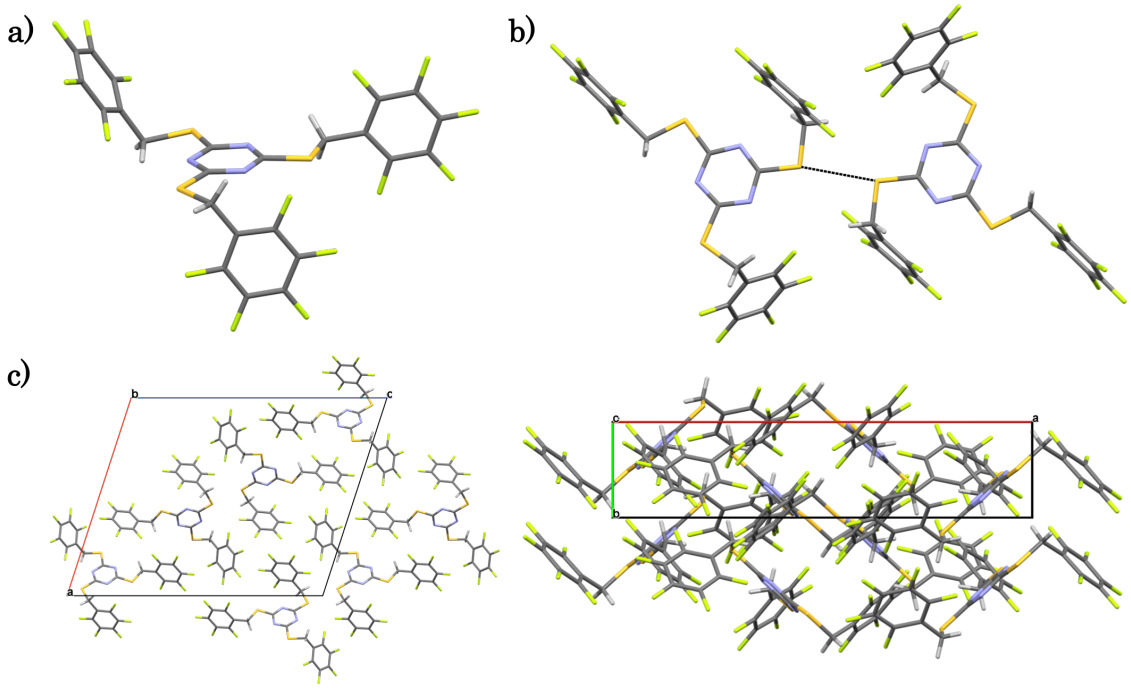

Figure 5. Solid state structure of **1** displaying its (a) monomer geometry, (b) dimer interaction with short S–S interactions, and (c) packing down the b (left) and c (right) axes of the repeated unit cell.

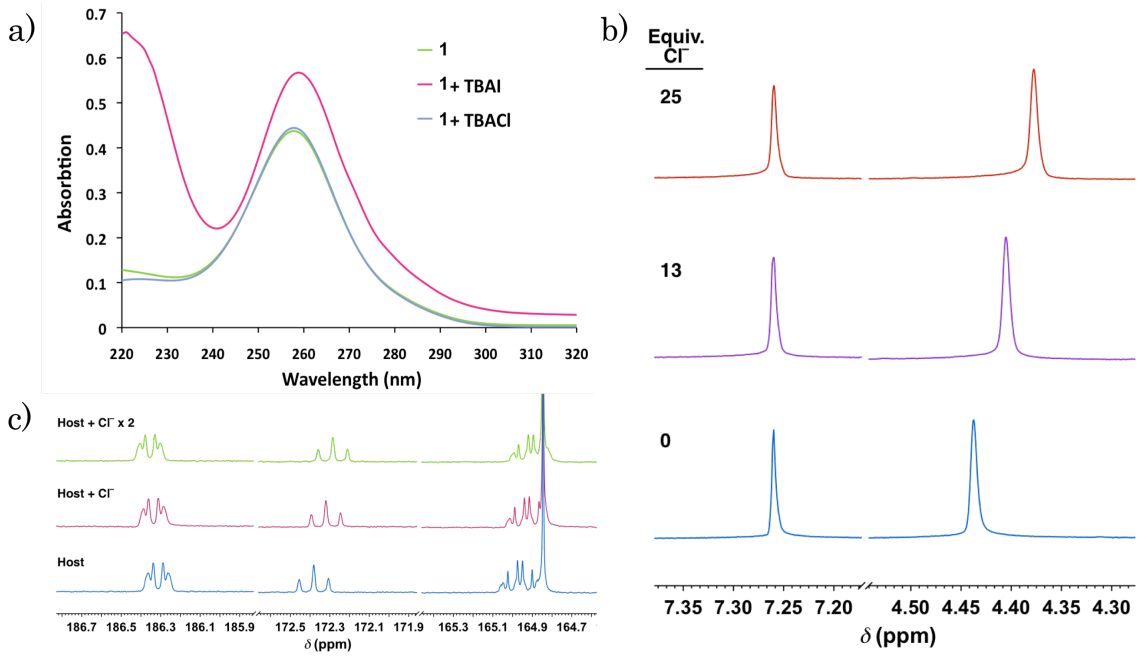

Figure 6. Characterization spectra for monitoring anion binding of **1**: (a) UV-Vis spectra of host **1** before and after the addition of excess tetrabutylammonium chloride or iodide ([**1**] = 8.4 μM). (b) ^{1}H NMR spectra from the titration of TBACl into a 5.0 mM solution of **1**, displaying a linear trend of shifts even past 100 equivalents of guest. (c) ^{19}F NMR spectra before and after the addition of excess chloride to **1**.

likely the case. Both bromide and iodide produced smaller peak shifts than chloride. In addition, highly symmetric **1** possesses only a single ^{1}H NMR spectroscopic handle, which is not an aromatic proton. If anion–π interactions occur this benzylic proton would not be greatly affected due to its distance from the aromatic ring. Experiments with ^{19}F NMR spectroscopy were also performed to monitor anion binding. Similar studies have shown ^{19}F NMR to be a suitable spectroscopic handle to observe anion–π interactions, with changes in chemical shift ranging between approximately 0.5 – 3 ppm.[18-23] Unfortunately, our results showed essentially no change in chemical shift ($\Delta\delta_{max} \approx 0.01$) when internally referenced to hexafluorobenzene for additions of TBACl (Figure 6c), nor TBABr with external reference to trifluoroacetic acid. Finally, attempts to obtain crystals of the host interacting with anions provided only host. Overall, no spectroscopic methods gave indication of **1** binding anions through anion–π or other anion–arene interactions. At this time, more promising alternatives for binding anions through arene interactions were initiated using the arylethynyl scaffold as will be discussed in Chapter III.

II.2.3. Altering Substitutions of the Tripod

In the interest of expanding upon this tripodal system and utilizing other anion–arene interactions, a series of receptors **2**-**7** were envisioned (Figure 7). It is possible these receptors could still lead to observation of anion–π interactions – most likely in the solid state – through an enforced proximity approach. Receptors **2**, **4**, and **6** posses iodo-substitutions to allow for halogen bonding interactions to the arene while **3**, **5**, and **7** lack a substitution at the *para*, *meta*, and *ortho* positions respectively allowing for C_{aryl}–H hydrogen bond interactions in solution. For all of the proposed receptors, original tripod **1** can serve as a control.

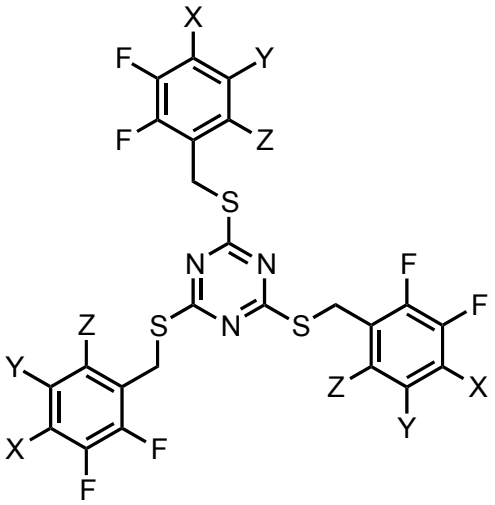

Figure 7. Proposed tripodal triazine receptor series with iodo-substitutions or no substitution in the *para*, *meta*, and *ortho* positions.

Based on geometry, *meta*-substituted and unsubstituted tetrafluorobenzyl substituted receptors **4** and **5** were synthesized first (Scheme 3 and 4). Tetrafluoroiodobenzyl chloride precursors were previously prepared from tetrafluorobenzyl halides with *p*- and *m*-iodo substitutions through reaction with butyl lithium and iodide.[18] Complications arose in the butyl lithium reaction during the synthesis of **4** due to side product formation resulting from homo-coupling of the benzyl chloride to the arene. Changing from the literature procedure's required -78 °C temperature to a colder -95 °C diminished the amount of unwanted side product. Reaction of crude 2,4,5,6-tetrafluoro-3-iodochloromethylbenzene with thiocyanuric acid was performed at room temperature and yielded receptor **4** in ~90 % yield. Initial experiments with tetrabutylammonium anion salts in chloroform showed no color changes of **4**, indicating strong charge-transfer complexes are not occurring.

Receptors capable of C_{aryl}–H interactions are interesting for this system as it gives a better spectroscopic handle by which to monitor anion binding. Initial attempts to synthesize *meta*-unsubstituted receptor **5** were low-yielding. Likely, performing this

Scheme 3. Synthesis of 2,4,5,6-tetrafluoro-3-iodochloromethylbenzene – precursor to receptor **4**.

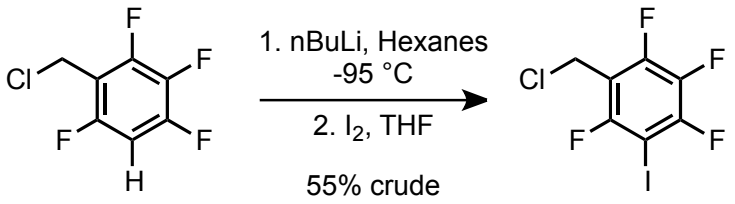

Scheme 4. Synthesis of tripodal receptors **4** and **5**.

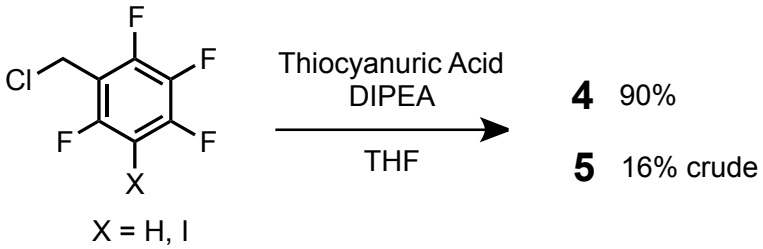

reaction at reflux in comparison to at room temperature will provide better yields. This compound has not been purified for investigation with anions as of yet.

II.3. Conclusions

Receptors were designed with no hydrogen bonding functionalities, except where specifically desired. The original ideas behind this project focused on engineering receptors with detectable binding through anion–π interactions. The preorganization of the cryptand has the potential to maximize weak interactions, although synthesis attempts proved nonproductive. To better realize the goals of the project, a tripodal equivalent with electron-deficient arenes was synthesized. As of yet, no experimental evidence has indicated binding of any form with anions. Ways to expand this project beyond anion–π interactions includes the aryl halogen and hydrogen bonding motifs proposed and synthesized in this chapter.

II.4. Experimental

General Methods. ^{1}H, ^{13}C, and ^{19}F NMR spectra were obtained on a Varian Mercury 300 MHz spectrometer (^{1}H: 300.09, ^{19}F: 282.33 MHz), Inova 500 MHz spectrometer (^{1}H: 500.10 MHz, ^{13}C: 125.75 MHz, ^{19}F: 470.53 MHz), or Bruker Avance III HD 600 MHz NMR Spectrometer with Prodigy multinuclear broadband BBO CryoProbe (^{1}H: 600.02 MHz, ^{13}C: 150.89 MHz). ^{1}H and ^{13}C NMR spectra were referenced to residual solvent peaks while ^{19}F NMR spectra were referenced to an internal standard of 1 % C_6F_6 in $CDCl_3$ (^{19}F -164.9 ppm) or an external standard of 100 % trifluoroacetic acid (^{19}F -76.55 ppm). Chemical shifts (δ) are expressed in ppm downfield from tetramethylsilane (TMS) using non-deuterated solvent present in the bulk deuterated solvent ($CDCl_3$: ^{1}H 7.26 ppm, ^{13}C 77.16 ppm; d_6-DMSO: ^{1}H 2.50 ppm ^{13}C 39.52 ppm). All NMR spectra were processed using MestReNova NMR processing software. All materials were synthesized following literature procedures or were obtained from TCI-America, Sigma-Aldrich, or Acros and used as received. X-ray crystal data were obtained on a Bruker Apex CCD or a Bruker Apex2 CCD diffractometer.

Perfluoro-tripodal triazine 1. In an oven dried round bottom flask thiocyanuric acid (0.3 g, 1.69 mmol) and DIPEA (1 mL, 5.92 mmol) were dissolved in THF (35 mL). The solution was placed under N_2. Pentafluorobenzyl bromide (0.84 mL, 5.92 mmol) was added and the solution was allowed to reflux overnight under N_2 followed by dilution with ethyl acetate, washes with water (3x) and brine, drying over $MgSO_4$, and removal of solvent *in vacuo* provided the crude product. Purification with flash chromatography over silica gel with 3:2 Hex:DCM yielded the product as a white solid (0.94 g, 77 %). The compound is further purified by crystallizing from DCM through the addition of hexanes. ^{1}H NMR (600 MHz, $CDCl_3$): δ 4.44 (s). ^{19}F NMR (282

MHz, $CDCl_3$, C_6F_6 internal ref.): δ -164.79 (m, 2F), -157.36 (t, J = 20.8 Hz, 1F), -143.43 (m, 2F). ^{19}F NMR (282 MHz, $CDCl_3$, TFA external ref.): δ -162.49 (m, 2F), -155.08 (t, J = 20.9 Hz, 1F), -141.15 (m, 2F). ^{13}C NMR (151 MHz, $CDCl_3$): δ 21.73 (s), 110.64 (td, J = 17.3, 4.0 Hz), 137.74 (dt, J = 255.9, 16.3 Hz), 143.14-139.02 (m), 147.31-143.39 (m), 178.71 (s). MS (APCI+) m/z = 718 $[M+H]^+$, 720 $[M(^{34}S)+H]^+$.

***m*-Iodo-substituted trisperfluoroaryl triazine 4.** In an oven dried round bottom flask thiocyanuric acid (50.0 mg, 0.28 mmol) and DIPEA (0.17 mL, 0.99 mmol) were dissolved in dry THF (5 mL). The solution was placed under Ar. 2,4,5,6-tetrafluoro-3-iodochloromethylbenzene[18] (0.34 g, 0.99 mmol) was added and the solution was allowed to stir at room temperature overnight. Purification with flash chromatography over silica gel with gradient Hex:DCM yielded the product as an off white solid (0.26 g, 90 % crude). Small impurities present. ^{1}H NMR (300 MHz, $CDCl_3$) δ 4.43 (s). ^{19}F NMR (471 MHz, $CDCl_3$)[a] δ -97.07 (d, J = 9.9 Hz), -112.40 (dd, J = 22.8, 6.9 Hz), -132.11 (dd, J = 20.9, 6.8 Hz), -160.88 (td, J = 21.8, 9.9 Hz). ^{13}C NMR (126 MHz, $CDCl_3$) δ 178.62 , 155.64 (ddt, J = 245.1, 8.2, 3.5 Hz), 152.59–150.57 (m), 150.48–148.38 (m), 136.80 (dtd, J = 253.5, 17.1, 5.2 Hz), 110.48 (ddd, J = 21.3, 16.4, 3.7 Hz), 66.14 (ddd, J = 32.2, 26.8, 4.7 Hz), 22.21.

***m*-Unsubstituted tristetrafluoroaryl triazine 5.** In an oven dried round bottom flask thiocyanuric acid (0.13 g, 0.72 mmol) and DIPEA (0.44 mL, 2.52 mmol) were dissolved in dry THF (15 mL). The solution was placed under Ar. 2,4,5,6-tetrafluorochloromethylbenzene (0.34 mL, 2.52 mmol) was added and the solution was allowed to stir at room temperature overnight. Purification with flash chromatography over silica gel with gradient Hex:DCM yielded the product (80.5 mg, 16 % crude). Impurities present. ^{1}H NMR (300 MHz, $CDCl_3$) δ 6.80 (tdd, J = 9.5, 5.9, 2.3 Hz, 3H), 4.43 (s, 6H). ^{19}F NMR (282 MHz, $CDCl_3$)[a] δ -115.95 (t, J = 10.3 Hz), -132.07 (dt, J = 21.2, 7.8 Hz), -132.97 (dd, J = 21.0, 5.9 Hz), -164.39 (tdd, J = 20.9, 11.2, 5.9 Hz).

II.5. Notes

[a] No reference was utilized in the ^{19}F NMR spectra.

II.6. Bridge to Chapter III

This chapter focused on my initial project designs to better understand and isolate anion–π interactions in solution studies. Chapter III will introduce the project in which this goal was realized, utilizing the arylethynyl scaffolding introduced in Chapter I.

CHAPTER III

SELECTIVE NITRATE BINDING IN COMPETITIVE HYDROGEN BONDING SOLVENTS: DO ANION–π INTERACTIONS FACILITATE NITRATE SELECTIVITY?

The work in Chapter III was published in volume 52 of the journal *Angewandte Chemie, International Edition* in September 2013. Dr. Lev Zakharov collected and solved the diffraction data for the crystal structure of **1**, **1**•NO_3^-, and **1**•Cl^-. My advisors and principle investigators, Profs. Darren W. Johnson and Michael M. Haley, conceptualized this research and provided editorial assistance for this publication.

III.1. Introduction

Anions are increasingly recognized as problematic environmental contaminants. For example, excess nitrate in soil from over-fertilization has led to contamination in water sources worldwide.[1] Nitrate run-off into water sources causes algal blooms, a process known as eutrophication, which ultimately deprives water of oxygen and leads to dead zones in the world's lakes and oceans. Given the negative impact nitrate has on water sources, there has been considerable interest in the design and synthesis of receptors capable of sensing the molecule in solution. A number of studies have reported synthetic neutral receptors capable of binding nitrate in solution; however, most exhibit low affinity.[2-8] Some reports have shown enhanced nitrate binding in polar solvents, such as $CHCl_3$,[9-12] and even a few demonstrate high nitrate binding in

more competitive solvents;[13-19] however, selectivity for nitrate remains rare.[2,4,8,18,19] We report new tripodal receptor **1** that exhibits strong binding of nitrate in polar, competitive solvents and shows modest selectivity for nitrate over common interferents, such as chloride. Control receptor **2**, lacking an electron-deficient aromatic ring, exhibits no such selectivity for nitrate. A close contact between nitrate and an alkyne within the receptor suggests an anion–π-type interaction may enhance nitrate binding.

Recently, examples indicating the presence of anion–π interactions in solution have emerged, often accompanied by complementary solid-state evidence. A functionalized naphthalenediimide chain has shown a high selectivity for transporting nitrate over acetate in vesicles.[20] Similarly, a perfluorobenzene calixarene-based ditopic receptor showed chloride ion transport across a lipid membrane, despite a lack of detectable chloride binding from ^{19}F NMR spectroscopy.[21] Attempts to quantify non-charge-transfer anion–π interactions have proved difficult because of their innate weakness; however, an "enforced proximity" approach has been used to quantify a small but favorable anion–π interaction in a nitro-substituted octamethyl calix[4]pyrroles.[22] Most recently, nitrate–π interactions have been further quantified for a series of disubstituted calix[4]pyrroles in which nitrate is likely sandwiched between two electron-deficient aryl substituents.[23] Two such receptors showed selectivity for the transport of nitrate over chloride across lipid membranes.[23] The work presented herein suggests an influence of anion–π-type interactions in the observed nitrate selectivity.[a]

III.2. Results and Discussion

We have previously modified a bis(arylethynyl)pyridine scaffold to make a series of receptors studied for their anion-binding capabilities.[24-27] Binding of these systems has been characterized through an electronic response by fluorescence. In the work presented herein, we sought to design and synthesize a three-fold symmetric receptor

(**1**) for binding nitrate. Molecular models suggested the tripodal structure and urea functionalities are likely to bind trigonal planar anions. Nitrate should be able to accommodate six hydrogen bond donors, which is more easily accomplished with diprotic donors, such as ureas.[28,29] Furthermore, the electron-deficient central arene of **1** would enhance the chances of a three-fold symmetric binding motif. For comparison, an unsubstituted, more electron-rich analogue (**2**) was synthesized. The 1,3,5-trifluorobenzene core (**3**) was obtained in 93 % yield through a Sonogashira cross-coupling at 70 °C between 1,3,5-trifluoro-2,4,6-triiodobenzene[30] and 4-*tert*-butyl-2-ethynylaniline (Scheme 1).[27,31] Similarly, the unsubstituted core (4) was synthesized in 60 % yield from triiodobenzene.[32,33] Subsequent reaction of **3** and **4** with *p*-nitrophenylisocyanate in toluene provided receptor **1** in 67 % yield and **2** in 57 % yield, respectively.

Scheme 1. Synthesis of tripodal receptors **1** and **2**.

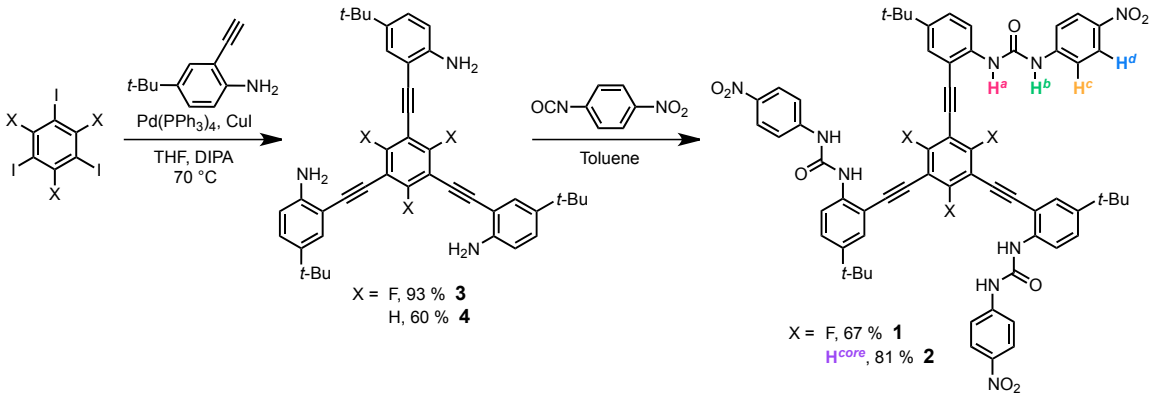

Single crystals of **1** were obtained by vapor diffusion of pentane into acetone. The solid state structure shows a tight dimer held together by an intricate network of hydrogen bonds (Figure 1). Two monomers stack on top of each other through slip-stacked π–π interactions of the central benzene. Two urea arms on one host molecule bind two urea arms on the second host with one as the donor, the other as the acceptor. The urea protons not involved in interactions of self-association bind acetone

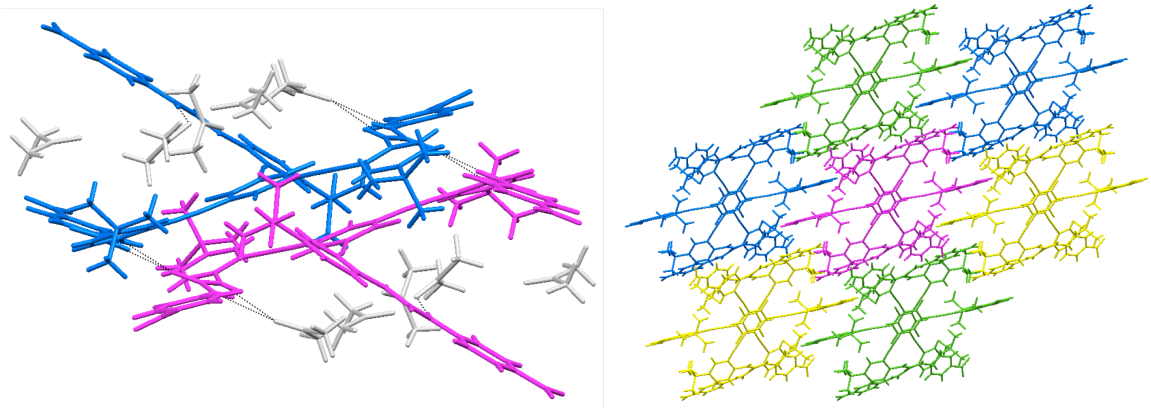

Figure 1. Crystal packing of **1** (left) showing a dimer capped by a total of eight acetone molecules and (right) showing these dimers are mostly discrete, interacting with each other through only π-stacking (solvent omitted for clarity).

molecules. The third arm of each monomer sticks out of the plane defined by the core and the other two arms. The dimer is capped on each side by a total of eight acetone molecules. Each dimer interacts with another through π-stacking of the third protruding arm.

Interaction of 1 with anions in solution was investigated by ^{1}H NMR spectroscopy. Initial titration experiments were performed at 0.5 mM of **1** in d_6-acetone owing to its limited solubility in other solvents, despite the potential solvent competition as a hydrogen bond acceptor. Addition of tetrabutylammonium (TBA) salts of chloride, bromide, and nitrate resulted in a downfield shift of both urea protons H^a and H^b (labels refer to assignments shown in Scheme 1). Changes in chemical shifts of phenyl protons H^c and H^d were also observed, but to a lesser extent, with H^d moving upfield (Figure 2). Large downfield shifts of the urea protons indicate hydrogen bonds of the ureas to the anion as the main mode of binding. Change in chemical shift corresponding to the addition of NO_3^- or Br^- begins to maximize at approximately 0.5 equiv. of guest, indicating a possible 2:1 binding model in acetone. Non-linear regression analysis[34] of these data failed to provide reproducible binding constants with 1:1 or 2:1 models for NO_3^- or Br^-. The sharp transition seen in the binding curves often

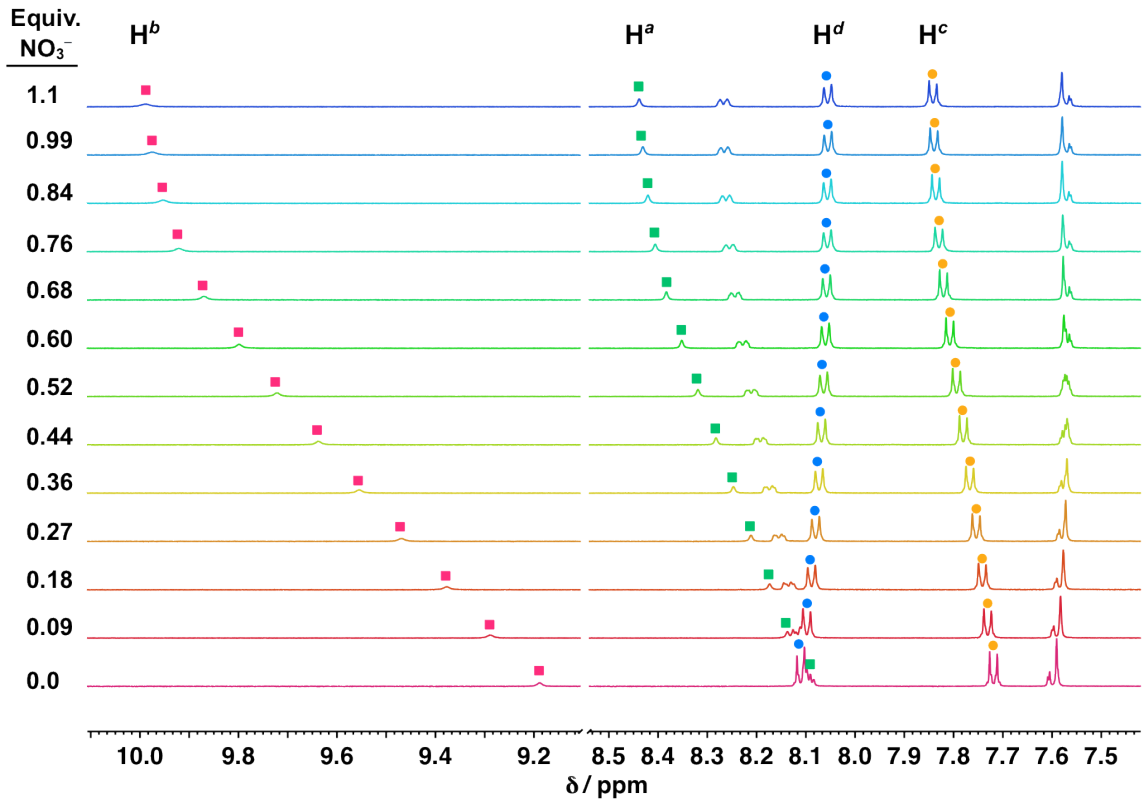

Figure 2. Example of a stacked ^{1}H NMR spectra for the titration of nitrate into a 1 mM solution of receptor **1** in 10 % d_6-acetone.

indicates strong binding with $K_a > 10^4$ M^{-1}, which is typically too large to be accurately determined by NMR spectroscopy.[b] Titrations with Cl^- showed the $\Delta\delta$ maximizing closer to 1 equiv. of guest. Non-linear regression analysis[34] of these data provided a 1:1 binding constant for Cl^- of 8620 ± 1170 M^{-1}. This evidence alone is not enough to demonstrate the proposed stronger binding of NO_3^- or Cl^- for **1**; however, it does indicate a strong binding of NO_3^- in acetone and suggests a lower limit for the NO_3^- association constant.[c] For comparison, to the best of our knowledge, the largest association constants previously reported in the literature for nitrate binding of neutral receptors in acetone are 3470 M^{-1} for a *p*-ureapyridine-based receptor[16] and 910 M^{-1} for a 1,4-diaryl triazole oligomer.[15]

Preferential binding of chloride and nitrate to **1** over the competitive solvent acetone was also demonstrated in the solid state (Figure 3). Single crystals of **1** binding TBACl and $TBANO_3$ were grown through vapor diffusion of pentane into acetone. Comparison of the solid state structures shows the packing of **1** with Cl^- (Figure 3b,d) and with NO_3^- (Figure 3f,h) to be remarkably similar. A single host molecule binds two anions through hydrogen bonds to the ureas of two arms (Figure 3a,e). The hydrogen bonds between **1** and NO_3^- are shorter than those of **1** and Cl^-, with $N_{urea}\cdots O_{nitrate}$ distances of 2.874(6) and 3.089(6) Å for one urea and 3.008(5) and 2.887(5) Å for the other, compared to $N_{urea}\cdots Cl^-$ distances of 3.324(3) and 3.244(3) Å for one urea and 3.175(3) and 3.314(3) Å for the other. Each anion is located over the alkyne of a single monomer. Once again, NO_3^- is held closer to the monomer than Cl^-, as seen in Figure 3c,g. The closest interaction of Cl^- to the monomer is to one alkyne carbon with a distance of 3.796 Å. However, for nitrate the anionic π-system appears to align with

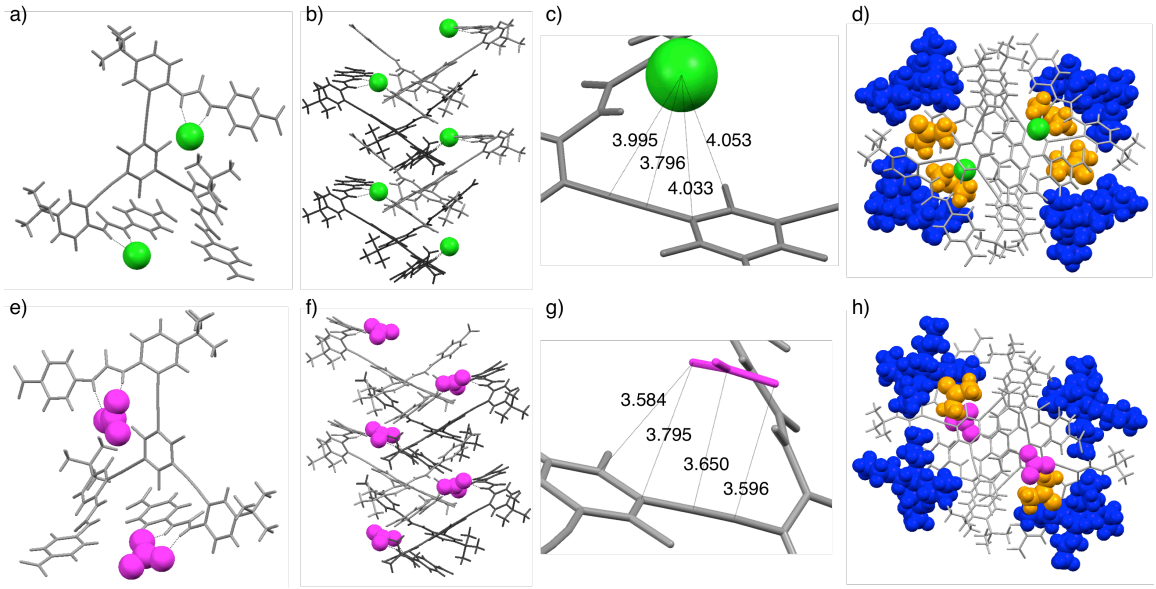

Figure 3. Crystal packing of **1** with (a-d) TBACl and (e-h) $TBANO_3$, highlighting the overall 1:1 interactions between host and anionic guest in the (a,e) monomer, (b,f) stacked column, and with the conjugated π-system (c,g). Cation (blue) and solvent (orange) interactions are shown in d and h.

the π-system of the receptor, supporting some intermolecular distances less than 3.7 Å (Figure 3g). Crystal packing shows an overall 1:1 binding where the host and anion are arranged in an infinite chain of host–guest–host–guest, and so on (Figure 3b,f). As mentioned, the anion is bound to the host through hydrogen bonds to both urea hydrogens on a single arm of the structure. The urea carbonyl of the same arm is hydrogen bonded to an arm on the receptor, which shares binding to the anion. TBA countercations form solvent-separated ion pairs with both Cl^- (Figure 3d) and NO_3^- (Figure 3h) and are in approximately the same location in each crystal structure.

To simplify the mode of binding in these receptors, as well as to lower the association constant of nitrate and bromide to a measurable amount, other solvent systems were investigated. Low solubility of the tripodal receptors limited the solvent possibilities. We also aimed to maintain competition between binding of the anion and solvent molecules to provide further evidence for the strong binding of nitrate in competitive solvents, a critical feature for applications in environmental monitoring. Increasing concentrations of DMSO in chloroform have been shown to simplify binding models by breaking up self-association and, as a result, higher order binding.[15,18,19,35] Furthermore, DMSO is a strong hydrogen-bond acceptor, and thus a lower association constant would be expected.[d] Initial upfield shifts, followed by downfield shifts of the urea protons, were observed upon the addition of $TBANO_3$ to 1 mM solutions of **1** in 2 % d_6-DMSO/$CDCl_3$ and 5 % d_6-DMSO/$CDCl_3$. The titration curves indicate a more complicated system than a 1:1 model (Figure 4 and Figure 5); however, the data still could not be fit to a standard model.[e] Raising the DMSO concentration to 10 % d_6-DMSO/$CDCl_3$ decreased the overall change in chemical shift of the urea protons (Figure 6), but a smooth binding curve is observed, indicating self-association (and likely ion-pairing) is no longer occurring. As suspected, titrations of

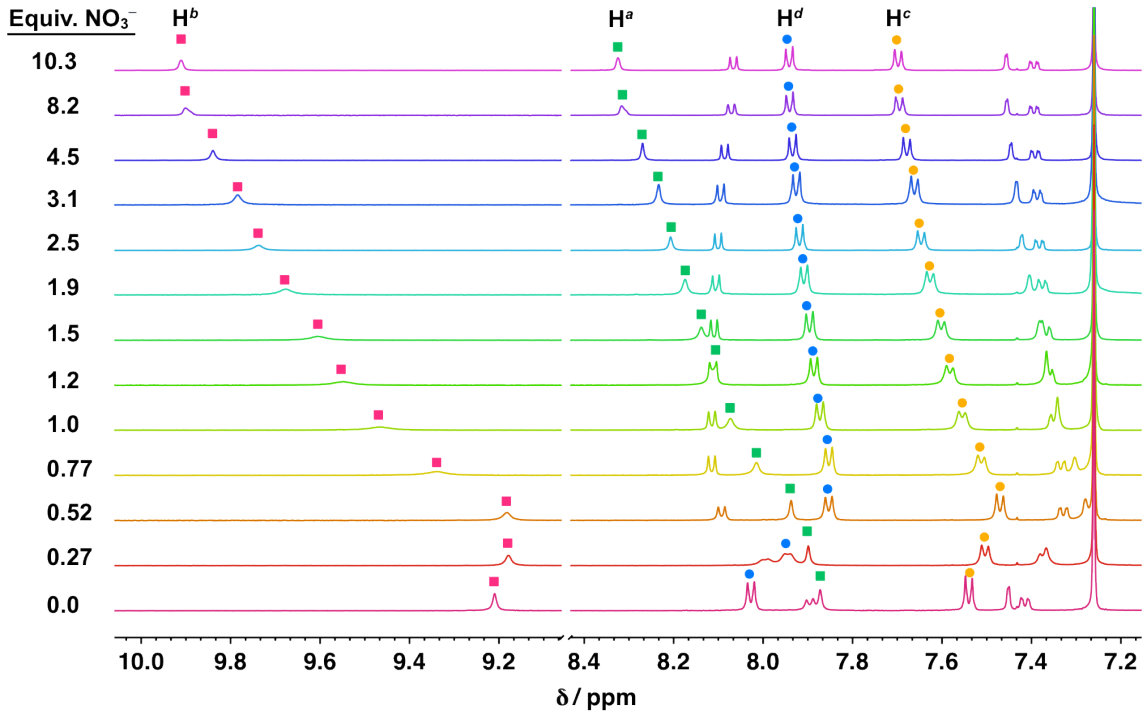

Figure 4. Example of stacked ^{1}H NMR spectra for the titration of nitrate into a 1 mM solution of receptor **1** in 2 % d_6-DMSO/$CDCl_3$.

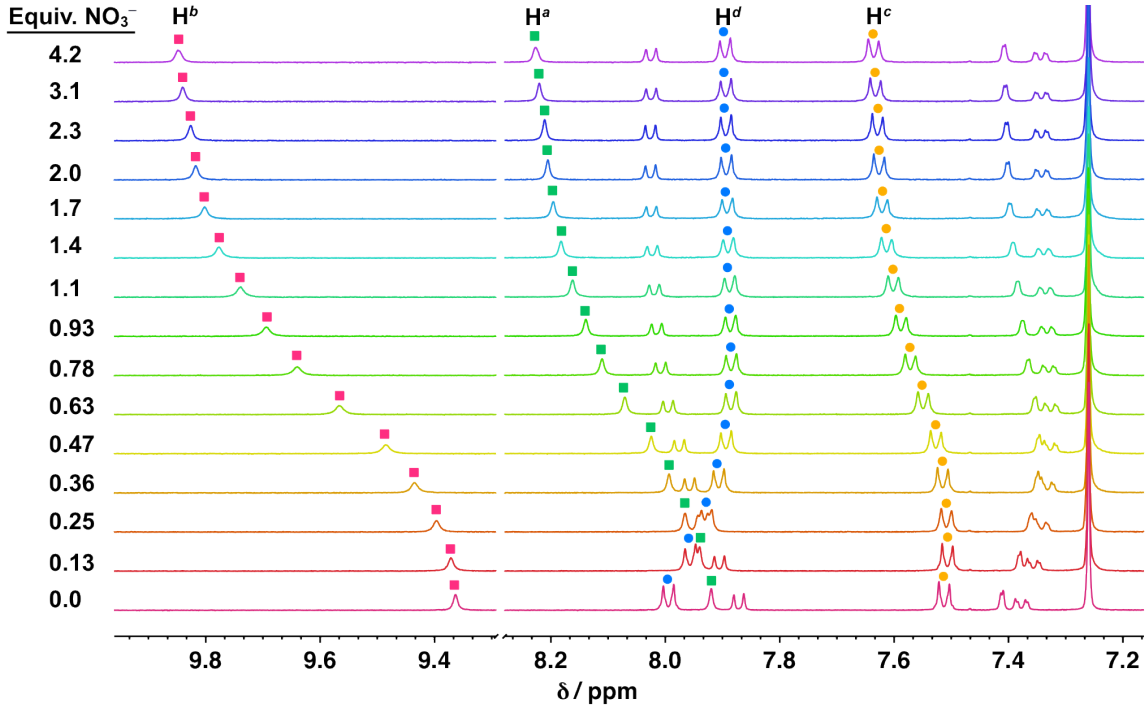

Figure 5. Example of stacked ^{1}H NMR spectra for the titration of nitrate into a 1 mM solution of receptor **1** in 5 % d_6-DMSO/$CDCl_3$.

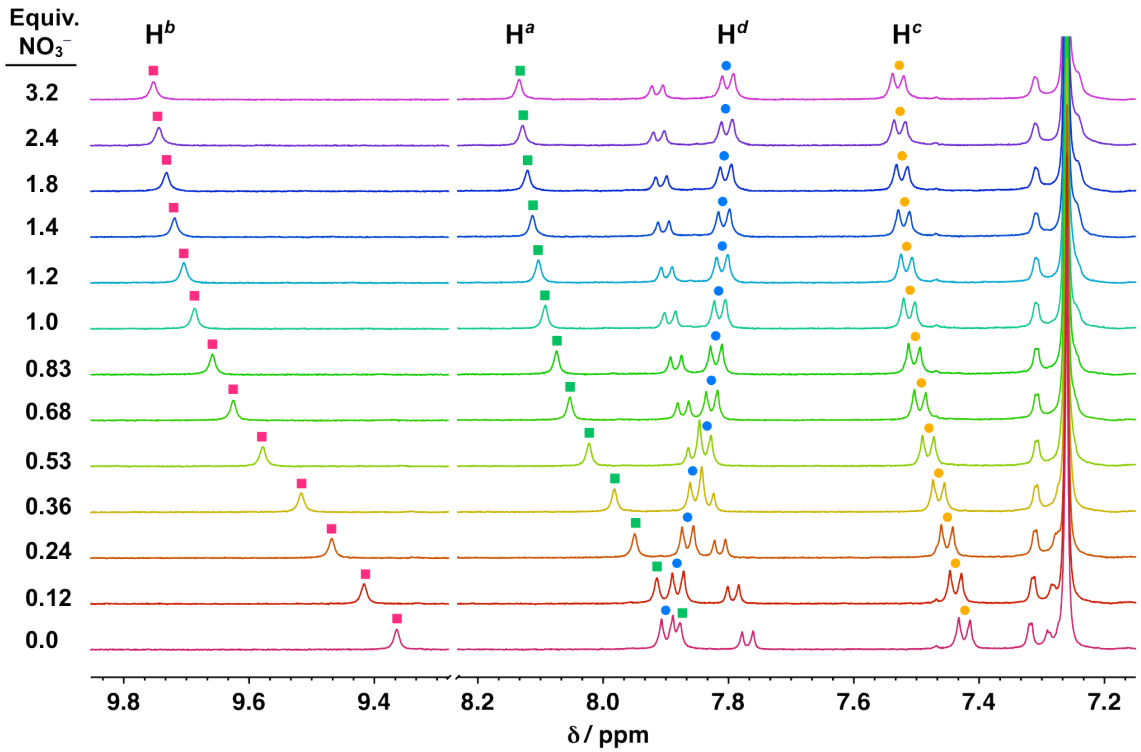

Figure 6. Example of a stacked ^{1}H NMR spectra for the titration of nitrate into a 1 mM solution of receptor **1** in 10 % d_6-DMSO/$CDCl_3$.

TBA salts of nitrate, bromide, chloride, and iodide fit to a 1:1 model when performed in 10 % d_6-DMSO/$CDCl_3$ (Table 1).

Titrations in 10 % d_6-DMSO/$CDCl_3$ were performed at a constant 1 mM concentration of **1**. The change in chemical shift was monitored throughout the titration and fit to a 1:1 model using non-linear regression analysis.[34] Titrations of NO_3^-, Cl^-, and Br^- performed with **1** showed $\Delta\delta$ level off at approximately 1 equiv. of guest, while I^- began to maximize closer to 3 equiv. (Appendix C). The binding constants of each anion investigated and the calculated total $\Delta\delta$ values based on the determined constant are presented in Table 1. The largest changes in chemical shift for each anion are observed in the urea protons of **1**, namely H^a and H^b. H^b moves farthest downfield, demonstrating a stronger hydrogen bond between the anion and this proton.

Table 1. Association constants (K_a, M^{-1}) of **1** and **2** in 10 % DMSO-d_6/$CDCl_3$ determined by monitoring urea protons H^a and H^b and *p*-$NO_2C_6H_4$ protons H^c and H^d during ^1H NMR titrations.[i]

	1			**2**			
	Δδ (ppm)			Δδ (ppm)			
Anion[ii]	H^a [iii]	H^b [iii]	K_a (M^{-1}) [iv]	H^a [iii]	H^b [iii]	H^{core} [v]	K_a (M^{-1}) [iv]
NO_3^-	0.26	0.39	24100 (1050)	0.19	0.27	<0.01	11800 (1570)
Cl^-	0.21	0.99	12200 (934)	0.12	0.97	0.31	63700 (814)
Br^-	0.16	0.62	8320 (876)				—[vii]
I^- [vi]	0.12	0.29	755 (85)				—[vii]

[i] Determined at 25 °C. [ii] Anions added as tetrabutylammonium salts. [iii] Averaged calculated values are based on the determined binding constants. [iv] Values are an average of three titrations. Standard deviation is given in parenthesis. All errors are < 15 %. [v] Averaged values from the observed changes in chemical shift. [vi] Δδ(H) values are over a larger equivalency range for iodide than nitrate, chloride, or bromide. [vii] Not determined.

Chloride has the largest shift in H^b but its measured K_a of 12,200 M^{-1} was not the highest observed association with **1**.

The largest association constant of 24,100 M^{-1} was obtained with NO_3^-, which also had the largest observed shift in H^a, Δδ = 0.26 ppm versus Δδ = 0.21, 0.16, and 0.12 ppm for Cl^-, Br^-, and I^-, respectively. Comparing the other values of H^a with the binding constants, a trend is observed – the larger shift in H^a, the higher the measured 1:1 association constant. Not only is **1** capable of binding anions out of competitive media, the binding of nitrate is significantly higher than chloride.[f] The only comparison in 10 % d_6-DMSO/$CDCl_3$ these authors are aware of is a neutral tripodal cyclic peptide with a 1:1 NO_3^- binding constant of 126 M^{-1} and no selectivity for NO_3^- is observed.[14] Selectivity for NO_3^- over Cl^- and I^- has been demonstrated in 100 % d_6-DMSO for a NHBoc-substituted macrocyclic triamide with a NO_3^- association constant of 20 M^{-1}.[18,19] To the best of our knowledge, tripodal host **1** exhibits the strongest nitrate binding for a neutral receptor in competitive solvents, and an anion–π interaction appears to facilitate, if not enhance, this binding.

More detailed analysis of the binding modes of anions with **1** and the selectivity of NO_3^- in this system will be investigated in the near future; however, some

observations are worth noting. The trend in binding constants corresponds to the observed $\Delta\delta$ values of H^a. A larger value of $\Delta\delta$ would typically indicate a stronger and shorter hydrogen bond of the urea proton to the anion, which would correspond to the anion being in closer proximity to the aryl core. This presents an argument for the presence of an anion–π interaction. The crystal structure of the nitrate-bound host supports this hypothesis, and reveals a clear interaction between the nitrate anion and the π-system of the aryl core and the alkyne (for example, see Figure 3g showing $N/O_{nitrate}\cdots C_{alkynyl}$ contacts distances of 3.596 and 3.650 Å). As previously discussed, the distances of NO_3^- to the aryl core and alkyne are significantly shorter than those of Cl^-. An electrostatic potential map of **1** indicates a lack of electron density in the arene as well as the conjugated alkynes (Appendix C). The question arises as to why nitrate would have a stronger interaction with the π-system than chloride. Nitrate itself possesses a conjugated π-system, so this could be suggestive of a favorable π–π type interaction; nevertheless, one of the partners in this interaction is anionic making this a clear example of an anion–π interaction of some type or a "π–π-assisted anion–π" interaction.

To further investigate this claim, unsubstituted and more electron-rich receptor **2** was synthesized for comparison to electron-deficient **1**. Along with the change in the electronics providing weakened anion–π interactions, the extra proton in **2**, H^{core}, could provide further insight into the binding mode.

Similar to **1**, host–guest complexes of **2** were investigated through ^1H NMR spectroscopy titrations in 10 % d_6-DMSO/$CDCl_3$. Titrations were performed at approximately 1 mM **2** with TBA salts of Cl^- and NO_3^-. The urea protons (H^a and H^b), nitrophenyl protons (H^c and H^d), and core proton (H^{core}) were monitored throughout the titrations. For consistency, only H^a, H^b, H^c, and H^d were used to fit the data to a 1:1 model, as was done with **1**. All changes in chemical shift began to level off near 1

equiv. of anion and are presented in Table 1 with association constants corresponding to NO_3^- and Cl^-. The values reported for H^a and H^b are averages derived from the individual association constants of each titration, while the values for H^{core} are averaged from the observed changes during the titration.

Replacing the fluorine atoms with hydrogens changes not only the electronics, but also the number of hydrogen bond donors. This combination leads to a loss in selectivity for NO_3^- over Cl^-. Chloride binding is now enhanced, with an association constant for **2** of 63,700 M^{-1}, whereas nitrate binding is weakened to 11,800 M^{-1}. Any anion–π interactions would be weakened or now repulsive owing to the change in electronics within the central ring, so weakening of the binding would be expected, as seen with NO_3^-. The large increase in K_a for Cl^- can be attributed to the addition of a hydrogen bond with H^{core},[36] assigned from the titration of **2** (Figure 7). This hydrogen bond is observably stronger ($\Delta\delta$ = 0.31 ppm versus $\Delta\delta$ = 0.12 ppm) than that of H^a, which correlated to K_a for **1**. The association constant for NO_3^- with **2** trends with the noted correlation and indicates **2** may bind NO_3^- by a similar mode as **1**, but binds Cl^- through a different mode. More importantly, no significant shift of H^{core} occurs upon the addition of nitrate to **2** (Figure 6), thus there is no hydrogen bonding of the anion to H^{core}, indicating an anion–π interaction may still be the preferred mode of binding, despite the more electron-rich arene. Three important results stem from the investigation of **2**: nitrate selectivity is lost, the association constant of nitrate is diminished, and nitrate binds via a different mode than chloride. These data support a model in which nitrate binds to the receptor through an anion–π-type interaction regardless of the electronics, while chloride prefers to bind through a hydrogen bond to the core of **2** rather than to the π-system, effectively raising the association constant.

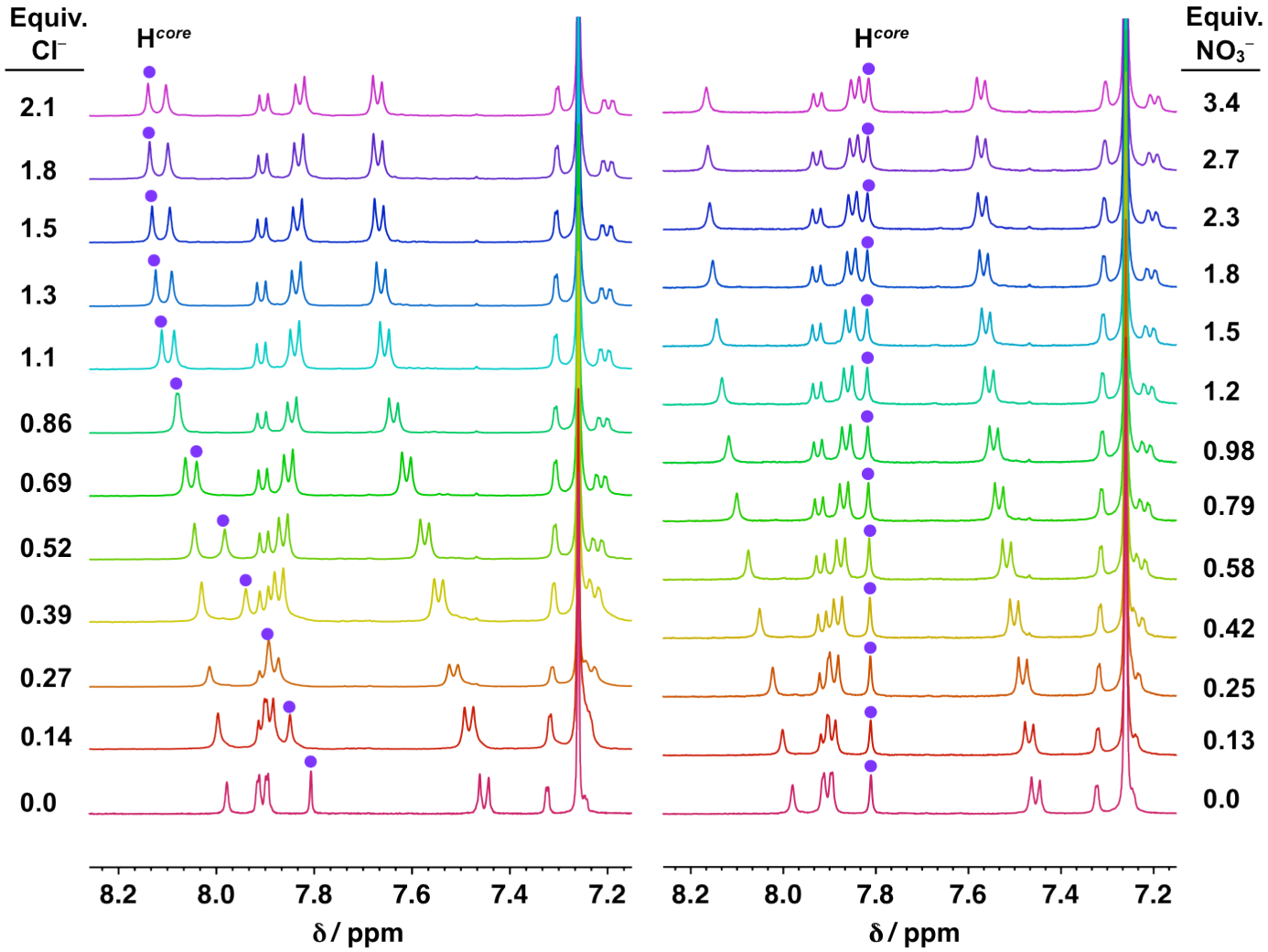

Figure 7. Stacked ^{1}H NMR spectra for the titration of Cl^{-} (left) and NO_3^{-} (right) into a 1 mM solution of receptor **2** in 10 % d_6-DMSO/$CDCl_3$.

III.3. Conclusions

The tripodal receptors presented herein demonstrate preferential binding of anions over competitive hydrogen bonding solvents, namely d_6-acetone and 10 % d_6-DMSO/$CDCl_3$. The binding of nitrate and bromide to **1** in d_6-acetone could not be accurately determined. The association of chloride to **1** is actually higher in the 10 % d_6-DMSO/$CDCl_3$ solution than in d_6-acetone, whereas the association of both bromide and nitrate are lower. Receptors **1** and **2** bind anions out of 10 % d_6-DMSO/$CDCl_3$ in a 1:1 stoichiometry. A strong affinity for the anions is observed even in the presence of d_6-DMSO and the binding of **1** trends: $NO_3^- > Cl^- > Br^- > I^-$, with a moderate selectivity for nitrate possibly resulting from an anion–π interaction. Binding studies of **2** support the existence of a favorable anion–π interaction by demonstrating a loss in nitrate selectivity and indicating an anion–π-type interaction still is the preferred mode of binding for nitrate. We intend to expand the investigation of **1** and **2** to other anionic substrates as well as further probing the influence of an anion–π interaction.

III.4. Experimental

Trifluorobenzene/trianiline core 3. In a sealable flask 1,3,5-trifluoro-2,4,6-triiodobenzene (2.824 g, 5.54 mmol) was dissolved in DIPA (100 mL) and THF (100 mL), then CuI (0.105 g, 0.551 mmol) was added. The mixture was purged with Ar for 30 min, then $Pd(PPh_3)_4$ (0.510 g, 0.441 mmol) was carefully added. An Ar-purged solution of 4-*tert*-butyl-2-ethynylaniline (4.80 g, 27.7 mmol) in DIPA (40 mL) and THF (40 mL) was then transferred into the flask via cannula. The flask was sealed and heated to 70 °C overnight. After cooling, the solvent was removed *in vacuo*, and the residue run through a plug of silica using CH_2Cl_2. The crude product, suitable for continuation, was obtained by precipitation out of the CH_2Cl_2 solution using hexanes. Pure product **3** was obtained by column chromatography (4:1 CH_2Cl_2:hexanes) as an

off-white solid (3.33 g, 93 % yield.) ^{1}H NMR (600 MHz, $CDCl_3$) δ 7.40 (d, J = 2.2 Hz, 3H), 7.25 (dd, J = 8.5, 2.2 Hz, 3H), 6.71 (d, J = 8.5 Hz, 3H), 4.26 (s, 6H), 1.30 (s, 27H). ^{13}C NMR (151 MHz, $CDCl_3$) δ 160.83 (dt, J = 251.9, 7.1 Hz), 146.15, 140.99, 128.64, 128.44, 114.57, 106.13, 100.35 (m), 97.79, 79.29, 34.08, 31.51. LRMS (ESI) *m/e* 646.3 (M^+,100), 323.7 (60). HRMS (ESI) for $C_{42}H_{43}N_3F_3$ [M^+]: calcd 646.3409, found 646.3387.

Benzene/trianiline core 4. Following the procedure for synthesis of **3**, 1,3,5-triiodobenzene (0.364 g, 0.80 mmol) was reacted with 4-*tert*-butyl-2-ethynylaniline (0.691 g, 4.00 mmol) in the presence of THF (5 mL), DIPA (5 mL), CuI (0.015 g, 0.078 mmol) and $Pd(PPh_3)_4$ (0.075 g, 0.065 mmol). Pure product **4** was obtained as an off-white solid by precipitation out of CH_2Cl_2 using hexanes (0.285 g, 60 % yield.) ^{1}H NMR (600 MHz, $CDCl_3$) δ 7.67 (s, 3H), 7.41 (d, J = 2.3 Hz, 3H), 7.23 (dd, J = 8.5, 2.3 Hz, 3H), 6.71 (d, J = 8.5 Hz, 3H), 4.20 (s, 6H), 1.32 (s, 27H). ^{13}C NMR (151 MHz, $CDCl_3$) δ 145.73, 141.03, 133.50, 128.92, 127.65, 124.34, 114.53, 107.01, 92.79, 88.00, 34.03, 31.51. LRMS (ESI) *m/e* 592.4 (M^+, 100), 296.7 (65). HRMS (ESI) for $C_{42}H_{46}N_3$ [M^+]: calcd 592.3692, found 592.3674.

Receptor 1. In oven dried glassware, trisaniline **3** (0.300 g, 0.465 mmol) and *p*-nitrophenyl isocyanate (0.457 g, 2.787 mmol) were dissolved in freshly distilled toluene (75 mL). The reaction mixture was stirred overnight, quenched with acetone, and product **1** was precipitated cleanly with hexanes (0.354 g, 67 % yield). ^{1}H NMR (600 MHz, DMSO-d_6) δ 9.95 (s, 3H), 8.45 (s, 3H), 8.12 (d, J = 9.2 Hz, 6H), 7.89 (d, J = 8.7 Hz, 3H), 7.65 (d, J = 9.2 Hz, 6H), 7.55 (dd, J = 8.7, 2.4 Hz, 3H), 7.49 (d, J = 2.4 Hz, 3H), 1.28 (s, 27H). ^{13}C NMR (151 MHz, DMSO-d_6) δ 161.36 (dt, J = 261.1, 7.4 Hz), 151.82, 146.05, 146.01, 141.13, 137.48, 128.65, 128.26, 125.08, 121.45, 117.50, 111.54, 99.57 (m), 96.78, 78.75, 39.52, 34.07, 30.89. LRMS (ESI) *m/e* 1138.4 (M^+, 90), 242.3 (100). HRMS (ESI) for $C_{63}H_{55}N_9O_9F_3$ [M^+]: calcd 1138.4075, found 1138.4045.

Receptor 2. In oven dried glassware, trisaniline **4** (85 mg, 0.144 mmol) and *p*-nitrophenyl isocyanate (0.148 g, 0.862 mmol) were dissolved in freshly distilled toluene (15 mL). The reaction mixture was stirred overnight, quenched with acetone, and product **2** was obtained cleanly by repeated precipitation from acetone with hexanes (89 mg, 57 % yield). ^{1}H NMR (600 MHz, DMSO-d_6) δ 10.20 (s, 3H), 8.46 (s, 3H), 8.10 (d, J = 8.8 Hz, 6H), 8.07 (s, 3H), 8.03 (d, J = 8.7 Hz, 3H), 7.69 (d, J = 8.9 Hz, 6H), 7.57 (d, J = 2.4 Hz, 3H), 7.50 (dd, J = 9.0, 2.4 Hz, 3H), 1.31 (s, 27H). ^{13}C NMR (151 MHz, DMSO-d_6) δ151.78, 146.07, 145.44, 141.07, 137.28, 134.27, 128.94, 127.34, 125.05, 123.52, 120.25, 117.49, 111.37, 92.99, 87.45, 34.05, 30.97. LRMS (ESI) *m/e* 1084.4 (M^+, 98), 208.0 (100). HRMS (ESI) for $C_{63}H_{58}N_9O_9$ [M^+]: calcd 1084.4358, found 1084.4368.

III.5. Notes

[a] We recognize the observed interaction between nitrate and the π-system may simply be π-stacking between nitrate and an arylalkyne; however, such an interaction might still be broadly described as "anion–π" since one partner in the association is anionic.

[b] Values obtained using the 1:1 Thordarson fitting program consistently gave association constants on the order of 10^4 M^{-1} for bromide and 10^5 M^{-1} for nitrate, albeit high errors and poor overall fit.

[c] Given the possibility of 2:1 binding modes for NO_3^- or Br^- in d_6-acetone, and evidence of solid state dimerization, self-association of **1** in acetone was investigated. The data obtained could not be fit to a self-association/dimerization model (even when dimerization was assumed). While this evidence provides little assistance in fitting NO_3^- or Br^- titration data, it shows the receptor aggregates in acetone. This, coupled to the potential for association constants larger than 10^4 M^{-1}, led us to investigate the binding in other solvents.

[d] No changes in chemical shift were observed upon titration of nitrate into **1** in neat d_6-DMSO.

[e] Results indicate a 2:1 binding model breaking up to 1:1 upon the further addition of anion. The 2:1 model likely results from self-aggregation of the receptor in these polar solvent mixtures.

[f] Statistical significance determined by a t-test comparing the values obtained for nitrate binding versus those of chloride binding. The difference between the two was found to be significant with 99.9 % certainty.

III.6. Bridge to Chapter IV

Chapter III introduced tripodal tris-urea receptors which bound anions in a competitive solvent system. These systems demonstrated binding through anion–π interactions in solution, a notoriously difficult task. This interaction was demonstrated to be pivotal for the selectivity of nitrate over chloride in the fluoro-substituted receptor. Chapter IV expands on this receptor series with a methoxy-substitution on the phenyl urea moieties. In addition, the anion binding studies are continued to include tetrahedral and more basic anions.

CHAPTER IV

ANION BINDING PROPERTIES OF TRIPODAL ARYLETHYNYL-BASED RECEPTORS

Chapter IV is comprised of unpublished co-authored work, which will be submitted to the journal *Chemical Science* later this year. I wrote the document and performed many of the spectroscopic titrations within. This work is supplemented by synthetic advances and additional titrations performed by an undergraduate student I advised, John Houlihan. The crystal structure data was collected and solved by Dr. Lev Zakharov. Editing was performed by my advisors and principle investigators, Profs. Darren W. Johnson and Michael M. Haley.

IV.1. Introduction

Anions are ubiquitous in the environment and biological systems – naturally occurring or as contaminants. Many of our bis(urea) receptors have taken advantage of a chloride selective turn-on fluorescent response, often in conjunction with aggregation, for future applications in biological sensors.[1-4] A water-soluble version of these bis(ureas) will be discussed in Chapter V. While most of these compounds are studied for potential applications in cell imaging, some versions of our arylethynyl receptors have potential applications in sensing anions in the environment, including nitrate and phosphates. Over fertilization in agriculture results in excess nitrates and phosphates running off into rivers and streams, ultimately leading to eutrophication of larger water bodies. As a result, the UN lists nitrate as the number one contaminant in the world's

aquifers.[5] Levels of perchlorate in the environment can be traced back to fireworks and fuel propellants,[6] while pertechnetate is released in the processing of nuclear fuel.[7] Due to the radioactivity of pertechnetate, perrhenate is often used as a model for binding studies. Accurate sensing of these and other pertinent anions depends significantly on selectively binding a single anionic species of interest.

Previously, we synthesized two tris(urea) arylethynyl receptors with a trifluorobenzene- and phenyl-based core (**1** and **2**, Figure 1).[8] Anion binding properties of both receptors were reported for nitrate and chloride, as well as bromide and iodide with **1**. The arene-based core was determined to bind nitrate, in part, using anion–π type interactions, regardless of the electron density of the arene. More electron-deficient core **1** was selective for nitrate over the halogens due to this phenomenon. When the core was switched to benzene (**2**) from trifluorobenzene (**1**), the electron-density of the arene was increased and this selectivity was lost. Receptor **2** binds chloride more strongly than receptor **1** via a hydrogen bond interaction between the halide and proton on the core arene.

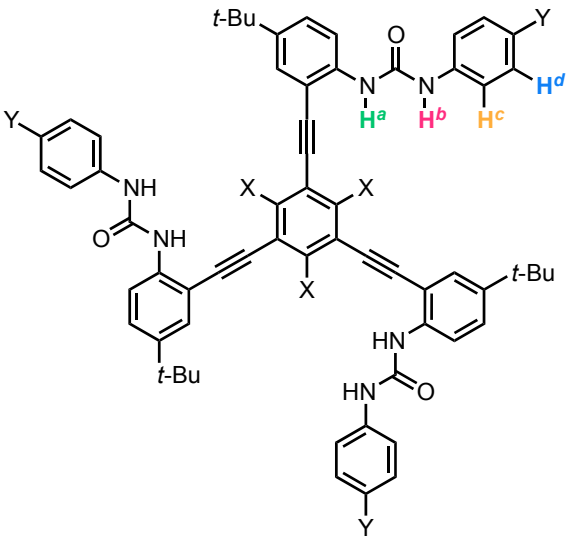

1 X = F, Y = NO_2
2 X = H^{core}, Y = NO_2
3 X = H^{core}, Y = OMe

Figure 1. Tripodal receptors **1**, **2**, and **3**.

To expand further on this receptor series, methoxy substituted analogues were envisioned in place of the nitro substitution of **1** and **2**. Receptor **3** possesses an electron-donating group on the peripheral arenes which will affect the binding of the ureas as well as possibly change the fluorescent properties of the receptor class. While receptors **1** and **2** are non-fluorescent with and without the presence of a guest, **3** is

inherently fluorescent. Unfortunately, this fluorescence is also not affected by the presence of guest thus far. Additionally, we sought to further investigate the selectivity of our system by expanding our anion set.

IV.2. Synthesis

The synthesis of receptors **1** and **2** were previously reported in Chapter III.[8] Synthesis of **3** is performed in the same manner as the prior receptors through reaction of the unsubstituted trisaniline core with *p*-methoxyphenyl isocyanate in toluene with a 57 % yield (Appendix D). A fourth receptor with X = F, Y = OMe was synthesized, however purification proved problematic.

IV.3. Crystal Structure of 2

Crystals of diffraction quality were obtained through slow evaporation of either acetone or DMSO. The structure of **2•DMSO** is disordered throughout the solvent molecules and within the *t*-butyl groups. Monomers of **2•DMSO** and **2•Acetone** mirror each other with one arm essentially in the plane of the central arene and the other two arms oriented above and below the plane, similar what is also observed in the crystal structure of **1** (Figure 2). The main difference between **1** and **2** observable in the monomer is the extent to which the arms are oriented out of the plane of the central arene. The arm directed furthest from the plane sits 52.8°, 60.4°, and 53.4° in

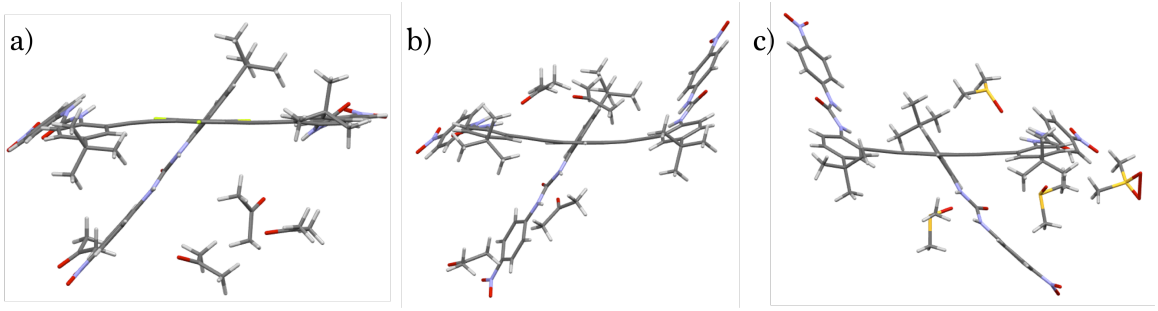

Figure 2. Solid state conformation of the (a) **1•Acetone**, (b) **2•Acetone**, and (c) **2•DMSO** monomers.

1•Acetone, **2•Acetone**, and **2•DMSO**, respectively. The remaining two arms of **1•Acetone** has two arms close to the plane of the central arene with dihedral angles of 9.81° and 7.55°. In contrary, solvates of **2** have one arm close to the plane with dihedral angles from the central arene of 9.21° and 12.8°, while the last arm extends further from the plane by 22.0° and 29.0° for **2•Acetone**, and **2•DMSO**, respectively. The differences in the orientation of monomers **1** and **2** (clearly shown in Figure 2) may result from the dimer formed by **1** (see Chapter III), which is not observed in **2**. While not dimerized, monomers are connected via C_{aryl}–H···O_{urea}, N_{urea}–H···O_{nitro}, and C_{aryl}–H···O_{nitro} hydrogen bonds in an infinite network, with the remaining interactions associated with π-stacking (Figure 3). While the solvates of **2** are similar in orientation with regards to the monomer structure, the intermolecular interactions of **2•DMSO** are minimized in the crystal lattice in comparison to **2•Acetone**. Only C_{aryl}–H···O_{urea} hydrogen bonds and π-stacking interactions are found in the crystal packing of **2•DMSO** (Figure 4). A large volume of solvent molecules are present in **2•DMSO** which accept hydrogen bonds from **2**, occupying all the donating sites of urea moieties. This aligns with previous solution results for **1** which demonstrate the weakening of intramolecular hydrogen bonding in DMSO in comparison to acetone. Crystal growth of **2** with anions has only yielded structures of solvates of **2** thus far.

IV.4. ^{1}H NMR Titrations

Following with the previous study, titrations were typically performed in 10 % d_6-DMSO/$CDCl_3$ at a constant concentration of 1 mM. This study includes titrations of receptors **1**, **2**, and **3** – expanding upon the anions already investigated. The changes in chemical shift of H^a, H^b, H^c, H^d, and H^{core} (when applicable) were monitored throughout the titration. In each case, four protons[a] were globally fit to a 1:1 model

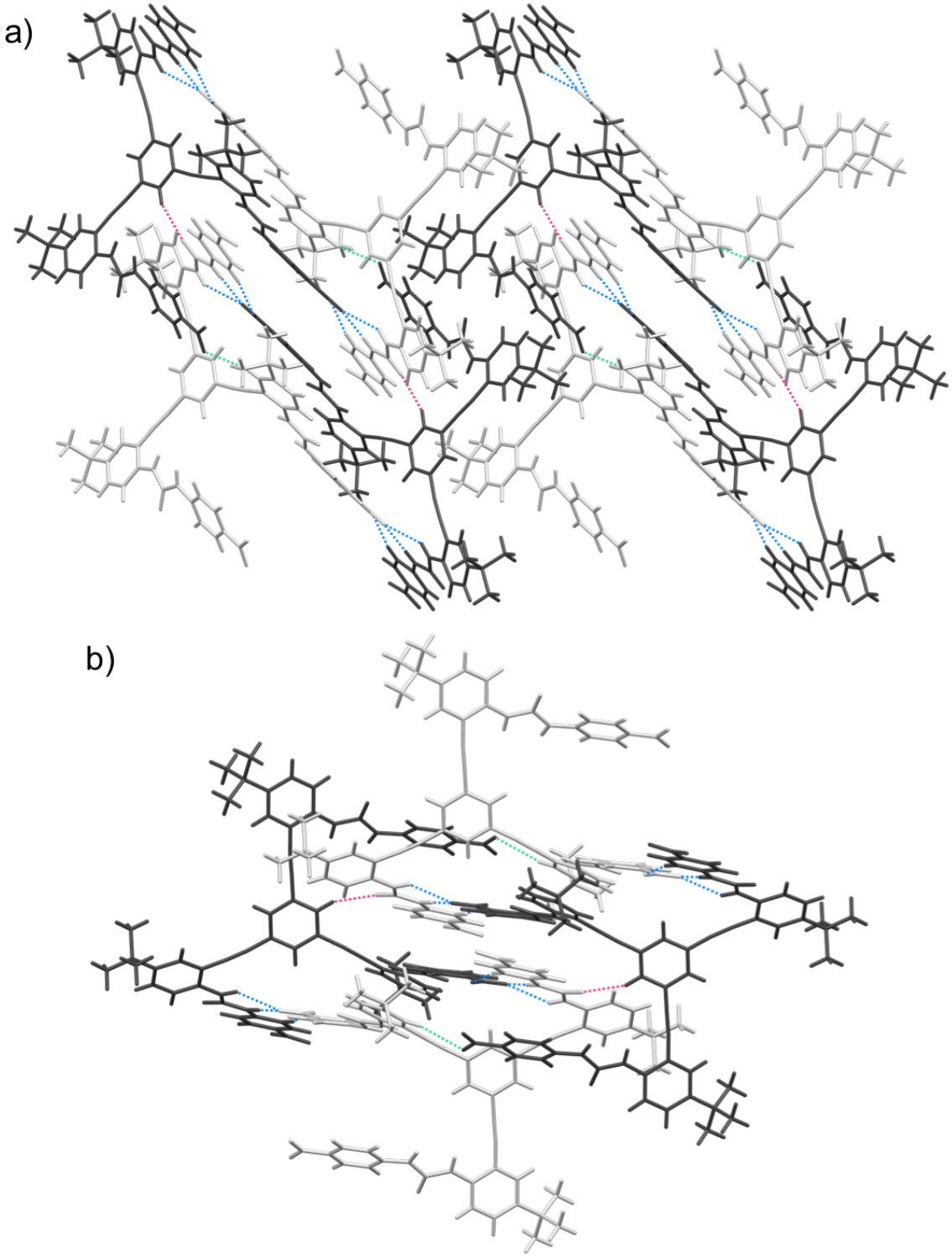

Figure 3. Crystal packing of **2•Acetone** highlighting (a) the hydrogen bond network (C_{aryl}–H···O_{urea}: pink, N_{urea}–H···O_{nitro}: blue, C_{aryl}–H···O_{nitro}: green) and (b) the π-stacking of the arms. (Acetone molecules not shown for clarity)

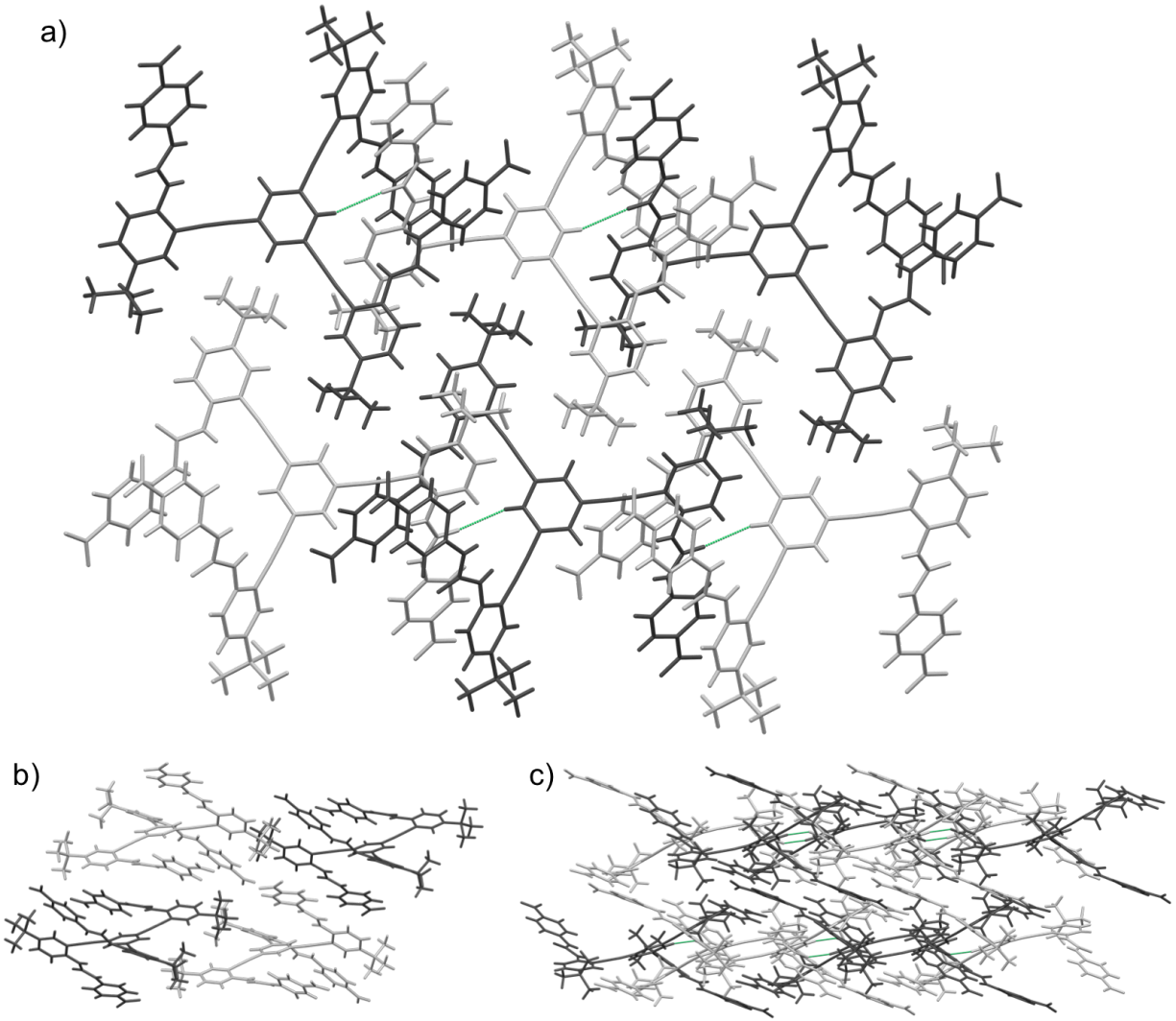

Figure 4. Crystal packing of **2•DMSO** highlighting (a) the hydrogen bond network (C_{aryl}–H···O_{nitro}: green) and (b,c) the layers of host molecules which have no interaction due to their separation by DMSO molecules (not shown for clarity).

using non-linear regression analysis.[9] A summary of the determined 1:1 association constants and the corresponding $\Delta\delta$ values are presented in Table 1.

IV.4.1. ^{1}H NMR Titrations of 1

Initial investigation of this class of receptors focused on the binding of nitrate in comparison to halogens, particularly chloride, as receptors are rarely selective for nitrate over chloride. In this chapter, we seek to expand upon the anions investigated to determine the selectivity of **1** with regards to oxyanions. Beyond those previously determined, association constants of TBA hydrogen sulfate, sulfate, acetate, dihydrogen phosphate, perchlorate and perrhenate were sought. Tris(urea) receptors have been demonstrated to bind tetrahedral anions more effectively than trigonal planar ones via computations.[10] This study explored binding configurations by simplifying the receptor to the configuration of urea groups and did not consider the potential effect of the tethering moiety.

Titrations of hydrogen sulfate performed in 10 % d_6-DMSO/$CDCl_3$ produced steep changes in chemical shifts of H^a, H^b, H^c, and H^d (Figure 5a), similar to those seen in the titrations of nitrate in acetone, indicating strong association. Large error across a set of triplicate titrations further established the inability to determine a 1:1 binding constant for **1•HSO_4^-** in 10 % d_6-DMSO/$CDCl_3$. Following with our previous study, the concentration of DMSO was increased to weaken association and minimize competing equilibria. The curve produced by the change in chemical shift of H^b in 15 % d_6-DMSO/$CDCl_3$ is indicative of multiple equilibria, while a 20 % volume ratio of DMSO results in a 1:1 fit (Figure 5a,b). As previously observed, downfield shifts result from the addition of anion to **1** for the H^a, H^b, and H^d peaks and an upfield shift for H^c. The association constant for hydrogen sulfate is 7240 M^{-1} in 20 % DMSO. To best compare binding strength, a nitrate association constant was also determined at this

Table 1. Association constants (K_a, M^{-1}) of **1**, **2**, and **3** in volume ratios of DMSO-d_6/$CDCl_3$ determined by a global fit using non-linear regression analysis.

			1			**2**				**3**			
				$\Delta\delta$ (ppm)[iii]			$\Delta\delta$ (ppm)[iii]				$\Delta\delta$ (ppm)[iii]		
Anion[i]	% Volume DMSO	Temp (°C)	K_a (M^{-1})[ii]	H^a	H^b	K_a (M^{-1})[ii]	H^a	H^b	H^{core}	K_a (M^{-1})[ii]	H^a	H^b	H^{core}
Cl^-	10	25	12200 ± 930	0.21	0.99	63700 ± 810	0.12	0.97	0.31	1300 ± 180	0.16	1.10	0.40
Br^-	10	25	8320 ± 880	0.16	0.62	9130 ± 1540[iv]	0.04	0.52	0.24	700 ± 70[v]	0.06	0.49	0.22
I^-	10	25	760 ± 90	0.12	0.29	330 ± 50	0.02	0.22	0.13	30 ± 2	0.03	0.43	0.13
NO_3^-	10	25	24100 ± 1050	0.26	0.39	11800 ± 1570	0.19	0.27	~0	1080 ± 60	0.18	0.35	0.04
	20	25	2200 ± 300	0.15	0.22	—	—	—	—	—	—	—	—
ClO_4^-	10	25	400 ± 90[iv]	-0.01	-0.15	110 ± 15	-0.03	-0.14	~0	—	—	—	—
ReO_4^-	10	25	530 ± 135[vi]	0.04	-0.13	250 ± 50[iv]	0.03	-0.13	-0.02	—	—	—	—
HSO_4^-	10	25	—[vii]	0.23[viii]	0.35[viii]	—	—	—	—	—	—	—	—
	20	25	7240 ± 650	0.17	0.24	—[vii]	0.23[viii],[ix]	0.11[viii],[ix]	0.08[viii],[ix]	—	—	—	—
	30	25	—	—	—	(660)[ix]	0.19[ix]	0.11[ix]	0.09[ix]	—	—	—	—
SO_4^{2-}	10	25	—[x]	—[x]	—[x]	—[x]	—[x]	—[x]	—[x]	—	—	—	—
	10	-20	—[x]	—[x]	—[x]	—	—	—	—	—	—	—	—
AcO^-	10	25	—[vii]	0.96[viii],[ix]	1.89[viii],[ix]	—[vii]	1.28[viii],[ix]	1.94[viii],[ix]	~0	—	—	—	—
	10	30	—	—	—	—[vii]	1.19[viii],[ix]	1.87[viii],[ix]	~0	—	—	—	—
	20	25	—[vii]	0.89[viii],[ix]	1.76[viii],[ix]	—	—	—	—	—	—	—	—
	50	25	—[vii],[xi]	0.79[viii],[ix]	1.56[viii],[ix]	—	—	—	—	—	—	—	—
$H_2PO_4^-$	10	25	—[x]	0.57[viii],[ix]	—[x]	—[vii]	0.89[viii],H	1.95[viii],[ix]	—[xii]	—	—	—	—
	20	25	—	—	—	—[vii]	0.86[viii],[ix]	1.82[viii],[ix]	—[xii]	—	—	—	—

[i] Anions added as tetrabutylammonium salts. [ii] Values are an average of at least three titrations. All errors are < 15 % unless otherwise noted. [iii] Averaged from the calculated values based on the determined binding constants, unless otherwise noted. [iv] An average of > 5 titrations. Error 15 - 23 %. [v] Determined with H^a, H^b, H^d, and H^{core}. [vi] Not a final value, more titrations still need to be performed. [vii] Does not fit well to a 1:1 model. [viii] Averaged values from the observed changes in chemical shift. [ix] Results are from a single titration. [x] Cannot be determined due to broadening. [xi] New peaks appear during the titration. [xii] The overall shift of H^{core} is ~0 ppm, however the peak shifts downfield and back upfield during the titration.

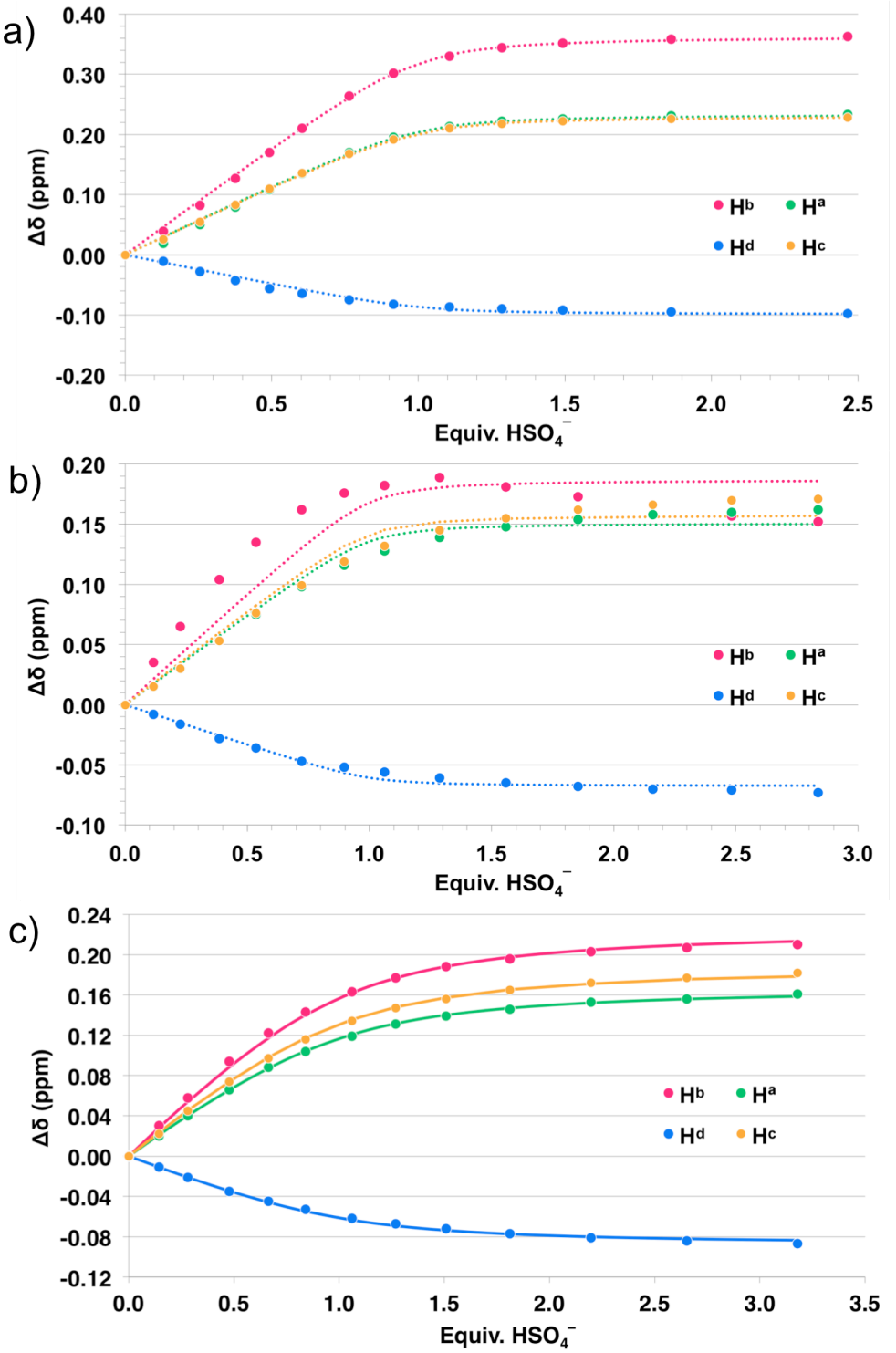

Figure 5. Example plots of observed $\Delta\delta$ (points) upon the titration of tetrabutylammonium hydrogen sulfate in (a) 10 %, (b) 15 %, and (c) 20 % d_6-DMSO/$CDCl_3$ with calculated 1:1 fits (lines: dotted represent unreliable fits, solid represent data used to determine association constants).

volume ratio. Overall, 1:1 nitrate binding with **1** in 20 % d_6-DMSO/$CDCl_3$ is weaker than hydrogen sulfate with an association constant of 2200 M^{-1}, thus suggesting tetrahedral ligands bind this tripodal series more strongly.

With strong association to hydrogen sulfate even at 20 % DMSO, we were interested if we could obtained measurable binding with **1** to perchlorate or perrhenate in 10 % d_6-DMSO/$CDCl_3$. Perchlorate and pertechnetate anions are problematic environmental contaminants which are also known for their weak association. Typically perchlorate is even used as a control or non-bonding anion in binding studies. Upon the addition of TBA perchlorate to **1**, all four proton resonances produced 1:1 titration curves, albeit with minimal shifts in the case of H^a (Fig). H^c and H^d shifted downfield and upfield, respectively, as is typical throughout this receptor class. H^b and H^a, however, both moved upfield whereas the other anions studied thus far cause downfield shifts in these two protons. Similarly, the titration of TBA perrhenate also produced 1:1 binding isotherms. In the case of perrhenate (as a model for pertechnetate) we still observe a deviation from the $\Delta\delta$s in comparison to previous results – H^b once again moves upfield while H^a returns to its typical trend of shifting downfield. Both anions require the addition of at least 7 equivalents of guest to reach saturated 1:1 binding, with similar association constants of 400 and 530[b] M^{-1} for perchlorate and perrhenate respectively.

Investigation of sulfate binding with **1** produced intriguing results. We were interested to compare the binding of HSO_4^- to SO_4^{2-} and determine if binding would be affected by the increase in negative charge or if a variation in binding equilibria would occur. Titration of **1** with SO_4^{2-} in 10 % d_6-DMSO/$CDCl_3$ at 25 °C, however, resulted in a large degree of peak broadening for both the host and tetrabutylammonium proton resonances (Appendix D). To resolve what is occurring in solution, a titration monitoring both ^1H and ^{19}F spectra was performed at -20 °C. Low

temperature spectra indicated complete loss of symmetry of tripodal receptor **1** at half of an equivalent of TBA_2SO_4, based on broad ^1H peaks which appear to be six inequivalent urea resonances (Figure 6a). In addition, the singlet ^{19}F resonance observed at 25 °C split into four signals at 0.5 equivalents of sulfate suggesting an exchange process now slow on the NMR time scale (Figure 6b). Continual addition of sulfate results in further symmetry change of **1**, and at a large excess (8 equiv.) the urea peaks are no longer discernable (Appendix D).

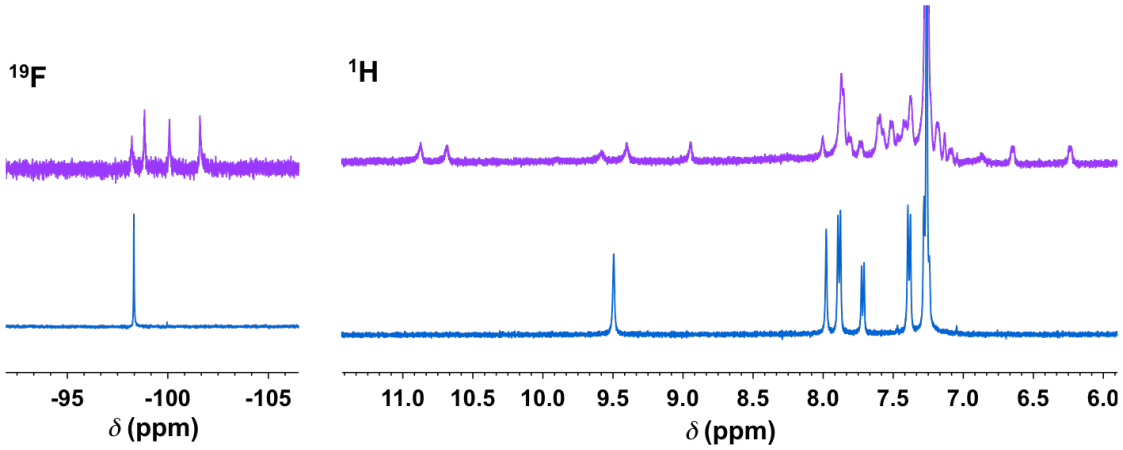

Figure 6. Example stacked ^{19}F (left) and ^1H (right) NMR spectra taken at -20 °C during the titration of tetrabutylammonium sulfate to **1** in 10 % d_6-DMSO/$CDCl_3$. Spectra shown represent **1** at -20 °C with no guest present (bottom) and after the addition of 0.5 equiv. of $TBA_2SO_4^{2-}$ (top).

Addition of acetate produced the largest observed $\Delta\delta$ values thus far in this class of receptors indicating a strong association in 10 % d_6-DMSO/$CDCl_3$, with $\Delta\delta(H^a) \approx 1.0$ ppm and $\Delta\delta(H^b) \approx 1.9$ ppm. Broadening of H^b occurs upon the first addition of TBAOAc, although the peak is still distinguishable, and sharpens once saturation of the receptor is achieved. In addition, $\Delta\delta(H^c)$ is sigmoidal in shape throughout the titration, indicating more than the 1:1 equilibrium is present in solution at a 10 % DMSO volume ratio to $CDCl_3$. Once again, increasing concentrations of DMSO were used to diminish the presence of competing equilibria and elucidate a 1:1 association

constant. Titration in 20 % d_6-DMSO/$CDCl_3$ results in diminished competition; however, a reasonable fit of the binding isotherm to a 1:1 model is still not obtained. DMSO was further increased up to 50 % v/v and while fitting results are improved with regards to error in the 1:1 isotherm fit, new peaks appear during the progress of the titration. We believe the data obtained at 20 % DMSO could fit to a 1:1 model but the binding strength is too large to be determined utilizing NMR spectroscopy. Thus, UV-Vis titrations may provide reliable association constants for acetate.

The final anion we were interested in investigating was dihydrogen phosphate. Upon initial addition of $TBAH_2PO_4$ to **1**, broadening of the H^b and H^a peaks is observed (Appendix D). As the titration proceeds to 1 equiv. of guest, broadening of both peaks increases until H^b is no longer discernable from the baseline. Broadening also occurs with the remaining peaks of **1**, but proton resonances corresponding to the tetrabutylammonium cation remain sharp throughout the titration. A binding constant cannot be determined via NMR spectroscopy at this time.

IV.4.2. ^{1}H NMR Titrations of 2

In the previous publication (Chapter III), the 1:1 association constants of **2** with chloride and nitrate were determined for comparison to **1**. Results showed the change in electron density of the central arene not only weakens anion–π interactions as anticipated for nitrate, but also demonstrated a loss of selectivity due to a change in binding mode from anion–π to C_{aryl}–H hydrogen bonding with chloride. To further compare the effect of the electron-richness of the arene to **1**, titrations of **2** were continued to include all the anions also investigated with **1**. Of great interest with this system is the continued determination for preference of binding mode – either an anion–π interaction or C_{aryl}–H hydrogen bond to the central arene.

Firstly, the halogen series was completed. Addition of TBA bromide or iodide to a 1 mM 10 % d_6-DMSO/$CDCl_3$ solution of **2** results in downfield shifts of H^a, H^b, and

H^c with H^d moving upfield as previously observed. Examination of H^{core} shows it again posseses a larger $\Delta\delta$ than H^a, indicating a stronger hydrogen bond, but weaker than that of H^b. 1:1 association constants were determined as 9130 M^{-1} and 330 M^{-1} for bromide and iodide, respectively. In comparison to the results previously obtained for **2**, these values fit in the typical binding strength trend of $Cl^- > Br^- > I^-$, all of which appear to bind **2** through the same binding mode – urea and C_{aryl}–H hydrogen bonds. Interestingly, the association constant of Br^- is of similar strength to the binding of NO_3^-, which was previously established to bind **2** through a different mode – urea hydrogen bonds and an anion–π interaction to the extended conjugated core. Since bromine and iodide bind the core via a hydrogen bond in **2**, we anticipated the binding strength to be greater than that of **1**, which would bind the anions via anion–π and urea hydrogen bonds or solely through the ureas. Interestingly, bromide binds **1** and **2** to the same degree within error, while iodide is held more strongly to **1** than **2**. Seeing as the shift of the core proton is small in comparison to the urea, any hydrogen bond is weak (likely possessing a $X^-\cdots H\text{-}C_{aryl}$ angle much less than 180°) or a σ-complex may dominate (Figure 7).

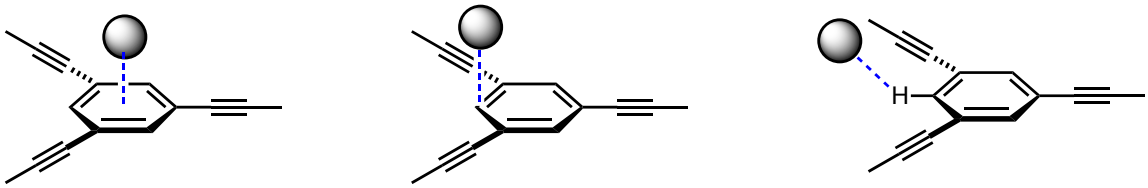

Figure 7. Possible binding modes for halogen association with **2**.

Based on the binding strength with **1** and for comparison purposes, hydrogen sulfate was titrated into **2** as a solution in 20 % d_6-DMSO/$CDCl_3$. Initial results indicate a 1:1 binding model may not provide the best fit for this data (Figure 8a). As before, the volume ratio of DMSO was further increased to 30 % to elucidate a 1:1

association constant (Figure 8b). While data from a single titration did provide a better fit with regards to error, further titrations need to be performed to report a reliable value.[c] The most intriguing result from both of these titrations is the relative Δδs. In all other titrations with this class of receptors, the proton shifts of H^b have always resulted in a larger change due to the addition of anions than H^a; whereas the addition of hydrogen sulfate to receptor **2** specifically induces a larger change in the H^a urea resonance than H^b. A ~0.1 ppm shift of H^{core} is observed throughout either titration.

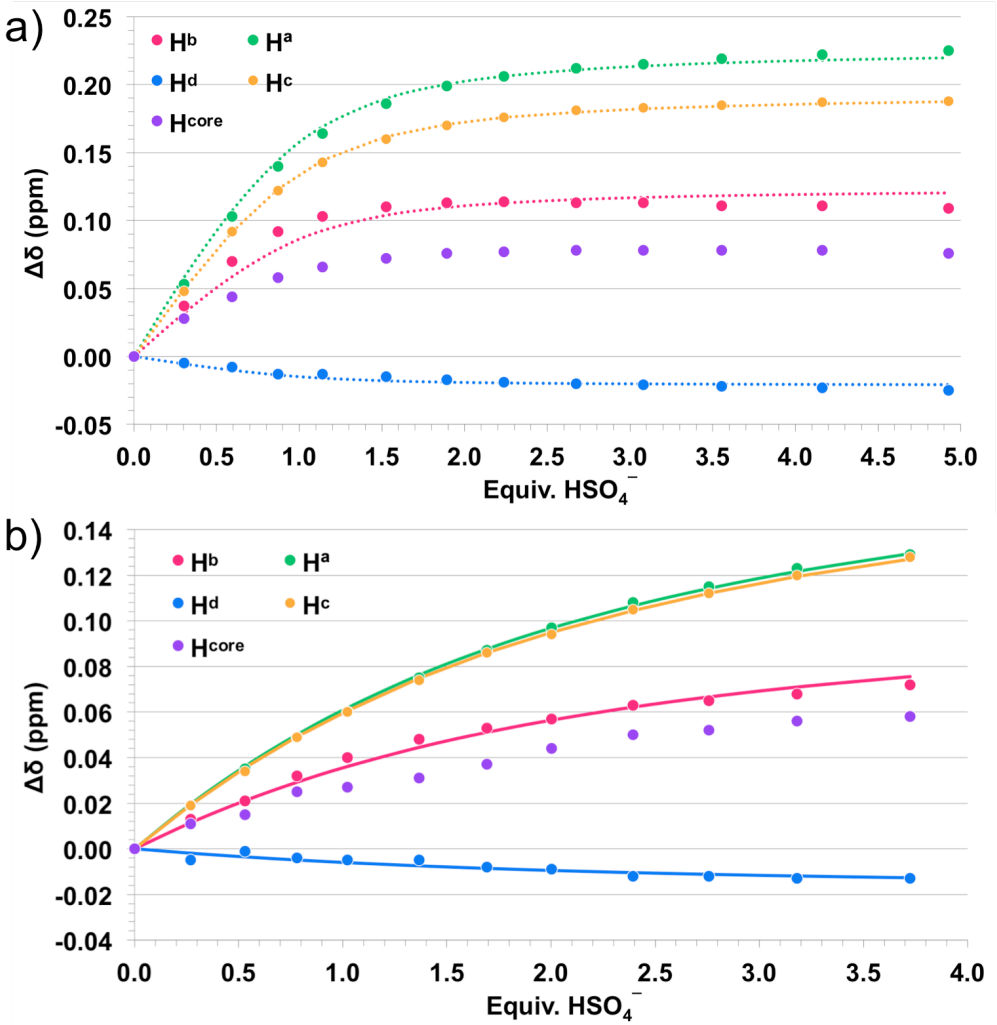

Figure 8. Example plots of observed Δδ (points) upon the titration of tetrabutylammonium hydrogen sulfate into a solution of **2** in (a) 20 % and (b) 30 % d_6-DMSO/$CDCl_3$ with calculated 1:1 fits.

Association of perchlorate and perrhenate were also determined for **2**. The same trend is observed in this system as in **1** – H^b moves upfield upon the titration of either anion and H^a moves upfield with the addition of perchlorate and downfield with perrhenate contrary to the shifts resulting from the addition of all other anions. Association of each anion is weaker for **2** than **1**, with 110 M^{-1} and 250 M^{-1} 1:1 binding for perchlorate and perrhenate, respectively, in 10 % d_6-DMSO/$CDCl_3$. Due to the opposite trend in shifts, binding of TBA could be occurring in these systems. Examination of the $\Delta\delta$ values of the TBA proton resonances shows the largest change in peak shift is ~0.02 ppm, which is rather insignificant compared to other anions but is on par with $\Delta\delta$ of both H^a and H^{core} for perchlorate and perrhenate additions. Binding of TBA can be further elucidated by titration with a TBA salt of a larger non-coordinating anion such as $BAr^F{}_4^-$.

The binding response of acetate, sulfate, and dihydrogen phosphate was also investigated with **2**. As the errors in the 1:1 fit of **1**•AcO^- were postulated to, in part, result from binding strength, we expected binding with **2** to be more easily elucidated as the association would be weakened if it followed the trend of the halogens. Initial titration in 10 % d_6-DMSO/$CDCl_3$ resulted in broadening of the proton resonances of **2**, although the peaks could still be followed throughout the titration. The binding isotherm does not fit well to a 1:1 model. To sharpen the spectra throughout the titration, and ideally weaken the equilibria, the titration temperature was raised to 30 °C. Higher temperatures beyond this were not required for further resolution of the peaks. The addition of acetate with **2** at 30 °C provided resolution for H^c, H^d, and H^{core} throughout the titration, while H^a and H^b still broadened into the baseline at the initial addition of acetate and resharpened once binding reached saturation at ~ 1 equiv. of guest. Unfortunately, errors from the 1:1 fit of the binding isotherm are still high.

2•Sulfate binding was investigated at 10 % d_6-DMSO/$CDCl_3$ and 25 °C. Similar to the results observed with **1**•$H_2PO_4^-$, broadening and coalescence of the receptor peaks occurred as the equivalents of anion were increased. Once again, the TBA proton resonances remained sharp throughout the titration. As a result of the broadening, the changes in chemical shift were unable to be followed or fit to a binding model. Change in temperature during titration with sulfate provided no resolution for the peaks of **2**.

Titration of **2** with dihydrogen phosphate in 10 % DMSO gave an interesting response with regards to H^{core}. While the other proton resonances monitored through the addition of $H_2PO_4^-$ produced typical binding isotherms, H^{core} shifted downfield and then back upfield producing a parabolic shape when plotted against the equivalents of anion (Figure 9). Once again, the proton resonances of **2** broaden as the titration progresses with the ureas disappearing into the baseline. The volume ratio of DMSO was increased with this system to 20 % DMSO, however the same parabolic trend of H^{core} as well as broadening of the proton resonances of **2** was still observed (Appendix

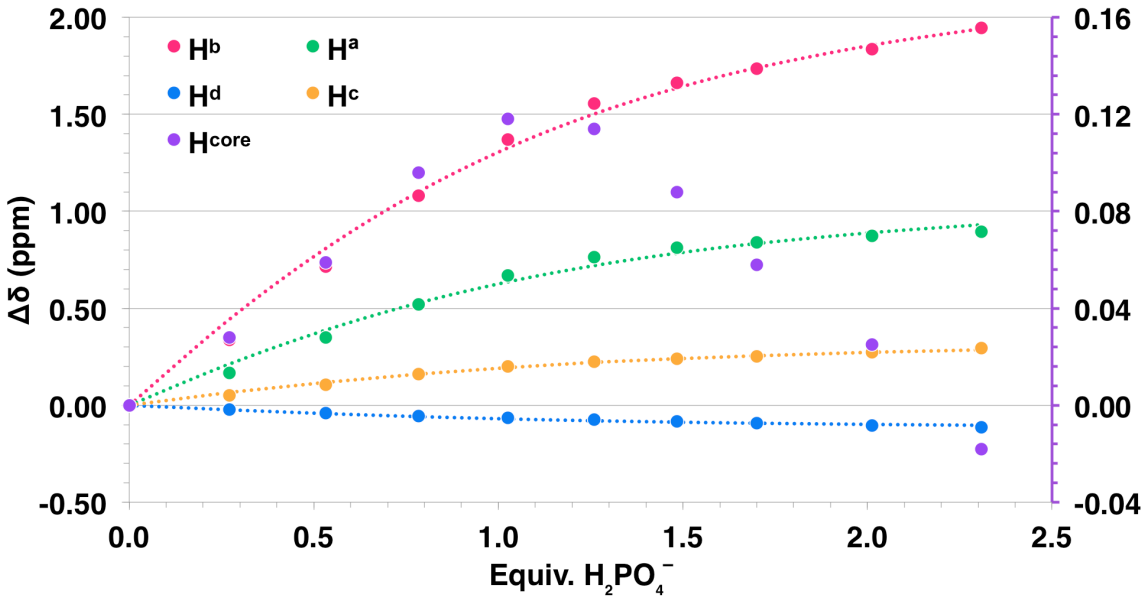

Figure 9. Example plot of observed $\Delta\delta$ (points) upon the titration of tetrabutylammonium dihydrogen phosphate into **2** in 10 % d_6-DMSO/$CDCl_3$ with the calculated 1:1 fit.

D). A slightly different trend of H^a and H^b is observed in the larger concentration of DMSO solution: both broaden into the baseline, but resharpen at ~1 equiv. of $H_2PO_4^-$, only to immediately begin to broaden back and eventually are undetectable in the noise. In both 10 % and 20 % DMSO titrations, H^c and H^d coalesce at high equivalencies of guest. This was also observed in the binding of chloride and bromide with **1**.

IV.4.3. ^{1}H NMR Titrations of 3

Due to the previous issues observed with many of the oxyanions investigated, the binding properties of receptor **3** were only determined for nitrate and the halogens. We expect the ureas to be weakened as hydrogen bond donors as a result of the electron-donating character of the methoxy substituents, thus diminishing binding with anions overall. All four anions induced the typical changes in chemical shift previously observed in this series of receptors with H^b shifting the furthest over H^a, H^c, H^d, and H^{core}.

Association constants of **3** followed the Hofmeister series with $Cl^- > NO_3^- > Br^- > I^-$. As expected, binding of all the anions investigated is weaker with **3** in comparison to **1** and **2**. Binding was fit to a 1:1 more for **3**, with determined association constants of 1300, 700, 30, and 1080 M^{-1} for TBA chloride, bromide, iodide, and nitrate, respectively. Overall, approximately an order of magnitude difference is observed when nitro (**2**) is replaced with methoxy (**3**) for the binding of bromide, iodide, and nitrate whereas chloride binding is considerably weaker in comparison (Table 1). Titration of all four anions results in the characteristic changes in chemical shift, with $\Delta\delta(H^b)$ as the most significant. In fact, chloride induces a calculated 1.10 ppm overall peak shift in H^b of **3**, which is slightly more than the shifts determined for titration with **1** or **2**. Once again chloride induces the largest change in chemical shift for H^{core}, which lessens (or weakens) down the series of halogens as a result of size. While a shift of the H^{core} peaks

can be observed upon the titration of nitrate, the overall change is minimal indicating an anion–π-type interaction is still present with receptor **3**.

IV.5. Conclusions

The titration data for receptors **1**, **2**, and **3** is summarized in Table 1. Of the association constants elucidated, tripodal receptor **1** binds hydrogen sulfate the strongest. Acetate appears to have a strong association constant with **1** as well, and future titrations monitored with UV-Vis spectroscopy may provide a reliable binding constant. Weak but measurable associations of **1** and **2** were determined with perchlorate and perrhenate, however these associations need to be confirmed to result from the anion and not the TBA cation. Both changes in temperature and variation in the volume ratio of DMSO were utilized in the study presented herein to isolate 1:1 equilibria and clarify the solution state binding. While this proved successful with hydrogen sulfate, binding with several of the other oxyanions studied remained unclear. Evidence was presented herein of multiple binding equilibria in solution throughout the titrations. In the case of **1**•SO_4^{2-}, a loss of three fold symmetry is apparent in both ^{1}H and ^{19}F NMR spectra when the sample containing 0.25 equivalents of guest is cooled to -20 °C.

Based on the associations determined, receptor **2** binds all anions weaker than **1** with the exception of chloride. This is still suspected to be the result of a strong hydrogen bond to the core C_{aryl}–H, demonstrating once again the influence of binding pocket size (which is ideal for chloride) on binding strength. One of the most perplexing results with receptor **2** was the effect of hydrogen sulfate on the overall changes of the proton resonances – a greater shift of H^a over H^b was observed for the first time. We have not yet elucidated the implications this provides with regards to the binding geometry in solution. A second intriguing and yet unexplained result was

observed for the addition of dihydrogen phosphate. Titrations in 10 or 20 % DMSO produced what appears to be the transition between two binding modes of **2**, where H^{core} at first participates in binding as its proton resonance moves downfield, and then the biding geometry changes where H^{core} no longer interacts with dihydrogen phosphate and moves back upfield.

Receptor **3** was titrated with our originally studied anions (nitrate and the halogens) for comparison with regards to electron density of the urea moieties. Binding was weakened across the board in comparison to **2**, and showed no deviation from the Hofmeister bias. While the binding of many of the anions investigated within remains unclear, overall trends were still observed and interpreted. Future work with this system truncated to a one-armed receptor (Chapter VI), may provide simplified binding with fewer arms. The anion–π binding nature of these systems with nitrate and other anions can also be further elucidated.

IV.6. Notes

[a] In all cases, H^a, H^b, H^c, and H^d were fit except when one of the four protons (H^a and H^d) could not be accurately followed; H^{core} was used in place of this proton. Titrations providing accurate values for all five protons were fit using various proton resonances and provided the same association constant within error.

[b] Not a final association constant. Average of three titrations, however more need to be performed to improve the error for perrhenate.

[c] K_a of the single titration at 30 % d_6-DMSO/$CDCl_3$ was 660 M^{-1} regardless of whether H^a, H^b, H^c, and H^d or H^a, H^b, H^c, and H^{core} were used to determine the global fit.

IV.7. Bridge to Chapter V

Chapter IV continued our investigation of tripodal analogues of our traditional arylethynyl receptors. Chapter V will look at a water soluble analogue of the bis(urea) receptor class and the characterization of its turn-on fluorescent response to chloride.

CHAPTER V

"OFF-ON" AGGREGATE-BASED FLUORESCENT SENSOR FOR THE DETECTION OF CHLORIDE IN WATER

Chapter V is a revised and unpublished manuscript draft originally written by previous graduate student, Jeff Engle. Jeff also performed the original experiments with the assistance of undergraduate Timothy Robitshek. I have reperformed many experiments, expanded on the data contained within, and rewrote the original manuscript. Cell lysate experiments were performed by Chris Vonnegut and HeLa cells were prepared by Aaron Docter. Editing was performed by Profs. Darren W. Johnson and Michael M. Haley. The final manuscript will be submitted to the journal *Organic and Biomolecular Chemistry* later this year as an invited article.

V.1. Introduction

Interest in supramolecular sensors for the detection of anions has received considerable attention over the past two decades.[1,2] Such systems exploit non-covalent interactions between a guest molecule and a host molecule to induce a change in the host (e.g., NMR shift, color, fluorescence, electrochemical behavior, etc.). Supramolecular sensors are advantageous when compared to chemodosimeters because non-covalent interactions are reversible, providing dynamic monitoring of an analyte.

Arguably the most powerful of these sensors exploit a fluorescence change due to their inherent sensitivity.[3]

"Aggregation induced emission" (AIE) or dye aggregates with active photophysical properties typically contain highly conjugated backbones with moieties capable of having their inherent rotational freedom restricted by non-covalent interactions or crystal packing forces.[4,5] Often acting through J-aggregation, these systems have been known since 1935.[5] However, AIE or dye aggregate molecules have more recently been exploited as fluorophores for analytes.[5,6] Under most conditions the molecules rotate freely and are non-fluorescent, but upon application of an external or internal stimuli, such as changes in solvent or temperature, rotational freedom becomes restricted.[4] Ultimately the molecules aggregate together and an atypical turn-on fluorescent response occurs. AIE has been used as a sensing platform for analytes, such as cyanide,[7] carbohydrates,[8] amino acids,[9] CO_2,[10] and electron deficient aromatics.[11] Aggregation-based fluorescence responses could allow for turn-on fluorescence sensors to be further developed for use in detecting analytes typically viewed as quenching agents, such as halides.[4]

Our previously reported bisethynylpyridine based compounds have shown considerable promise towards selective turn-on anion sensing, as discussed in Chapter I.[12-15] This chapter reports the synthesis and characterization of a turn-on sensor ($\mathbf{1}^+$) activated by aggregation with anions and selective for chloride over other biologically relevant anions in water under acidic conditions. To the best of our knowledge this is the first example of a fully organic turn-on fluorescence sensor selective for chloride in water. Chloride's importance in biology is increasingly appreciated as more studies demonstrate its involvement in biological processes, including regulation of cellular volume and nerve transduction.[16-18]

Existing fluorescent organic sensors for halides are either based upon a 6-methoxyquinolinium scaffold[19-21] or modified yellow fluorescent proteins.[22,23] Both classes of sensors undergo collisional quenching in the presence of halides and the concentration of chloride can be determined using a Stern-Volmer relationship.[24] While these sensors are widely used and available commercially, it would be desirable to have a turn-on sensor to allow for improved spacial resolution. Furthermore, existing sensors are susceptible to interference from other halides, "pseudohalides", and dissolved oxygen making more selective alternatives desirable.[19,24]

V.2. Results and Discussion

Synthesis of receptor **1** is achieved through a typical Sonogashira cross-coupling reaction (Scheme 1). Reaction of two equivalents of urea **2**[25] with 2,6-dibromo-4-nitropyridine in the presence of Pd(0) and Cu(I) provides precursor **3** in 84 % yield. S_NAr reaction of **3** with 2-dimethylaminoethanol and potassium carbonate produces **1** in 67 % yield. Previous results with similar pyridine receptors[12-14] demonstrated the dependence of the turn-on fluorescent response to chloride and other anions on the protonation of the host. The addition of more than two equivalents of trifluoroacetic acid (TFA) in acetonitrile provides the final water-soluble chloride sensor, denoted here as $\mathbf{1}^+$ (the plus sign symbolizes only the protonated state of the receptor, not the charge

Scheme 1. Synthesis of receptor **1.**

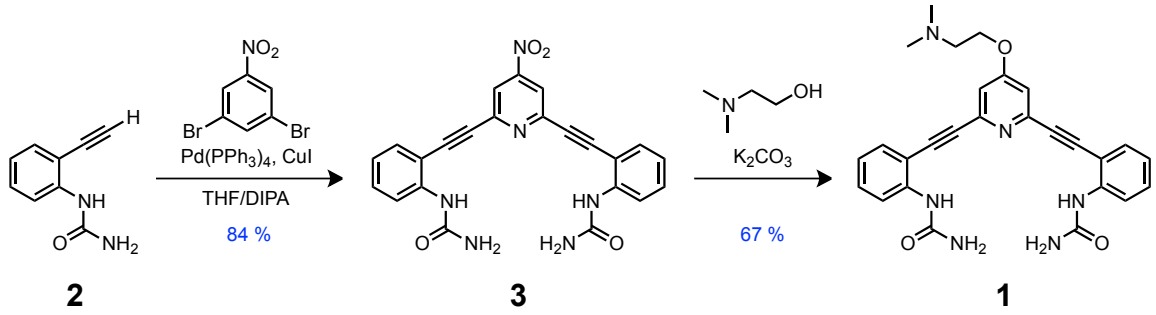

of the receptor complex). Unprotonated receptor **1** is not soluble in aqueous solutions; however, pre-protonated $\mathbf{1}^+$ is soluble in water with 1 % TFA up to ~0.5 mM; solubility is diminished without the presence of 1 % TFA to ~0.1 mM.

V.2.1. Fluorescent Response to Anions

To first determine selectivity of $\mathbf{1}^+$, excess equivalents (>500) of various anions were added to 0.5 mM aqueous solutions of $\mathbf{1}^+$ as sodium salts in the presence of 1 % TFA (Figure 1). Dihydrogen phosphate is excluded from these results due to its protonation state at the pH of these solutions, as well as experimental evidence indicating its ability to deprotonate the receptor (V.2.4). Upon addition of a sodium salt to $\mathbf{1}^+$, a visible color change was observed from pale to dark yellow. Excitation at 365 nm via a hand-held long wave UV lamp demonstrated the selective response of the protonated host to chloride – a blue to bright yellow-green fluorescence is observed dependent on concentration or equivalents of chloride (Figure 1).

A notable feature is the presence of aggregates in the samples which demonstrate turn-on fluorescence (Figure 1c). Most of the other anions investigated produced little to no turn-on response, except for sodium fluoride and sodium perchlorate – critical with regards to their environmental impact but not typically biologically relevant with regards to the applications of this receptor series for sensing chloride in a cellular environment. This selectivity is further highlighted in the emission spectra collected when the complexes are excited at $\lambda_{max}(\mathbf{1}^+\bullet\mathbf{Cl}^-)$ = 425 nm (Figure 1a,b) – the intensity ratio of $\mathbf{1}^+\bullet\mathbf{Cl}^-$ is four times larger than the next most fluorescent anion complex, $\mathbf{1}^+\bullet\mathbf{ClO_4}^-$. In addition, $\mathbf{1}^+\bullet\mathbf{Cl}^-$ is red-shifted by 75 nm in comparison to 6-methoxyquinolinium derivatives currently commercially used, making it more amenable for use in cells.

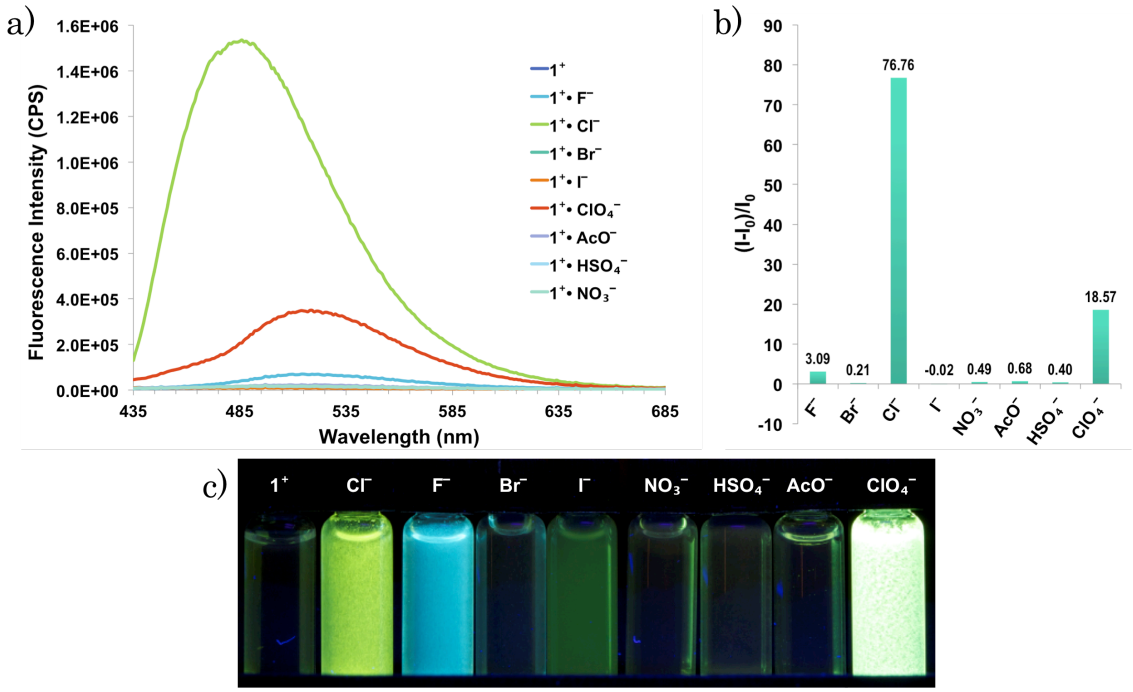

Figure 1. Emission profiles of host $\mathbf{1}^+$ with various anions depicted through (a) fluorescence spectra, (b) intensity ratios in comparison to $\mathbf{1}^+$ without the presence of anion, and (c) visual emission under a long-wave, 365 nm fluorescent lamp.

V.2.2. Fluorescent Character of $\mathbf{1}^+\bullet\mathbf{Cl}^-$ Aggregates

To demonstrate the emission and aggregation of $\mathbf{1}^+$ in the presence of chloride the percent volume of water was varied with a solvent capable of solubilizing $\mathbf{1}^+\bullet\mathbf{Cl}^-$. Aggregation was observed when mixing $\mathbf{1}^+$ with a source of chloride in nearly all solvents investigated, except for DMSO. Due to the highly solubilizing nature of DMSO, the AIE character was determined at relatively high concentrations of $\mathbf{1}^+$ and equivalents of chloride. A series of 0.5 mM $\mathbf{1}^+$ and 1.5 M LiCl solutions were made with the volume ratio of water ranging from 0 % to 90 % in 1% TFA/DMSO. The concentration of TFA and $\mathbf{1}^+$ were held constant throughout the solutions and the equivalencies of chloride are nearly identical. A change in the yellow intensity of the solutions under visible light is, once again, observable upon mixture with chloride. $\mathbf{1}^+$ possesses a blue fluorescence in DMSO but switches closer to a white fluorescence upon the addition of chloride (Appendix E). As water is introduced to the DMSO

solution up to 70 % this fluorescence is quenched (Figure 2). At 80 % water in DMSO, $\mathbf{1}^{+}\bullet\mathbf{Cl}^{-}$ begins to aggregate and fluorescence is dramatically turned on. Once 90 % water is reached, the solution is still highly fluorescent and the visible concentration of aggregates is further increased (Figure 2b); however, the measured fluorescence at excitation 425 nm is quenched in comparison to the 80 % water solution (Figure 2a). This observation could be caused by the large concentration of aggregates (which typically results in quenching for non-AIE active compounds) and may not be observed if the solution was at less of a large excess of chloride or below the concentration limit of $\mathbf{1}^{+}$ in water.

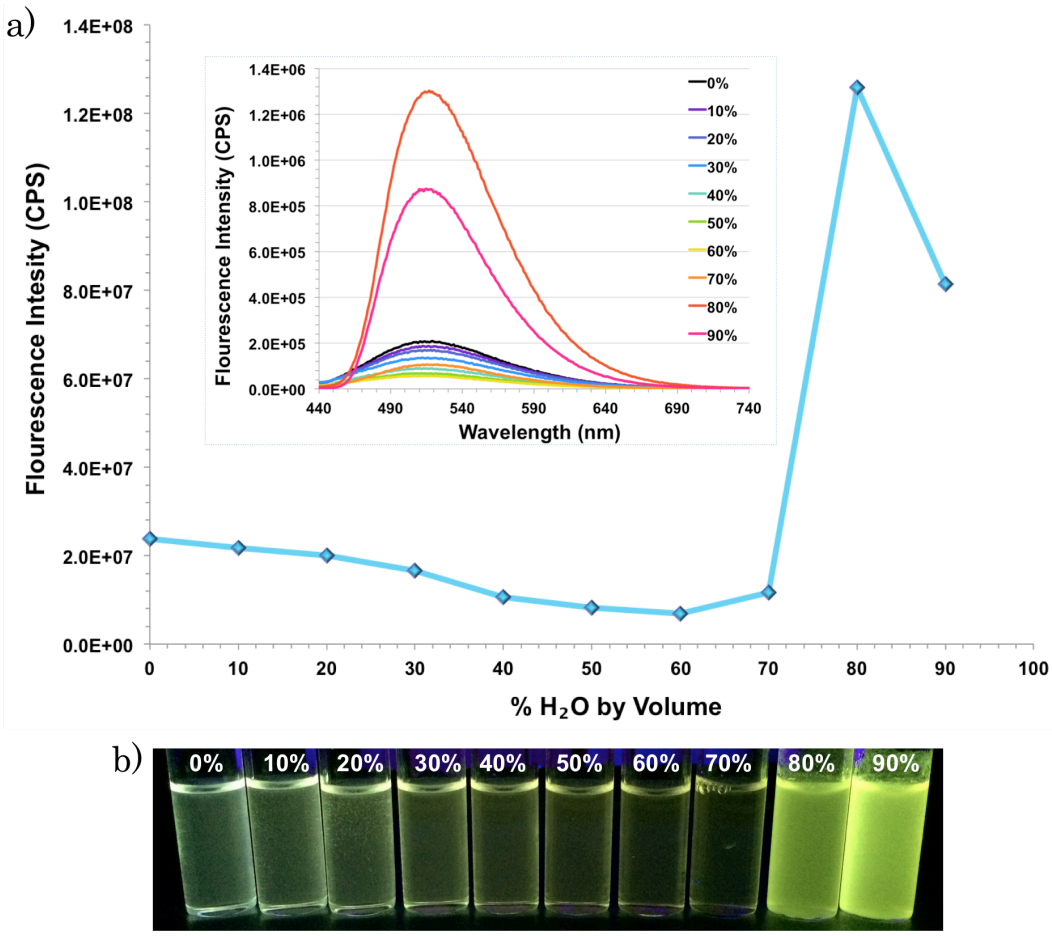

Figure 2. Emission profiles of $\mathbf{1}^{+}\bullet\mathbf{Cl}^{-}$ in solutions of 1 % TFA in H_2O/DMSO mixtures with water ranging from 0 - 90 % depicted through a plot of the total intensity from 440-740 nm determined from the fluorescence spectra excited at 425 nm (a) and the visual emission under a long-wave, 365 nm fluorescent lamp (b).

V.2.3. Aggregate Structure of $\mathbf{1}^{+}\bullet\mathbf{Cl}^{-}$

Samples of $\mathbf{1}^{+}\bullet\mathbf{Cl}^{-}$ were visualized under a Scanning Electron Microscope (SEM) (Figure 3). A 0.3 mM solution of $\mathbf{1}^{+}$ in water spiked with 1 % TFA was distributed into two samples with ~10^3 equivalents and ~2 x 10^3 equivalents of chloride (NaCl). Would there be a difference in aggregate shape or size based on the equivalents of guest? 10 µL of each solution was pipetted onto an untreated silica wafer and allowed to dry. The excess of NaCl produced many crystalline structures on the surface of the dried $\mathbf{1}^{+}\bullet\mathbf{Cl}^{-}$. The latter sample with a larger concentration of chloride produced only flat translucent sheets amidst the NaCl crystals. These sheets were previously observed during SEM on a treated silica wafer on a sample prepped from a suspension of **1** in water after the addition HCl gas (no TFA present) (Figure 3a). When the sample with 10^3 equivalents

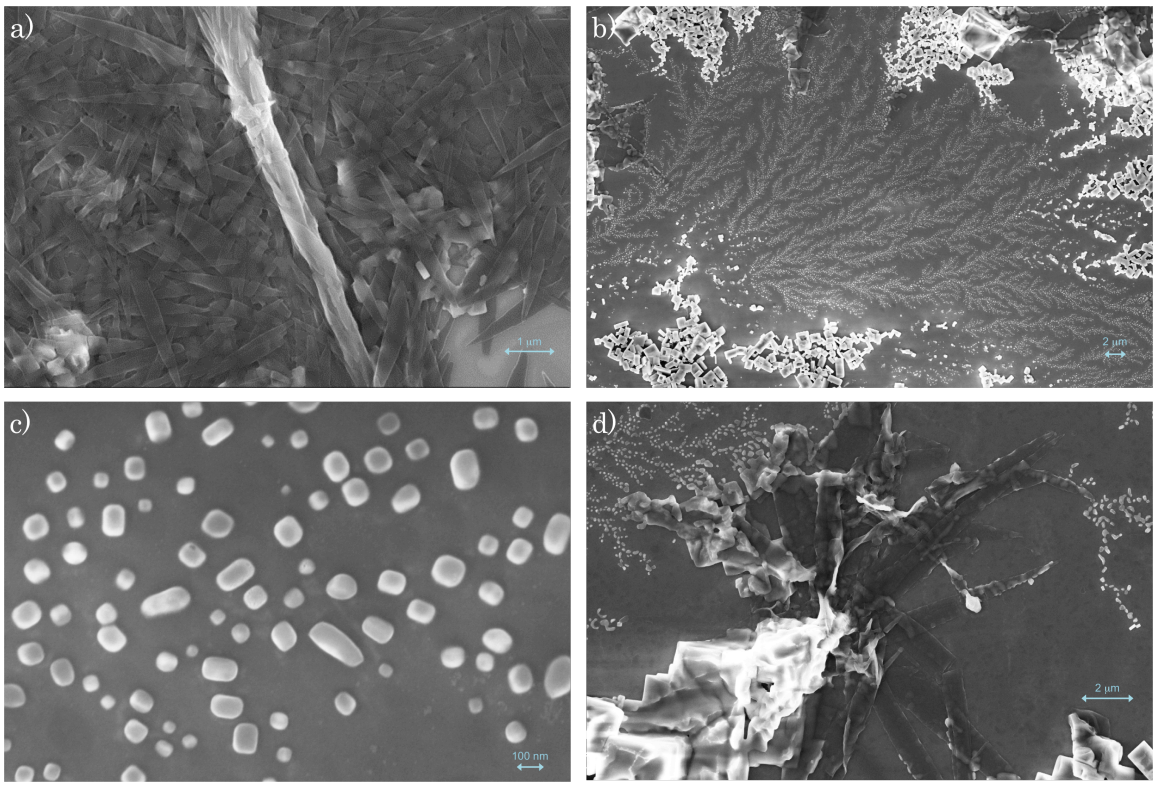

Figure 3. SEM images of aggregated samples evaporated onto silica wafers: (a) HCl gas bubbled through a suspension of $\mathbf{1}^{+}$ in water. (b-d) Addition of ~10^3 equiv. of NaCl to $\mathbf{1}^{+}$ in 1 % TFA/water.

of chloride was visualized, a river delta or dendritic formation was observed (Figure 3b). Closer inspection this pattern (Figure 3c) revealed small featureless nano-sized particles. This formation also terminated into the translucent sheets previously observed, which assembled into larger featureless clusters (Figure 3d). Sensitivity of the energy-dispersive X-ray spectrometer, particularly with regards to resolution, has prevented the confirmation of chloride present in the particles or sheets thus far.

V.2.4. ^{1}H NMR Spectroscopic Titrations of $\mathbf{1}^+$

While aggregation in this class of receptors is beneficial for their fluorescent turn-on responses to anions such as chloride, it is often detrimental in the determination of association constants, making it difficult to compare the strength of binding to current receptors. The overall weak association in strong hydrogen bonding solvents and the time-dependent nature of the fluorescent response of $\mathbf{1}^+\bullet\mathbf{Cl}^-$, lead to the investigation of binding in d_6-DMSO monitored via ^{1}H NMR spectroscopy.

Titration experiments were typically performed at 1.5 mM of **1** in d_6-DMSO spiked with 0.5 % H_2O. Water was added to minimize the effect of DMSO's natural absorption of water throughout the titration. Addition of TBA salts of nitrate, iodide, hydrogen sulfate, and perchlorate resulted in little to no change in chemical shift of any protons. Dihydrogen phosphate, as mentioned previously, deprotonates the host – indicated by the immediate loss of the R_3N^+H resonance upon the first addition of salt and the change of chemical shifts to match **1** at the end of the titration (Appendix E). Titration of TBA chloride and bromide result in the downfield shift of four proton resonances on $\mathbf{1}^+$: R_3N^+H, HN_{urea}, H_2N_{urea}, and HC_{Py}. These four shifts were fit to 1:1 association using the Thordarson fitting program.[26]

The protonated ethanolamine (R_3N^+H) moiety produces the largest change in chemical shift observed for chloride ($\Delta\delta \approx 1.0$ ppm) with the pyridine proton (HC_{Py})

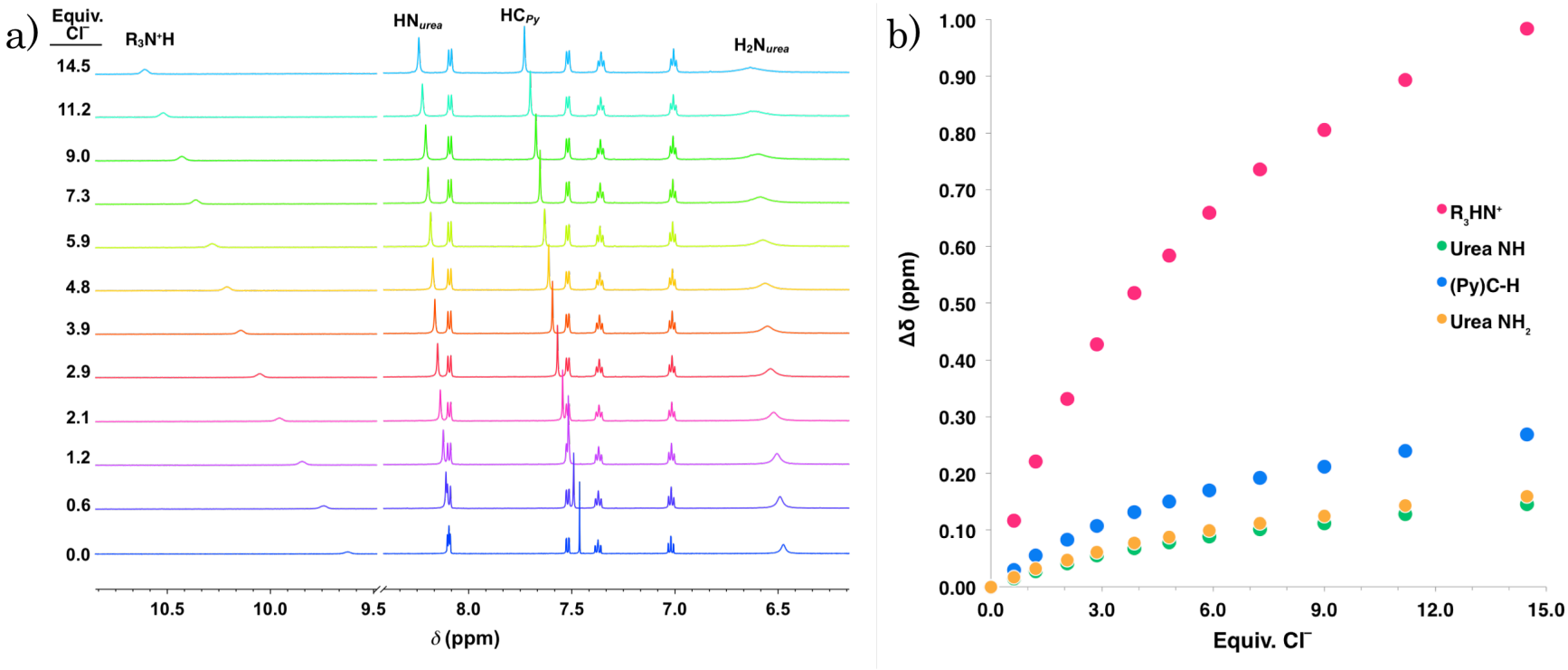

Figure 4. Example (a) stacked ^{1}H NMR spectra and (b) plot of $\Delta\delta$ for the titration of TBACl into $\mathbf{1}^{+}$.

resonance producing the second largest shift ($\Delta\delta \approx 0.3$ ppm) (Figure 4). The titration of the seemingly 1:1 chloride association ends at ~15 equivalents. Beyond 15 equivalents new peaks appear in the ^{1}H NMR spectra indicating the presence of an additional equilibrium, slow on the NMR time scale. Bromide also appears to fit well to a 1:1 association, but exhibits a weaker association than chloride, with the largest changes in chemical shifts also corresponding to R_3N^+H and HC_{Py} ($\Delta\delta \approx 0.2$ ppm for both resonances). In the case of bromide, however, a new peak appears before the titration is finished at ~30 equivalents (Appendix E). Unfortunately, error between titrations is currently too high to report binding constants for chloride or bromide. The difficulties with this system correspond to the possible additional equilibria, weak association overall ($K_a \leq 100$ M^{-1}), and the degradation of $\mathbf{1}^+$ as a solid.[a] Results may be more easily obtained if the host is freshly protonated before each titration.

V.2.5. Binding Conformations of $\mathbf{1}^+$

We believe most of our bisurea systems, particularly the pyridine- and phenyl-based receptors, bind in a typical **U** conformation.[14,27,28] This precluded us to hypothesize receptor $\mathbf{1}^+$ would also posses a similar **U** conformation with a five-point binding site involving the electrostatic pyridinium moiety (Figure 5). Keeping in mind, however, that crystal and solution studies have also demonstrated the existence of **W** and **S** conformations in this general class of bisurea arylethynyl receptors.[29]

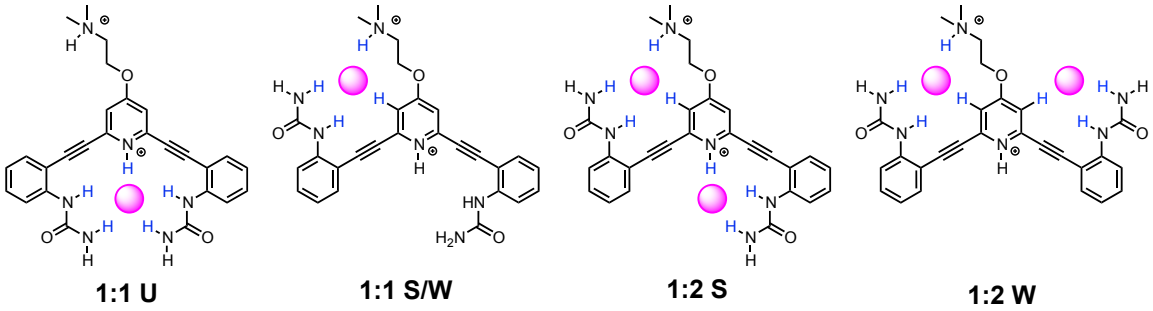

Figure 5. Possible binding conformations for 1:1 or 1:2 arrangements of $\mathbf{1}^+\bullet\mathbf{X}^-$.

Firstly, binding conformation would be affected by the protonation state of $\mathbf{1}^+$. Two sites on $\mathbf{1}^+$ are available for protonation: the pyridine and the ethanolamine moiety. While this chapter focuses on the theory in which both are protonated, data only provides confirmation of the protonated amine (via ^{1}H NMR spectroscopy as previously discussed). However, the observed change in yellow intensity upon addition of excess TFA for protonation in solution and when $\mathbf{1}^+$ is isolated as a solid provides indication for the presence of pyridinium, based on our previous receptors of this class.[14,15] Overall, two conformations can be envisioned for 1:1 binding: **U** and **S/W** (the second arm would freely rotate in solution essentially providing either an **S** or **W** type arrangement).

Based on the observed changes in ^{1}H chemical shift for both bromide and chloride, we can begin to speculate further upon the binding conformation of $\mathbf{1}^+$ with chloride or bromide (**U**, **S**, or **W**, Figure 5) – at least for a solution in DMSO. Seeing as the most significant proton shifts, and therefore likely the strongest hydrogen bonds, occur with R_3N^+H and HC_{Py}, conformation **1:1 U** is highly unlikely (Figure 5). Chloride must sit inside the cleft formed from an **S** or **W** arrangement in order to hydrogen bond to the R_3N^+H and HC_{Py} protons, similar to what is observed when our bipyridine-based receptor binds chloride or bromide (referred to as the Z arrangement).[29] As discussed, additional equilibria appear to come into play during the titration of bromide or chloride into $\mathbf{1}^+$, likely indicating a competing 1:2 interaction. What is unclear is whether this secondary equilibrium occurs with the pyridinium NH proton (**1:2 S**) or CH proton (**1:2 W**). While the binding conformation is of interest, the important aspect of this system lies within its fluorescence response.

V.2.6. Chloride Detection in Cell Lysates

For initial proof of concept of $\mathbf{1}^+$ sensing chloride in cells, we turned to a study with HeLa cell lysates (Figure 6). A 0.12 mM solution of $\mathbf{1}^+$ in water was diluted to 0.08 mM with a HeLa cell lysate suspension. Upon mixture of the lysate suspension with $\mathbf{1}^+$, turn on fluorescence was observed (cellular concentration of chloride is ~50 mM[b]). Addition of further excess chloride as NaCl increases the fluorescent response, demonstrating the dependence of the sensor on equivalents of chloride to induce more aggregation and therefore more emission.[c] Fluorescence emission spectra were obtained of each sample by exciting at 316 nm.[d] While the data obtained cannot be considered quantitatively, it clearly indicates the ability of $\mathbf{1}^+$ to sense chloride in a cellular environment. A time-lapse fluorescent study was performed which demonstrated the stability of the turn-on response over an hour (Appendix E). While initial signal depression began around 30 min., loss of fluorescence was slow and minimal in comparison to its magnitude.

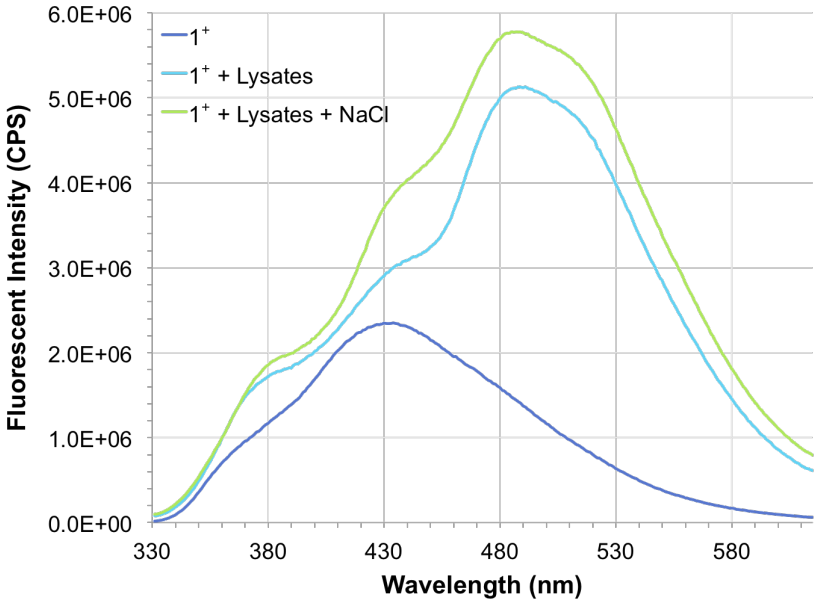

Figure 6. Fluorescence emission spectra obtained at excitation wavelength 316 nm demonstrating the ability of cell lysates with a inherent chloride concentration of 50 mM to turn on fluorescence of $\mathbf{1}^+$ even when dilute.

V.2.7. Potential Counter-Cation Dependence

In preparation for the demonstration of AIE character of $\mathbf{1}^{+}\bullet\mathbf{Cl}^{-}$, a problem was encountered with regards to the solubility of sodium chloride in DMSO which had been used in all experiments thus far. Other more soluble chloride salts were investigated to verify they would elicit the same positive turn-on response with $\mathbf{1}^{+}$. A 0.3 mM solution of $\mathbf{1}^{+}$ in water spiked with 1 % TFA was mixed with preweighed amounts of sodium chloride, potassium chloride, lithium chloride, and magnesium chloride corresponding to more than 2,000 equivalents of chloride anion. Results indicated all four salts induced aggregation and turned on fluorescence in comparison to the protonated receptor (Figure 7). Interestingly, differences in fluorescence intensity were

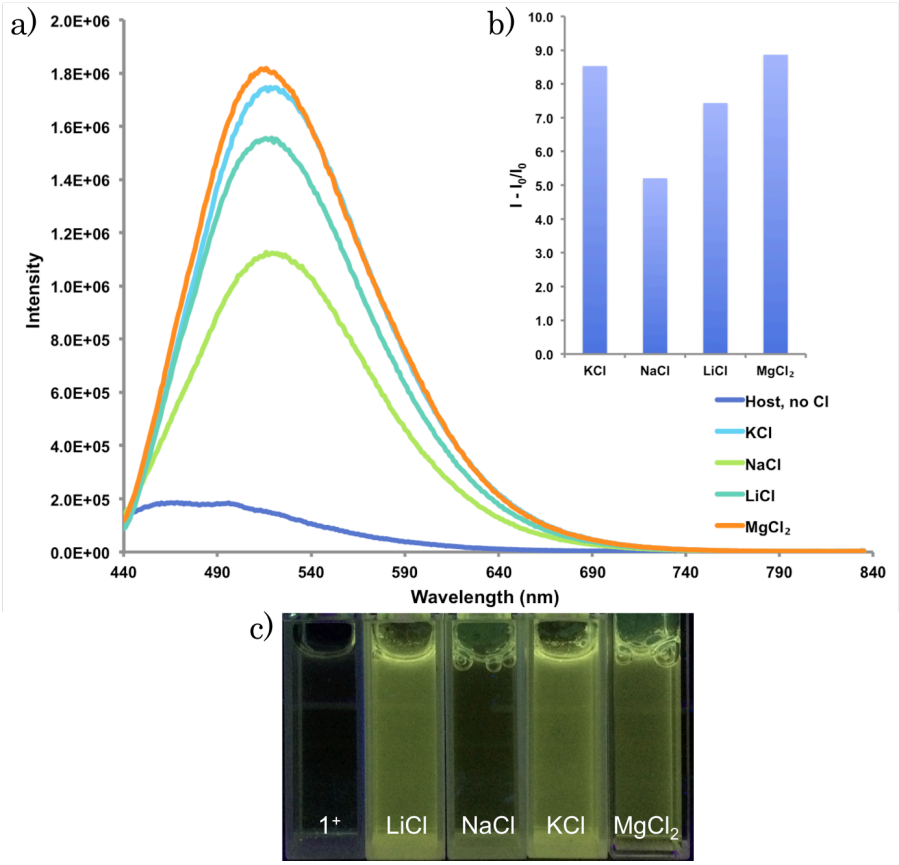

Figure 7. Emission profiles of host $\mathbf{1}^{+}$ with various chloride salts depicted through (a) fluorescence spectra when excited at 425 nm, (b) intensity ratios in comparison to $\mathbf{1}^{+}$ without the presence of anion, and (c) visual emission under a long-wave, 365 nm fluorescent lamp.

evident even by the eye between the various cations (Figure 7c), despite the chloride equivalents being essentially held constant.[e] Most surprisingly, sodium chloride – the salt used throughout all our initial fluorescent investigations – produced the weakest fluorescent intensity of all the chloride salts tested. Each chloride salt was shown to be more than fives times more fluorescent overall than the protonated host at this concentration and equivalency range. This experiment should be performed with higher quality salt sources to minimize interfering analytes and a more consistent chloride equivalency to confirm these findings. Regardless, this is an intriguing initial result.

V.3. Conclusions

The detection of chloride has proved problematic with existing sensor technologies. Fully organic sensors for aqueous chloride typically undergo fluorescence quenching or suffer from competition with other anions. By using chloride as a template for fluorophore aggregation, $\mathbf{1}^+$ makes advances to overcome these obstacles. Other biologically relevant anions investigated appear to template non-emissive or significantly blue shifted aggregates, when produced. While this receptor still suffers from consistency likely dependent on pH or analyte and sensor concentration, $\mathbf{1}^+$ provides proof of concept towards the further design of aggregation-based turn-on chloride sensors.

V.4. Notes

[a] $\mathbf{1}^+$ degrades or further reacts with itself as a solid. Therefore cannot be stored as a protonated solid. We have verified its stability in DMSO for over 6 months. We have not yet confirmed the stability of $\mathbf{1}^+$ in water for extended periods of time.

[b] Cellular concentration of chloride varies according to cell type: mammalian embryonic motorneurons = ~50 mM,[30] Jurkat T-cells = 58 mM,[31] and epithelial cells = ~40 mM.[32]

[c] Varying the concentration of $\mathbf{1}^+$ from 0.1 to 0.4 mM and observing the fluorescent response with 500 equivalents of chloride has also demonstrated this dependence (Appendix E).

[d] Early results directed fluorescent emission scans to be performed at both excitation of 316 and 425 nm. Overall 425 nm excitation was determined to best demonstrate the selectivity and intensity of $\mathbf{1}^+$. However the initial lysate studies presented here were performed at the early 316 nm excitation.

[e] Equivalents of chloride from the sodium, potassium, and magnesium salts were ~2,200, whereas the lithium salt was higher with ~2,700 equivalents.

V.5. Bridge to Chapter VI

Chapter V focused on a bis(urea) receptor which was designed for selectively binding chloride in water. Chapter VI will introduce another form of our arylethynyl urea receptors – a single-armed mono(urea) receptor which is based off the studies seen in Chapter III and IV.

CHAPTER VI

FUTURE WORK OF A ONE-ARMED UREA RECEPTOR

Chapter VI consists of unpublished work conceptualized by my advisors, Profs. Darren Johnson and Mike Haley, and myself. My advisors also performed editing.

VI.1. Introduction

In Chapter III, anion–π interactions were shown to influence selectivity for nitrate over chloride in our newly developed tripodal class of receptors. Chapter IV expanded upon these receptors through additional substitution and anionic guests. Next, we would like to determine if the tripodal tris(urea) structure of this receptor class is necessary to observe the preference for anion–π over C_{aryl}–H hydrogen bond interactions. A series of simplified one-armed arylethynyl urea receptors (Figure 1) is being synthesized to address this question. The basic structure of the one-armed receptors will provide a more easily tuned central arene to further enhance our selectivity for nitrate over chloride, as well as provide selectivity over tetrahedral anions which typically bind more strongly to tripodal structures.

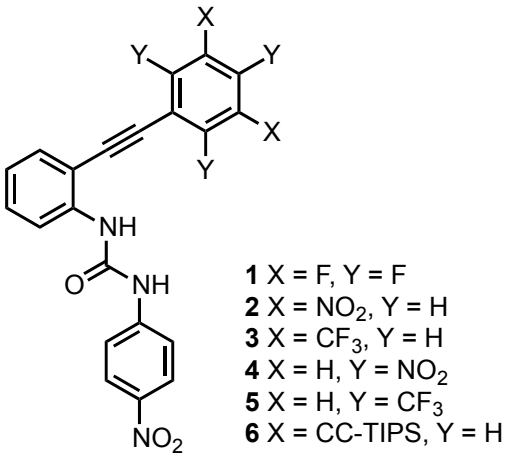

Figure 1. Proposed one-armed arylethynyl receptors.

VI.2. Receptor Design

The one-arm receptor is modeled after our series of arylethynyl receptors and is similar in design to the original perfluoroarylsulfonamide receptor.[1] Initial one-armed receptors **1**-**6** are proposed for comparison to our tripodal and phenyl bis(urea) receptor classes. **1**, **4**, and **5**, with Y substitutions, prevent hydrogen bonding to the phenyl core, thus encouraging more anion–π interactions. The substitution pattern on **2**, **3**, and **6** leaves these hydrogen bonding locations open to allow for competition between the two interactions, provided the sterics of the adjacent substituents do not prevent hydrogen bonding to anionic guests. Receptor **6** will provide the most equivalent core to our unsubstituted tripodal receptor for comparison. **6** could also be modified with X = F to best compare to our trifluoro-based tripodal system.

Receptor **2** has been initially synthesized but additional synthesis is currently underway to study the anion binding properties of **2.** Sonogashira cross coupling of 4-*tert*-butyl-2-ethynylaniline and 3,5-dinitroiodobenene provides the dinitro one-arm core **7** (Scheme 1). Subsequent reaction with *p*-nitrophenyl isocyanate provides receptor **2.** Both reactions require further optimization with regards to purification and yield.

Scheme 1. Synthesis of receptor **2.**

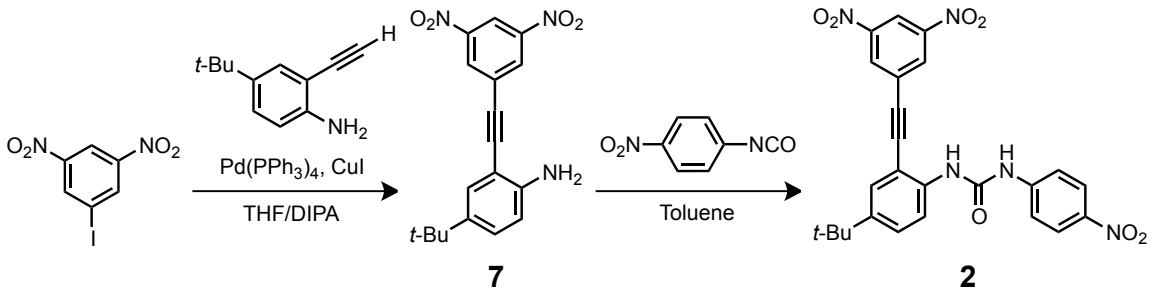

VI.3. Conclusions

The design and synthesis of single-armed receptors probes multiple fundamental questions: Does our arylethynyl urea receptor class require two or three arms to observe

similar selectivity and fluorescence responses to those previously noted? To what extent is strength of binding lost or gained with respect to the loss of urea moieties and addition of electron-deficient π-surfaces? And, can anion–π interactions be observed in solution with a single urea-binding site?

VI.4. Experimental

3,5-Dinitro aniline core 7. In a round bottom flask 3,5-dinitroiodobenzene (0.30 g, 1.02 mmol) was dissolved in DIPA (5 mL) and THF (5 mL), then CuI (19.4 mg, 0.102 mmol) was added. The mixture was purged with Ar for 30 min, then $Pd(PPh_3)_4$ (94.3 mg, 0.082 mmol) was carefully added. An Ar-purged solution of 4-*tert*-butyl-2-ethynylaniline (2.65 g, 1.53 mmol) in DIPA (5 mL) and THF (5 mL) was then transferred into the flask via cannula. After stirring at room temperature overnight, the solvent was removed *in vacuo*, and the residue run through a plug of silica using a gradient of Hexanes/CH_2Cl_2. Crude product, suitable for continuation, was obtained by precipitation out of the CH_2Cl_2 solution using hexanes (0.21 g, 62 % crude yield.) ^{1}H NMR (300 MHz, $CDCl_3$) δ 8.95 (t, J = 1.9 Hz, 1H), 8.64 (d, J = 2.0 Hz, 2H), 7.40 (d, J = 2.2 Hz, 1H), 7.28 (dd, J = 8.7, 2.3 Hz, 1H), 6.72 (d, J = 8.5 Hz, 1H), 4.22 (s, 2H), 1.30 (s, 9H). (Figure 2)

Receptor 2. In oven dried glassware, aniline **7** (0.150 g, 0.442 mmol) and *p*-nitrophenyl isocyanate (0.110 g, 0.663 mmol) were dissolved in freshly distilled toluene (40 mL). The reaction mixture was stirred overnight, quenched with acetone, and crude product **2** was precipitated with hexanes. ^{1}H NMR (300 MHz, Acetone-d_6) δ 9.05 (s, 1H), 8.94 – 8.85 (m, 1H), 8.76 (d, J = 2.0 Hz, 2H), 8.18 (d, J = 9.7 Hz, 1H), 8.11 (d, J = 9.3 Hz, 2H), 7.76 (s, 0H), 7.72 (d, J = 9.1 Hz, 2H), 7.61 (d, J = 2.1 Hz, 1H), 7.48 (dd, J = 9.0, 2.3 Hz, 1H), 1.32 (s, 6H). (Figure 3)

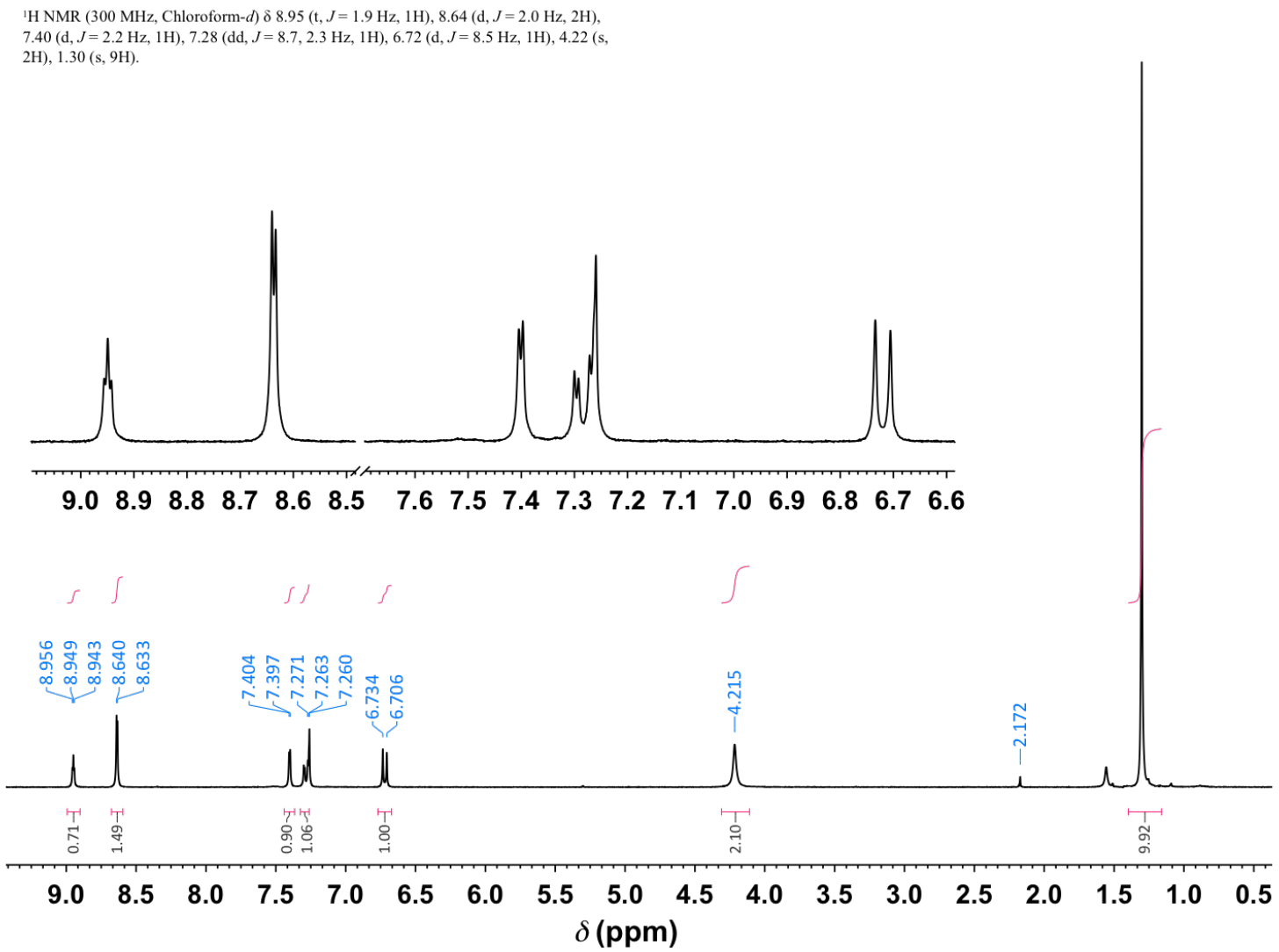

Figure 2. ^{1}H NMR of dinitro core **7**, 300 MHz.

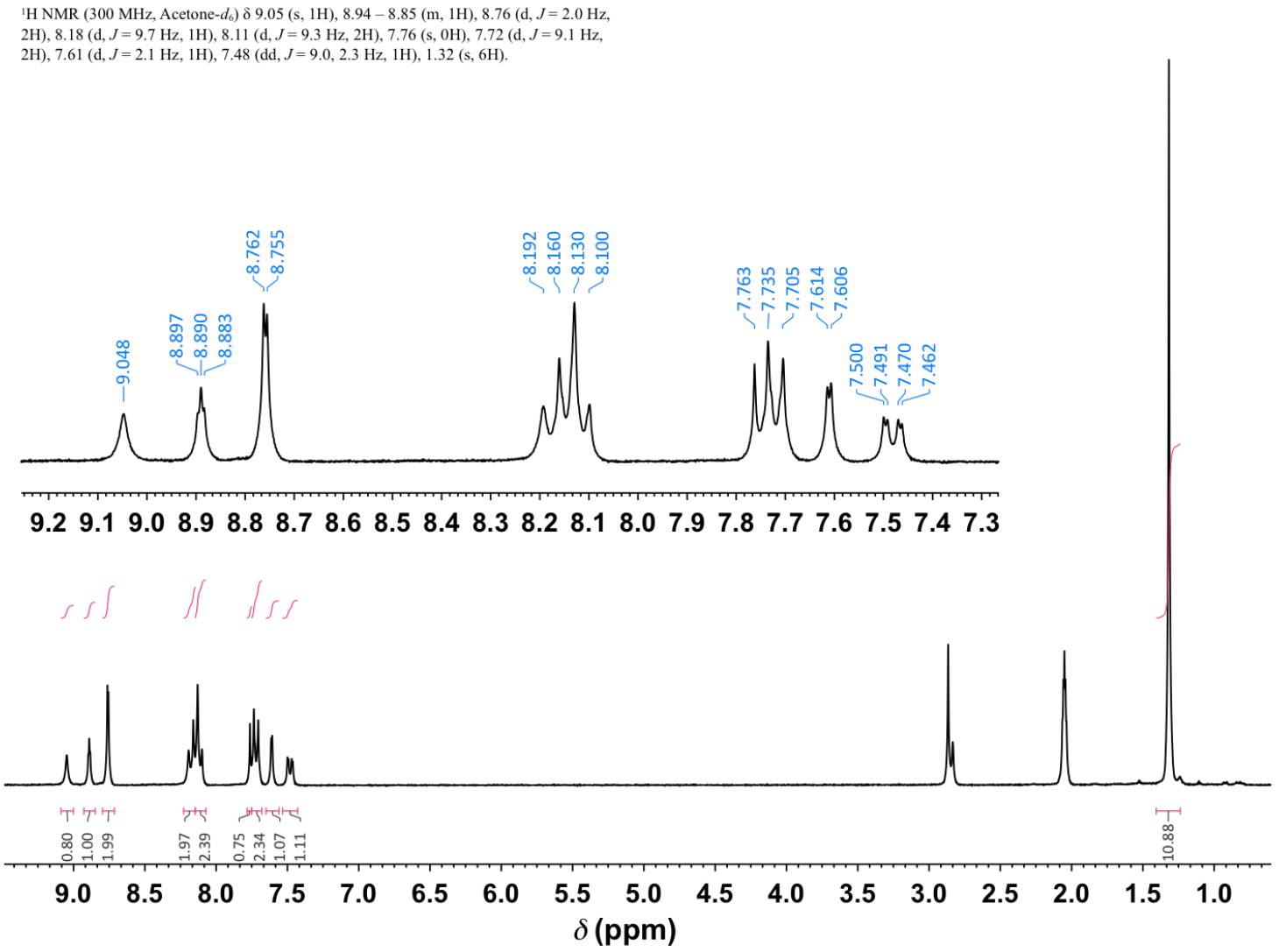

Figure 3. ^{1}H NMR of receptor **2**, 300 MHz.

APPENDIX A

MAIN GROUP CATION–ARENE INTERACTIONS

This appendix consists of the rest of the published review in volume 46 of the journal *Accounts of Chemical Research* in April 2013. Chapter I was comprised of a portion of this original manuscript, prior to its final editing for publication, as well as an unpublished summary of other relevant studies. Mary Collins wrote the original version of this main group cation section of the manuscript. I rewrote and edited this portion of the manuscript as it appears in the publication. My advisor and principle investigator Prof. Darren W. Johnson conceptualized the original research and provided editorial assistance for this publication.

A.1. Main Group Supramolecular Coordination Chemistry – Group 15

Over the last two decades, a diverse compilation of supramolecular coordination complexes emerged from self-assembly between a *d*-block, or less commonly an *f*-block metal, and a multidentate ligand. The resulting metal–ligand self-assemblies typically have square-planar, tetrahedral, or octahedral coordination geometries. Development of self-assembled complexes featuring main group metalloid ions has received less attention, perhaps due to the unusual and sometimes unpredictable coordination geometries of main group elements. The result is a lack of highly specific chelators for toxic ions such as arsenic (As). With this in mind, we launched a program in 2004 to investigate a "supramolecular approach" to toxic metal coordination chemistry and

initially targeted arsenic by employing stabilizing secondary bonding contacts, more specifically, an ion–π interaction, to direct self-assembly.

A.2. Brief Overview of Interactions between Main Group Cations and Aromatic Rings

Recently the role of weak intermolecular forces for complex formation between arenes and heavier metals of Groups 13-16 was highlighted.[1] In low-oxidation states, post-transition metals with stereochemically active lone pairs, such as As, Sb, and Bi, produce stable arene complexes. Recent measurements of binding enthalpies between $SbCl_3$ and neutral arenes (*ca.* 5-10 kcal mol^{-1}) are in the typical range for other "weak interactions",[1] suggesting these interactions might serve as a motif for directing the formation of supramolecular self-assemblies. This weak, predominately electrostatic interaction has been described both as a traditional Lewis acid (main group metalloid) to π-base (arene ring) interaction[1] (Figure 1) and as an electron transfer between As (lone pair) and the π-aryl ring.[2] In the latter description, calculations show the intrinsic molecular dipole of $AsCl_3$ induces polarization in the arene ring upon complexation, revealing a weak sharing of electrons between the As center and each C atom of the arene ring ($As_{lone\text{-}pair}$–π_{aryl} interactions). In the Lewis acid to π-base interaction, sometimes referred to as "Menshutkin complexes", donor orbitals on the arene interact with acceptor orbitals on the metal center. Such a description explains the shortening of the metalloid–π distances in ECl_3•arene complexes (E = As, Sb, Bi), as the metalloids become more Lewis acidic going down the group.

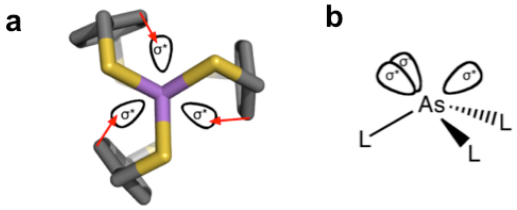

Figure 1. Illustrative depiction of pnictogen–π interactions in supramolecular assemblies. (a) View down the As–As axis of $As_2(\mathbf{L})_3$ showing the possibility of interactions (red arrows) between the π-systems of the arene spacers and the σ* orbitals of As. (b) Locations of σ* orbitals in the primary coordination sphere about an As(III) center.

Along with this, it is important to note dispersion forces may become dominant for heavier congeners of the Group.[3]

The evidence illustrating the significance of π_{aryl} interactions upon complexation with Group 15 metal cations sparked our interest in applying this weak and reversible force as part of a design strategy for forming self-assembled supramolecular main group coordination complexes. The self-assembly of the macrocycles, cryptands, and metallocycles described below all proceed with the apparent assistance of stabilizing As–π_{aryl} interactions.

A.3. Pnictogen–π Interactions and "Supramolecular" Ligand Design

Our supramolecular design strategy focuses on the self-assembly of an As(III) source and an organothiol ligand (Chart 1). The As–thiolate bond is attractive due to its lability and reversibility, as well as the predictable trigonal-pyramidal coordination geometry of As(III)–thiolates. Our first approach for self-assembled As(III)–organothiolate complexes exploiting a stabilizing As–π interaction utilized a rigid, multidendate 1,4-bis(mercaptomethyl)benzene (H_2**L**) ligand.[4] When treated with stoichiometric amounts of $AsCl_3$ and KOH in THF/methanol, a discrete dinuclear As_2**L**$_3$ complex emerges, with As positioned *endo* relative to the ligands, allowing for the stereochemically active lone pair to be directed inside the small cavity of the cryptand (Scheme 1). The crystal structure revealed six short As–C_{aryl} contacts with distances between 3.18 and 3.33 Å, indicating a stabilizing metal–π interaction between the arene and the As lone pair (Figure 2). DFT calculations of this weak force in an $AsCl_3$–benzene dimer suggest the As–π interaction is strong (7.3 kcal mol^{-1}), with a shallow potential for its preferred geometry.

Chart 1. Ligands used to prepare pnictogen-containing supramolecular assemblies.

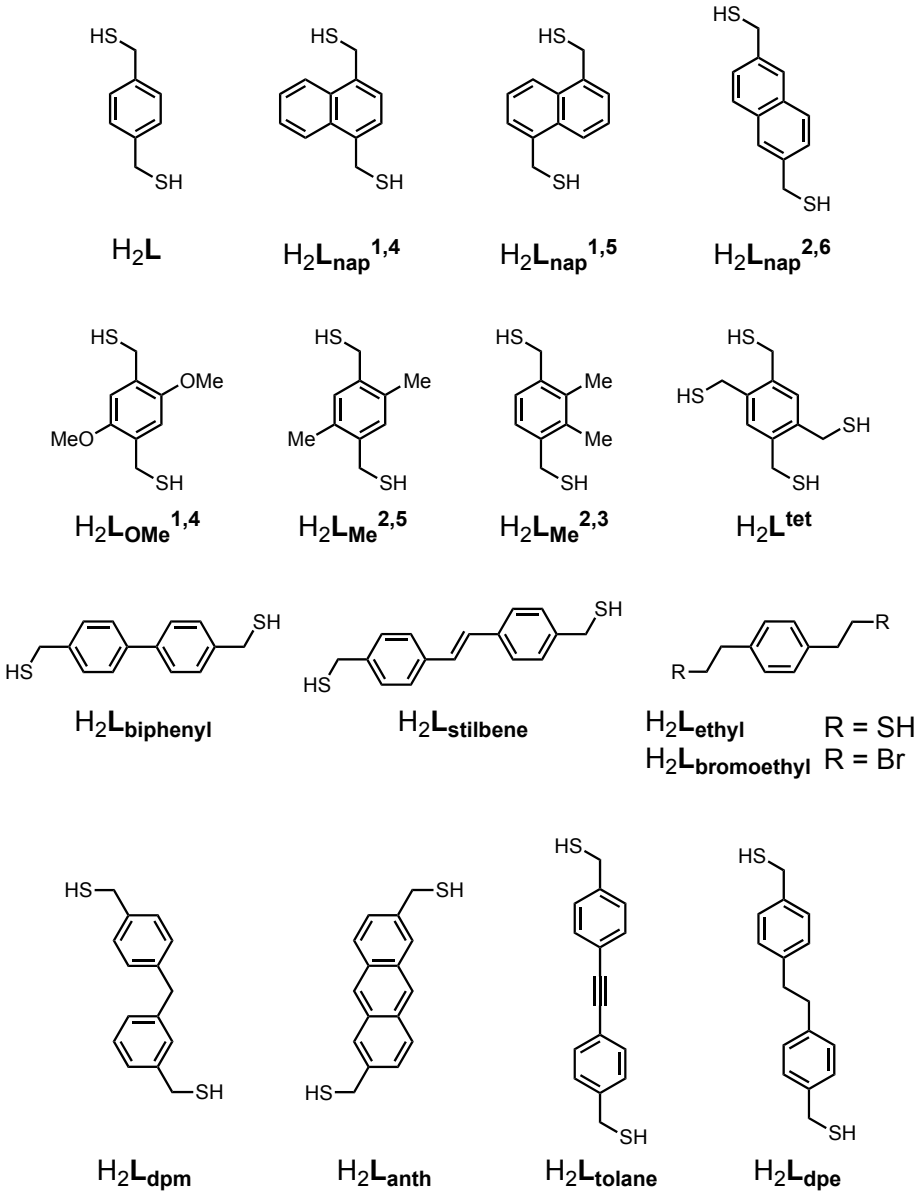

Scheme 1. Synthesis of $As_2\mathbf{L}_3$ assemblies.

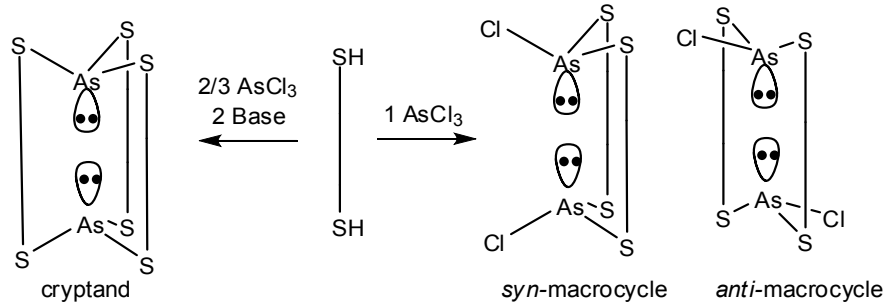

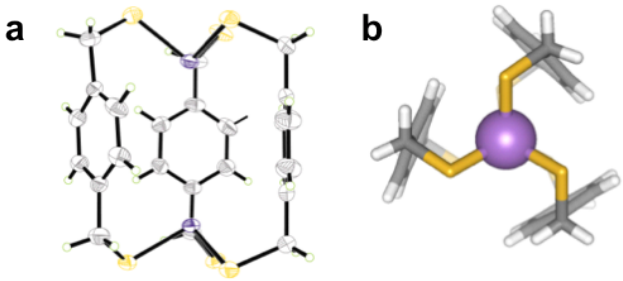

Figure 2. (a) ORTEP representation of the X-ray crystal structure of $As_2\mathbf{L}_3$. (b) Wire frame representations with arsenic atoms shown as space-filling spheres.

In the absence of base, a macrocyclic $As_2\mathbf{L}_2Cl_2$ complex forms as a mixture of *syn* and *anti* diastereomers as seen by ^{1}H NMR spectroscopy.[5] However, either stereoisomer can be selectively isolated by altering crystallization conditions (Figure 3). Structural analysis of the *anti* conformer displays two As–Cl bonds pointing in opposite directions. In the *anti* conformation, the aromatic rings are parallel and the As(III) centers twist, allowing each As(III) center, providing a short As1–As1a separation (4.65 Å) and decreased As–C_{aryl} distances (3.16 Å, far smaller than the sum of the van der Waals radii of 3.70 Å). In the *syn*-$As_2\mathbf{L}_2Cl_2$ diastereomer, both As–Cl bonds point in the same direction. In contrast to the case of its diastereomeric partner, the two As(III) centers in the syn conformation align along the ligand axis (As1–As1a = 5.02 Å), and correspondingly longer As–π interactions were observed (avg. As–C_{aryl} = 3.25 Å). When molecular mechanics modeling was examined, both *syn*-$As_2\mathbf{L}_2Cl_2$ and *anti*-$As_2\mathbf{L}_2Cl_2$ macrocycles were shown to have more torsional freedom to shift the As ion away from the aryl rings than the $As_2\mathbf{L}_3$ cryptand.[6] Nevertheless, both macrocycles show closer As–π contacts than those for the cryptand, indicating As–π interactions might play a more significant role in the self-assembly of the macrocycle than the apparently more

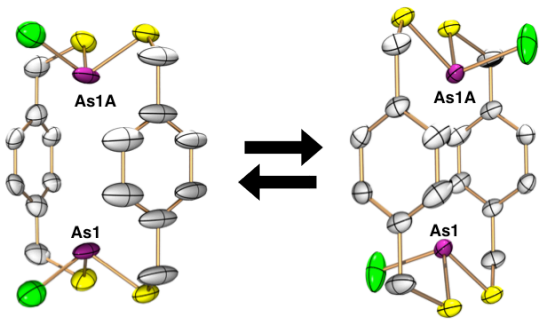

Figure 3. ORTEP representation of the single crystal X-ray structure of *syn*-$As_2\mathbf{L}_2Cl_2$ and *anti*-$As_2\mathbf{L}_2Cl_2$ macrocycle with 50 % probability ellipsoids and hydrogen atoms omitted.

thermodynamically stable cryptand. Interestingly, ^{1}H NMR spectroscopy reveals a slow equilibrium between *syn* and *anti*, slightly favoring the formation of the *anti* macrocycle (diastereomeric ratio ca. 5:4). This suggests the shorter As–π interaction observed in the solid state might persist in solution to provide a stronger stabilization to the *anti* macrocycle.

The directing role of As–π interactions was further investigated by expanding the choice of organothiol ligand to achiral, isomeric bis(mercaptomethyl)naphthalene ligands ($H_2\mathbf{L}_{\mathbf{nap}}^{\mathbf{1,4}}$, $H_2\mathbf{L}_{\mathbf{nap}}^{\mathbf{1,5}}$, $H_2\mathbf{L}_{\mathbf{nap}}^{\mathbf{2,6}}$).[7] As before, a secondary As–π interaction directs the formation of each *syn* and *anti* macrocycle; however, the choice of naphthalene ligand dictates the *syn*-to-*anti* ratio. The variation in substitution pattern alters the environment of the As–Cl bond upon complexation and directs formation of the major diastereomer: the isomer that places the chlorine ligands farthest from the electron-rich arene ring is favored. Given this repulsive interaction, crystallization gave the following expected isomers as the preferred products: a nearly equal mixture of *anti*-$As_2(\mathbf{L}_{\mathbf{nap}}^{\mathbf{2,6}})_2Cl_2$ and *syn*-$As_2(\mathbf{L}_{\mathbf{nap}}^{\mathbf{2,6}})_2Cl_2$, primarily *anti*-$As_2(\mathbf{L}_{\mathbf{nap}}^{\mathbf{1,5}})_2Cl_2$, and last, *syn*-$As_2(\mathbf{L}_{\mathbf{nap}}^{\mathbf{1,4}})_2Cl_2$, all of which minimize the unfavorable steric interactions (Figure 4). The As–As distances vary (7.45, 5.64, 4.66 Å) for each macrocycle, but the As–C_{aryl} distances remain comparable (3.30, 3.22, 3.14 Å).

We also sought to explore the host–guest chemistry of macrocycles featuring larger interior cavities assembled from extended ligands (e.g., biphenyl, stilbene, anthracene linkers). The assembly expansion revealed no effect on the As–π interaction, although the presence of the interaction itself may inhibit guests from fitting entirely within the cavity.[8] In each case, the macrocycles were too small to completely surround a guest molecule but were large enough to accommodate one or two guests on the periphery of the macrocyclic cavity (Figure 5). Each macrocycle displays multiple

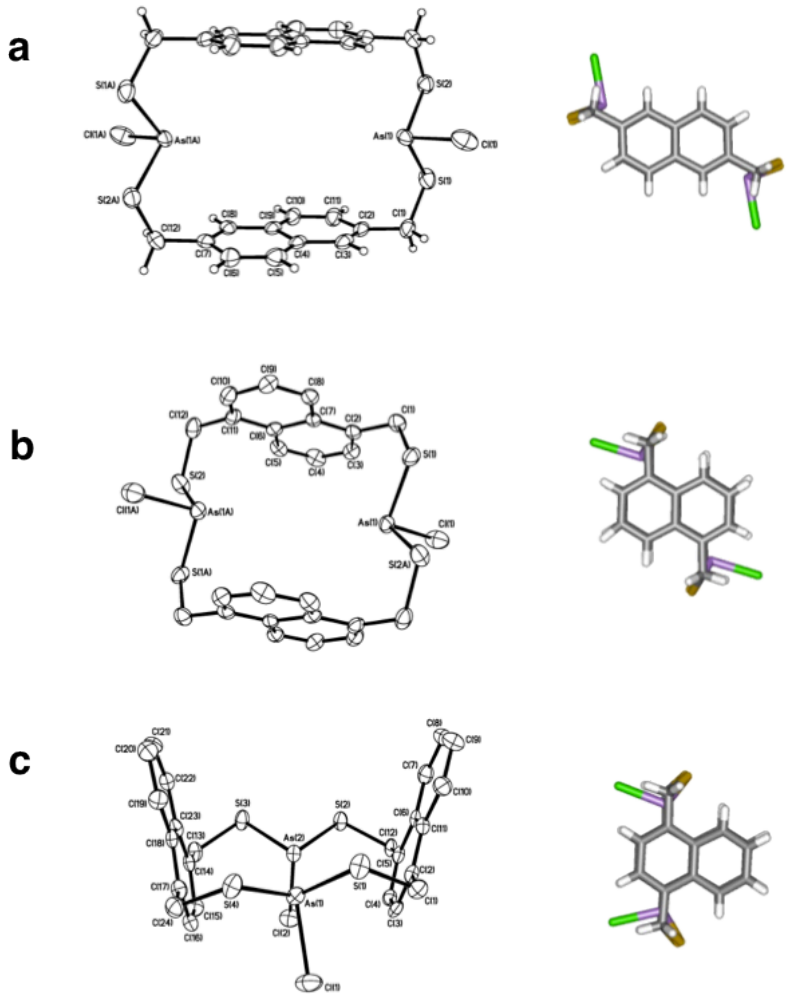

Figure 4. ORTEP (30 % probability ellipsoids) and wire frame representations of single-crystal X-ray structures for (a) *anti*-$As_2(\mathbf{L_{nap}}^{2,6})_2Cl_2$, (b) *anti*-$As_2(\mathbf{L_{nap}}^{1,5})_2Cl_2$, and (c) *syn*-$As_2(\mathbf{L_{nap}}^{1,4})_2Cl_2$ macrocycles.

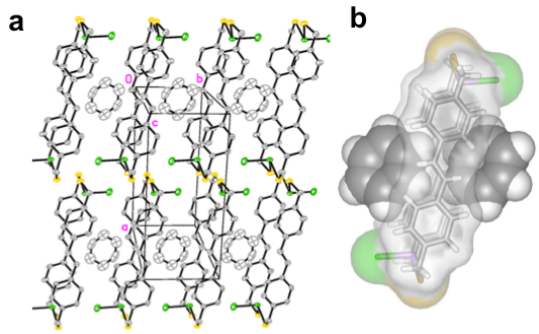

Figure 5. (a) Packing diagram of [*anti*-$As_2(\mathbf{L_{stilbene}})_2Cl_2$•benzene] along the macrocyclic axis. (b) Space-filling representation of inclusion complex.

intramolecular As–π interactions. Self-assembly of $H_2\mathbf{L_{OMe}}^{1,4}$ and $AsCl_3$ provided a macrocycle wide enough to host a guest due to the protruding methoxy substituents (Figure 6). When crystallized from a solvent that serves as a suitable guest, such as *p*-xylene, the macrocycle forms a homodimer

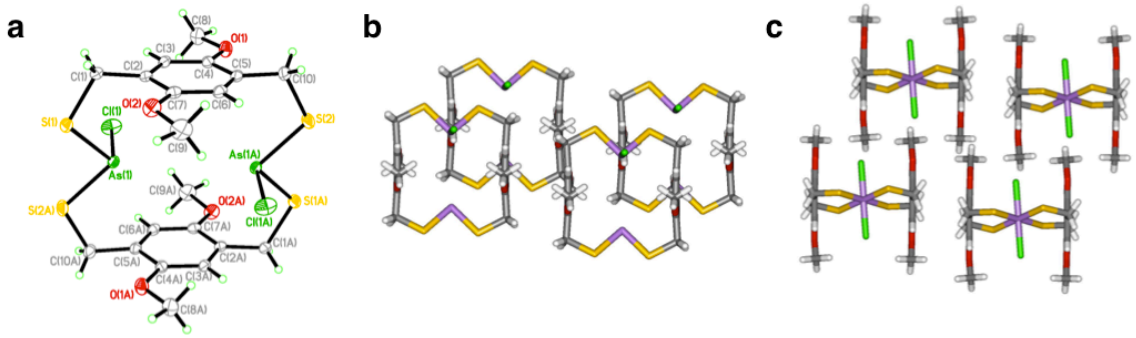

Figure 6. ORTEP (30 % probability ellipsoids) representation of single-crystal X-ray structure of (a) *anti*-$As_2(\mathbf{L_{OMe}}^{1,4})_2Cl_2$. Stick representation showing the packing from (b) side and (c) top views.

[(*syn*-$As_2(\mathbf{L_{OMe}}^{1,4})_2Cl_2)_2$•*p*-xylene], where the ligand walls of one macrocycle tilt out of parallel allowing one end of the cavity to open and share a guest molecule with the cavity of a second macrocycle (Figure 7). A slight tilt of one ligand from parallel with the other clearly indicates guest inclusion in the macrocyclic dimeric "capsule" does not destroy the As–π interaction, and therefore, the guest alone may control the diastereoselectivity during the crystallization. When no suitable guest molecules are present, the *anti* macrocycle is crystallized exclusively and the As–π interaction is shorter than in any other macrocycles reported to date (As–C_{aryl} = 3.11 Å), presumably due to the increased π-basicity of $H_2\mathbf{L_{OMe}}^{1,4}$.

To expand preliminary work probing the role of steric repulsions in self-assembly of the macrocycles, two types of dimethyl-substituted phenyl ligands were synthesized: $H_2\mathbf{L_{Me}}^{2,5}$ and $H_2\mathbf{L_{Me}}^{2,3}$.[9] Each showed facile formation of the *anti* macrocycle, indicating the bulky methyl groups do not disrupt the apparently strong directing effect of the As–π interaction. In the crystal structure of *anti*-$As_2(\mathbf{L_{Me}}^{2,5})_2Cl_2$, the two chloride ligands point away from the methyl groups, avoiding unfavorable steric repulsions while maintaining favorable As–π interactions (Figure 8a,c). Preferential formation of the sterically disfavored *anti*-$As_2(\mathbf{L_{Me}}^{2,3})_2Cl_2$ macrocycle was surprising, since one of the *anti*-conformers has one chloride ligand folded into the

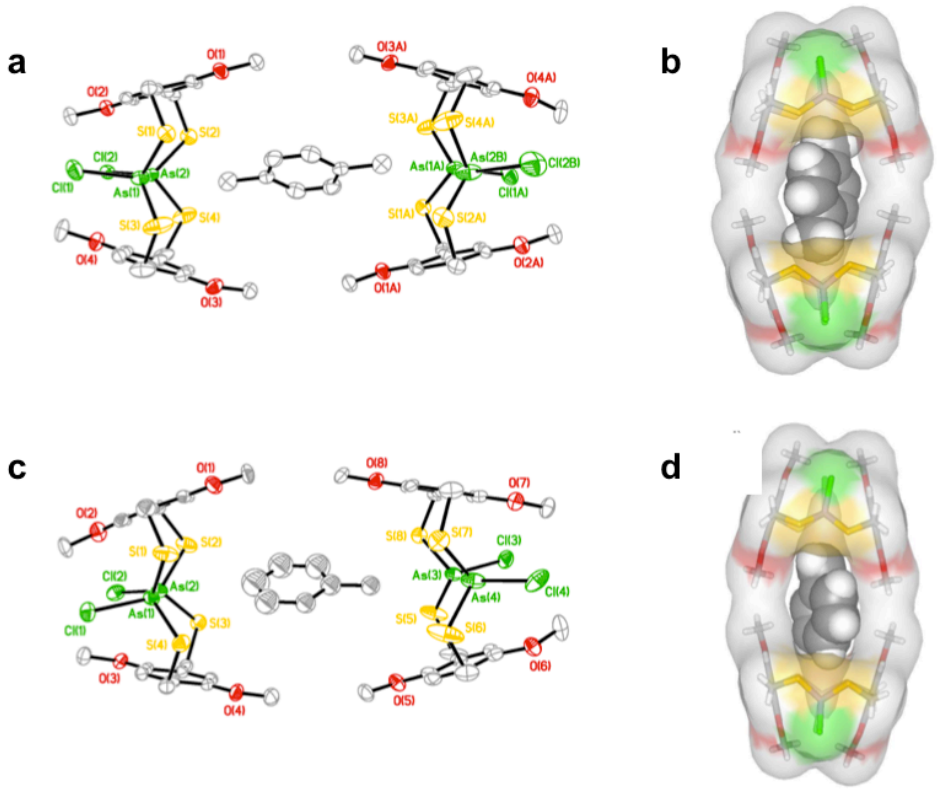

Figure 7. ORTEP (30 % probability ellipsoids) and space-filling representations of single-crystal X-ray structures of (a,b) [(*syn*-$As_2(\mathbf{L_{OMe}}^{1,4})_2Cl_2)_2$•*p*-xylene] and (c,d) [(*syn*-$As_2(\mathbf{L_{OMe}}^{1,4})_2Cl_2)_2$•toluene].

cavity of the macrocycle to avoid steric repulsions with the methyl groups (Figure 8b,d). Rather than participating in potential weak anion–p interactions, this "folded in" chloride ligand participates in secondary bonding interactions (SBIs) with an As center in an adjacent macrocycle. As anticipated, this conformation does not disrupt intramolecular As–π interactions, maintaining As–C_{aryl} distances of 3.27 and 3.32 Å with the thiol ligand (Figure 9).

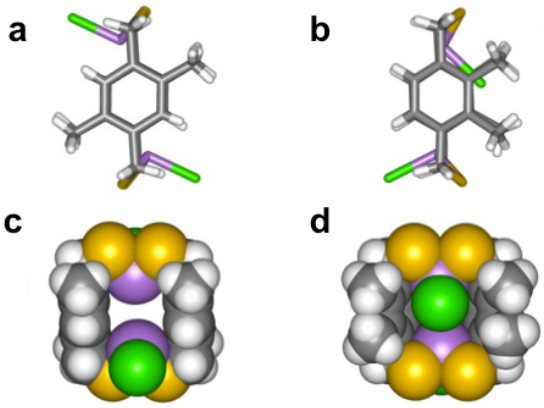

Figure 8. Molecular structures in stick and space-filling representations of (a,c) $As_2(\mathbf{L_{Me}}^{2,5})_2Cl_2$ and (b,d) $As_2(\mathbf{L_{Me}}^{2,3})_2Cl_2$.

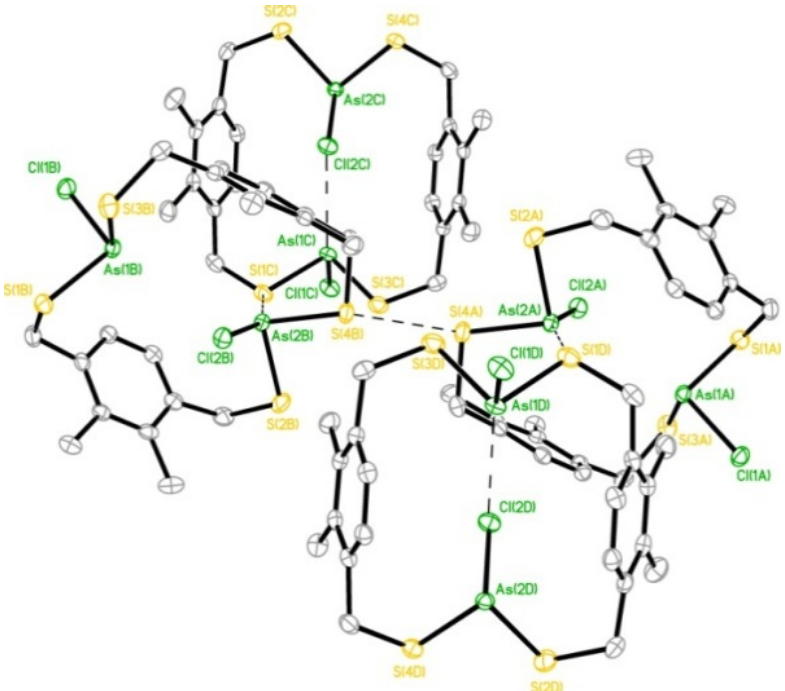

Figure 9. Fragment of the crystal packing structure of $As_2(\mathbf{L_{Me}}^{2,3})_2Cl_2$ showing As-Cl, As-S, and S-S SBIs (dash lines).

Another example where this interaction imparts stereochemical direction upon self-assembly of organo–arsenic coordination complexes is in the structure of a tetranuclear arsenic(III) $As_4(\mathbf{L_{tet}})_2Cl_4$ S_4 metallacyclophane (Chart 1 and Figure 10).[10] This unusual S_4-symmetric coordination complex co-crystallizes with two *cis*- and *trans*-$As_2\mathbf{L}^{\mathbf{tet}}Cl_2$ intermediates in a single crystal. The S_4-symmetry complex houses four As–π interactions per aryl ring (As–C_{aryl} range: 3.24 and 3.45 Å), with the four As(III) metalloids pointing their lone pairs directly into the cavity, in an endo configuration. Surprisingly, no intramolecular As–π contacts were observed in the *cis*- and *trans*-$As_2\mathbf{L}^{\mathbf{tet}}Cl_2$ complexes (Figure 10).

These supramolecular approaches to coordination chemistry helped us develop generalized rules for designing ligands for specific arsenic(III) coordination.[11,12] However, it was uncertain if the ligands always needed to be as rigid as those previously described. To probe this constraint, diphenylmethane ligand $H_2\mathbf{L_{dpm}}$ (4,4′-

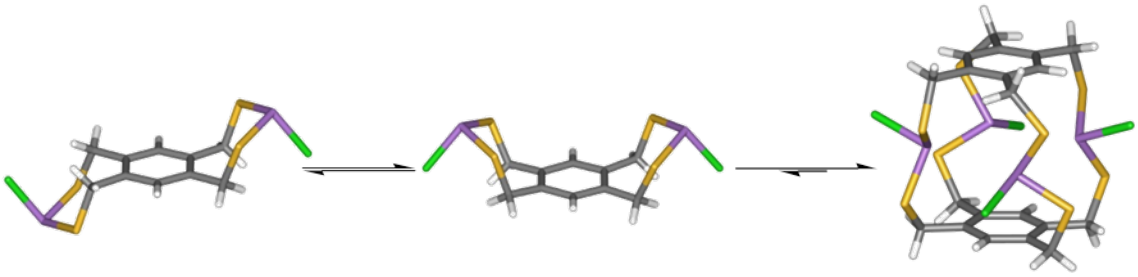

Figure 10. Wire frame representations of the three discrete complexes observed in a single crystal: (a) *trans*-[$As_2\mathbf{L}^{tet}Cl_2$], (b) *cis*-[$As_2\mathbf{L}^{tet}Cl_2$], and (c) the [$As_4(\mathbf{L}^{tet})_2Cl_4$] metallacyclophane.

dimercaptomethyl-diphenylmethane) was utilized,[12] where the methyl spacer between the two phenyl rings would possibly lengthen the cavity of the cryptand and the added flexibility might also widen it. The solid state structure of $As_2(\mathbf{L}_{dpm})_3$ reveals a distorted mesocate in which the three ligands are unevenly distributed around the metalloid centers. The diphenylmethane aryl rings are twisted to direct their edges toward the inner cavity, resulting in an "imploded" cryptand that fills its own cavity interior (Figure 11). Despite the distorted geometry, the structure still maintains multiple intramolecular As–π interactions, with one ligand folded into the cavity shortening the metal–metal distance to 9.19 Å.

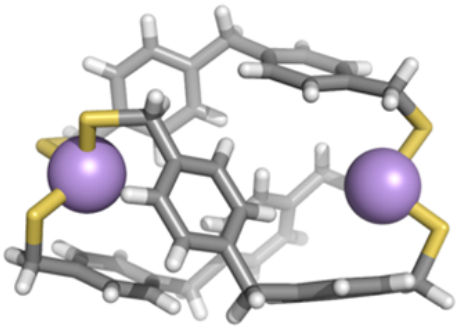

Figure 11. Molecular structure of $As_2(\mathbf{L}_{dpm})_3$ shown as a wire frame; spheres represent arsenic atoms.

Successful incorporation of arsenic into supramolecular self-assemblies led us to explore other Group 15 metalloids. Early work in our lab revealed two dinuclear complexes, $Sb_2\mathbf{L}_3$ cryptand and $Sb_2\mathbf{L}_2Cl_2$ macrocycle, can be formed upon treatment of $H_2\mathbf{L}$ with $SbCl_3$, featuring intramolecular Sb–π contacts (Sb–C_{aryl} contact distances range from 3.20 to 3.61 Å).[13] Self-assembly of related bismuth- and antimony-containing cryptands, $E_2(\mathbf{L}_{nap}^{1,4})_3$ was

achieved using $H_2\mathbf{L}_{\mathbf{nap}}^{\mathbf{1,4}}$, DIPEA, and ECl_3 (E = Bi, Sb).[14] The metalloid–metalloid (E–E) distances decrease from $As_2(\mathbf{L}_{\mathbf{nap}}^{\mathbf{1,4}})_3$ (5.11 Å) to $Sb_2(\mathbf{L}_{\mathbf{nap}}^{\mathbf{1,4}})_3$ (4.83 Å) to $Bi_2(\mathbf{L}_{\mathbf{nap}}^{\mathbf{1,4}})_3$ (4.68 Å) to compensate for longer E–S bonds and smaller S–E–S angles, thus allowing the ligands to retain near identical positions in each cryptand. Previous research[1,15-17] reports E–π interactions to be stronger for larger pnictogens, typically resulting in a decrease in the E–C_{aryl} distance. Due to the constraints of the cryptand structure, the trend is reversed; the shortest observed E–C_{aryl} distance increases slightly from As (3.30 Å) to Sb (3.34 Å) to Bi (3.36 Å) complexes. This does not necessarily indicate a weakening of the E–π interactions, but an increasing ionic radius of E giving the longer E–S bond lengths and constricted metal coordination inside the cavity. In addition to E–π interactions, all of the cryptands formed from $H_2\mathbf{L}_{\mathbf{nap}}^{\mathbf{1,4}}$ maintain favorable intramolecular edge-to-face aromatic interactions, giving the complex a propeller twist (Figure 12).

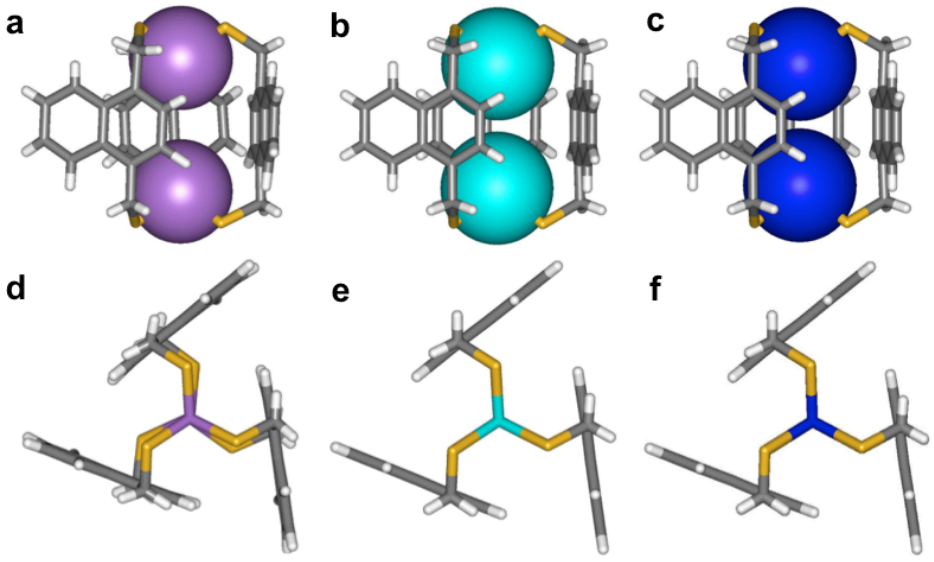

Figure 12. Stick and space-filling representations of the molecular structures of symmetric cryptands (a,d) $As_2(\mathbf{L}_{\mathbf{nap}}^{\mathbf{1,4}})_3$, (b,e) $Sb_2(\mathbf{L}_{\mathbf{nap}}^{\mathbf{1,4}})_3$, and (e,f) $Bi_2(\mathbf{L}_{\mathbf{nap}}^{\mathbf{1,4}})_3$.

The dynamic solution behavior of these supramolecular complexes allowed us to experimentally measure the relative stability of each complex by subjecting each pnictogen cryptand to a different trivalent Group 15 metalloid. Upon addition of $AsCl_3$ to dissolved crystals of the $Sb_2(L_{nap}^{1,4})_3$ cryptand, a transmetalation reaction was observed to provide the $As_2(L_{nap}^{1,4})_3$ cryptand within a week. The weaker Sb–Cl bonds likely help drive the formation of the more thermodynamically stable As cryptand. This "transmetalation" reaction has since allowed us to synthesize a new phosphorus-containing supramolecular complex, which was unattainable by direct methods (Figure 13).[14] The $P_2(\mathbf{L_{nap}^{1,4}})_3$ crystal structure reveals the same endohedral coordination as the As, Sb, and Bi cryptands with the phosphorus lone pairs directed inside the small cryptand cavity. Despite close P–C_{aryl} contacts (3.54 Å, sum of the van der Waals radii: 3.50 Å), the presence of P–π interactions is not apparent. Such interactions are typically only observed in more Lewis acidic cationic phosphorus complexes.[18]

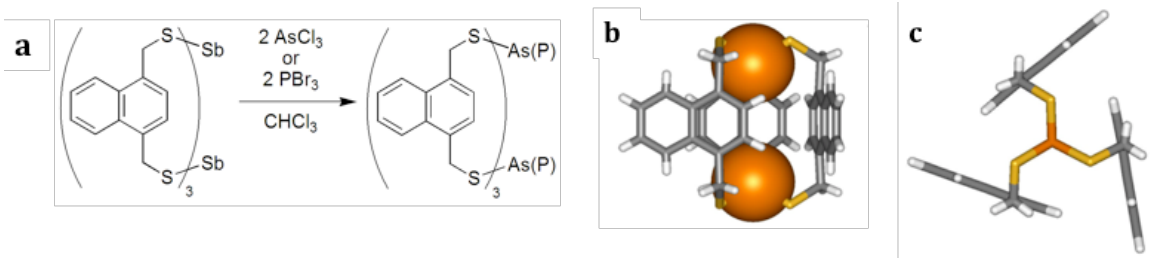

Figure 13. (a) Transmetalation of $Sb_2(\mathbf{L_{nap}^{1,4}})_3$. (b,c) Stick and space-filling representations of the molecular structures of symmetric cryptands $P_2(\mathbf{L_{nap}^{1,4}})_3$.

Surprisingly, closer inspection of the homometallic cryptands $E_2(\mathbf{L_{nap}^{1,4}})_3$ (E = As, Sb, Bi) in solution identified the presence of a second, less symmetric species, *asym*-E_2-$(\mathbf{L_{nap}^{1,4}})_3$, in which one ligand has "flipped", perturbing the C_3 symmetry of the complex (Figure 14).[19] Each conformer maintains numerous intramolecular E–π interactions. The asymmetric species is in equilibrium with the C_{3h}-symmetric cryptand

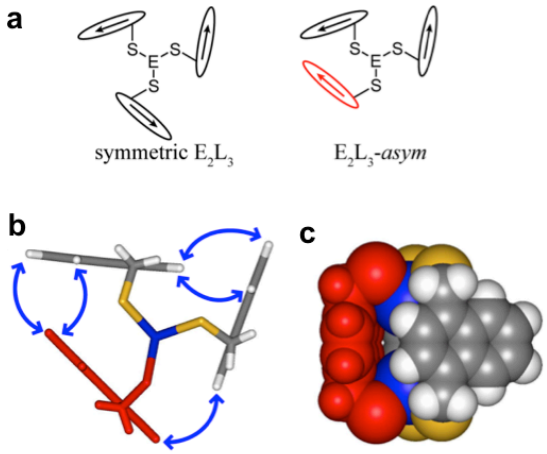

Figure 14. Cartoon representations of (a) symmetric $E_2(\mathbf{L}_{nap}^{1,4})_3$ (left) and *asym*-$E_2(\mathbf{L}_{nap}^{1,4})_3$ (right), in which the ligands are represented by arrows. The DFT-calculated structure of *asym*-$Bi_2(\mathbf{L}_{nap}^{1,4})_3$ is shown in (b) a stick and (c) a space-filling representation. The "flipped" ligand is indicated in red; blue arrows indicate the protons correlated by their NOEs in solution.

in solution and is increasingly favored in the heavier pnictogens (< 5 % component for As, 47 % for Sb, 60 % for Bi).

We also have pursued a systematic study of E_2L_3 cryptands formed from a variety of different organic ligand backbones, each with small structural alterations to change the electronics, cavity size, and flexibility of the aromatic framework ($H_2\mathbf{L}_{anth}$, $H_2\mathbf{L}_{tolane}$, $H_2\mathbf{L}_{stilbene}$, $H_2\mathbf{L}_{dpm}$, $H_2\mathbf{L}_{dpe}$; Chart 1).[20] Despite the diversity of the ligands, each of the cryptands synthesized showed clear As–π interactions, with varied metal–metal distances depending on the distance between the two thiolate functional groups (5.03-12.28 Å). Again, the same somewhat surprising trend appears in comparing these $As_2\mathbf{L}_3$ cryptands to their $Sb_2\mathbf{L}_3$ congeners: the C_{aryl}–E contacts are approximately the same distance in the arsenic complexes (3.25-3.31 Å) as in the antimony cryptands (3.31-3.36 Å), despite the higher Lewis acidity of Sb. As a comparison, while the S–S distances in H2L and $H_2\mathbf{L}_{nap}^{1,4}$ are identical, the Sb–Sb distances in the corresponding cryptands vary dramatically (Figure 15b,d): 4.30 Å for $Sb_2\mathbf{L}_3$ compared to 4.83 Å for $Sb_2(\mathbf{L}_{nap}^{1,4})_3$. This greater than 0.5 Å difference is even more remarkable when one considers that the As–As distances in $As_2\mathbf{L}_3$ and $As_2(\mathbf{L}_{nap}^{1,4})_3$ vary by *less than 0.1 Å*. The result is a profound helical twist in the $Sb_2\mathbf{L}_3$ cryptand (Figure 15).

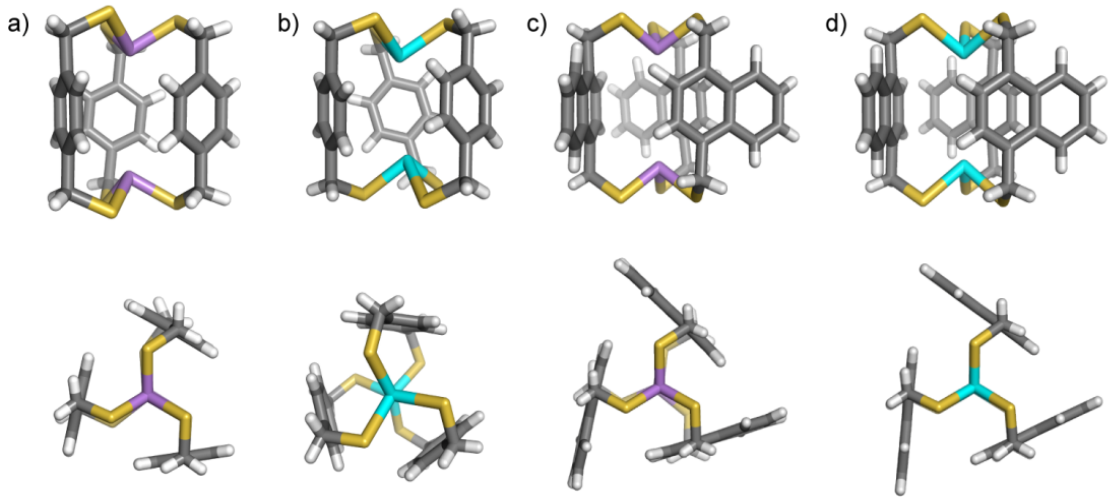

Figure 15. Stick representations of the molecular structures of previously reported E_2L_3 cryptands: (a) $As_2\mathbf{L}_3$, (b) $Sb_2\mathbf{L}_3$, (c) $As_2(\mathbf{L_{nap}}^{1,4})_3$, (d) $Sb_2(\mathbf{L_{nap}}^{1,4})_3$.

The observed endohedral directionality of the As centers in our complexes can perhaps be attributed to the intramolecular As–π interaction, meaning its stability (whether *endo* or *exo* at the metal center for similar systems with stereochemically active lone pairs) depends on the macrocycle's ring size and the steric strain imposed. The presence of such short interactions in the pnictogen macrocycles and cryptands could result from strong mechanical coupling in the self-assembled complex due to the constraints imposed by the rigid ligand framework. Interestingly, the endo conformation also appears to be the more stable geometry in de novo designed and native proteins that bind As(III) as well, suggesting another mechanism for outer sphere metal coordination may explain some modes of metal ion toxicity in vivo.[21]

APPENDIX B

SUPPLEMENTARY INFORMATION FOR CHAPTER II

B.1. Characterization Data of 1

^{1}H NMR (600 MHz, $CDCl_3$) δ 4.44.

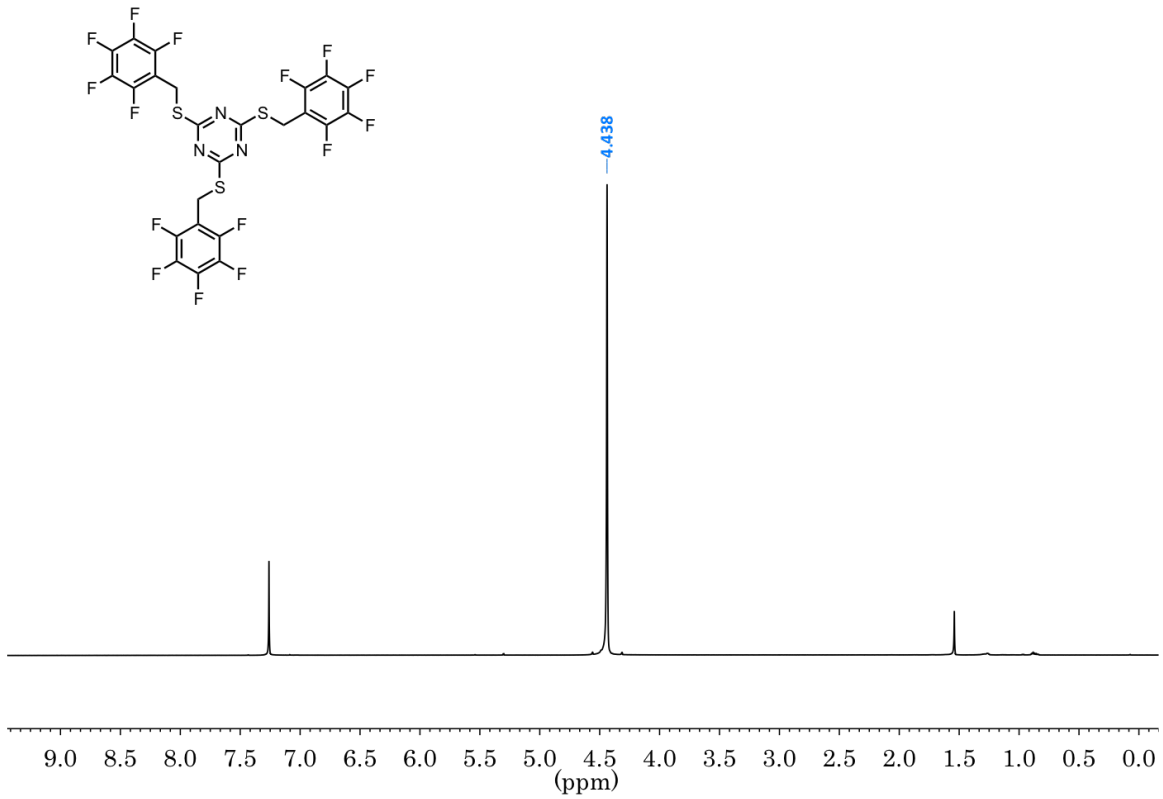

Figure 1. ^{1}H NMR spectrum of **1** in $CDCl_3$, 600 MHz.

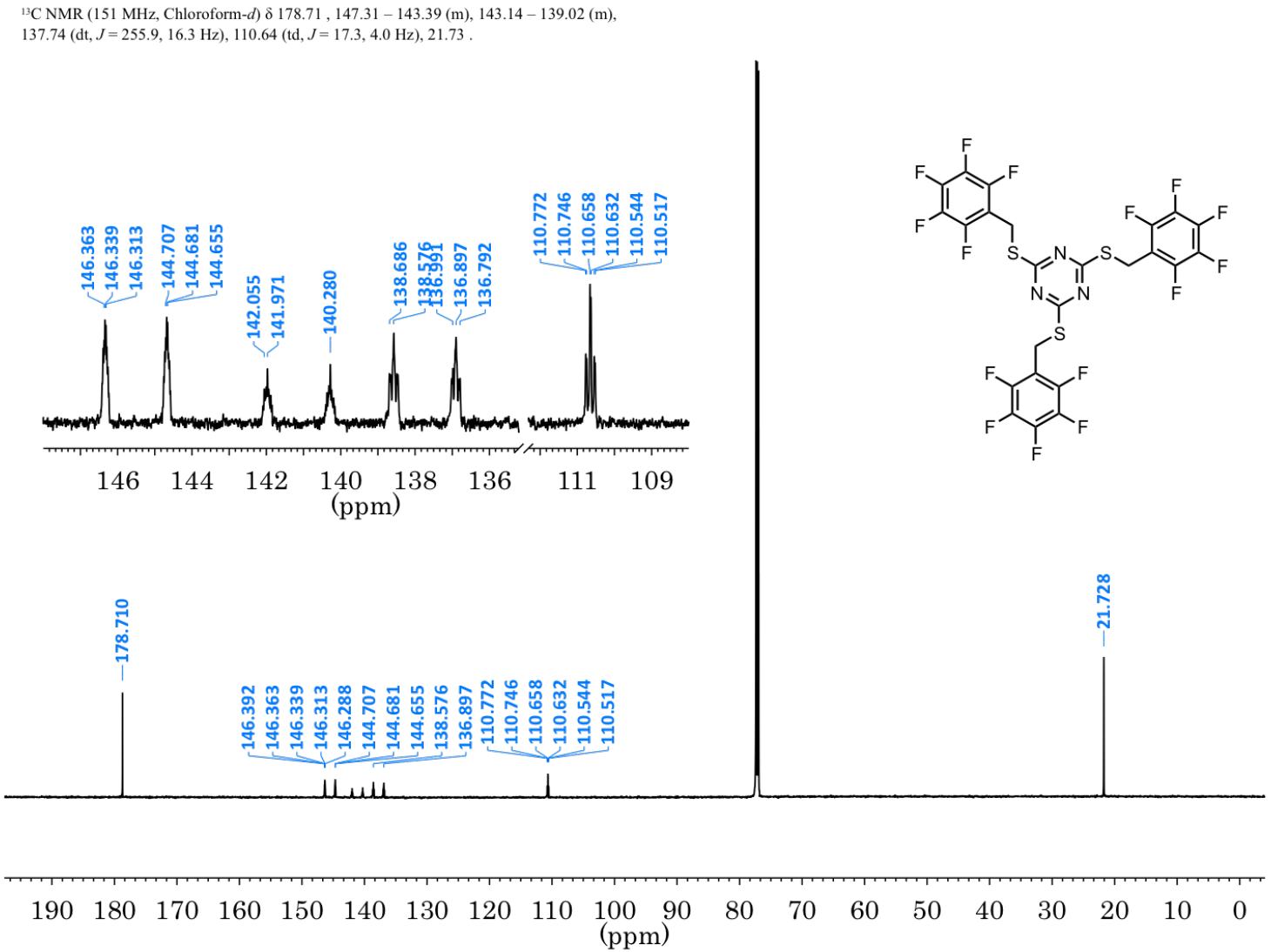

Figure 2. ^{13}C NMR spectrum of **1** in $CDCl_3$, 151 MHz.

[19]F NMR (282 MHz, Chloroform-*d*) δ -143.43 (m), -157.36 (t, *J* = 20.8 Hz), -164.79 (m).

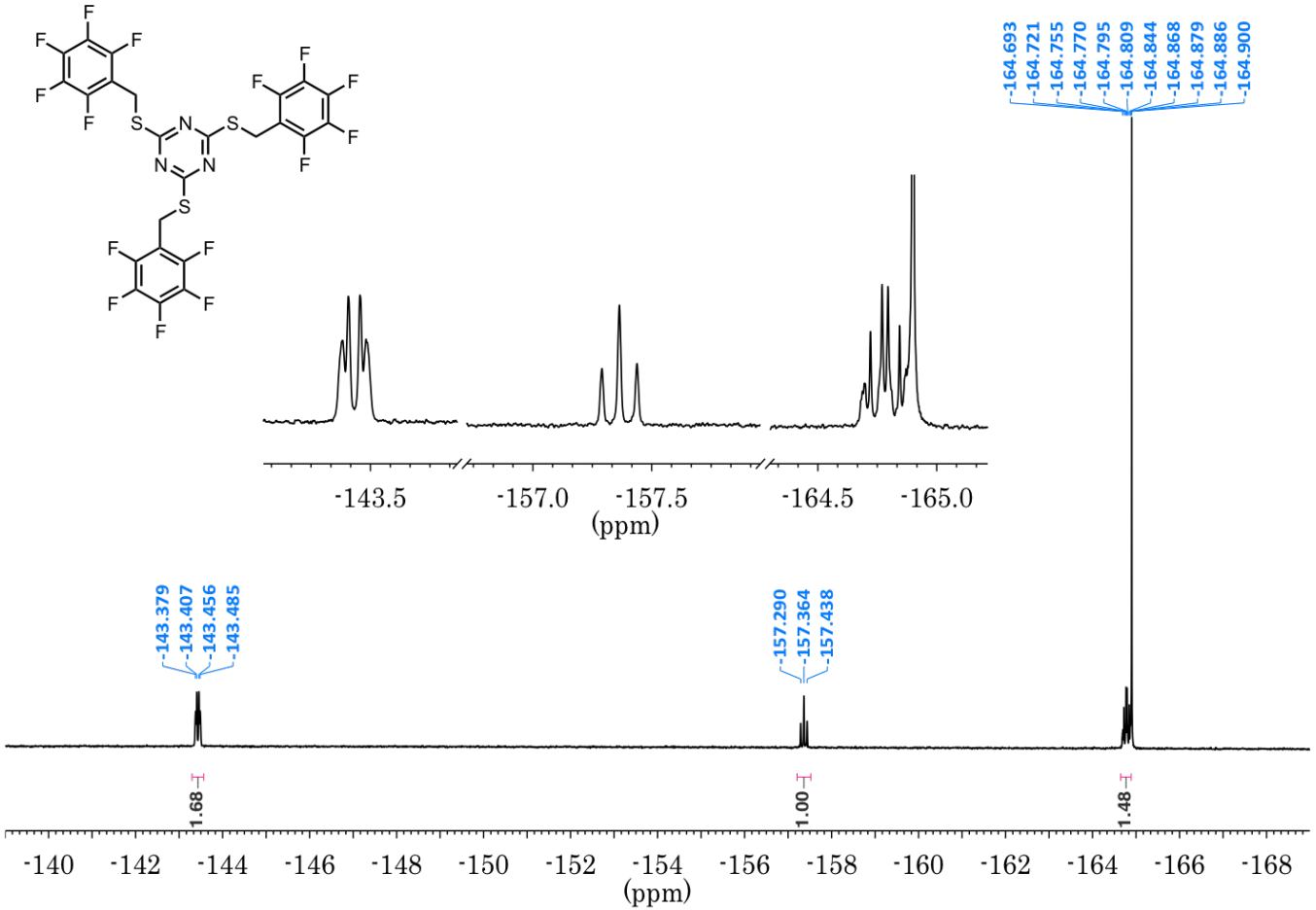

Figure 3. [19]F NMR spectrum of **1** in $CDCl_3$, 282 MHz with internal reference, C_6F_6 (δ = -164.9 ppm relative to $CFCl_3$).

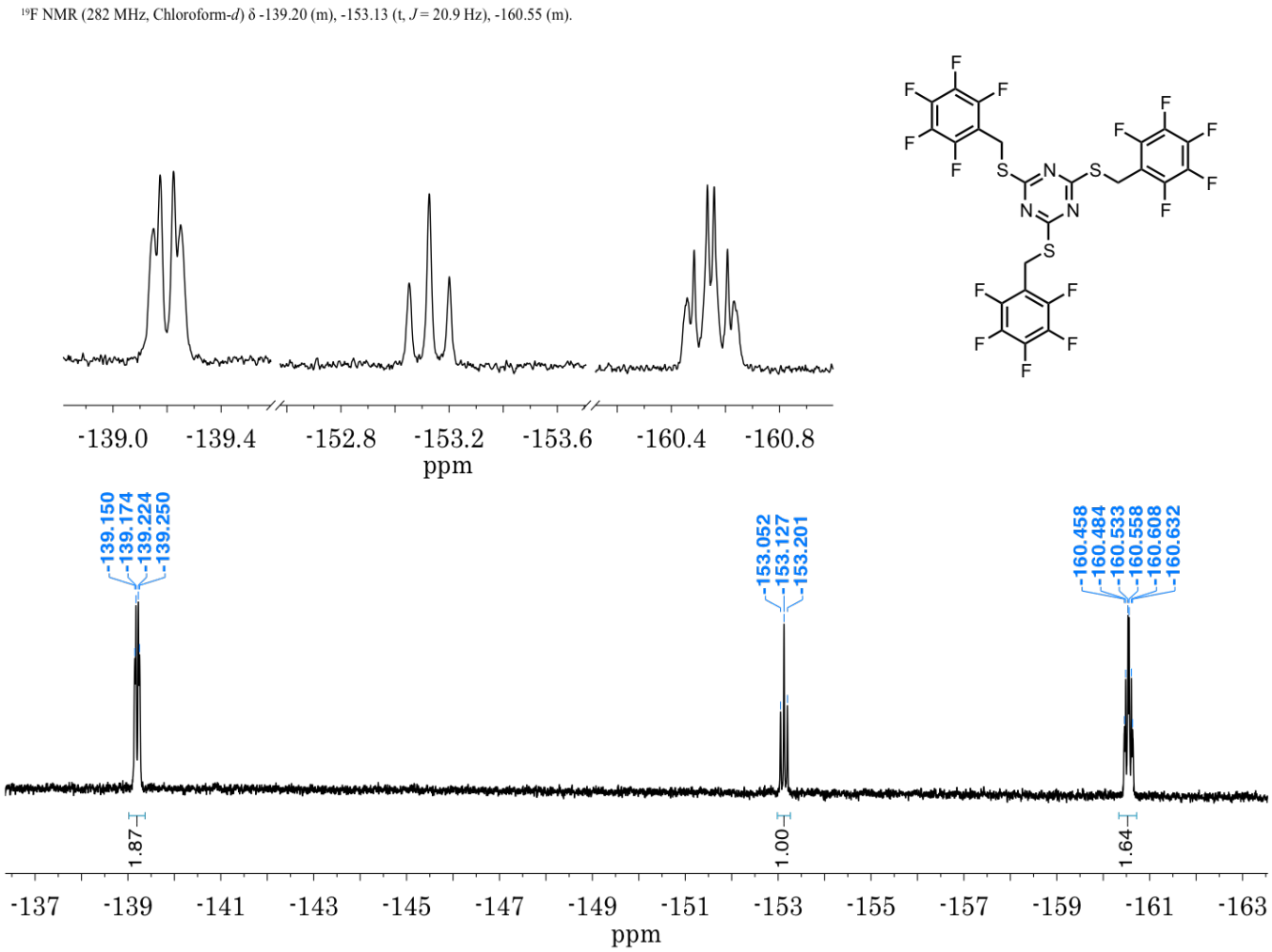

Figure 4. ^{19}F NMR spectrum of **1** in $CDCl_3$, 282 MHz with external reference, CF_3COOH (δ = -76.55 ppm relative to $CFCl_3$).

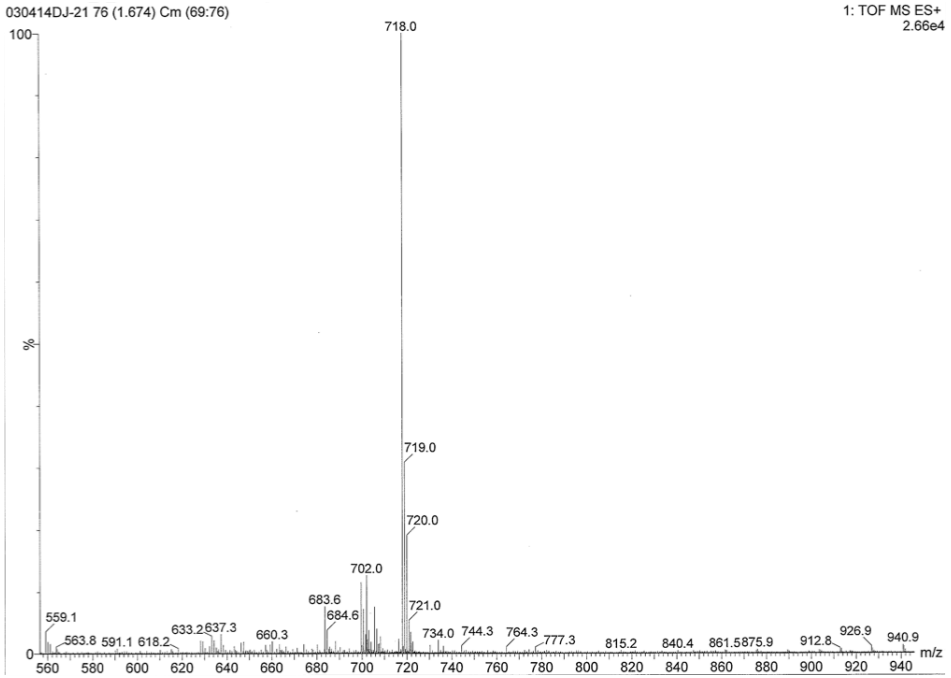

Figure 5. Low resolution ESI mass spectrum of **1.**

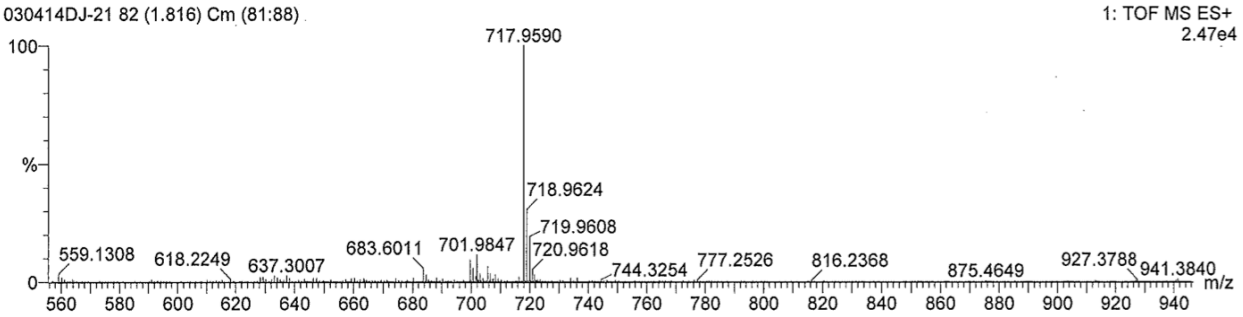

Figure 6. High resolution ESI mass spectrum of **1.**

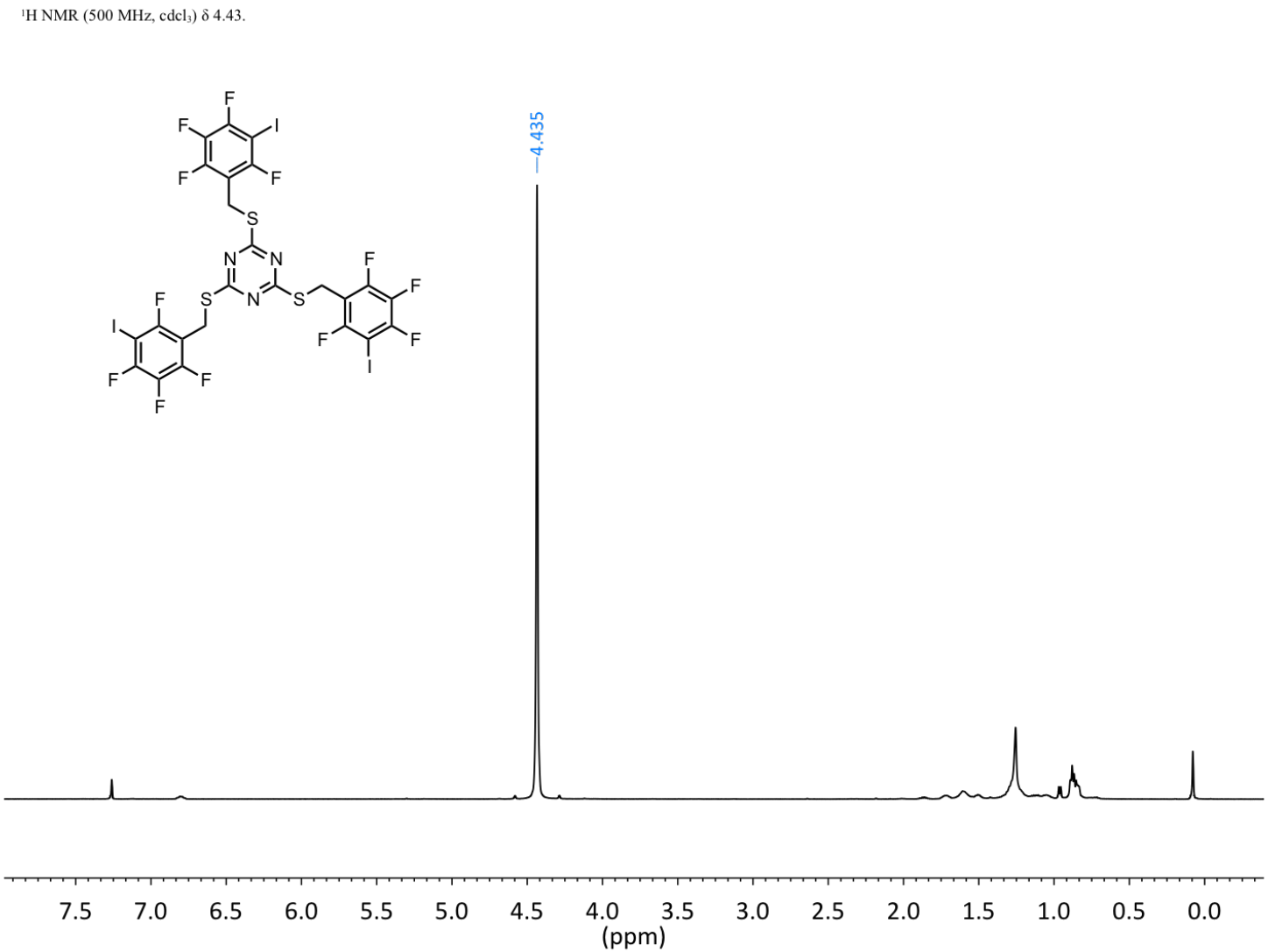

Figure 7. ^{1}H NMR spectrum of **4** in $CDCl_3$, 500 MHz.

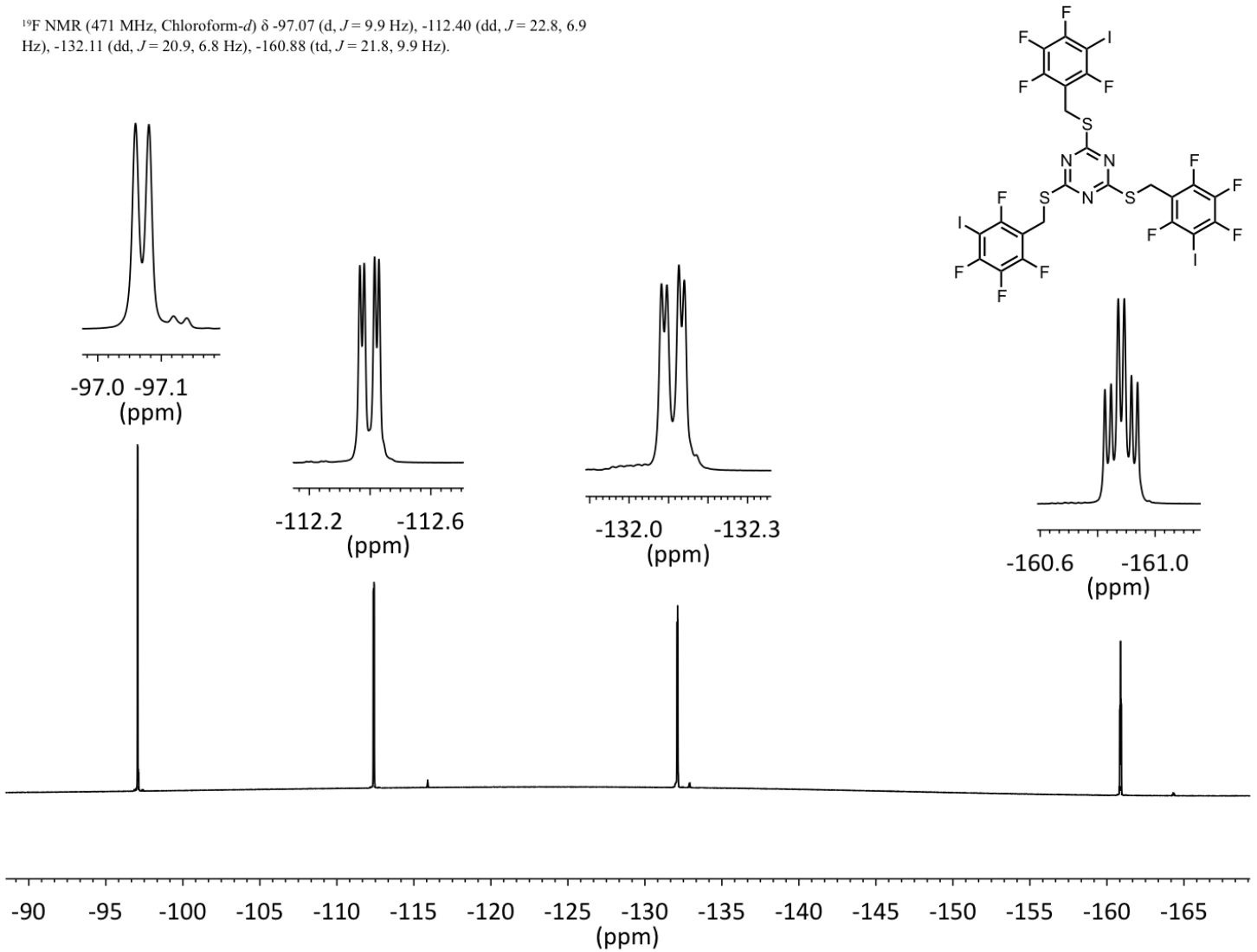

Figure 8. ^{19}F NMR spectrum of **4** in $CDCl_3$, 471 MHz. Spectrum in not referenced to a fluorine source.

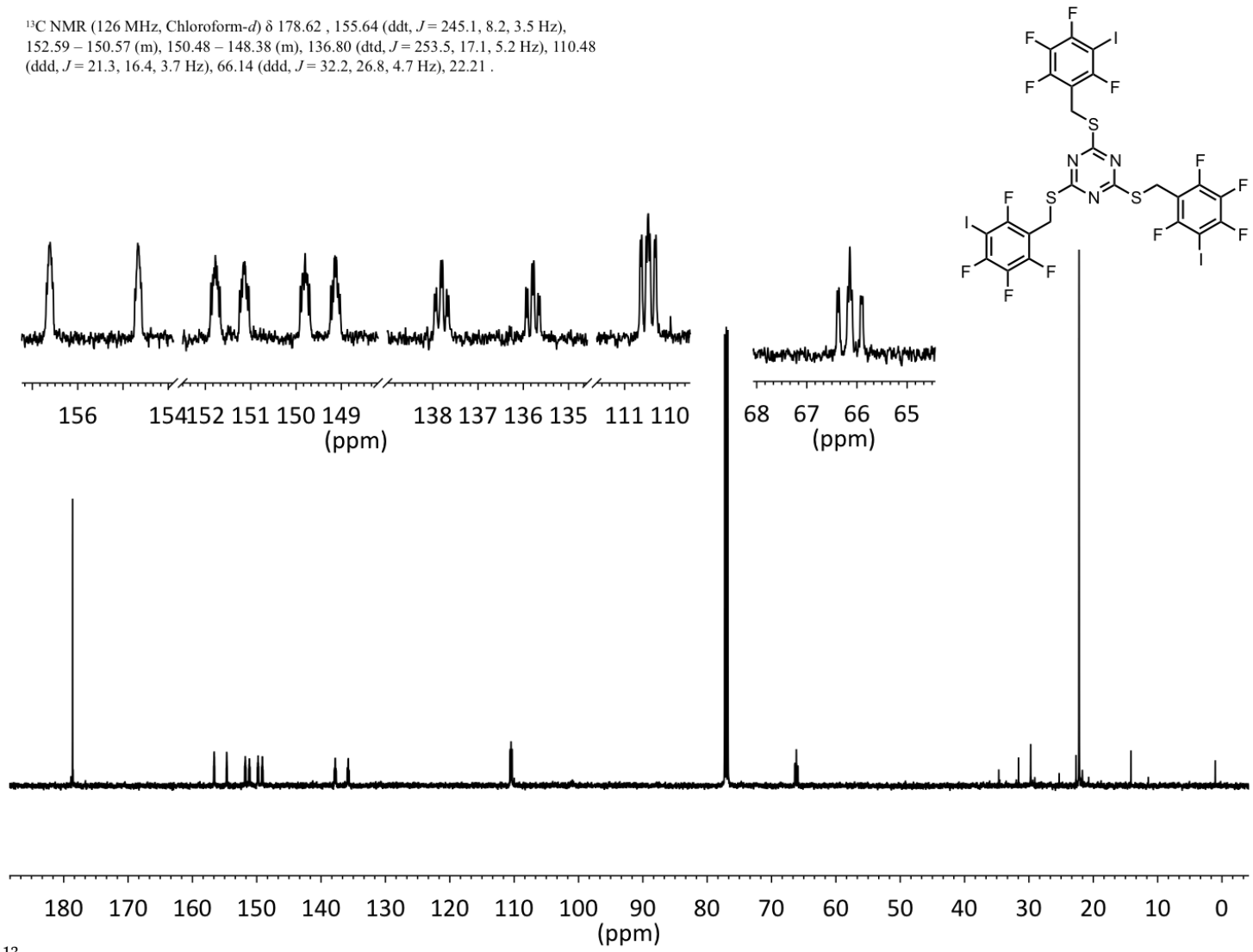

Figure 9. ^{13}C NMR spectrum of **4** in $CDCl_3$, 126 MHz.

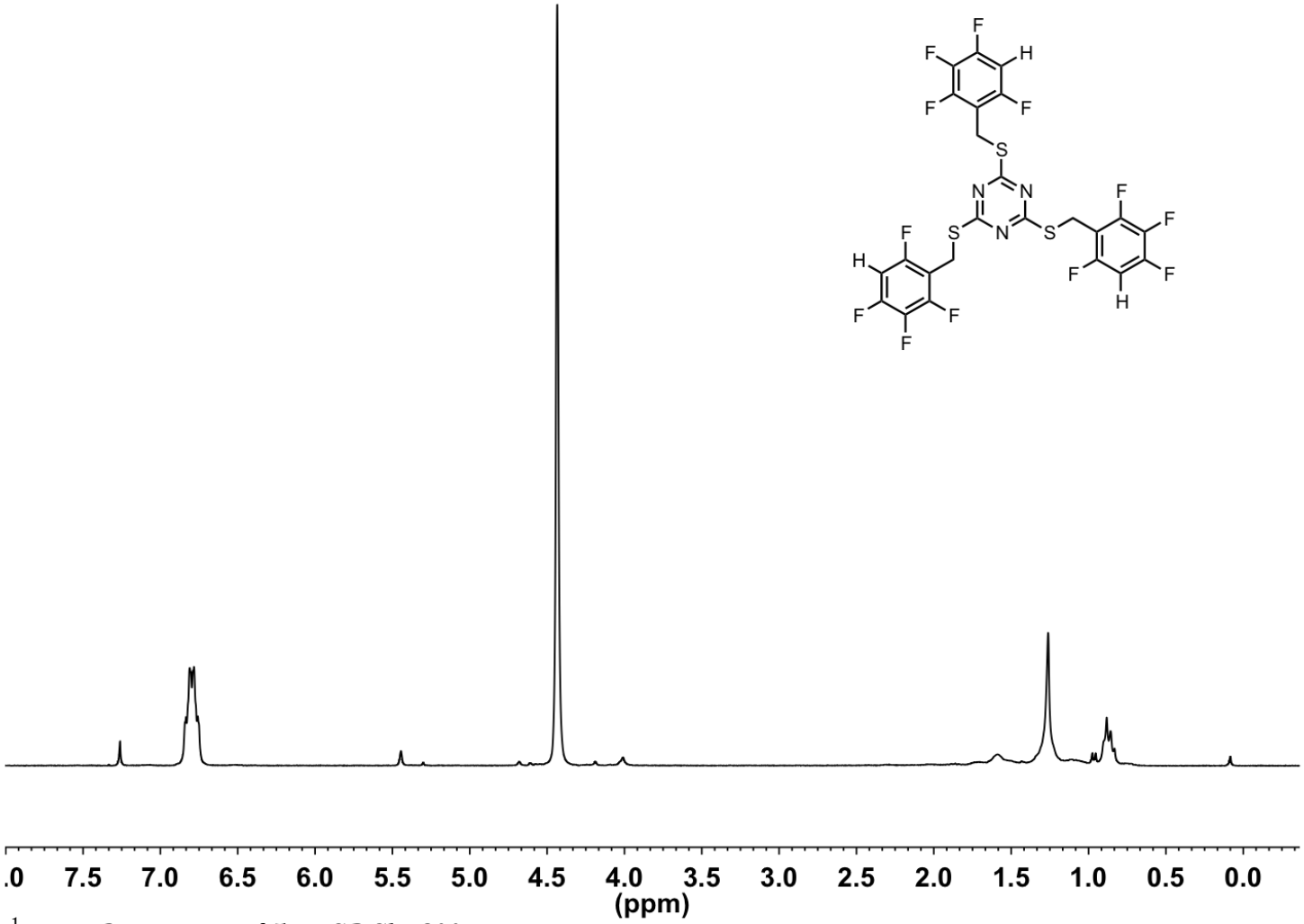

Figure 10. ^{1}H NMR spectrum of **5** in $CDCl_3$, 300 MHz.

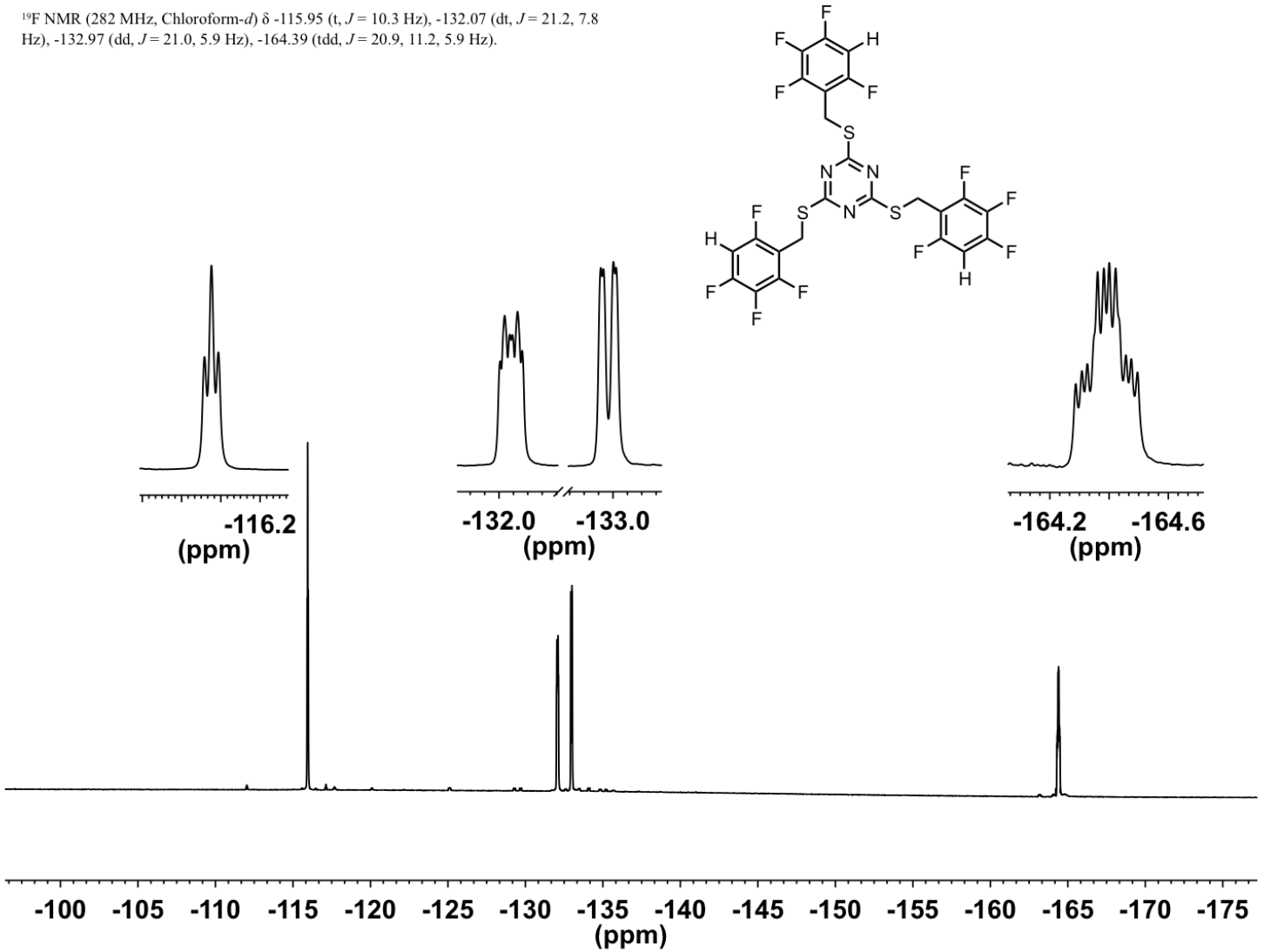

Figure 11. ^{19}F NMR spectrum of **4** in $CDCl_3$, 282 MHz.

B.2. X-Ray Crystallography Data

Table 1. Crystal data and structure refinement for **1.**

Identification code	mwatt3	
Empirical formula	C24 H6 F15 N3 S3	
Formula weight	717.50	
Temperature	173(2) K	
Wavelength	0.71073 Å	
Crystal system	Monoclinic	
Space group	P2(1)/n	
Unit cell dimensions	a = 21.460(2) Å b = 4.6550(5) Å c = 26.363(3) Å	a= 90°. b= 107.970(2)°. g = 90°.
Volume	2505.1(4) $Å^3$	
Z	4	
Density (calculated)	1.902 Mg/m^3	
Absorption coefficient	0.432 mm^{-1}	
F(000)	1416	
Crystal size	0.32 x 0.28 x 0.11 mm^3	
Theta range for data collection	1.07 to 27.00°.	
Index ranges	-27<=h<=27, -5<=k<=5, -33<=l<=31	
Reflections collected	15747	
Independent reflections	5417 [R(int) = 0.0210]	
Completeness to theta = 27.00°	99.5 %	
Absorption correction	Semi-empirical from equivalents	
Max. and min. transmission	0.9540 and 0.8741	
Refinement method	Full-matrix least-squares on F^2	
Data / restraints / parameters	5417 / 0 / 430	
Goodness-of-fit on F^2	1.077	
Final R indices [I>2sigma(I)]	R1 = 0.0342, wR2 = 0.0883	
R indices (all data)	R1 = 0.0403, wR2 = 0.0980	
Largest diff. peak and hole	0.352 and -0.263 $e.Å^{-3}$	

Table 2. Atomic coordinates (x 10^4) and equivalent isotropic displacement parameters ($Å^2$ x 10^3) for **1.** U(eq) is defined as one third of the trace of the orthogonalized U^{ij} tensor.

Atom	X	Y	Z	U(eq)
S(1)	7839(1)	11698(1)	800(1)	26(1)
S(2)	9640(1)	4913(1)	487(1)	26(1)
S(3)	9288(1)	5366(1)	2371(1)	30(1)
N(1)	8776(1)	8163(3)	696(1)	23(1)

Table 2 Continued.

Atom	X	Y	Z	U(eq)
N(2)	9396(1)	5249(3)	1420(1)	24(1)
N(3)	8580(1)	8445(3)	1537(1)	24(1)
C(1)	8465(1)	9163(4)	1024(1)	22(1)
C(2)	9236(1)	6194(4)	924(1)	22(1)
C(3)	9052(1)	6506(4)	1709(1)	23(1)
C(4)	7857(1)	12498(4)	128(1)	28(1)
C(5)	7365(1)	10882(4)	-307(1)	25(1)
C(6)	7538(1)	8836(4)	-619(1)	28(1)
C(7)	7085(1)	7409(4)	-1024(1)	32(1)
C(8)	6429(1)	8036(5)	-1134(1)	36(1)
C(9)	6236(1)	10100(5)	-839(1)	35(1)
C(10)	6701(1)	11473(4)	-432(1)	29(1)
C(11)	10245(1)	2488(4)	907(1)	28(1)
C(12)	10745(1)	3887(4)	1367(1)	24(1)
C(13)	10808(1)	3170(4)	1892(1)	29(1)
C(14)	11257(1)	4495(5)	2317(1)	33(1)
C(15)	11660(1)	6591(4)	2225(1)	32(1)
C(16)	11624(1)	7320(4)	1712(1)	28(1)
C(17)	11171(1)	5962(4)	1294(1)	24(1)
C(18)	8735(1)	7505(5)	2622(1)	35(1)
C(19)	8787(1)	6472(4)	3173(1)	25(1)
C(20)	8382(1)	4343(4)	3256(1)	32(1)
C(21)	8422(1)	3362(5)	3757(1)	44(1)
C(22)	8875(1)	4510(6)	4190(1)	47(1)
C(23)	9285(1)	6636(6)	4130(1)	45(1)
C(24)	9238(1)	7581(5)	3621(1)	32(1)
F(1)	8173(1)	8181(3)	-534(1)	36(1)
F(2)	7274(1)	5387(3)	-1306(1)	46(1)
F(3)	5984(1)	6642(3)	-1522(1)	54(1)
F(4)	5602(1)	10751(3)	-945(1)	51(1)
F(5)	6507(1)	13494(3)	-148(1)	40(1)
F(6)	10432(1)	1092(3)	1997(1)	39(1)
F(7)	11306(1)	3749(3)	2817(1)	50(1)
F(8)	12089(1)	7949(3)	2633(1)	46(1)
F(9)	12021(1)	9335(3)	1622(1)	37(1)
F(10)	11146(1)	6721(2)	795(1)	30(1)
F(11)	7936(1)	3148(3)	2835(1)	52(1)
F(12)	8020(1)	1273(3)	3816(1)	73(1)
F(13)	8918(1)	3539(4)	4677(1)	85(1)
F(14)	9722(1)	7802(4)	4551(1)	78(1)
F(15)	9642(1)	9668(3)	3568(1)	53(1)

Table 3. Bond lengths for **1.**

Atoms	Å	Atoms	Å
S(1)-C(1)	1.7484(18)	S(3)-C(18)	1.822(2)
S(1)-C(4)	1.822(2)	N(1)-C(1)	1.328(2)
S(2)-C(2)	1.7474(18)	N(1)-C(2)	1.345(2)
S(2)-C(11)	1.815(2)	N(2)-C(2)	1.321(2)
S(3)-C(3)	1.7420(18)	N(2)-C(3)	1.347(2)

Table 3 Continued.

Atoms	Å	Atoms	Å
N(3)-C(3)	1.328(2)	C(13)-C(14)	1.378(3)
N(3)-C(1)	1.342(2)	C(14)-F(7)	1.336(2)
C(4)-C(5)	1.501(3)	C(14)-C(15)	1.374(3)
C(4)-H(4A)	0.98(2)	C(15)-F(8)	1.339(2)
C(4)-H(4B)	0.89(2)	C(15)-C(16)	1.374(3)
C(5)-C(6)	1.382(3)	C(16)-F(9)	1.337(2)
C(5)-C(10)	1.387(3)	C(16)-C(17)	1.378(3)
C(6)-F(1)	1.346(2)	C(17)-F(10)	1.345(2)
C(6)-C(7)	1.372(3)	C(18)-C(19)	1.502(3)
C(7)-F(2)	1.339(2)	C(18)-H(18A)	0.96(3)
C(7)-C(8)	1.377(3)	C(18)-H(18B)	0.98(3)
C(8)-F(3)	1.333(2)	C(19)-C(24)	1.375(3)
C(8)-C(9)	1.378(3)	C(19)-C(20)	1.380(3)
C(9)-F(4)	1.336(2)	C(20)-F(11)	1.342(2)
C(9)-C(10)	1.375(3)	C(20)-C(21)	1.374(3)
C(10)-F(5)	1.345(2)	C(21)-F(12)	1.340(3)
C(11)-C(12)	1.499(3)	C(21)-C(22)	1.361(4)
C(11)-H(11A)	0.94(2)	C(22)-F(13)	1.336(2)
C(11)-H(11B)	0.96(2)	C(22)-C(23)	1.366(4)
C(12)-C(17)	1.385(3)	C(23)-F(14)	1.328(3)
C(12)-C(13)	1.389(3)	C(23)-C(24)	1.387(3)
C(13)-F(6)	1.342(2)	C(24)-F(15)	1.338(2)

Table 4. Bond angles for **1**.

Atoms	°	Atoms	°
C(1)-S(1)-C(4)	102.78(9)	C(10)-C(5)-C(4)	120.75(18)
C(2)-S(2)-C(11)	102.60(9)	F(1)-C(6)-C(7)	117.35(18)
C(3)-S(3)-C(18)	100.17(9)	F(1)-C(6)-C(5)	120.03(17)
C(1)-N(1)-C(2)	113.21(15)	C(7)-C(6)-C(5)	122.63(18)
C(2)-N(2)-C(3)	113.24(15)	F(2)-C(7)-C(6)	120.55(19)
C(3)-N(3)-C(1)	113.43(15)	F(2)-C(7)-C(8)	119.80(19)
N(1)-C(1)-N(3)	126.58(16)	C(6)-C(7)-C(8)	119.64(19)
N(1)-C(1)-S(1)	120.35(13)	F(3)-C(8)-C(7)	120.1(2)
N(3)-C(1)-S(1)	113.07(13)	F(3)-C(8)-C(9)	120.3(2)
N(2)-C(2)-N(1)	126.97(16)	C(7)-C(8)-C(9)	119.62(19)
N(2)-C(2)-S(2)	120.53(14)	F(4)-C(9)-C(10)	120.3(2)
N(1)-C(2)-S(2)	112.50(13)	F(4)-C(9)-C(8)	120.25(19)
N(3)-C(3)-N(2)	126.53(16)	C(10)-C(9)-C(8)	119.43(19)
N(3)-C(3)-S(3)	120.24(14)	F(5)-C(10)-C(9)	118.97(18)
N(2)-C(3)-S(3)	113.23(13)	F(5)-C(10)-C(5)	118.49(17)
C(5)-C(4)-S(1)	114.87(14)	C(9)-C(10)-C(5)	122.53(19)
C(5)-C(4)-H(4A)	109.9(13)	C(12)-C(11)-S(2)	114.96(14)
S(1)-C(4)-H(4A)	101.0(13)	C(12)-C(11)-H(11A)	111.8(13)
C(5)-C(4)-H(4B)	110.6(14)	S(2)-C(11)-H(11A)	102.0(13)
S(1)-C(4)-H(4B)	107.2(14)	C(12)-C(11)-H(11B)	110.4(13)
H(4A)-C(4)-H(4B)	113(2)	S(2)-C(11)-H(11B)	107.1(13)
C(6)-C(5)-C(10)	116.13(18)	H(11A)-C(11)-H(11B)	110.1(19)
C(6)-C(5)-C(4)	123.08(17)	C(17)-C(12)-C(13)	116.23(17)

Table 4 Continued.

Atoms	°	Atoms	°
C(17)-C(12)-C(11)	121.90(17)	S(3)-C(18)-H(18B)	107.1(15)
C(13)-C(12)-C(11)	121.87(17)	H(18A)-C(18)-H(18B)	109(2)
F(6)-C(13)-C(14)	117.93(17)	C(24)-C(19)-C(20)	116.41(18)
F(6)-C(13)-C(12)	119.96(18)	C(24)-C(19)-C(18)	122.22(19)
C(14)-C(13)-C(12)	122.09(18)	C(20)-C(19)-C(18)	121.36(19)
F(7)-C(14)-C(15)	119.79(19)	F(11)-C(20)-C(21)	118.3(2)
F(7)-C(14)-C(13)	120.6(2)	F(11)-C(20)-C(19)	119.33(18)
C(15)-C(14)-C(13)	119.64(18)	C(21)-C(20)-C(19)	122.4(2)
F(8)-C(15)-C(14)	120.52(18)	F(12)-C(21)-C(22)	120.4(2)
F(8)-C(15)-C(16)	119.32(19)	F(12)-C(21)-C(20)	120.1(2)
C(14)-C(15)-C(16)	120.15(18)	C(22)-C(21)-C(20)	119.5(2)
F(9)-C(16)-C(15)	120.23(17)	F(13)-C(22)-C(21)	119.6(3)
F(9)-C(16)-C(17)	120.68(17)	F(13)-C(22)-C(23)	120.0(3)
C(15)-C(16)-C(17)	119.09(18)	C(21)-C(22)-C(23)	120.4(2)
F(10)-C(17)-C(16)	117.84(17)	F(14)-C(23)-C(22)	120.9(2)
F(10)-C(17)-C(12)	119.40(16)	F(14)-C(23)-C(24)	120.1(3)
C(16)-C(17)-C(12)	122.76(17)	C(22)-C(23)-C(24)	119.0(2)
C(19)-C(18)-S(3)	108.28(14)	F(15)-C(24)-C(19)	119.36(19)
C(19)-C(18)-H(18A)	111.2(16)	F(15)-C(24)-C(23)	118.4(2)
S(3)-C(18)-H(18A)	110.3(16)	C(19)-C(24)-C(23)	122.2(2)
C(19)-C(18)-H(18B)	110.6(15)		

Table 5. Torsion angles for **1**.

Atoms	°	Atoms	°
C(2)-N(1)-C(1)-N(3)	1.7(3)	C(4)-C(5)-C(6)-C(7)	-178.72(18)
C(2)-N(1)-C(1)-S(1)	-178.89(12)	F(1)-C(6)-C(7)-F(2)	2.1(3)
C(3)-N(3)-C(1)-N(1)	-0.9(3)	C(5)-C(6)-C(7)-F(2)	-178.20(17)
C(3)-N(3)-C(1)-S(1)	179.59(13)	F(1)-C(6)-C(7)-C(8)	-178.87(17)
C(4)-S(1)-C(1)-N(1)	-5.24(17)	C(5)-C(6)-C(7)-C(8)	0.8(3)
C(4)-S(1)-C(1)-N(3)	174.29(13)	F(2)-C(7)-C(8)-F(3)	-0.3(3)
C(3)-N(2)-C(2)-N(1)	-1.1(3)	C(6)-C(7)-C(8)-F(3)	-179.33(18)
C(3)-N(2)-C(2)-S(2)	178.17(13)	F(2)-C(7)-C(8)-C(9)	179.42(18)
C(1)-N(1)-C(2)-N(2)	-0.6(3)	C(6)-C(7)-C(8)-C(9)	0.4(3)
C(1)-N(1)-C(2)-S(2)	-179.85(12)	F(3)-C(8)-C(9)-F(4)	-1.0(3)
C(11)-S(2)-C(2)-N(2)	-2.08(17)	C(7)-C(8)-C(9)-F(4)	179.27(19)
C(11)-S(2)-C(2)-N(1)	177.27(13)	F(3)-C(8)-C(9)-C(10)	178.64(18)
C(1)-N(3)-C(3)-N(2)	-1.1(3)	C(7)-C(8)-C(9)-C(10)	-1.1(3)
C(1)-N(3)-C(3)-S(3)	178.40(13)	F(4)-C(9)-C(10)-F(5)	-0.6(3)
C(2)-N(2)-C(3)-N(3)	2.0(3)	C(8)-C(9)-C(10)-F(5)	179.69(18)
C(2)-N(2)-C(3)-S(3)	-177.53(13)	F(4)-C(9)-C(10)-C(5)	-179.74(18)
C(18)-S(3)-C(3)-N(3)	-0.03(18)	C(8)-C(9)-C(10)-C(5)	0.6(3)
C(18)-S(3)-C(3)-N(2)	179.50(15)	C(6)-C(5)-C(10)-F(5)	-178.55(16)
C(1)-S(1)-C(4)-C(5)	97.34(16)	C(4)-C(5)-C(10)-F(5)	-1.0(3)
S(1)-C(4)-C(5)-C(6)	-113.09(18)	C(6)-C(5)-C(10)-C(9)	0.6(3)
S(1)-C(4)-C(5)-C(10)	69.6(2)	C(4)-C(5)-C(10)-C(9)	178.06(18)
C(10)-C(5)-C(6)-F(1)	178.42(16)	C(2)-S(2)-C(11)-C(12)	-63.34(16)
C(4)-C(5)-C(6)-F(1)	1.0(3)	S(2)-C(11)-C(12)-C(17)	-61.9(2)
C(10)-C(5)-C(6)-C(7)	-1.3(3)	S(2)-C(11)-C(12)-C(13)	118.29(18)

Table 5 Continued.

Atoms	°	Atoms	°
C(17)-C(12)-C(13)-F(6)	-177.20(16)	S(3)-C(18)-C(19)-C(20)	-91.0(2)
C(11)-C(12)-C(13)-F(6)	2.7(3)	C(24)-C(19)-C(20)-F(11)	-179.22(17)
C(17)-C(12)-C(13)-C(14)	1.6(3)	C(18)-C(19)-C(20)-F(11)	0.7(3)
C(11)-C(12)-C(13)-C(14)	-178.51(17)	C(24)-C(19)-C(20)-C(21)	0.0(3)
F(6)-C(13)-C(14)-F(7)	-1.0(3)	C(18)-C(19)-C(20)-C(21)	179.91(18)
C(12)-C(13)-C(14)-F(7)	-179.82(17)	F(11)-C(20)-C(21)-F(12)	-0.3(3)
F(6)-C(13)-C(14)-C(15)	178.68(17)	C(19)-C(20)-C(21)-F(12)	-179.53(18)
C(12)-C(13)-C(14)-C(15)	-0.2(3)	F(11)-C(20)-C(21)-C(22)	179.19(19)
F(7)-C(14)-C(15)-F(8)	-1.9(3)	C(19)-C(20)-C(21)-C(22)	-0.1(3)
C(13)-C(14)-C(15)-F(8)	178.49(17)	F(12)-C(21)-C(22)-F(13)	0.1(3)
F(7)-C(14)-C(15)-C(16)	178.32(17)	C(20)-C(21)-C(22)-F(13)	-179.35(19)
C(13)-C(14)-C(15)-C(16)	-1.3(3)	F(12)-C(21)-C(22)-C(23)	179.9(2)
F(8)-C(15)-C(16)-F(9)	1.0(3)	C(20)-C(21)-C(22)-C(23)	0.5(3)
C(14)-C(15)-C(16)-F(9)	-179.18(17)	F(13)-C(22)-C(23)-F(14)	-1.2(3)
F(8)-C(15)-C(16)-C(17)	-178.55(17)	C(21)-C(22)-C(23)-F(14)	179.0(2)
C(14)-C(15)-C(16)-C(17)	1.3(3)	F(13)-C(22)-C(23)-C(24)	179.02(19)
F(9)-C(16)-C(17)-F(10)	0.3(3)	C(21)-C(22)-C(23)-C(24)	-0.8(3)
C(15)-C(16)-C(17)-F(10)	179.86(16)	C(20)-C(19)-C(24)-F(15)	-179.51(17)
F(9)-C(16)-C(17)-C(12)	-179.26(16)	C(18)-C(19)-C(24)-F(15)	0.6(3)
C(15)-C(16)-C(17)-C(12)	0.3(3)	C(20)-C(19)-C(24)-C(23)	-0.4(3)
C(13)-C(12)-C(17)-F(10)	178.73(15)	C(18)-C(19)-C(24)-C(23)	179.74(19)
C(11)-C(12)-C(17)-F(10)	-1.1(3)	F(14)-C(23)-C(24)-F(15)	0.1(3)
C(13)-C(12)-C(17)-C(16)	-1.7(3)	C(22)-C(23)-C(24)-F(15)	179.90(19)
C(11)-C(12)-C(17)-C(16)	178.45(17)	F(14)-C(23)-C(24)-C(19)	-179.03(19)
C(3)-S(3)-C(18)-C(19)	170.96(16)	C(22)-C(23)-C(24)-C(19)	0.8(3)
S(3)-C(18)-C(19)-C(24)	88.9(2)		

Table 6. Anisotropic displacement parameters ($Å^2$ x 10^3) for **1**. The anisotropic displacement factor exponent takes the form: $-2p^2[h^2a^{*2}U^{11} + ... + 2hka^*b^*U^{12}]$.

Atom	U^{11}	U^{22}	U^{33}	U^{23}	U^{13}	U^{12}
S(1)	26(1)	27(1)	25(1)	3(1)	7(1)	4(1)
S(2)	24(1)	33(1)	21(1)	-5(1)	9(1)	-1(1)
S(3)	34(1)	36(1)	22(1)	7(1)	13(1)	12(1)
N(1)	23(1)	26(1)	20(1)	0(1)	7(1)	-2(1)
N(2)	23(1)	28(1)	22(1)	1(1)	8(1)	1(1)
N(3)	26(1)	25(1)	21(1)	2(1)	9(1)	3(1)
C(1)	21(1)	20(1)	24(1)	-1(1)	5(1)	-3(1)
C(2)	22(1)	22(1)	21(1)	-4(1)	7(1)	-5(1)
C(3)	23(1)	26(1)	21(1)	0(1)	7(1)	-2(1)
C(4)	28(1)	27(1)	27(1)	6(1)	6(1)	-2(1)
C(5)	28(1)	24(1)	23(1)	9(1)	7(1)	0(1)
C(6)	31(1)	28(1)	25(1)	10(1)	11(1)	4(1)
C(7)	44(1)	30(1)	25(1)	3(1)	14(1)	-1(1)
C(8)	41(1)	38(1)	26(1)	2(1)	4(1)	-11(1)
C(9)	24(1)	40(1)	38(1)	12(1)	4(1)	-1(1)
C(10)	30(1)	27(1)	30(1)	5(1)	11(1)	2(1)
C(11)	27(1)	24(1)	34(1)	-6(1)	12(1)	0(1)
C(12)	23(1)	22(1)	26(1)	-1(1)	9(1)	5(1)

Table 6 Continued.

Atom	U^{11}	U^{22}	U^{33}	U^{23}	U^{13}	U^{12}
C(13)	31(1)	25(1)	34(1)	7(1)	15(1)	7(1)
C(14)	39(1)	36(1)	23(1)	7(1)	9(1)	14(1)
C(15)	31(1)	33(1)	24(1)	-4(1)	-1(1)	8(1)
C(16)	24(1)	26(1)	32(1)	-1(1)	7(1)	2(1)
C(17)	24(1)	25(1)	23(1)	1(1)	7(1)	5(1)
C(18)	43(1)	39(1)	28(1)	8(1)	20(1)	16(1)
C(19)	28(1)	27(1)	25(1)	4(1)	14(1)	7(1)
C(20)	28(1)	31(1)	40(1)	-1(1)	17(1)	5(1)
C(21)	53(1)	33(1)	64(2)	14(1)	45(1)	12(1)
C(22)	68(2)	51(2)	34(1)	18(1)	33(1)	30(1)
C(23)	47(1)	58(2)	26(1)	-9(1)	3(1)	21(1)
C(24)	29(1)	32(1)	38(1)	-4(1)	13(1)	4(1)
F(1)	33(1)	43(1)	35(1)	8(1)	15(1)	10(1)
F(2)	68(1)	40(1)	34(1)	-6(1)	22(1)	1(1)
F(3)	53(1)	61(1)	41(1)	-7(1)	2(1)	-22(1)
F(4)	24(1)	65(1)	60(1)	7(1)	4(1)	0(1)
F(5)	38(1)	37(1)	47(1)	0(1)	17(1)	9(1)
F(6)	43(1)	33(1)	48(1)	14(1)	22(1)	4(1)
F(7)	68(1)	55(1)	25(1)	13(1)	14(1)	16(1)
F(8)	46(1)	49(1)	30(1)	-8(1)	-7(1)	3(1)
F(9)	30(1)	37(1)	42(1)	-5(1)	8(1)	-10(1)
F(10)	32(1)	36(1)	24(1)	0(1)	11(1)	-4(1)
F(11)	34(1)	49(1)	72(1)	-19(1)	11(1)	-6(1)
F(12)	85(1)	40(1)	130(2)	22(1)	83(1)	7(1)
F(13)	137(2)	90(1)	47(1)	37(1)	59(1)	62(1)
F(14)	73(1)	100(1)	41(1)	-28(1)	-11(1)	28(1)
F(15)	38(1)	43(1)	80(1)	-14(1)	21(1)	-12(1)

Table 7. Hydrogen coordinates (x 10^4) and isotropic displacement parameters ($Å^2$ x 10^3) for **1**.

Atom	X	Y	Z	U(eq)
H(4A)	7750(11)	14540(50)	103(9)	35(6)
H(4B)	8261(11)	12140(50)	121(8)	35(6)
H(11A)	10435(11)	1700(50)	663(8)	32(6)
H(11B)	10008(11)	1030(50)	1032(9)	34(6)
H(18A)	8843(13)	9510(60)	2623(10)	56(8)
H(18B)	8290(13)	7200(60)	2379(10)	50(7)

APPENDIX C

SUPPLEMENTARY INFORMATION FOR CHAPTER III

C.1. General Experimental Details

^{1}H and ^{13}C NMR spectra were obtained on a Varian Mercury 300 MHz spectrometer (^{1}H: 300.09), Inova 500 MHz spectrometer (^{1}H: 500.10 MHz, ^{13}C: 125.75 MHz), or Bruker Avance III HD 600 MHz NMR Spectrometer with Prodigy multinuclear broadband BBO CryoProbe (^{1}H: 600.02 MHz, ^{13}C: 150.89 MHz). Chemical shifts (δ) are expressed in ppm downfield from tetramethylsilane (TMS) using non-deuterated solvent present in the bulk deuterated solvent ($CDCl_3$: ^{1}H 7.26 ppm, ^{13}C 77.16 ppm; d_6-DMSO: ^{1}H 2.50 ppm ^{13}C 39.52 ppm). All NMR spectra were processed using MestReNova NMR processing software. All materials were synthesized following literature procedures or were obtained from TCI-America, Sigma-Aldrich, or Acros and used as received. X-ray crystal data were obtained on a Bruker Apex CCD or a Bruker Apex2 CCD diffractometer. Characterization spectra corresponding to the synthetic procedures of Receptors **1** and **2** and precursors **3** and **4** presented in Chapter III are shown in Figures 1-16.

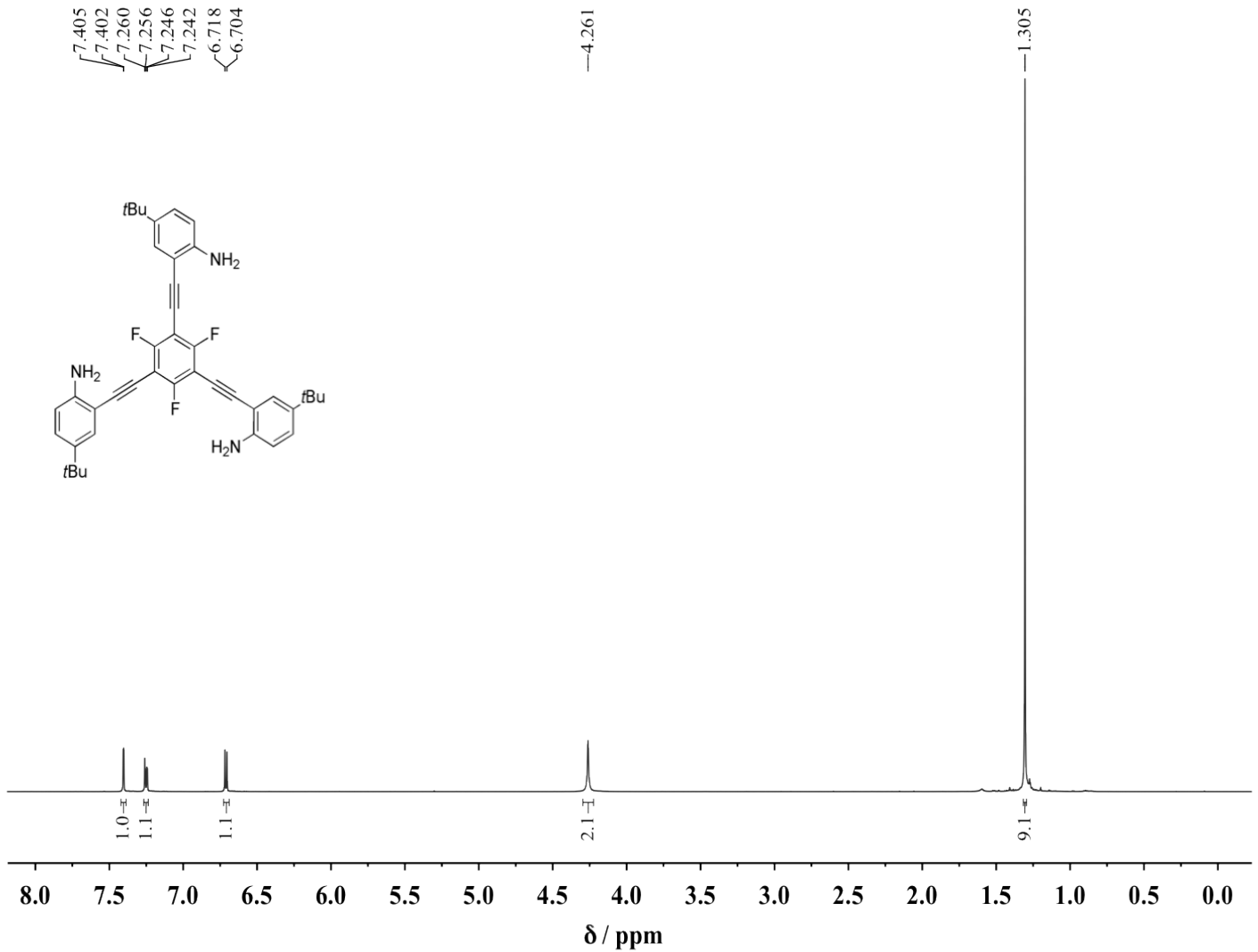

Figure 1. ^{1}H NMR spectrum of **3** in $CDCl_3$, 600 MHz.

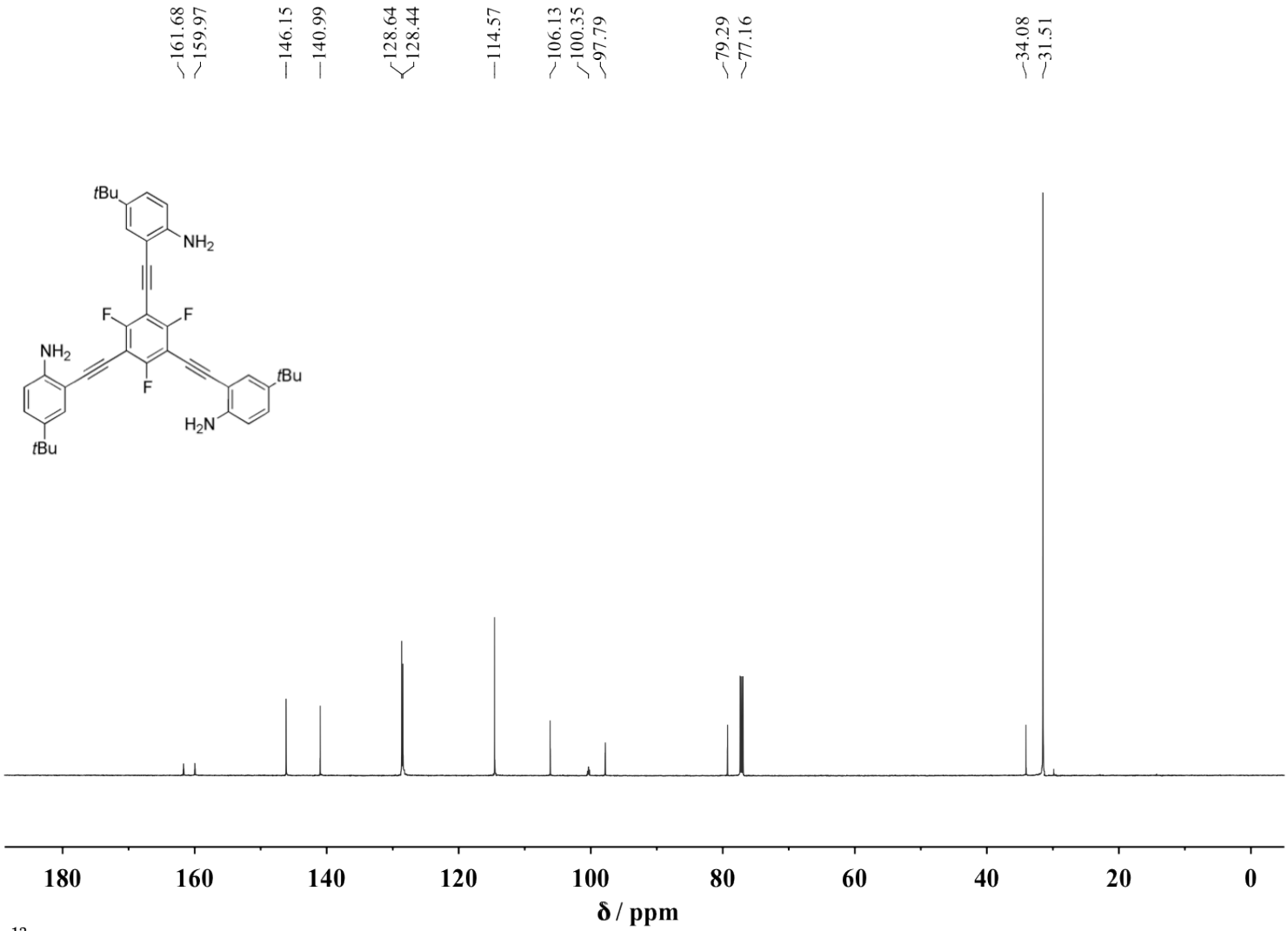

Figure 2. ^{13}C NMR spectrum of **3** in $CDCl_3$, 151 MHz.

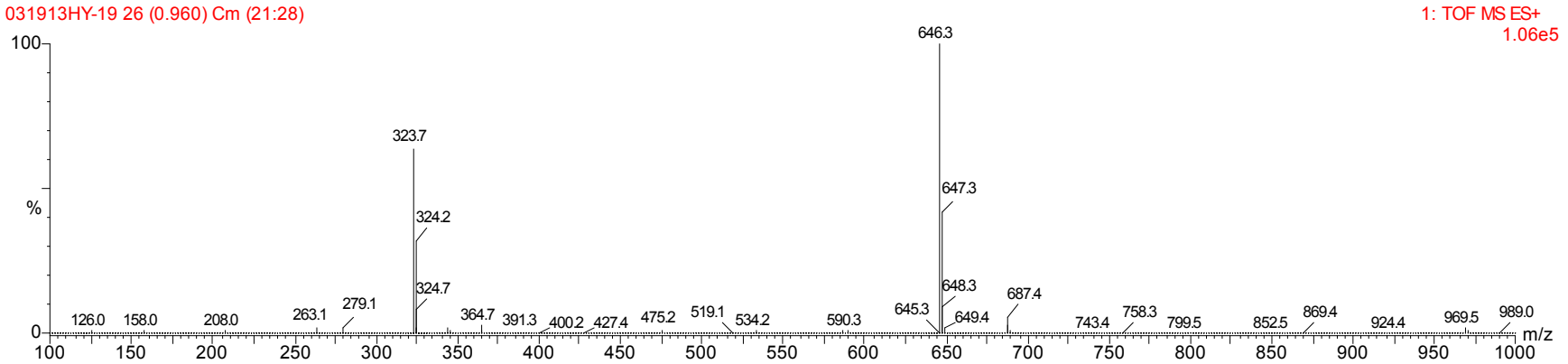

Figure 3. Low resolution ESI mass spectrum of **3.**

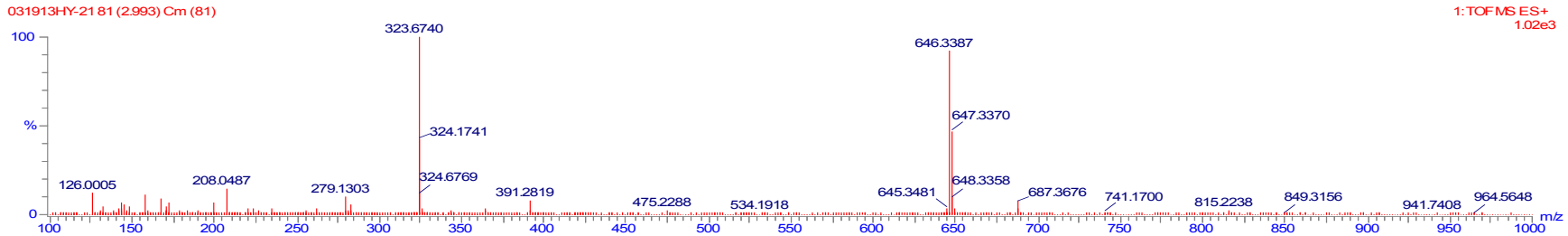

Figure 4. High resolution ESI mass spectrum of **3.**

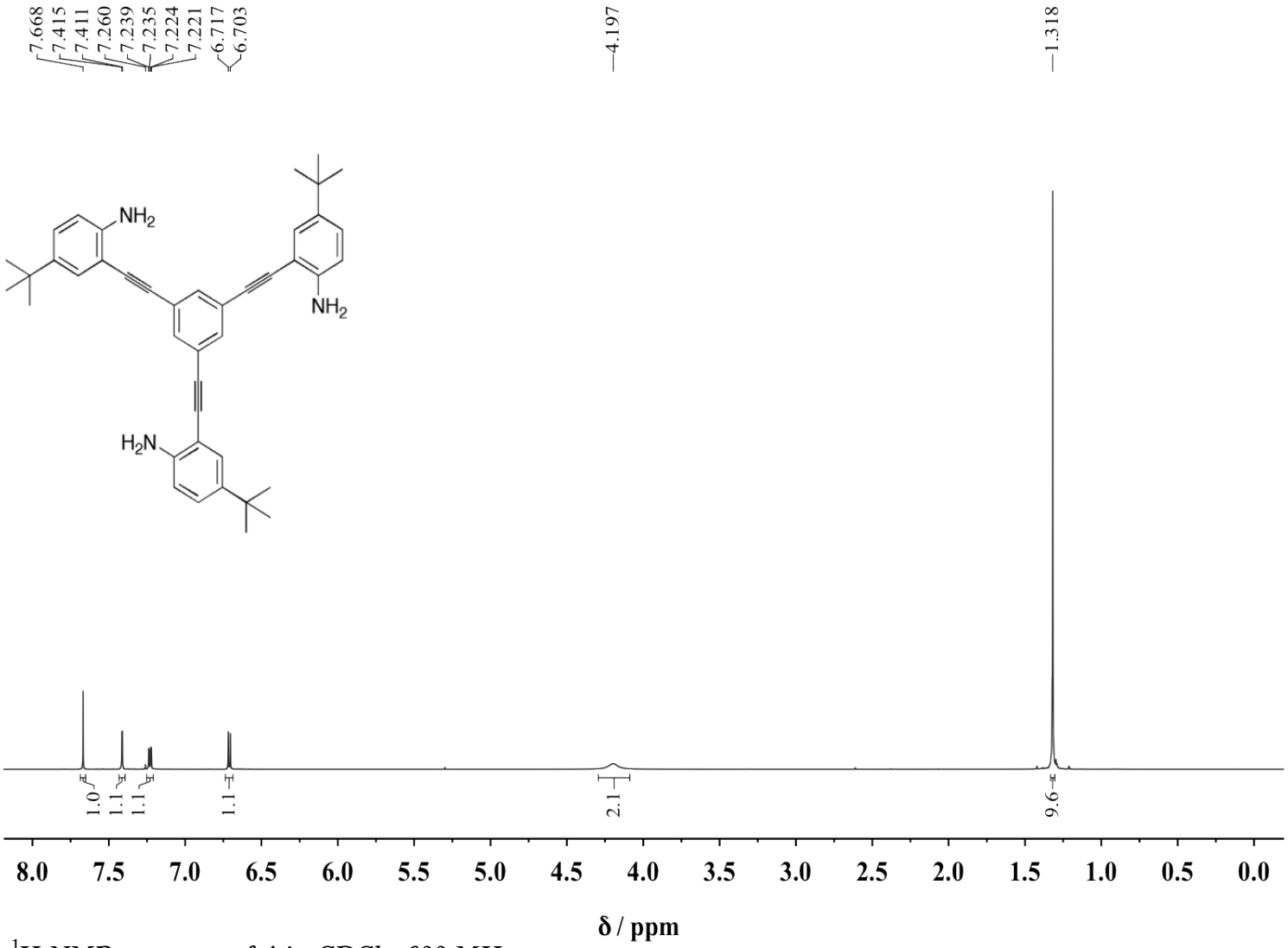

Figure 5. ^{1}H NMR spectrum of **4** in $CDCl_3$, 600 MHz.

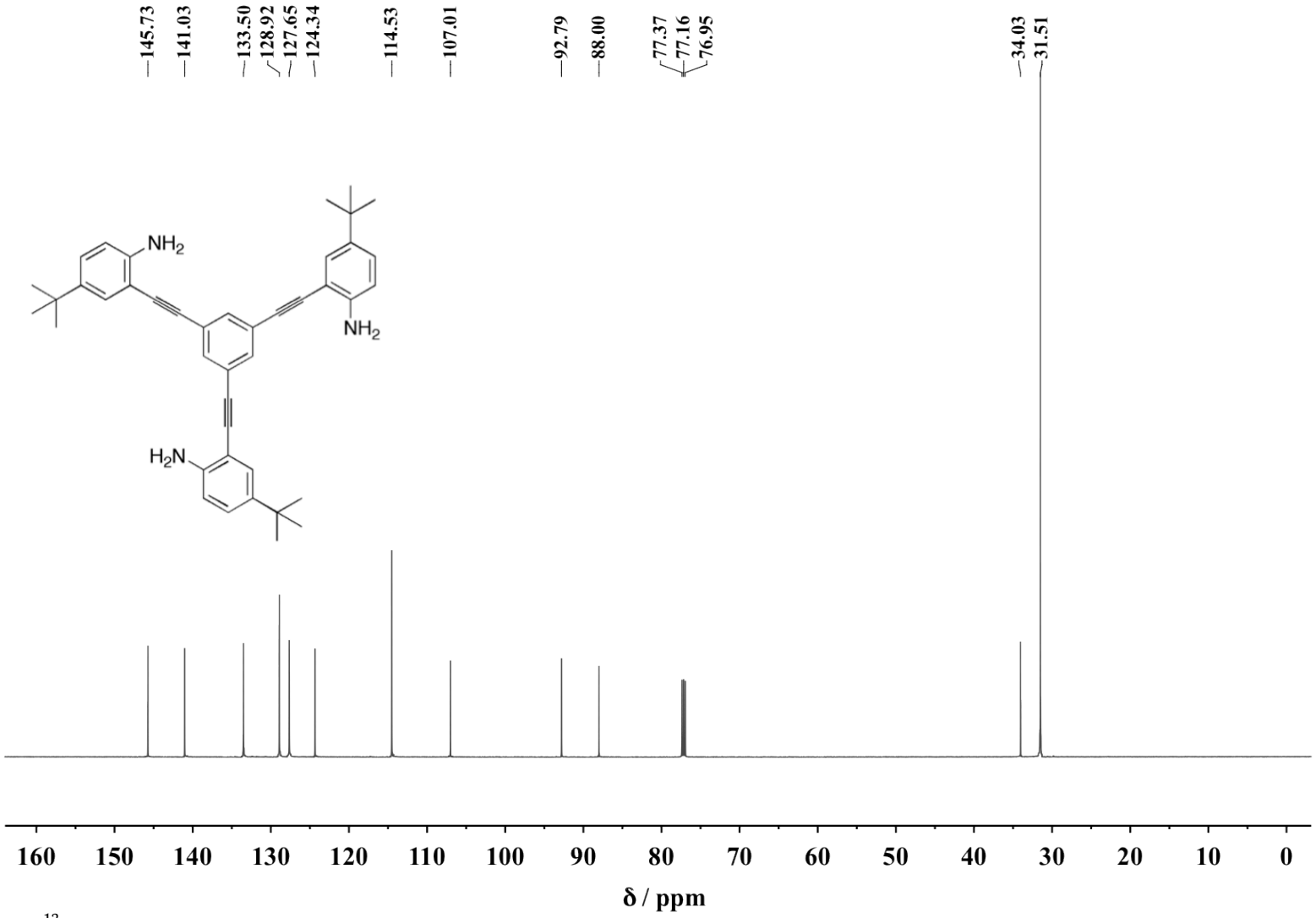

Figure 6. ^{13}C NMR spectrum of **4** in $CDCl_3$, 151 MHz.

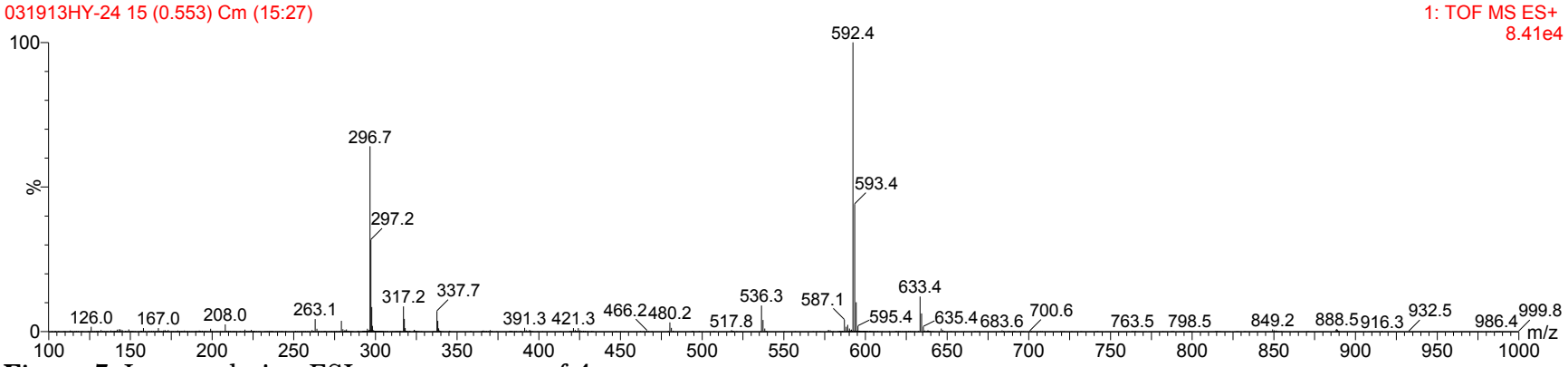

Figure 7. Low resolution ESI mass spectrum of **4.**

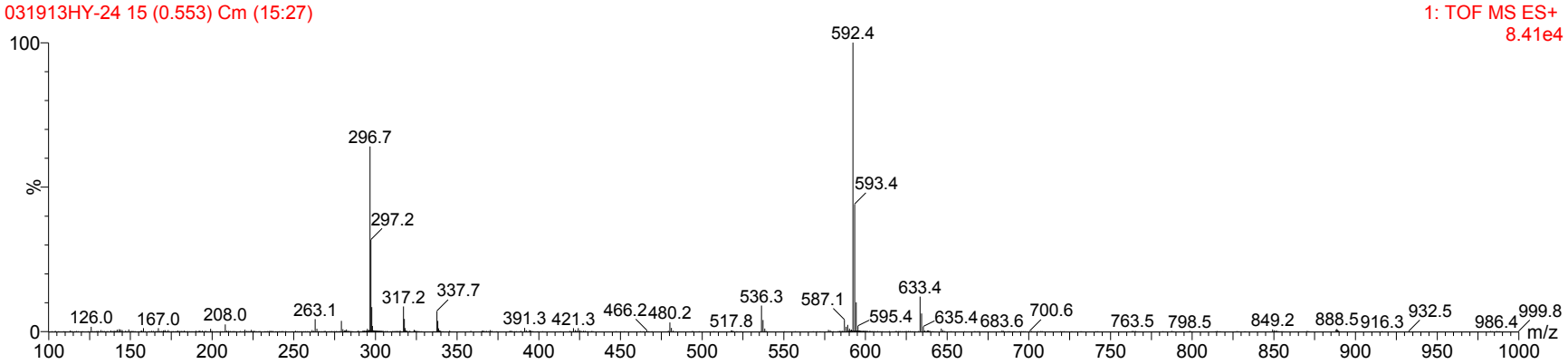

Figure 8. High resolution ESI mass spectrum of **4.**

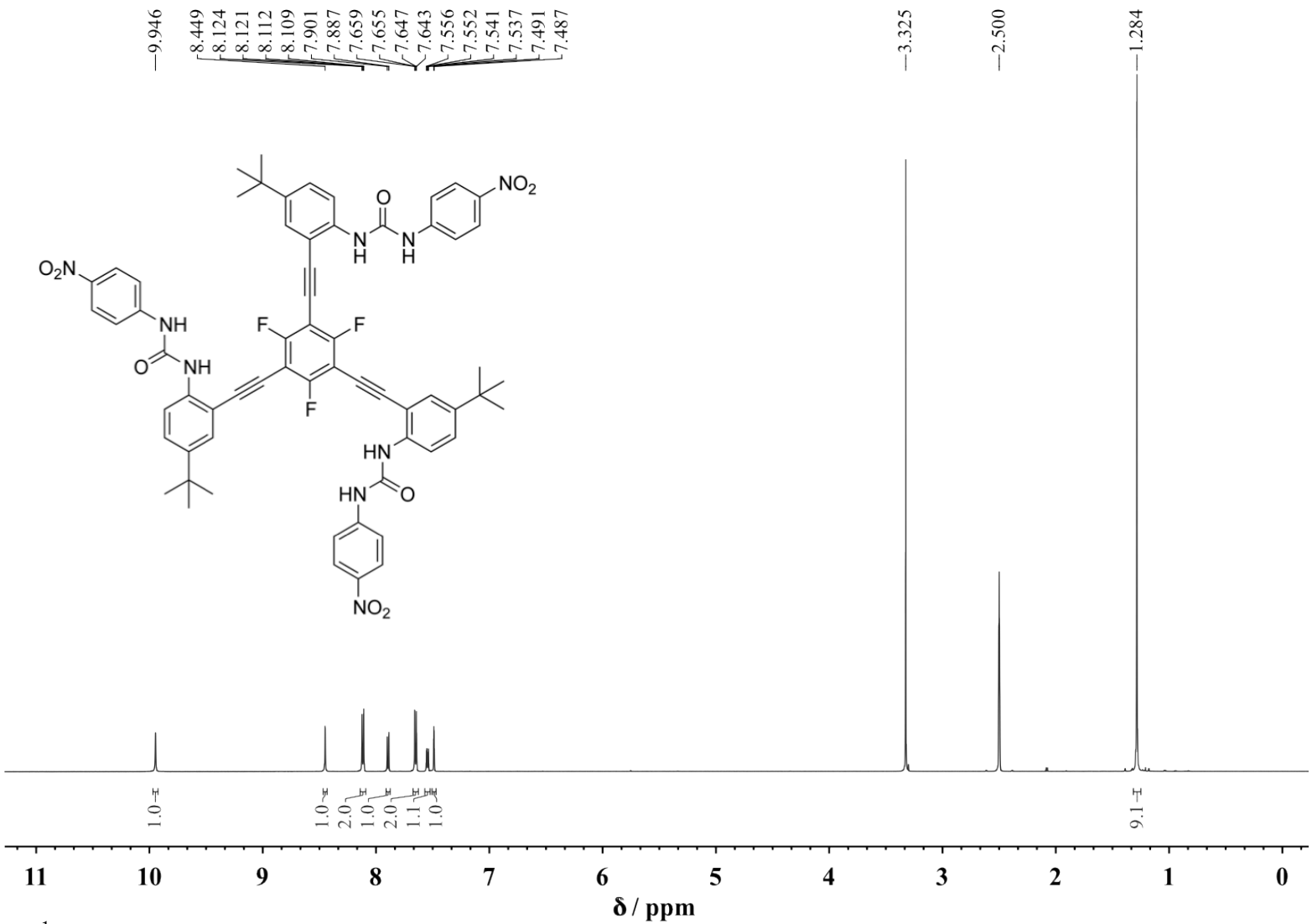

Figure 9. ^{1}H NMR spectrum of **1** in d_6-DMSO, 600 MHz.

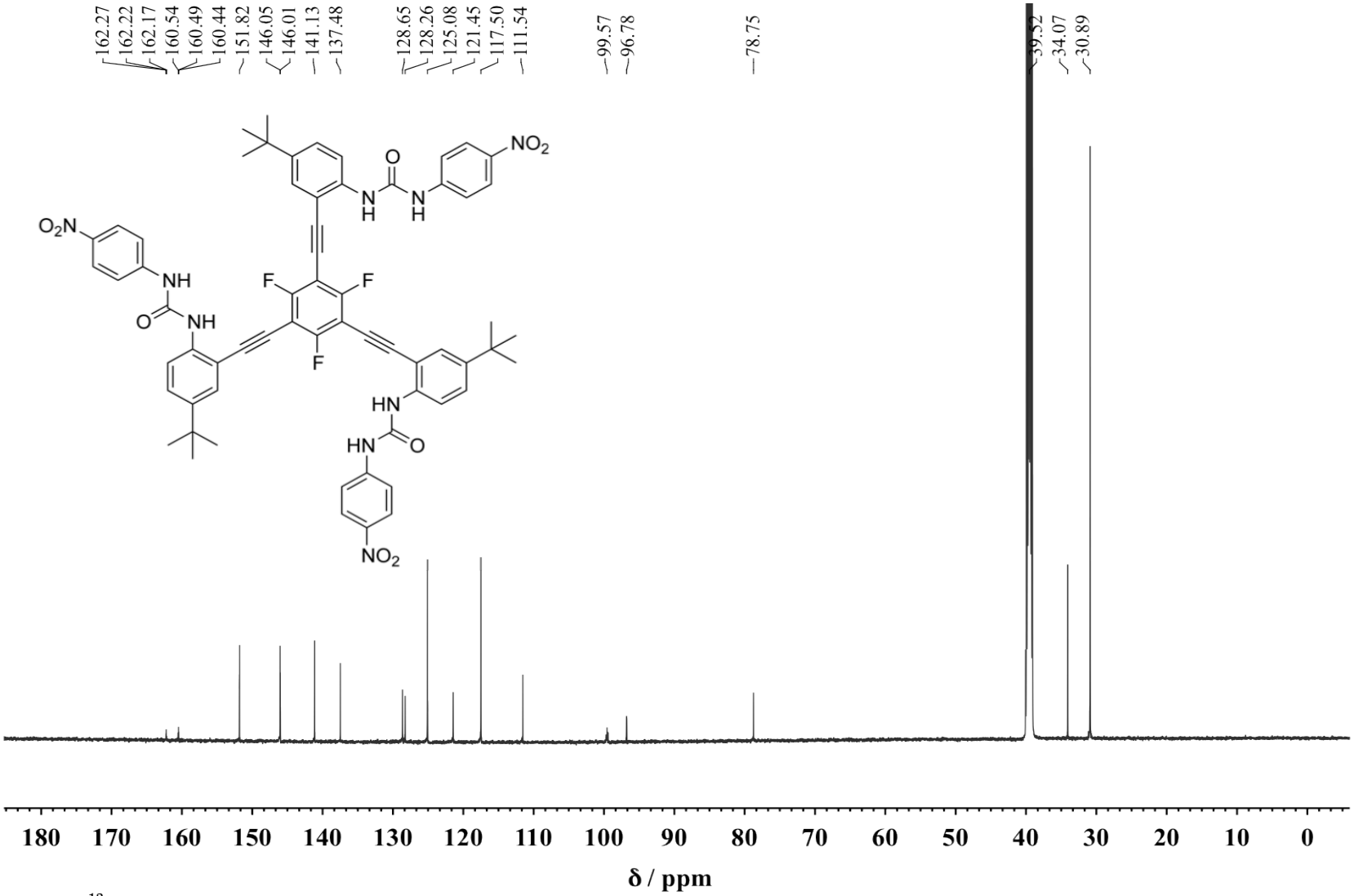

Figure 10. ^{13}C NMR spectrum of **1** in d_6-DMSO, 151 MHz.

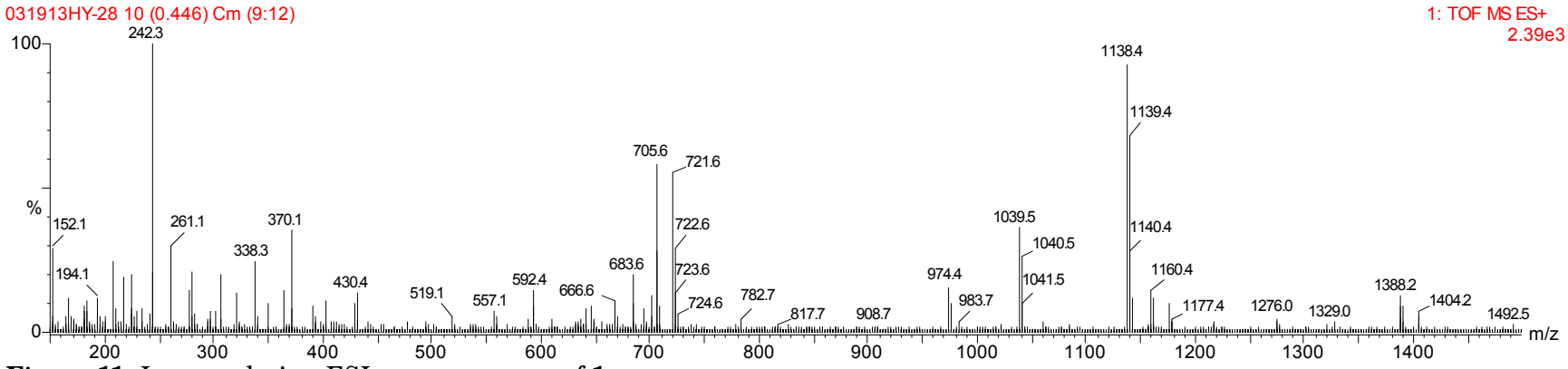

Figure 11. Low resolution ESI mass spectrum of **1.**

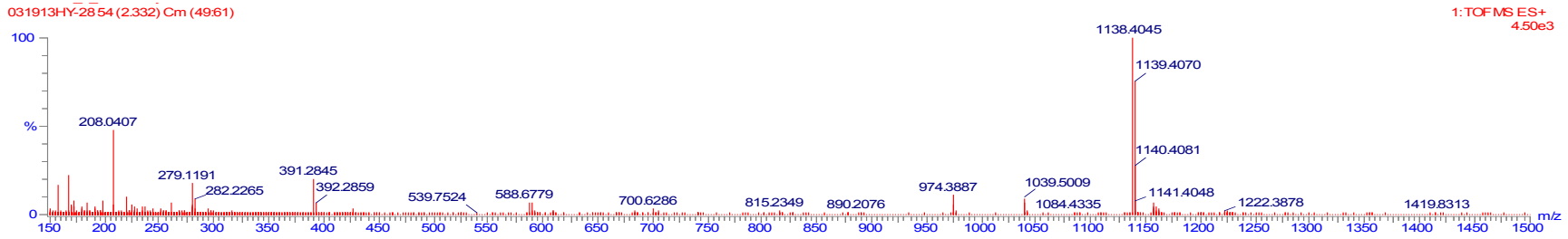

Figure 12. High resolution ESI mass spectrum of **1.**

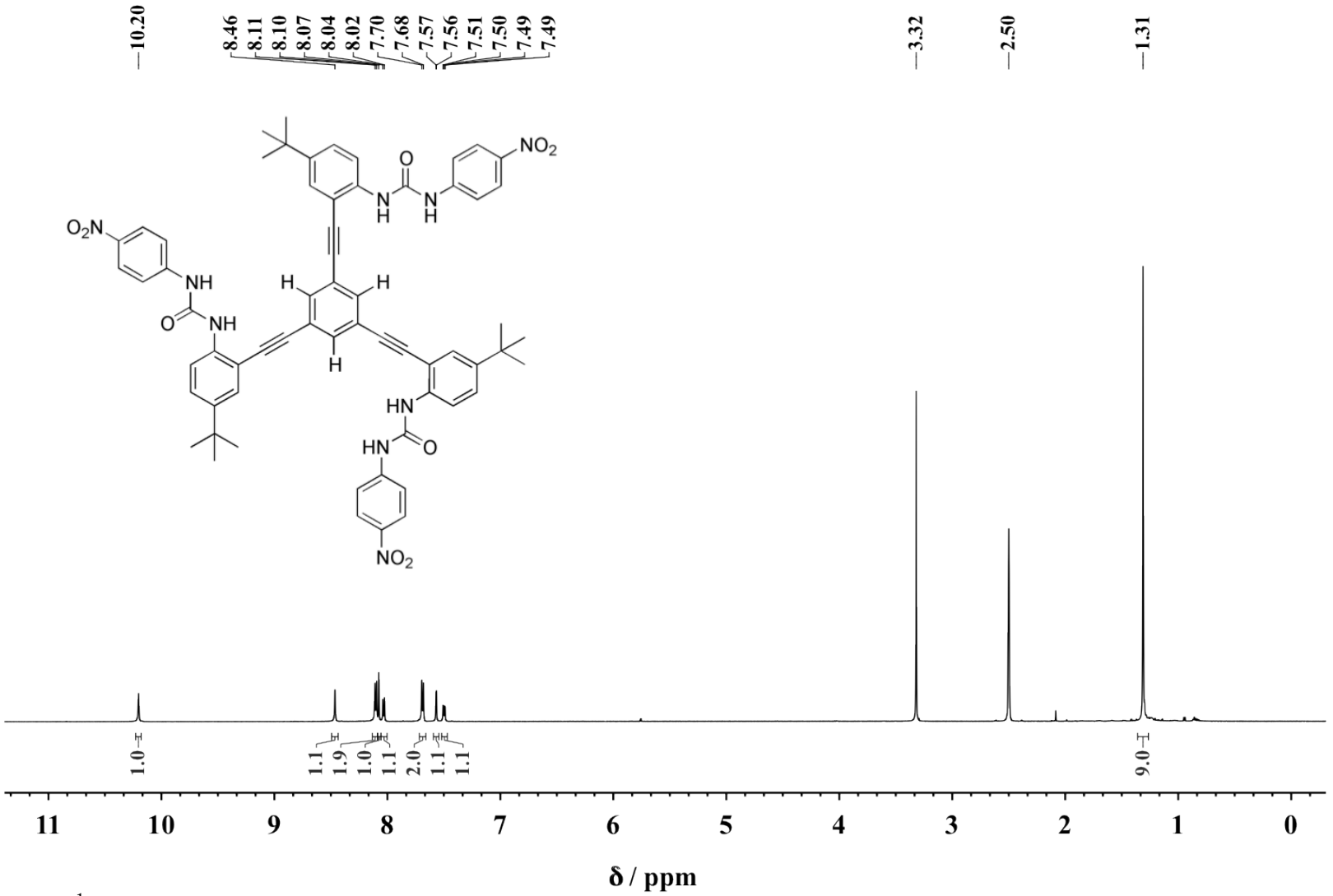

Figure 13. ^{1}H NMR spectrum of **2** in d_6-DMSO, 600 MHz.

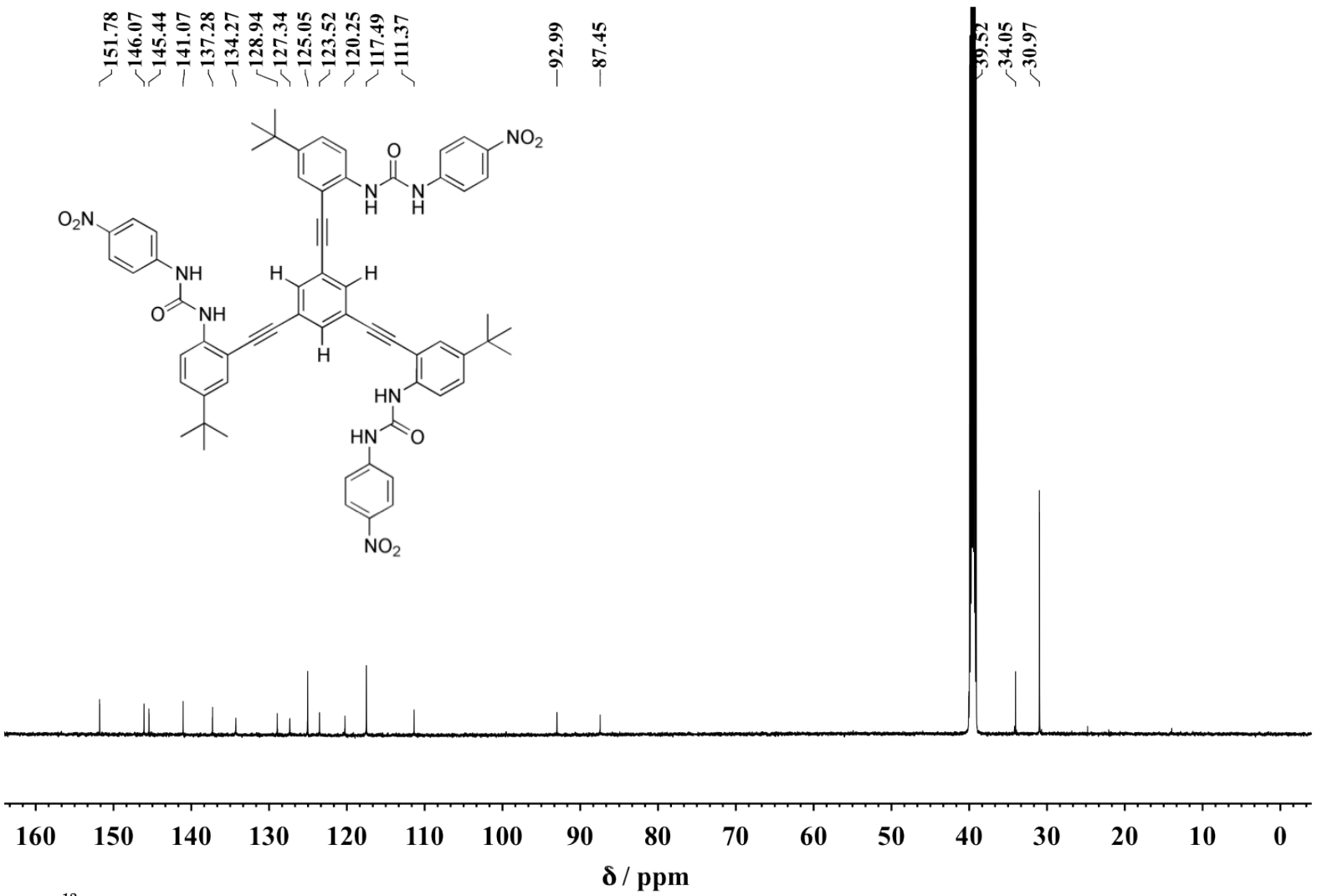

Figure 14. ^{13}C NMR spectrum of **2** in d_6-DMSO, 151 MHz.

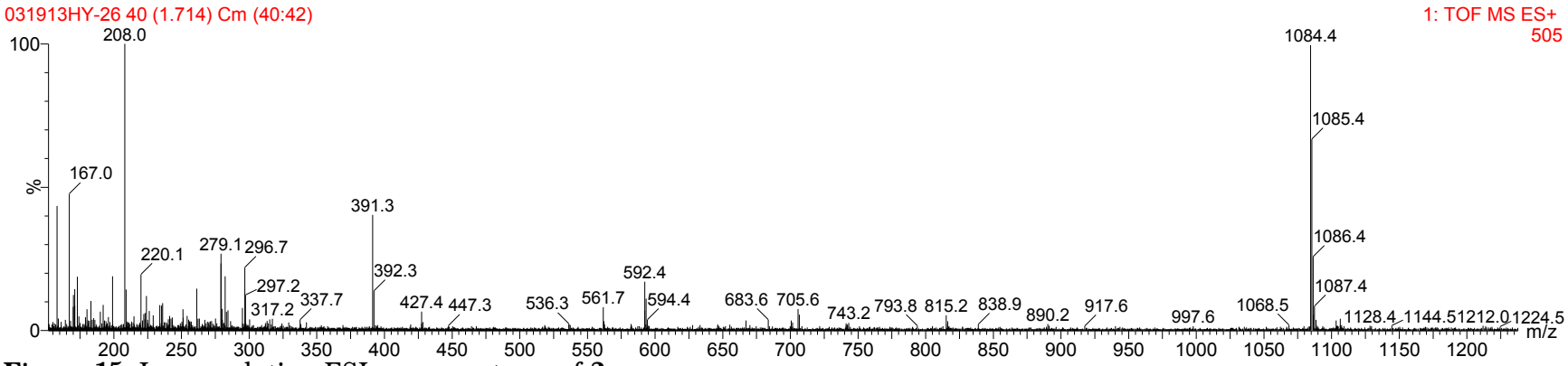

Figure 15. Low resolution ESI mass spectrum of **2.**

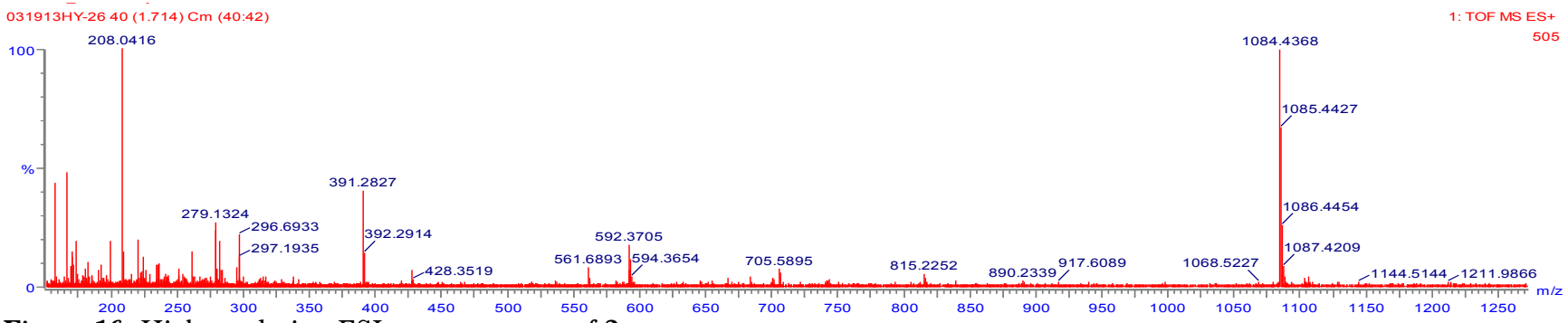

Figure 16. High resolution ESI mass spectrum of **2.**

C.2. X-ray Crystallography

Diffraction intensities were collected at 173(2) K (**1**), 193(2) K (**1**•TBACl) and 100(2) K (**1**•$TBANO_3$) on a Bruker Apex CCD diffractometer using MoK radiation = 0.71073 Å (**1**, **1**•TBACl) and Bruker Apex2 CCD diffractometer using CuK radiation = 1.54178 Å (**1**•$TBANO_3$). Space groups were determined based on systematic absences (**1**•TBACl and **1**•$TBANO_3$) and intensity statistics (**1**). Absorption corrections were applied by SADABS.[1] Structure was solved by direct methods and Fourier techniques and refined on F^2 using full matrix least-squares procedures. All non-H atoms were refined with anisotropic thermal parameters. Some of the terminal $-CH_2-CH_2-CH_3$ groups in NBu_4^+ in **1**•TBACl and **1**•$TBANO_3$ are disordered over two positions. These disordred groups were refined with restrictions; the standard C–C bond distances were used in the refinement as the targets for corresponding bond distances. All H atoms in **1**•TBACl, **1**•$TBANO_3$, and H atoms in solvent acetone molecules in **1** were refined in calculated positions in a rigid group model. Other H atoms in **1** were found from the residual density map and refined with isotropic thermal parameters. All calculations were performed by the Bruker SHELXTL (v. 6.10) package.[2]

X-ray data for 1: $C_{75}H_{78}F_3N_9O_{13}$, M = 1370.46, 0.26 x 0.26 x 0.06 mm, triclinic, space group $P\bar{1}$, (N 2), a = 13.1669(6) Å, b = 16.5153(7) Å, c = 18.4829(8) Å, α = 64.727(1)°, β = 77.710(1)°, γ = 81.612(1)°, V = 3544.3(3) $Å^3$, Z = 2, D_c = 1.284 Mg/m^3, μ = 0.094 mm^{-1}, $F(000)$ = 1444, $2\Theta_{max}$ = 50.00°, T = 173 K, 34533 reflections, 12473 independent reflections [R_{int} = 0.0327], $R1$ = 0.0809, w$R2$ = 0.1694 and GOF = 1.144 for 12473 reflections (1117 parameters) with $I>2\sigma(I)$, $R1$ = 0.0930, w$R2$ = 0.1758 and GOF = 1.144 for all reflections, max/min residual electron density +0.301/–0.335 $eÅ^3$. CCDC 928631 contains the supplementary crystallographic data for these compounds. These data can be obtained free of charge from The Cambridge Crystallographic Data Centre via www.ccdc.cam.ac.uk/data_request/cif.

X-ray data for 1•TBACl: $C_{85}H_{102}ClF_3N_{10}O_{11}$, M = 1532.22, 0.26 x 0.17 x 0.05 mm, orthorhombic, space group $P2_12_12_1$ (N 19), a = 11.850(1) Å, b = 21.883(2) Å, c = 31.984(3) Å, V = 8294(1) Å^3, Z = 4, D_c = 1.227 Mg/m^3, μ = 0.117 mm^{-1}, F(000) = 3256, $2\Theta_{max}$ = 50.00°, T = 193 K, 58785 reflections, 14595 independent reflections [R_{int} = 0.0716], $R1$ = 0.0579, w$R2$ = 0.1261 and GOF = 1.021 for 14595 reflections (1001 parameters) with $I>2\sigma(I)$, $R1$ = 0.1054, w$R2$ = 0.1529 and GOF = 1.023 for all reflections, the Flack = 0.01(8), max/min residual electron density +0.289/–0.269 eÅ^3. CCDC 928629 contains the supplementary crystallographic data for these compounds. These data can be obtained free of charge from The Cambridge Crystallographic Data Centre via www.ccdc.cam.ac.uk/data_request/cif.

X-ray data for 1•TBANO$_3$: $C_{82}H_{96}F_3N_{11}O_{13}$, M = 1500.70, 0.42 x 0.27 x 0.18 mm, orthorhombic, space group $P2_12_12_1$ (N 19), a = 11.1237(3) Å, b = 21.7241(5) Å, c = 32.5573(8) Å, V = 7867.5(3) Å^3, Z = 4, D_c = 1.267 Mg/m^3, μ = 0.752 mm^{-1}, F(000) = 3184, $2\Theta_{max}$ = 130.00°, T = 100 K, 41890 reflections, 10960 independent reflections [R_{int} = 0.0502], $R1$ = 0.0723, w$R2$ = 0.1952 and GOF = 1.045 for 10960 reflections (942 parameters) with $I>2\sigma(I)$, $R1$ = 0.0859, w$R2$ = 0.2106 and GOF = 1.049 for all reflections, the Flack = 0.1(2), max/min residual electron density +0.563/–0.498 eÅ^3. CCDC 928630 contains the supplementary crystallographic data for these compounds. These data can be obtained free of charge from The Cambridge Crystallographic Data Centre via www.ccdc.cam.ac.uk/data_request/cif.

C.3. Titration Details

Tetrabutylammonium salts were dried at 50 °C under vacuum and stored in a calcium carbonate filled dessicator. In all titrations the receptor concentration was kept constant during the titration. A stock solution of receptor was prepared and the host-guest solution was prepared with the stock receptor solution. All additions were

performed with a Hamilton μL syringe. Titrations were carried out in triplicate and the reported binding constants represent the average of the fits from three titrations. Association constants (K_a) were calculated by nonlinear curve fitting of the obtained titration isotherms using Thordarson fitting programs via Matlab. Representative data are provided for each set.

C.3.1. NMR Titration Conditions

^{1}H NMR titrations in 10 % DMSO-d_6/$CDCl_3$ were carried out on an Inova 500 MHz spectrometer (^{1}H 500.10 MHz) at 298 K. ^{1}H NMR titrations in acetone-d_6 were carried out on an Agilent VNMRS 600 spectrometer (^{1}H: 600.02 MHz, ^{13}C: 150.89 MHz) at 298 K. Chemical shifts (δ) are expressed in ppm downfield from tetramethylsilane (TMS) using non-deuterated solvent present in the bulk deuterated solvent (Acetone-d_6: ^{1}H 2.05 ppm; $CDCl_3$: ^{1}H 7.26 ppm).

Table 1. Example titration for the addition of tetrabutylammonium chloride to **1** in d_6-acetone.

Addition (μL)	Total Volume Anion (μL)	[TBACl] (M)	Equiv. Cl^-	$\delta(H^a)$ (ppm)	$\delta(H^b)$ (ppm)	$\delta(H^c)$ (ppm)	$\delta(H^d)$ (ppm)
0	0	0.000E+00	0	8.084	9.191	8.102	7.726
5	5	9.212E-05	0.187	8.198	9.588	8.062	7.749
5	10	1.824E-04	0.369	8.284	9.970	8.032	7.789
5	15	2.710E-04	0.549	8.359	10.352	8.012	7.846
5	20	3.578E-04	0.725	8.422	10.704	8.000	7.913
5	25	4.430E-04	0.897	8.493	10.925	7.998	7.937
5	30	5.266E-04	1.067	8.564	11.083	7.996	7.949
5	35	6.087E-04	1.233	8.626	11.229	7.995	7.958
10	45	7.682E-04	1.556	8.724	11.442	7.993	7.973
10	55	9.220E-04	1.867	8.794	11.592	7.993	7.982
10	65	1.070E-03	2.168	8.840	11.690	7.993	7.990
20	85	1.352E-03	2.738	8.895	11.804	7.994	7.994
20	105	1.615E-03	3.270	8.925	11.862	7.996	7.996
20	125	1.861E-03	3.768	8.949	11.902	7.997	7.997

C.3.2. NMR Titrations of 1 in Acetone-d_6

Tetrabutylammonium chloride. A 5 mL stock solution of **1** (2.81 mg, [R] = 0.49 mM) in acetone-d_6 was prepared and used in the preparation of a 3.5 mL TBACl guest solution (9.05 mg, [G] = 9.30 mM). Starting volume of 500 µL. (Table 1, Figures 17 and 18)

Tetrabutylammonium bromide and nitrate. Titrations were as listed with tetrabutylammonium chloride, but the data could not be fit in a reliable fashion. A comparison was performed for the change in chemical shift of the urea protons in **1** for the titration of chloride, bromide and nitrate. (Figure 19)

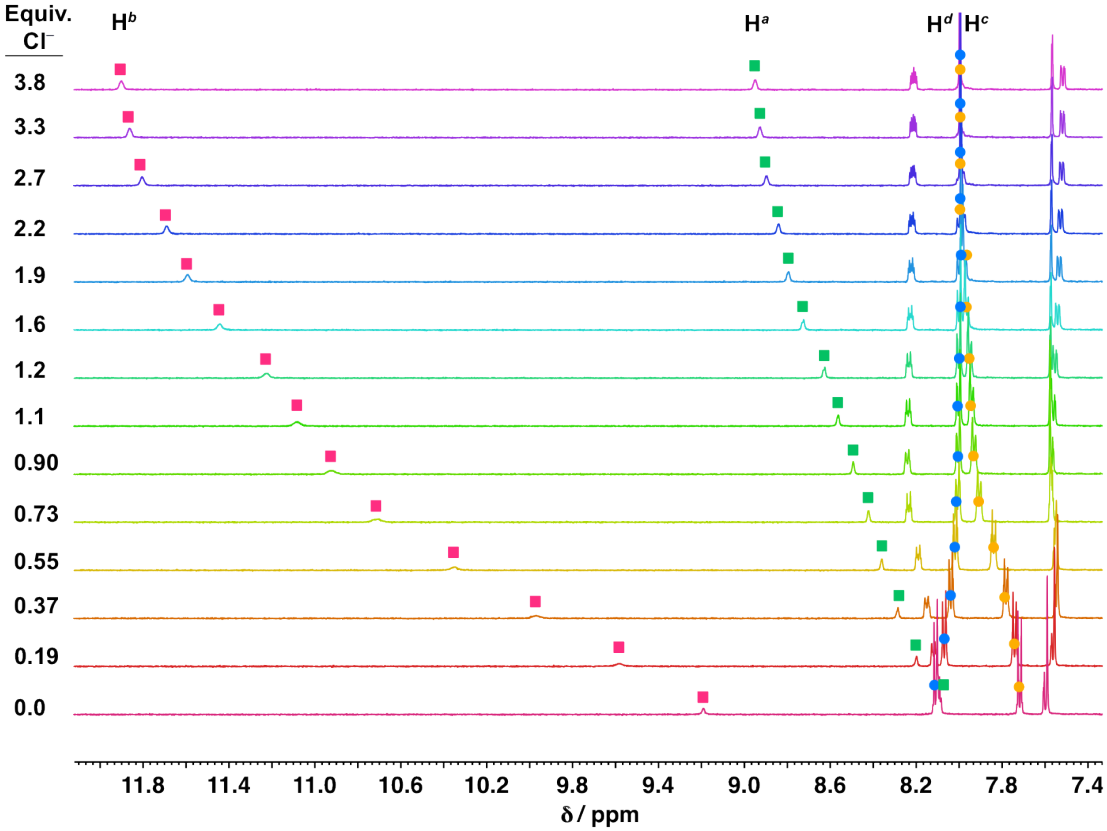

Figure 17. Example stacked spectra from the titration for the addition of tetrabutylammonium chloride to **1** in d_6-acetone.

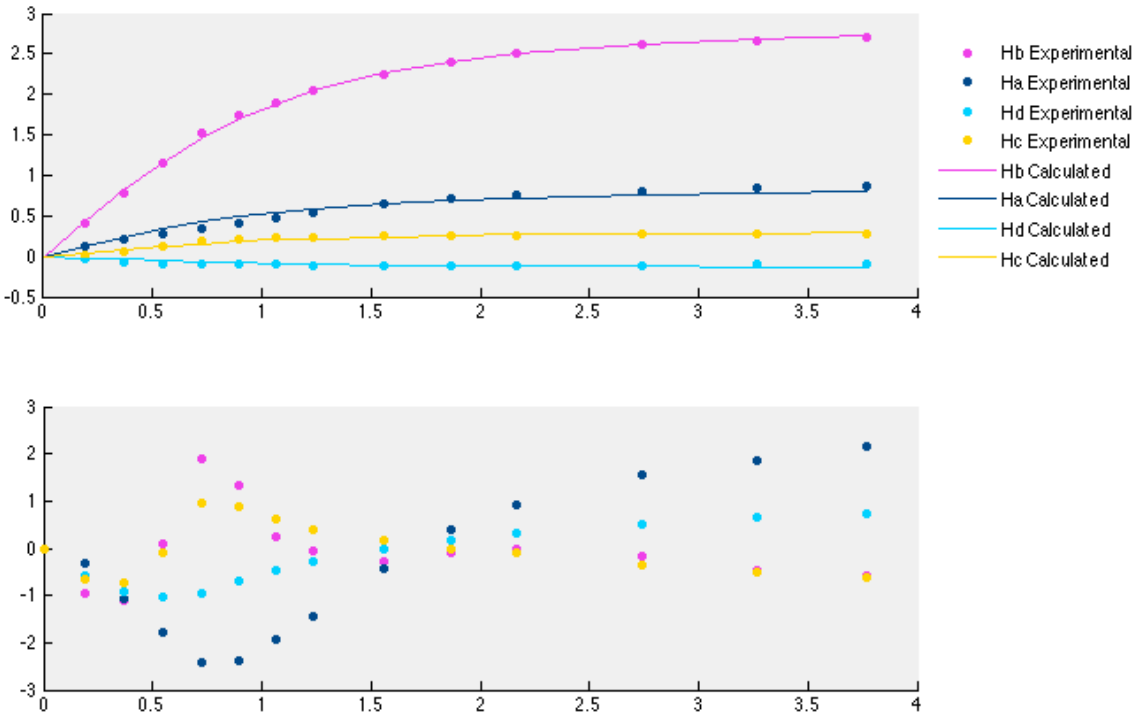

Figure 18. Example 1:1 fitting using non-linear regression from the data obtained for the titration of tetrabutylammonium chloride into **1** in d_6-acetone.

C.3.3. NMR Titrations of 1 in 2 % DMSO-d_6/$CDCl_3$

Tetrabutylammonium nitrate. A 3 mL stock solution of **1** (3.42 mg, [R] = 1.00 mM) in 2 % DMSO-d_6/$CDCl_3$ was prepared and used in the preparation of a 2.5 mL $TBANO_3$ guest solution (10.35 mg, [G] = 13.6 mM). Starting volume of 500 µL.

C.3.4. NMR Titrations of 1 in 5 % DMSO-d_6/$CDCl_3$

Tetrabutylammonium nitrate. A 3 mL stock solution of **1** (3.42 mg, [R] = 1.00 mM) in 5 % DMSO-d_6/$CDCl_3$ was prepared and used in the preparation of a 2.5 mL $TBANO_3$ guest solution (4.87 mg, [G] = 6.40 mM). Starting volume of 500 µL.

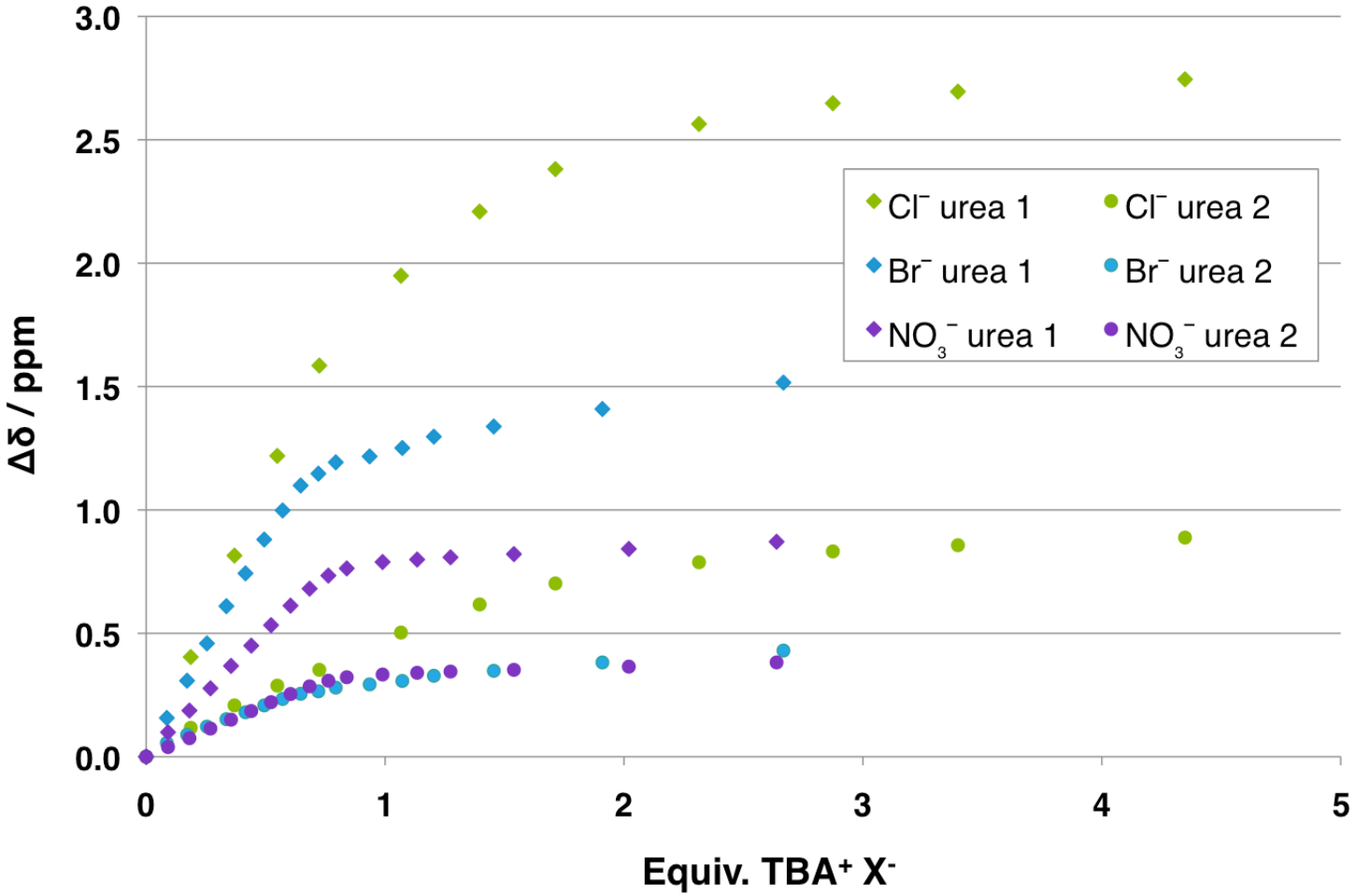

Figure 19. Comparison of the change in chemical shifts for the titration of tetrabutylammonium chloride, bromide, and nitrate into **1** in d_6-acetone.

C.3.5. NMR Titrations of 1 in 10 % DMSO-d_6/$CDCl_3$

Tetrabutylammonium nitrate. A 3 mL stock solution of **1** (3.34 mg, [R] = 0.98 mM) in 10 % DMSO-d_6/$CDCl_3$ was prepared and used in the preparation of a 2 mL $TBANO_3$ guest solution (4.36 mg, [G] = 6.23 mM). Starting volume of 500 µL. (Table 2, Figure 20)

Tetrabutylammonium chloride. A 3 mL stock solution of **1** (3.51 mg, [R] = 1.03 mM) in 10 % DMSO-d_6/$CDCl_3$ was prepared and used in the preparation of a 2 mL TBACl guest solution (2.72 mg, [G] = 4.89 mM). Starting volume of 500 µL. (Table 3, Figures 21 and 22)

Tetrabutylammonium bromide. A 3 mL stock solution of **1** (3.59 mg, [R] = 1.05 mM) in 10 % DMSO-d_6/$CDCl_3$ was prepared and used in the preparation of a 2 mL TBABr guest solution (3.47 mg, [G] = 5.38 mM). Starting volume of 500 µL. (Table 4, Figures 23 and 24)

Table 2. Example titration for the addition of tetrabutylammonium nitrate to **1** in 10 % d_6-DMSO/$CDCl_3$.

Addition (µL)	Total Volume Anion (µL)	[$TBANO_3$] (M)	Equiv. NO_3^-	$\delta(H^a)$ (ppm)	$\delta(H^b)$ (ppm)	$\delta(H^c)$ (ppm)	$\delta(H^d)$ (ppm)
0	0	0.000E+00	0	7.878	9.365	7.433	7.889
10	10	1.221E-04	0.125	7.915	9.417	7.447	7.872
10	20	2.395E-04	0.245	7.950	9.468	7.460	7.856
10	30	3.524E-04	0.360	7.982	9.517	7.474	7.843
15	45	5.141E-04	0.526	8.022	9.578	7.491	7.828
15	60	6.671E-04	0.682	8.053	9.625	7.504	7.818
15	75	8.121E-04	0.830	8.074	9.659	7.513	7.810
20	95	9.941E-04	1.016	8.092	9.686	7.521	7.805
20	115	1.164E-03	1.190	8.103	9.704	7.525	7.801
30	145	1.400E-03	1.431	8.113	9.718	7.529	7.798
50	195	1.747E-03	1.786	8.121	9.732	7.532	7.795
100	295	2.310E-03	2.362	8.128	9.743	7.535	7.794
200	495	3.097E-03	3.166	8.135	9.753	7.538	7.792

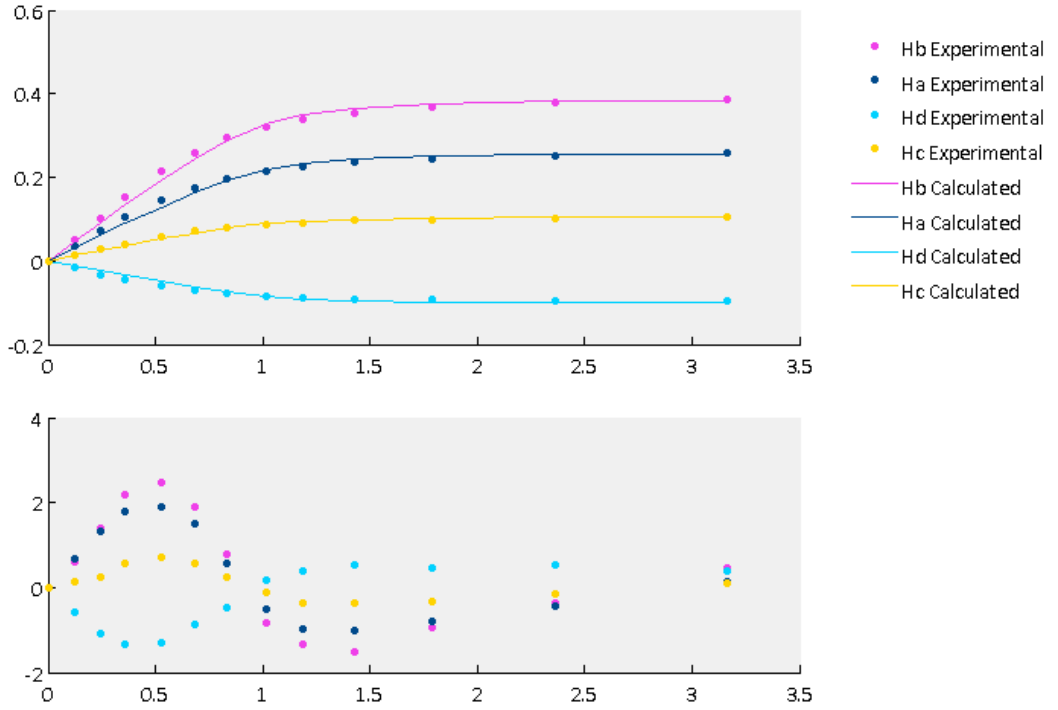

Figure 20. Example 1:1 fitting using non-linear regression from the data obtained for the titration of tetrabutylammonium nitrate into **1** in 10 % d_6-DMSO/$CDCl_3$.

Table 3. Example titration for the addition of tetrabutylammonium chloride to **1** in 10 % d_6-DMSO/$CDCl_3$.

Addition (µL)	Total Volume Anion (µL)	[TBACl] (M)	Equiv. Cl^-	$\delta(H^a)$ (ppm)	$\delta(H^b)$ (ppm)	$\delta(H^c)$ (ppm)	$\delta(H^d)$ (ppm)
0	0	0.000E+00	0	7.884	9.378	7.437	7.888
25	25	2.330E-04	0.227	7.925	9.553	7.466	7.859
25	50	4.449E-04	0.433	7.966	9.732	7.496	7.831
25	75	6.383E-04	0.621	8.001	9.897	7.525	7.808
25	100	8.156E-04	0.793	8.027	10.030	7.549	7.791
40	140	1.070E-03	1.041	8.053	10.164	7.574	7.775
50	190	1.347E-03	1.311	8.068	10.242	7.589	7.766
75	265	1.695E-03	1.649	8.077	10.289	7.596	7.760
100	365	2.065E-03	2.009	8.084	10.315	7.600	7.756
200	565	2.596E-03	2.525	8.089	10.336	7.601	7.753
300	865	3.101E-03	3.017	8.092	10.340	7.601	7.751

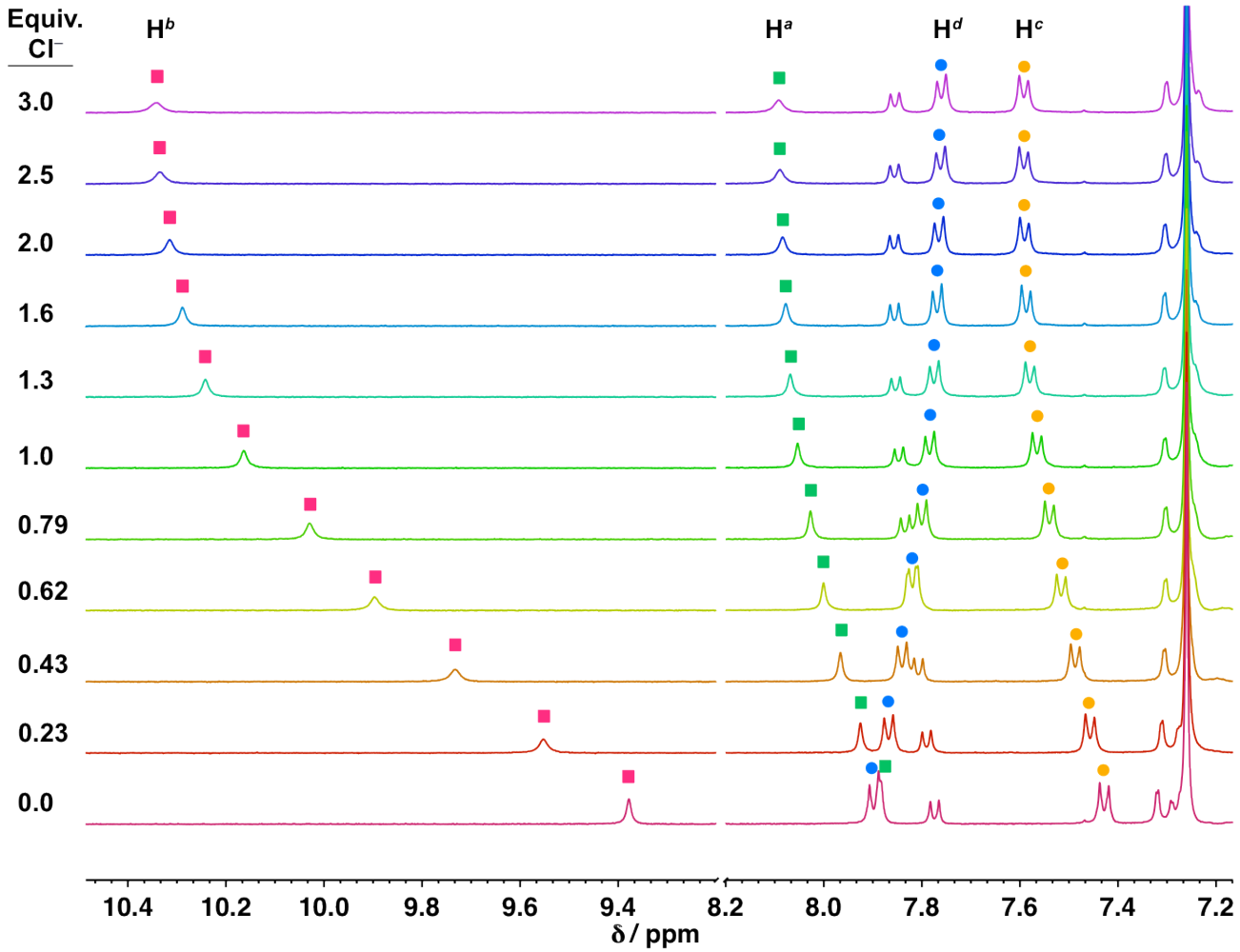

Figure 21. Example stacked spectra from the titration for the addition of tetrabutylammonium chloride to **1** in 10 % d_6-DMSO/$CDCl_3$.

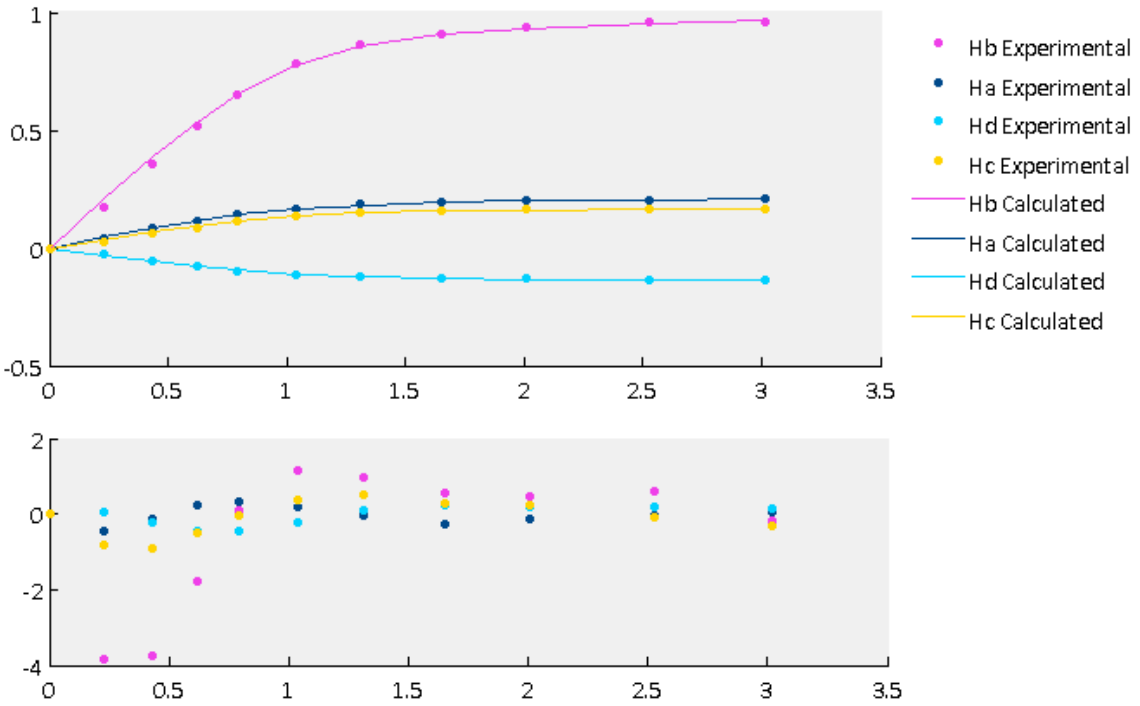

Figure 22. Example 1:1 fitting using non-linear regression from the data obtained for the titration of tetrabutylammonium chloride into **1** in 10 % d_6-DMSO/$CDCl_3$.

Table 4. Example titration for the addition of tetrabutylammonium bromide to **1** in 10 % d_6-DMSO/$CDCl_3$.

Addition (µL)	Total Volume Anion (µL)	[TBABr] (M)	Equiv. Br^-	$\delta(H^a)$ (ppm)	$\delta(H^b)$ (ppm)	$\delta(H^c)$ (ppm)	$\delta(H^d)$ (ppm)
0	0	0.000E+00	0	7.880	9.362	7.436	7.893
10	10	1.055E-04	0.100	7.895	9.414	7.451	7.883
10	20	2.070E-04	0.197	7.909	9.468	7.466	7.872
15	35	3.521E-04	0.335	7.930	9.544	7.487	7.858
15	50	4.893E-04	0.465	7.948	9.612	7.506	7.846
20	70	6.609E-04	0.629	7.967	9.684	7.526	7.833
20	90	8.210E-04	0.781	7.981	9.740	7.542	7.824
30	120	1.042E-03	0.991	7.996	9.797	7.558	7.815
40	160	1.305E-03	1.241	8.009	9.846	7.571	7.807
50	210	1.592E-03	1.514	8.017	9.881	7.581	7.800
75	285	1.954E-03	1.858	8.025	9.913	7.589	7.795
150	435	2.504E-03	2.381	8.032	9.941	7.596	7.789

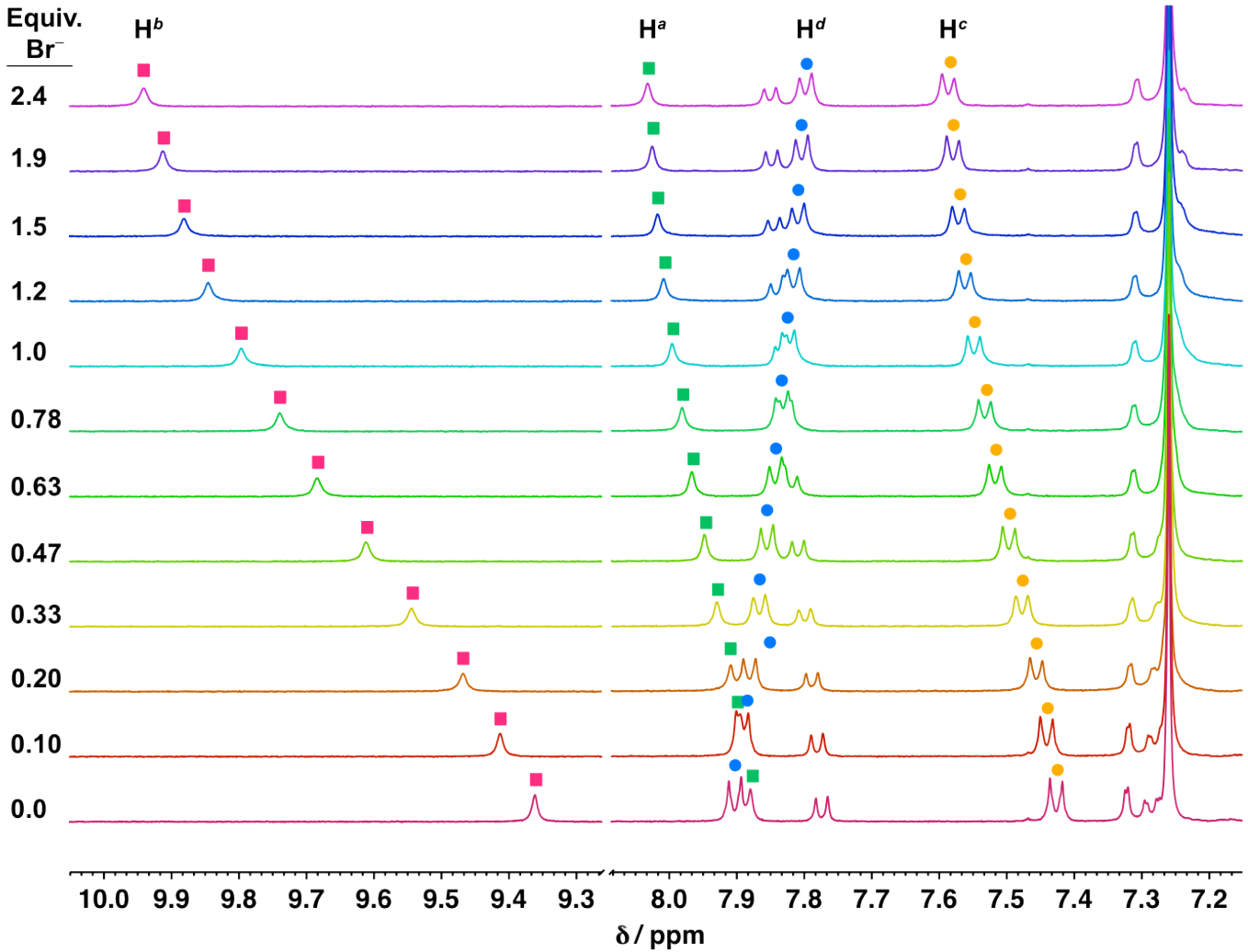

Figure 23. Example stacked spectra from the titration for the addition of tetrabutylammonium bromide to **1** in 10 % d_6-DMSO/$CDCl_3$.

Tetrabutylammonium iodide. A 3 mL stock solution of **1** (3.35 mg, [R] = 0.98 mM) in 10 % DMSO-d_6/$CDCl_3$ was prepared and used in the preparation of a 2 mL TBAI guest solution (11.67 mg, [G] = 15.8 mM). Starting volume of 500 µL. (Table 5, Figures 25 and 26)

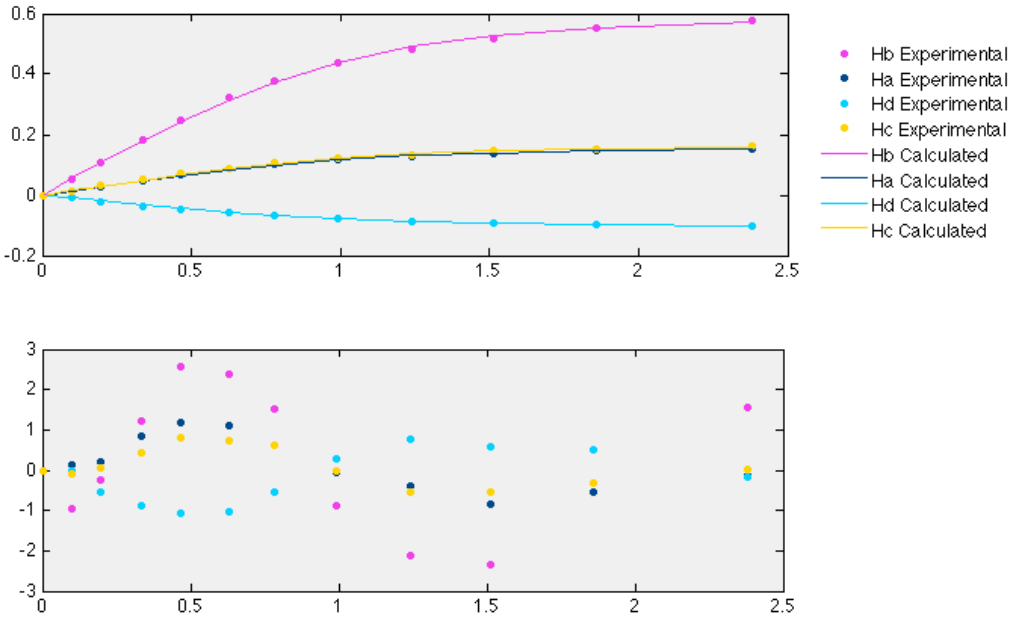

Figure 24. Example 1:1 fitting using non-linear regression from the data obtained for the titration of tetrabutylammonium bromide into **1** in 10 % d_6-DMSO/$CDCl_3$.

Table 5. Example titration for the addition of tetrabutylammonium iodide to **1** in 10 % d_6-DMSO/$CDCl_3$.

Addition (µL)	Total Volume Anion (µL)	[TBAI] (M)	Equiv. I^-	$\delta(H^a)$ (ppm)	$\delta(H^b)$ (ppm)	$\delta(H^c)$ (ppm)	$\delta(H^d)$ (ppm)
0	0	0.000E+00	0	7.879	9.359	7.434	7.892
5	5	1.564E-04	0.159	7.889	9.388	7.447	7.887
10	15	4.601E-04	0.469	7.903	9.421	7.465	7.877
15	30	8.942E-04	0.911	7.920	9.458	7.486	7.870
20	50	1.436E-03	1.464	7.933	9.488	7.503	7.863
25	75	2.061E-03	2.100	7.944	9.513	7.517	7.857
30	105	2.742E-03	2.794	7.953	9.533	7.530	7.852
40	145	3.551E-03	3.620	7.960	9.551	7.539	7.847
50	195	4.432E-03	4.518	7.967	9.567	7.548	7.844
50	245	5.195E-03	5.295	7.972	9.578	7.554	7.841
100	345	6.450E-03	6.574	7.978	9.591	7.562	7.836
150	495	7.859E-03	8.010	7.983	9.603	7.570	7.835
200	695	9.187E-03	9.364	7.987	9.611	7.575	7.834

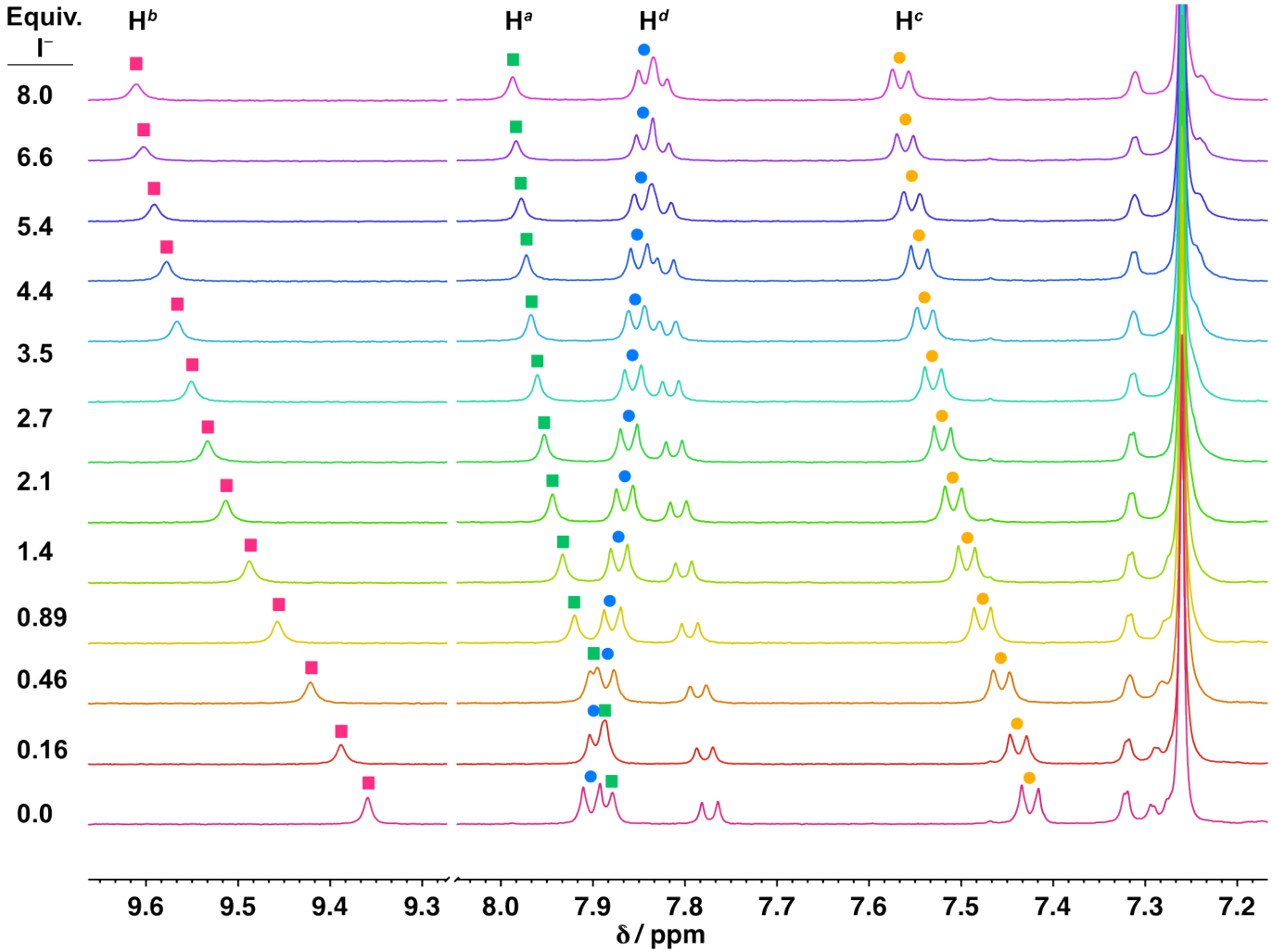

Figure 25. Example stacked spectra from the titration for the addition of tetrabutylammonium iodide to **1** in 10 % d_6-DMSO/$CDCl_3$.

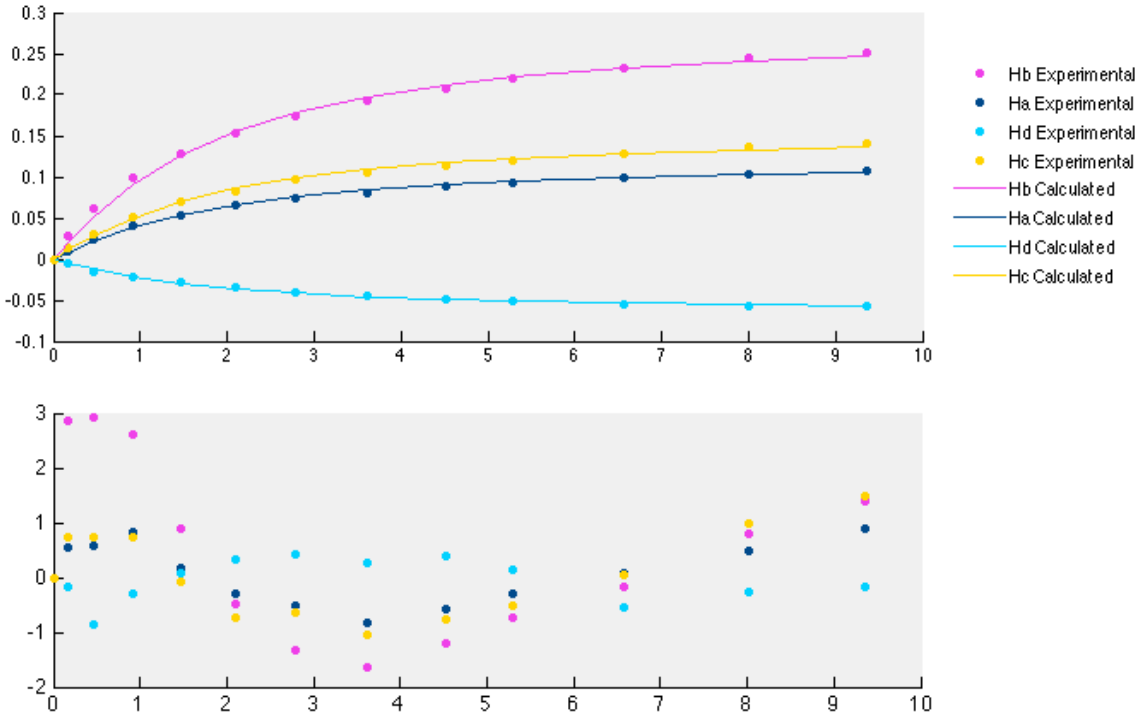

Figure 26. Example 1:1 fitting using non-linear regression from the data obtained for the titration of tetrabutylammonium iodide into **1** in 10 % d_6-DMSO/$CDCl_3$.

C.3.5. NMR Titrations of 2 in 10 % DMSO-d_6/$CDCl_3$

Tetrabutylammonium nitrate. A 3 mL stock solution of **2** (2.99 mg, [R] = 0.92 mM) in 10 % DMSO-d_6/$CDCl_3$ was prepared and used in the preparation of a 2 mL $TBANO_3$ guest solution (3.58 mg, [G] = 5.88 mM). Starting volume of 500 µL. (Table 6, Figures 27 and 28)

Tetrabutylammonium chloride. A 3 mL stock solution of **2** (3.24 mg, [R] = 1.00 mM) in 10 % DMSO-d_6/$CDCl_3$ was prepared and used in the preparation of a 2 mL TBACl guest solution (3.86 mg, [G] = 6.94 mM). Starting volume of 500 µL. (Table 7, Figures 29 and 30)

Table 6. Example titration for the addition of tetrabutylammonium nitrate to **2** in 10 % d_6-DMSO/$CDCl_3$.

Addition (µL)	Total Volume Anion (µL)	[$TBANO_3$] (M)	Equiv. NO_3^-	$\delta(H^a)$ (ppm)	$\delta(H^b)$ (ppm)	$\delta(H^c)$ (ppm)	$\delta(H^a)$ (ppm)
0	0	0.000E+00	0	7.980	9.595	7.464	7.894
10	10	1.153E-04	0.125	8.002	9.626	7.478	7.887
10	20	2.261E-04	0.246	8.023	9.656	7.492	7.881
15	35	3.846E-04	0.418	8.052	9.696	7.510	7.873
15	50	5.345E-04	0.581	8.075	9.730	7.526	7.867
20	70	7.220E-04	0.785	8.101	9.766	7.543	7.860
20	90	8.968E-04	0.976	8.118	9.791	7.554	7.855
25	115	1.099E-03	1.196	8.132	9.812	7.564	7.851
35	150	1.357E-03	1.476	8.144	9.828	7.572	7.847
50	200	1.680E-03	1.827	8.153	9.840	7.576	7.844
75	275	2.086E-03	2.269	8.159	9.847	7.580	7.841
100	375	2.520E-03	2.741	8.163	9.853	7.581	7.839
200	575	3.145E-03	3.421	8.166	9.856	7.582	7.836

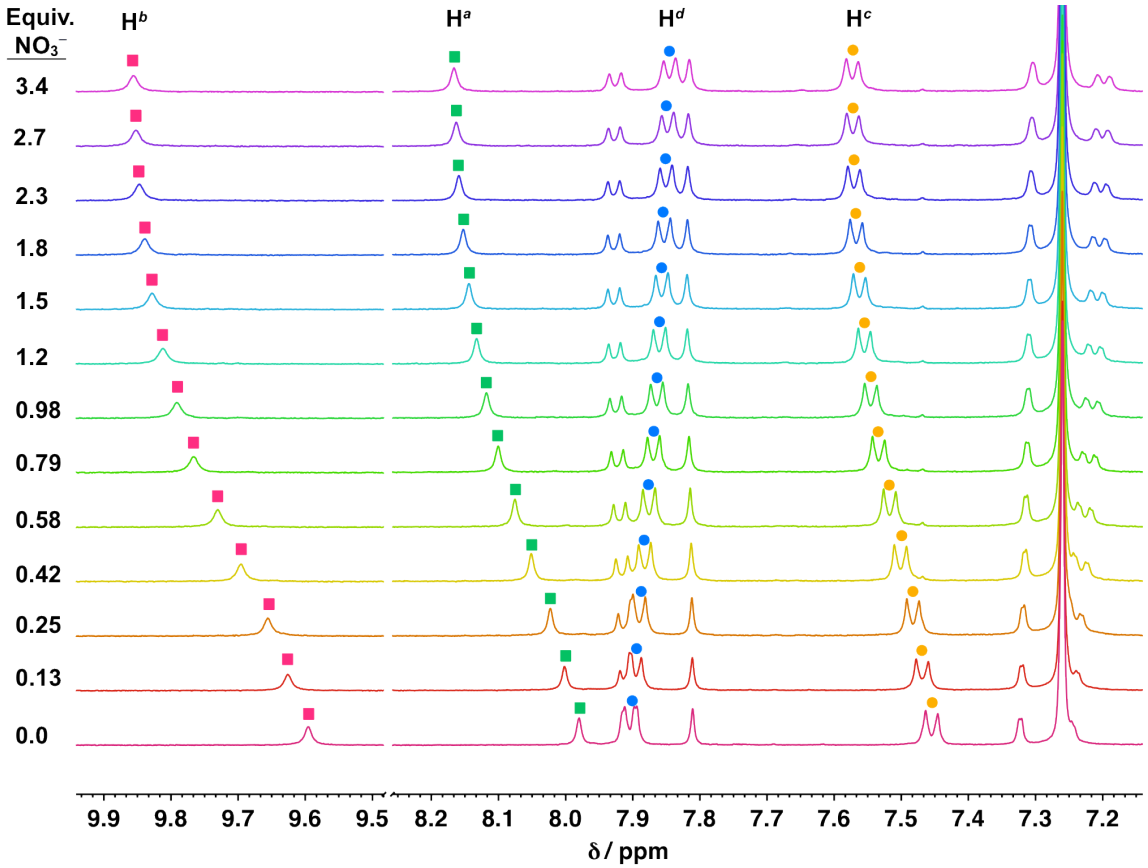

Figure 27. Example stacked spectra from the titration for the addition of tetrabutylammonium nitrate to **2** in 10 % d_6-DMSO/$CDCl_3$.

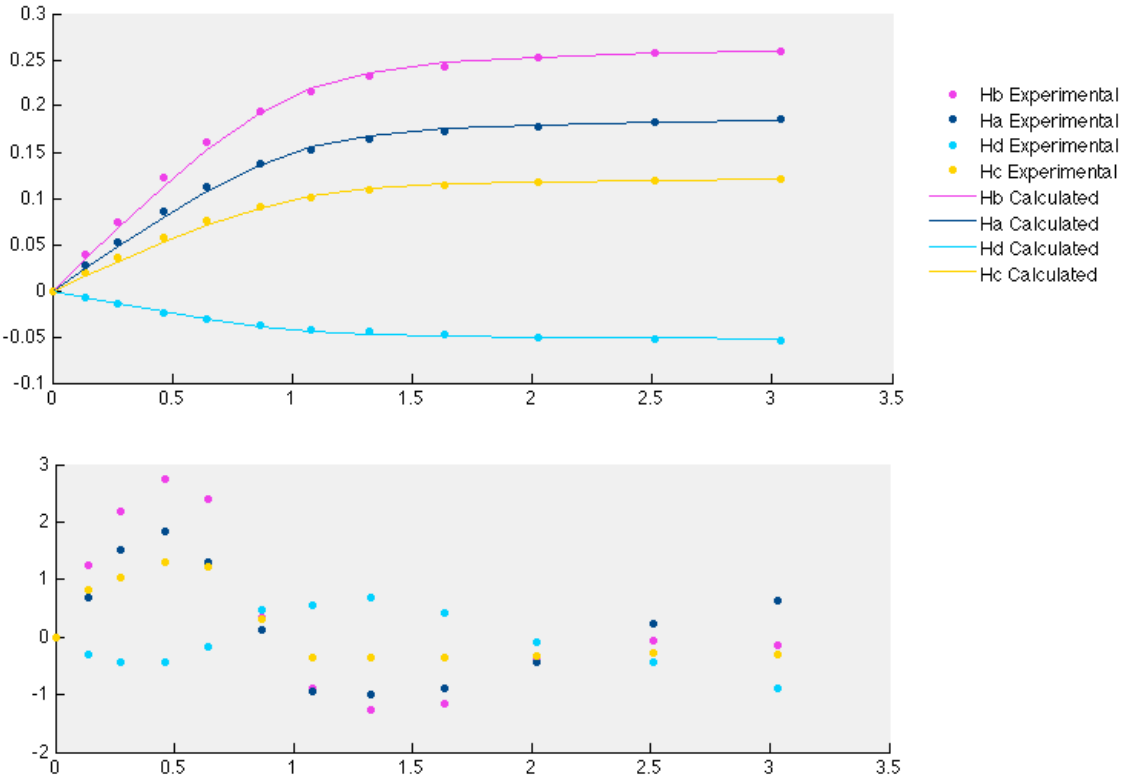

Figure 28. Example 1:1 fitting using non-linear regression from the data obtained for the titration of tetrabutylammonium nitrate into **2** in 10 % d_6-DMSO/$CDCl_3$.

Table 7. Example titration for the addition of tetrabutylammonium chloride to **2** in 10 % d_6-DMSO/$CDCl_3$.

Addition (µL)	Total Volume Anion (µL)	[TBACl] (M)	Equiv. Cl^-	$\delta(H^a)$ (ppm)	$\delta(H^b)$ (ppm)	$\delta(H^c)$ (ppm)	$\delta(H^d)$ (ppm)
0	0	0.000E+00	0	7.979	9.582	7.461	7.894
10	10	1.362E-04	0.137	7.996	9.724	7.492	7.884
10	20	2.671E-04	0.268	8.014	9.866	7.524	7.873
10	30	3.931E-04	0.395	8.031	10.004	7.555	7.864
10	40	5.144E-04	0.516	8.045	10.134	7.583	7.855
15	55	6.882E-04	0.691	8.064	10.300	7.620	7.844
15	70	8.528E-04	0.856	8.078	10.417	7.647	7.836
20	90	1.059E-03	1.063	8.086	10.501	7.665	7.830
20	110	1.252E-03	1.257	8.091	10.538	7.673	7.827
25	135	1.476E-03	1.482	8.095	10.562	7.677	7.825
35	170	1.762E-03	1.769	8.099	10.580	7.679	7.822
50	220	2.122E-03	2.130	8.103	10.595	7.680	7.820

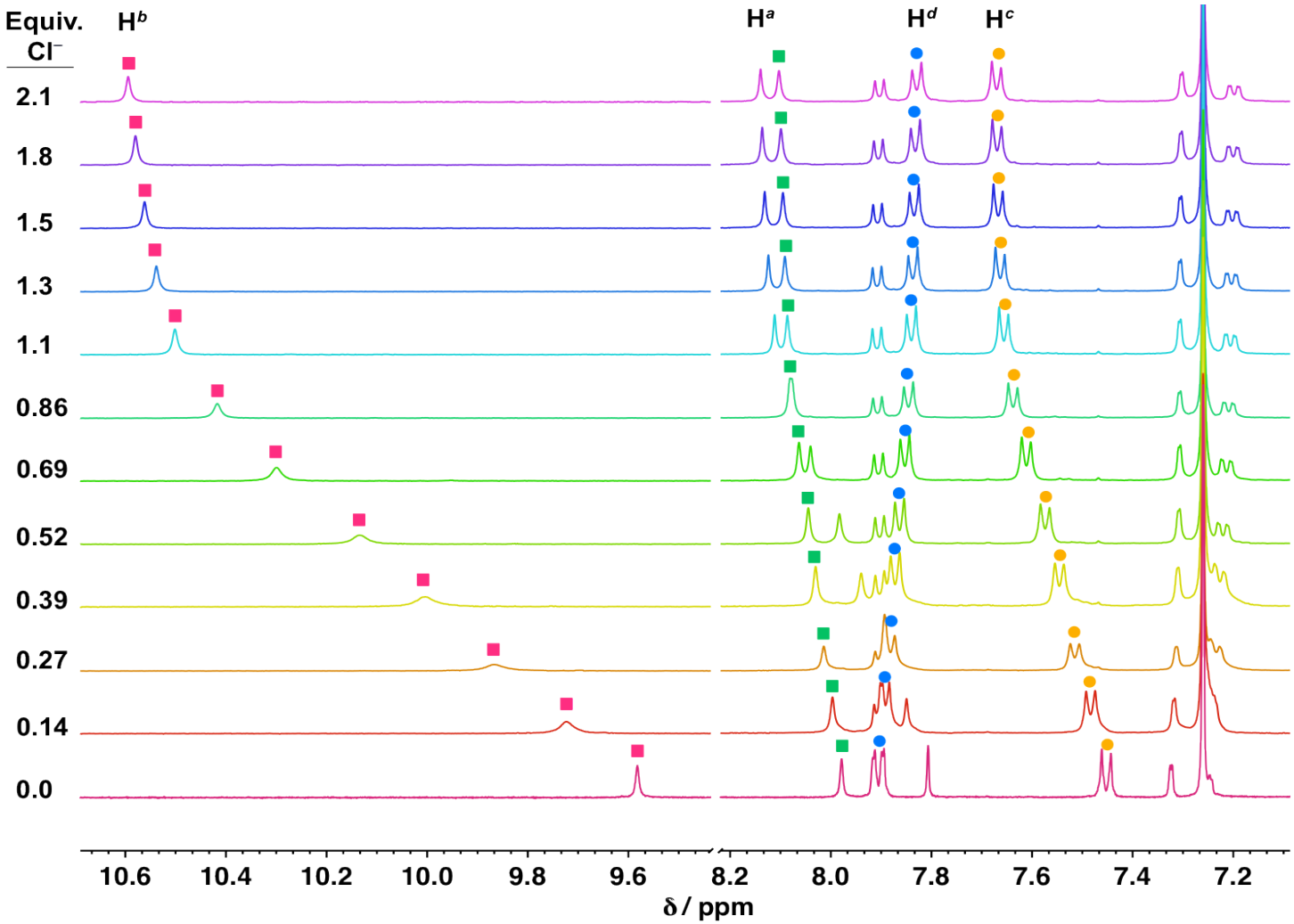

Figure 29. Example stacked spectra from the titration for the addition of tetrabutylammonium chloride to **2** in 10 % d_6-DMSO/$CDCl_3$.

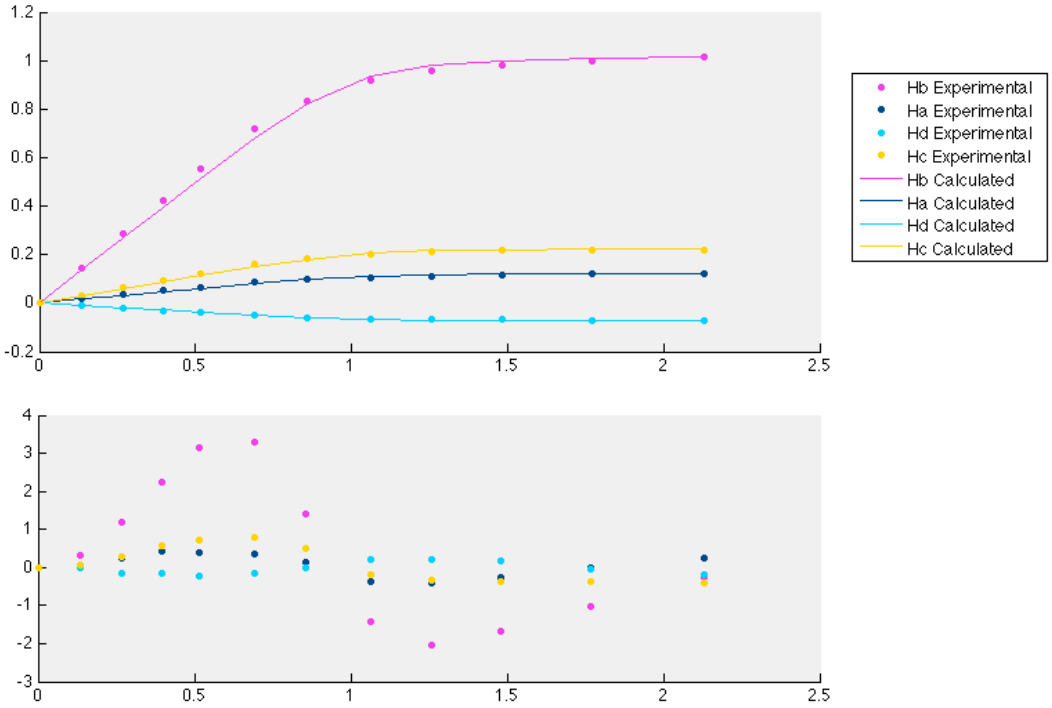

Figure 30. Example 1:1 fitting using non-linear regression from the data obtained for the titration of tetrabutylammonium chloride into **2** in 10 % d_6-DMSO/$CDCl_3$.

C.4. Computational Details

For the purposes of obtaining a simple visual representation of the electron density in host **1**, a geometry was used where the arms are spread out and more planar. In addition, methyl groups were used in place of the *t*-butyl units for ease of computation. Minimization of this geometry was performed at PM6 and the electrostatic potential surface map was calculated using Spartan'10 (Wavefunction, Inc.). In the following figure red represents areas of high electron density and blue represents low.

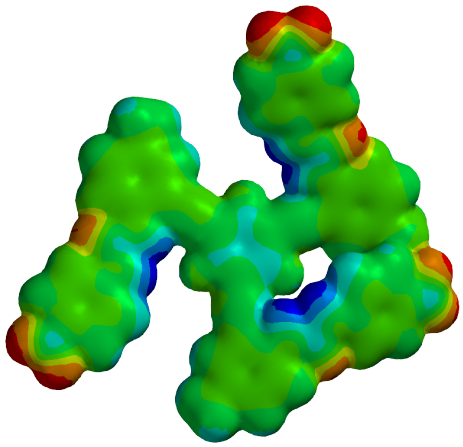

Figure 31. Electrostatic potential map of **1** showing the electron deficient core.

Table 8. X, Y, Z Coordinates for PM6 minimized geometry.

Atom	X	Y	Z	Atom	X	Y	Z
C	1.890855	0.979702	-6.982650	H	0.730353	-5.675270	-9.715795
H	1.801835	3.485213	-4.002144	C	-1.437017	6.148805	-2.535853
H	1.915697	0.284210	-7.831580	C	-0.405205	7.321946	-4.842182
H	2.306606	2.690815	-8.213154	C	-1.112853	7.521120	-2.536101
C	3.119799	-8.057940	1.648831	C	-1.268508	5.370107	-3.709886
H	4.077418	-8.362654	2.097616	C	-0.752051	5.957753	-4.854075
H	2.503954	-8.964972	1.554009	C	-0.600769	8.103638	-3.687296
C	2.344480	4.701296	-6.387923	H	-1.264848	8.126469	-1.632420
H	1.523203	5.172357	-6.959015	H	-1.533435	4.313936	-3.722543
H	2.464230	5.287826	-5.468182	H	-0.605387	5.369443	-5.768603
C	-2.665317	5.885364	6.564716	H	-0.341121	9.169627	-3.706640
H	-1.938443	6.629955	6.925184	N	0.170708	7.927225	-6.047156
H	-2.499599	4.969349	7.147195	O	0.370649	9.130375	-6.048204
H	-3.666112	6.255997	6.832444	O	0.423269	7.182947	-6.986925
N	-2.225023	5.047726	0.907490	N	0.366248	-8.091187	-8.575214
H	-2.286263	4.062244	0.639049	O	0.362299	-8.078315	-9.795882
C	-2.048380	6.040488	-0.079319	O	0.219710	-9.093346	-7.891232
O	-2.005127	7.232511	0.137840	H	3.340929	-7.714256	0.629836
N	-1.909284	5.466371	-1.388213	N	0.504875	-4.072841	4.857123
H	-2.157129	4.481976	-1.526065	H	0.355085	-3.178921	4.380291
H	3.258554	4.855020	-6.981149	C	0.077937	-4.230434	6.196012
H	2.409514	-5.516783	0.925471	O	0.208256	-5.247672	6.845523
N	1.424543	-0.883447	-5.397083	N	-0.535521	-3.046007	6.717143
H	1.358523	-1.127745	-4.405309	H	-0.618171	-2.219984	6.117695
C	1.304634	-1.893766	-6.378598	C	-1.055130	-2.911806	8.032501
O	1.359053	-1.700572	-7.575628	C	-2.112464	-2.498871	10.577700
N	1.106514	-3.192292	-5.807127	C	-1.016586	-3.951613	8.983209
H	1.088189	-3.293328	-4.788854	C	-1.629358	-1.658489	8.363673
C	0.928291	-4.388909	-6.552064	C	-2.154606	-1.458047	9.632417
C	0.560646	-6.813138	-7.876639	C	-1.543757	-3.743689	10.250901
C	0.922179	-4.422305	-7.961094	H	-0.573130	-4.924054	8.729071
C	0.749311	-5.581076	-5.805912	H	-1.664144	-0.850581	7.635509
C	0.566694	-6.785745	-6.470306	H	-2.603513	-0.496329	9.909199
C	0.738581	-5.631223	-8.619102	H	-1.521579	-4.542249	11.003528
H	1.062077	-3.500317	-8.541899	N	-2.668771	-2.280951	11.920083
H	0.753165	-5.564931	-4.717817	O	-2.612426	-3.204069	12.716698
H	0.426301	-7.719552	-5.912161	O	-3.155849	-1.185992	12.159928

APPENDIX D

SUPPLEMENTARY INFORMATION FOR CHAPTER IV

D.1. General Experimental Details

^{1}H and ^{13}C NMR spectra were obtained on a Varian Mercury 300 MHz spectrometer (^{1}H: 300.09), Inova 500 MHz spectrometer (^{1}H: 500.10 MHz, ^{13}C: 125.75 MHz), or Bruker Avance III HD 600 MHz NMR Spectrometer with Prodigy multinuclear broadband BBO CryoProbe (^{1}H: 600.02 MHz, ^{13}C: 150.89 MHz). Chemical shifts (δ) are expressed in ppm downfield from tetramethylsilane (TMS) using non-deuterated solvent present in the bulk deuterated solvent ($CDCl_3$: ^{1}H 7.26 ppm, ^{13}C 77.16 ppm; d_6-DMSO: ^{1}H 2.50 ppm ^{13}C 39.52 ppm). All NMR spectra were processed using MestReNova NMR processing software. All materials were synthesized following literature procedures or were obtained from TCI-America, Sigma-Aldrich, or Acros and used as received. X-ray crystal data were obtained on a Bruker Apex CCD diffractometer.

D.2. Synthesis of Receptor 3

In oven dried glassware, trisaniline **4** (300 mg, 0.507 mmol) and *p*-methoxyphenyl isocyanate (0.40 mL, 3.04 mmol) were dissolved in freshly distilled toluene (50 mL) (Scheme 1). The reaction mixture was stirred overnight, quenched with acetone, and product **3** was obtained cleanly by repeated precipitation from acetone with hexanes (300 mg, 57 % yield). ^{1}H NMR (600 MHz, d_6-DMSO) δ 9.26 (s, 3H),

Scheme 1. Synthesis of receptor **3** from previously reported core molecule **4**.

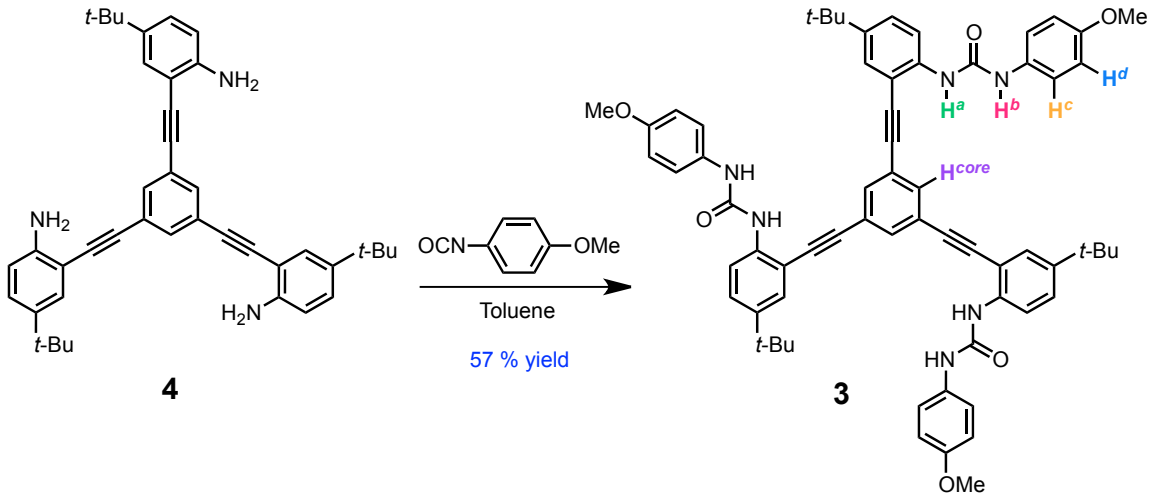

8.13 (s, 3H), 8.05 (d, J = 8.8 Hz, 3H), 8.04 (s, 3H), 7.54 (d, J = 2.4 Hz, 3H), 7.45 (dd, J = 8.8, 2.4 Hz, 3H), 7.37 (d, J = 9.0 Hz, 6H), 6.83 (d, J = 9.0 Hz, 6H), 3.69 (s, 9H), 1.30 (s, 27H). ^{13}C NMR (151 MHz, d_6-DMSO) δ 154.63, 152.40, 144.44, 138.19, 134.09, 132.35, 128.83, 127.25, 123.64, 120.28, 119.72, 114.01, 110.48, 92.81, 87.65, 55.10, 33.96, 31.01. LRMS (ESI) m/e 1039.5 (M^+, 100). HRMS (ESI) for $C_{66}H_{67}N_6O_6$ [M^+]: calcd 1039.5122, found 1039.5084. (Figures 1-4)

D.3. Titration Details

Tetrabutylammonium salts were dried at 50 °C under vacuum and stored in a calcium carbonate filled desiccator. Tetrabutylammonium sulfate was purchased as a 50 % solution in water. In all titrations the receptor concentration was kept constant during the titration. A stock solution of receptor was prepared and the host-guest solution was prepared with the stock receptor solution. Final guest amounts were obtained through drying an aliquot of a freshly prepared stock solution for each titration unless desires masses could accurately be weighed out. All additions were performed with a Hamilton µL syringe. Titrations were carried out in at least triplicate and the reported binding constants represent the average of the fits from the titrations.

^{1}H NMR (600 MHz, DMSO-d_6) δ 9.26 (s, 3H), 8.13 (s, 3H), 8.05 (d, J = 8.8 Hz, 3H), 8.04 (s, 3H), 7.54 (d, J = 2.4 Hz, 3H), 7.45 (dd, J = 8.8, 2.4 Hz, 3H), 7.37 (d, J = 9.0 Hz, 6H), 6.83 (d, J = 9.0 Hz, 6H), 3.69 (s, 9H), 1.30 (s, 27H).

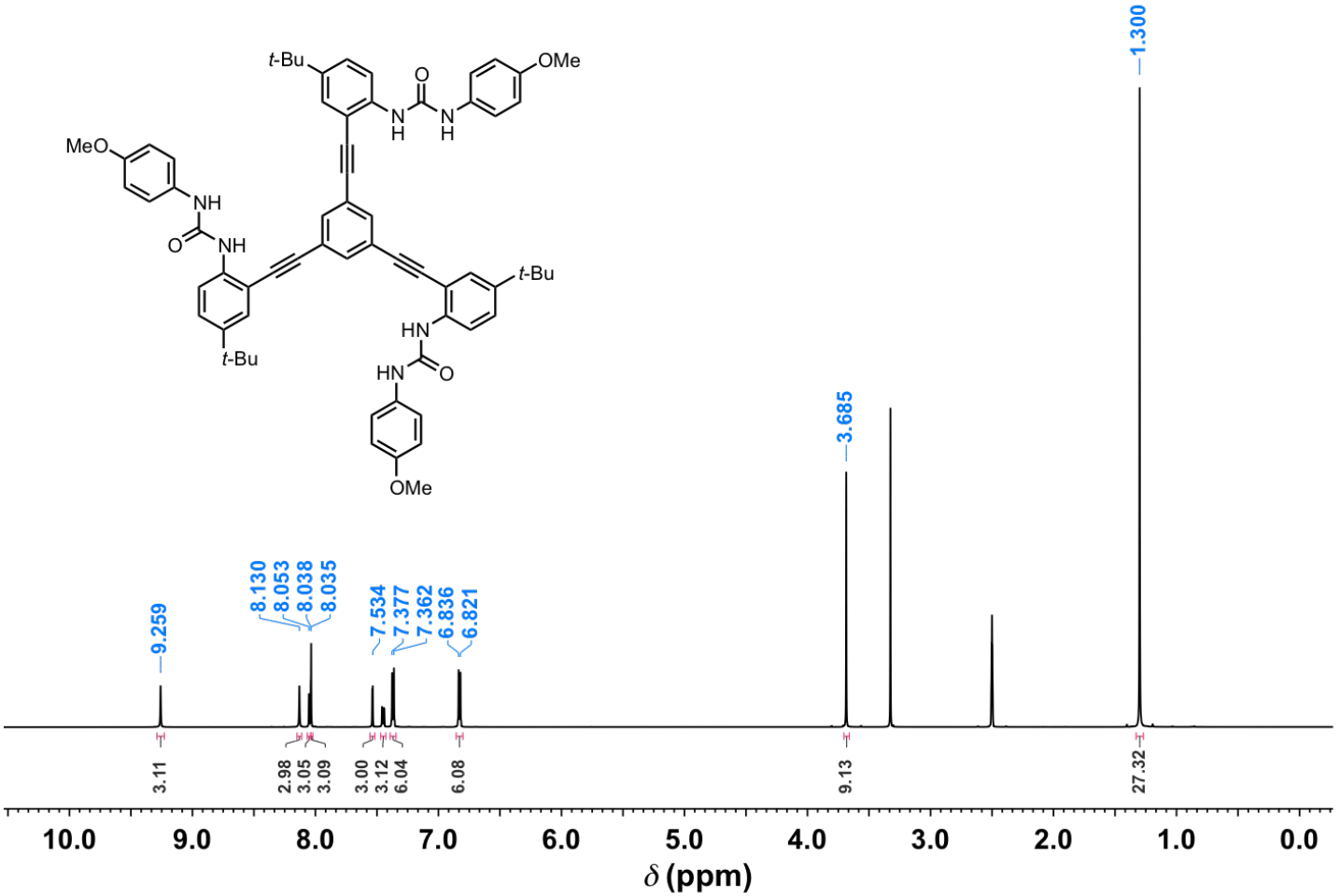

Figure 1. ^{1}H NMR spectrum of **3** in $CDCl_3$, 600 MHz.

^{13}C NMR (151 MHz, DMSO) δ 154.63, 152.40, 144.44, 138.19, 134.09, 132.35, 128.83, 127.25, 123.64, 120.28, 119.72, 114.01, 110.48, 92.81, 87.65, 55.10, 33.96, 31.01.

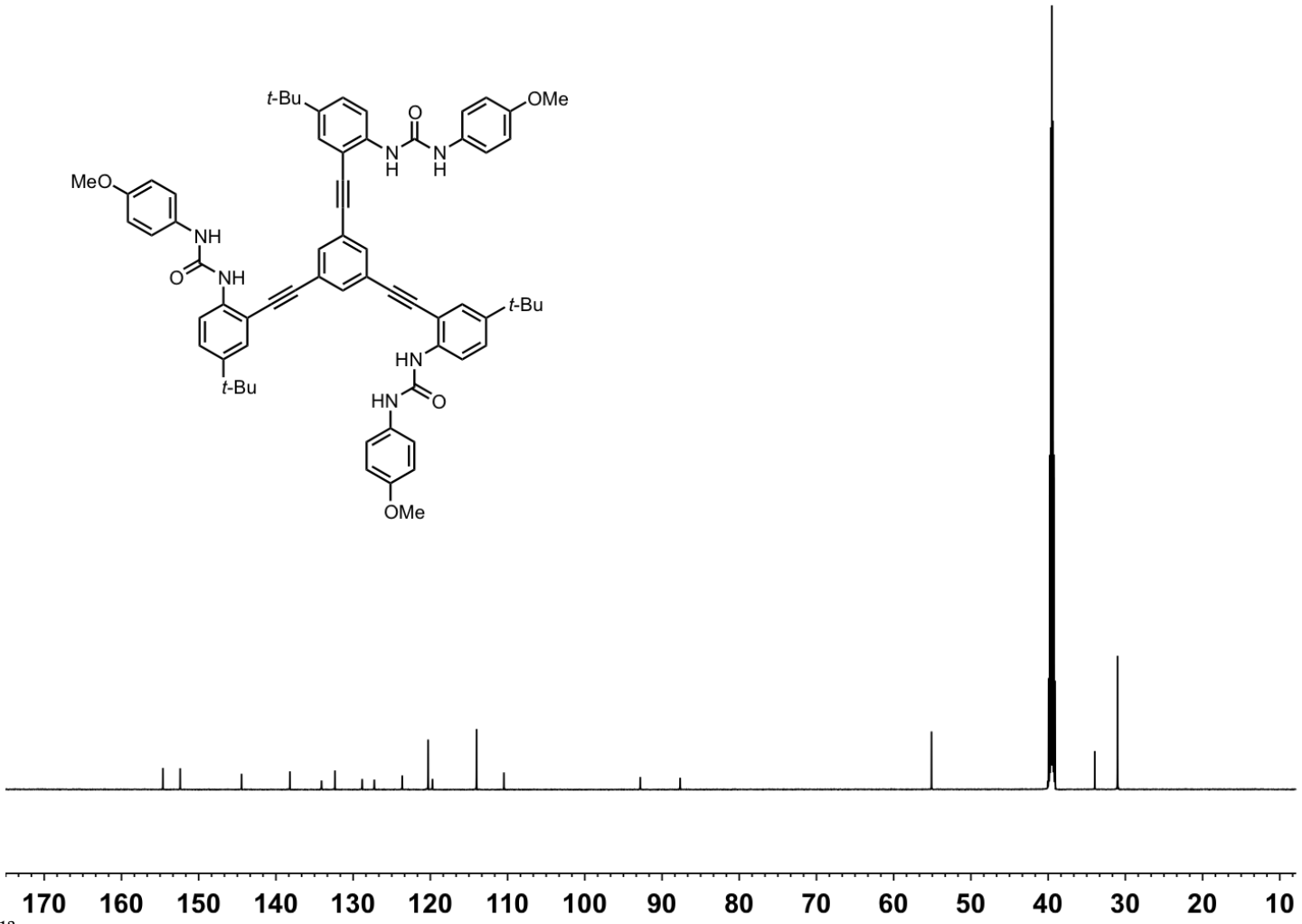

Figure 2. ^{13}C NMR spectrum of **3** in $CDCl_3$, 151 MHz.

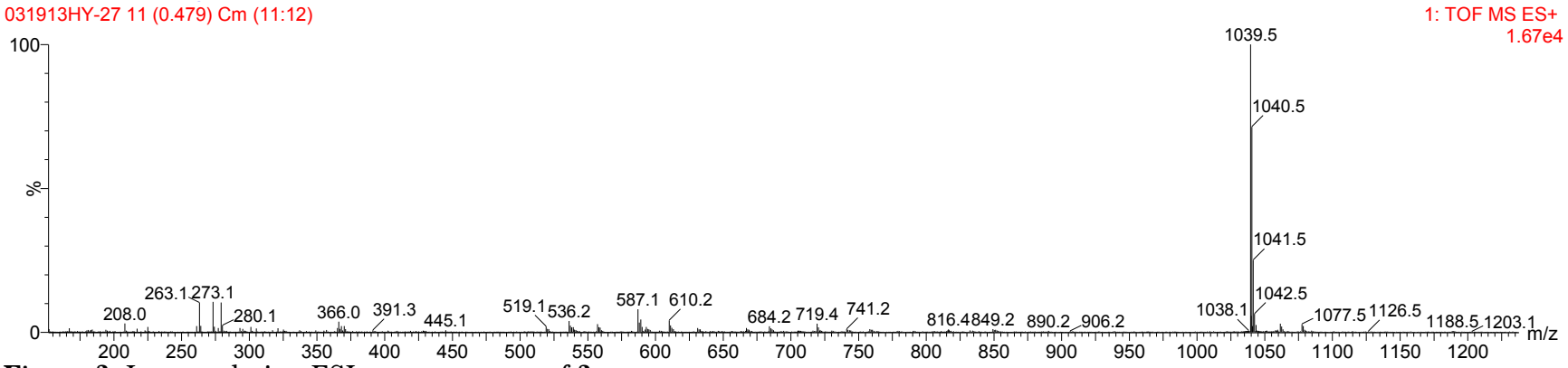

Figure 3. Low resolution ESI mass spectrum of **3.**

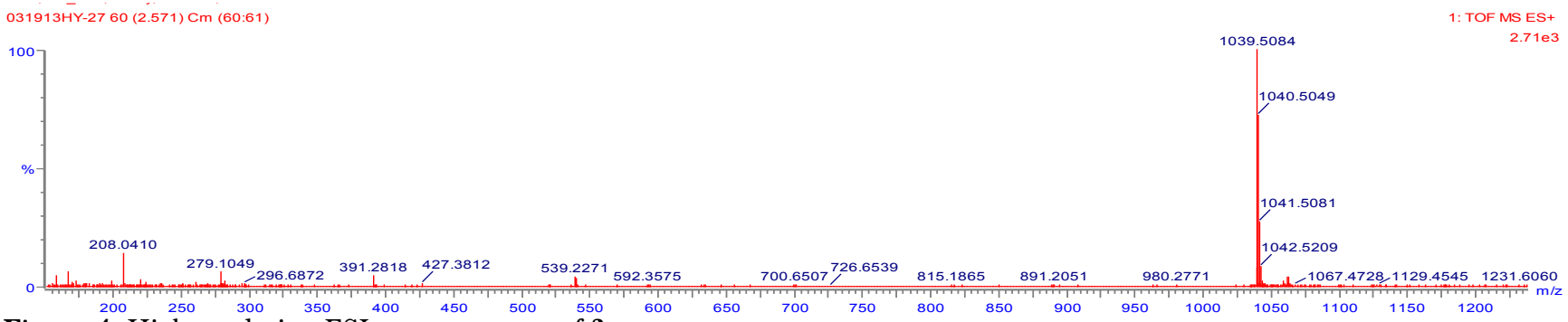

Figure 4. High resolution ESI mass spectrum of **3.**

Association constants (K_a) were calculated by nonlinear curve fitting of the obtained titration isotherms using Thordarson fitting programs via Matlab. Representative data are provided for each set.

^{1}H NMR titrations were carried out on an Inova 500 MHz spectrometer (^{1}H 500.10 MHz) at 298 K unless otherwise noted. Chemical shifts (δ) are expressed in ppm downfield from tetramethylsilane (TMS) using non-deuterated solvent present in the bulk deuterated solvent ($CDCl_3$: ^{1}H 7.26 ppm). Chemical shifts of urea protons broadened into the baseline were determined using line broadening.

D.3.1. NMR Titrations of 3

Tetrabutylammonium nitrate, 10 % DMSO-d_6/$CDCl_3$. A 3 mL stock solution of **3** (3.24 mg, [R] = 1.04 mM) in 10 % DMSO-d_6/$CDCl_3$ was prepared and used in the preparation of a 2 mL $TBANO_3$ guest solution (5.00 mg, [G] = 8.21 mM). Starting volume of 500 µL. (Table 1, Figures 5 and 6)

Table 1. Example titration for the addition of tetrabutylammonium nitrate to **3** in 10 % d_6-DMSO/$CDCl_3$.

Addition (µL)	Total Volume Anion (µL)	[$TBANO_3$] (M)	Equiv. NO_3^-	$\delta(H^a)$ (ppm)	$\delta(H^b)$ (ppm)	$\delta(H^c)$ (ppm)	$\delta(H^d)$ (ppm)	$\delta(H^{core})$ (ppm)
0	0	0.00E+00	0	7.696	8.675	7.150	6.590	6.590
10	10	1.61E-04	0.15	7.710	8.704	7.160	6.593	6.593
10	20	3.16E-04	0.30	7.720	8.729	7.164	6.589	6.589
10	30	4.64E-04	0.45	7.736	8.752	7.169	6.585	6.585
10	40	6.08E-04	0.58	7.741	8.770	7.172	6.581	6.581
10	50	7.46E-04	0.72	7.744	8.787	7.176	6.578	6.578
15	65	9.44E-04	0.91	7.761	8.809	7.179	6.574	6.574
15	80	1.13E-03	1.09	7.770	8.827	7.182	6.570	6.570
20	100	1.37E-03	1.32	7.780	8.848	7.186	6.566	6.566
20	120	1.59E-03	1.53	7.788	8.862	7.189	6.563	6.563
25	145	1.84E-03	1.78	7.797	8.880	7.192	6.559	6.559
35	180	2.17E-03	2.09	7.806	8.894	7.197	6.557	6.557
50	230	2.59E-03	2.49	7.817	8.915	7.199	6.552	6.552

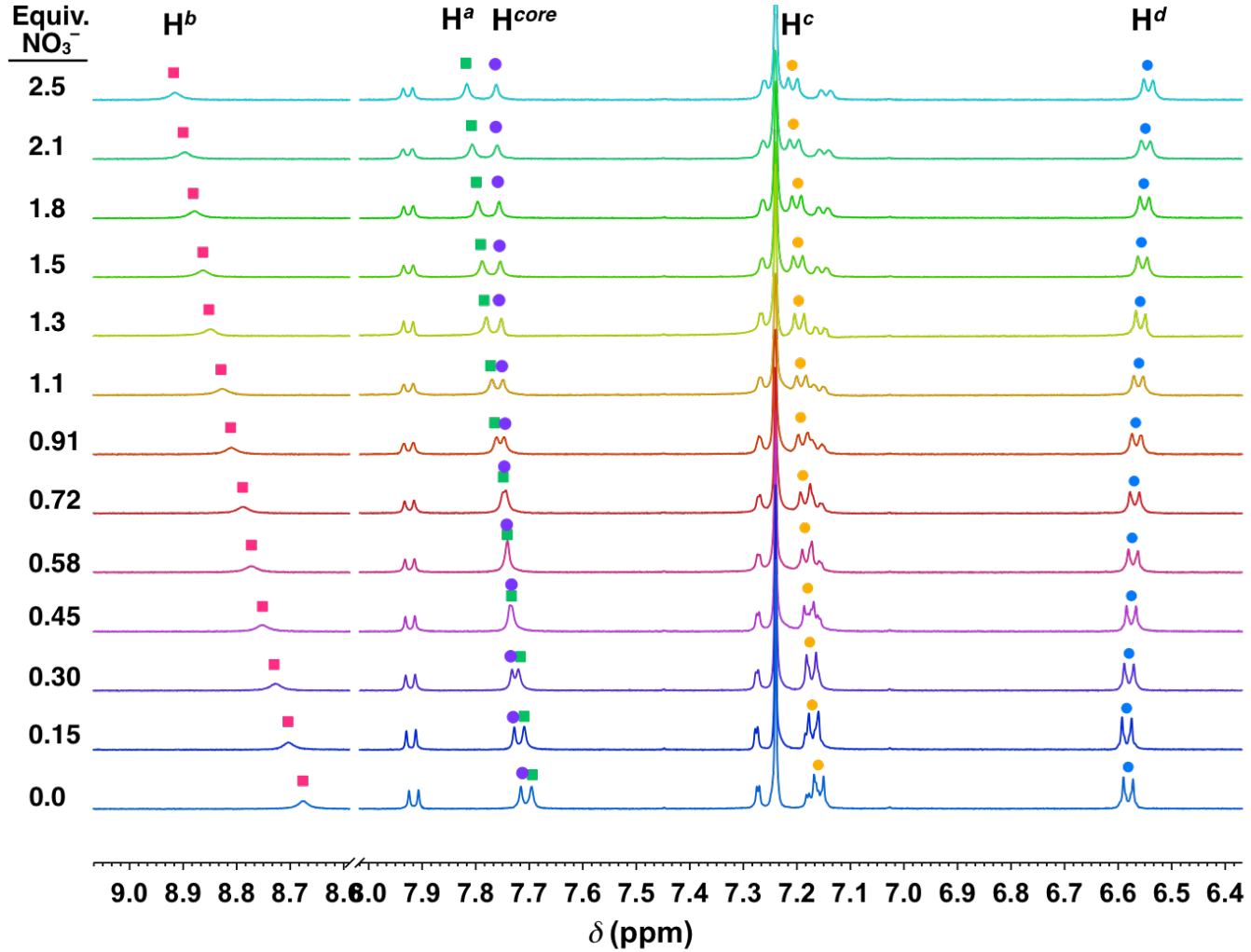

Figure 5. Example stacked spectra from the titration for the addition of tetrabutylammonium nitrate to **3** in 10 % d_6-DMSO/$CDCl_3$.

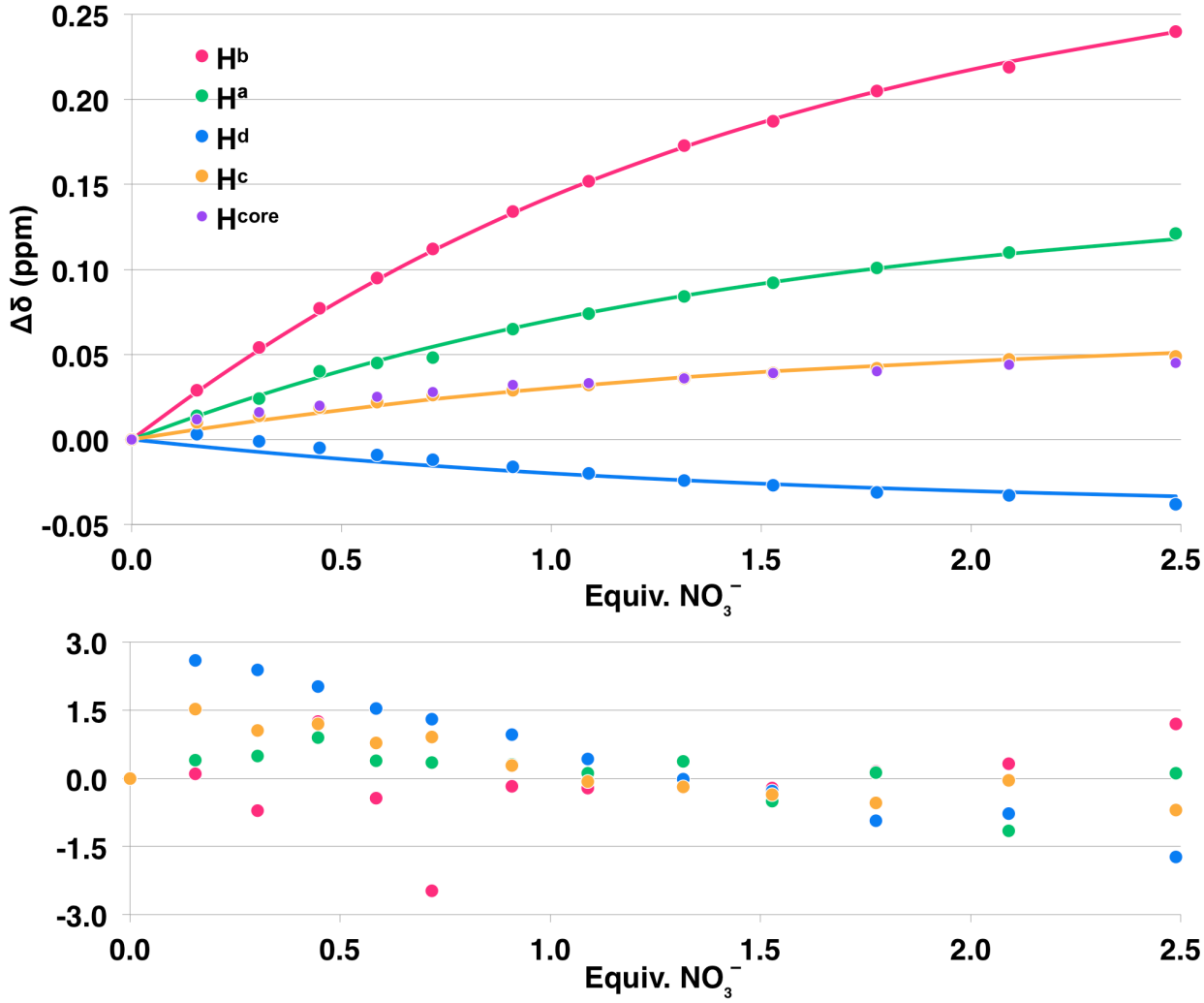

Figure 6. Example 1:1 fitting using non-linear regression from the data obtained for the titration of tetrabutylammonium nitrate into **3** in 10 % d_6-DMSO/$CDCl_3$.

Tetrabutylammonium chloride, 10 % DMSO-d_6/$CDCl_3$. A 3 mL stock solution of **3** (3.51 mg, [R] = 1.13 mM) in 10 % DMSO-d_6/$CDCl_3$ was prepared and used in the preparation of a 2 mL TBACl guest solution (5.24 mg, [G] = 9.43 mM). Starting volume of 500 µL. (Table 2, Figures 7 and 8)

Tetrabutylammonium bromide, 10 % DMSO-d_6/$CDCl_3$. A 3 mL stock solution of **3** (3.31 mg, [R] = 1.06 mM) in 10 % DMSO-d_6/$CDCl_3$ was prepared and used in the preparation of a 2 mL TBABr guest solution (5.04 mg, [G] = 7.81 mM). Starting volume of 500 µL. (Table 3, Figures 9 and 10)

Tetrabutylammonium iodide, 10 % DMSO-d_6/$CDCl_3$. A 3 mL stock solution of **3** (6.47 mg, [R] = 2.08 mM) in 10 % DMSO-d_6/$CDCl_3$ was prepared and used in the preparation of a 2 mL TBAI guest solution (81.49 mg, [G] = 110.3 mM). Starting volume of 500 µL. (Table 4, Figures 11 and 12)

Table 2. Example titration for the addition of tetrabutylammonium chloride to **3** in 10 % d_6-DMSO/$CDCl_3$.

Addition (µL)	Total Volume Anion (µL)	[TBACl] (M)	Equiv. Cl^-	$\delta(H^a)$ (ppm)	$\delta(H^b)$ (ppm)	$\delta(H^c)$ (ppm)	$\delta(H^d)$ (ppm)	$\delta(H^{core})$ (ppm)
0	0	0.00E+00	0	7.713	8.693	7.187	6.614	7.741
10	10	1.85E-04	0.16	7.727	8.793	7.200	6.606	7.775
10	20	3.63E-04	0.32	7.739	8.891	7.213	6.595	7.810
10	30	5.34E-04	0.47	7.751	8.978	7.225	6.587	7.842
10	40	6.99E-04	0.62	7.763	9.057	7.236	6.580	7.870
10	50	8.58E-04	0.76	7.771	9.116	7.245	6.574	7.894
15	65	1.09E-03	0.96	7.782	9.198	—	6.568	7.926
15	80	1.30E-03	1.16	7.791	9.258	—	6.561	7.945
20	100	1.57E-03	1.40	7.800	9.328	7.273	6.556	7.973
20	120	1.83E-03	1.62	7.807	9.379	7.276	6.551	7.992
25	145	2.12E-03	1.88	7.814	9.422	7.285	6.546	8.010
35	180	2.50E-03	2.22	7.822	9.473	7.293	6.542	8.030
50	230	2.97E-03	2.64	7.828	9.524	7.297	6.537	8.048

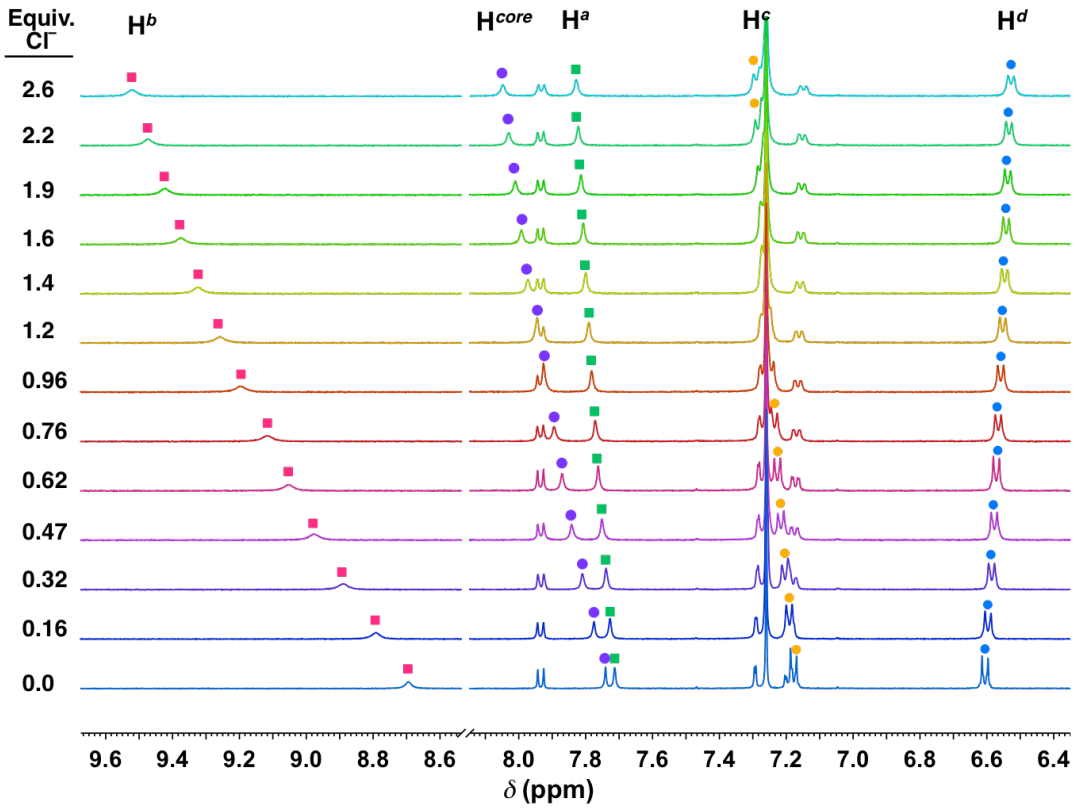

Figure 7. Example stacked spectra from the titration for the addition of tetrabutylammonium chloride to **3** in 10 % d_6-DMSO/$CDCl_3$.

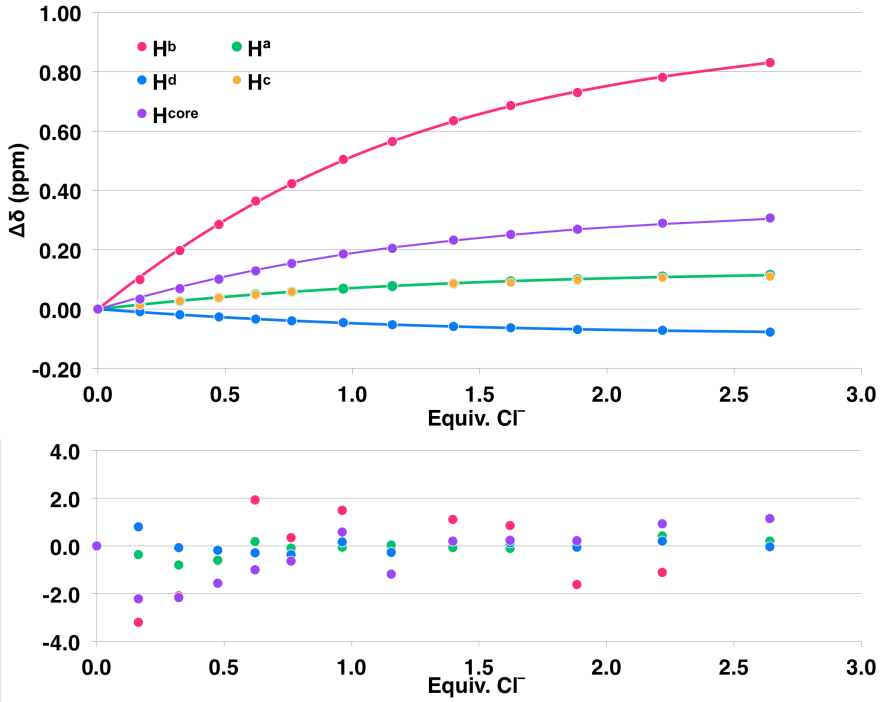

Figure 8. Example 1:1 fitting using non-linear regression from the data obtained for the titration of tetrabutylammonium chloride into **3** in 10 % d_6-DMSO/$CDCl_3$.

Table 3. Example titration for the addition of tetrabutylammonium bromide to **3** in 10 % d_6-DMSO/$CDCl_3$.

Addition (µL)	Total Volume Anion (µL)	[TBABr] (M)	Equiv. Br^-	$\delta(H^a)$ (ppm)	$\delta(H^b)$ (ppm)	$\delta(H^c)$ (ppm)	$\delta(H^d)$ (ppm)	$\delta(H^{core})$ (ppm)
0	0	0.00E+00	0	7.712	8.696	7.168	6.614	7.740
10	10	1.53E-04	0.14	7.716	8.725	7.174	6.609	7.753
10	20	3.00E-04	0.28	7.719	8.751	7.178	6.605	7.764
10	30	4.42E-04	0.42	7.721	8.770	7.182	6.602	7.773
10	40	5.78E-04	0.54	7.723	8.791	7.186	6.599	7.781
15	55	7.74E-04	0.73	7.726	8.814	7.190	6.595	7.792
15	70	9.59E-04	0.90	7.728	8.834	7.194	6.592	7.802
20	90	1.19E-03	1.12	7.731	8.861	7.198	6.589	7.813
20	110	1.41E-03	1.33	7.733	8.879	7.203	6.586	7.822
25	135	1.66E-03	1.56	7.735	8.903	7.206	6.582	7.832
25	160	1.89E-03	1.78	7.736	8.921	7.209	6.579	7.841
35	195	2.19E-03	2.06	7.739	8.943	7.214	6.575	7.850
50	245	2.57E-03	2.42	7.742	8.965	7.218	6.572	7.861

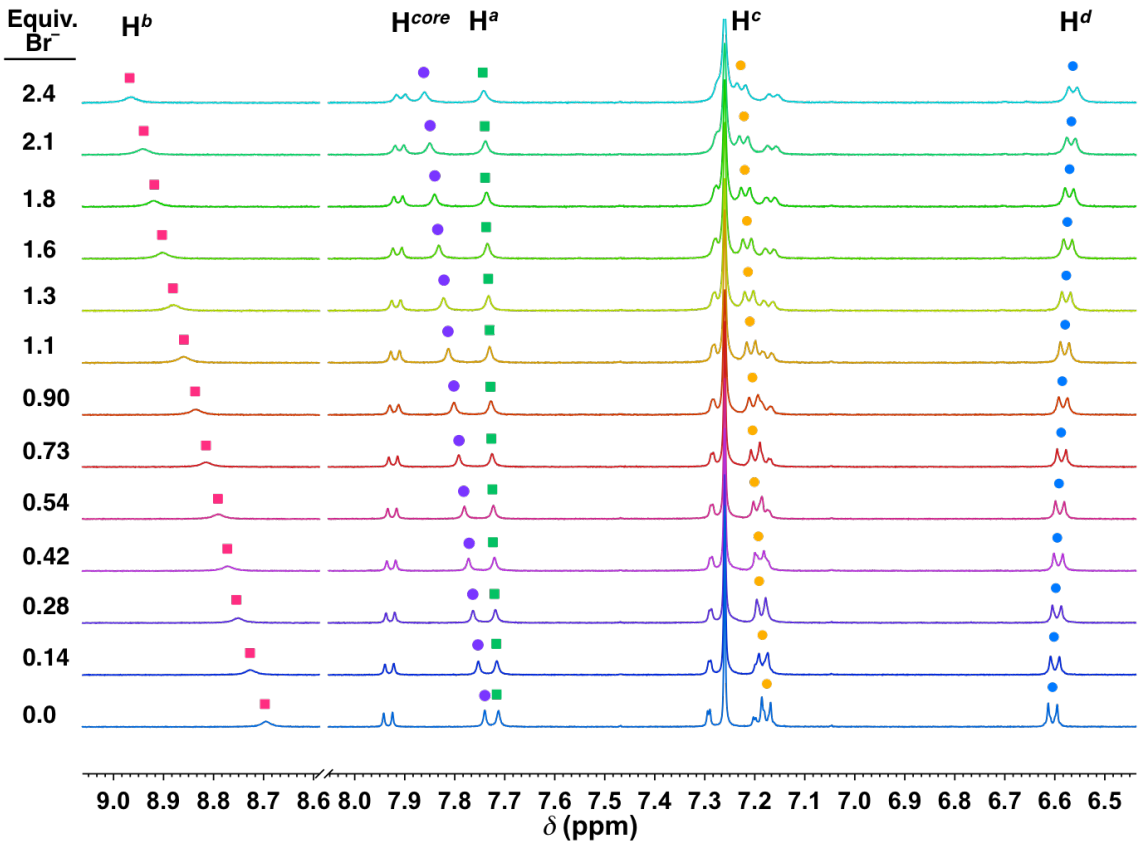

Figure 9. Example stacked spectra from the titration for the addition of tetrabutylammonium bromide to **3** in 10 % d_6-DMSO/$CDCl_3$.

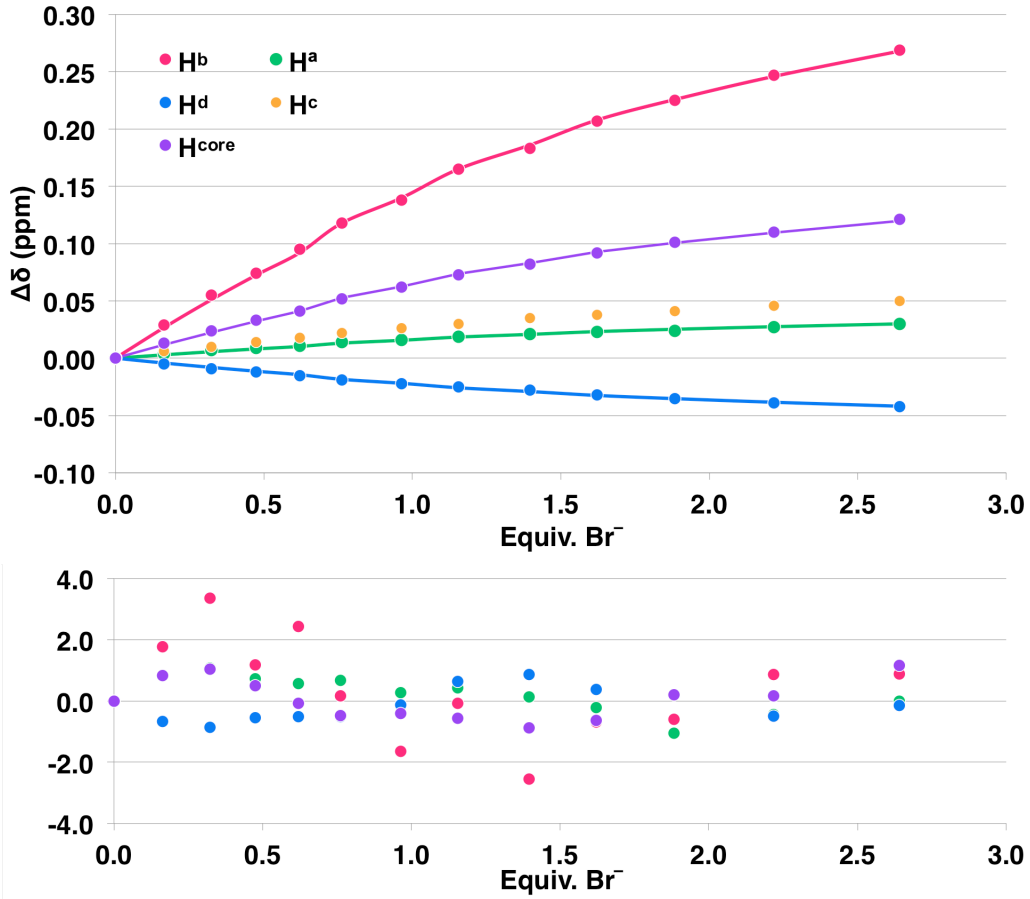

Figure 10. Example 1:1 fitting using non-linear regression from the data obtained for the titration of tetrabutylammonium bromide into **3** in 10 % d_6-DMSO/$CDCl_3$.

Table 4. Example titration for the addition of tetrabutylammonium iodide to **3** in 10 % d_6-DMSO/$CDCl_3$.

Addition (µL)	Total Volume Anion (µL)	[TBAI] (M)	Equiv. I^-	$\delta(H^a)$ (ppm)	$\delta(H^b)$ (ppm)	$\delta(H^c)$ (ppm)	$\delta(H^d)$ (ppm)	$\delta(H^{core})$ (ppm)
0	0	0.00E+00	0	7.707	8.689	7.159	6.607	7.736
5	5	1.09E-03	0.53	7.708	8.699	7.163	6.603	7.747
10	15	3.21E-03	1.55	7.709	8.716	7.168	6.598	7.755
10	25	5.25E-03	2.53	7.710	8.729	7.173	6.595	7.770
15	40	8.17E-03	3.94	7.711	8.745	7.180	6.590	7.789
20	60	1.18E-02	5.70	7.711	8.763	7.186	6.584	7.811
20	80	1.52E-02	7.33	7.712	8.776	7.191	6.578	7.828
25	105	1.91E-02	9.23	7.712	8.792	7.196	6.573	7.845
25	130	2.28E-02	10.97	7.713	8.803	7.199	6.570	7.859
35	165	2.74E-02	13.19	7.712	8.814	7.201	6.564	7.876
35	200	3.15E-02	15.19	7.712	8.825	7.206	6.561	7.888
50	250	3.68E-02	17.72	7.712	8.840	7.208	6.555	7.898
75	325	4.35E-02	20.94	7.710	8.852	7.211	6.547	7.911

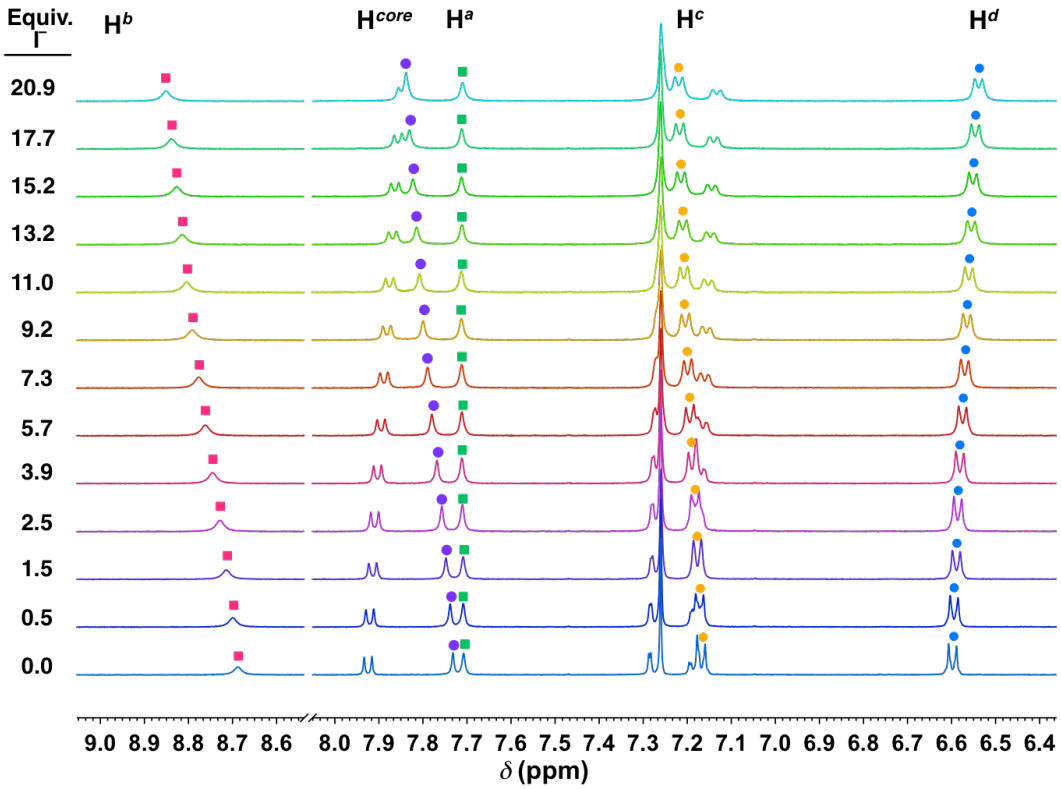

Figure 11. Example stacked spectra from the titration for the addition of tetrabutylammonium iodide to **3** in 10 % d_6-DMSO/$CDCl_3$.

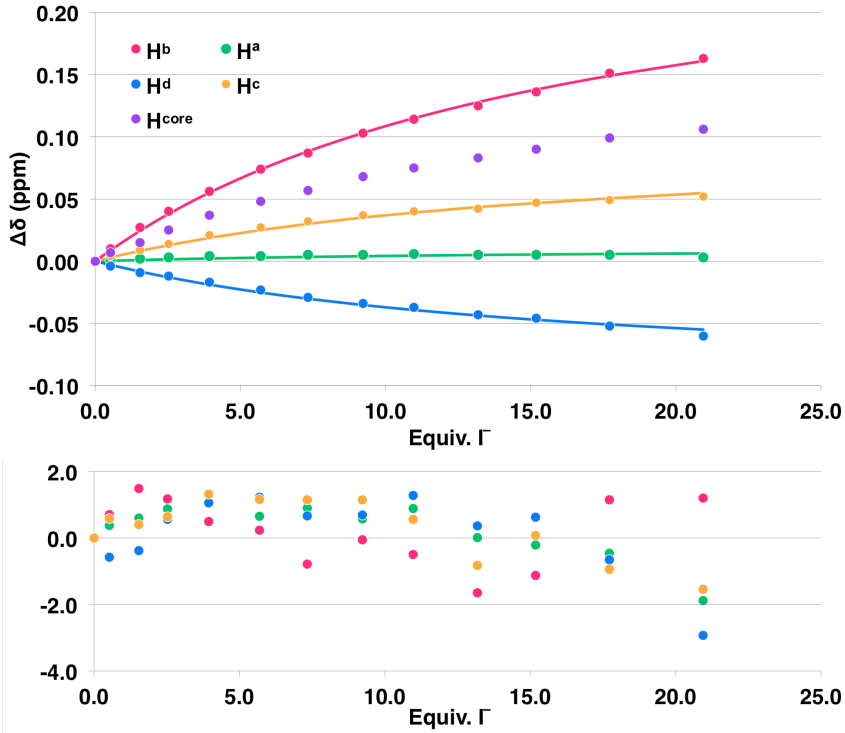

Figure 12. Example 1:1 fitting using non-linear regression from the data obtained for the titration of tetrabutylammonium iodide into **3** in 10 % d_6-DMSO/$CDCl_3$.

D.3.2. NMR Titrations of 1

Tetrabutylammonium perchlorate, 10 % DMSO-d_6/$CDCl_3$. A 3 mL stock solution of **1** (3.49 mg, [R] = 1.02 mM) in 10 % DMSO-d_6/$CDCl_3$ was prepared and used in the preparation of a 2 mL $TBAClO_4$ guest solution (9.29 mg, [G] = 13.59 mM). Starting volume of 500 µL. (Table 5, Figures 13 and 14)

Tetrabutylammonium perrhenate, 10 % DMSO-d_6/$CDCl_3$. A 3 mL stock solution of **1** (3.51 mg, [R] = 1.03 mM) in 10 % DMSO-d_6/$CDCl_3$ was prepared and used in the preparation of a 2 mL $TBAReO_4$ guest solution (11.62 mg, [G] = 13.52 mM). Starting volume of 500 µL. (Table 6, Figures 15 and 16)

Tetrabutylammonium hydrogen sulfate, 10 % DMSO-d_6/$CDCl_3$. A 3 mL stock solution of **1** (3.27 mg, [R] = 0.96 mM) in 10 % DMSO-d_6/$CDCl_3$ was prepared and used in the preparation of a 2 mL $TBAHSO_4$ guest solution (4.32 mg, [G] = 6.36 mM). Starting volume of 500 µL. (Table 7, Figures 17 and 18)

Table 5. Example titration for the addition of tetrabutylammonium perchlorate to **1** in 10 % d_6-DMSO/$CDCl_3$.

Addition (µL)	Total Volume Anion (µL)	[$TBAClO_4$] (M)	Equiv. ClO_4^-	$\delta(H^a)$ (ppm)	$\delta(H^b)$ (ppm)	$\delta(H^c)$ (ppm)	$\delta(H^d)$ (ppm)
0	0	0.00E+00	0	7.895	9.416	7.442	7.881
15	15	3.96E-04	0.39	7.893	9.400	7.449	7.878
15	30	7.69E-04	0.75	7.893	9.389	7.454	7.875
20	50	1.24E-03	1.21	7.891	9.378	7.459	7.872
20	70	1.67E-03	1.63	7.889	9.368	7.462	7.870
25	95	2.17E-03	2.12	7.890	9.361	7.466	7.867
30	125	2.72E-03	2.66	7.890	9.354	7.469	7.864
35	160	3.29E-03	3.22	7.890	9.347	7.471	7.863
40	200	3.88E-03	3.80	7.890	9.341	7.474	7.861
50	250	4.53E-03	4.43	7.890	9.336	7.476	7.859
60	310	5.20E-03	5.09	7.890	9.329	7.477	7.856
80	390	5.95E-03	5.83	7.889	9.325	7.479	7.853
125	515	6.90E-03	6.75	7.890	9.320	7.480	7.851
200	715	8.00E-03	7.82	7.889	9.316	7.480	7.849

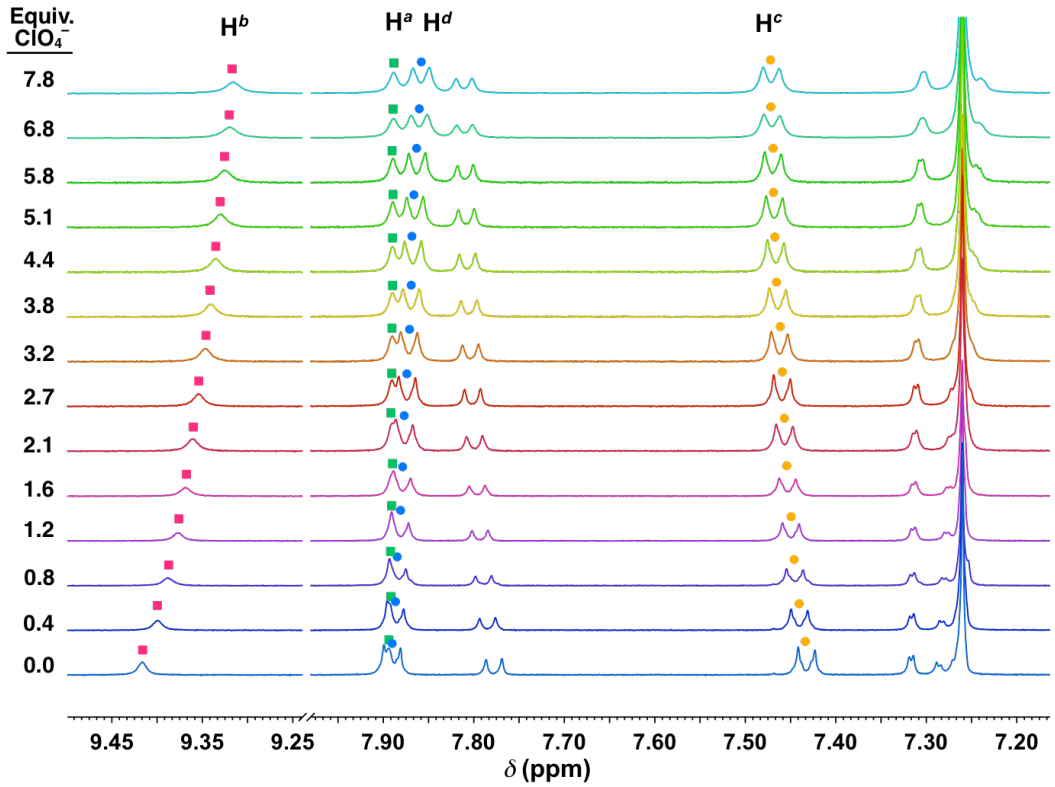

Figure 13. Example stacked spectra from the titration for the addition of tetrabutylammonium perchlorate to **1** in 10 % d_6-DMSO/$CDCl_3$.

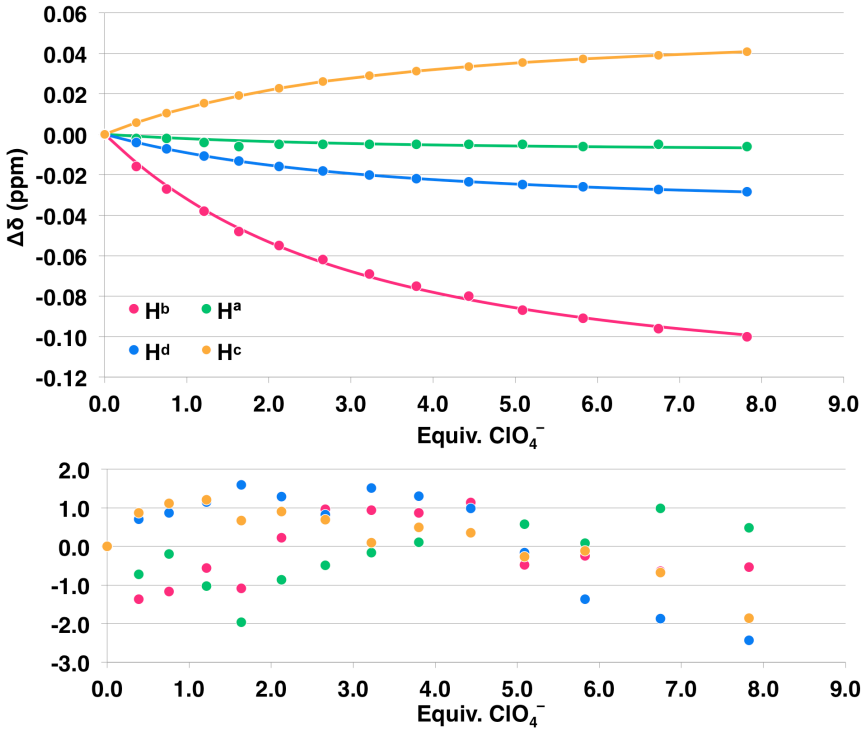

Figure 14. Example 1:1 fitting using non-linear regression from the data obtained for the titration of tetrabutylammonium perchlorate into **1** in 10 % d_6-DMSO/$CDCl_3$.

Table 6. Example titration for the addition of tetrabutylammonium perrhenate to **1** in 10 % d_6-DMSO/$CDCl_3$.

Addition (µL)	Total Volume Anion (µL)	[$TBAReO_4$] (M)	Equiv. ReO_4^-	$\delta(H^a)$ (ppm)	$\delta(H^b)$ (ppm)	$\delta(H^c)$ (ppm)	$\delta(H^d)$ (ppm)
0	0	0.00E+00	0	7.916	9.440	7.445	7.872
15	15	3.94E-04	0.38	7.921	9.419	7.454	7.869
20	35	8.85E-04	0.86	7.924	9.402	7.461	7.866
25	60	1.45E-03	1.41	7.927	9.387	7.468	7.864
30	90	2.06E-03	2.01	7.930	9.375	7.472	7.861
35	125	2.70E-03	2.63	7.930	9.364	7.478	7.857
40	165	3.36E-03	3.26	7.933	9.356	7.483	7.858
50	215	4.07E-03	3.96	7.933	9.347	7.484	7.860
60	275	4.80E-03	4.67	7.934	9.341	7.486	7.855
80	355	5.62E-03	5.46	7.934	9.334	7.487	7.854
100	455	6.44E-03	6.27	7.934	9.329	7.490	7.854
150	605	7.40E-03	7.20	7.934	9.324	7.489	7.854

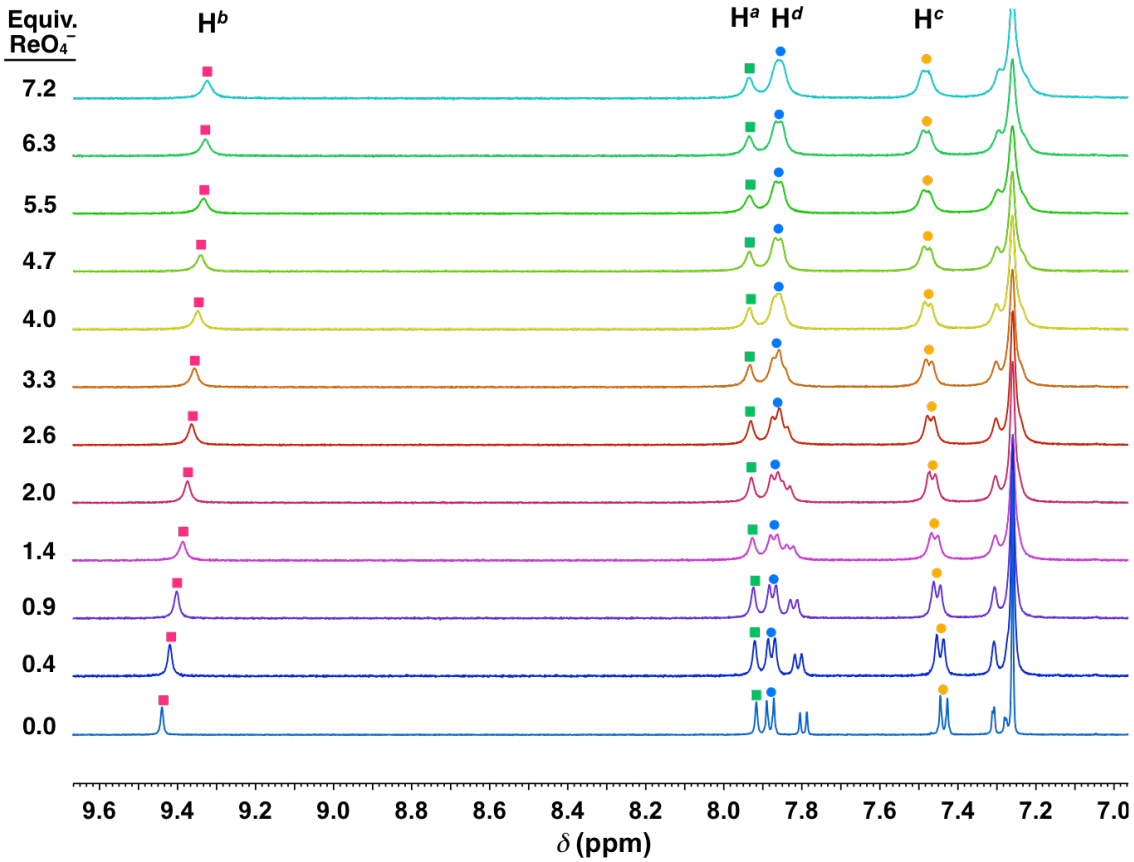

Figure 15. Example stacked spectra from the titration for the addition of tetrabutylammonium perrhenate to **1** in 10 % d_6-DMSO/$CDCl_3$.

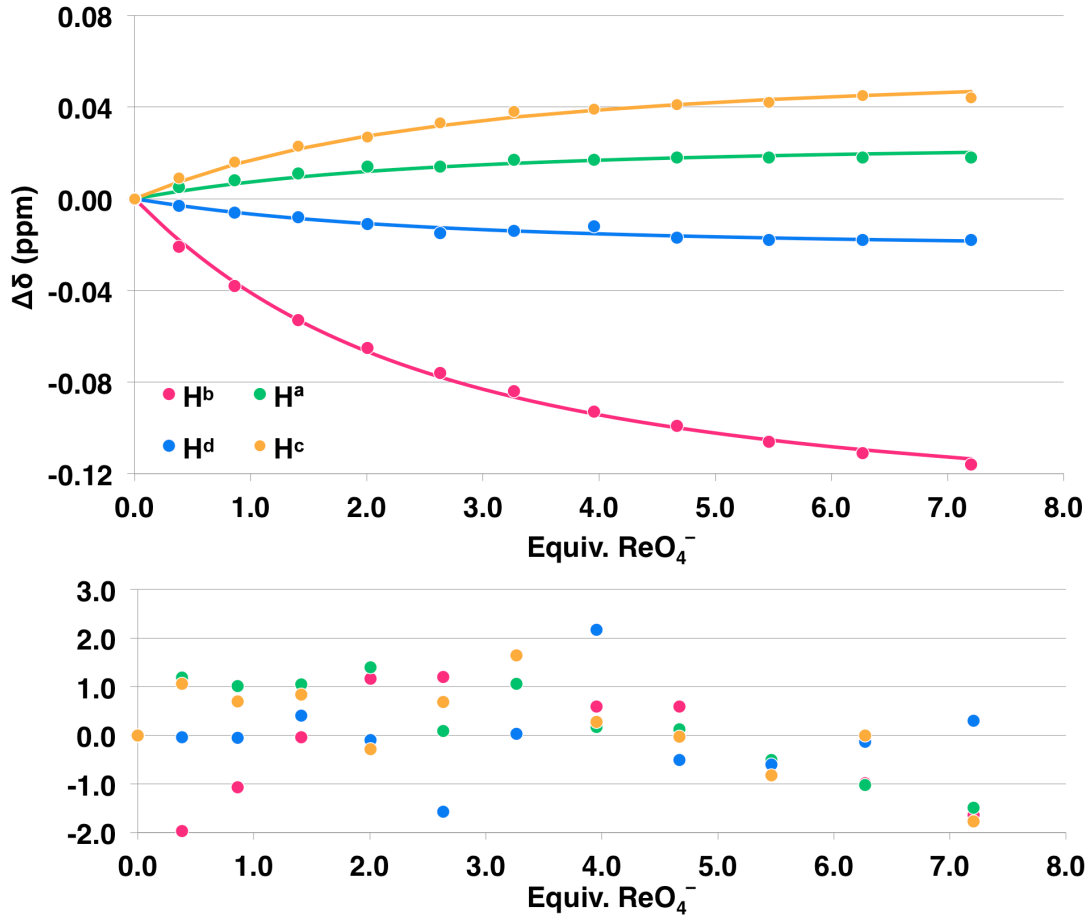

Figure 16. Example 1:1 fitting using non-linear regression from the data obtained for the titration of tetrabutylammonium perrhenate into **1** in 10 % d_6-DMSO/$CDCl_3$.

Table 7. Example titration for the addition of tetrabutylammonium hydrogen sulfate to **1** in 10 % d_6-DMSO/$CDCl_3$.

Addition (µL)	Total Volume Anion (µL)	[$TBAHSO_4$] (M)	Equiv. HSO_4^-	$\delta(H^a)$ (ppm)	$\delta(H^b)$ (ppm)	$\delta(H^c)$ (ppm)	$\delta(H^d)$ (ppm)
0	0	0.00E+00	0	7.889	9.367	7.434	7.882
10	10	1.25E-04	0.13	7.908	9.406	7.460	7.871
10	20	2.45E-04	0.26	7.939	9.449	7.489	7.854
10	30	3.60E-04	0.38	7.968	9.494	7.517	7.839
10	40	4.71E-04	0.49	7.997	9.537	7.544	7.826
10	50	5.78E-04	0.60	8.024	9.577	7.570	7.818
15	65	7.32E-04	0.76	8.059	9.631	7.602	7.807
15	80	8.77E-04	0.92	8.084	9.669	7.626	7.800
20	100	1.06E-03	1.11	8.102	9.697	7.644	7.795
20	120	1.23E-03	1.29	8.111	9.711	7.652	7.792
25	145	1.43E-03	1.49	8.115	9.719	7.656	7.790
50	195	1.78E-03	1.86	8.120	9.725	7.660	7.787
100	295	2.36E-03	2.46	8.122	9.730	7.662	7.784

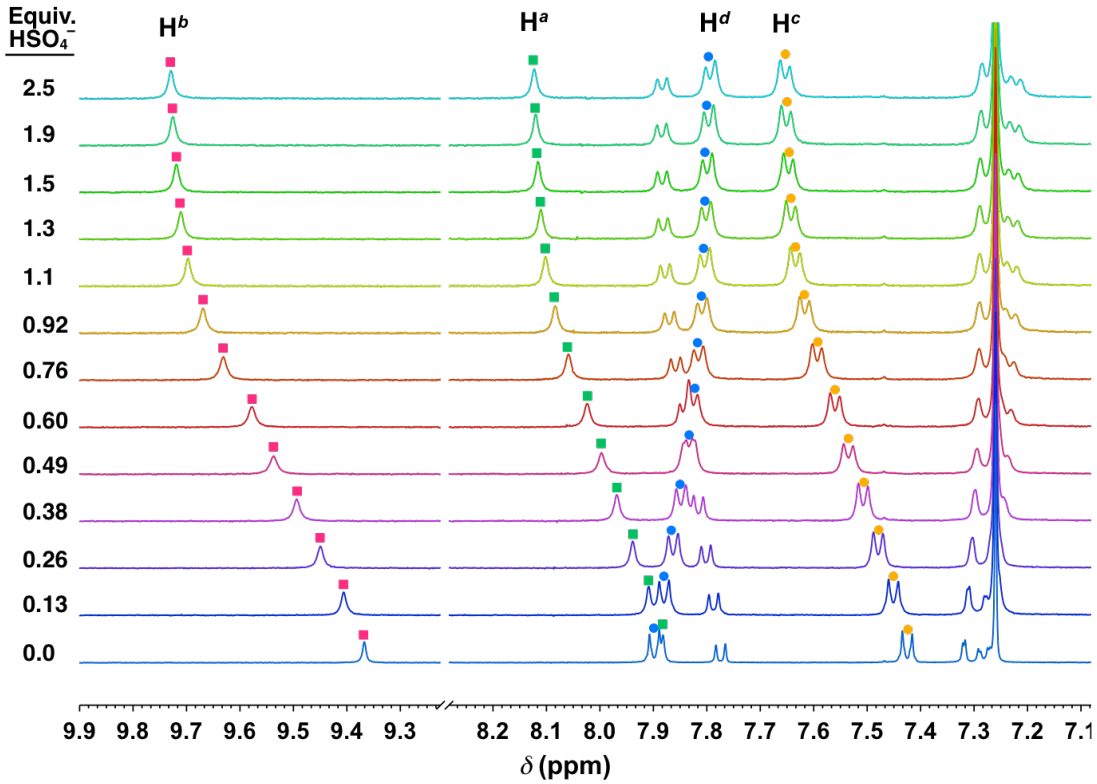

Figure 17. Example stacked spectra from the titration for the addition of tetrabutylammonium hydrogen sulfate to **1** in 10 % d_6-DMSO/$CDCl_3$.

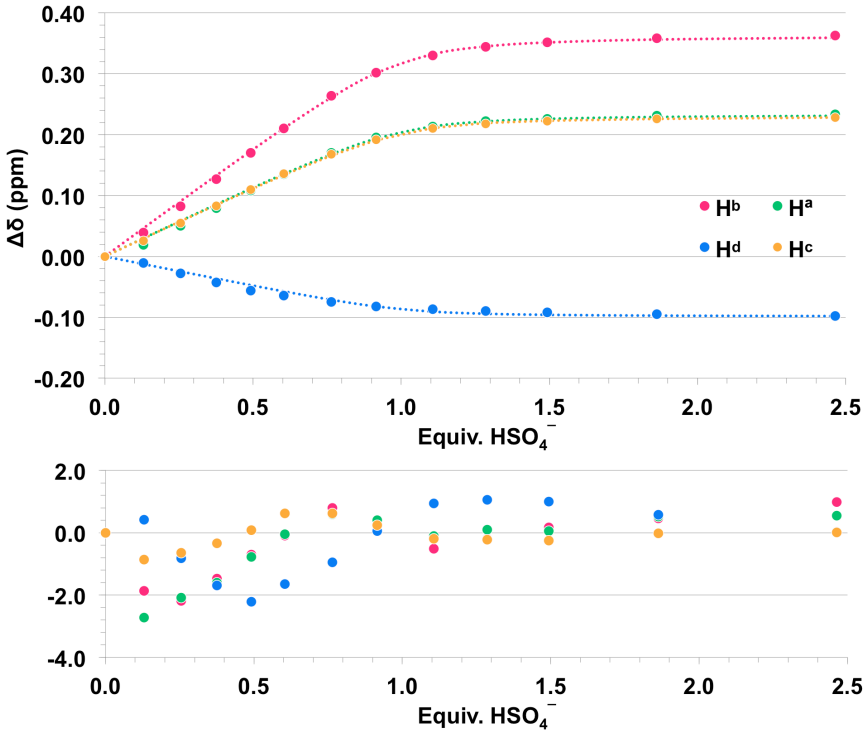

Figure 18. Plot of the change in chemical shift versus equivalents added of $TBAHSO_4$ during the titration in 10 % DMSO-d_6/$CDCl_3$.

Tetrabutylammonium hydrogen sulfate, 15 % DMSO-d_6/$CDCl_3$. A 3 mL stock solution of **1** (3.35 mg, [R] = 0.98 mM) in 15 % DMSO-d_6/$CDCl_3$ was prepared and used in the preparation of a 2 mL $TBAHSO_4$ guest solution (3.92 mg, [G] = 5.77 mM). Starting volume of 500 µL. (Table 8, Figures 19 and 20)

Tetrabutylammonium hydrogen sulfate, 20 % DMSO-d_6/$CDCl_3$. A 3 mL stock solution of **1** (3.43 mg, [R] = 1.00 mM) in 20 % DMSO-d_6/$CDCl_3$ was prepared and used in the preparation of a 2 mL $TBAHSO_4$ guest solution (4.98 mg, [G] = 7.34 mM). Starting volume of 500 µL. (Table 9, Figures 21 and 22)

Tetrabutylammonium sulfate, 10 % DMSO-d_6/$CDCl_3$, 25 °C. A 3 mL stock solution of **1** (3.34 mg, [R] = 1.03 mM) in 10 % DMSO-d_6/$CDCl_3$ was prepared and used in the preparation of a 2 mL $TBASO_4$ guest solution (10.0 µL, 9.9 mg, [G] = 8.53 mM). Starting volume of 500 µL. ^{1}H NMR spectra were taken of 0.0 µL (0.0 µL total, 0.0 mM [$TBASO_4$]), 15.0 µL (15.0 µL total, 0.25 mM [$TBASO_4$]), and then 20.0 µL (35.0 µL total, 0.56 mM [$TBASO_4$]) additions of the sulfate•host solution. (Figures 23)

Table 8. Example titration for the addition of tetrabutylammonium hydrogen sulfate to **1** in 15 % d_6-DMSO/$CDCl_3$.

Addition (µL)	Total Volume Anion (µL)	[$TBAHSO_4$] (M)	Equiv. HSO_4^-	$\delta(H^a)$ (ppm)	$\delta(H^b)$ (ppm)	$\delta(H^c)$ (ppm)	$\delta(H^d)$ (ppm)
0	0	0.00E+00	0	7.871	9.543	7.378	7.758
10	10	1.13E-04	0.12	7.886	9.578	7.393	7.750
10	20	2.22E-04	0.23	7.901	9.608	7.408	7.742
15	35	3.78E-04	0.39	7.924	9.647	7.431	7.730
15	50	5.25E-04	0.54	7.946	9.678	7.454	7.722
20	70	7.09E-04	0.72	7.969	9.705	7.477	7.711
20	90	8.81E-04	0.90	7.987	9.719	7.497	7.706
20	110	1.04E-03	1.06	7.999	9.725	7.510	7.702
30	140	1.26E-03	1.29	8.010	9.732	7.523	7.697
40	180	1.53E-03	1.56	8.019	9.724	7.533	7.693
50	230	1.82E-03	1.85	8.025	9.716	7.540	7.690
60	290	2.12E-03	2.16	8.029	9.709	7.544	7.688
75	365	2.44E-03	2.48	8.031	9.700	7.548	7.687
100	465	2.78E-03	2.84	8.033	9.695	7.549	7.685

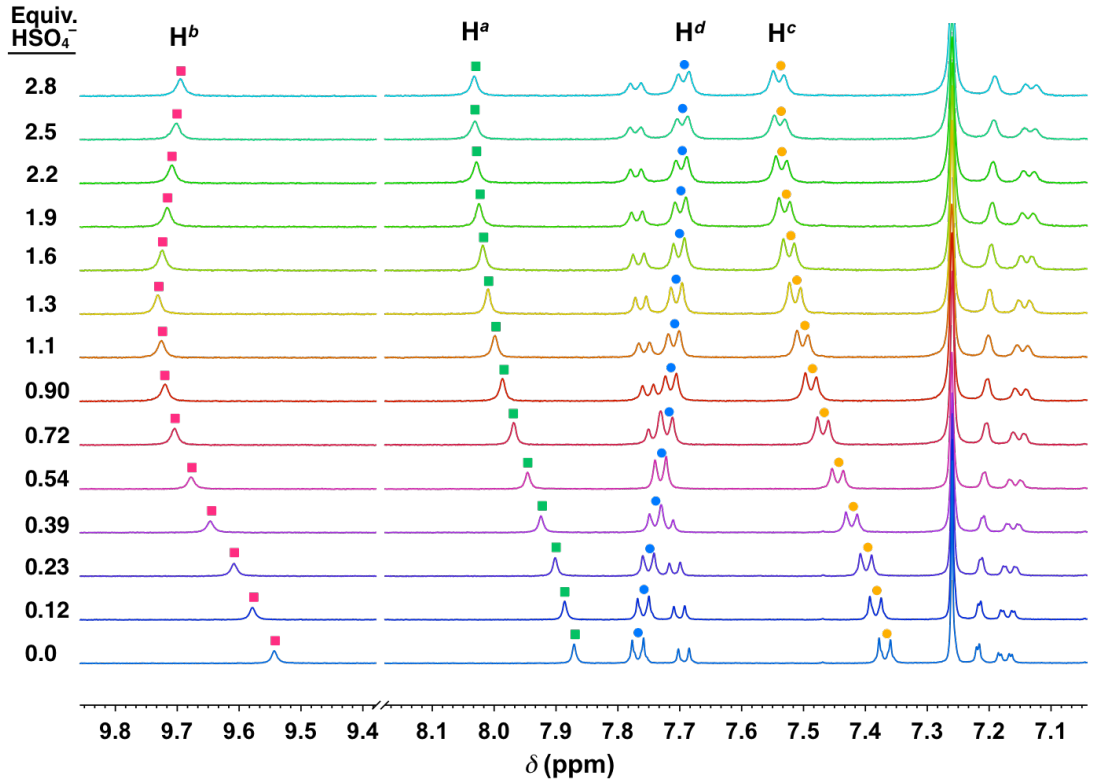

Figure 19. Example stacked spectra from the titration for the addition of tetrabutylammonium hydrogen sulfate to **1** in 15 % d_6-DMSO/$CDCl_3$.

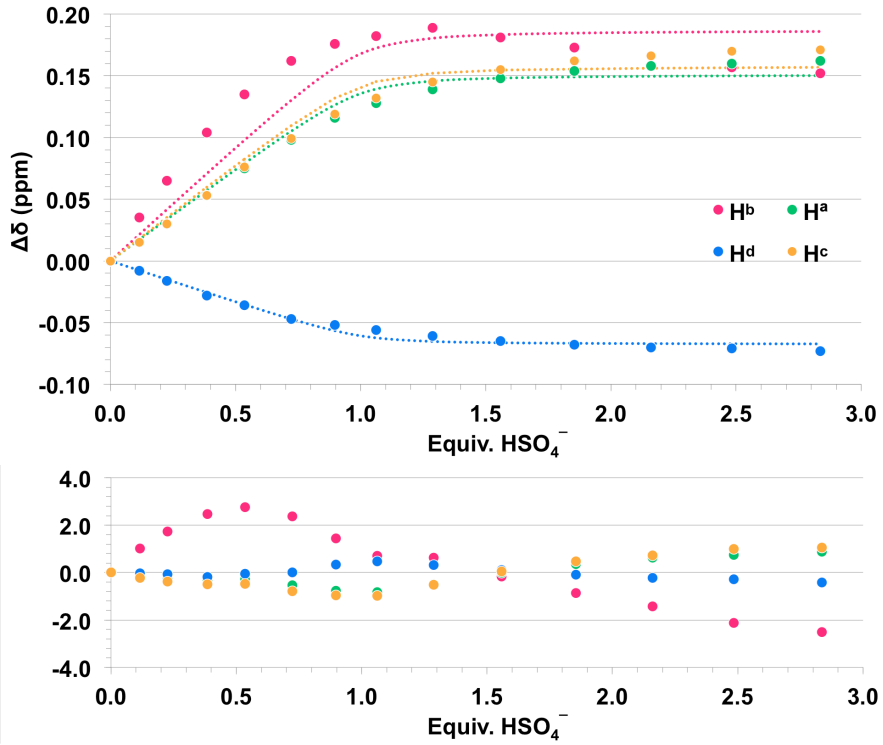

Figure 20. Plot of the change in chemical shift versus equivalents added of $TBAHSO_4$ during the titration in 15 % DMSO-d_6/$CDCl_3$.

Table 9. Example titration for the addition of tetrabutylammonium hydrogen sulfate to **1** in 20 % d_6-DMSO/$CDCl_3$.

Addition (µL)	Total Volume Anion (µL)	[$TBAHSO_4$] (M)	Equiv. HSO_4^-	$\delta(H^a)$ (ppm)	$\delta(H^b)$ (ppm)	$\delta(H^c)$ (ppm)	$\delta(H^d)$ (ppm)
0	0	0.00E+00	0	7.772	9.329	7.249	7.672
10	10	1.44E-04	0.14	7.792	9.358	7.271	7.661
10	20	2.82E-04	0.28	7.812	9.387	7.294	7.651
15	35	4.80E-04	0.48	7.838	9.423	7.323	7.637
15	50	6.67E-04	0.66	7.860	9.451	7.346	7.627
15	65	8.44E-04	0.84	7.876	9.472	7.365	7.619
20	85	1.07E-03	1.06	7.891	9.492	7.383	7.610
20	105	1.27E-03	1.27	7.903	9.506	7.396	7.605
25	130	1.51E-03	1.51	7.911	9.517	7.405	7.600
35	165	1.82E-03	1.81	7.918	9.525	7.414	7.595
50	215	2.21E-03	2.20	7.925	9.532	7.421	7.591
70	285	2.66E-03	2.65	7.928	9.536	7.426	7.588
100	385	3.19E-03	3.18	7.933	9.539	7.431	7.585

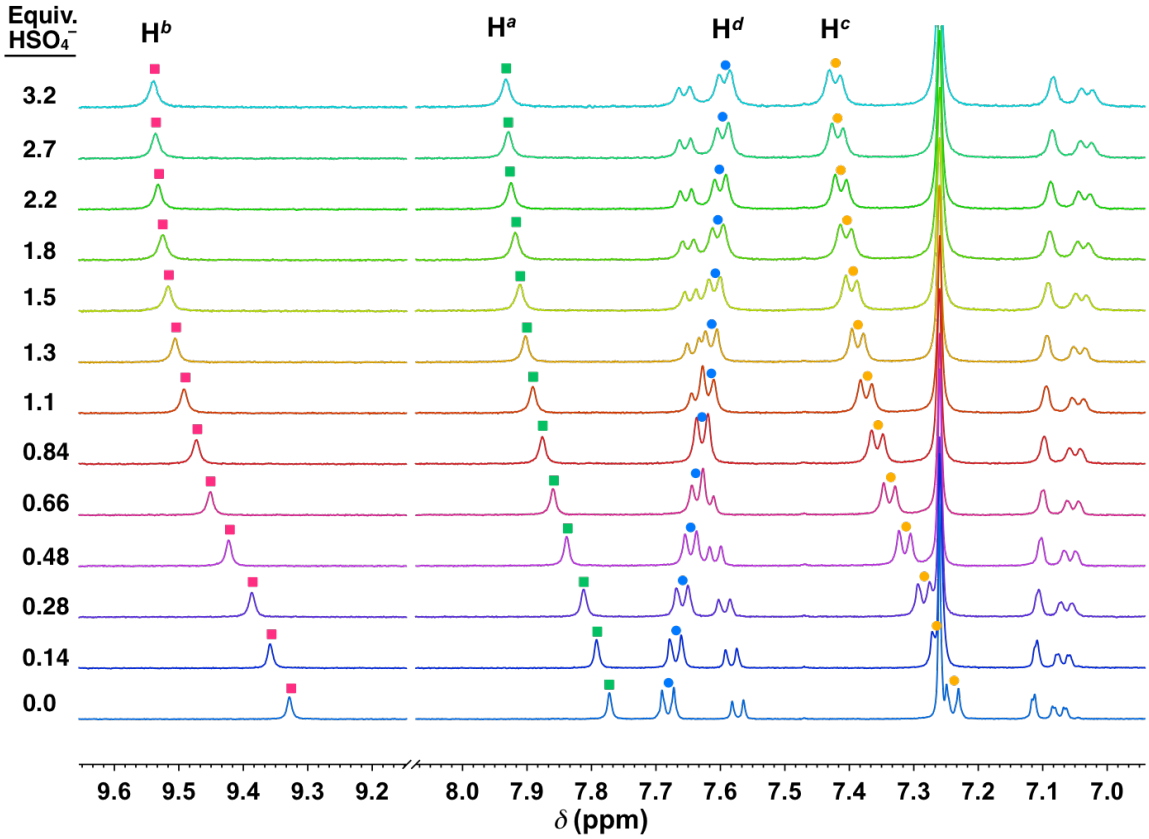

Figure 21. Example stacked spectra from the titration for the addition of tetrabutylammonium hydrogen sulfate to **1** in 20 % d_6-DMSO/$CDCl_3$.

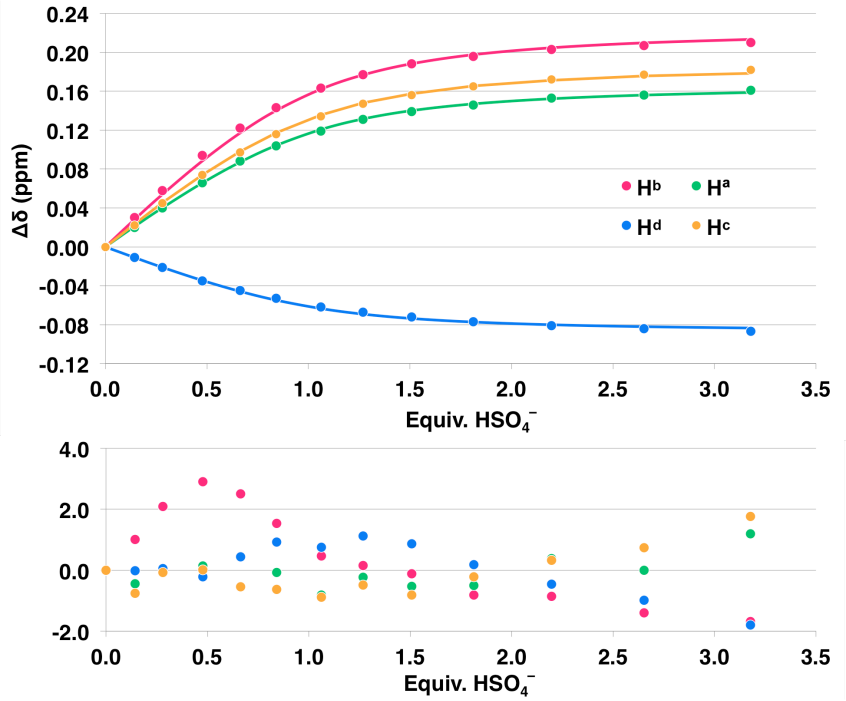

Figure 22. Example 1:1 fitting using non-linear regression from the data obtained for the titration of tetrabutylammonium hydrogen sulfate into **1** in 20 % d_6-DMSO/$CDCl_3$.

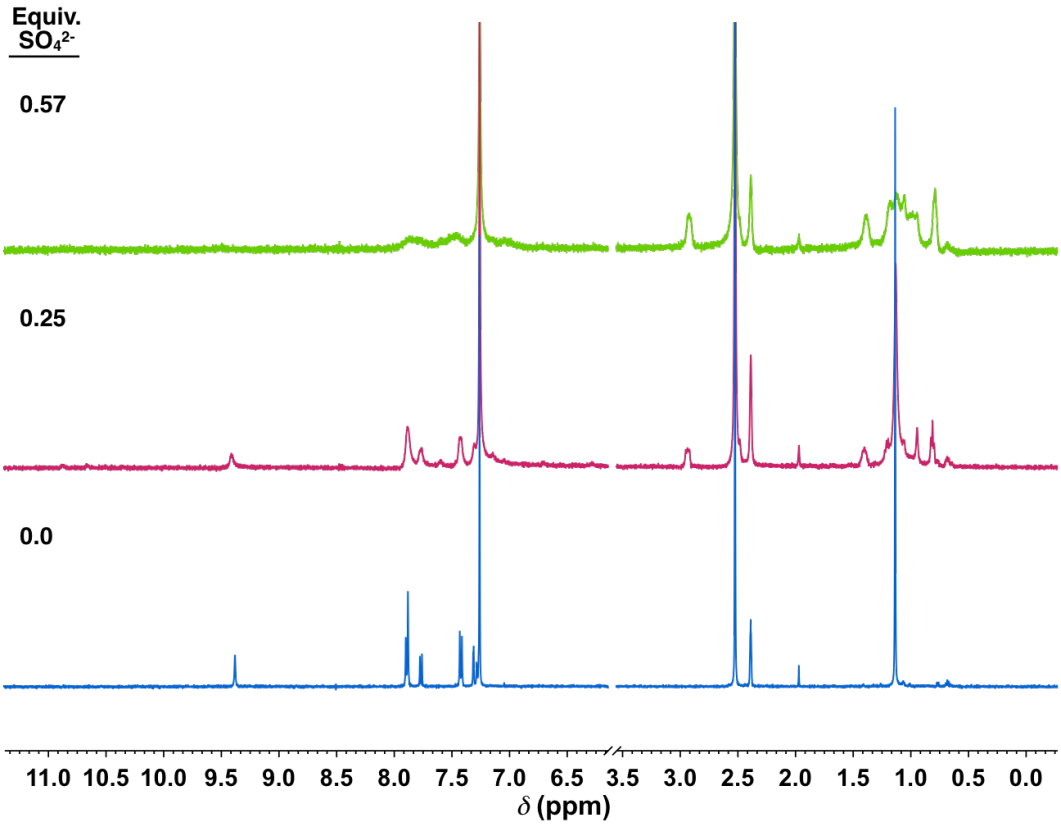

Figure 23. Example stacked spectra taken at 25 °C from the titration for the addition of tetrabutylammonium sulfate to **1** in 10 % d_6-DMSO/$CDCl_3$.

Tetrabutylammonium sulfate, 10 % DMSO-d_6/$CDCl_3$, -20 °C. A 3 mL stock solution of **1** (3.58 mg, [R] = 1.05 mM) in 10 % DMSO-d_6/$CDCl_3$ was prepared and used in the preparation of a 2 mL $TBASO_4$ guest solution (10.0 µL, 9.9 mg, [G] = 8.53 mM). Starting volume of 500 µL. ^1H and ^{19}F NMR spectra were taken of 0.0 µL (0.0 µL total, 0.0 mM [$TBASO_4$]), 35.0 mL (35.0 mL total, 0.56 mM [$TBASO_4$]), 35.0 µL (70.0 µL total, 1.05 mM [$TBASO_4$]), and lastly 45.0 µL (115.0 µL total, 1.60 mM [$TBASO_4$]) additions of the sulfate•host solution. ^{19}F NMR spectra are shown with line broadening applied (0.3). (Figures 24 and 25)

Tetrabutylammonium acetate, 10 % DMSO-d_6/$CDCl_3$. A 3 mL stock solution of **1** (3.53 mg, [R] = 1.03 mM) in 10 % DMSO-d_6/$CDCl_3$ was prepared and used in the preparation of a 2 mL TBAOAc guest solution (4.13 mg, [G] = 6.86 mM). Starting volume of 500 µL. (Table 10, Figures 26 and 27)

Tetrabutylammonium acetate, 20 % DMSO-d_6/$CDCl_3$. A 3 mL stock solution of **1** (3.36 mg, [R] = 0.98 mM) in 20 % DMSO-d_6/$CDCl_3$ was prepared and used in the preparation of a 2 mL TBAOAc guest solution (5.86 mg, [G] = 9.72 mM). Starting volume of 500 µL. (Table 11, Figures 28 and 29)

Tetrabutylammonium acetate, 50 % DMSO-d_6/$CDCl_3$. A 3 mL stock solution of **1** (3.39 mg, [R] = 0.99 mM) in 50 % DMSO-d_6/$CDCl_3$ was prepared and used in the preparation of a 2 mL TBAOAc guest solution (6.44 mg, [G] = 10.68 mM). Starting volume of 500 µL. (Table 12, Figures 30, 31, and 32)

Tetrabutylammonium dihydrogen phosphate, 10 % DMSO-d_6/$CDCl_3$. A 3 mL stock solution of **1** (3.28 mg, [R] = 0.96 mM) in 10 % DMSO-d_6/$CDCl_3$ was prepared and used in the preparation of a 2 mL $TBAH_2PO_4$ guest solution (2.68 mg, [G] = 6.94 mM). Starting volume of 500 µL. Reliable data is unobtainable near saturation of the host's binding sites. (Table 13, Figure 33 and 34)

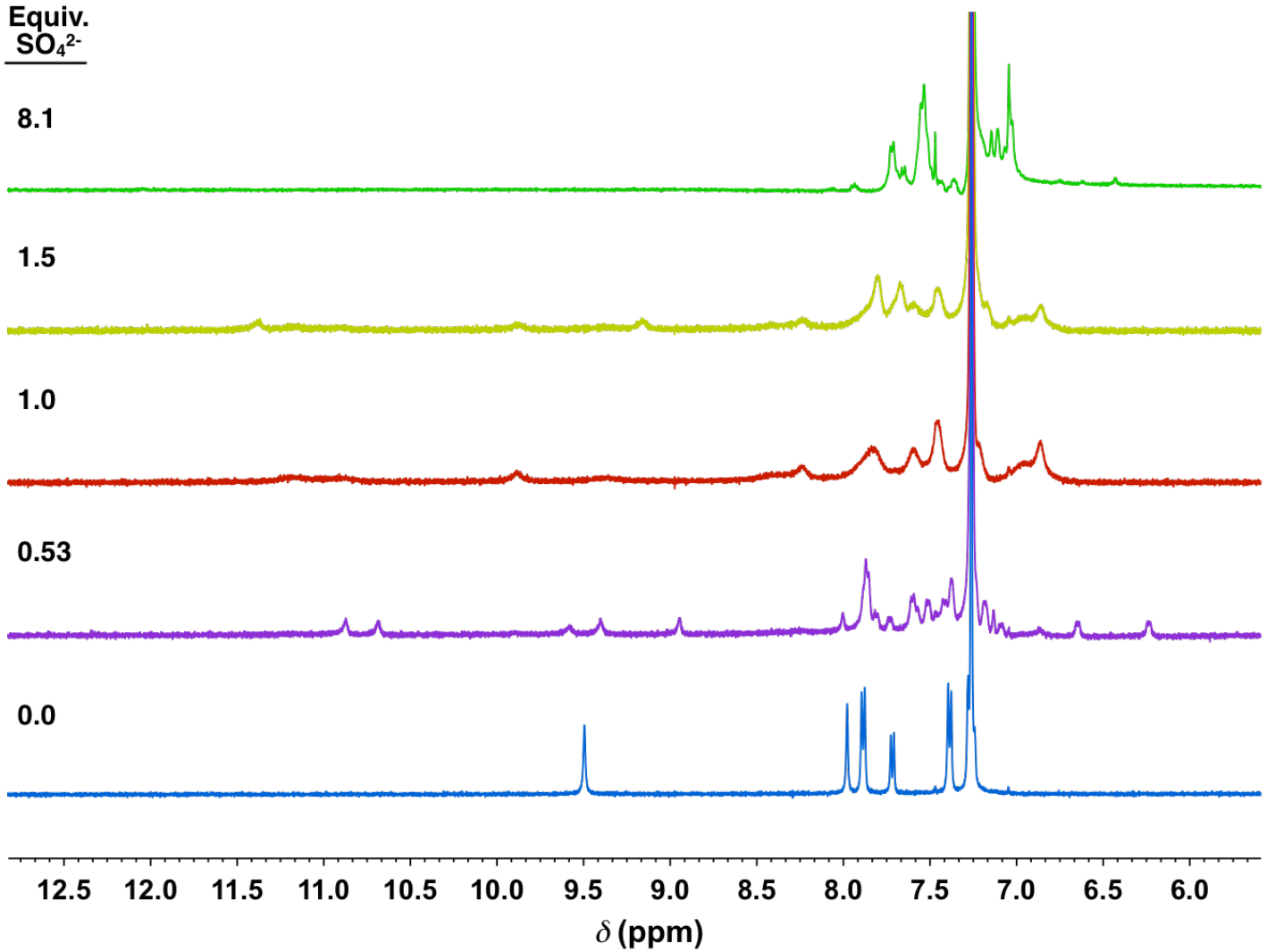

Figure 24. Example stacked ^{1}H NMR spectra taken at -20 °C from the titration for the addition of tetrabutylammonium sulfate to **1** in 10 % d_6-DMSO/$CDCl_3$.

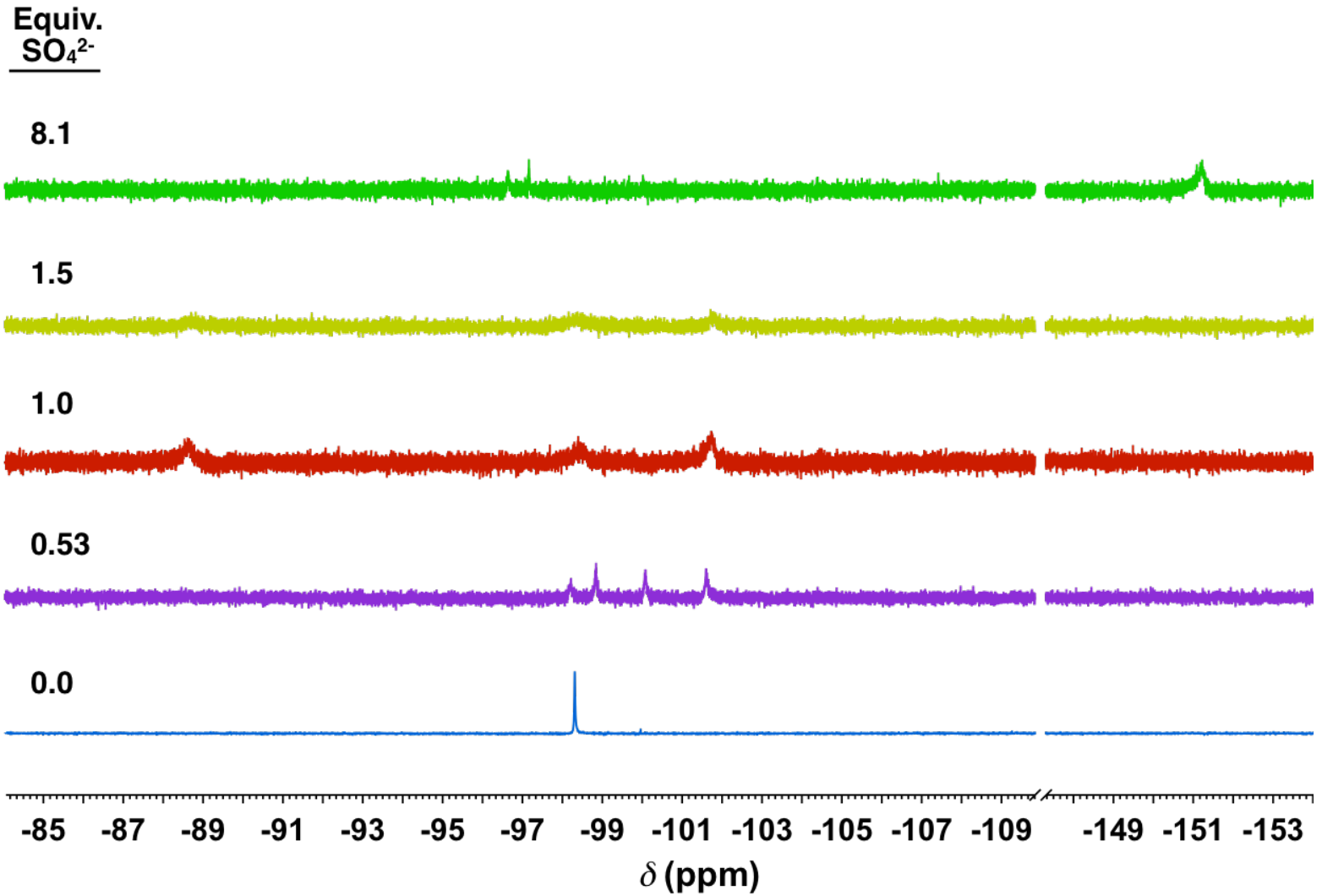

Figure 25. Example stacked ^{19}F NMR spectra taken at -20 °C from the titration for the addition of tetrabutylammonium sulfate to **1** in 10 % d_6-DMSO/$CDCl_3$.

Table 10. Example titration for the addition of tetrabutylammonium acetate to **1** in 10 % d_6-DMSO/$CDCl_3$.

Addition (µL)	Total Volume Anion (µL)	[TBAOAc] (M)	Equiv. AcO^-	$\delta(H^a)$ (ppm)	$\delta(H^b)$ (ppm)	$\delta(H^c)$ (ppm)	$\delta(H^d)$ (ppm)
0	0	0.00E+00	0	7.902	9.372	7.437	7.887
10	10	1.34E-04	0.13	7.986	9.545	7.436	7.853
10	20	2.64E-04	0.26	8.086	9.732	7.440	7.822
10	30	3.88E-04	0.38	8.177	9.934	7.448	7.797
10	40	5.08E-04	0.49	8.264	10.130	7.465	7.780
10	50	6.23E-04	0.60	8.336	10.315	7.487	7.776
15	65	7.89E-04	0.76	8.434	10.587	7.524	7.776
15	80	9.46E-04	0.91	8.515	10.828	7.557	7.781
20	100	1.14E-03	1.11	8.596	11.000	7.583	7.785
20	120	1.33E-03	1.28	8.654	11.071	7.591	7.783
25	145	1.54E-03	1.49	8.713	11.129	7.597	7.781
35	180	1.81E-03	1.76	8.781	11.192	7.603	7.779
50	230	2.16E-03	2.09	8.857	11.261	7.608	7.775

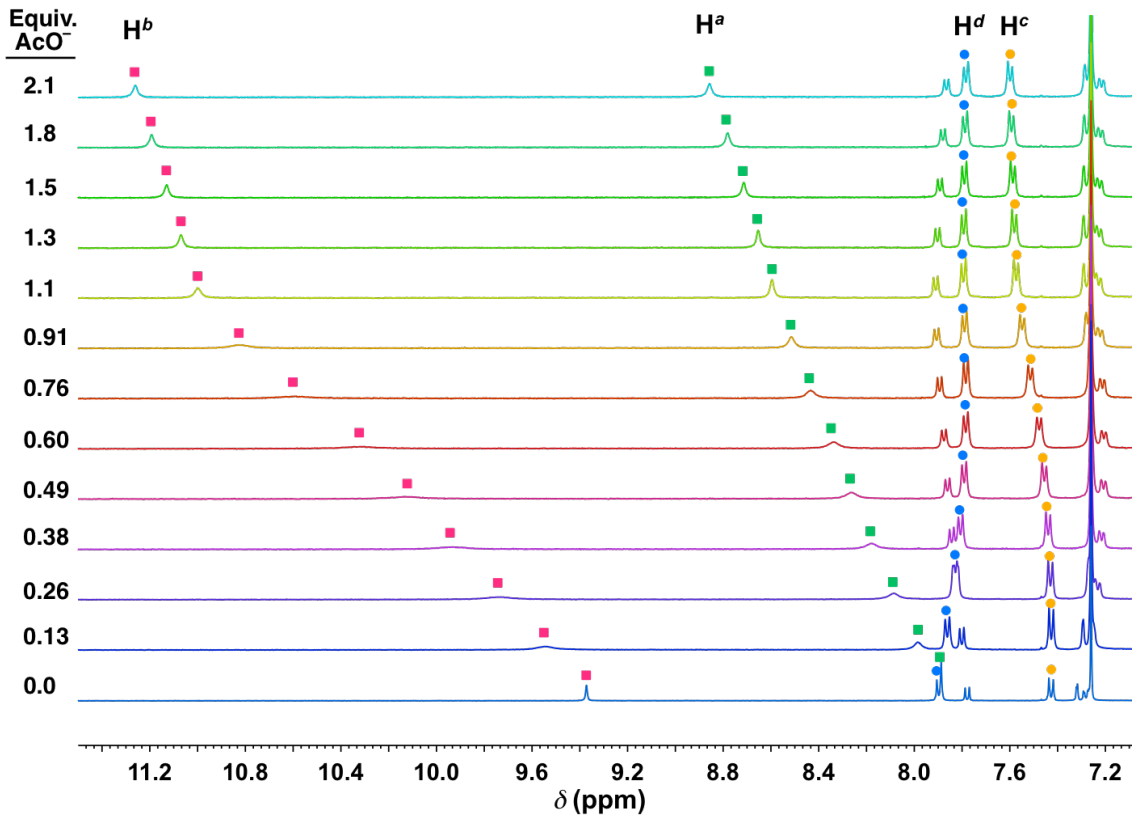

Figure 26. Example stacked spectra from the titration for the addition of tetrabutylammonium acetate to **1** in 10 % d_6-DMSO/$CDCl_3$.

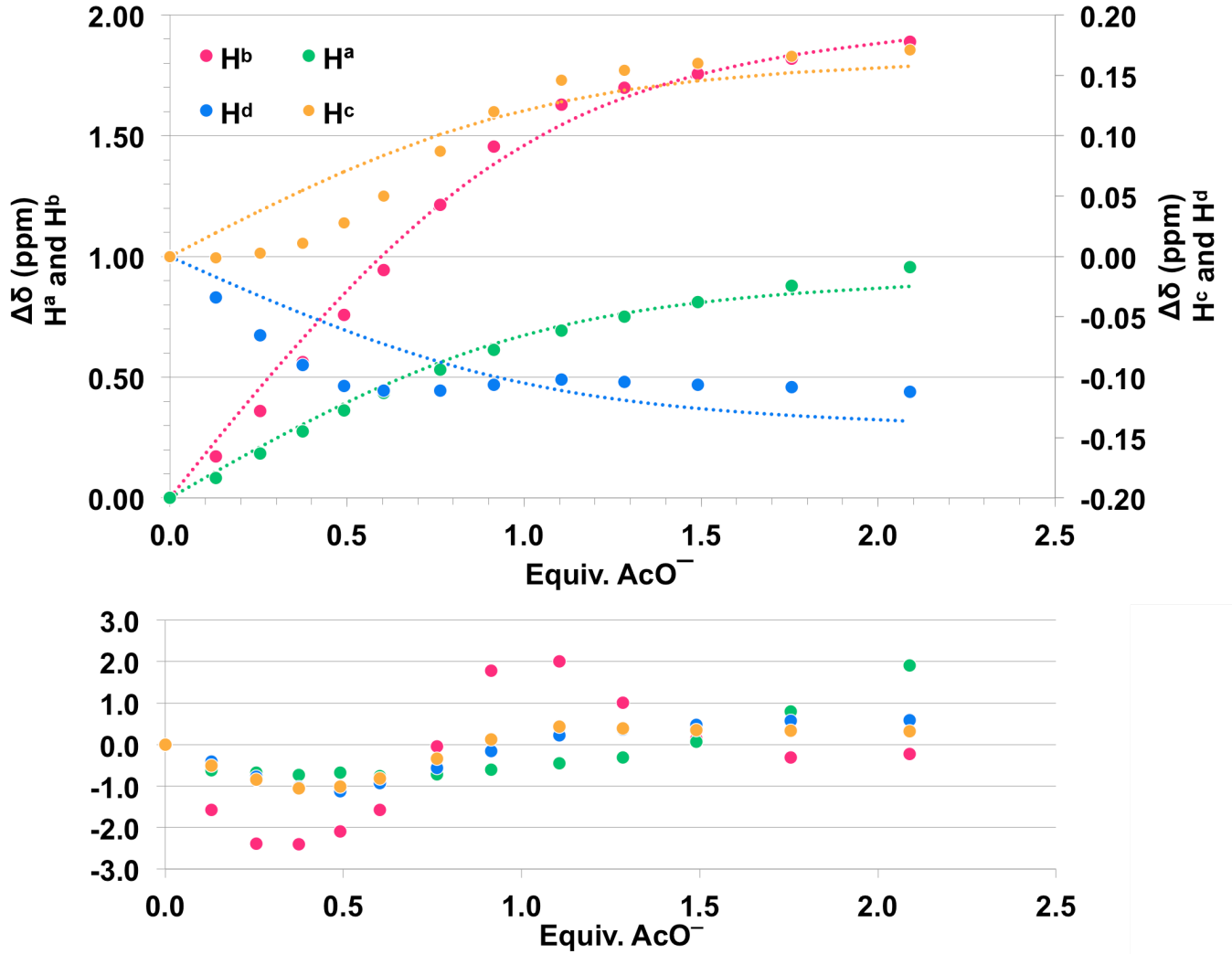

Figure 27. Plot of the change in chemical shift versus equivalents added of TBAOAc during the titration in 10 % DMSO-d_6/$CDCl_3$.

Table 11. Example titration for the addition of tetrabutylammonium acetate to **1** in 20 % d_6-DMSO/$CDCl_3$.

Addition (µL)	Total Volume Anion (µL)	[TBAOAc] (M)	Equiv. AcO^-	$\delta(H^a)$ (ppm)	$\delta(H^b)$ (ppm)	$\delta(H^c)$ (ppm)	$\delta(H^d)$ (ppm)
0	0	0.00E+00	0	7.761	9.288	7.240	7.675
10	10	1.91E-04	0.19	7.871	9.528	7.260	7.650
10	20	3.74E-04	0.38	7.993	9.816	7.280	7.628
10	30	5.50E-04	0.56	8.107	10.097	7.305	7.611
10	40	7.20E-04	0.73	8.210	10.339	7.329	7.597
15	55	9.63E-04	0.98	8.340	10.656	7.364	7.584
15	70	1.19E-03	1.21	8.420	10.814	7.381	7.579
15	85	1.41E-03	1.44	8.468	10.874	7.387	7.576
20	105	1.69E-03	1.71	8.521	10.929	7.390	7.573
25	130	2.01E-03	2.04	8.580	10.986	7.395	7.568
35	165	2.41E-03	2.45	8.648	11.051	7.400	7.564

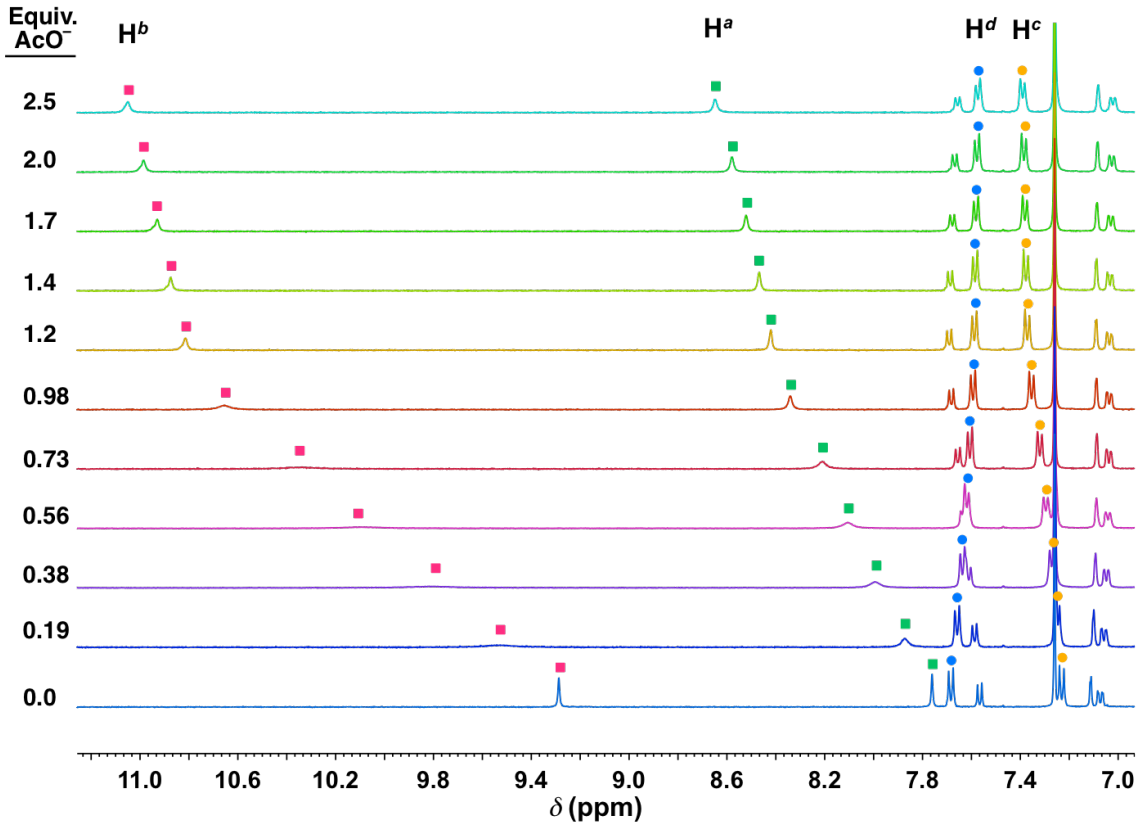

Figure 28. Example stacked spectra from the titration for the addition of tetrabutylammonium acetate to **1** in 20 % d_6-DMSO/$CDCl_3$.

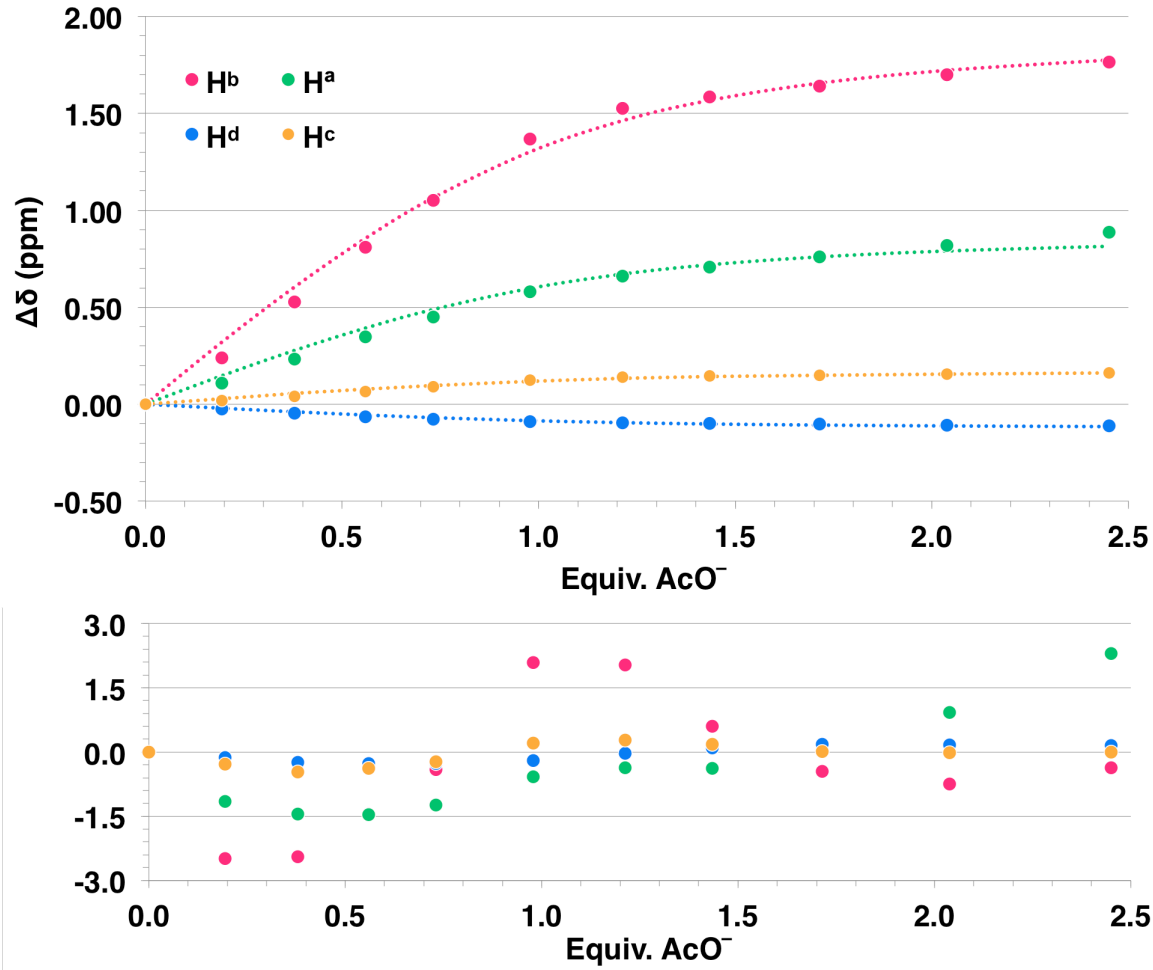

Figure 29. Example 1:1 fitting using non-linear regression from the data obtained for the titration of tetrabutylammonium acetate into **1** in 20 % d_6-DMSO/$CDCl_3$.

Table 12. Example titration for the addition of tetrabutylammonium acetate to **1** in 50 % d_6-DMSO/$CDCl_3$.

Addition (µL)	Total Volume Anion (µL)	[TBAOAc] (M)	Equiv. AcO^-	$\delta(H^a)$ (ppm)	$\delta(H^b)$ (ppm)	$\delta(H^c)$ (ppm)	$\delta(H^d)$ (ppm)
0	0	0.00E+00	0	7.498	9.031	6.837	7.252
10	10	2.09E-04	0.21	7.580	9.221	6.851	7.239
10	20	4.11E-04	0.41	7.675	9.442	6.869	7.225
10	30	6.05E-04	0.61	7.763	9.640	6.886	7.213
10	40	7.91E-04	0.80	7.844	9.826	6.901	7.200
10	50	9.71E-04	0.98	7.913	9.977	6.914	7.191
10	60	1.14E-03	1.15	7.971	10.104	6.923	7.182
15	75	1.39E-03	1.40	8.038	10.235	6.935	7.176
20	95	1.71E-03	1.72	8.102	10.345	6.943	7.167
30	125	2.14E-03	2.15	8.168	10.441	6.950	7.162
40	165	2.65E-03	2.67	8.233	10.519	6.956	7.158
50	215	3.21E-03	3.23	8.293	10.591	6.961	7.153

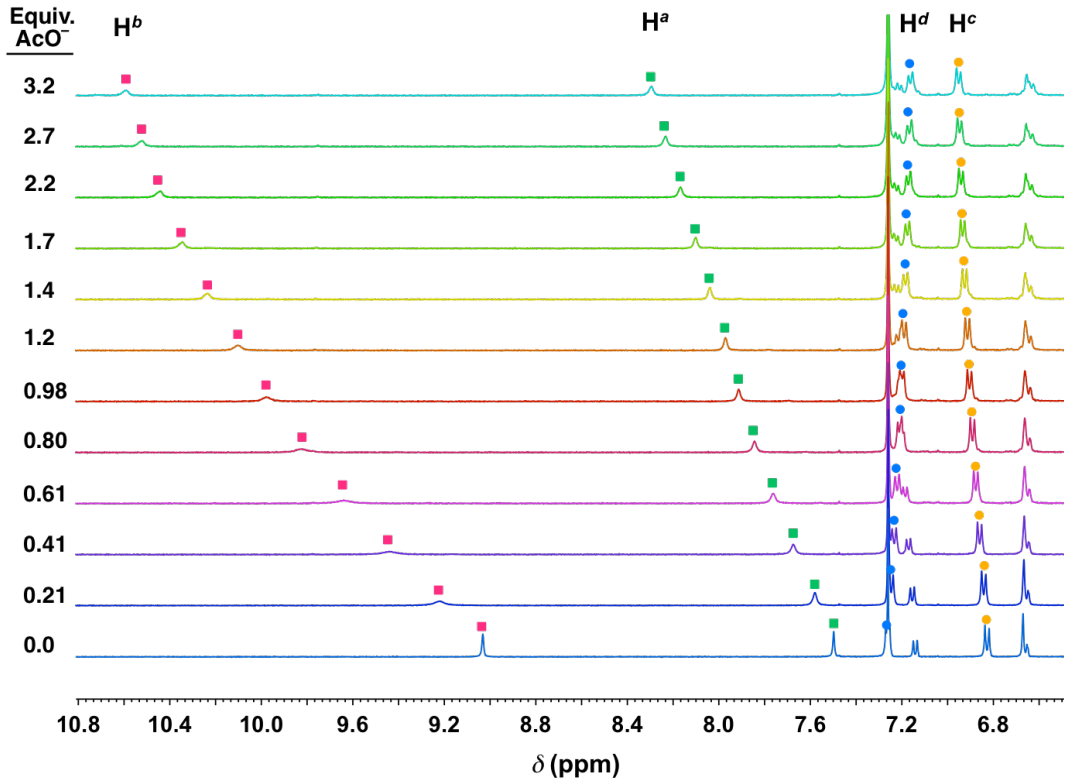

Figure 30. Stacked spectra from the titration for the addition of tetrabutylammonium acetate to **1** in 50 % d_6-DMSO/$CDCl_3$.

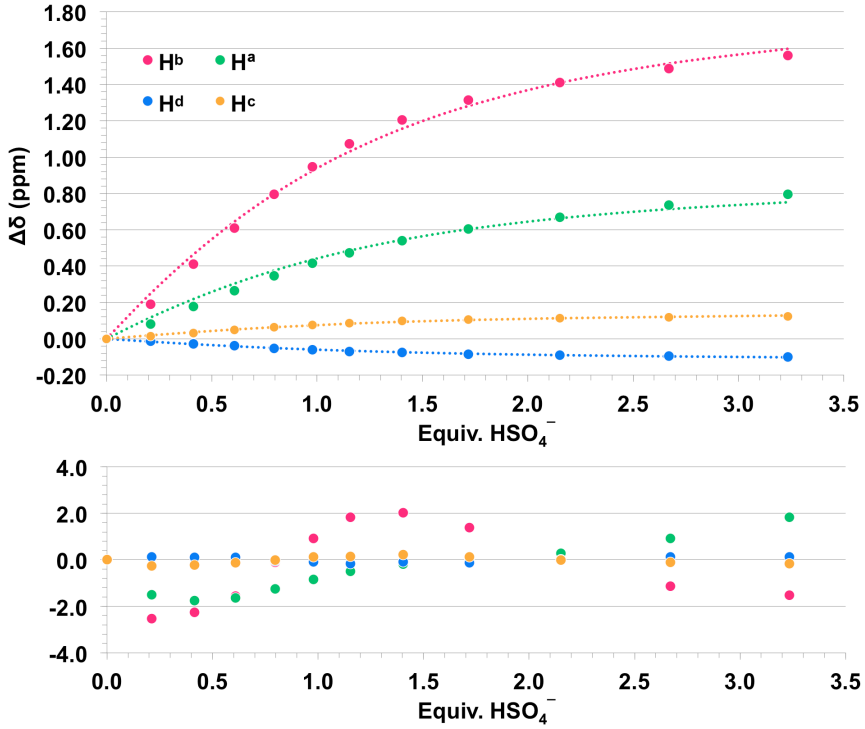

Figure 31. Example 1:1 fitting using non-linear regression from the data obtained for the titration of tetrabutylammonium acetate into **1** in 50 % d_6-DMSO/$CDCl_3$.

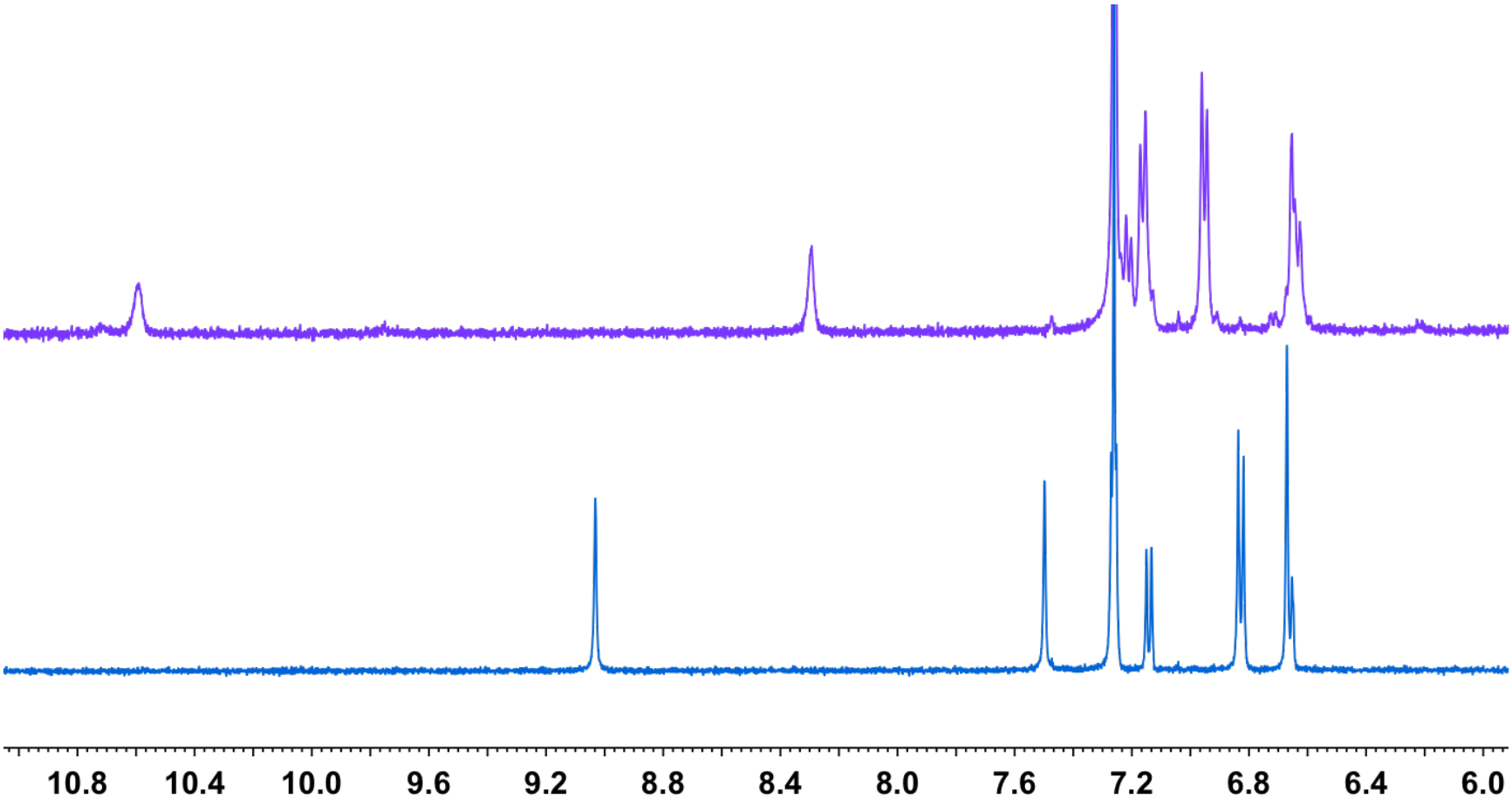

Figure 32. Host **1** in 50 % d_6-DMSO/$CDCl_3$ before addition of tetrabutylammonium acetate (bottom) and after saturation (top).

Table 13. Example titration for the addition of tetrabutylammonium dihydrogen phosphate to **1** in 10 % d_6-DMSO/$CDCl_3$.

Addition (µL)	Total Volume Anion (µL)	[$TBAH_2PO_4$] (M)	Equiv. $H_2PO_4^-$	$\delta(H^a)$ (ppm)	$\delta(H^b)$ (ppm)	$\delta(H^c)$ (ppm)	$\delta(H^d)$ (ppm)
0	0	0.00E+00	0	7.880	9.365	7.433	7.890
20	20	1.52E-04	0.16	7.994	9.600	7.465	7.850
20	40	2.92E-04	0.30	8.094	9.828	7.493	7.814
20	60	4.22E-04	0.44	8.182	10.018	7.516	7.789
20	80	5.44E-04	0.57	8.250	10.184	7.543	7.771
25	105	6.84E-04	0.71	8.311	10.368	7.552	7.747
25	130	8.14E-04	0.85	8.364	10.523	7.563	7.729
30	160	9.56E-04	1.00	8.411	—	7.579	7.709
40	200	1.13E-03	1.17	8.454	—	7.602	7.692

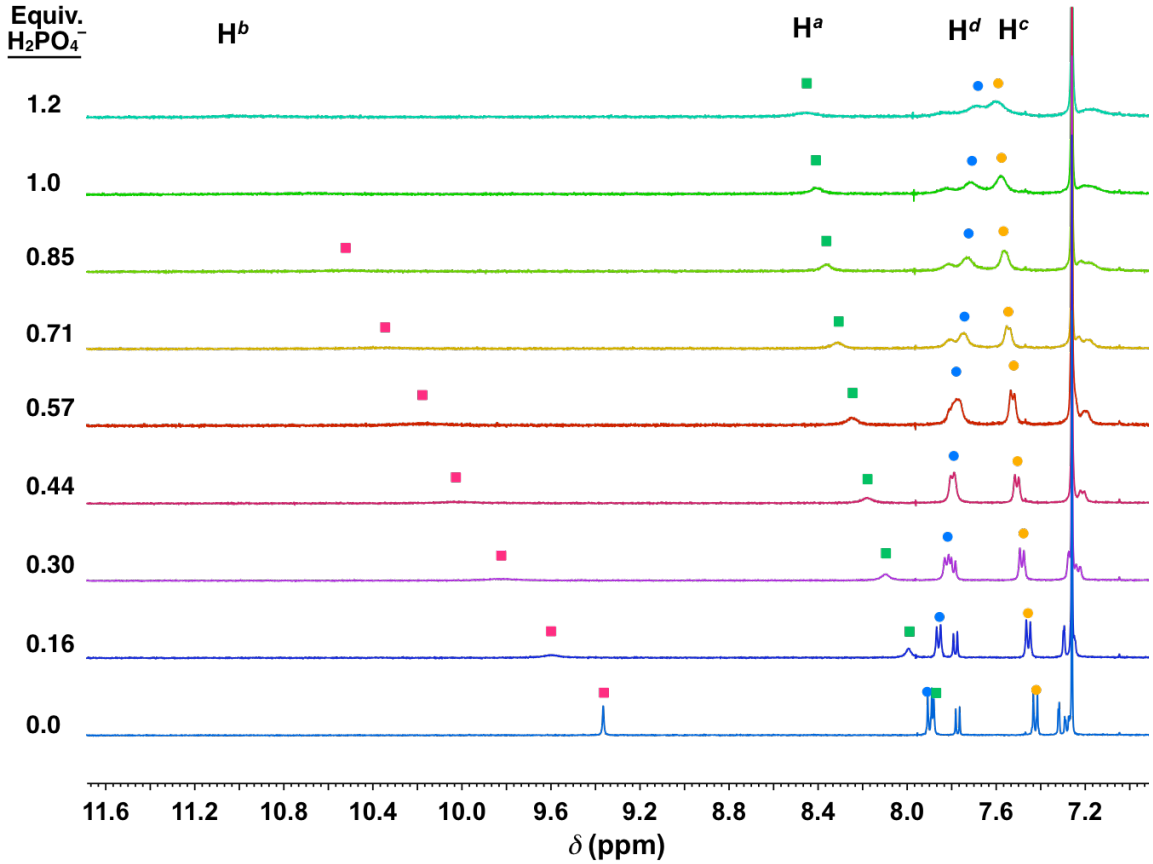

Figure 33. Example stacked spectra from the titration for the addition of tetrabutylammonium dihydrogen phosphate to **1** in 10 % d_6-DMSO/$CDCl_3$. Line broadening was employed elucidate chemical shifts of broadened peaks.

Tetrabutylammonium nitrate, 20 % DMSO-d_6/$CDCl_3$. A 3 mL stock solution of **1** (3.27 mg, [R] = 0.96 mM) in 20 % DMSO-d_6/$CDCl_3$ was prepared and used in the preparation of a 2 mL $TBANO_3$ guest solution (6.00 mg, [G] = 9.95 mM). Starting volume of 500 µL. (Table 14, Figures 34 and 35)

Table 14. Example titration for the addition of tetrabutylammonium nitrate to **1** in 20 % d_6-DMSO/$CDCl_3$.

Addition (µL)	Total Volume Anion (µL)	[$TBANO_3$] (M)	Equiv. NO_3^-	$\delta(H^a)$ (ppm)	$\delta(H^b)$ (ppm)	$\delta(H^c)$ (ppm)	$\delta(H^d)$ (ppm)
0	0	0.00E+00	0	7.765	9.298	7.244	7.677
10	10	1.95E-04	0.20	7.789	9.334	7.255	7.667
10	20	3.83E-04	0.40	7.808	9.363	7.260	7.658
10	30	5.63E-04	0.59	7.825	9.388	7.269	7.651
15	45	8.21E-04	0.86	7.843	9.417	7.277	7.641
15	60	1.07E-03	1.11	7.858	9.439	7.281	7.635
20	80	1.37E-03	1.43	7.873	9.462	7.289	7.629
20	100	1.66E-03	1.73	7.884	9.477	7.292	7.623
25	125	1.99E-03	2.08	7.895	9.494	7.297	7.619
35	160	2.41E-03	2.52	7.902	9.506	7.300	7.614
50	210	2.94E-03	3.07	7.913	9.520	7.303	7.609
70	280	3.57E-03	3.73	7.919	9.527	7.304	7.603

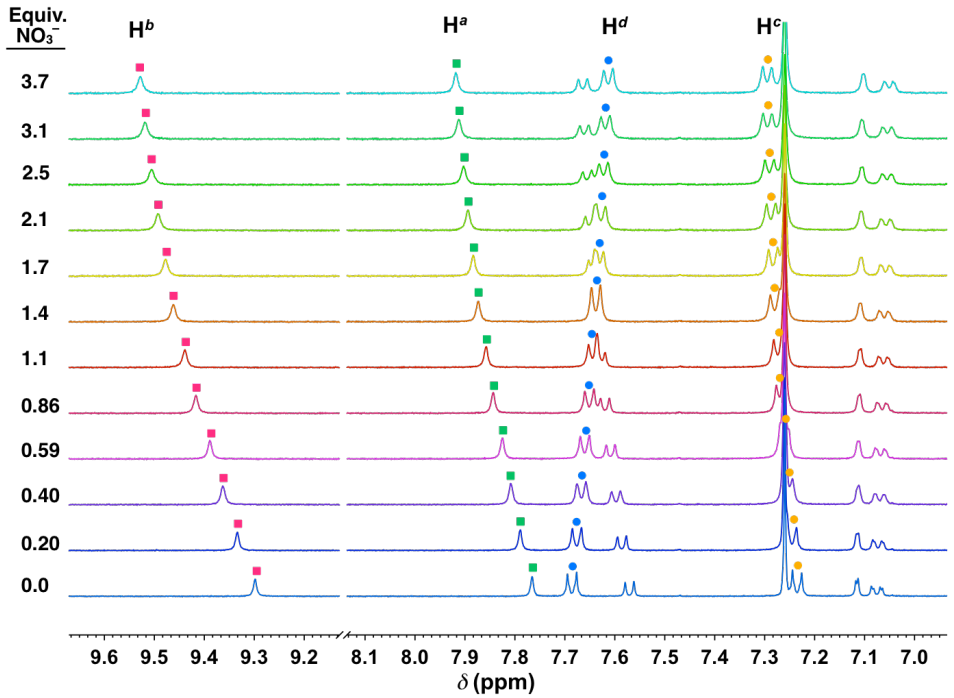

Figure 34. Example stacked spectra from the titration for the addition of tetrabutylammonium nitrate to **1** in 20 % d_6-DMSO/$CDCl_3$.

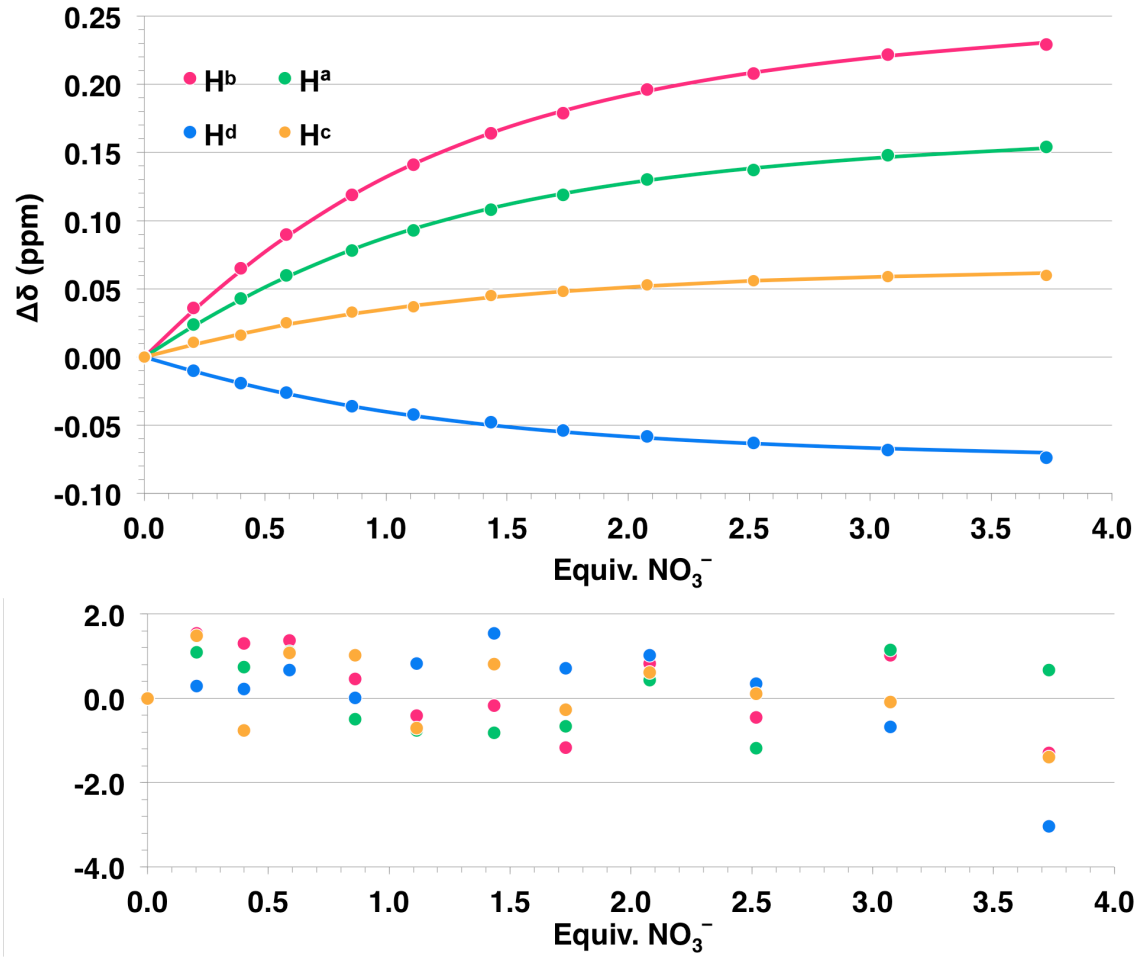

Figure 35. Example 1:1 fitting using non-linear regression from the data obtained for the titration of tetrabutylammonium nitrate into **1** in 20 % d_6-DMSO/$CDCl_3$.

D.3.3. NMR Titrations of 2

Tetrabutylammonium bromide, 10 % DMSO-d_6/$CDCl_3$. A 3 mL stock solution of **2** (3.36 mg, [R] = 1.03 mM) in 10 % DMSO-d_6/$CDCl_3$ was prepared and used in the preparation of a 2 mL TBABr guest solution (5.44 mg, [G] = 8.44 mM). Starting volume of 500 µL. (Table 15, Figures 36 and 37)

Tetrabutylammonium iodide, 10 % DMSO-d_6/$CDCl_3$. A 3 mL stock solution of **2** (3.07 mg, [R] = 0.94 mM) in 10 % DMSO-d_6/$CDCl_3$ was prepared and used in the preparation of a 2 mL TBAI guest solution (36.63 mg, [G] = 49.58 mM). Starting volume of 500 µL. (Table 16, Figures 38 and 39)

Table 15. Example titration for the addition of tetrabutylammonium bromide to **2** in 10 % d_6-DMSO/$CDCl_3$.

Addition (µL)	Total Volume Anion (µL)	[TBABr] (M)	Equiv. Br^-	$\delta(H^a)$ (ppm)	$\delta(H^b)$ (ppm)	$\delta(H^c)$ (ppm)	$\delta(H^d)$ (ppm)	$\delta(H^{core})$ (ppm)
0	0	0.00E+00	0	7.975	9.590	7.457	7.887	7.805
10	10	1.65E-04	0.16	7.983	9.681	7.493	7.879	7.846
10	20	3.24E-04	0.31	7.990	9.758	7.525	7.873	7.882
10	30	4.77E-04	0.46	7.995	9.824	7.551	7.867	7.913
10	40	6.25E-04	0.60	8.001	9.876	7.572	7.864	7.939
15	55	8.36E-04	0.81	8.005	9.938	7.596	7.858	7.967
15	70	1.04E-03	1.00	8.009	9.979	7.613	7.854	7.989
15	85	1.23E-03	1.19	8.011	10.011	7.624	7.851	8.004
20	105	1.46E-03	1.42	8.015	10.039	7.635	7.848	8.016
20	125	1.69E-03	1.63	8.016	10.058	7.644	7.846	8.026
25	150	1.95E-03	1.88	8.018	10.076	7.650	7.844	8.034
25	175	2.19E-03	2.12	8.019	10.086	7.655	7.843	8.039
50	225	2.62E-03	2.53	8.020	10.104	7.659	7.841	8.047

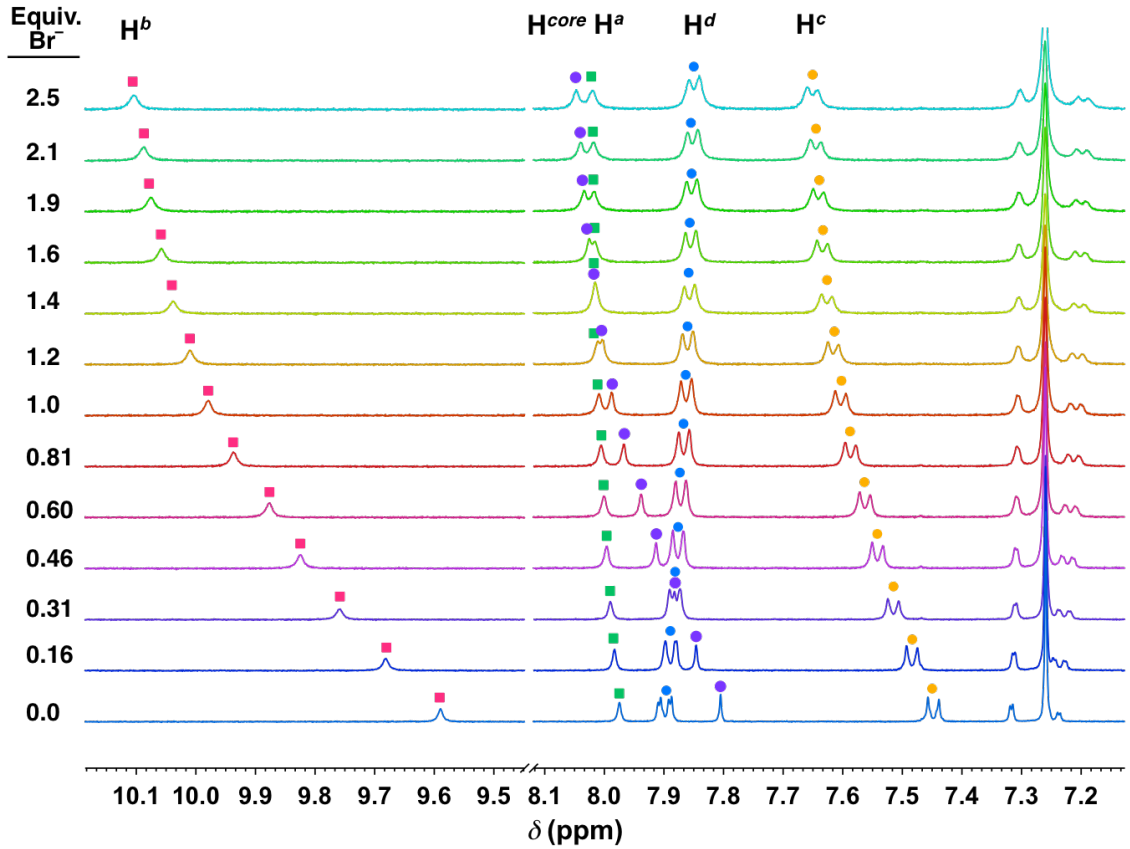

Figure 36. Example stacked spectra from the titration for the addition of tetrabutylammonium bromide to **2** in 10 % d_6-DMSO/$CDCl_3$.

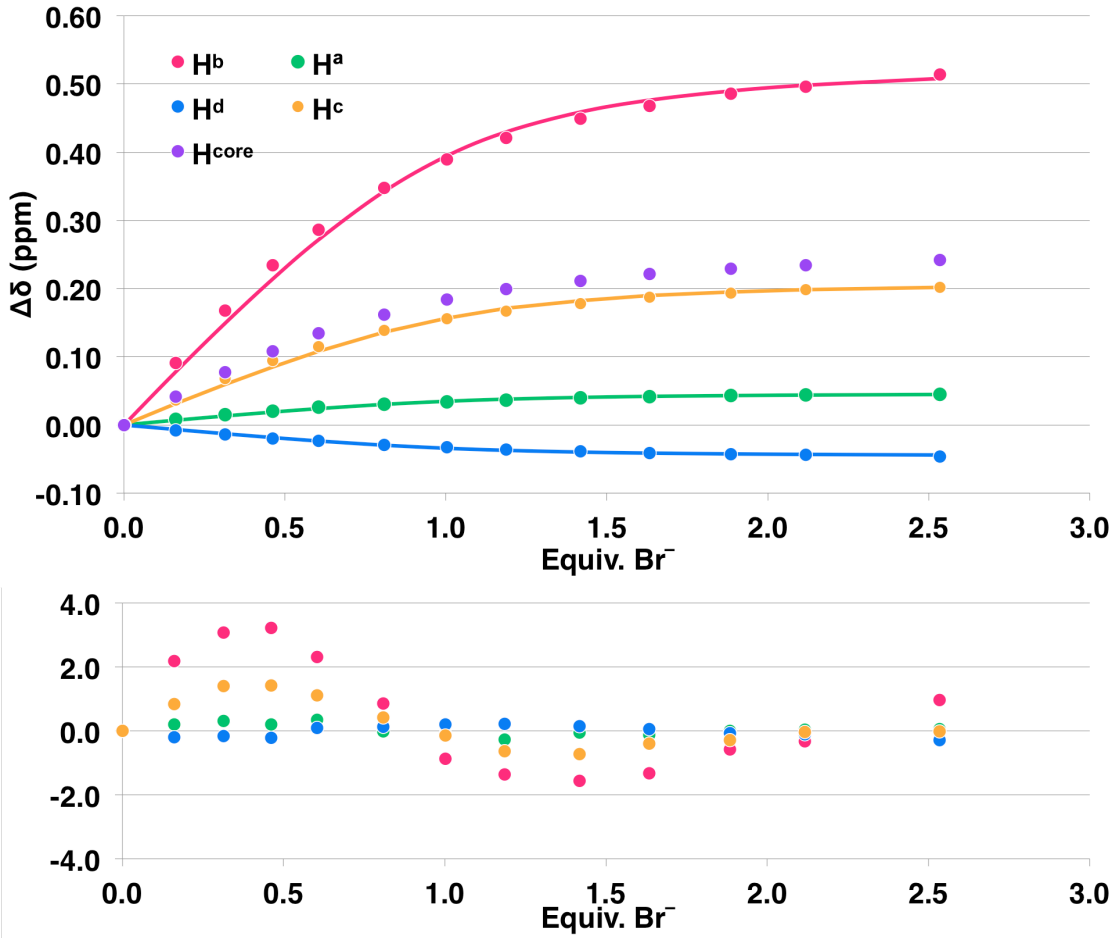

Figure 37. Example 1:1 fitting using non-linear regression from the data obtained for the titration of tetrabutylammonium bromide into **2** in 10 % d_6-DMSO/$CDCl_3$.

Table 16. Example titration for the addition of tetrabutylammonium iodide to **2** in 10 % d_6-DMSO/$CDCl_3$.

Addition (µL)	Total Volume Anion (µL)	[TBAI] (M)	Equiv. I^-	$\delta(H^a)$ (ppm)	$\delta(H^b)$ (ppm)	$\delta(H^c)$ (ppm)	$\delta(H^d)$ (ppm)	$\delta(H^{core})$ (ppm)
0	0	0.00E+00	0	7.982	9.642	7.468	7.884	7.821
5	5	4.91E-04	0.52	7.986	9.677	7.495	7.880	7.844
10	15	1.44E-03	1.53	7.988	9.707	7.524	7.870	7.870
10	25	2.36E-03	2.50	7.989	9.730	7.541	7.870	7.886
10	35	3.24E-03	3.44	7.991	9.747	7.555	7.867	7.896
10	45	4.09E-03	4.34	7.993	9.762	7.564	7.864	7.905
15	60	5.31E-03	5.63	7.995	9.777	7.574	7.863	7.913
15	75	6.47E-03	6.85	7.997	9.789	7.581	7.859	7.920
15	90	7.56E-03	8.01	8.000	9.807	7.587	7.856	7.925
20	110	8.94E-03	9.47	8.001	9.817	7.592	7.853	7.929
25	135	1.05E-02	11.17	8.003	9.825	7.597	7.850	7.935
35	170	1.26E-02	13.33	8.004	9.839	7.602	7.847	7.940
50	220	1.52E-02	16.05	8.002	9.843	7.606	7.841	7.944

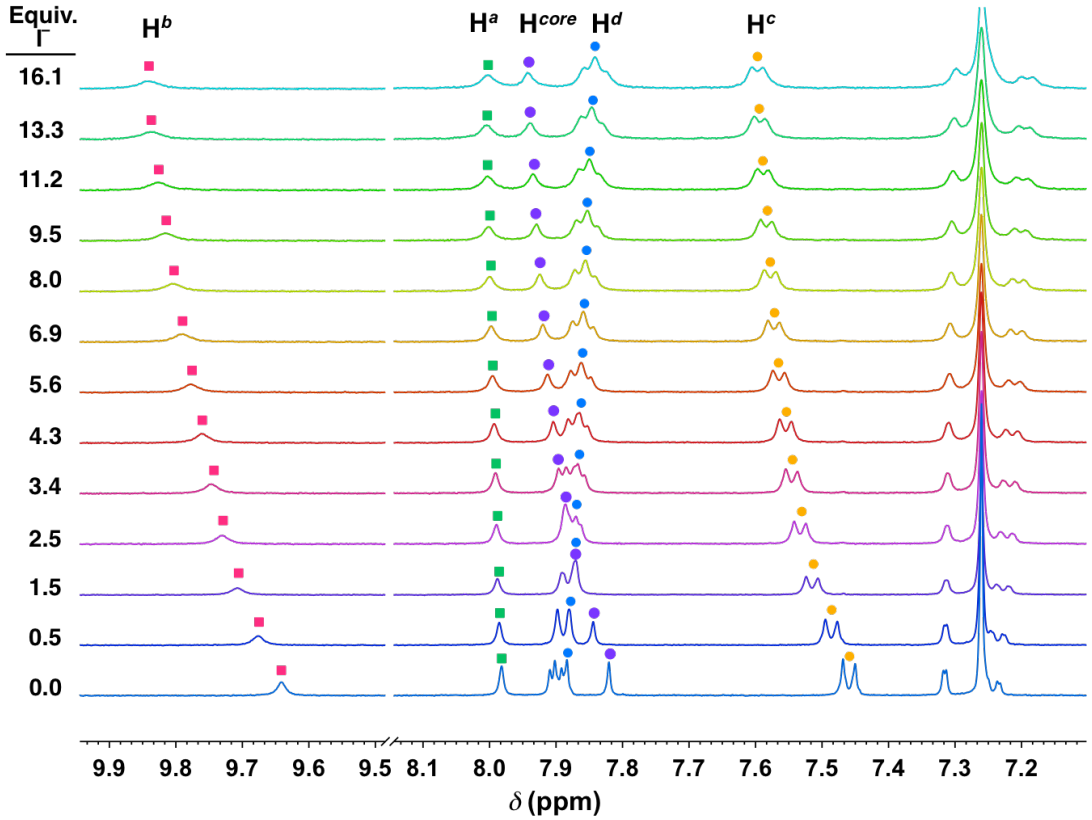

Figure 38. Example stacked spectra from the titration for the addition of tetrabutylammonium iodide to **2** in 10 % d_6-DMSO/$CDCl_3$.

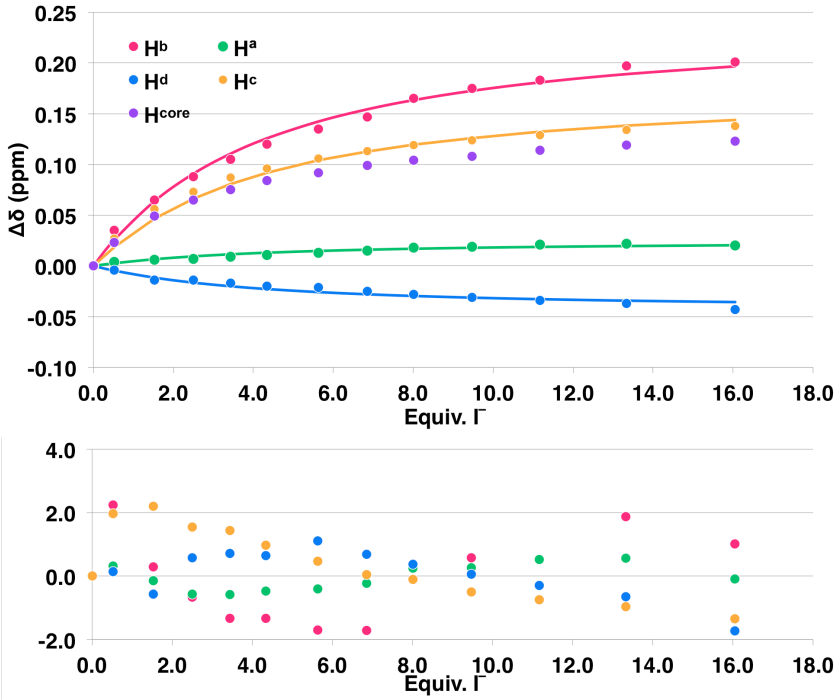

Figure 39. Example 1:1 fitting using non-linear regression from the data obtained for the titration of tetrabutylammonium iodide into **2** in 10 % d_6-DMSO/$CDCl_3$.

Tetrabutylammonium perchlorate, 10 % DMSO-d_6/$CDCl_3$. A 3 mL stock solution of **2** (3.23 mg, [R] = 0.99 mM) in 10 % DMSO-d_6/$CDCl_3$ was prepared and used in the preparation of a 2 mL $TBAReO_4$ guest solution (77.46 mg, [G] = 0.113 M). Starting volume of 500 µL. (Table 17, Figures 40 and 41)

Tetrabutylammonium perrhenate, 10 % DMSO-d_6/$CDCl_3$. A 3 mL stock solution of **2** (3.49 mg, [R] = 1.07 mM) in 10 % DMSO-d_6/$CDCl_3$ was prepared and used in the preparation of a 2 mL $TBAReO_4$ guest solution (60.26 mg, [G] = 70.12 mM). Starting volume of 500 µL. (Table 18, Figures 42 and 43)

Tetrabutylammonium hydrogen sulfate, 20 % DMSO-d_6/$CDCl_3$. A 3 mL stock solution of **2** (3.14 mg, [R] = 0.97 mM) in 20 % DMSO-d_6/$CDCl_3$ was prepared and used in the preparation of a 2 mL $TBAHSO_4$ guest solution (10.10 mg, [G] = 14.87 mM). Starting volume of 500 µL. (Table 19, Figures 44 and 45)

Tetrabutylammonium hydrogen sulfate, 30 % DMSO-d_6/$CDCl_3$. A 3 mL stock solution of **2** (3.33 mg, [R] = 1.02 mM) in 30 % DMSO-d_6/$CDCl_3$ was prepared and used in the preparation of a 2 mL $TBAHSO_4$ guest solution (9.59 mg, [G] = 14.12 mM). Starting volume of 500 µL. (Table 20, Figures 46 and 47)

Table 17. Example titration for the addition of tetrabutylammonium perchlorate to **2** in 10 % d_6-DMSO/$CDCl_3$.

Addition (µL)	Total Volume Anion (µL)	[$TBAReO_4$] (M)	Equiv. ReO_4^-	$\delta(H^a)$ (ppm)	$\delta(H^b)$ (ppm)	$\delta(H^c)$ (ppm)	$\delta(H^d)$ (ppm)	$\delta(H^{core})$ (ppm)
0	0	0.00E+00	0	7.977	9.599	7.459	7.887	7.808
5	5	1.12E-03	1.28	7.973	9.579	7.467	7.886	7.808
5	10	2.22E-03	2.51	7.971	9.568	7.471	7.884	7.809
10	20	4.36E-03	3.70	7.968	9.551	7.478	7.882	7.809
10	30	6.41E-03	4.84	7.966	9.540	7.482	7.880	7.808
10	40	8.39E-03	5.94	7.965	9.531	7.486	7.878	7.808
10	50	1.03E-02	7.00	7.964	9.524	7.488	7.877	7.808
15	65	1.30E-02	8.52	7.962	9.515	7.492	7.875	7.807
15	80	1.56E-02	10.43	7.961	9.508	7.494	7.873	7.807
20	100	1.89E-02	12.22	7.960	9.499	7.496	7.871	7.806
20	120	2.19E-02	14.30	7.958	9.494	7.498	7.870	7.806

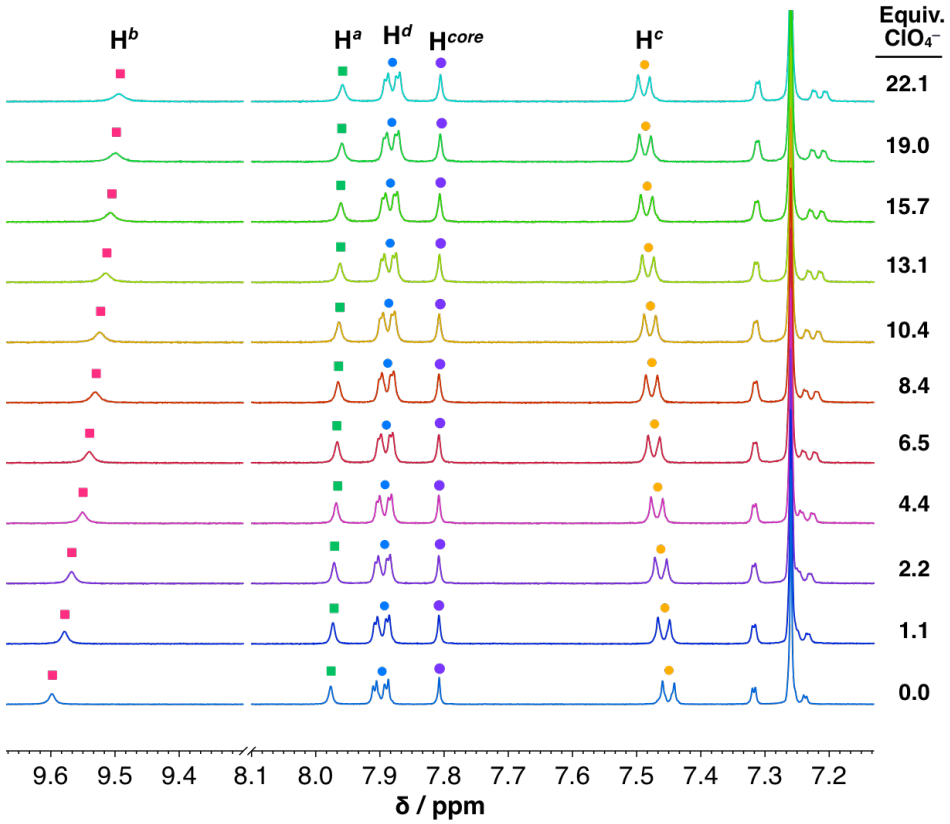

Figure 40. Example stacked spectra from the titration for the addition of tetrabutylammonium perchlorate to **2** in 10 % d_6-DMSO/$CDCl_3$.

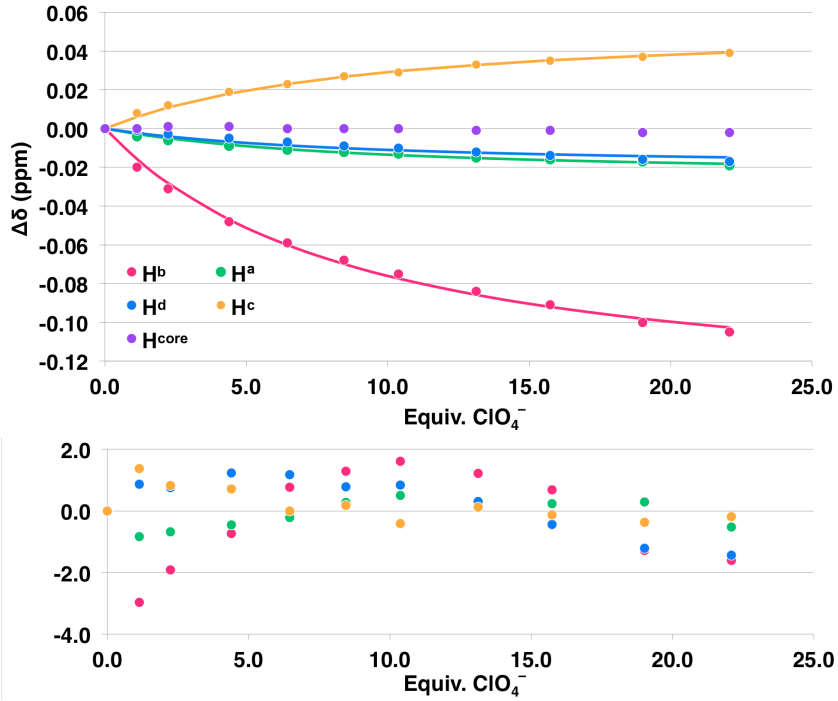

Figure 41. Example 1:1 fitting using non-linear regression from the data obtained for the titration of tetrabutylammonium perchlorate into **2** in 10 % d_6-DMSO/$CDCl_3$.

Table 18. Example titration for the addition of tetrabutylammonium perrhenate to **2** in 10 % d_6-DMSO/$CDCl_3$.

Addition (µL)	Total Volume Anion (µL)	[$TBAReO_4$] (M)	Equiv. ReO_4^-	$\delta(H^a)$ (ppm)	$\delta(H^b)$ (ppm)	$\delta(H^c)$ (ppm)	$\delta(H^d)$ (ppm)	$\delta(H^{core})$ (ppm)
0	0	0.00E+00	0	7.975	9.599	7.456	7.882	7.804
10	10	1.37E-03	1.28	7.981	9.565	7.470	7.881	7.798
10	20	2.70E-03	2.51	7.985	9.547	7.479	7.879	7.795
10	30	3.97E-03	3.70	7.987	9.533	7.484	7.878	7.792
10	40	5.19E-03	4.84	7.989	9.523	7.488	7.876	7.789
10	50	6.37E-03	5.94	7.991	9.516	7.492	7.876	7.788
10	60	7.51E-03	7.00	7.992	9.510	7.494	7.874	7.786
15	75	9.15E-03	8.52	7.995	9.504	7.499	7.873	7.784
20	95	1.12E-02	10.43	7.997	9.494	7.501	7.872	7.781
20	115	1.31E-02	12.22	7.997	9.486	7.503	7.870	7.779
25	140	1.53E-02	14.30	7.998	9.481	7.504	7.867	7.776

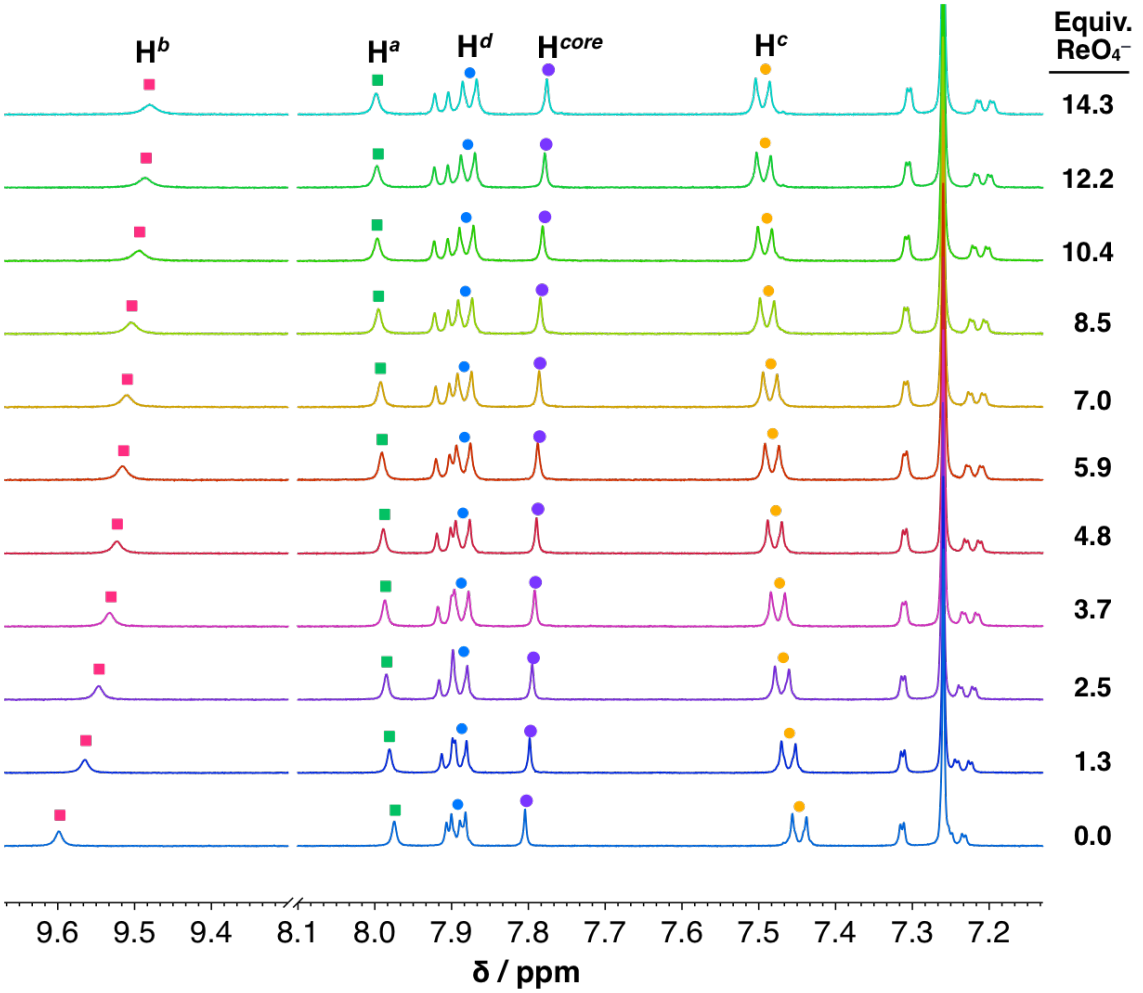

Figure 42. Example stacked spectra from the titration for the addition of tetrabutylammonium perrhenate to **2** in 10 % d_6-DMSO/$CDCl_3$.

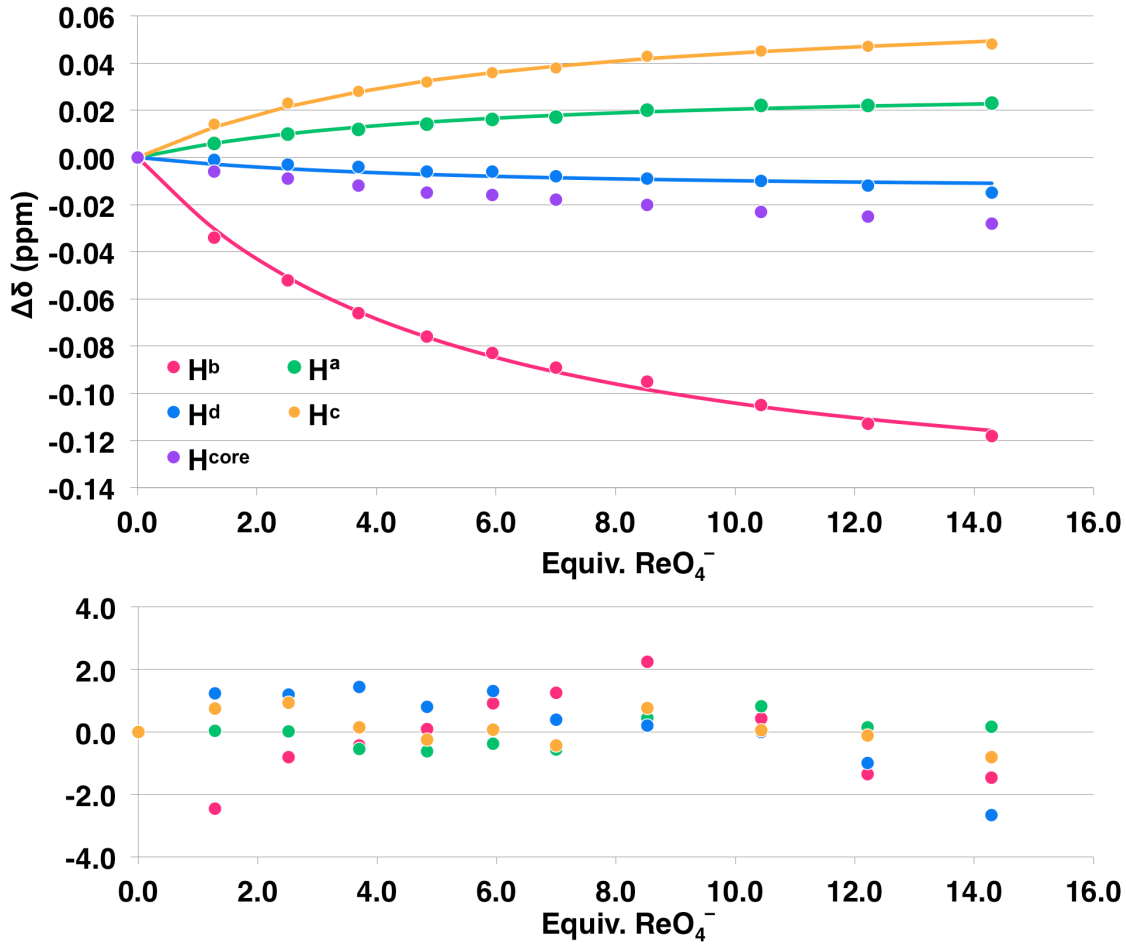

Figure 43. Example 1:1 fitting using non-linear regression from the data obtained for the titration of tetrabutylammonium perrhenate into **2** in 10 % d_6-DMSO/$CDCl_3$.

Table 19. Example titration for the addition of tetrabutylammonium hydrogen sulfate to **2** in 20 % d_6-DMSO/$CDCl_3$.

Addition (µL)	Total Volume Anion (µL)	[$TBAHSO_4$] (M)	Equiv. HSO_4^-	$\delta(H^a)$ (ppm)	$\delta(H^b)$ (ppm)	$\delta(H^c)$ (ppm)	$\delta(H^d)$ (ppm)	$\delta(H^{core})$ (ppm)
0	0	0.00E+00	0	7.859	9.569	7.299	7.689	7.669
10	10	2.92E-04	0.30	7.912	9.605	7.347	7.684	7.697
10	20	5.72E-04	0.59	7.962	9.639	7.391	7.681	7.713
10	30	8.42E-04	0.87	7.999	9.661	7.421	7.676	7.727
10	40	1.10E-03	1.14	8.023	9.672	7.442	7.676	7.735
15	55	1.47E-03	1.53	8.045	9.678	7.459	7.674	7.741
15	70	1.83E-03	1.89	8.058	9.682	7.469	7.672	7.745
15	85	2.16E-03	2.24	8.065	9.683	7.475	7.670	7.746
20	105	2.58E-03	2.67	8.071	9.682	7.480	7.669	7.747
20	125	2.97E-03	3.08	8.074	9.682	7.482	7.668	7.747
25	150	3.43E-03	3.56	8.078	9.680	7.484	7.667	7.747
35	185	4.02E-03	4.16	8.081	9.680	7.486	7.666	7.747
50	235	4.76E-03	4.93	8.084	9.678	7.487	7.664	7.745

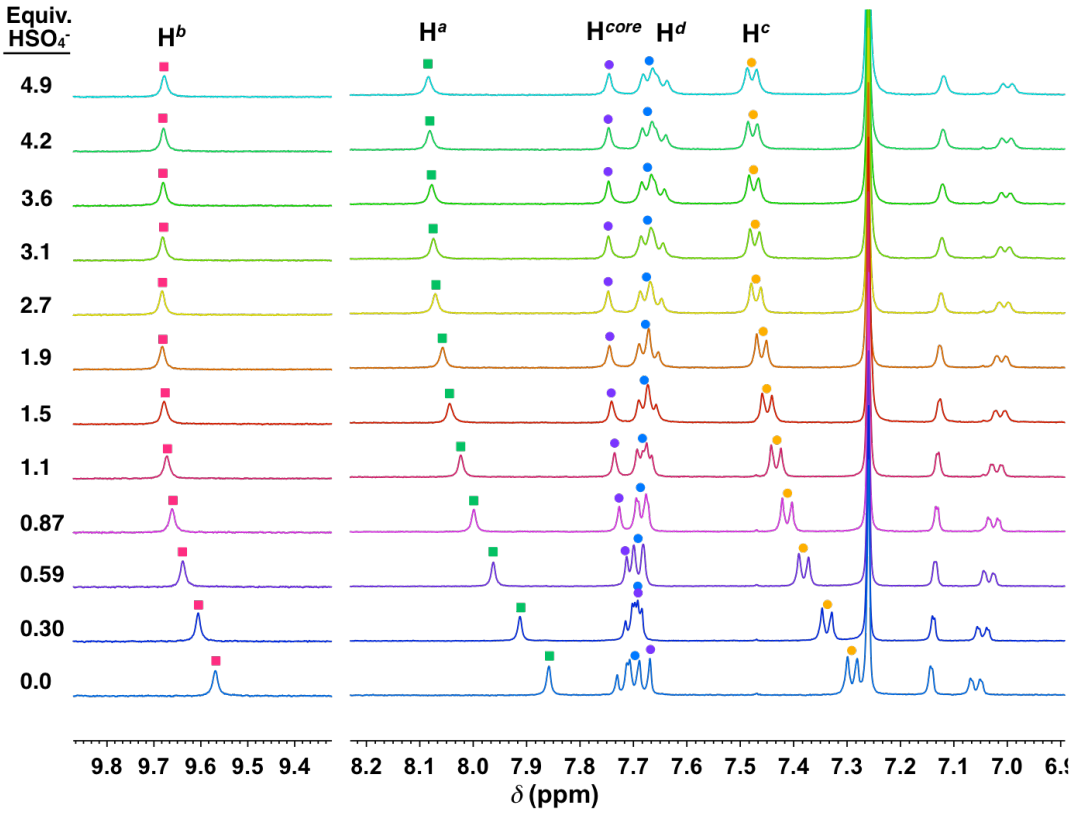

Figure 44. Example stacked spectra from the titration for the addition of tetrabutylammonium hydrogen sulfate to **2** in 20 % d_6-DMSO/$CDCl_3$.

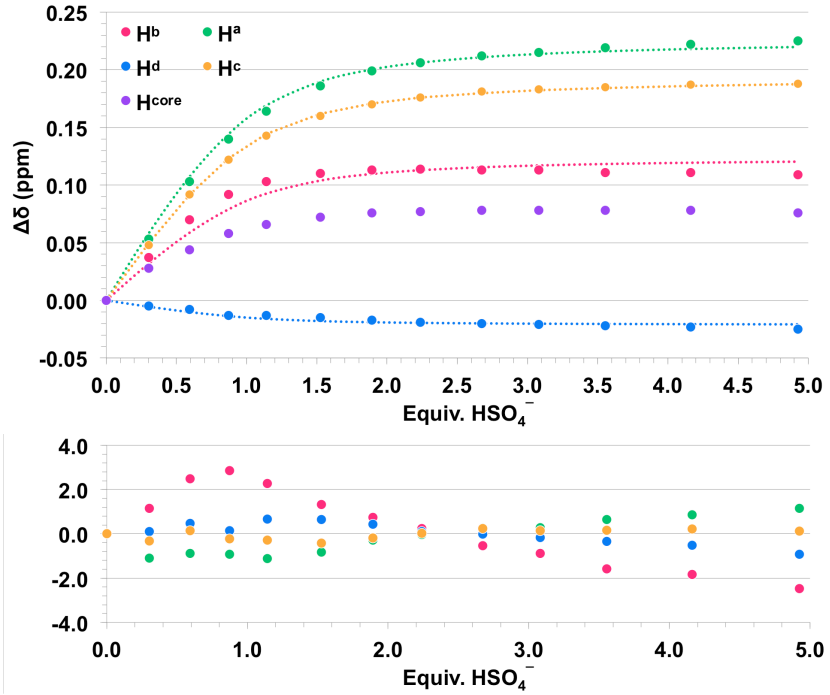

Figure 45. Example 1:1 fitting using non-linear regression from the data obtained for the titration of tetrabutylammonium perrhenate into **2** in 10 % d_6-DMSO/$CDCl_3$.

Table 20. Example titration for the addition of tetrabutylammonium hydrogen sulfate to **2** in 30 % d_6-DMSO/$CDCl_3$.

Addition (µL)	Total Volume Anion (µL)	[$TBAHSO_4$] (M)	Equiv. HSO_4^-	$\delta(H^a)$ (ppm)	$\delta(H^b)$ (ppm)	$\delta(H^c)$ (ppm)	$\delta(H^d)$ (ppm)	$\delta(H^{core})$ (ppm)
0	0	0.00E+00	0	7.705	9.397	7.096	7.485	7.469
10	10	2.77E-04	0.27	7.724	9.410	7.115	7.480	7.480
10	20	5.43E-04	0.53	7.740	9.418	7.130	7.484	7.484
10	30	7.99E-04	0.78	7.754	9.429	7.145	7.481	7.494
10	40	1.05E-03	1.02	7.765	9.437	7.156	7.480	7.496
15	55	1.40E-03	1.37	7.780	9.445	7.170	7.480	7.500
15	70	1.73E-03	1.69	7.792	9.450	7.182	7.477	7.506
15	85	2.05E-03	2.00	7.802	9.454	7.190	7.476	7.513
20	105	2.45E-03	2.39	7.813	9.460	7.201	7.473	7.519
20	125	2.82E-03	2.76	7.820	9.462	7.208	7.473	7.521
25	150	3.26E-03	3.18	7.828	9.465	7.216	7.472	7.525
35	185	3.81E-03	3.72	7.834	9.469	7.224	7.472	7.527

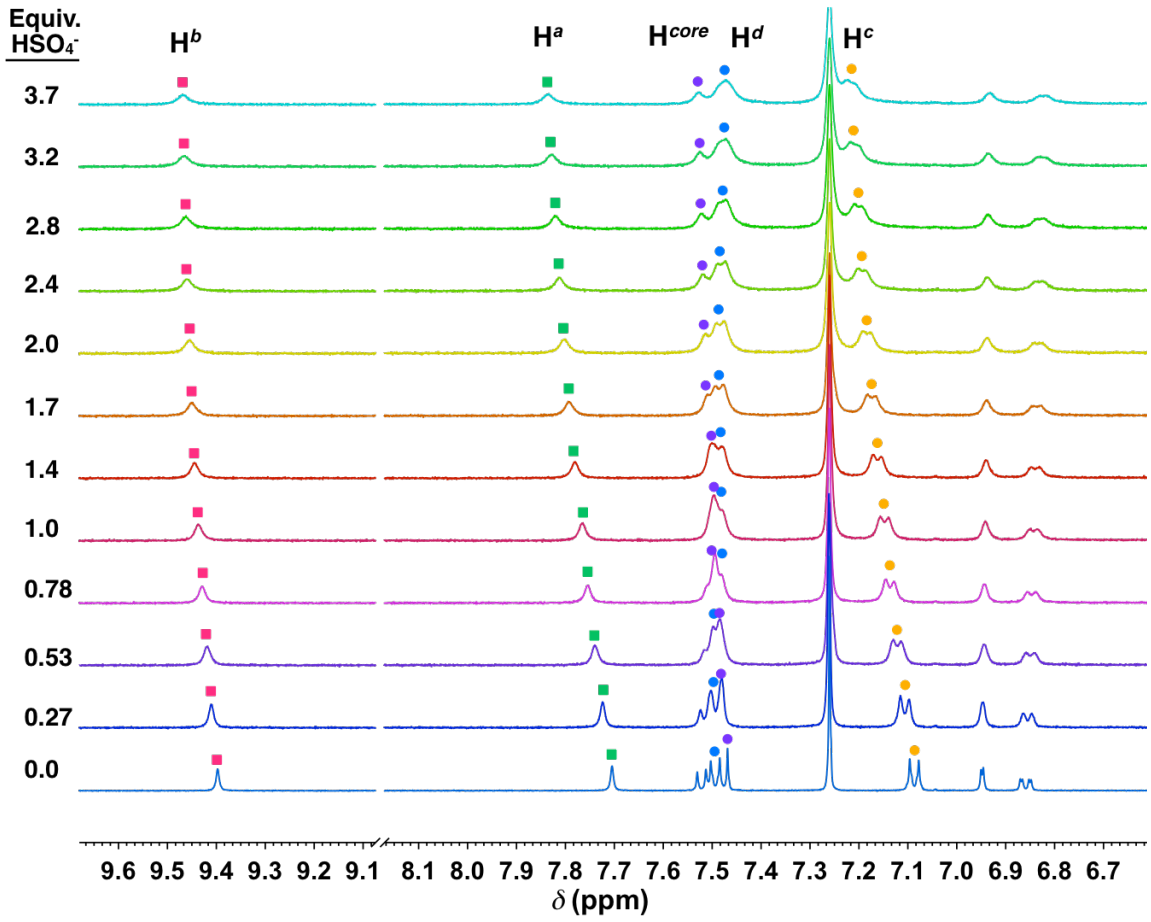

Figure 46. Example stacked spectra from the titration for the addition of tetrabutylammonium hydrogen sulfate to **2** in 30 % d_6-DMSO/$CDCl_3$.

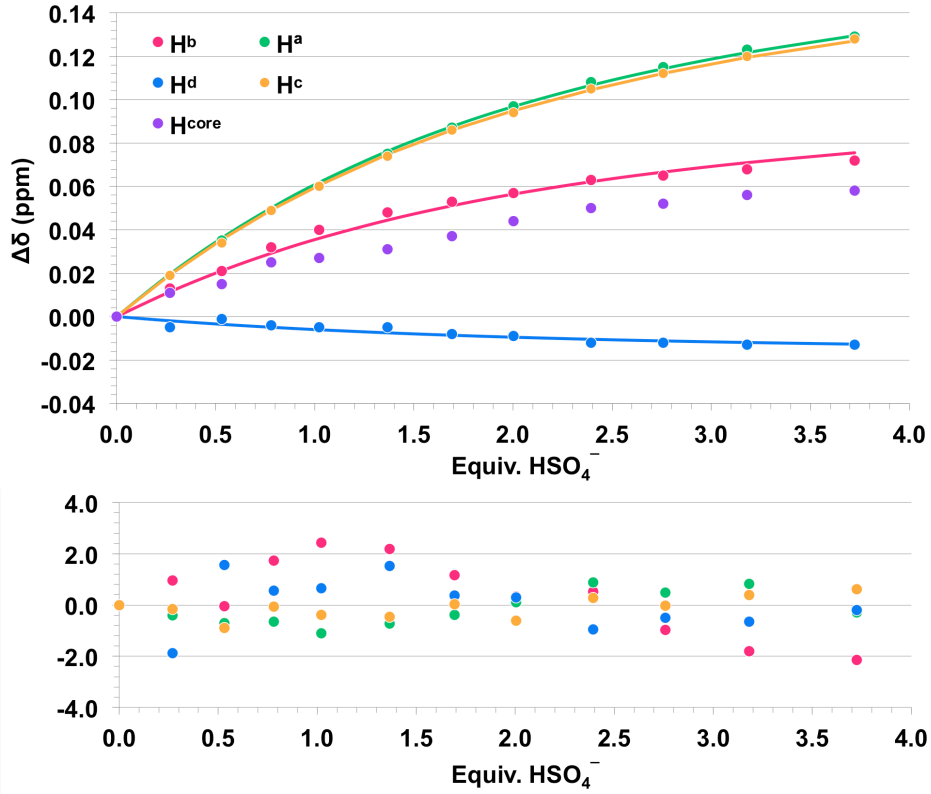

Figure 47. Example 1:1 fitting using non-linear regression from the data obtained for the titration of tetrabutylammonium perrhenate into **2** in 10 % d_6-DMSO/$CDCl_3$.

Tetrabutylammonium sulfate, 10 % DMSO-d_6/$CDCl_3$. A 3 mL stock solution of **2** (3.21 mg, [R] = 0.99 mM) in 10 % DMSO-d_6/$CDCl_3$ was prepared and used in the preparation of a 2 mL $TBASO_4$ guest solution (10.0 µL, 9.9 mg, [G] = 8.53 mM). Starting volume of 500 µL. (Table 21, Figures 48)

Table T. Example titration for the addition of tetrabutylammonium sulfate to **2** in 10 % d_6-DMSO/$CDCl_3$.

Addition (µL)	Total Volume Anion (µL)	[TBA_2SO_4] (M)	Equiv. SO_4^{2-}	$\delta(H^a)$ (ppm)	$\delta(H^b)$ (ppm)	$\delta(H^c)$ (ppm)	$\delta(H^d)$ (ppm)	$\delta(H^{core})$ (ppm)
0	0	0.00E+00	0.25	7.977	9.604	7.460	7.885	7.809
15	15	2.49E-04	0.49	7.983	9.628	7.468	7.886	7.816
15	30	4.83E-04	0.79	7.992	9.663	7.469	7.884	7.829
20	50	7.76E-04	1.44	—	—	—	—	—
50	100	1.42E-03	2.47	—	—	—	—	—
100	200	2.44E-03	3.24	—	—	—	—	—
100	300	3.20E-03	4.32	—	—	—	—	—
200	500	4.27E-03	5.77	—	—	—	—	—
500	1000	5.69E-03	0.25	—	—	—	—	—

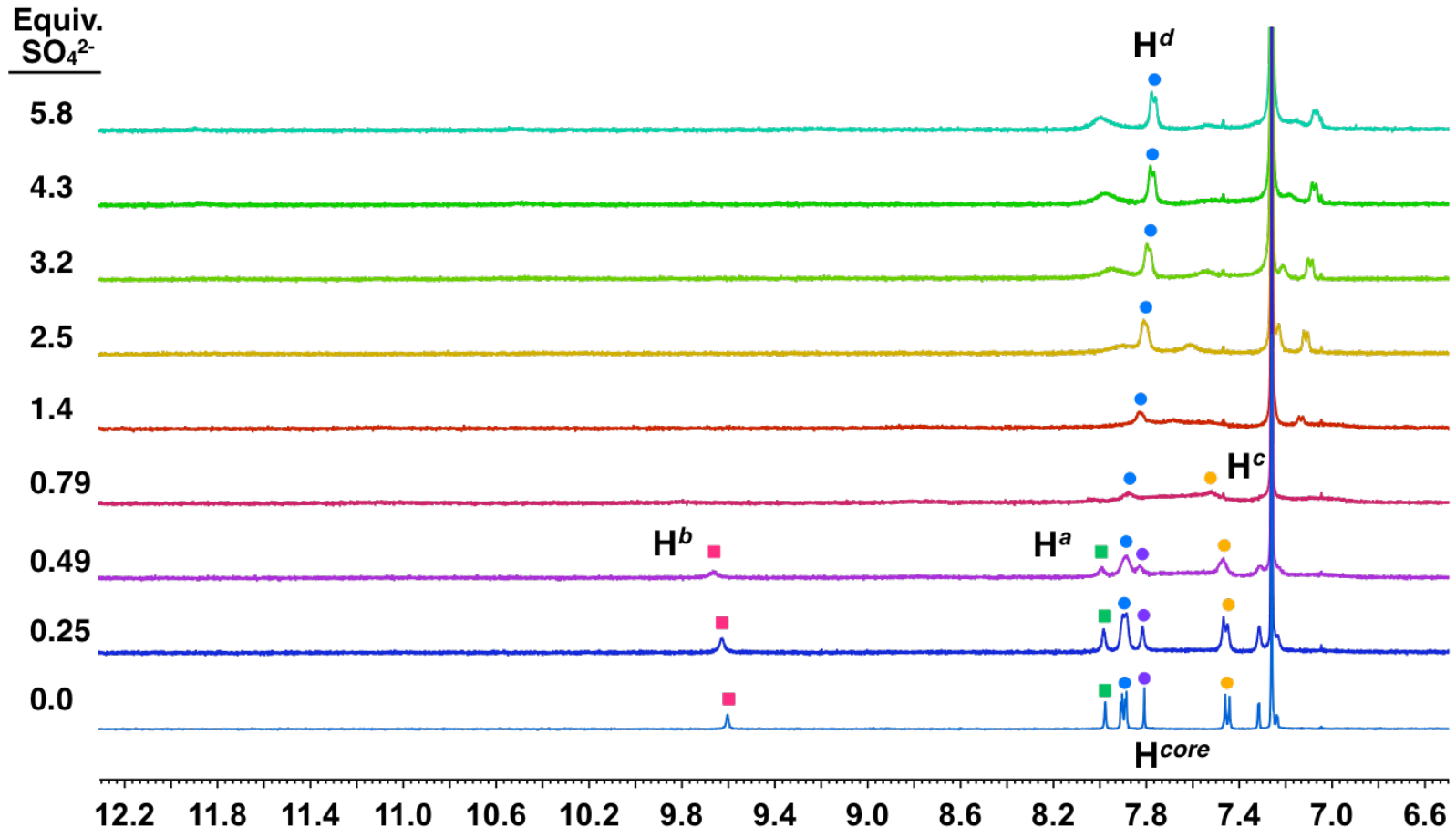

Figure 48. Example stacked spectra from the titration for the addition of tetrabutylammonium sulfate to **2** in 10 % d_6-DMSO/$CDCl_3$.

Tetrabutylammonium acetate, 10 % DMSO-d_6/$CDCl_3$, 25 °C. A 3 mL stock solution of **2** (3.20 mg, [R] = 0.98 mM) in 10 % DMSO-d_6/$CDCl_3$ was prepared and used in the preparation of a 2 mL TBAOAc guest solution (8.97 mg, [G] = 14.88 mM). Starting volume of 500 µL. (Table 22, Figures 49 and 50)

Tetrabutylammonium acetate, 10 % DMSO-d_6/$CDCl_3$, 30 °C. A 3 mL stock solution of **2** (3.17 mg, [R] = 0.97 mM) in 10 % DMSO-d_6/$CDCl_3$ was prepared and used in the preparation of a 2 mL TBAOAc guest solution (7.42 mg, [G] = 12.31 mM). Starting volume of 500 µL. (Table 23, Figures 51 and 52)

Tetrabutylammonium dihydrogen phosphate, 10 % DMSO-d_6/$CDCl_3$. A 3 mL stock solution of **2** (3.19 mg, [R] = 0.98 mM) in 10 % DMSO-d_6/$CDCl_3$ was prepared and used in the preparation of a 2 mL $TBAHPO_4$ guest solution (9.22 mg, [G] = 13.58 mM). Starting volume of 500 µL. (Table 24, Figures W1 and W2)

Tetrabutylammonium dihydrogen phosphate, 20 % DMSO-d_6/$CDCl_3$. A 3 mL stock solution of **2** (3.17 mg, [R] = 0.97 mM) in 20 % DMSO-d_6/$CDCl_3$ was prepared and used in the preparation of a 2 mL $TBAHPO_4$ guest solution (6.29 mg, [G] = 9.26 mM). Starting volume of 500 µL. (Table 25, Figures X1 and X2)

Table 22. Example titration for the addition of tetrabutylammonium acetate to **2** in 10 % d_6-DMSO/$CDCl_3$ at 25 °C.

Addition (µL)	Total Volume Anion (µL)	[TBAOAc] (M)	Equiv. AcO^-	$\delta(H^a)$ (ppm)	$\delta(H^b)$ (ppm)	$\delta(H^c)$ (ppm)	$\delta(H^d)$ (ppm)	$\delta(H^{core})$ (ppm)
0	0	0.00E+00	0	7.976	9.597	7.458	7.885	7.806
10	10	2.92E-04	0.30	8.195	10.024	7.498	7.854	7.804
10	20	5.72E-04	0.58	8.416	10.485	7.540	7.826	7.812
10	30	8.42E-04	0.86	8.618	10.878	7.579	7.806	7.821
10	40	1.10E-03	1.12	8.767	11.086	7.589	7.794	7.805
10	50	1.35E-03	1.37	8.867	11.181	7.595	7.791	7.801
10	60	1.59E-03	1.62	8.951	11.257	7.599	7.785	7.799
10	70	1.83E-03	1.86	9.022	11.323	7.605	7.781	7.798
15	85	2.16E-03	2.20	9.110	11.405	7.610	7.776	7.797
15	100	2.48E-03	2.52	9.182	11.464	7.614	7.772	7.798
20	120	2.88E-03	2.93	9.259	11.534	7.620	7.769	7.800

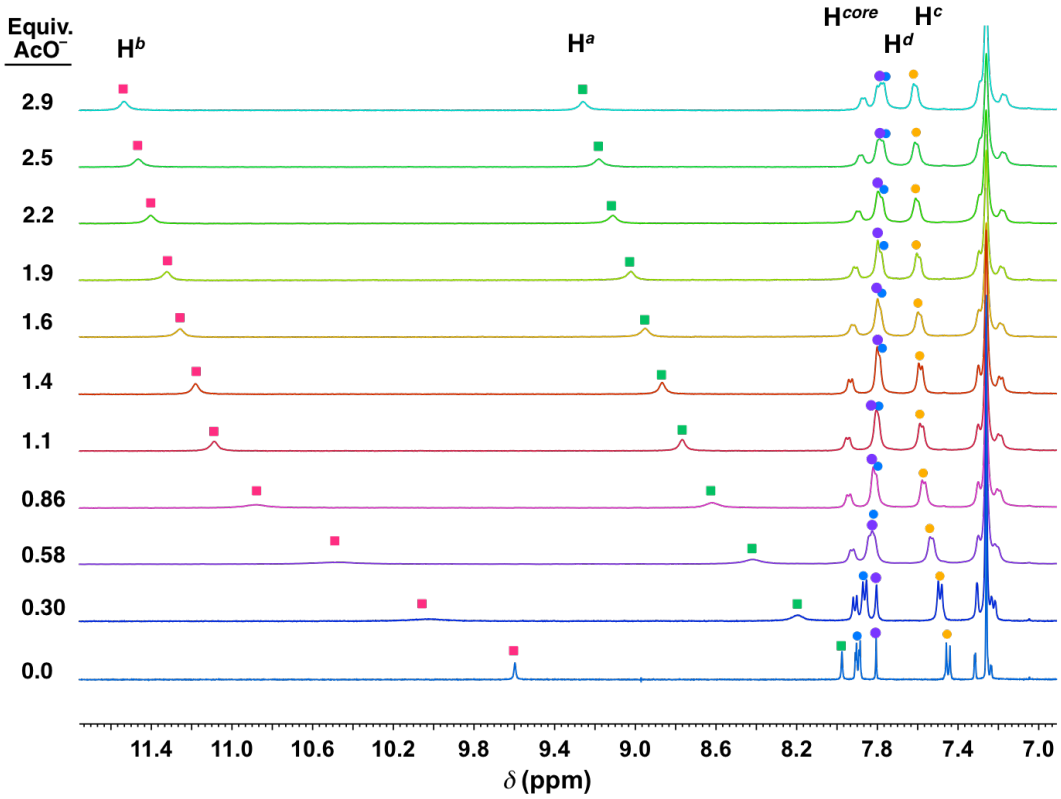

Figure 49. Example stacked spectra from the titration for the addition of tetrabutylammonium acetate to **2** in 10 % d_6-DMSO/$CDCl_3$ taken at 25 °C.

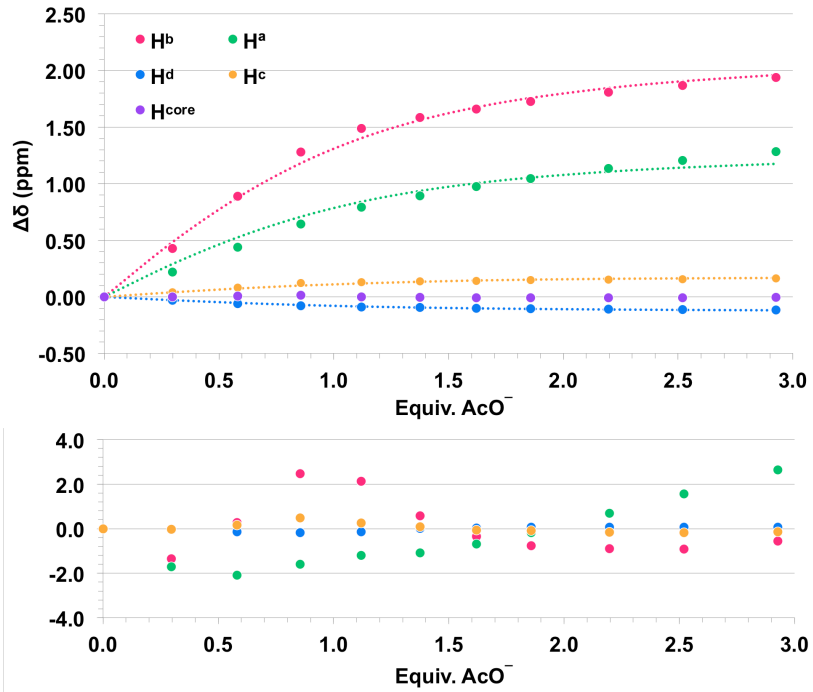

Figure 50. Example 1:1 fitting using non-linear regression from the data obtained for the titration of tetrabutylammonium acetate into **2** in 10 % d_6-DMSO/$CDCl_3$ taken at 25 °C.

Table 23. Example titration for the addition of tetrabutylammonium acetate to **2** in 10 % d_6-DMSO/$CDCl_3$ at 30 °C.

Addition (µL)	Total Volume Anion (µL)	[TBAOAc] (M)	Equiv. AcO^-	$\delta(H^a)$ (ppm)	$\delta(H^b)$ (ppm)	$\delta(H^c)$ (ppm)	$\delta(H^d)$ (ppm)	$\delta(H^{core})$ (ppm)
0	0	0.00E+00	0.00	7.965	9.574	7.461	7.888	7.802
10	10	2.41E-04	0.25	8.147	9.929	7.494	7.862	7.802
10	20	4.73E-04	0.49	8.332	10.308	7.529	7.837	7.807
10	30	6.97E-04	0.71	8.514	10.675	7.564	7.816	7.816
10	40	9.12E-04	0.94	8.672	10.973	7.591	7.800	7.818
10	50	1.12E-03	1.15	8.780	11.098	7.595	7.793	7.811
10	60	1.32E-03	1.35	8.857	11.172	7.600	7.789	7.806
10	70	1.51E-03	1.55	8.924	11.234	7.604	7.785	7.803
15	85	1.79E-03	1.83	9.009	11.312	7.610	7.781	7.800
15	100	2.05E-03	2.10	9.078	11.375	7.615	7.777	7.804
20	120	2.38E-03	2.44	9.154	11.446	7.620	7.773	7.804

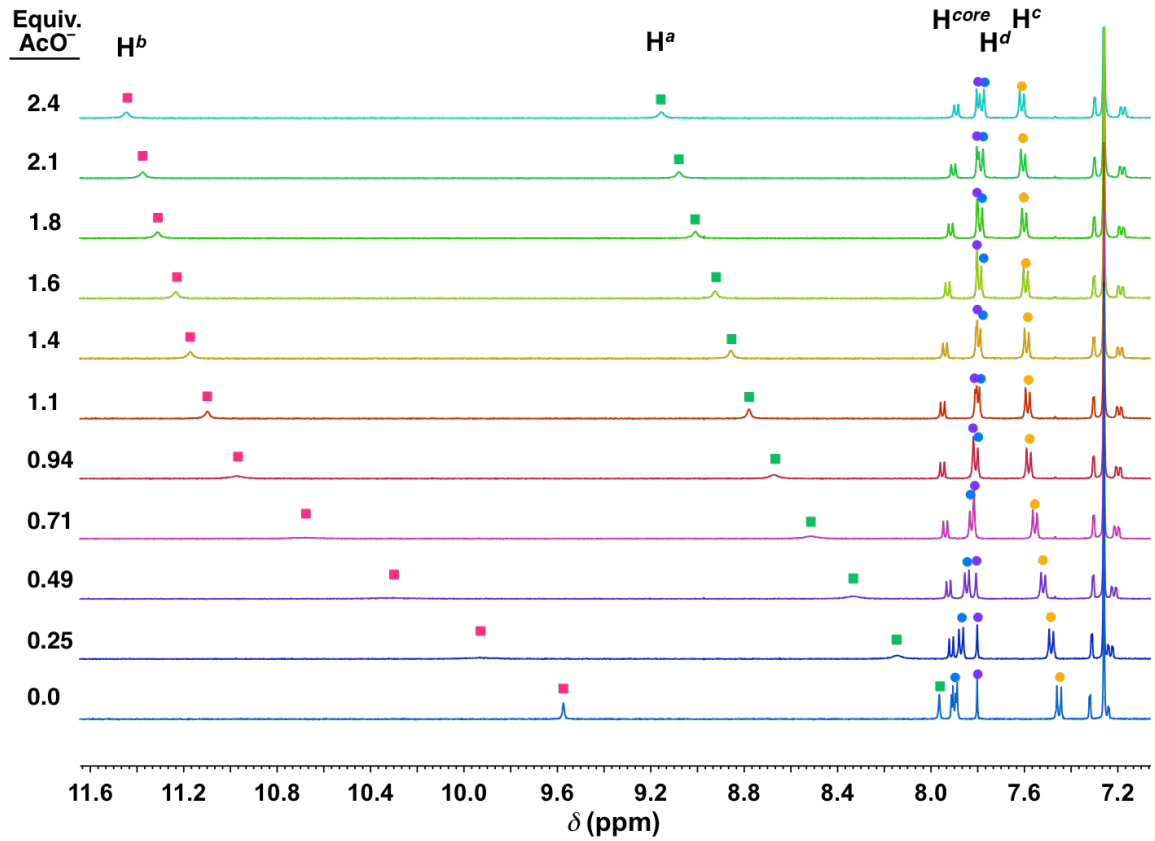

Figure 51. Example stacked spectra from the titration for the addition of tetrabutylammonium acetate to **2** in 10 % d_6-DMSO/$CDCl_3$ taken at 30 °C.

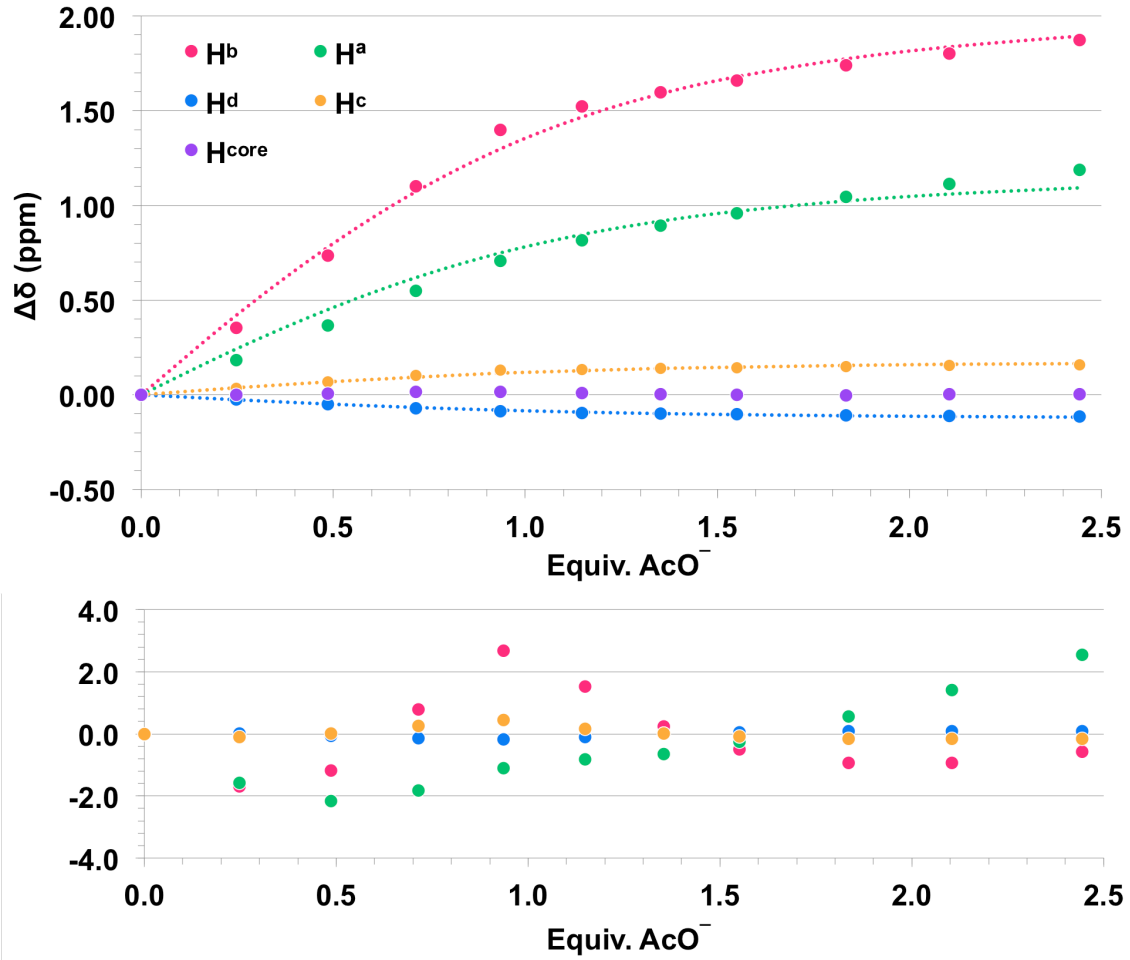

Figure 52. Example 1:1 fitting using non-linear regression from the data obtained for the titration of tetrabutylammonium acetate into **2** in 10 % d_6-DMSO/$CDCl_3$ taken at 30 °C.

Table 24. Example titration for the addition of tetrabutylammonium hydrogen phosphate to **2** in 10 % d_6-DMSO/$CDCl_3$.

Addition (µL)	Total Volume Anion (µL)	[$TBAH_2PO_4$] (M)	Equiv. $H_2PO_4^-$	$\delta(H^a)$ (ppm)	$\delta(H^b)$ (ppm)	$\delta(H^c)$ (ppm)	$\delta(H^d)$ (ppm)	$\delta(H^{core})$ (ppm)
0	0	0.00E+00	0	7.978	9.598	7.461	7.889	7.809
10	10	2.66E-04	0.27	8.143	9.936	7.512	7.868	7.837
10	20	5.22E-04	0.53	8.326	10.312	7.568	7.849	7.868
10	30	7.69E-04	0.78	8.499	10.677	7.621	7.834	7.905
10	40	1.01E-03	1.03	8.647	10.968	7.661	7.823	7.927
10	50	1.23E-03	1.26	8.741	11.152	7.685	7.814	7.923
10	60	1.46E-03	1.48	8.789	11.261	7.700	7.806	7.897
10	70	1.67E-03	1.70	8.817	11.333	7.713	7.797	7.867
15	85	1.97E-03	2.01	8.851	11.434	7.733	7.785	7.834
15	100	2.26E-03	2.31	8.871	11.543	7.754	7.775	7.791

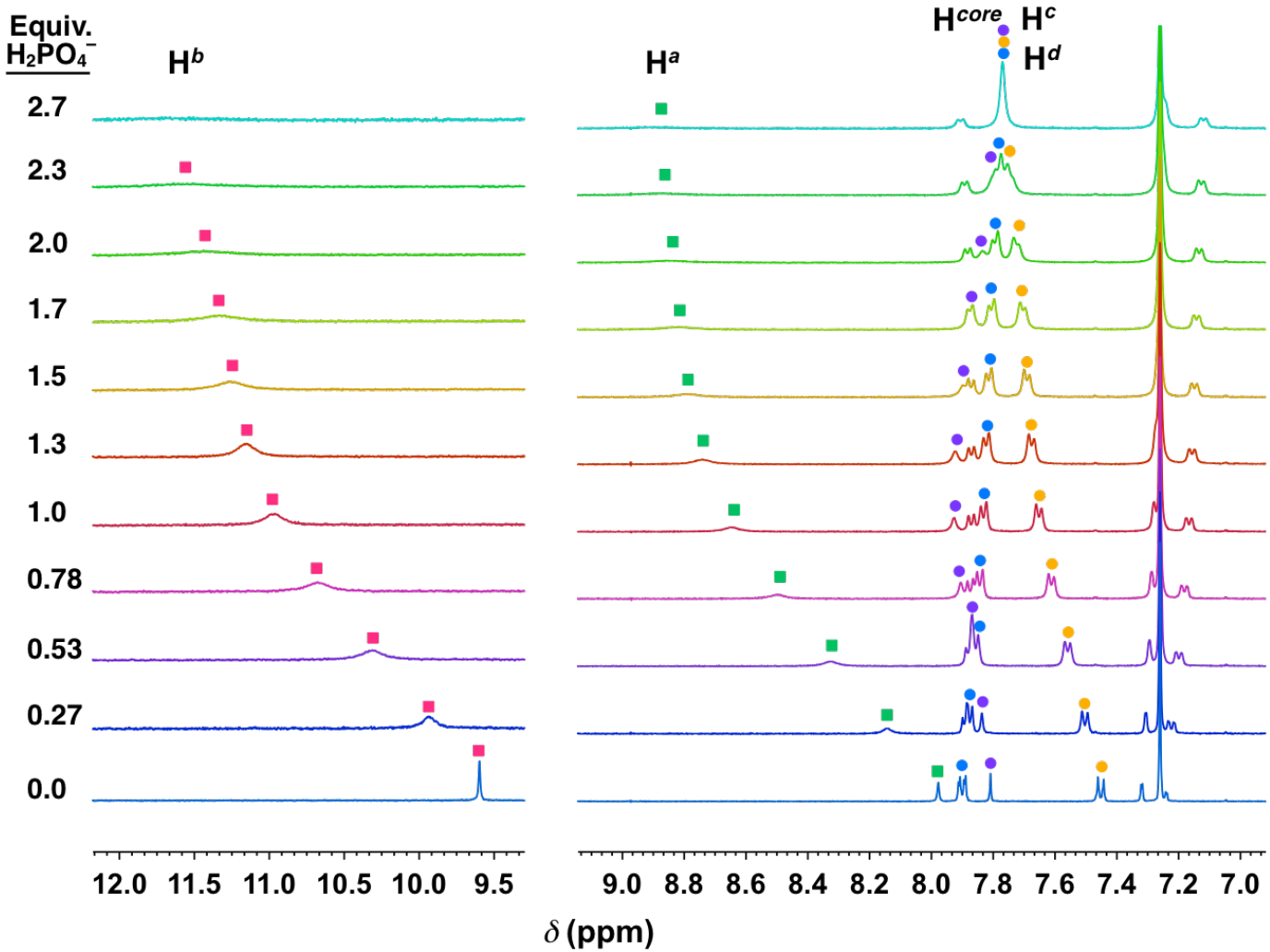

Figure 53. Example stacked spectra from the titration for the addition of tetrabutylammonium dihydrogen phosphate to **2** in 10 % d_6-DMSO/$CDCl_3$. Line broadening was employed elucidate chemical shifts of broadened peaks.

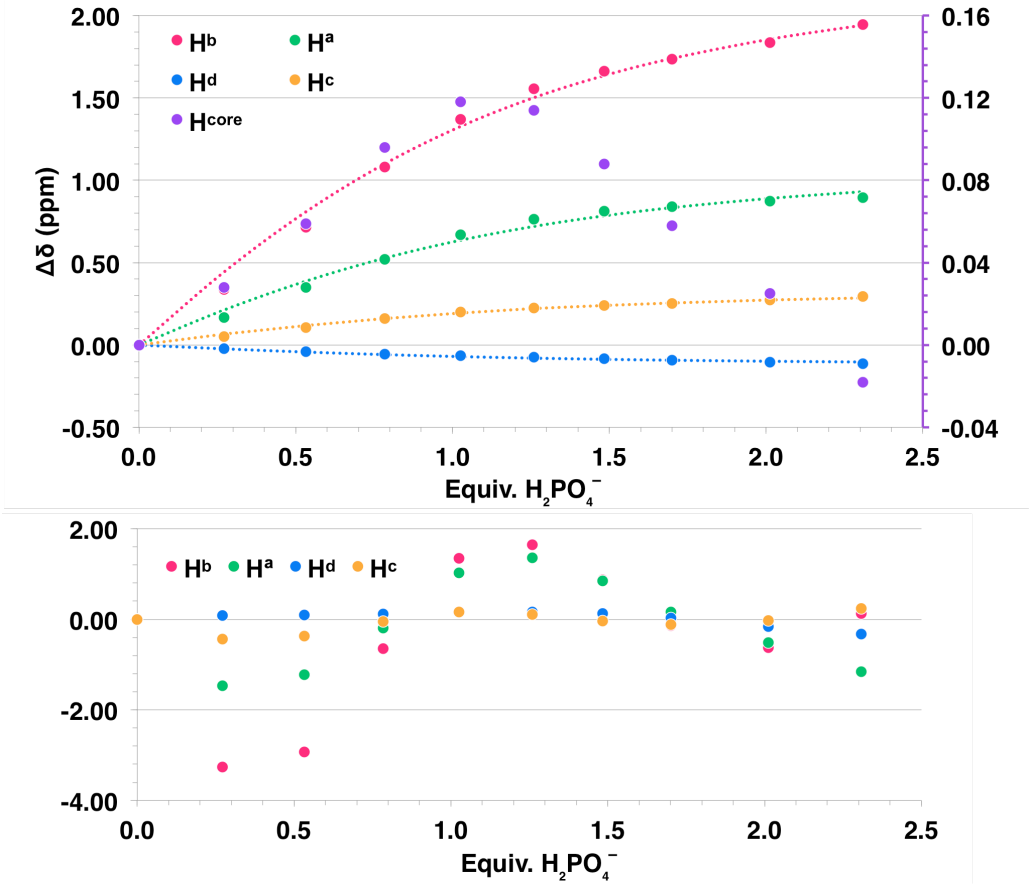

Figure 54. Example stacked spectra from the titration for the addition of tetrabutylammonium dihydrogen phosphate to **2** in 10 % d_6-DMSO/$CDCl_3$.

Table 25. Example titration for the addition of tetrabutylammonium hydrogen phosphate to **2** in 20 % d_6-DMSO/$CDCl_3$.

Addition (µL)	Total Volume Anion (µL)	[$TBAH_2PO_4$] (M)	Equiv. $H_2PO_4^-$	$\delta(H^a)$ (ppm)	$\delta(H^b)$ (ppm)	$\delta(H^c)$ (ppm)	$\delta(H^d)$ (ppm)	$\delta(H^{core})$ (ppm)
0	0	0.00E+00	0	7.840	9.508	7.271	7.675	7.636
15	15	2.70E-04	0.28	7.988	9.773	7.319	7.664	7.669
15	30	5.24E-04	0.54	8.177	10.193	7.375	7.651	7.710
15	45	7.65E-04	0.78	8.365	10.600	7.427	7.640	7.745
15	60	9.92E-04	1.02	8.525	10.921	7.473	7.631	7.776
15	75	1.21E-03	1.24	8.628	11.121	7.501	7.623	7.789
15	90	1.41E-03	1.45	8.653	11.173	7.508	7.616	7.777
15	105	1.61E-03	1.65	8.668	11.203	7.515	7.609	7.758
20	125	1.85E-03	1.90	8.683	11.245	7.522	7.599	7.736
20	145	2.08E-03	2.14	8.691	11.270	7.528	7.591	7.715
25	170	2.35E-03	2.41	8.697	11.323	7.537	7.584	7.696
100	270	3.25E-03	3.33	—	—	7.564	7.564	7.646

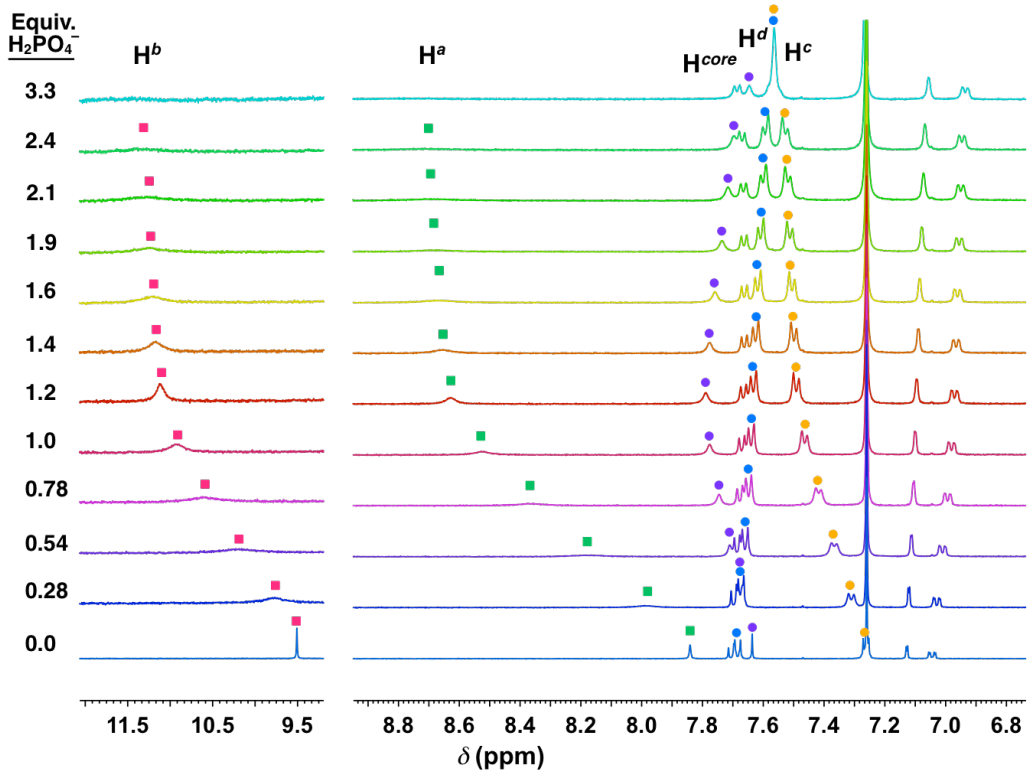

Figure 55. Example stacked spectra from the titration for the addition of tetrabutylammonium dihydrogen phosphate to **2** in 20 % d_6-DMSO/$CDCl_3$. Line broadening was employed elucidate chemical shifts of broadened peaks.

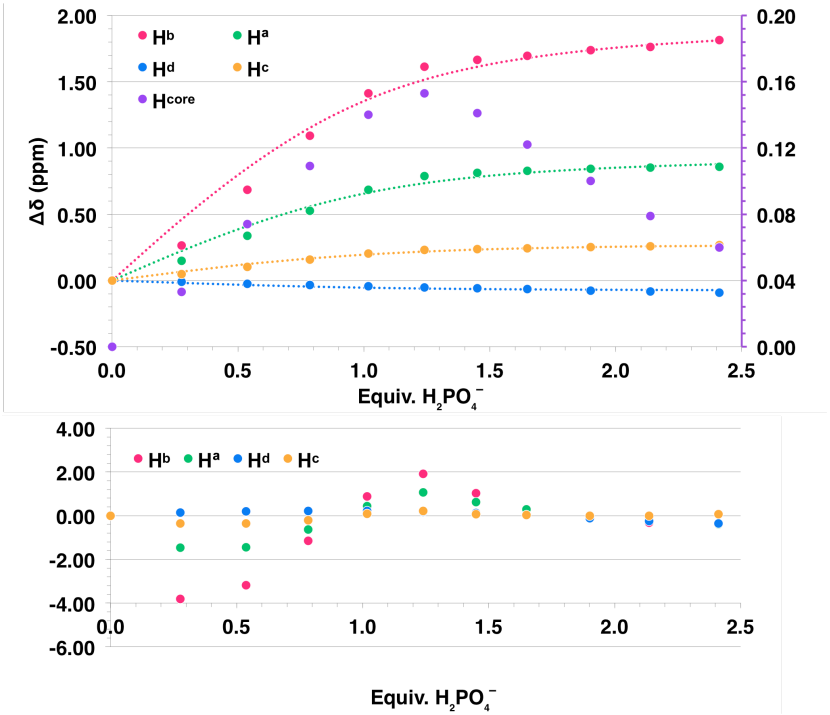

Figure 56. Example stacked spectra from the titration for the addition of tetrabutylammonium dihydrogen phosphate to **2** in 20 % d_6-DMSO/$CDCl_3$.

D.4. X-ray Crystallography

Table 26. Crystal data and structure refinement for **2•Acetone.**

Identification code	mh82	
Empirical formula	C75 H81 N9 O13	
Formula weight	1316.49	
Temperature	173(2) K	
Wavelength	0.71073 Å	
Crystal system	Triclinic	
Space group	P-1	
Unit cell dimensions	a = 12.2820(17) Å	a= 83.428(2)°.
	b = 13.7330(19) Å	b= 78.604(2)°.
	c = 21.485(3) Å	g = 87.611(2)°.
Volume	3528.4(8) Å3	
Z	2	
Density (calculated)	1.239 Mg/m^3	
Absorption coefficient	0.086 mm^{-1}	
F(000)	1396	
Crystal size	0.42 x 0.27 x 0.18 mm^3	
Theta range for data collection	1.49 to 27.00°.	
Index ranges	-15<=h<=15, -17<=k<=17, -27<=l<=27	
Reflections collected	39977	
Independent reflections	15274 [R(int) = 0.0363]	
Completeness to theta = 27.00°	99.2 %	
Absorption correction	Semi-empirical from equivalents	
Max. and min. transmission	0.9847 and 0.9649	
Refinement method	Full-matrix least-squares on F2	
Data / restraints / parameters	15274 / 0 / 898	
Goodness-of-fit on F2	1.019	
Final R indices [I>2sigma(I)]	R1 = 0.0540, wR2 = 0.1325	
R indices (all data)	R1 = 0.0804, wR2 = 0.1512	
Largest diff. peak and hole	0.421 and -0.322 e.$Å^{-3}$	

Table 27. Atomic coordinates (x 10^4) and equivalent isotropic displacement parameters ($Å^2$ x 10^3) for **2•Acetone.** U(eq) is defined as one third of the trace of the orthogonalized U^{ij} tensor.

Atom	X	Y	Z	U(eq)
O(1)	13138(1)	5084(1)	2533(1)	46(1)
O(2)	14058(2)	10002(1)	1793(1)	91(1)
O(3)	12918(2)	10324(1)	1141(1)	95(1)
O(4)	545(1)	3985(1)	4525(1)	49(1)
O(5)	-945(2)	8303(1)	2406(1)	66(1)
O(6)	-2071(2)	7102(1)	2552(1)	79(1)
O(7)	3583(1)	7121(1)	24(1)	48(1)
O(8)	332(2)	3452(2)	-1052(1)	96(1)
O(9)	-142(2)	4952(2)	-1293(1)	78(1)
N(1)	11711(1)	4252(1)	2319(1)	33(1)
N(2)	11977(1)	5853(1)	1912(1)	35(1)

Table 27 Continued.

Atom	X	Y	Z	U(eq)
N(3)	13356(2)	9757(2)	1507(1)	67(1)
N(4)	2409(1)	3914(1)	4503(1)	33(1)
N(5)	1657(1)	5201(1)	3956(1)	33(1)
N(6)	-1209(2)	7462(1)	2615(1)	50(1)
N(7)	4705(1)	6416(1)	687(1)	35(1)
N(8)	3418(1)	5498(1)	384(1)	37(1)
N(9)	395(2)	4331(2)	-1016(1)	61(1)
C(1)	7804(1)	3637(1)	2782(1)	26(1)
C(2)	6960(1)	3198(1)	3249(1)	27(1)
C(3)	5869(1)	3549(1)	3304(1)	25(1)
C(4)	5608(1)	4321(1)	2871(1)	25(1)
C(5)	6445(1)	4760(1)	2400(1)	25(1)
C(6)	7540(1)	4420(1)	2362(1)	28(1)
C(7)	8934(1)	3314(1)	2766(1)	29(1)
C(8)	9862(1)	3057(1)	2803(1)	29(1)
C(9)	10952(1)	2730(1)	2884(1)	28(1)
C(10)	11097(2)	1801(1)	3193(1)	31(1)
C(11)	12124(2)	1444(1)	3303(1)	32(1)
C(12)	13011(2)	2068(1)	3096(1)	37(1)
C(13)	12898(2)	2996(1)	2785(1)	36(1)
C(14)	11871(1)	3342(1)	2667(1)	29(1)
C(15)	12222(2)	418(1)	3656(1)	39(1)
C(16)	11768(2)	-346(2)	3320(1)	57(1)
C(17)	11543(2)	419(2)	4336(1)	58(1)
C(18)	13421(2)	138(2)	3703(1)	62(1)
C(19)	12345(1)	5064(1)	2276(1)	32(1)
C(20)	12367(2)	6812(1)	1821(1)	35(1)
C(21)	13242(2)	7100(2)	2078(1)	45(1)
C(22)	13551(2)	8069(2)	1977(1)	53(1)
C(23)	13005(2)	8737(2)	1619(1)	49(1)
C(24)	12146(2)	8468(2)	1356(1)	54(1)
C(25)	11825(2)	7508(2)	1460(1)	47(1)
C(26)	5035(1)	3145(1)	3823(1)	27(1)
C(27)	4362(1)	2827(1)	4275(1)	28(1)
C(28)	3488(1)	2489(1)	4793(1)	26(1)
C(29)	3616(1)	1632(1)	5189(1)	28(1)
C(30)	2762(1)	1263(1)	5673(1)	28(1)
C(31)	1774(2)	1812(1)	5756(1)	33(1)
C(32)	1630(2)	2680(1)	5384(1)	34(1)
C(33)	2483(1)	3030(1)	4891(1)	28(1)
C(34)	2922(2)	313(1)	6098(1)	33(1)
C(35)	1810(2)	-138(2)	6419(1)	59(1)
C(36)	3532(2)	552(2)	6615(1)	57(1)
C(37)	3616(2)	-440(1)	5711(1)	51(1)
C(38)	1460(2)	4333(1)	4343(1)	31(1)
C(39)	897(1)	5745(1)	3647(1)	29(1)
C(40)	-59(2)	5342(1)	3532(1)	34(1)
C(41)	-744(2)	5910(2)	3192(1)	38(1)
C(42)	-480(2)	6867(1)	2970(1)	35(1)
C(43)	460(2)	7283(1)	3080(1)	34(1)
C(44)	1141(2)	6719(1)	3424(1)	32(1)
C(45)	6212(1)	5571(1)	1962(1)	28(1)
C(46)	6099(1)	6275(1)	1595(1)	30(1)
C(47)	6020(2)	7159(1)	1180(1)	30(1)
C(48)	6666(2)	7947(1)	1226(1)	34(1)
C(49)	6638(2)	8835(1)	847(1)	39(1)

Table 27 Continued.

Atom	X	Y	Z	U(eq)
C(50)	5914(2)	8906(1)	424(1)	45(1)
C(51)	5259(2)	8138(1)	368(1)	41(1)
C(52)	5311(2)	7243(1)	735(1)	33(1)
C(53)	7368(2)	9674(2)	915(1)	47(1)
C(54)	7113(2)	9926(2)	1603(1)	55(1)
C(55)	8590(2)	9352(2)	743(1)	74(1)
C(56)	7148(3)	10606(2)	489(1)	89(1)
C(57)	3881(2)	6407(1)	340(1)	35(1)
C(58)	2630(2)	5254(2)	44(1)	36(1)
C(59)	1982(2)	5945(2)	-258(1)	46(1)
C(60)	1245(2)	5636(2)	-601(1)	50(1)
C(61)	1143(2)	4655(2)	-636(1)	47(1)
C(62)	1753(2)	3955(2)	-330(1)	47(1)
C(63)	2491(2)	4260(2)	9(1)	42(1)
O(1S)	4000(1)	5586(1)	3922(1)	54(1)
C(1S)	4790(2)	6106(2)	3839(1)	47(1)
C(2S)	4830(3)	7058(2)	3438(2)	93(1)
C(3S)	5771(3)	5814(3)	4124(2)	109(1)
O(2S)	4745(1)	4147(1)	1078(1)	57(1)
C(4S)	4859(2)	3287(2)	1265(1)	46(1)
C(5S)	3985(3)	2574(2)	1256(1)	70(1)
C(6S)	5857(2)	2914(2)	1512(1)	60(1)
O(3S)	7277(3)	2377(2)	5407(1)	150(1)
C(7S)	7904(2)	2764(2)	4957(1)	66(1)
C(8S)	8870(2)	2230(2)	4621(2)	78(1)
C(9S)	7743(2)	3799(2)	4707(1)	63(1)
O(4S)	-937(2)	2035(2)	1291(2)	124(1)
C(10S)	-72(3)	1705(2)	1415(1)	72(1)
C(11S)	1002(3)	2210(3)	1161(2)	118(1)
C(12S)	-19(3)	824(2)	1873(1)	81(1)

Table 28. Bond lengths for **2•Acetone**.

Atoms	Å	Atoms	Å
O(1)-C(19)	1.213(2)	N(4)-H(4N)	0.86(2)
O(2)-N(3)	1.230(3)	N(5)-C(38)	1.374(2)
O(3)-N(3)	1.227(3)	N(5)-C(39)	1.394(2)
O(4)-C(38)	1.212(2)	N(5)-H(5N)	0.90(2)
O(5)-N(6)	1.223(2)	N(6)-C(42)	1.455(2)
O(6)-N(6)	1.225(2)	N(7)-C(57)	1.371(2)
O(7)-C(57)	1.214(2)	N(7)-C(52)	1.408(2)
O(8)-N(9)	1.225(3)	N(7)-H(7N)	0.87(2)
O(9)-N(9)	1.228(3)	N(8)-C(57)	1.378(3)
N(1)-C(19)	1.371(2)	N(8)-C(58)	1.394(2)
N(1)-C(14)	1.409(2)	N(8)-H(8N)	0.84(2)
N(1)-H(1N)	0.89(2)	N(9)-C(61)	1.457(3)
N(2)-C(19)	1.377(2)	C(1)-C(6)	1.394(2)
N(2)-C(20)	1.399(2)	C(1)-C(2)	1.395(2)
N(2)-H(2N)	0.86(2)	C(1)-C(7)	1.434(2)
N(3)-C(23)	1.462(3)	C(2)-C(3)	1.394(2)
N(4)-C(38)	1.366(2)	C(2)-H(2B)	0.9500
N(4)-C(33)	1.403(2)	C(3)-C(4)	1.398(2)

Table 28 Continued.

Atoms	Å	Atoms	Å
C(3)-C(26)	1.433(2)	C(35)-H(35C)	0.9800
C(4)-C(5)	1.394(2)	C(36)-H(36A)	0.9800
C(4)-H(4B)	0.9500	C(36)-H(36B)	0.9800
C(5)-C(6)	1.395(2)	C(36)-H(36C)	0.9800
C(5)-C(45)	1.430(2)	C(37)-H(37A)	0.9800
C(6)-H(6A)	0.9500	C(37)-H(37B)	0.9800
C(7)-C(8)	1.195(2)	C(37)-H(37C)	0.9800
C(8)-C(9)	1.431(2)	C(39)-C(44)	1.391(2)
C(9)-C(10)	1.391(2)	C(39)-C(40)	1.395(3)
C(9)-C(14)	1.406(2)	C(40)-C(41)	1.381(3)
C(10)-C(11)	1.388(2)	C(40)-H(40A)	0.9500
C(10)-H(10A)	0.9500	C(41)-C(42)	1.376(3)
C(11)-C(12)	1.386(3)	C(41)-H(41A)	0.9500
C(11)-C(15)	1.534(3)	C(42)-C(43)	1.381(3)
C(12)-C(13)	1.384(3)	C(43)-C(44)	1.380(2)
C(12)-H(12A)	0.9500	C(43)-H(43A)	0.9500
C(13)-C(14)	1.389(2)	C(44)-H(44A)	0.9500
C(13)-H(13A)	0.9500	C(45)-C(46)	1.197(2)
C(15)-C(16)	1.521(3)	C(46)-C(47)	1.434(2)
C(15)-C(18)	1.527(3)	C(47)-C(48)	1.392(3)
C(15)-C(17)	1.533(3)	C(47)-C(52)	1.406(2)
C(16)-H(16A)	0.9800	C(48)-C(49)	1.390(2)
C(16)-H(16B)	0.9800	C(48)-H(48A)	0.9500
C(16)-H(16C)	0.9800	C(49)-C(50)	1.386(3)
C(17)-H(17A)	0.9800	C(49)-C(53)	1.526(3)
C(17)-H(17B)	0.9800	C(50)-C(51)	1.382(3)
C(17)-H(17C)	0.9800	C(50)-H(50A)	0.9500
C(18)-H(18A)	0.9800	C(51)-C(52)	1.389(2)
C(18)-H(18B)	0.9800	C(51)-H(51A)	0.9500
C(18)-H(18C)	0.9800	C(53)-C(54)	1.526(3)
C(20)-C(25)	1.393(3)	C(53)-C(56)	1.532(3)
C(20)-C(21)	1.392(3)	C(53)-C(55)	1.533(4)
C(21)-C(22)	1.380(3)	C(54)-H(54A)	0.9800
C(21)-H(21A)	0.9500	C(54)-H(54B)	0.9800
C(22)-C(23)	1.369(3)	C(54)-H(54C)	0.9800
C(22)-H(22A)	0.9500	C(55)-H(55A)	0.9800
C(23)-C(24)	1.373(3)	C(55)-H(55B)	0.9800
C(24)-C(25)	1.372(3)	C(55)-H(55C)	0.9800
C(24)-H(24A)	0.9500	C(56)-H(56A)	0.9800
C(25)-H(25A)	0.9500	C(56)-H(56B)	0.9800
C(26)-C(27)	1.199(2)	C(56)-H(56C)	0.9800
C(27)-C(28)	1.433(2)	C(58)-C(63)	1.396(3)
C(28)-C(29)	1.393(2)	C(58)-C(59)	1.399(3)
C(28)-C(33)	1.406(2)	C(59)-C(60)	1.383(3)
C(29)-C(30)	1.390(2)	C(59)-H(59A)	0.9500
C(29)-H(29A)	0.9500	C(60)-C(61)	1.370(3)
C(30)-C(31)	1.393(2)	C(60)-H(60A)	0.9500
C(30)-C(34)	1.533(2)	C(61)-C(62)	1.380(3)
C(31)-C(32)	1.383(2)	C(62)-C(63)	1.375(3)
C(31)-H(31A)	0.9500	C(62)-H(62A)	0.9500
C(32)-C(33)	1.391(2)	C(63)-H(63A)	0.9500
C(32)-H(32A)	0.9500	O(1S)-C(1S)	1.202(2)
C(34)-C(35)	1.525(3)	C(1S)-C(3S)	1.477(4)
C(34)-C(37)	1.527(3)	C(1S)-C(2S)	1.478(4)
C(34)-C(36)	1.528(3)	C(2S)-H(2SA)	0.9800
C(35)-H(35A)	0.9800	C(2S)-H(2SB)	0.9800
C(35)-H(35B)	0.9800	C(2S)-H(2SC)	0.9800

Table 28 Continued.

Atoms	Å	Atoms	Å
C(3S)-H(3SA)	0.9800	C(8S)-H(8SA)	0.9800
C(3S)-H(3SB)	0.9800	C(8S)-H(8SB)	0.9800
C(3S)-H(3SC)	0.9800	C(8S)-H(8SC)	0.9800
O(2S)-C(4S)	1.214(2)	C(9S)-H(9SA)	0.9800
C(4S)-C(6S)	1.479(3)	C(9S)-H(9SB)	0.9800
C(4S)-C(5S)	1.488(3)	C(9S)-H(9SC)	0.9800
C(5S)-H(5SA)	0.9800	O(4S)-C(10S)	1.205(4)
C(5S)-H(5SB)	0.9800	C(10S)-C(12S)	1.477(4)
C(5S)-H(5SC)	0.9800	C(10S)-C(11S)	1.492(4)
C(6S)-H(6SA)	0.9800	C(11S)-H(11A)	0.9800
C(6S)-H(6SB)	0.9800	C(11S)-H(11B)	0.9800
C(6S)-H(6SC)	0.9800	C(11S)-H(11C)	0.9800
O(3S)-C(7S)	1.198(3)	C(12S)-H(12B)	0.9800
C(7S)-C(8S)	1.475(4)	C(12S)-H(12C)	0.9800
C(7S)-C(9S)	1.480(4)	C(12S)-H(12D)	0.9800

Table 29. Bond angles for **2•Acetone**.

Atoms	°	Atoms	°
C(19)-N(1)-C(14)	125.49(16)	C(4)-C(3)-C(26)	120.75(15)
C(19)-N(1)-H(1N)	116.1(14)	C(5)-C(4)-C(3)	120.11(15)
C(14)-N(1)-H(1N)	116.9(14)	C(5)-C(4)-H(4B)	119.9
C(19)-N(2)-C(20)	127.11(17)	C(3)-C(4)-H(4B)	119.9
C(19)-N(2)-H(2N)	115.8(14)	C(4)-C(5)-C(6)	119.54(15)
C(20)-N(2)-H(2N)	117.1(14)	C(4)-C(5)-C(45)	121.50(15)
O(3)-N(3)-O(2)	123.7(2)	C(6)-C(5)-C(45)	118.94(15)
O(3)-N(3)-C(23)	118.0(2)	C(1)-C(6)-C(5)	120.77(15)
O(2)-N(3)-C(23)	118.3(2)	C(1)-C(6)-H(6A)	119.6
C(38)-N(4)-C(33)	126.01(16)	C(5)-C(6)-H(6A)	119.6
C(38)-N(4)-H(4N)	117.8(14)	C(8)-C(7)-C(1)	174.65(19)
C(33)-N(4)-H(4N)	115.3(14)	C(7)-C(8)-C(9)	176.87(19)
C(38)-N(5)-C(39)	126.44(16)	C(10)-C(9)-C(14)	119.77(15)
C(38)-N(5)-H(5N)	116.7(13)	C(10)-C(9)-C(8)	119.33(16)
C(39)-N(5)-H(5N)	116.8(13)	C(14)-C(9)-C(8)	120.89(16)
O(5)-N(6)-O(6)	123.07(19)	C(11)-C(10)-C(9)	122.55(17)
O(5)-N(6)-C(42)	118.60(19)	C(11)-C(10)-H(10A)	118.7
O(6)-N(6)-C(42)	118.31(19)	C(9)-C(10)-H(10A)	118.7
C(57)-N(7)-C(52)	125.52(16)	C(12)-C(11)-C(10)	116.52(16)
C(57)-N(7)-H(7N)	118.2(13)	C(12)-C(11)-C(15)	123.59(16)
C(52)-N(7)-H(7N)	116.3(13)	C(10)-C(11)-C(15)	119.86(17)
C(57)-N(8)-C(58)	125.74(17)	C(13)-C(12)-C(11)	122.47(16)
C(57)-N(8)-H(8N)	117.4(15)	C(13)-C(12)-H(12A)	118.8
C(58)-N(8)-H(8N)	116.0(15)	C(11)-C(12)-H(12A)	118.8
O(8)-N(9)-O(9)	122.6(2)	C(12)-C(13)-C(14)	120.66(17)
O(8)-N(9)-C(61)	118.9(2)	C(12)-C(13)-H(13A)	119.7
O(9)-N(9)-C(61)	118.6(2)	C(14)-C(13)-H(13A)	119.7
C(6)-C(1)-C(2)	119.26(15)	C(13)-C(14)-C(9)	118.00(16)
C(6)-C(1)-C(7)	121.05(15)	C(13)-C(14)-N(1)	123.54(16)
C(2)-C(1)-C(7)	119.59(15)	C(9)-C(14)-N(1)	118.39(15)
C(3)-C(2)-C(1)	120.49(15)	C(16)-C(15)-C(18)	108.79(18)
C(3)-C(2)-H(2B)	119.8	C(16)-C(15)-C(17)	109.40(19)
C(1)-C(2)-H(2B)	119.8	C(18)-C(15)-C(17)	107.99(19)
C(2)-C(3)-C(4)	119.78(15)	C(16)-C(15)-C(11)	110.41(16)
C(2)-C(3)-C(26)	119.40(15)	C(18)-C(15)-C(11)	112.09(17)

Table 29 Continued.

Atoms	°	Atoms	°
C(17)-C(15)-C(11)	108.09(16)	C(32)-C(33)-N(4)	123.46(15)
C(15)-C(16)-H(16A)	109.5	C(32)-C(33)-C(28)	118.34(15)
C(15)-C(16)-H(16B)	109.5	N(4)-C(33)-C(28)	118.15(15)
H(16A)-C(16)-H(16B)	109.5	C(35)-C(34)-C(37)	108.53(17)
C(15)-C(16)-H(16C)	109.5	C(35)-C(34)-C(36)	108.76(18)
H(16A)-C(16)-H(16C)	109.5	C(37)-C(34)-C(36)	108.60(18)
H(16B)-C(16)-H(16C)	109.5	C(35)-C(34)-C(30)	111.36(16)
C(15)-C(17)-H(17A)	109.5	C(37)-C(34)-C(30)	111.05(15)
C(15)-C(17)-H(17B)	109.5	C(36)-C(34)-C(30)	108.48(15)
H(17A)-C(17)-H(17B)	109.5	C(34)-C(35)-H(35A)	109.5
C(15)-C(17)-H(17C)	109.5	C(34)-C(35)-H(35B)	109.5
H(17A)-C(17)-H(17C)	109.5	H(35A)-C(35)-H(35B)	109.5
H(17B)-C(17)-H(17C)	109.5	C(34)-C(35)-H(35C)	109.5
C(15)-C(18)-H(18A)	109.5	H(35A)-C(35)-H(35C)	109.5
C(15)-C(18)-H(18B)	109.5	H(35B)-C(35)-H(35C)	109.5
H(18A)-C(18)-H(18B)	109.5	C(34)-C(36)-H(36A)	109.5
C(15)-C(18)-H(18C)	109.5	C(34)-C(36)-H(36B)	109.5
H(18A)-C(18)-H(18C)	109.5	H(36A)-C(36)-H(36B)	109.5
H(18B)-C(18)-H(18C)	109.5	C(34)-C(36)-H(36C)	109.5
O(1)-C(19)-N(1)	123.63(17)	H(36A)-C(36)-H(36C)	109.5
O(1)-C(19)-N(2)	123.94(17)	H(36B)-C(36)-H(36C)	109.5
N(1)-C(19)-N(2)	112.43(16)	C(34)-C(37)-H(37A)	109.5
C(25)-C(20)-C(21)	119.22(18)	C(34)-C(37)-H(37B)	109.5
C(25)-C(20)-N(2)	117.13(18)	H(37A)-C(37)-H(37B)	109.5
C(21)-C(20)-N(2)	123.64(18)	C(34)-C(37)-H(37C)	109.5
C(22)-C(21)-C(20)	119.6(2)	H(37A)-C(37)-H(37C)	109.5
C(22)-C(21)-H(21A)	120.2	H(37B)-C(37)-H(37C)	109.5
C(20)-C(21)-H(21A)	120.2	O(4)-C(38)-N(4)	124.03(17)
C(23)-C(22)-C(21)	119.9(2)	O(4)-C(38)-N(5)	123.71(17)
C(23)-C(22)-H(22A)	120.0	N(4)-C(38)-N(5)	112.26(16)
C(21)-C(22)-H(22A)	120.0	C(44)-C(39)-N(5)	117.70(16)
C(22)-C(23)-C(24)	121.4(2)	C(44)-C(39)-C(40)	119.51(16)
C(22)-C(23)-N(3)	119.2(2)	N(5)-C(39)-C(40)	122.73(16)
C(24)-C(23)-N(3)	119.4(2)	C(41)-C(40)-C(39)	119.66(17)
C(25)-C(24)-C(23)	119.1(2)	C(41)-C(40)-H(40A)	120.2
C(25)-C(24)-H(24A)	120.5	C(39)-C(40)-H(40A)	120.2
C(23)-C(24)-H(24A)	120.5	C(42)-C(41)-C(40)	119.76(18)
C(24)-C(25)-C(20)	120.7(2)	C(42)-C(41)-H(41A)	120.1
C(24)-C(25)-H(25A)	119.6	C(40)-C(41)-H(41A)	120.1
C(20)-C(25)-H(25A)	119.6	C(41)-C(42)-C(43)	121.60(17)
C(27)-C(26)-C(3)	176.99(19)	C(41)-C(42)-N(6)	119.44(18)
C(26)-C(27)-C(28)	175.30(18)	C(43)-C(42)-N(6)	118.96(18)
C(29)-C(28)-C(33)	119.99(15)	C(44)-C(43)-C(42)	118.65(17)
C(29)-C(28)-C(27)	121.14(15)	C(44)-C(43)-H(43A)	120.7
C(33)-C(28)-C(27)	118.87(15)	C(42)-C(43)-H(43A)	120.7
C(30)-C(29)-C(28)	122.22(15)	C(43)-C(44)-C(39)	120.81(17)
C(30)-C(29)-H(29A)	118.9	C(43)-C(44)-H(44A)	119.6
C(28)-C(29)-H(29A)	118.9	C(39)-C(44)-H(44A)	119.6
C(29)-C(30)-C(31)	116.39(15)	C(46)-C(45)-C(5)	174.85(18)
C(29)-C(30)-C(34)	121.12(15)	C(45)-C(46)-C(47)	175.45(19)
C(31)-C(30)-C(34)	122.48(15)	C(48)-C(47)-C(52)	120.01(16)
C(32)-C(31)-C(30)	122.88(16)	C(48)-C(47)-C(46)	118.26(16)
C(32)-C(31)-H(31A)	118.6	C(52)-C(47)-C(46)	121.73(16)
C(30)-C(31)-H(31A)	118.6	C(49)-C(48)-C(47)	122.39(17)
C(31)-C(32)-C(33)	120.12(16)	C(49)-C(48)-H(48A)	118.8
C(31)-C(32)-H(32A)	119.9	C(47)-C(48)-H(48A)	118.8
C(33)-C(32)-H(32A)	119.9	C(50)-C(49)-C(48)	116.41(18)

Table 29 Continued.

Atoms	°	Atoms	°
C(50)-C(49)-C(53)	123.33(17)	C(3S)-C(1S)-C(2S)	117.2(3)
C(48)-C(49)-C(53)	120.25(17)	C(1S)-C(2S)-H(2SA)	109.5
C(51)-C(50)-C(49)	122.59(18)	C(1S)-C(2S)-H(2SB)	109.5
C(51)-C(50)-H(50A)	118.7	H(2SA)-C(2S)-H(2SB)	109.5
C(49)-C(50)-H(50A)	118.7	C(1S)-C(2S)-H(2SC)	109.5
C(50)-C(51)-C(52)	120.81(18)	H(2SA)-C(2S)-H(2SC)	109.5
C(50)-C(51)-H(51A)	119.6	H(2SB)-C(2S)-H(2SC)	109.5
C(52)-C(51)-H(51A)	119.6	C(1S)-C(3S)-H(3SA)	109.5
C(51)-C(52)-C(47)	117.75(17)	C(1S)-C(3S)-H(3SB)	109.5
C(51)-C(52)-N(7)	124.06(17)	H(3SA)-C(3S)-H(3SB)	109.5
C(47)-C(52)-N(7)	118.19(16)	C(1S)-C(3S)-H(3SC)	109.5
C(54)-C(53)-C(49)	109.70(18)	H(3SA)-C(3S)-H(3SC)	109.5
C(54)-C(53)-C(56)	107.2(2)	H(3SB)-C(3S)-H(3SC)	109.5
C(49)-C(53)-C(56)	111.70(18)	O(2S)-C(4S)-C(6S)	121.7(2)
C(54)-C(53)-C(55)	109.2(2)	O(2S)-C(4S)-C(5S)	120.5(2)
C(49)-C(53)-C(55)	108.95(18)	C(6S)-C(4S)-C(5S)	117.8(2)
C(56)-C(53)-C(55)	110.1(2)	C(4S)-C(5S)-H(5SA)	109.5
C(53)-C(54)-H(54A)	109.5	C(4S)-C(5S)-H(5SB)	109.5
C(53)-C(54)-H(54B)	109.5	H(5SA)-C(5S)-H(5SB)	109.5
H(54A)-C(54)-H(54B)	109.5	C(4S)-C(5S)-H(5SC)	109.5
C(53)-C(54)-H(54C)	109.5	H(5SA)-C(5S)-H(5SC)	109.5
H(54A)-C(54)-H(54C)	109.5	H(5SB)-C(5S)-H(5SC)	109.5
H(54B)-C(54)-H(54C)	109.5	C(4S)-C(6S)-H(6SA)	109.5
C(53)-C(55)-H(55A)	109.5	C(4S)-C(6S)-H(6SB)	109.5
C(53)-C(55)-H(55B)	109.5	H(6SA)-C(6S)-H(6SB)	109.5
H(55A)-C(55)-H(55B)	109.5	C(4S)-C(6S)-H(6SC)	109.5
C(53)-C(55)-H(55C)	109.5	H(6SA)-C(6S)-H(6SC)	109.5
H(55A)-C(55)-H(55C)	109.5	H(6SB)-C(6S)-H(6SC)	109.5
H(55B)-C(55)-H(55C)	109.5	O(3S)-C(7S)-C(8S)	121.5(3)
C(53)-C(56)-H(56A)	109.5	O(3S)-C(7S)-C(9S)	121.6(3)
C(53)-C(56)-H(56B)	109.5	C(8S)-C(7S)-C(9S)	116.8(2)
H(56A)-C(56)-H(56B)	109.5	C(7S)-C(8S)-H(8SA)	109.5
C(53)-C(56)-H(56C)	109.5	C(7S)-C(8S)-H(8SB)	109.5
H(56A)-C(56)-H(56C)	109.5	H(8SA)-C(8S)-H(8SB)	109.5
H(56B)-C(56)-H(56C)	109.5	C(7S)-C(8S)-H(8SC)	109.5
O(7)-C(57)-N(7)	123.92(18)	H(8SA)-C(8S)-H(8SC)	109.5
O(7)-C(57)-N(8)	122.87(18)	H(8SB)-C(8S)-H(8SC)	109.5
N(7)-C(57)-N(8)	113.21(16)	C(7S)-C(9S)-H(9SA)	109.5
N(8)-C(58)-C(63)	117.32(18)	C(7S)-C(9S)-H(9SB)	109.5
N(8)-C(58)-C(59)	123.76(19)	H(9SA)-C(9S)-H(9SB)	109.5
C(63)-C(58)-C(59)	118.92(19)	C(7S)-C(9S)-H(9SC)	109.5
C(60)-C(59)-C(58)	119.7(2)	H(9SA)-C(9S)-H(9SC)	109.5
C(60)-C(59)-H(59A)	120.2	H(9SB)-C(9S)-H(9SC)	109.5
C(58)-C(59)-H(59A)	120.2	O(4S)-C(10S)-C(12S)	122.2(3)
C(61)-C(60)-C(59)	119.9(2)	O(4S)-C(10S)-C(11S)	122.0(3)
C(61)-C(60)-H(60A)	120.1	C(12S)-C(10S)-C(11S)	115.6(3)
C(59)-C(60)-H(60A)	120.1	C(10S)-C(11S)-H(11A)	109.5
C(60)-C(61)-C(62)	121.7(2)	C(10S)-C(11S)-H(11B)	109.5
C(60)-C(61)-N(9)	119.8(2)	H(11A)-C(11S)-H(11B)	109.5
C(62)-C(61)-N(9)	118.5(2)	C(10S)-C(11S)-H(11C)	109.5
C(63)-C(62)-C(61)	118.6(2)	H(11A)-C(11S)-H(11C)	109.5
C(63)-C(62)-H(62A)	120.7	H(11B)-C(11S)-H(11C)	109.5
C(61)-C(62)-H(62A)	120.7	C(10S)-C(12S)-H(12B)	109.5
C(62)-C(63)-C(58)	121.2(2)	C(10S)-C(12S)-H(12C)	109.5
C(62)-C(63)-H(63A)	119.4	H(12B)-C(12S)-H(12C)	109.5
C(58)-C(63)-H(63A)	119.4	C(10S)-C(12S)-H(12D)	109.5
O(1S)-C(1S)-C(3S)	121.5(3)	H(12B)-C(12S)-H(12D)	109.5
O(1S)-C(1S)-C(2S)	121.3(2)	H(12C)-C(12S)-H(12D)	109.5

Table 30. Torsion angles for **2•Acetone**.

Atoms	°	Atoms	°
C(6)-C(1)-C(2)-C(3)	-1.2(3)	N(2)-C(20)-C(25)-C(24)	179.10(19)
C(7)-C(1)-C(2)-C(3)	175.22(16)	C(2)-C(3)-C(26)-C(27)	68(4)
C(1)-C(2)-C(3)-C(4)	2.6(3)	C(4)-C(3)-C(26)-C(27)	-109(3)
C(1)-C(2)-C(3)-C(26)	-174.40(16)	C(3)-C(26)-C(27)-C(28)	121(3)
C(2)-C(3)-C(4)-C(5)	-2.2(2)	C(26)-C(27)-C(28)-C(29)	156(2)
C(26)-C(3)-C(4)-C(5)	174.76(16)	C(26)-C(27)-C(28)-C(33)	-23(2)
C(3)-C(4)-C(5)-C(6)	0.4(2)	C(33)-C(28)-C(29)-C(30)	2.4(3)
C(3)-C(4)-C(5)-C(45)	-177.94(16)	C(27)-C(28)-C(29)-C(30)	-176.67(16)
C(2)-C(1)-C(6)-C(5)	-0.7(3)	C(28)-C(29)-C(30)-C(31)	-1.9(3)
C(7)-C(1)-C(6)-C(5)	-177.02(16)	C(28)-C(29)-C(30)-C(34)	179.35(16)
C(4)-C(5)-C(6)-C(1)	1.1(3)	C(29)-C(30)-C(31)-C(32)	-0.2(3)
C(45)-C(5)-C(6)-C(1)	179.44(16)	C(34)-C(30)-C(31)-C(32)	178.59(17)
C(6)-C(1)-C(7)-C(8)	123.4(19)	C(30)-C(31)-C(32)-C(33)	1.7(3)
C(2)-C(1)-C(7)-C(8)	-53(2)	C(31)-C(32)-C(33)-N(4)	-178.55(17)
C(1)-C(7)-C(8)-C(9)	32(5)	C(31)-C(32)-C(33)-C(28)	-1.1(3)
C(7)-C(8)-C(9)-C(10)	45(4)	C(38)-N(4)-C(33)-C(32)	-30.0(3)
C(7)-C(8)-C(9)-C(14)	-133(3)	C(38)-N(4)-C(33)-C(28)	152.55(18)
C(14)-C(9)-C(10)-C(11)	0.4(3)	C(29)-C(28)-C(33)-C(32)	-0.8(3)
C(8)-C(9)-C(10)-C(11)	-178.29(17)	C(27)-C(28)-C(33)-C(32)	178.26(16)
C(9)-C(10)-C(11)-C(12)	0.8(3)	C(29)-C(28)-C(33)-N(4)	176.72(16)
C(9)-C(10)-C(11)-C(15)	179.03(17)	C(27)-C(28)-C(33)-N(4)	-4.2(2)
C(10)-C(11)-C(12)-C(13)	-1.1(3)	C(29)-C(30)-C(34)-C(35)	-159.56(19)
C(15)-C(11)-C(12)-C(13)	-179.24(18)	C(31)-C(30)-C(34)-C(35)	21.8(3)
C(11)-C(12)-C(13)-C(14)	0.2(3)	C(29)-C(30)-C(34)-C(37)	-38.5(2)
C(12)-C(13)-C(14)-C(9)	1.1(3)	C(31)-C(30)-C(34)-C(37)	142.82(19)
C(12)-C(13)-C(14)-N(1)	-175.94(18)	C(29)-C(30)-C(34)-C(36)	80.8(2)
C(10)-C(9)-C(14)-C(13)	-1.4(3)	C(31)-C(30)-C(34)-C(36)	-97.9(2)
C(8)-C(9)-C(14)-C(13)	177.30(17)	C(33)-N(4)-C(38)-O(4)	0.5(3)
C(10)-C(9)-C(14)-N(1)	175.83(16)	C(33)-N(4)-C(38)-N(5)	179.82(16)
C(8)-C(9)-C(14)-N(1)	-5.5(3)	C(39)-N(5)-C(38)-O(4)	-9.1(3)
C(19)-N(1)-C(14)-C(13)	-28.5(3)	C(39)-N(5)-C(38)-N(4)	171.51(17)
C(19)-N(1)-C(14)-C(9)	154.48(17)	C(38)-N(5)-C(39)-C(44)	162.73(18)
C(12)-C(11)-C(15)-C(16)	-126.1(2)	C(38)-N(5)-C(39)-C(40)	-20.0(3)
C(10)-C(11)-C(15)-C(16)	55.8(2)	C(44)-C(39)-C(40)-C(41)	0.8(3)
C(12)-C(11)-C(15)-C(18)	-4.7(3)	N(5)-C(39)-C(40)-C(41)	-176.46(17)
C(10)-C(11)-C(15)-C(18)	177.29(19)	C(39)-C(40)-C(41)-C(42)	-0.1(3)
C(12)-C(11)-C(15)-C(17)	114.2(2)	C(40)-C(41)-C(42)-C(43)	-0.1(3)
C(10)-C(11)-C(15)-C(17)	-63.8(2)	C(40)-C(41)-C(42)-N(6)	-179.67(18)
C(14)-N(1)-C(19)-O(1)	0.9(3)	O(5)-N(6)-C(42)-C(41)	-177.90(19)
C(14)-N(1)-C(19)-N(2)	-178.78(16)	O(6)-N(6)-C(42)-C(41)	3.6(3)
C(20)-N(2)-C(19)-O(1)	-6.1(3)	O(5)-N(6)-C(42)-C(43)	2.5(3)
C(20)-N(2)-C(19)-N(1)	173.54(17)	O(6)-N(6)-C(42)-C(43)	-176.0(2)
C(19)-N(2)-C(20)-C(25)	-176.40(18)	C(41)-C(42)-C(43)-C(44)	-0.4(3)
C(19)-N(2)-C(20)-C(21)	2.5(3)	N(6)-C(42)-C(43)-C(44)	179.20(17)
C(25)-C(20)-C(21)-C(22)	0.6(3)	C(42)-C(43)-C(44)-C(39)	1.1(3)
N(2)-C(20)-C(21)-C(22)	-178.33(19)	N(5)-C(39)-C(44)-C(43)	176.11(16)
C(20)-C(21)-C(22)-C(23)	-0.7(3)	C(40)-C(39)-C(44)-C(43)	-1.3(3)
C(21)-C(22)-C(23)-C(24)	0.1(3)	C(4)-C(5)-C(45)-C(46)	150(2)
C(21)-C(22)-C(23)-N(3)	-179.0(2)	C(6)-C(5)-C(45)-C(46)	-29(2)
O(3)-N(3)-C(23)-C(22)	173.9(2)	C(5)-C(45)-C(46)-C(47)	-34(4)
O(2)-N(3)-C(23)-C(22)	-7.2(3)	C(45)-C(46)-C(47)-C(48)	6(3)
O(3)-N(3)-C(23)-C(24)	-5.2(3)	C(45)-C(46)-C(47)-C(52)	-174(2)
O(2)-N(3)-C(23)-C(24)	173.7(2)	C(52)-C(47)-C(48)-C(49)	0.4(3)
C(22)-C(23)-C(24)-C(25)	0.6(3)	C(46)-C(47)-C(48)-C(49)	-179.45(18)
N(3)-C(23)-C(24)-C(25)	179.7(2)	C(47)-C(48)-C(49)-C(50)	1.1(3)
C(23)-C(24)-C(25)-C(20)	-0.7(3)	C(47)-C(48)-C(49)-C(53)	-179.70(19)
C(21)-C(20)-C(25)-C(24)	0.1(3)	C(48)-C(49)-C(50)-C(51)	-0.8(3)

Table 30 Continued.

Atoms	°	Atoms	°
C(53)-C(49)-C(50)-C(51)	180.0(2)	C(58)-N(8)-C(57)-O(7)	5.3(3)
C(49)-C(50)-C(51)-C(52)	-0.8(3)	C(58)-N(8)-C(57)-N(7)	-174.69(17)
C(50)-C(51)-C(52)-C(47)	2.2(3)	C(57)-N(8)-C(58)-C(63)	162.16(19)
C(50)-C(51)-C(52)-N(7)	-177.30(19)	C(57)-N(8)-C(58)-C(59)	-17.8(3)
C(48)-C(47)-C(52)-C(51)	-2.0(3)	N(8)-C(58)-C(59)-C(60)	177.98(19)
C(46)-C(47)-C(52)-C(51)	177.80(18)	C(63)-C(58)-C(59)-C(60)	-1.9(3)
C(48)-C(47)-C(52)-N(7)	177.57(17)	C(58)-C(59)-C(60)-C(61)	0.8(3)
C(46)-C(47)-C(52)-N(7)	-2.6(3)	C(59)-C(60)-C(61)-C(62)	0.8(3)
C(57)-N(7)-C(52)-C(51)	-9.0(3)	C(59)-C(60)-C(61)-N(9)	-177.84(19)
C(57)-N(7)-C(52)-C(47)	171.41(17)	O(8)-N(9)-C(61)-C(60)	178.6(2)
C(50)-C(49)-C(53)-C(54)	121.9(2)	O(9)-N(9)-C(61)-C(60)	-0.8(3)
C(48)-C(49)-C(53)-C(54)	-57.3(3)	O(8)-N(9)-C(61)-C(62)	0.0(3)
C(50)-C(49)-C(53)-C(56)	3.3(3)	O(9)-N(9)-C(61)-C(62)	-179.50(19)
C(48)-C(49)-C(53)-C(56)	-175.9(2)	C(60)-C(61)-C(62)-C(63)	-1.1(3)
C(50)-C(49)-C(53)-C(55)	-118.6(2)	N(9)-C(61)-C(62)-C(63)	177.50(18)
C(48)-C(49)-C(53)-C(55)	62.2(3)	C(61)-C(62)-C(63)-C(58)	-0.1(3)
C(52)-N(7)-C(57)-O(7)	0.8(3)	N(8)-C(58)-C(63)-C(62)	-178.33(18)
C(52)-N(7)-C(57)-N(8)	-179.25(17)	C(59)-C(58)-C(63)-C(62)	1.6(3)

Table 31. Anisotropic displacement parameters ($Å^2$ x 10^3) for **2•Acetone**. The anisotropic displacement factor exponent takes the form: $-2p^2[h^2a^{*2}U^{11} + ... + 2hka^*b^*U^{12}]$.

Atom	U^{11}	U^{22}	U^{33}	U^{23}	U^{13}	U^{12}
O(1)	34(1)	38(1)	70(1)	-3(1)	-22(1)	-5(1)
O(2)	78(1)	49(1)	145(2)	-6(1)	-21(1)	-25(1)
O(3)	147(2)	45(1)	91(2)	16(1)	-25(2)	-28(1)
O(4)	30(1)	48(1)	65(1)	22(1)	-11(1)	-6(1)
O(5)	70(1)	50(1)	77(1)	16(1)	-28(1)	15(1)
O(6)	70(1)	76(1)	105(2)	6(1)	-60(1)	3(1)
O(7)	65(1)	35(1)	52(1)	3(1)	-34(1)	2(1)
O(8)	88(2)	107(2)	110(2)	-36(1)	-42(1)	-24(1)
O(9)	55(1)	124(2)	56(1)	16(1)	-25(1)	-27(1)
N(1)	23(1)	32(1)	45(1)	0(1)	-11(1)	-1(1)
N(2)	32(1)	34(1)	39(1)	-2(1)	-7(1)	-6(1)
N(3)	76(2)	37(1)	79(2)	-4(1)	8(1)	-15(1)
N(4)	25(1)	29(1)	40(1)	8(1)	-2(1)	1(1)
N(5)	26(1)	28(1)	42(1)	5(1)	-9(1)	0(1)
N(6)	51(1)	51(1)	50(1)	-3(1)	-21(1)	14(1)
N(7)	45(1)	29(1)	33(1)	3(1)	-17(1)	2(1)
N(8)	43(1)	36(1)	35(1)	2(1)	-15(1)	2(1)
N(9)	42(1)	100(2)	41(1)	-5(1)	-5(1)	-22(1)
C(1)	22(1)	26(1)	29(1)	1(1)	-7(1)	-1(1)
C(2)	27(1)	23(1)	30(1)	5(1)	-8(1)	-1(1)
C(3)	21(1)	24(1)	29(1)	1(1)	-6(1)	-3(1)
C(4)	20(1)	27(1)	29(1)	0(1)	-8(1)	0(1)
C(5)	26(1)	24(1)	25(1)	2(1)	-9(1)	-1(1)
C(6)	23(1)	30(1)	28(1)	5(1)	-3(1)	-4(1)
C(7)	27(1)	26(1)	33(1)	5(1)	-6(1)	-3(1)
C(8)	25(1)	26(1)	34(1)	1(1)	-5(1)	-2(1)
C(9)	22(1)	31(1)	33(1)	-5(1)	-8(1)	2(1)
C(10)	26(1)	32(1)	37(1)	-3(1)	-7(1)	0(1)
C(11)	30(1)	31(1)	37(1)	-6(1)	-12(1)	6(1)

Table 31 Continued.

Atom	U^{11}	U^{22}	U^{33}	U^{23}	U^{13}	U^{12}
C(12)	26(1)	37(1)	50(1)	-7(1)	-16(1)	7(1)
C(13)	23(1)	36(1)	51(1)	-7(1)	-11(1)	-1(1)
C(14)	25(1)	30(1)	35(1)	-6(1)	-8(1)	2(1)
C(15)	42(1)	32(1)	46(1)	-3(1)	-19(1)	8(1)
C(16)	67(2)	37(1)	73(2)	-10(1)	-31(1)	5(1)
C(17)	73(2)	49(1)	50(1)	6(1)	-17(1)	7(1)
C(18)	52(1)	46(1)	90(2)	3(1)	-33(1)	15(1)
C(19)	25(1)	33(1)	35(1)	-6(1)	-2(1)	-2(1)
C(20)	33(1)	33(1)	35(1)	-4(1)	5(1)	-4(1)
C(21)	31(1)	36(1)	67(1)	-7(1)	-4(1)	-2(1)
C(22)	36(1)	39(1)	80(2)	-13(1)	1(1)	-7(1)
C(23)	51(1)	35(1)	53(1)	-5(1)	11(1)	-12(1)
C(24)	73(2)	38(1)	45(1)	7(1)	-5(1)	-6(1)
C(25)	60(1)	40(1)	39(1)	3(1)	-8(1)	-10(1)
C(26)	23(1)	24(1)	34(1)	4(1)	-7(1)	1(1)
C(27)	25(1)	24(1)	33(1)	3(1)	-7(1)	0(1)
C(28)	24(1)	25(1)	28(1)	-1(1)	-2(1)	-2(1)
C(29)	24(1)	25(1)	32(1)	1(1)	-2(1)	1(1)
C(30)	30(1)	25(1)	27(1)	-1(1)	-3(1)	-2(1)
C(31)	30(1)	33(1)	29(1)	2(1)	4(1)	0(1)
C(32)	29(1)	33(1)	33(1)	-1(1)	2(1)	7(1)
C(33)	28(1)	24(1)	29(1)	1(1)	-5(1)	1(1)
C(34)	33(1)	28(1)	34(1)	6(1)	0(1)	1(1)
C(35)	44(1)	41(1)	76(2)	22(1)	10(1)	-3(1)
C(36)	75(2)	49(1)	48(1)	7(1)	-24(1)	8(1)
C(37)	61(1)	29(1)	50(1)	7(1)	8(1)	8(1)
C(38)	30(1)	28(1)	34(1)	1(1)	-5(1)	2(1)
C(39)	30(1)	28(1)	27(1)	-3(1)	-3(1)	5(1)
C(40)	37(1)	29(1)	38(1)	-3(1)	-9(1)	-1(1)
C(41)	35(1)	42(1)	42(1)	-6(1)	-16(1)	1(1)
C(42)	37(1)	37(1)	33(1)	-4(1)	-11(1)	10(1)
C(43)	38(1)	28(1)	33(1)	-1(1)	-4(1)	5(1)
C(44)	29(1)	29(1)	36(1)	-2(1)	-6(1)	1(1)
C(45)	25(1)	31(1)	29(1)	2(1)	-9(1)	-2(1)
C(46)	29(1)	31(1)	29(1)	1(1)	-8(1)	0(1)
C(47)	36(1)	29(1)	24(1)	2(1)	-7(1)	5(1)
C(48)	43(1)	31(1)	30(1)	3(1)	-13(1)	2(1)
C(49)	56(1)	29(1)	33(1)	3(1)	-16(1)	0(1)
C(50)	74(2)	29(1)	37(1)	7(1)	-26(1)	-1(1)
C(51)	60(1)	33(1)	35(1)	3(1)	-24(1)	3(1)
C(52)	43(1)	29(1)	27(1)	-1(1)	-10(1)	4(1)
C(53)	67(2)	33(1)	43(1)	7(1)	-22(1)	-8(1)
C(54)	64(2)	49(1)	59(2)	-10(1)	-26(1)	-3(1)
C(55)	71(2)	62(2)	82(2)	-12(1)	7(2)	-26(1)
C(56)	159(3)	42(1)	82(2)	22(1)	-74(2)	-35(2)
C(57)	42(1)	34(1)	28(1)	-3(1)	-9(1)	3(1)
C(58)	34(1)	44(1)	29(1)	-1(1)	-4(1)	-2(1)
C(59)	43(1)	47(1)	49(1)	5(1)	-14(1)	-4(1)
C(60)	38(1)	67(2)	45(1)	12(1)	-12(1)	-8(1)
C(61)	34(1)	74(2)	31(1)	-2(1)	-2(1)	-17(1)
C(62)	42(1)	55(1)	43(1)	-11(1)	-2(1)	-8(1)
C(63)	39(1)	46(1)	40(1)	-4(1)	-7(1)	0(1)
O(1S)	41(1)	47(1)	73(1)	-17(1)	-1(1)	-10(1)
C(1S)	42(1)	50(1)	51(1)	-21(1)	-4(1)	-8(1)
C(2S)	98(2)	73(2)	97(2)	4(2)	7(2)	-28(2)
C(3S)	89(2)	126(3)	141(3)	-59(3)	-69(2)	15(2)
O(2S)	73(1)	37(1)	63(1)	4(1)	-23(1)	3(1)

Table 31 Continued.

Atom	U^{11}	U^{22}	U^{33}	U^{23}	U^{13}	U^{12}
C(4S)	67(2)	37(1)	33(1)	-2(1)	-10(1)	0(1)
C(5S)	98(2)	63(2)	51(2)	1(1)	-16(1)	-29(2)
C(6S)	84(2)	54(1)	45(1)	-9(1)	-24(1)	19(1)
O(3S)	195(3)	85(2)	119(2)	5(2)	82(2)	-8(2)
C(7S)	83(2)	62(2)	51(2)	-11(1)	3(1)	-23(1)
C(8S)	76(2)	51(2)	103(2)	-4(2)	-5(2)	-11(1)
C(9S)	67(2)	74(2)	46(1)	-9(1)	-7(1)	3(1)
O(4S)	127(2)	88(2)	173(3)	39(2)	-87(2)	-39(2)
C(10S)	96(2)	60(2)	66(2)	2(1)	-29(2)	-25(2)
C(11S)	106(3)	96(3)	127(3)	25(2)	17(2)	-19(2)
C(12S)	92(2)	85(2)	70(2)	15(2)	-35(2)	-31(2)

Table 32. Hydrogen coordinates (x 10^4) and isotropic displacement parameters ($Å^2$ x 10^3) for **2•Acetone.**

Atom	X	Y	Z	U(eq)
H(2B)	7132	2656	3533	32
H(4B)	4860	4546	2897	30
H(6A)	8112	4726	2046	33
H(10A)	10469	1395	3334	38
H(12A)	13723	1852	3171	44
H(13A)	13529	3399	2650	43
H(16A)	12201	-347	2885	85
H(16B)	10989	-187	3302	85
H(16C)	11822	-995	3556	85
H(17A)	10770	605	4318	87
H(17B)	11856	890	4560	87
H(17C)	11570	-238	4566	87
H(18A)	13871	127	3273	92
H(18B)	13445	-513	3941	92
H(18C)	13718	620	3925	92
H(21A)	13624	6633	2322	54
H(22A)	14142	8272	2155	63
H(24A)	11780	8939	1106	64
H(25A)	11226	7317	1283	56
H(29A)	4310	1290	5127	33
H(31A)	1172	1579	6082	39
H(32A)	948	3038	5465	40
H(35A)	1411	-295	6091	88
H(35B)	1366	329	6682	88
H(35C)	1939	-740	6690	88
H(36A)	4248	844	6414	85
H(36B)	3657	-52	6884	85
H(36C)	3082	1016	6878	85
H(37A)	3232	-603	5379	76
H(37B)	3718	-1035	5994	76
H(37C)	4342	-167	5512	76
H(40A)	-238	4681	3687	41
H(41A)	-1396	5640	3111	46
H(43A)	635	7944	2922	41
H(44A)	1783	6998	3509	38
H(48A)	7143	7875	1527	41
H(50A)	5866	9506	161	54
H(51A)	4767	8224	75	50
H(54A)	7256	9348	1890	82

Table 32 Continued.

Atom	X	Y	Z	U(eq)
H(54B)	6332	10131	1716	82
H(54C)	7589	10460	1646	82
H(55A)	8723	8760	1021	110
H(55B)	9064	9877	803	110
H(55C)	8765	9213	297	110
H(56A)	6366	10806	603	133
H(56B)	7319	10475	41	133
H(56C)	7620	11131	550	133
H(59A)	2048	6624	-228	55
H(60A)	809	6102	-812	60
H(62A)	1663	3277	-353	56
H(63A)	2915	3786	222	51
H(2SA)	4136	7169	3278	140
H(2SB)	5457	7052	3077	140
H(2SC)	4922	7585	3694	140
H(3SA)	5644	5175	4379	164
H(3SB)	5894	6304	4399	164
H(3SC)	6426	5767	3783	164
H(5SA)	3372	2915	1086	105
H(5SB)	3706	2272	1692	105
H(5SC)	4300	2064	985	105
H(6SA)	6361	3456	1493	90
H(6SB)	6236	2415	1250	90
H(6SC)	5636	2624	1955	90
H(8SA)	8890	1556	4827	117
H(8SB)	9553	2559	4639	117
H(8SC)	8807	2218	4174	117
H(9SA)	7080	4076	4966	94
H(9SB)	7647	3832	4263	94
H(9SC)	8394	4174	4727	94
H(11A)	882	2781	863	176
H(11B)	1537	1756	938	176
H(11C)	1293	2423	1515	176
H(12B)	-755	531	1999	121
H(12C)	219	1008	2252	121
H(12D)	514	347	1672	121
H(1N)	11066(19)	4351(15)	2190(10)	47(6)
H(2N)	11436(18)	5741(15)	1729(10)	43(6)
H(4N)	3034(18)	4151(15)	4301(10)	44(6)
H(5N)	2342(19)	5444(15)	3899(10)	45(6)
H(7N)	4861(16)	5875(15)	905(10)	37(6)
H(8N)	3705(18)	5030(17)	583(11)	49(7)

Table 33. Crystal data and structure refinement for **2•DMSO**.

Identification code	mh82
Empirical formula	C75 H81 N9 O13
Formula weight	1316.49
Temperature	173(2) K
Wavelength	0.71073 Å
Crystal system	Triclinic
Space group	P-1

Table 33 Continued.

Unit cell dimensions	a = 12.2820(17) Å	a= 83.428(2)°.
	b = 13.7330(19) Å	b= 78.604(2)°.
	c = 21.485(3) Å	g = 87.611(2)°.
Volume	3528.4(8) Å3	
Z	2	
Density (calculated)	1.239 Mg/m^3	
Absorption coefficient	0.086 mm^{-1}	
F(000)	1396	
Crystal size	0.42 x 0.27 x 0.18 mm^3	
Theta range for data collection	1.49 to 27.00°.	
Index ranges	-15<=h<=15, -17<=k<=17, -27<=l<=27	
Reflections collected	39977	
Independent reflections	15274 [R(int) = 0.0363]	
Completeness to theta = 27.00°	99.2 %	
Absorption correction	Semi-empirical from equivalents	
Max. and min. transmission	0.9847 and 0.9649	
Refinement method	Full-matrix least-squares on F2	
Data / restraints / parameters	15274 / 0 / 898	
Goodness-of-fit on F2	1.019	
Final R indices [I>2sigma(I)]	R1 = 0.0540, wR2 = 0.1325	
R indices (all data)	R1 = 0.0804, wR2 = 0.1512	
Largest diff. peak and hole	0.421 and -0.322 e.$Å^{-3}$	

Table 34. Atomic coordinates (x 10^4) and equivalent isotropic displacement parameters ($Å^2$ x 10^3) for **2•DMSO**. U(eq) is defined as one third of the trace of the orthogonalized U^{ij} tensor.

Atom	X	Y	Z	U(eq)
O(1)	-6508(2)	5447(2)	2601(1)	45(1)
O(2)	-7565(3)	10308(2)	1963(2)	81(1)
O(3)	-5854(3)	10861(2)	1567(2)	75(1)
O(4)	4656(2)	3787(2)	4657(1)	60(1)
O(5)	7613(2)	8331(2)	2469(2)	72(1)
O(6)	8712(2)	7165(2)	2748(2)	72(1)
O(7)	5778(2)	5917(2)	492(1)	48(1)
O(8)	8550(3)	1366(3)	1569(2)	86(1)
O(9)	9584(3)	2321(2)	714(2)	84(1)
N(1)	-4800(2)	4746(2)	2362(1)	36(1)
N(2)	-4938(2)	6393(2)	2034(1)	37(1)
N(3)	-6550(3)	10184(2)	1797(2)	58(1)
N(4)	2848(2)	3733(2)	4579(1)	40(1)
N(5)	3961(3)	5086(2)	4042(1)	39(1)
N(6)	7770(3)	7497(2)	2756(2)	55(1)
N(7)	3859(2)	5774(2)	850(1)	38(1)
N(8)	4923(3)	4418(2)	917(1)	41(1)
N(9)	8668(3)	2073(3)	1112(2)	64(1)
C(1)	-1202(2)	3892(2)	2843(1)	31(1)
C(2)	-737(2)	3388(2)	3336(2)	30(1)
C(3)	314(2)	3662(2)	3379(1)	31(1)
C(4)	923(3)	4425(2)	2899(2)	33(1)
C(5)	479(2)	4918(2)	2392(2)	32(1)
C(6)	-596(2)	4666(2)	2371(2)	34(1)
C(7)	-2305(3)	3631(2)	2824(2)	34(1)
C(8)	-3244(3)	3415(2)	2843(2)	34(1)
C(9)	-4373(2)	3112(2)	2897(2)	34(1)
C(10)	-4702(3)	2146(3)	3184(2)	38(1)

Table 34 Continued.

Atom	X	Y	Z	U(eq)
C(11)	-5781(3)	1791(2)	3258(2)	39(1)
C(12)	-6513(3)	2461(3)	3008(2)	43(1)
C(13)	-6210(3)	3419(3)	2711(2)	39(1)
C(14)	-5143(2)	3774(2)	2663(2)	34(1)
C(15)	-6112(3)	736(3)	3606(2)	47(1)
C(16)	-5344(4)	75(3)	3262(3)	62(1)
C(17)	-6017(5)	585(4)	4308(2)	69(1)
C(18)	-7340(4)	512(3)	3635(3)	68(2)
C(16A)	-7000(20)	594(19)	4215(15)	62(1)
C(17A)	-6500(30)	230(20)	3133(14)	69(1)
C(18A)	-5090(20)	30(19)	3756(17)	68(2)
C(19)	-5499(3)	5521(2)	2352(2)	34(1)
C(20)	-5391(3)	7315(2)	1983(1)	36(1)
C(21)	-6544(3)	7487(3)	2159(2)	45(1)
C(22)	-6915(3)	8427(3)	2095(2)	50(1)
C(23)	-6153(3)	9192(3)	1863(2)	46(1)
C(24)	-5014(3)	9043(3)	1686(2)	50(1)
C(25)	-4639(3)	8112(3)	1745(2)	45(1)
C(26)	751(2)	3177(2)	3918(2)	36(1)
C(27)	1094(3)	2793(2)	4377(2)	35(1)
C(28)	1568(2)	2359(2)	4909(2)	34(1)
C(29)	1130(3)	1481(2)	5341(2)	39(1)
C(30)	1577(3)	1031(2)	5852(2)	39(1)
C(31)	2493(3)	1506(3)	5920(2)	44(1)
C(32)	2939(3)	2380(3)	5508(2)	41(1)
C(33)	2480(3)	2826(2)	4997(2)	35(1)
C(34)	1072(3)	80(3)	6336(2)	50(1)
C(35)	1971(4)	-557(3)	6567(3)	90(2)
C(36)	234(5)	322(4)	6913(3)	120(3)
C(37)	474(5)	-519(3)	6023(3)	94(2)
C(38)	3886(3)	4168(2)	4442(2)	39(1)
C(39)	4923(3)	5670(2)	3760(2)	36(1)
C(40)	6004(3)	5287(3)	3653(2)	42(1)
C(41)	6923(3)	5890(3)	3332(2)	45(1)
C(42)	6784(3)	6874(2)	3117(2)	42(1)
C(43)	5728(3)	7273(3)	3227(2)	43(1)
C(44)	4803(3)	6670(2)	3550(2)	39(1)
C(45)	1134(2)	5683(2)	1892(2)	35(1)
C(46)	1721(3)	6292(2)	1475(2)	38(1)
C(47)	2468(3)	7009(2)	984(2)	36(1)
C(48)	2118(3)	7963(2)	815(2)	40(1)
C(49)	2795(3)	8681(2)	346(2)	41(1)
C(50)	3854(3)	8401(3)	54(2)	46(1)
C(51)	4241(3)	7475(3)	214(2)	43(1)
C(52)	3554(3)	6749(2)	681(2)	36(1)
C(53)	2392(3)	9722(2)	133(2)	49(1)
C(54)	1333(3)	9938(3)	622(2)	69(1)
C(55)	2124(4)	9828(3)	-524(2)	67(1)
C(56)	3317(3)	10461(2)	62(2)	54(1)
C(57)	4925(3)	5414(2)	730(2)	37(1)
C(58)	5859(3)	3838(2)	939(2)	41(1)
C(59)	6931(3)	4130(3)	534(2)	51(1)
C(60)	7832(3)	3539(3)	578(2)	56(1)
C(61)	7682(3)	2655(3)	1037(2)	51(1)
C(62)	6625(3)	2328(3)	1420(2)	51(1)
C(63)	5718(3)	2912(3)	1359(2)	46(1)
S(1S)	1717(1)	3387(1)	1250(1)	40(1)
O(1S)	2623(2)	3859(2)	1425(1)	49(1)

Table 34 Continued.

Atom	X	Y	Z	U(eq)
C(1S)	2415(4)	2601(3)	761(2)	47(1)
C(2S)	1077(4)	2470(3)	1949(2)	49(1)
S(2S)	8018(1)	6793(1)	984(1)	52(1)
O(2S)	7451(2)	6200(2)	1651(1)	56(1)
C(3S)	8878(4)	5983(3)	586(2)	81(1)
C(4S)	9114(3)	7468(3)	1083(2)	61(1)
S(3S)	628(2)	6185(2)	4225(1)	50(1)
O(3S)	1642(2)	5500(2)	4106(1)	60(1)
C(5S)	1005(8)	7327(6)	3824(4)	42(2)
C(6S)	-571(14)	5614(12)	4199(8)	56(4)
S(3SA)	999(1)	6115(1)	3672(1)	44(1)
O(3SA)	1642(2)	5500(2)	4106(1)	60(1)
C(5SA)	895(10)	7105(8)	3553(6)	118(4)
C(6SA)	-436(10)	5801(8)	4093(6)	67(4)
S(4S)	7316(2)	2355(1)	5078(1)	111(1)
O(4S)	7263(5)	2066(4)	5711(3)	76(2)
O(4SA)	8196(6)	1878(5)	4986(3)	92(2)
C(7S)	6369(5)	2078(3)	4668(3)	86(2)
C(8S)	7257(4)	3634(3)	4836(2)	61(1)

Table 35. Bond lengths for **2•DMSO**.

Atoms	Å	Atoms	Å
O(1)-C(19)	1.216(4)	C(1)-C(6)	1.393(4)
O(2)-N(3)	1.223(4)	C(1)-C(7)	1.432(4)
O(3)-N(3)	1.230(4)	C(2)-C(3)	1.395(4)
O(4)-C(38)	1.214(4)	C(2)-H(2)	0.92(3)
O(5)-N(6)	1.229(4)	C(3)-C(4)	1.393(4)
O(6)-N(6)	1.228(4)	C(3)-C(26)	1.433(4)
O(7)-C(57)	1.214(4)	C(4)-C(5)	1.387(4)
O(8)-N(9)	1.215(4)	C(4)-H(4)	0.87(3)
O(9)-N(9)	1.236(4)	C(5)-C(6)	1.396(4)
N(1)-C(19)	1.367(4)	C(5)-C(45)	1.435(4)
N(1)-C(14)	1.403(4)	C(6)-H(6)	0.92(3)
N(1)-H(1N)	0.77(3)	C(7)-C(8)	1.193(4)
N(2)-C(19)	1.373(4)	C(8)-C(9)	1.434(4)
N(2)-C(20)	1.389(4)	C(9)-C(10)	1.388(4)
N(2)-H(2N)	0.79(4)	C(9)-C(14)	1.407(4)
N(3)-C(23)	1.456(5)	C(10)-C(11)	1.391(4)
N(4)-C(38)	1.367(4)	C(10)-H(10)	0.90(3)
N(4)-C(33)	1.398(4)	C(11)-C(12)	1.394(5)
N(4)-H(4N)	0.81(4)	C(11)-C(15)	1.521(5)
N(5)-C(38)	1.371(4)	C(12)-C(13)	1.374(5)
N(5)-C(39)	1.384(4)	C(12)-H(12)	0.94(3)
N(5)-H(5N)	0.78(3)	C(13)-C(14)	1.391(4)
N(6)-C(42)	1.457(4)	C(13)-H(13)	0.92(3)
N(7)-C(57)	1.370(4)	C(15)-C(16A)	1.46(3)
N(7)-C(52)	1.402(4)	C(15)-C(16)	1.500(6)
N(7)-H(7N)	0.81(3)	C(15)-C(17)	1.538(6)
N(8)-C(57)	1.370(4)	C(15)-C(18)	1.536(5)
N(8)-C(58)	1.390(4)	C(15)-C(18A)	1.62(3)
N(8)-H(8N)	0.74(4)	C(15)-C(17A)	1.57(3)
N(9)-C(61)	1.458(5)	C(16)-H(16A)	0.9800
C(1)-C(2)	1.384(4)	C(16)-H(16B)	0.9800

Table 35 Continued.

Atoms	Å	Atoms	Å
C(16)-H(16C)	0.9800	C(43)-C(44)	1.374(5)
C(17)-H(17A)	0.9800	C(43)-H(43)	0.92(3)
C(17)-H(17B)	0.9800	C(44)-H(44)	1.01(3)
C(17)-H(17C)	0.9800	C(45)-C(46)	1.193(4)
C(18)-H(18A)	0.9800	C(46)-C(47)	1.437(4)
C(18)-H(18B)	0.9800	C(47)-C(48)	1.393(5)
C(18)-H(18C)	0.9800	C(47)-C(52)	1.408(4)
C(16A)-H(16D)	0.9800	C(48)-C(49)	1.379(4)
C(16A)-H(16E)	0.9800	C(48)-H(48)	0.97(3)
C(16A)-H(16F)	0.9800	C(49)-C(50)	1.384(5)
C(17A)-H(17D)	0.9800	C(49)-C(53)	1.537(5)
C(17A)-H(17E)	0.9800	C(50)-C(51)	1.372(5)
C(17A)-H(17F)	0.9800	C(50)-H(50)	0.88(3)
C(18A)-H(18D)	0.9800	C(51)-C(52)	1.388(4)
C(18A)-H(18E)	0.9800	C(51)-H(51)	0.90(3)
C(18A)-H(18F)	0.9800	C(53)-C(56)	1.530(5)
C(20)-C(25)	1.395(5)	C(53)-C(54)	1.533(5)
C(20)-C(21)	1.396(5)	C(53)-C(55)	1.533(5)
C(21)-C(22)	1.378(5)	C(54)-H(54A)	0.9800
C(21)-H(21)	0.95(3)	C(54)-H(54B)	0.9800
C(22)-C(23)	1.369(5)	C(54)-H(54C)	0.9800
C(22)-H(22)	0.91(3)	C(55)-H(55A)	0.9800
C(23)-C(24)	1.373(5)	C(55)-H(55B)	0.9800
C(24)-C(25)	1.368(5)	C(55)-H(55C)	0.9800
C(24)-H(24)	0.95(4)	C(56)-H(56A)	0.9800
C(25)-H(25)	0.91(4)	C(56)-H(56B)	0.9800
C(26)-C(27)	1.193(4)	C(56)-H(56C)	0.9800
C(27)-C(28)	1.432(4)	C(58)-C(63)	1.395(5)
C(28)-C(29)	1.397(4)	C(58)-C(59)	1.397(5)
C(28)-C(33)	1.403(4)	C(59)-C(60)	1.370(5)
C(29)-C(30)	1.381(5)	C(59)-H(59)	1.01(3)
C(29)-H(29)	0.91(3)	C(60)-C(61)	1.387(5)
C(30)-C(31)	1.392(5)	C(60)-H(60)	0.95(5)
C(30)-C(34)	1.535(5)	C(61)-C(62)	1.379(5)
C(31)-C(32)	1.379(5)	C(62)-C(63)	1.376(5)
C(31)-H(31)	0.92(3)	C(62)-H(62)	0.93(4)
C(32)-C(33)	1.387(4)	C(63)-H(63)	0.93(3)
C(32)-H(32)	0.94(3)	S(1S)-O(1S)	1.498(2)
C(34)-C(35)	1.508(5)	S(1S)-C(2S)	1.773(4)
C(34)-C(36)	1.516(6)	S(1S)-C(1S)	1.780(4)
C(34)-C(37)	1.527(6)	C(1S)-H(1SA)	0.94(4)
C(35)-H(35A)	0.9800	C(1S)-H(1SB)	1.00(4)
C(35)-H(35B)	0.9800	C(1S)-H(1SC)	0.96(4)
C(35)-H(35C)	0.9800	C(2S)-H(2SA)	0.94(4)
C(36)-H(36A)	0.9800	C(2S)-H(2SB)	0.91(4)
C(36)-H(36B)	0.9800	C(2S)-H(2SC)	0.92(4)
C(36)-H(36C)	0.9800	S(2S)-O(2S)	1.502(2)
C(37)-H(37A)	0.9800	S(2S)-C(3S)	1.767(5)
C(37)-H(37B)	0.9800	S(2S)-C(4S)	1.769(4)
C(37)-H(37C)	0.9800	C(3S)-H(3SA)	0.9800
C(39)-C(44)	1.393(5)	C(3S)-H(3SB)	0.9800
C(39)-C(40)	1.398(5)	C(3S)-H(3SC)	0.9800
C(40)-C(41)	1.369(5)	C(4S)-H(4SA)	0.9800
C(40)-H(40)	0.94(4)	C(4S)-H(4SB)	0.9800
C(41)-C(42)	1.377(5)	C(4S)-H(4SC)	0.9800
C(41)-H(41)	0.96(3)	S(3S)-O(3S)	1.557(3)
C(42)-C(43)	1.381(5)	S(3S)-C(5S)	1.661(9)

Table 35 Continued.

Atoms	Å	Atoms	Å
S(3S)-C(6S)	1.728(16)	C(6SA)-H(6SE)	0.9800
C(5S)-H(5SA)	0.9800	C(6SA)-H(6SF)	0.9800
C(5S)-H(5SB)	0.9800	S(4S)-O(4SA)	1.249(7)
C(5S)-H(5SC)	0.9800	S(4S)-O(4S)	1.335(6)
C(6S)-H(6SA)	0.9800	S(4S)-C(7S)	1.752(5)
C(6S)-H(6SB)	0.9800	S(4S)-C(8S)	1.764(4)
C(6S)-H(6SC)	0.9800	O(4S)-O(4SA)	1.778(9)
S(3SA)-C(5SA)	1.371(12)	C(7S)-H(7SA)	0.9800
S(3SA)-C(6SA)	1.783(11)	C(7S)-H(7SB)	0.9800
C(5SA)-H(5SD)	0.9800	C(7S)-H(7SC)	0.9800
C(5SA)-H(5SE)	0.9800	C(8S)-H(8SA)	0.9800
C(5SA)-H(5SF)	0.9800	C(8S)-H(8SB)	0.9800
C(6SA)-H(6SD)	0.9800	C(8S)-H(8SC)	0.9800

Table 36. Bond angles for **2•DMSO**.

Atoms	°	Atoms	°
C(19)-N(1)-C(14)	124.9(3)	C(3)-C(4)-H(4)	120.5(19)
C(19)-N(1)-H(1N)	121(2)	C(4)-C(5)-C(6)	119.9(3)
C(14)-N(1)-H(1N)	114(2)	C(4)-C(5)-C(45)	119.6(3)
C(19)-N(2)-C(20)	126.8(3)	C(6)-C(5)-C(45)	120.5(3)
C(19)-N(2)-H(2N)	115(3)	C(5)-C(6)-C(1)	120.0(3)
C(20)-N(2)-H(2N)	117(3)	C(5)-C(6)-H(6)	121.5(19)
O(2)-N(3)-O(3)	122.8(3)	C(1)-C(6)-H(6)	118.4(19)
O(2)-N(3)-C(23)	118.5(3)	C(8)-C(7)-C(1)	176.3(3)
O(3)-N(3)-C(23)	118.8(3)	C(7)-C(8)-C(9)	176.8(3)
C(38)-N(4)-C(33)	127.0(3)	C(10)-C(9)-C(14)	119.9(3)
C(38)-N(4)-H(4N)	117(3)	C(10)-C(9)-C(8)	118.9(3)
C(33)-N(4)-H(4N)	116(3)	C(14)-C(9)-C(8)	121.2(3)
C(38)-N(5)-C(39)	126.8(3)	C(9)-C(10)-C(11)	122.7(3)
C(38)-N(5)-H(5N)	114(3)	C(9)-C(10)-H(10)	117.1(19)
C(39)-N(5)-H(5N)	119(3)	C(11)-C(10)-H(10)	120.2(19)
O(5)-N(6)-O(6)	123.4(3)	C(12)-C(11)-C(10)	115.9(3)
O(5)-N(6)-C(42)	117.9(3)	C(12)-C(11)-C(15)	123.7(3)
O(6)-N(6)-C(42)	118.8(3)	C(10)-C(11)-C(15)	120.5(3)
C(57)-N(7)-C(52)	127.2(3)	C(13)-C(12)-C(11)	123.0(3)
C(57)-N(7)-H(7N)	115(2)	C(13)-C(12)-H(12)	117(2)
C(52)-N(7)-H(7N)	118(2)	C(11)-C(12)-H(12)	120(2)
C(57)-N(8)-C(58)	126.5(3)	C(12)-C(13)-C(14)	120.6(3)
C(57)-N(8)-H(8N)	115(3)	C(12)-C(13)-H(13)	122.8(19)
C(58)-N(8)-H(8N)	117(3)	C(14)-C(13)-H(13)	116.5(19)
O(8)-N(9)-O(9)	122.9(4)	C(13)-C(14)-N(1)	122.4(3)
O(8)-N(9)-C(61)	118.2(4)	C(13)-C(14)-C(9)	117.9(3)
O(9)-N(9)-C(61)	119.0(4)	N(1)-C(14)-C(9)	119.7(3)
C(2)-C(1)-C(6)	119.5(3)	C(16A)-C(15)-C(16)	134.8(11)
C(2)-C(1)-C(7)	120.3(3)	C(16A)-C(15)-C(11)	115.2(10)
C(6)-C(1)-C(7)	120.2(3)	C(16)-C(15)-C(11)	109.6(3)
C(1)-C(2)-C(3)	121.0(3)	C(16A)-C(15)-C(17)	49.9(12)
C(1)-C(2)-H(2)	119.7(18)	C(16)-C(15)-C(17)	111.2(4)
C(3)-C(2)-H(2)	119.3(18)	C(11)-C(15)-C(17)	107.4(3)
C(4)-C(3)-C(2)	119.0(3)	C(16A)-C(15)-C(18)	58.8(12)
C(4)-C(3)-C(26)	120.5(3)	C(16)-C(15)-C(18)	109.6(3)
C(2)-C(3)-C(26)	120.4(3)	C(11)-C(15)-C(18)	111.3(3)
C(5)-C(4)-C(3)	120.4(3)	C(17)-C(15)-C(18)	107.8(4)
C(5)-C(4)-H(4)	119.1(19)	C(16A)-C(15)-C(18A)	107.0(17)

Table 36 Continued.

Atoms	°	Atoms	°
C(16)-C(15)-C(18A)	44.6(12)	C(21)-C(22)-H(22)	116(2)
C(11)-C(15)-C(18A)	115.9(9)	C(22)-C(23)-C(24)	121.3(3)
C(17)-C(15)-C(18A)	67.3(13)	C(22)-C(23)-N(3)	119.7(3)
C(18)-C(15)-C(18A)	131.7(9)	C(24)-C(23)-N(3)	119.0(3)
C(16A)-C(15)-C(17A)	109.2(16)	C(25)-C(24)-C(23)	119.1(4)
C(16)-C(15)-C(17A)	59.0(12)	C(25)-C(24)-H(24)	119(3)
C(11)-C(15)-C(17A)	108.9(10)	C(23)-C(24)-H(24)	121(3)
C(17)-C(15)-C(17A)	143.5(10)	C(24)-C(25)-C(20)	121.2(4)
C(18)-C(15)-C(17A)	54.7(12)	C(24)-C(25)-H(25)	119(2)
C(18A)-C(15)-C(17A)	99.4(17)	C(20)-C(25)-H(25)	120(2)
C(15)-C(16)-H(16A)	109.5	C(27)-C(26)-C(3)	177.9(3)
C(15)-C(16)-H(16B)	109.5	C(26)-C(27)-C(28)	176.7(3)
H(16A)-C(16)-H(16B)	109.5	C(29)-C(28)-C(33)	119.7(3)
C(15)-C(16)-H(16C)	109.5	C(29)-C(28)-C(27)	120.9(3)
H(16A)-C(16)-H(16C)	109.5	C(33)-C(28)-C(27)	119.5(3)
H(16B)-C(16)-H(16C)	109.5	C(30)-C(29)-C(28)	122.5(3)
C(15)-C(17)-H(17A)	109.5	C(30)-C(29)-H(29)	123.7(18)
C(15)-C(17)-H(17B)	109.5	C(28)-C(29)-H(29)	113.7(18)
H(17A)-C(17)-H(17B)	109.5	C(29)-C(30)-C(31)	116.3(3)
C(15)-C(17)-H(17C)	109.5	C(29)-C(30)-C(34)	122.2(3)
H(17A)-C(17)-H(17C)	109.5	C(31)-C(30)-C(34)	121.4(3)
H(17B)-C(17)-H(17C)	109.5	C(32)-C(31)-C(30)	122.7(3)
C(15)-C(18)-H(18A)	109.5	C(32)-C(31)-H(31)	116(2)
C(15)-C(18)-H(18B)	109.5	C(30)-C(31)-H(31)	121(2)
H(18A)-C(18)-H(18B)	109.5	C(33)-C(32)-C(31)	120.4(3)
C(15)-C(18)-H(18C)	109.5	C(33)-C(32)-H(32)	122(2)
H(18A)-C(18)-H(18C)	109.5	C(31)-C(32)-H(32)	118(2)
H(18B)-C(18)-H(18C)	109.5	C(32)-C(33)-N(4)	123.8(3)
C(15)-C(16A)-H(16D)	109.5	C(32)-C(33)-C(28)	118.3(3)
C(15)-C(16A)-H(16E)	109.5	N(4)-C(33)-C(28)	117.9(3)
H(16D)-C(16A)-H(16E)	109.5	C(35)-C(34)-C(36)	109.5(4)
C(15)-C(16A)-H(16F)	109.5	C(35)-C(34)-C(37)	106.3(4)
H(16D)-C(16A)-H(16F)	109.5	C(36)-C(34)-C(37)	109.3(4)
H(16E)-C(16A)-H(16F)	109.5	C(35)-C(34)-C(30)	111.6(3)
C(15)-C(17A)-H(17D)	109.5	C(36)-C(34)-C(30)	108.9(3)
C(15)-C(17A)-H(17E)	109.5	C(37)-C(34)-C(30)	111.2(3)
H(17D)-C(17A)-H(17E)	109.5	C(34)-C(35)-H(35A)	109.5
C(15)-C(17A)-H(17F)	109.5	C(34)-C(35)-H(35B)	109.5
H(17D)-C(17A)-H(17F)	109.5	H(35A)-C(35)-H(35B)	109.5
H(17E)-C(17A)-H(17F)	109.5	C(34)-C(35)-H(35C)	109.5
C(15)-C(18A)-H(18D)	109.5	H(35A)-C(35)-H(35C)	109.5
C(15)-C(18A)-H(18E)	109.5	H(35B)-C(35)-H(35C)	109.5
H(18D)-C(18A)-H(18E)	109.5	C(34)-C(36)-H(36A)	109.5
C(15)-C(18A)-H(18F)	109.5	C(34)-C(36)-H(36B)	109.5
H(18D)-C(18A)-H(18F)	109.5	H(36A)-C(36)-H(36B)	109.5
H(18E)-C(18A)-H(18F)	109.5	C(34)-C(36)-H(36C)	109.5
O(1)-C(19)-N(1)	123.5(3)	H(36A)-C(36)-H(36C)	109.5
O(1)-C(19)-N(2)	123.7(3)	H(36B)-C(36)-H(36C)	109.5
N(1)-C(19)-N(2)	112.8(3)	C(34)-C(37)-H(37A)	109.5
N(2)-C(20)-C(25)	117.5(3)	C(34)-C(37)-H(37B)	109.5
N(2)-C(20)-C(21)	124.0(3)	H(37A)-C(37)-H(37B)	109.5
C(25)-C(20)-C(21)	118.5(3)	C(34)-C(37)-H(37C)	109.5
C(22)-C(21)-C(20)	120.0(3)	H(37A)-C(37)-H(37C)	109.5
C(22)-C(21)-H(21)	118.7(19)	H(37B)-C(37)-H(37C)	109.5
C(20)-C(21)-H(21)	121.3(19)	O(4)-C(38)-N(4)	123.6(3)
C(23)-C(22)-C(21)	119.9(4)	O(4)-C(38)-N(5)	123.5(3)
C(23)-C(22)-H(22)	124(2)	N(4)-C(38)-N(5)	112.8(3)

Table 36 Continued.

Atoms	°	Atoms	°
N(5)-C(39)-C(44)	118.6(3)	C(53)-C(56)-H(56B)	109.5
N(5)-C(39)-C(40)	122.2(3)	H(56A)-C(56)-H(56B)	109.5
C(44)-C(39)-C(40)	119.1(3)	C(53)-C(56)-H(56C)	109.5
C(41)-C(40)-C(39)	119.9(3)	H(56A)-C(56)-H(56C)	109.5
C(41)-C(40)-H(40)	123(2)	H(56B)-C(56)-H(56C)	109.5
C(39)-C(40)-H(40)	117(2)	O(7)-C(57)-N(7)	124.0(3)
C(40)-C(41)-C(42)	120.1(3)	O(7)-C(57)-N(8)	123.6(3)
C(40)-C(41)-H(41)	124(2)	N(7)-C(57)-N(8)	112.4(3)
C(42)-C(41)-H(41)	116(2)	N(8)-C(58)-C(63)	118.9(3)
C(41)-C(42)-C(43)	121.2(3)	N(8)-C(58)-C(59)	122.5(3)
C(41)-C(42)-N(6)	119.1(3)	C(63)-C(58)-C(59)	118.5(3)
C(43)-C(42)-N(6)	119.7(3)	C(60)-C(59)-C(58)	120.4(4)
C(44)-C(43)-C(42)	119.0(3)	C(60)-C(59)-H(59)	121.9(18)
C(44)-C(43)-H(43)	122(2)	C(58)-C(59)-H(59)	117.7(19)
C(42)-C(43)-H(43)	119(2)	C(59)-C(60)-C(61)	119.7(4)
C(43)-C(44)-C(39)	120.8(3)	C(59)-C(60)-H(60)	119(3)
C(43)-C(44)-H(44)	117.8(18)	C(61)-C(60)-H(60)	121(3)
C(39)-C(44)-H(44)	121.4(18)	C(62)-C(61)-C(60)	121.0(4)
C(46)-C(45)-C(5)	176.9(3)	C(62)-C(61)-N(9)	120.2(4)
C(45)-C(46)-C(47)	177.6(3)	C(60)-C(61)-N(9)	118.8(3)
C(48)-C(47)-C(52)	120.3(3)	C(63)-C(62)-C(61)	118.8(4)
C(48)-C(47)-C(46)	119.8(3)	C(63)-C(62)-H(62)	123(3)
C(52)-C(47)-C(46)	119.9(3)	C(61)-C(62)-H(62)	119(3)
C(49)-C(48)-C(47)	122.4(3)	C(62)-C(63)-C(58)	121.2(4)
C(49)-C(48)-H(48)	119.1(19)	C(62)-C(63)-H(63)	119(2)
C(47)-C(48)-H(48)	118.5(19)	C(58)-C(63)-H(63)	120(2)
C(50)-C(49)-C(48)	115.9(3)	O(1S)-S(1S)-C(2S)	106.17(19)
C(50)-C(49)-C(53)	121.4(3)	O(1S)-S(1S)-C(1S)	106.10(18)
C(48)-C(49)-C(53)	122.7(3)	C(2S)-S(1S)-C(1S)	97.34(19)
C(51)-C(50)-C(49)	123.6(3)	S(1S)-C(1S)-H(1SA)	108(2)
C(51)-C(50)-H(50)	117(2)	S(1S)-C(1S)-H(1SB)	104(2)
C(49)-C(50)-H(50)	119(2)	H(1SA)-C(1S)-H(1SB)	115(3)
C(50)-C(51)-C(52)	120.5(3)	S(1S)-C(1S)-H(1SC)	104(2)
C(50)-C(51)-H(51)	124.5(19)	H(1SA)-C(1S)-H(1SC)	114(3)
C(52)-C(51)-H(51)	115.0(19)	H(1SB)-C(1S)-H(1SC)	110(3)
C(51)-C(52)-C(47)	117.3(3)	S(1S)-C(2S)-H(2SA)	110(3)
C(51)-C(52)-N(7)	124.2(3)	S(1S)-C(2S)-H(2SB)	108(2)
C(47)-C(52)-N(7)	118.4(3)	H(2SA)-C(2S)-H(2SB)	116(3)
C(56)-C(53)-C(49)	110.2(3)	S(1S)-C(2S)-H(2SC)	110(2)
C(56)-C(53)-C(54)	108.1(3)	H(2SA)-C(2S)-H(2SC)	98(3)
C(49)-C(53)-C(54)	112.0(3)	H(2SB)-C(2S)-H(2SC)	114(3)
C(56)-C(53)-C(55)	109.6(3)	O(2S)-S(2S)-C(3S)	106.05(19)
C(49)-C(53)-C(55)	107.8(3)	O(2S)-S(2S)-C(4S)	105.84(18)
C(54)-C(53)-C(55)	109.1(3)	C(3S)-S(2S)-C(4S)	97.5(2)
C(53)-C(54)-H(54A)	109.5	S(2S)-C(3S)-H(3SA)	109.5
C(53)-C(54)-H(54B)	109.5	S(2S)-C(3S)-H(3SB)	109.5
H(54A)-C(54)-H(54B)	109.5	H(3SA)-C(3S)-H(3SB)	109.5
C(53)-C(54)-H(54C)	109.5	S(2S)-C(3S)-H(3SC)	109.5
H(54A)-C(54)-H(54C)	109.5	H(3SA)-C(3S)-H(3SC)	109.5
H(54B)-C(54)-H(54C)	109.5	H(3SB)-C(3S)-H(3SC)	109.5
C(53)-C(55)-H(55A)	109.5	S(2S)-C(4S)-H(4SA)	109.5
C(53)-C(55)-H(55B)	109.5	S(2S)-C(4S)-H(4SB)	109.5
H(55A)-C(55)-H(55B)	109.5	H(4SA)-C(4S)-H(4SB)	109.5
C(53)-C(55)-H(55C)	109.5	S(2S)-C(4S)-H(4SC)	109.5
H(55A)-C(55)-H(55C)	109.5	H(4SA)-C(4S)-H(4SC)	109.5
H(55B)-C(55)-H(55C)	109.5	H(4SB)-C(4S)-H(4SC)	109.5
C(53)-C(56)-H(56A)	109.5	O(3S)-S(3S)-C(5S)	110.7(4)

Table 36 Continued.

Atoms	°	Atoms	°
C(5SA)-S(3SA)-C(6SA)	97.1(6)	S(3SA)-C(6SA)-H(6SF)	109.5
O(3S)-S(3S)-C(6S)	108.8(5)	H(6SD)-C(6SA)-H(6SF)	109.5
C(5S)-S(3S)-C(6S)	123.3(7)	H(6SE)-C(6SA)-H(6SF)	109.5
S(3S)-C(5S)-H(5SA)	109.5	O(4SA)-S(4S)-O(4S)	86.9(4)
S(3S)-C(5S)-H(5SB)	109.5	O(4SA)-S(4S)-C(7S)	111.8(4)
H(5SA)-C(5S)-H(5SB)	109.5	O(4S)-S(4S)-C(7S)	128.0(4)
S(3S)-C(5S)-H(5SC)	109.5	O(4SA)-S(4S)-C(8S)	125.0(4)
H(5SA)-C(5S)-H(5SC)	109.5	O(4S)-S(4S)-C(8S)	110.5(3)
H(5SB)-C(5S)-H(5SC)	109.5	C(7S)-S(4S)-C(8S)	97.6(2)
S(3S)-C(6S)-H(6SA)	109.5	S(4S)-O(4S)-O(4SA)	44.5(3)
S(3S)-C(6S)-H(6SB)	109.5	S(4S)-O(4SA)-O(4S)	48.6(3)
H(6SA)-C(6S)-H(6SB)	109.5	S(4S)-C(7S)-H(7SA)	109.5
S(3S)-C(6S)-H(6SC)	109.5	S(4S)-C(7S)-H(7SB)	109.5
H(6SA)-C(6S)-H(6SC)	109.5	H(7SA)-C(7S)-H(7SB)	109.5
H(6SB)-C(6S)-H(6SC)	109.5	S(4S)-C(7S)-H(7SC)	109.5
S(3SA)-C(5SA)-H(5SD)	109.5	H(7SA)-C(7S)-H(7SC)	109.5
S(3SA)-C(5SA)-H(5SE)	109.5	H(7SB)-C(7S)-H(7SC)	109.5
H(5SD)-C(5SA)-H(5SE)	109.5	S(4S)-C(8S)-H(8SA)	109.5
S(3SA)-C(5SA)-H(5SF)	109.5	S(4S)-C(8S)-H(8SB)	109.5
H(5SD)-C(5SA)-H(5SF)	109.5	H(8SA)-C(8S)-H(8SB)	109.5
H(5SE)-C(5SA)-H(5SF)	109.5	S(4S)-C(8S)-H(8SC)	109.5
S(3SA)-C(6SA)-H(6SD)	109.5	H(8SA)-C(8S)-H(8SC)	109.5
S(3SA)-C(6SA)-H(6SE)	109.5	H(8SB)-C(8S)-H(8SC)	109.5
H(6SD)-C(6SA)-H(6SE)	109.5		

Table 37. Torsion angles for **2•DMSO**.

Atoms	°	Atoms	°
C(6)-C(1)-C(2)-C(3)	2.0(4)	C(19)-N(1)-C(14)-C(13)	31.4(5)
C(7)-C(1)-C(2)-C(3)	-177.0(3)	C(19)-N(1)-C(14)-C(9)	-152.0(3)
C(1)-C(2)-C(3)-C(4)	-3.2(4)	C(10)-C(9)-C(14)-C(13)	-2.1(5)
C(1)-C(2)-C(3)-C(26)	175.6(3)	C(8)-C(9)-C(14)-C(13)	177.7(3)
C(2)-C(3)-C(4)-C(5)	1.4(4)	C(10)-C(9)-C(14)-N(1)	-178.9(3)
C(26)-C(3)-C(4)-C(5)	-177.4(3)	C(8)-C(9)-C(14)-N(1)	1.0(4)
C(3)-C(4)-C(5)-C(6)	1.5(5)	C(12)-C(11)-C(15)-C(16A)	-63.8(14)
C(3)-C(4)-C(5)-C(45)	-178.1(3)	C(10)-C(11)-C(15)-C(16A)	115.0(14)
C(4)-C(5)-C(6)-C(1)	-2.7(5)	C(12)-C(11)-C(15)-C(16)	122.1(4)
C(45)-C(5)-C(6)-C(1)	176.9(3)	C(10)-C(11)-C(15)-C(16)	-59.1(4)
C(2)-C(1)-C(6)-C(5)	1.0(4)	C(12)-C(11)-C(15)-C(17)	-117.0(4)
C(7)-C(1)-C(6)-C(5)	180.0(3)	C(10)-C(11)-C(15)-C(17)	61.8(4)
C(2)-C(1)-C(7)-C(8)	50(5)	C(12)-C(11)-C(15)-C(18)	0.7(5)
C(6)-C(1)-C(7)-C(8)	-129(5)	C(10)-C(11)-C(15)-C(18)	179.5(3)
C(1)-C(7)-C(8)-C(9)	-54(10)	C(12)-C(11)-C(15)-C(18A)	170.3(15)
C(7)-C(8)-C(9)-C(10)	-26(6)	C(10)-C(11)-C(15)-C(18A)	-10.9(15)
C(7)-C(8)-C(9)-C(14)	154(6)	C(12)-C(11)-C(15)-C(17A)	59.2(14)
C(14)-C(9)-C(10)-C(11)	-0.4(5)	C(10)-C(11)-C(15)-C(17A)	-122.0(13)
C(8)-C(9)-C(10)-C(11)	179.8(3)	C(14)-N(1)-C(19)-O(1)	-0.8(5)
C(9)-C(10)-C(11)-C(12)	1.8(5)	C(14)-N(1)-C(19)-N(2)	178.8(3)
C(9)-C(10)-C(11)-C(15)	-177.1(3)	C(20)-N(2)-C(19)-O(1)	4.8(5)
C(10)-C(11)-C(12)-C(13)	-0.7(5)	C(20)-N(2)-C(19)-N(1)	-174.9(3)
C(15)-C(11)-C(12)-C(13)	178.1(3)	C(19)-N(2)-C(20)-C(25)	168.2(3)
C(11)-C(12)-C(13)-C(14)	-1.8(5)	C(19)-N(2)-C(20)-C(21)	-11.2(5)
C(12)-C(13)-C(14)-N(1)	179.8(3)	N(2)-C(20)-C(21)-C(22)	179.5(3)
C(12)-C(13)-C(14)-C(9)	3.2(5)	C(25)-C(20)-C(21)-C(22)	0.1(5)

Table 37 Continued.

Atoms	°	Atoms	°
C(20)-C(21)-C(22)-C(23)	-0.5(6)	N(6)-C(42)-C(43)-C(44)	178.0(3)
C(21)-C(22)-C(23)-C(24)	0.5(6)	C(42)-C(43)-C(44)-C(39)	-0.5(5)
C(21)-C(22)-C(23)-N(3)	-179.9(3)	N(5)-C(39)-C(44)-C(43)	-175.5(3)
O(2)-N(3)-C(23)-C(22)	1.3(5)	C(40)-C(39)-C(44)-C(43)	1.7(5)
O(3)-N(3)-C(23)-C(22)	-177.5(4)	C(4)-C(5)-C(45)-C(46)	43(7)
O(2)-N(3)-C(23)-C(24)	-179.1(4)	C(6)-C(5)-C(45)-C(46)	-137(6)
O(3)-N(3)-C(23)-C(24)	2.0(5)	C(5)-C(45)-C(46)-C(47)	-29(14)
C(22)-C(23)-C(24)-C(25)	-0.1(6)	C(45)-C(46)-C(47)-C(48)	-139(9)
N(3)-C(23)-C(24)-C(25)	-179.7(3)	C(45)-C(46)-C(47)-C(52)	41(9)
C(23)-C(24)-C(25)-C(20)	-0.2(6)	C(52)-C(47)-C(48)-C(49)	1.0(5)
N(2)-C(20)-C(25)-C(24)	-179.2(3)	C(46)-C(47)-C(48)-C(49)	-179.7(3)
C(21)-C(20)-C(25)-C(24)	0.2(5)	C(47)-C(48)-C(49)-C(50)	-0.5(5)
C(4)-C(3)-C(26)-C(27)	96(9)	C(47)-C(48)-C(49)-C(53)	176.8(3)
C(2)-C(3)-C(26)-C(27)	-83(9)	C(48)-C(49)-C(50)-C(51)	-0.8(5)
C(3)-C(26)-C(27)-C(28)	-109(10)	C(53)-C(49)-C(50)-C(51)	-178.1(3)
C(26)-C(27)-C(28)-C(29)	-154(6)	C(49)-C(50)-C(51)-C(52)	1.5(6)
C(26)-C(27)-C(28)-C(33)	26(6)	C(50)-C(51)-C(52)-C(47)	-0.9(5)
C(33)-C(28)-C(29)-C(30)	-1.6(5)	C(50)-C(51)-C(52)-N(7)	176.5(3)
C(27)-C(28)-C(29)-C(30)	178.8(3)	C(48)-C(47)-C(52)-C(51)	-0.3(5)
C(28)-C(29)-C(30)-C(31)	0.6(5)	C(46)-C(47)-C(52)-C(51)	-179.5(3)
C(28)-C(29)-C(30)-C(34)	178.4(3)	C(48)-C(47)-C(52)-N(7)	-177.9(3)
C(29)-C(30)-C(31)-C(32)	0.3(5)	C(46)-C(47)-C(52)-N(7)	2.9(4)
C(34)-C(30)-C(31)-C(32)	-177.6(3)	C(57)-N(7)-C(52)-C(51)	18.5(5)
C(30)-C(31)-C(32)-C(33)	0.0(5)	C(57)-N(7)-C(52)-C(47)	-164.1(3)
C(31)-C(32)-C(33)-N(4)	176.7(3)	C(50)-C(49)-C(53)-C(56)	-45.7(5)
C(31)-C(32)-C(33)-C(28)	-1.0(5)	C(48)-C(49)-C(53)-C(56)	137.1(3)
C(38)-N(4)-C(33)-C(32)	24.2(5)	C(50)-C(49)-C(53)-C(54)	-166.1(3)
C(38)-N(4)-C(33)-C(28)	-158.2(3)	C(48)-C(49)-C(53)-C(54)	16.7(5)
C(29)-C(28)-C(33)-C(32)	1.7(5)	C(50)-C(49)-C(53)-C(55)	73.9(4)
C(27)-C(28)-C(33)-C(32)	-178.6(3)	C(48)-C(49)-C(53)-C(55)	-103.3(4)
C(29)-C(28)-C(33)-N(4)	-176.0(3)	C(52)-N(7)-C(57)-O(7)	5.2(5)
C(27)-C(28)-C(33)-N(4)	3.6(4)	C(52)-N(7)-C(57)-N(8)	-175.6(3)
C(29)-C(30)-C(34)-C(35)	145.9(4)	C(58)-N(8)-C(57)-O(7)	8.0(5)
C(31)-C(30)-C(34)-C(35)	-36.4(5)	C(58)-N(8)-C(57)-N(7)	-171.3(3)
C(29)-C(30)-C(34)-C(36)	-93.1(5)	C(57)-N(8)-C(58)-C(63)	155.3(3)
C(31)-C(30)-C(34)-C(36)	84.6(5)	C(57)-N(8)-C(58)-C(59)	-27.6(5)
C(29)-C(30)-C(34)-C(37)	27.4(5)	N(8)-C(58)-C(59)-C(60)	179.1(3)
C(31)-C(30)-C(34)-C(37)	-154.9(4)	C(63)-C(58)-C(59)-C(60)	-3.8(5)
C(33)-N(4)-C(38)-O(4)	3.0(6)	C(58)-C(59)-C(60)-C(61)	-1.3(6)
C(33)-N(4)-C(38)-N(5)	-176.2(3)	C(59)-C(60)-C(61)-C(62)	4.7(6)
C(39)-N(5)-C(38)-O(4)	8.3(5)	C(59)-C(60)-C(61)-N(9)	-175.2(4)
C(39)-N(5)-C(38)-N(4)	-172.5(3)	O(8)-N(9)-C(61)-C(62)	-9.2(6)
C(38)-N(5)-C(39)-C(44)	-159.2(3)	O(9)-N(9)-C(61)-C(62)	171.5(4)
C(38)-N(5)-C(39)-C(40)	23.6(5)	O(8)-N(9)-C(61)-C(60)	170.6(4)
N(5)-C(39)-C(40)-C(41)	175.5(3)	O(9)-N(9)-C(61)-C(60)	-8.7(6)
C(44)-C(39)-C(40)-C(41)	-1.6(5)	C(60)-C(61)-C(62)-C(63)	-2.7(6)
C(39)-C(40)-C(41)-C(42)	0.3(5)	N(9)-C(61)-C(62)-C(63)	177.2(3)
C(40)-C(41)-C(42)-C(43)	1.0(5)	C(61)-C(62)-C(63)-C(58)	-2.6(5)
C(40)-C(41)-C(42)-N(6)	-177.9(3)	N(8)-C(58)-C(63)-C(62)	-177.0(3)
O(5)-N(6)-C(42)-C(41)	167.1(3)	C(59)-C(58)-C(63)-C(62)	5.8(5)
O(6)-N(6)-C(42)-C(41)	-12.2(5)	C(7S)-S(4S)-O(4S)-O(4SA)	115.5(5)
O(5)-N(6)-C(42)-C(43)	-11.7(5)	C(8S)-S(4S)-O(4S)-O(4SA)	-126.3(4)
O(6)-N(6)-C(42)-C(43)	168.9(3)	C(7S)-S(4S)-O(4SA)-O(4S)	-130.0(4)
C(41)-C(42)-C(43)-C(44)	-0.9(5)	C(8S)-S(4S)-O(4SA)-O(4S)	112.9(4)

Table 38. Anisotropic displacement parameters ($Å^2$ x 10^3) for **2•DMSO**. The anisotropic displacement factor exponent takes the form: $-2p^2[h^2a^{*2}U^{11} + ... + 2hka^*b^*U^{12}]$.

Atom	U^{11}	U^{22}	U^{33}	U^{23}	U^{13}	U^{12}
O(1)	27(1)	42(1)	61(2)	-7(1)	-8(1)	-2(1)
O(2)	69(2)	52(2)	110(3)	-8(2)	-16(2)	17(2)
O(3)	82(2)	42(2)	91(2)	2(2)	-23(2)	-4(2)
O(4)	41(1)	58(2)	74(2)	16(1)	-28(1)	-11(1)
O(5)	70(2)	57(2)	75(2)	6(2)	-11(2)	-19(2)
O(6)	43(2)	78(2)	85(2)	-7(2)	-10(2)	-12(2)
O(7)	33(1)	47(1)	57(2)	-8(1)	-2(1)	-11(1)
O(8)	91(2)	78(2)	86(2)	-7(2)	-32(2)	27(2)
O(9)	45(2)	76(2)	122(3)	-18(2)	-13(2)	8(2)
N(1)	22(2)	43(2)	44(2)	-13(1)	-6(1)	-4(1)
N(2)	26(2)	44(2)	39(2)	-10(1)	-4(1)	-2(1)
N(3)	69(2)	45(2)	56(2)	-2(2)	-19(2)	7(2)
N(4)	34(2)	40(2)	44(2)	1(1)	-18(1)	-3(1)
N(5)	33(2)	38(2)	45(2)	-4(1)	-14(1)	-1(1)
N(6)	53(2)	56(2)	52(2)	-7(2)	-10(2)	-15(2)
N(7)	32(2)	38(2)	40(2)	-2(1)	-4(1)	-9(1)
N(8)	30(2)	41(2)	48(2)	-9(1)	-7(1)	-7(1)
N(9)	59(2)	58(2)	80(3)	-21(2)	-22(2)	12(2)
C(1)	22(2)	32(2)	39(2)	-8(1)	-8(1)	1(1)
C(2)	24(2)	30(2)	34(2)	-4(1)	-3(1)	-3(1)
C(3)	24(2)	32(2)	35(2)	-6(1)	-7(1)	3(1)
C(4)	20(2)	36(2)	44(2)	-10(1)	-8(1)	-2(1)
C(5)	25(2)	30(2)	37(2)	-7(1)	-4(1)	1(1)
C(6)	25(2)	37(2)	37(2)	-6(2)	-9(1)	2(1)
C(7)	30(2)	34(2)	37(2)	-5(1)	-10(1)	-1(1)
C(8)	29(2)	35(2)	37(2)	-7(1)	-10(1)	3(1)
C(9)	23(2)	43(2)	37(2)	-13(1)	-8(1)	-5(1)
C(10)	32(2)	44(2)	41(2)	-13(2)	-13(2)	3(2)
C(11)	33(2)	43(2)	42(2)	-14(2)	-5(1)	-9(2)
C(12)	27(2)	50(2)	57(2)	-22(2)	-10(2)	-3(2)
C(13)	29(2)	42(2)	51(2)	-17(2)	-13(2)	3(2)
C(14)	25(2)	39(2)	38(2)	-14(1)	-7(1)	-1(1)
C(15)	40(2)	43(2)	55(2)	-11(2)	-9(2)	-8(2)
C(16)	55(3)	43(3)	94(4)	-29(3)	-17(3)	-2(2)
C(17)	84(4)	49(3)	65(3)	2(2)	-15(3)	-18(3)
C(18)	47(3)	44(3)	105(4)	-13(3)	-10(3)	-15(2)
C(16A)	55(3)	43(3)	94(4)	-29(3)	-17(3)	-2(2)
C(17A)	84(4)	49(3)	65(3)	2(2)	-15(3)	-18(3)
C(18A)	47(3)	44(3)	105(4)	-13(3)	-10(3)	-15(2)
C(19)	29(2)	40(2)	34(2)	-8(1)	-12(1)	-1(1)
C(20)	38(2)	40(2)	30(2)	-7(1)	-10(1)	-2(2)
C(21)	36(2)	44(2)	54(2)	-9(2)	-15(2)	-2(2)
C(22)	38(2)	50(2)	58(2)	-6(2)	-16(2)	4(2)
C(23)	51(2)	44(2)	41(2)	-5(2)	-13(2)	5(2)
C(24)	60(2)	39(2)	45(2)	0(2)	-9(2)	-7(2)
C(25)	37(2)	48(2)	47(2)	-6(2)	-6(2)	-3(2)
C(26)	25(2)	37(2)	44(2)	-5(2)	-9(1)	-4(1)
C(27)	28(2)	36(2)	40(2)	-5(1)	-8(1)	-3(1)
C(28)	29(2)	36(2)	36(2)	-6(1)	-10(1)	4(1)
C(29)	27(2)	43(2)	48(2)	-8(2)	-13(2)	0(2)
C(30)	34(2)	37(2)	41(2)	-6(2)	-5(1)	5(1)
C(31)	43(2)	46(2)	41(2)	-1(2)	-19(2)	2(2)
C(32)	35(2)	47(2)	42(2)	-5(2)	-14(2)	-5(2)
C(33)	32(2)	35(2)	36(2)	-7(1)	-10(1)	3(1)
C(34)	48(2)	38(2)	57(2)	-1(2)	-10(2)	1(2)
C(35)	81(3)	53(3)	121(4)	22(3)	-43(3)	5(2)

Table 38 Continued.

Atom	U^{11}	U^{22}	U^{33}	U^{23}	U^{13}	U^{12}
C(36)	139(5)	55(3)	102(4)	3(3)	65(4)	-18(3)
C(37)	105(4)	55(3)	117(4)	22(3)	-56(3)	-28(3)
C(38)	36(2)	42(2)	40(2)	-9(2)	-12(2)	-1(2)
C(39)	39(2)	40(2)	31(2)	-10(1)	-11(1)	-2(2)
C(40)	44(2)	40(2)	42(2)	-14(2)	-9(2)	0(2)
C(41)	38(2)	48(2)	46(2)	-14(2)	-7(2)	2(2)
C(42)	45(2)	45(2)	36(2)	-10(2)	-8(2)	-10(2)
C(43)	54(2)	36(2)	40(2)	-5(2)	-17(2)	-4(2)
C(44)	42(2)	40(2)	36(2)	-7(2)	-11(2)	0(2)
C(45)	26(2)	34(2)	42(2)	-6(2)	-7(1)	1(1)
C(46)	30(2)	39(2)	43(2)	-7(2)	-9(2)	-1(2)
C(47)	36(2)	36(2)	35(2)	-5(1)	-9(1)	-8(1)
C(48)	34(2)	39(2)	44(2)	-10(2)	-6(2)	-6(2)
C(49)	45(2)	35(2)	42(2)	-6(2)	-10(2)	-11(2)
C(50)	44(2)	39(2)	43(2)	0(2)	-1(2)	-13(2)
C(51)	35(2)	43(2)	45(2)	-8(2)	0(2)	-6(2)
C(52)	36(2)	40(2)	33(2)	-8(1)	-8(1)	-8(1)
C(53)	52(2)	35(2)	55(2)	-7(2)	-10(2)	-6(2)
C(54)	57(3)	38(2)	103(4)	-12(2)	-8(2)	1(2)
C(55)	77(3)	47(2)	79(3)	-7(2)	-34(2)	-1(2)
C(56)	64(2)	35(2)	57(2)	-7(2)	-8(2)	-12(2)
C(57)	34(2)	43(2)	32(2)	-8(1)	-7(1)	-6(2)
C(58)	38(2)	44(2)	43(2)	-16(2)	-10(2)	-3(2)
C(59)	39(2)	50(2)	58(2)	-6(2)	-7(2)	-7(2)
C(60)	37(2)	52(2)	73(3)	-12(2)	-7(2)	-4(2)
C(61)	40(2)	53(2)	64(2)	-23(2)	-16(2)	6(2)
C(62)	63(3)	44(2)	42(2)	-12(2)	-7(2)	7(2)
C(63)	46(2)	45(2)	44(2)	-15(2)	1(2)	-3(2)
S(1S)	33(1)	32(1)	51(1)	-7(1)	-8(1)	-1(1)
O(1S)	39(1)	41(1)	68(2)	-16(1)	-9(1)	-10(1)
C(1S)	48(2)	46(2)	43(2)	-9(2)	-4(2)	-1(2)
C(2S)	47(2)	42(2)	50(2)	-12(2)	2(2)	-8(2)
S(2S)	36(1)	66(1)	46(1)	-2(1)	-9(1)	-3(1)
O(2S)	36(1)	71(2)	48(2)	3(1)	-5(1)	-7(1)
C(3S)	98(4)	71(3)	65(3)	-21(2)	1(3)	-16(3)
C(4S)	55(2)	53(2)	70(3)	-4(2)	-16(2)	-11(2)
S(3S)	46(1)	52(2)	52(2)	-14(1)	-15(1)	11(1)
O(3S)	53(2)	53(2)	75(2)	-14(1)	-24(1)	18(1)
S(3SA)	43(1)	44(1)	48(1)	-14(1)	-14(1)	12(1)
O(3SA)	53(2)	53(2)	75(2)	-14(1)	-24(1)	18(1)
S(4S)	209(2)	67(1)	92(1)	-30(1)	-97(1)	47(1)
C(7S)	114(4)	50(3)	95(4)	-17(2)	-31(3)	-2(3)
C(8S)	69(3)	61(3)	62(3)	-23(2)	-27(2)	6(2)
N(7)	45(1)	29(1)	33(1)	3(1)	-17(1)	2(1)
N(8)	43(1)	36(1)	35(1)	2(1)	-15(1)	2(1)
N(9)	42(1)	100(2)	41(1)	-5(1)	-5(1)	-22(1)
C(1)	22(1)	26(1)	29(1)	1(1)	-7(1)	-1(1)

Table 39. Hydrogen coordinates (x 10^4) and isotropic displacement parameters ($Å^2$ x 10^3) for **2•DMSO**.

Atom	X	Y	Z	U(eq)
H(16A)	-5540	77	2856	93
H(16B)	-5430	-587	3540	93
H(16C)	-4561	305	3164	93

Table 39 Continued.

Atom	X	Y	Z	U(eq)
H(17A)	-6621	931	4545	104
H(17B)	-5284	839	4303	104
H(17C)	-6086	-111	4521	104
H(18A)	-7704	1116	3474	101
H(18B)	-7746	215	4085	101
H(18C)	-7355	60	3364	101
H(16D)	-7652	976	4138	93
H(16E)	-6710	808	4537	93
H(16F)	-7217	-97	4377	93
H(17D)	-7127	587	2991	104
H(17E)	-6743	-441	3359	104
H(17F)	-5867	235	2754	104
H(18D)	-4743	260	4050	101
H(18E)	-4520	41	3348	101
H(18F)	-5384	-636	3959	101
H(35A)	2372	-207	6779	135
H(35B)	2504	-723	6195	135
H(35C)	1619	-1154	6877	135
H(36A)	616	703	7116	180
H(36B)	-80	-282	7229	180
H(36C)	-377	700	6766	180
H(37A)	159	-1121	6342	141
H(37B)	1015	-680	5652	141
H(37C)	-136	-142	5875	141
H(54A)	728	9472	675	104
H(54B)	1092	10600	463	104
H(54C)	1502	9880	1042	104
H(55A)	1527	9357	-477	100
H(55B)	2803	9706	-842	100
H(55C)	1871	10489	-674	100
H(56A)	3486	10393	483	81
H(56B)	3059	11121	-86	81
H(56C)	3998	10345	-256	81
H(3SA)	8401	5530	490	121
H(3SB)	9333	5616	867	121
H(3SC)	9377	6353	180	121
H(4SA)	8787	7975	1304	92
H(4SB)	9606	7771	656	92
H(4SC)	9554	7033	1344	92
H(5SA)	1688	7510	3925	64
H(5SB)	394	7760	3955	64
H(5SC)	1155	7384	3356	64
H(6SA)	-699	4991	4526	84
H(6SB)	-473	5499	3767	84
H(6SC)	-1221	6029	4291	84
H(5SD)	1630	7422	3319	177
H(5SE)	624	7294	3965	177
H(5SF)	355	7308	3288	177
H(6SD)	-582	5115	4125	101
H(6SE)	-931	6207	3856	101
H(6SF)	-585	5910	4530	101
H(7SA)	6292	1370	4747	129
H(7SB)	6653	2363	4201	129
H(7SC)	5632	2346	4827	129
H(8SA)	7757	3928	5024	91
H(8SB)	6482	3836	4988	91
H(8SC)	7500	3847	4361	91

Table 39 Continued.

Atom	X	Y	Z	U(eq)
H(1N)	-4160(30)	4820(20)	2256(15)	31(9)
H(1SA)	1860(30)	2220(30)	701(18)	60(12)
H(1SC)	2910(30)	2240(30)	1003(17)	47(10)
H(1SB)	2860(30)	3050(30)	358(18)	50(10)
H(2)	-1140(20)	2880(20)	3649(14)	28(8)
H(2N)	-4280(30)	6360(30)	1901(17)	43(11)
H(2SA)	740(40)	2750(30)	2300(20)	71(13)
H(2SB)	600(30)	2110(30)	1832(17)	52(11)
H(2SC)	1620(30)	2120(30)	2122(18)	55(12)
H(4)	1570(30)	4610(20)	2919(13)	24(8)
H(4N)	2420(30)	4000(30)	4373(18)	50(11)
H(5N)	3390(30)	5280(20)	3978(16)	39(10)
H(6)	-910(30)	4980(20)	2040(15)	33(8)
H(7N)	3360(30)	5370(20)	1050(16)	37(9)
H(8N)	4360(30)	4180(30)	1082(17)	41(11)
H(10)	-4180(30)	1740(20)	3321(14)	28(8)
H(12)	-7240(30)	2250(20)	3026(15)	43(9)
H(13)	-6680(30)	3850(20)	2520(14)	32(8)
H(21)	-7080(30)	6970(20)	2330(15)	35(8)
H(22)	-7680(30)	8490(20)	2219(16)	41(9)
H(24)	-4480(40)	9570(30)	1530(20)	79(14)
H(25)	-3880(30)	8010(20)	1657(16)	48(10)
H(29)	540(30)	1230(20)	5249(13)	25(7)
H(31)	2810(30)	1270(20)	6264(16)	36(9)
H(32)	3570(30)	2650(20)	5584(15)	40(9)
H(40)	6060(30)	4600(30)	3779(18)	62(11)
H(41)	7690(30)	5680(20)	3253(15)	41(9)
H(43)	5670(30)	7940(30)	3085(16)	42(9)
H(44)	4040(30)	6970(20)	3625(15)	41(9)
H(48)	1370(30)	8120(20)	1038(15)	38(9)
H(50)	4320(30)	8840(20)	-250(17)	44(10)
H(51)	4930(30)	7290(20)	36(14)	29(8)
H(59)	7010(30)	4790(20)	219(16)	41(9)
H(60)	8570(40)	3780(30)	320(20)	88(15)
H(62)	6550(40)	1710(30)	1690(20)	78(14)
H(63)	5000(30)	2690(20)	1606(17)	44(9)

APPENDIX E

SUPPLEMENTARY INFORMATION FOR CHAPTER V

E.1. Synthesis

E.1.1. General Methods

^{1}H and ^{13}C NMR spectra were obtained on a Varian 300 MHz spectrometer (^{1}H 299.95 Hz, ^{13}C 75.43 Hz), Inova 500 MHz spectrometer (^{1}H 500.10 MHz, ^{13}C 125.75 MHz) or Bruker Avance III HD 600 MHz NMR Spectrometer with Prodigy multinuclear broadband BBO CryoProbe (^{1}H: 600.02 MHz, ^{13}C: 150.89 MHz). Chemical shifts (δ) are expressed in ppm from solvent signal using non-deuterated solvent present in the bulk deuterated solvent ($(CD_3)_2SO$: ^{1}H 2.5 ppm, ^{13}C 39.52 ppm). Unless otherwise specified, solvents were obtained from distillation using published literature procedures directly before use. Mass spectra were acquired Waters LCT Premier ESI-MS in positive mode using acetone as a solvent. UV-Vis spectra were acquired with a Hewlett-Packard 8453 UV-Visible spectrophotometer equipped with a 250 nm cutoff filter. Fluorescence data was acquired with a Horiba Jobin-Yvon FluoroMax-4 fluorescence spectrophotometer.

E.1.2. Synthesis of Compound 3

To a stirred degassed solution of 2,6-dibromo-4-nitropyridine (0.298 g, 1.06 mmol) in 1:1 THF/DIPA (70 mL) CuI (0.020 g 0.11 mmol) and $Pd(PPh_3)_4$ (0.073 g, 0.064 mmol) were added at room temperature. The solution was degassed for an additional 30 min after which a degassed solution of alkyne **2**[ref] (0.373 g, 2.33 mmol) in

THF (50 mL) was added via cannulation, and the reaction mixture was stirred for 3 h at room temp. Upon completion the crude reaction mixture was run through a pad of silica and eluted with MeCN to remove the organic byproducts. Compound **3** was eluted with DMF and precipitated via the addition of water. The precipitated product was filtered, rinsed thoroughly with water and dried via high vacuum. No further purification was needed. Product was a bright orange solid (0.426g, 91 % yield). m.p. 198 °C (decomp.). ^{1}H NMR (300 MHz, DMSO-d_6) δ 8.55 (s, 2H), 8.19 (s, 2H), 8.13 (d, J = 8.3 Hz, 2H), 7.60 (d, J = 7.4 Hz, 2H), 7.41 (t, J = 7.8 Hz, 2H), 7.04 (t, J = 7.4 Hz, 2H), 6.50 (s, 4H). ^{13}C NMR (126 MHz, DMSO-d_6) δ 155.55, 154.32, 144.85, 141.95, 132.97, 130.94, 121.82, 119.88, 119.53, 109.22, 92.71, 88.18. UV-Vis (DMSO) λ_{max} 297 nm (17103 $cm^{-1}M^{-1}$), 379 nm (7234 $cm^{-1}M^{-1}$). HRMS (EI+) calcd for $C_{23}H_{17}N_6O_4^+$ [MH^+] 441.1311, found 441.1307. (Figures 1 and 2)

E.1.3. Synthesis of Compound 1

A suspension of compound **3** (0.408 g, 0.926 mmol) and potassium carbonate (0.640 g, 4.63 mmol) in *N*,*N*-dimethylethanolamine (9.28 mL, 92.6 mmol) was stirred at room temperature overnight. The mixture was concentrated under reduced pressure and purified by chromatography using a solution of 7:2:1 MeCN:H_2O:TEA as eluent. The product was concentrated under reduced pressure affording an off-white solid (0.300 g, 67 % yield). ^{1}H NMR (300 MHz, DMSO-d_6) δ 8.11 (d, J = 8.4 Hz, 2H), 8.03 (s, 2H), 7.52 (d, J = 7.6 Hz, 2H), 7.45 (s, 2H), 7.36 (t, J = 7.9 Hz, 2H), 7.01 (t, J = 7.6 Hz, 2H), 6.49 (s, 4H), 4.25 (t, J = 5.7 Hz, 2H), 2.67 (t, J = 5.4 Hz, 2H), 2.23 (s, 6H). HRMS (EI+) calcd for $C_{27}H_{27}N_6O_3^+$ [MH^+] 483.2145, found 483.2164. (Figure 3)

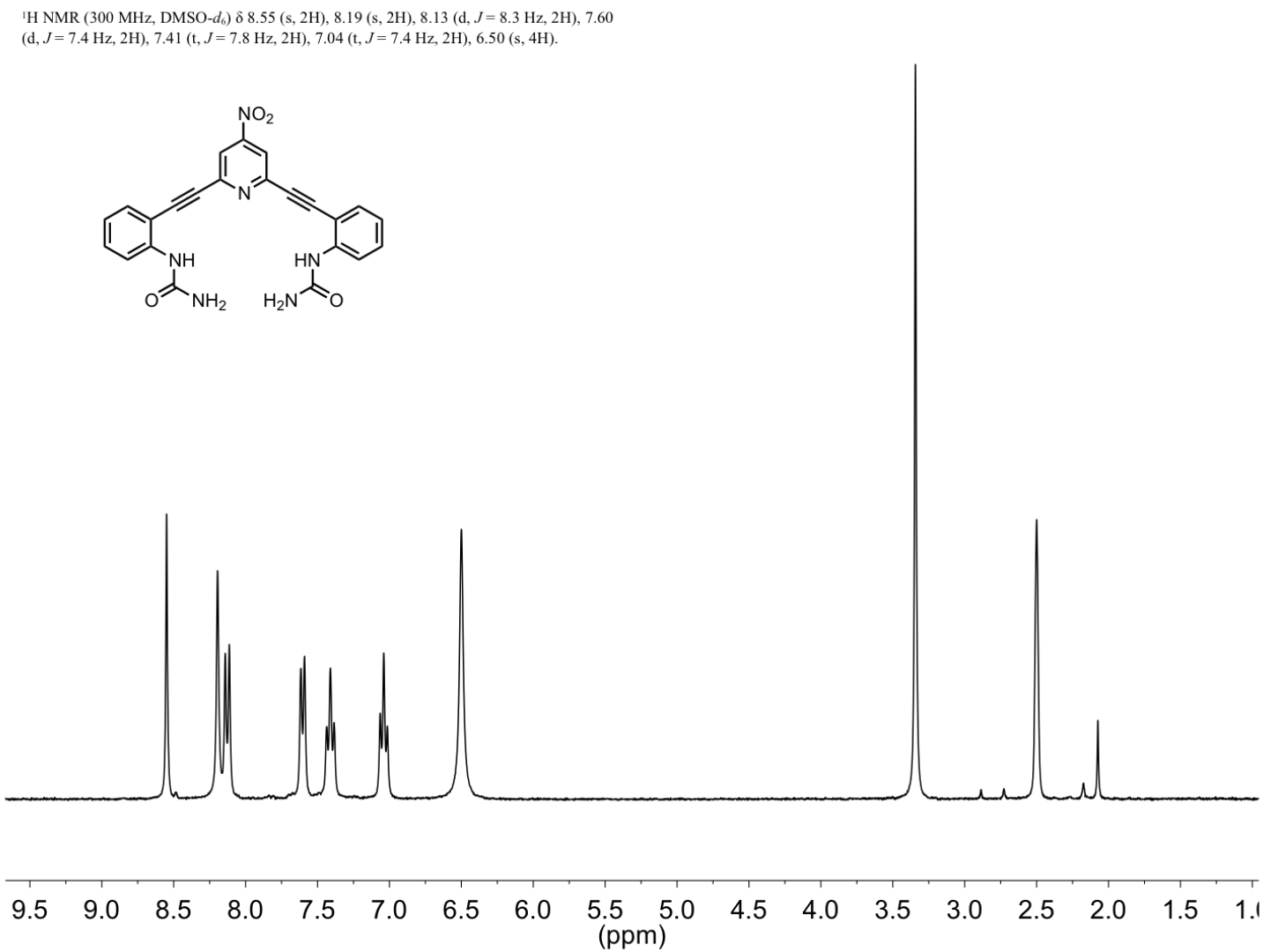

Figure 1. [1]H NMR spectrum of **3** in $CDCl_3$, 300 MHz.

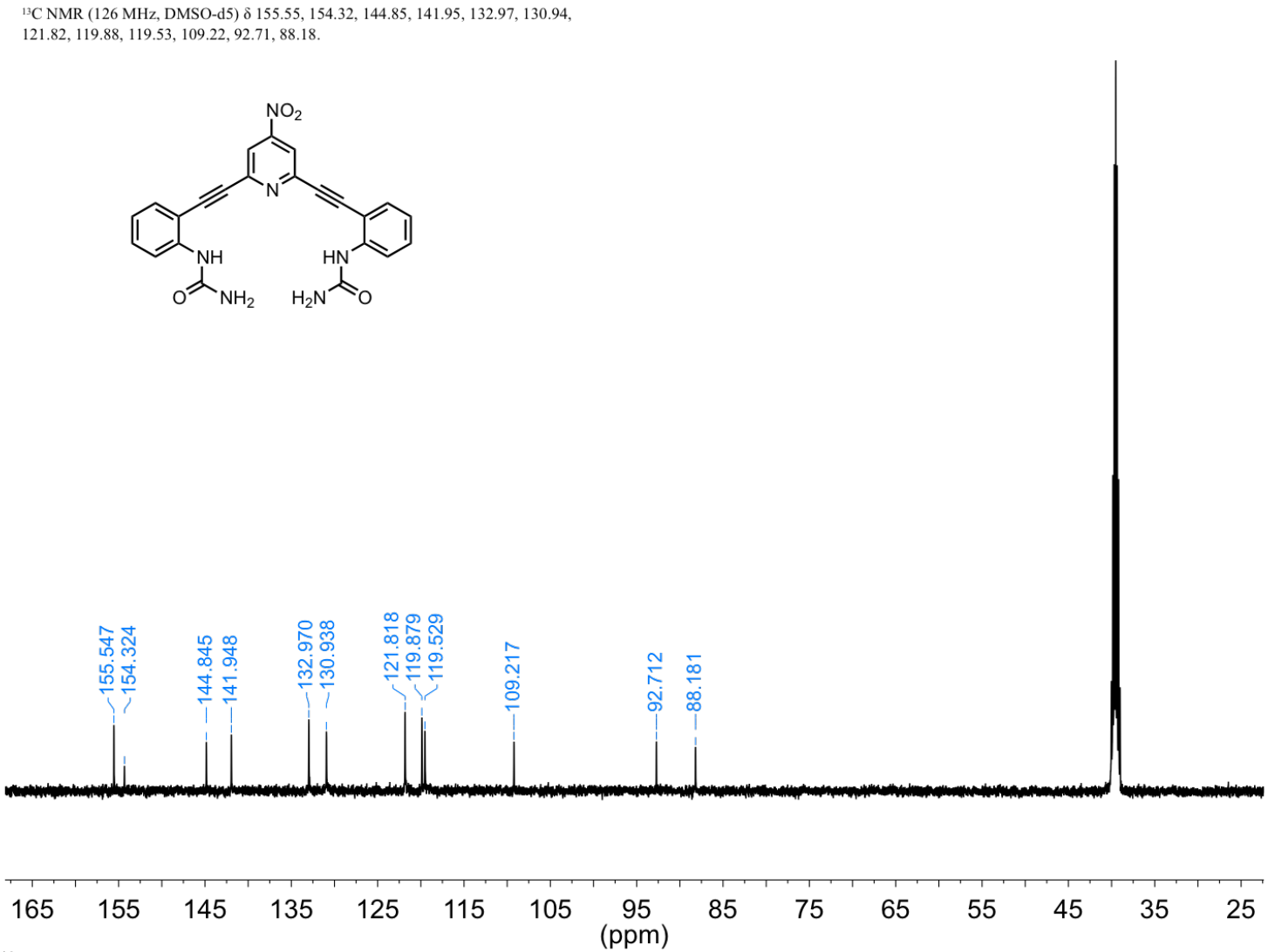

Figure 2. ^{13}C NMR spectrum of **3** in $CDCl_3$, 126 MHz.

^{1}H NMR (300 MHz, DMSO-d_6) δ 8.11 (d, J = 8.4 Hz, 2H), 8.03 (s, 2H), 7.52 (d, J = 7.6 Hz, 2H), 7.45 (s, 2H), 7.36 (t, J = 7.9 Hz, 2H), 7.01 (t, J = 7.6 Hz, 2H), 6.49 (s, 4H), 4.25 (t, J = 5.7 Hz, 2H), 2.67 (t, J = 5.4 Hz, 2H), 2.23 (s, 6H).

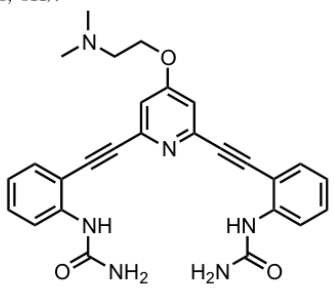

Figure 3. ^{1}H NMR spectrum of **1** in $CDCl_3$, 300 MHz.

E.1.4. Formation of 1^+

Compound **1** was protonated through the addition of trifluoroacetic acid to a suspension in MeCN and solvent removed via reduced pressure and high vacuum. On small scales a film is typically formed with MeCN. Dissolving the film in acetone followed by addition of hexanes to crash $\mathbf{1}^+$ with subsequent removal of solvent provides a dark yellow solid. ^{1}H NMR (600 MHz, DMSO-*d6*) δ 9.63 (s, 1H), 8.10 (d, J = 5.8 Hz, 2H), 8.09 (s, 2H), 7.52 (dd, J = 7.7, 1.6 Hz, 2H), 7.46 (s, 2H), 7.37 (ddd, J = 8.8, 7.4, 1.6 Hz, 2H), 7.02 (td, J = 7.5, 1.2 Hz, 2H), 6.47 (s, 4H), 4.53 (t, J = 5.0 Hz, 2H), 3.58 (m, 2H), 2.88 (s, 6H). ^{13}C NMR (151 MHz, DMSO) δ 163.97, 155.62, 143.89, 141.62, 132.66, 130.28, 121.67, 119.85, 114.22, 109.80, 93.58, 85.51, 63.05, 54.92, 42.81. UV-Vis (DMSO) λ_{max} 292 nm (20296 $cm^{-1}M^{-1}$), 331 nm (15982 $cm^{-1}M^{-1}$). (Figures 4 and 5)

E.2. Titration Details

Tetrabutylammonium salts were dried at 50 °C under vacuum and stored in a calcium carbonate filled desiccator. In all titrations the receptor concentration was kept constant during the titration. A stock solution of receptor was prepared in DMSO-d_6 and spiked with 0.5 % H_2O. The host-guest solution was prepared with the stock receptor solution. Final guest amounts were obtained through drying an aliquot of a freshly prepared stock solution for each titration unless desires masses could accurately be weighed out. All additions were performed with a Hamilton µL syringe. Representative data are provided for each set. ^{1}H NMR titrations were carried out on an Bruker Avance III HD 600 MHz NMR Spectrometer with Prodigy multinuclear broadband BBO CryoProbe (^{1}H: 600.02 MHz, ^{13}C: 150.89 MHz). Chemical shifts (δ) are expressed in ppm downfield from tetramethylsilane (TMS) using non-deuterated solvent present in the bulk deuterated solvent (DMSO: ^{1}H 2.50 ppm). Chemical shifts of urea protons broadened into the baseline were determined using line broadening.

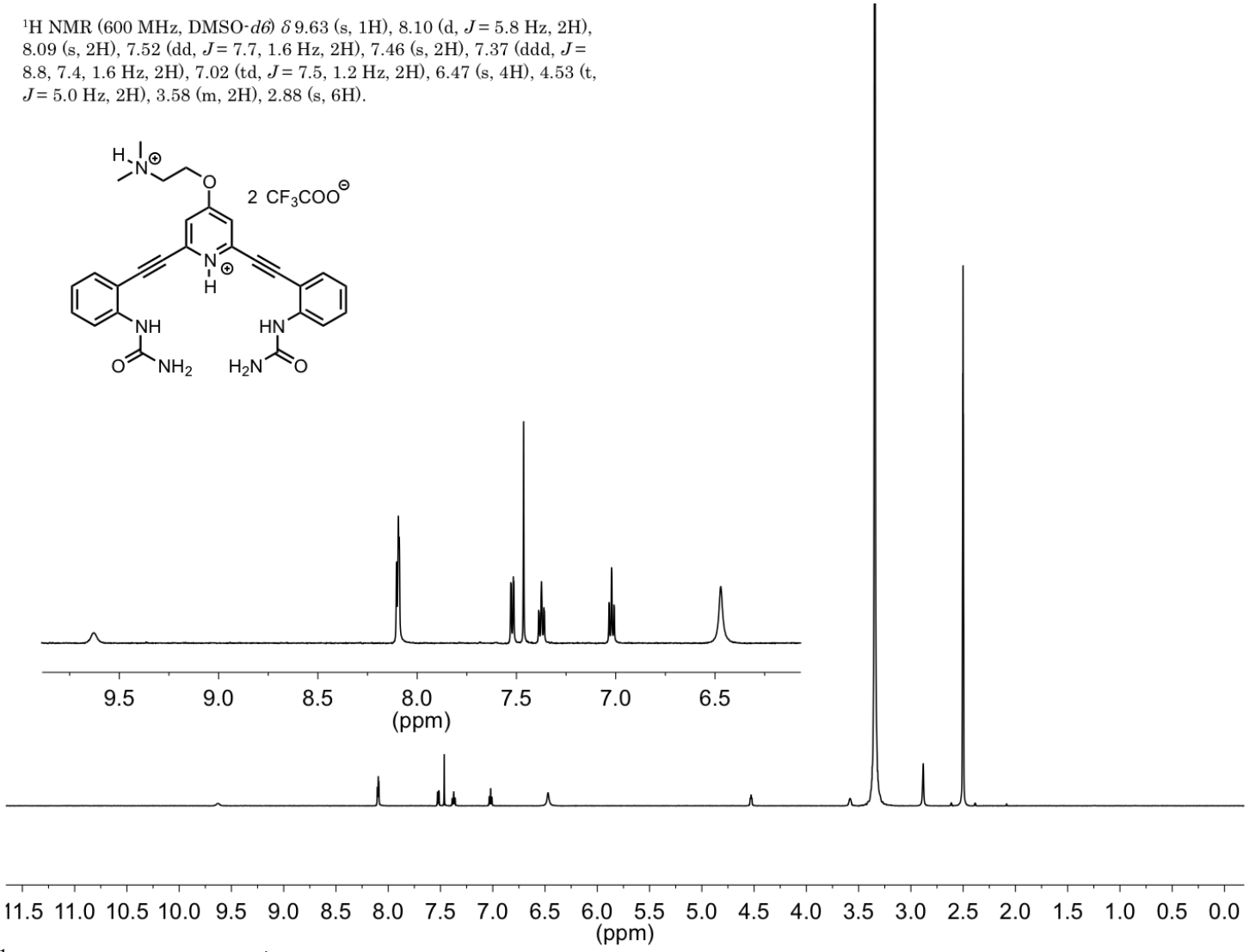

Figure 4. ^{1}H NMR spectrum of $\mathbf{1}^+$ in $CDCl_3$, 600 MHz.

^{13}C NMR (151 MHz, DMSO) δ 163.97, 155.62, 143.89, 141.62, 132.66, 130.28, 121.67, 119.85, 114.22, 109.80, 93.58, 85.51, 63.05, 54.92, 42.81.

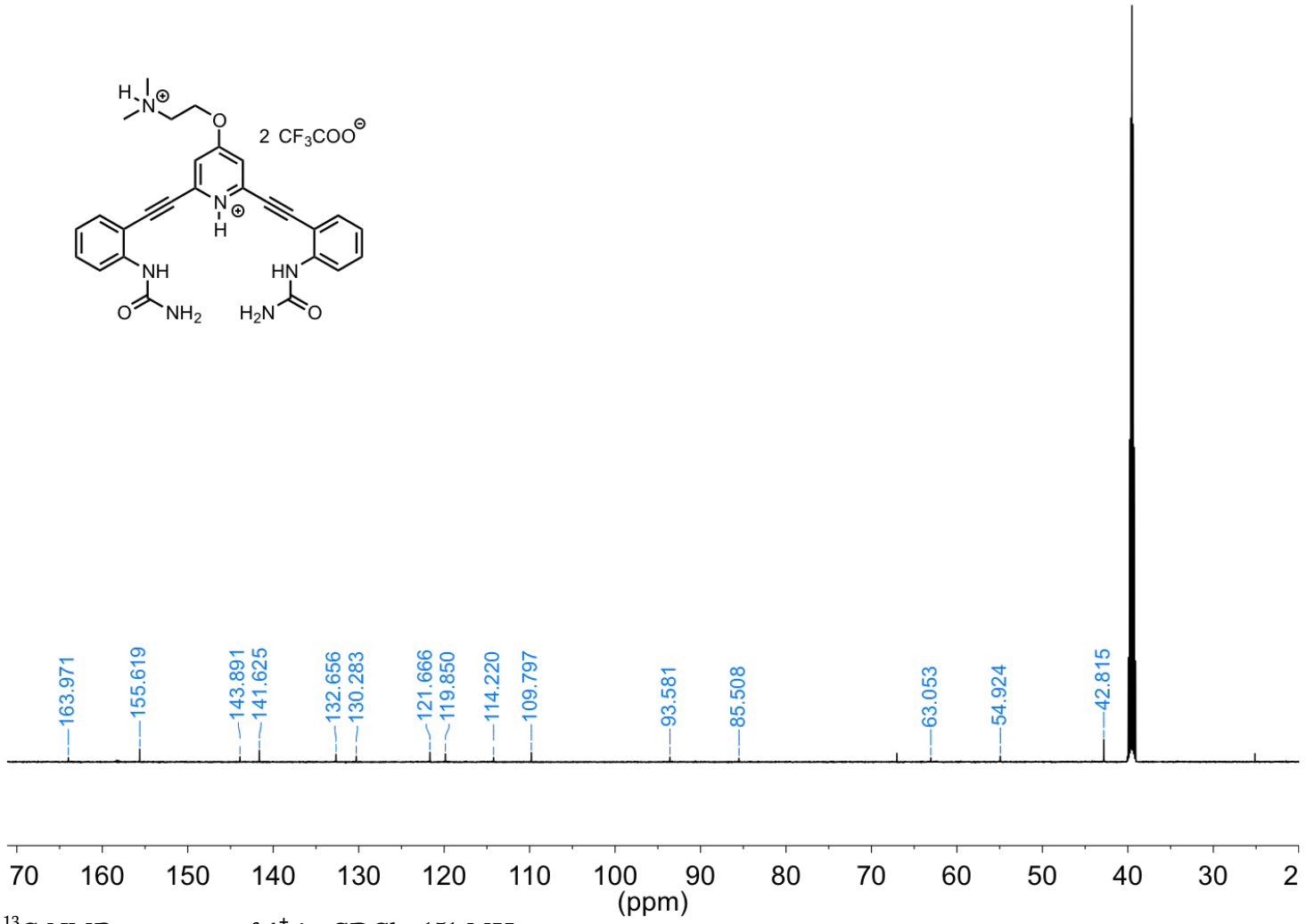

Figure 5. ^{13}C NMR spectrum of $\mathbf{1}^{+}$ in $CDCl_3$, 151 MHz.

E.2.1. NMR Titration of $\mathbf{1}^+$ with Tetrabutylammonium Chloride

A 3 mL stock solution of $\mathbf{1}^+$ (3.18 mg, [R] = 1.49 mM) in 0.5 % H_2O/DMSO-d_6 was prepared and used in the preparation of a 2 mL TBACl guest solution (21.43 mg, [G] = 47.0 mM). Starting volume of 500 µL. (Table 1, Figure 6)

Table 1. Example titration for the addition of tetrabutylammonium chloride to $\mathbf{1}^+$ in 0.5 % H_2O/d_6-DMSO.

Addition (µL)	Total Volume Anion (µL)	[TBACl] (M)	Equiv. Cl^-	$\delta(R_3HN^+)$ (ppm)	$\delta(C_{Py}H)$ (ppm)	$\delta(HN_{urea})$ (ppm)	$\delta(H_2N_{urea})$ (ppm)
0	0	0.00E+00	0.00	9.625	7.462	8.096	6.474
10	10	9.22E-04	0.62	9.742	7.491	8.110	6.491
10	20	1.81E-03	1.21	9.846	7.517	8.123	6.506
15	35	3.08E-03	2.06	9.956	7.545	8.137	6.521
15	50	4.27E-03	2.87	10.053	7.569	8.151	6.535
20	70	5.77E-03	3.87	10.143	7.594	8.164	6.551
20	90	7.17E-03	4.81	10.209	7.612	8.174	6.562
25	115	8.79E-03	5.89	10.284	7.632	8.185	6.573
35	150	1.09E-02	7.27	10.361	7.654	8.197	6.586
50	200	1.34E-02	9.01	10.431	7.674	8.208	6.599
75	275	1.67E-02	11.18	10.519	7.701	8.224	6.617
150	425	2.16E-02	14.48	10.609	7.730	8.242	6.634

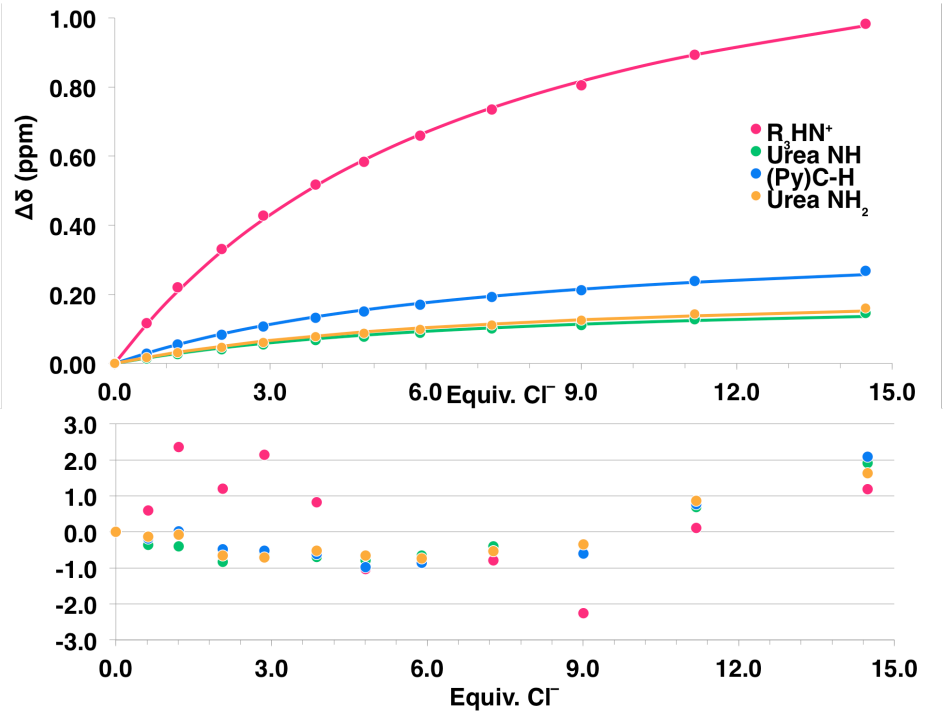

Figure 6. Example 1:1 fitting using non-linear regression from the data obtained for the titration of tetrabutylammonium chloride into $\mathbf{1}^+$ in 0.5 % H_2O/d_6-DMSO.

E.2.2. NMR Titration of $\mathbf{1}^+$ with Tetrabutylammonium Bromide

A 3 mL stock solution of $\mathbf{1}^+$ (1.00 mg, [R] = 0.47 mM) in 0.5 % H_2O/DMSO-d_6 was prepared and used in the preparation of a 2 mL TBABr guest solution (0.151 g, [G] = 0.235 M). Starting volume of 500 µL. (Table 2, Figure 7 and 8)

E.2.3. NMR Titration of $\mathbf{1}^+$ with Tetrabutylammonium Nitrate, Hydrogen Sulfate, Iodide, Perchlorate

1.5 mM $\mathbf{1}^+$ in 0.5 % H_2O/DMSO-d_6 was titrated with a $\mathbf{1}^+$•Guest solution up to 21.4 equivalents of guest for $TBANO_3$, $TBAHSO_4$, TBAI, and $TBAClO_4$. No changes in chemical shift were observed throughout the titrations. (Figure 9)

E.2.4. NMR Titration of $\mathbf{1}^+$ with Tetrabutylammonium Dihydrogen Phosphate

1.5 mM $\mathbf{1}^+$ in 0.5 % H_2O/DMSO-d_6 was titrated with a $\mathbf{1}^+$•$H_2PO_4^-$ solution up to 21.4 equivalents. (Figure 10)

Table 2. Example titration for the addition of tetrabutylammonium bromide to $\mathbf{1}^+$ in 0.5 % H_2O/d_6-DMSO.

Addition (µL)	Total Volume Anion (µL)	[TBABr] (M)	Equiv. Br^-	$\delta(R_3HN^+)$ (ppm)	$\delta(C_{Py}H)$ (ppm)	$\delta(HN_{urea})$ (ppm)	$\delta(H_2N_{urea})$ (ppm)
0	0	0.00E+00	0	9.775	7.481	8.108	6.485
25	25	1.12E-02	2.38	9.806	7.521	8.121	6.505
25	50	2.14E-02	4.54	9.831	7.547	8.130	6.516
30	80	3.24E-02	6.89	9.854	7.570	8.138	6.526
35	115	4.39E-02	9.33	9.875	7.589	8.144	6.536
40	155	5.56E-02	11.81	9.892	7.606	8.150	6.545
50	205	6.83E-02	14.52	9.909	7.622	8.156	6.554
70	275	8.33E-02	17.71	9.928	7.639	8.162	6.562
100	375	1.01E-01	21.39	9.948	7.656	8.169	6.568
150	525	1.20E-01	25.57	9.965	7.671	8.174	6.576
200	725	1.39E-01	29.55	9.986	7.687	8.180	6.589

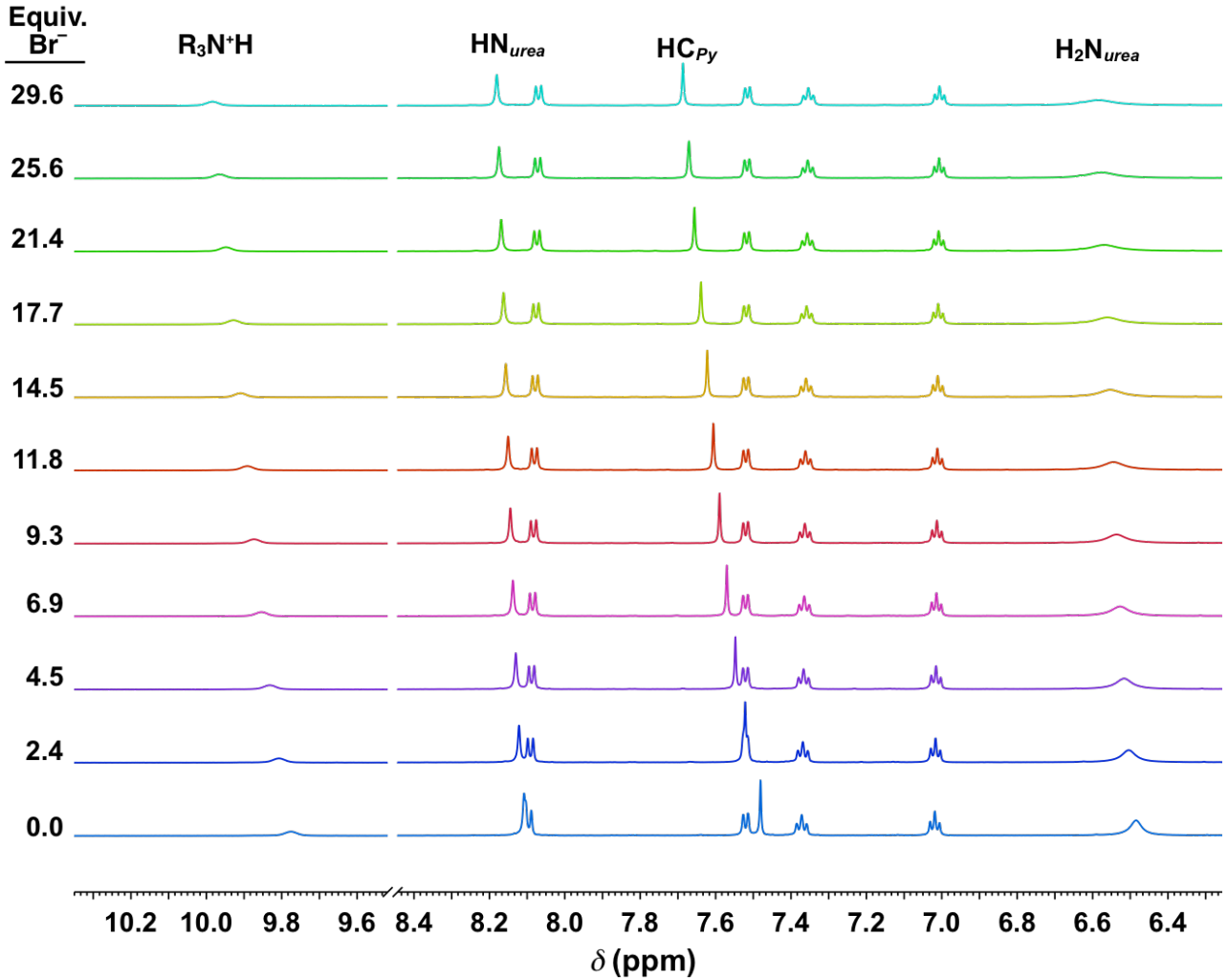

Figure 7. Example stacked spectra from the titration for the addition of tetrabutylammonium bromide to into $\mathbf{1}^+$ in 0.5 % H_2O/d_6-DMSO.

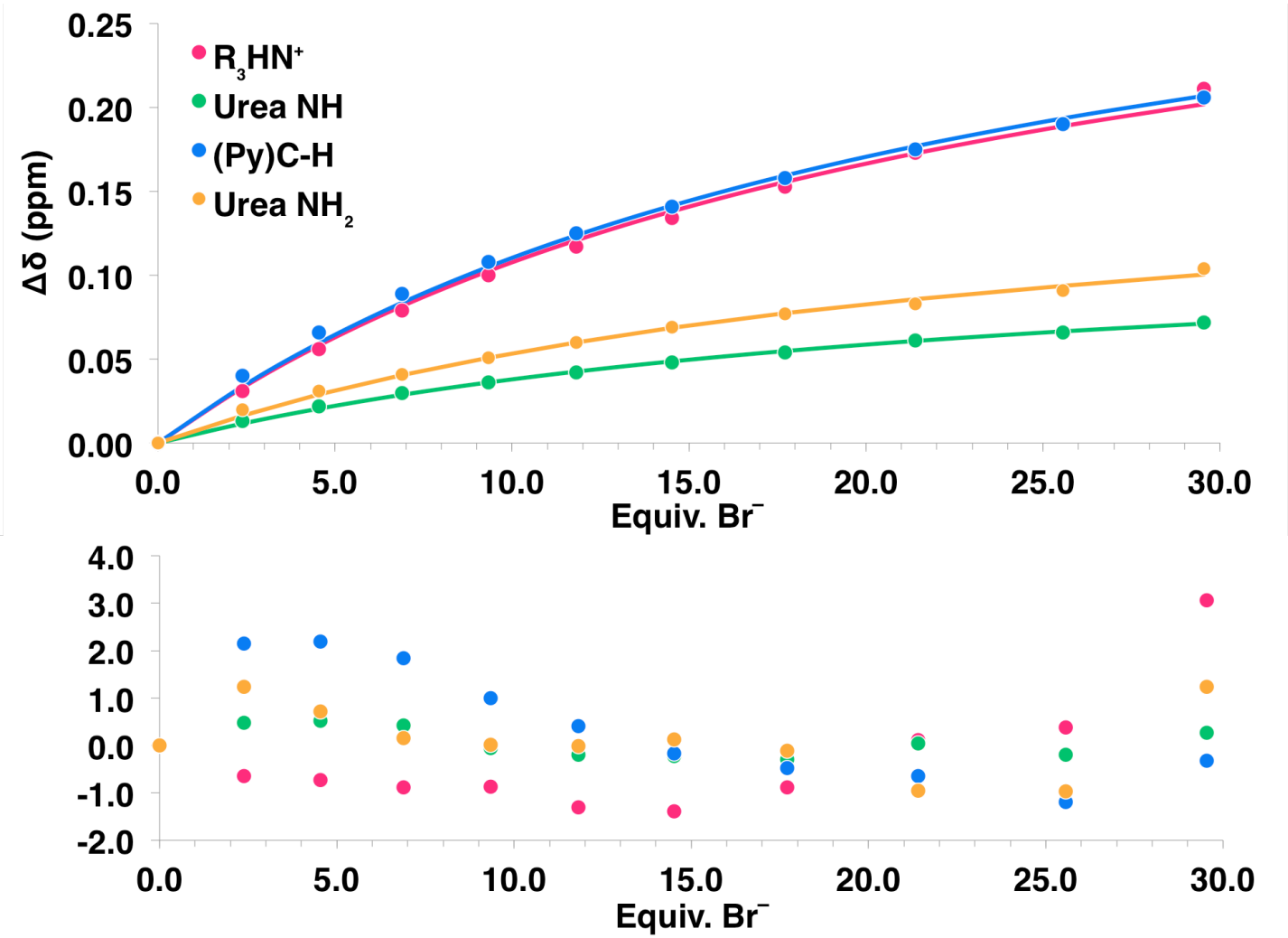

Figure 8. Example 1:1 fitting using non-linear regression from the data obtained for the titration of tetrabutylammonium bromide into $\mathbf{1}^+$ in 0.5 % H_2O/d_6-DMSO.

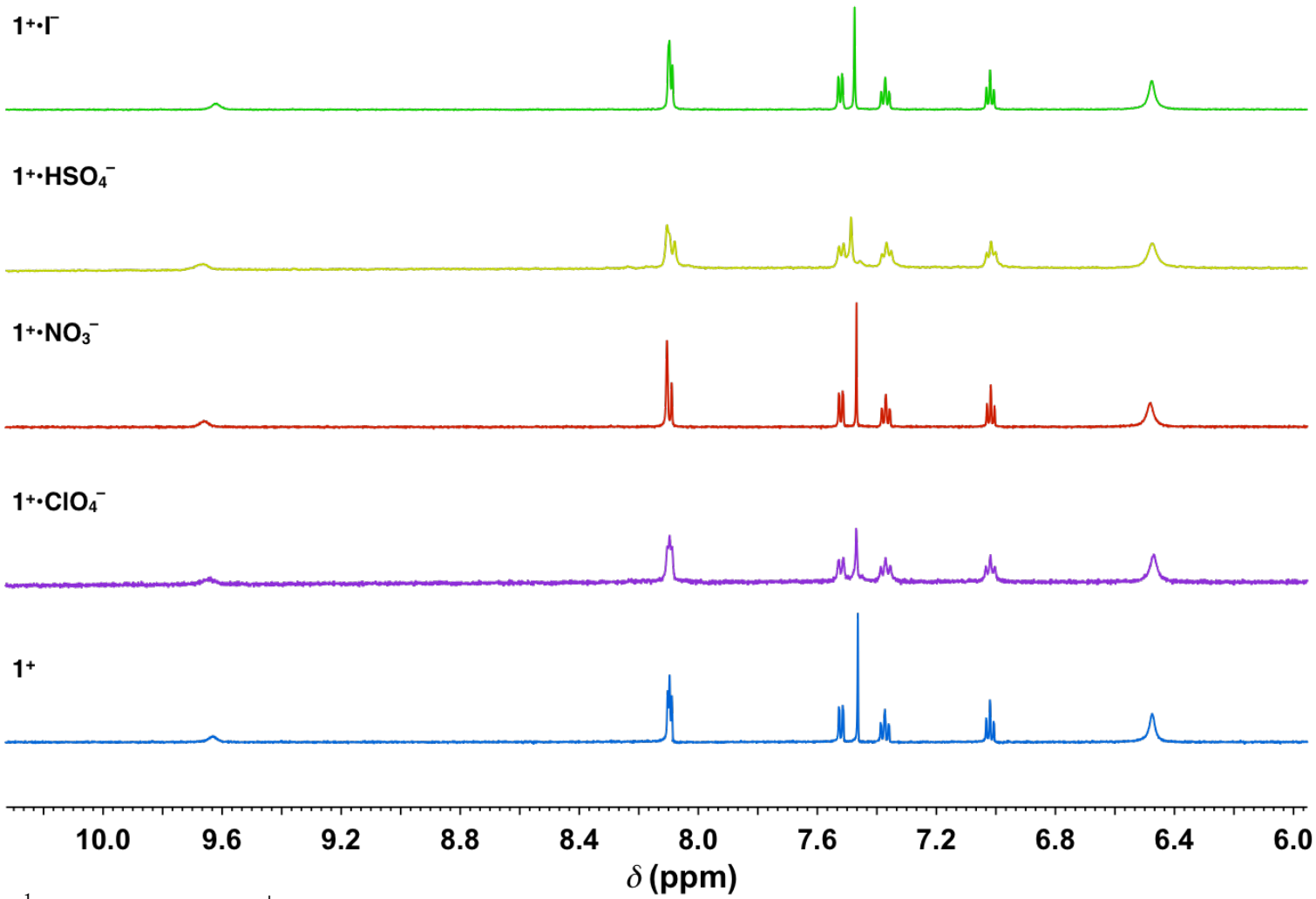

Figure 9. ^{1}H NMR spectra of $\mathbf{1}^{+}$ and 21.4 equivalents of TBA salts of perchlorate, nitrate, hydrogen sulfate, and iodide. Minimal to zero change in chemical shifts is observed throughout their titrations.

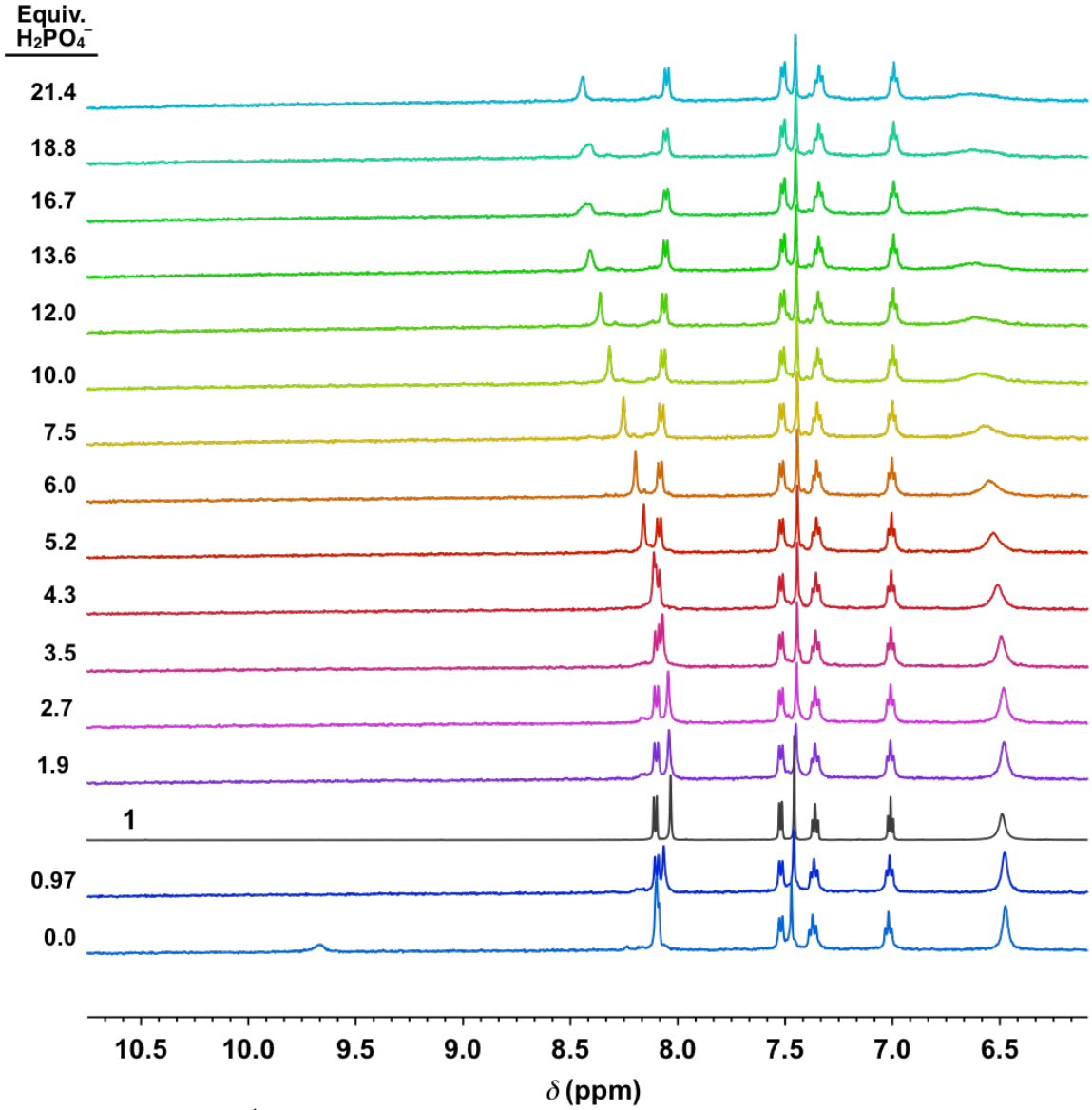

Figure 10. Stacked ^{1}H NMR spectra for the titration of tetrabutylammonium dihydrogen phosphate into $\mathbf{1}^{+}$. After the addition of 1 equivalent of guest, the $R_3N^{+}H$ proton resonance disappears and the other resonances return to the approximate shifts of unprotonated **1** (shown for comparison).

E.3. Determining the Fluorescent Character of $\mathbf{1}^{+}$•Cl^{-} Aggregates

Lithium chloride solutions were prepared by dissolving 1.74 g and 1.78 g in 1 % TFA/DMSO (spectroscopic grade) and 1 % TFA/H_2O (nanopure, 18 Ω) respectively (1.64 mM and 1.68 mM LiCl). 11.9 mg of **1** were protonated as previously noted and dissolved in 1 % TFA/DMSO. In each of ten vials, 0.3 mL of the $\mathbf{1}^{+}$ solution was

pipetted and diluted with volumes of LiCl solutions corresponding to 0, 10, 20, 30, 40, 50, 60, 70, 80, and 90 % water with 0.49 mM $\mathbf{1}^+$ and 3000 equivalents of chloride. Fluorescence spectra were obtained from 440-835 nm by exciting at 425 nm with slit widths of 2 nm and 2 nm. Intensity values represent the sum of intensity from 440-740 nm. Beyond 740 nm the fluorescence of each sample is in the baseline. (Figure 11)

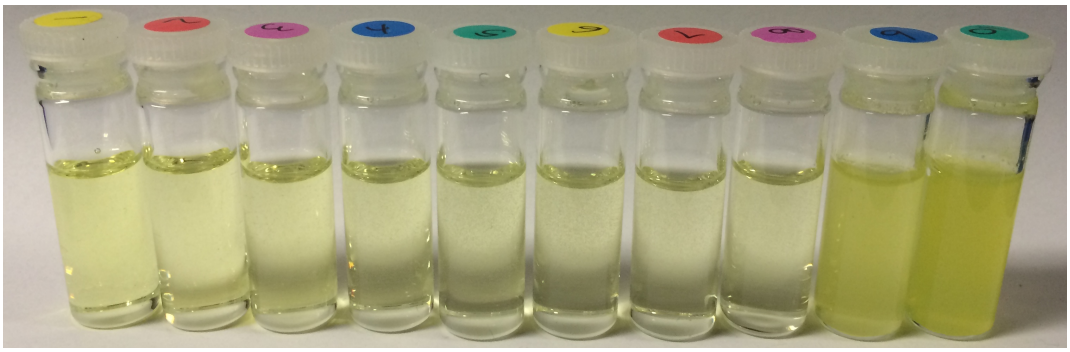

Figure 11. Observable color change based on the addition of chloride and variation in water percentage (0 – 90 % from left to right). Aggregates are clearly visible in the 80 and 90 % water/DMSO solutions.

E.3. SEM of $\mathbf{1}^+\bullet\mathbf{Cl}^-$ Aggregates

A $\mathbf{1}^+$ 0.29 mM solution was prepared by pre-protonating 0.69 mg of **1** and, after application of high vacuum, was dissolved in 1 % TFA/H_2O (nanopure, 18 Ω) respectively. This solution was mixed NaCl salt corresponding ~1200 and 2000 equivalents of chloride. A 10 µl drop of each $\mathbf{1}^+\bullet\mathbf{Cl}^-$ solution was pipette onto a 10 mm x 10 mm arsenic-doped silicon wafer and left to dry for 30 minutes. SEM images were taken using a Zeiss Ultra-55 SEM operating at 5 kV with a 20 µm aperture and an in-lens detector.

E.4. Dependence of $\mathbf{1}^+\bullet\mathbf{Cl}^-$ Aggregate Fluorescence on Concentration of $\mathbf{1}^+$

A 10 mL 0.36 mM $\mathbf{1}^+$ solution was made in 1 % TFA/H_2O (nanopure, 18 Ω) by protonating 1.76 mg of **1**. This solution was used to prepare 0.17 M NaCl host•guest solution which demonstrated turn-on fluorescence with the presence of aggregates.

Fluorescence spectra were obtained by excitation at 316 and 425 nm. Successive dilutions of the 500 equivalent $\mathbf{1}^{+}\bullet\mathbf{Cl}^{-}$ solution provided an assessment of turn-on fluorescence based on varying concentration in comparison to the simultaneous dilutions of a 0.36 mM $\mathbf{1}^{+}$ solution without guest. Intensity ratios comparing $\mathbf{1}^{+}$ with and without the presence of 500 equivalents of chloride were determined for each set (Figure 12). A sharp transition of turn-on fluorescence is observed between 0.25 and 0.30 mM $\mathbf{1}^{+}$.

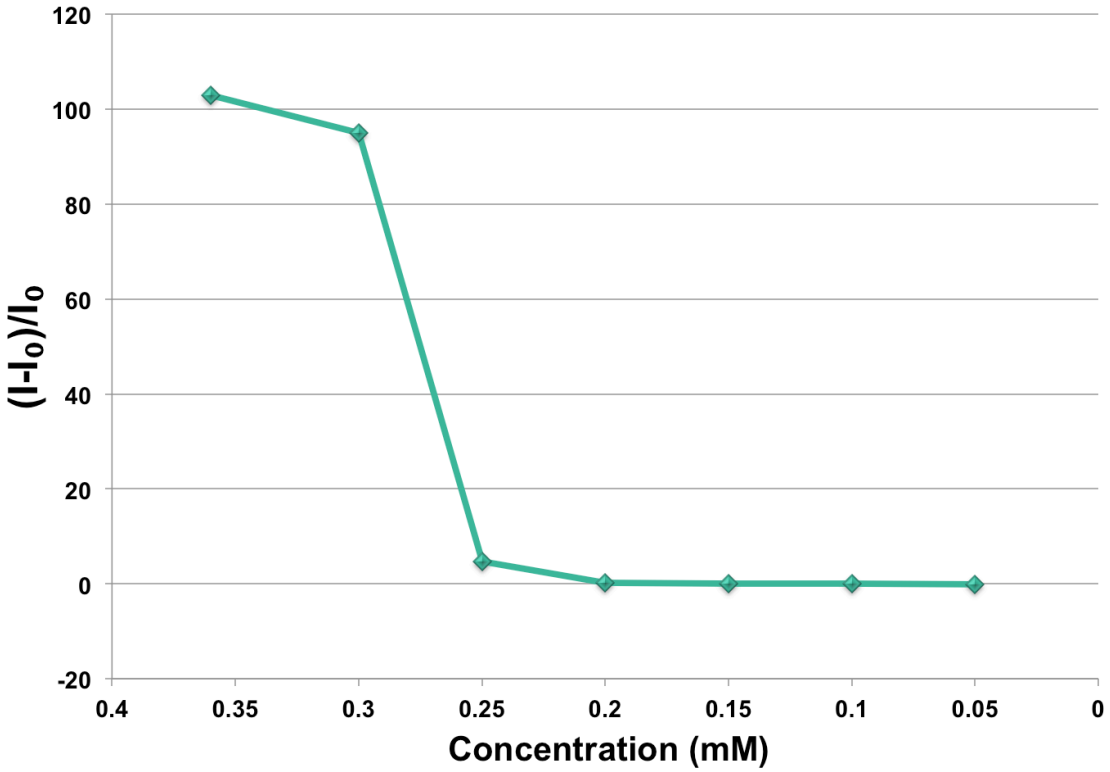

Figure 12. Plot of intensity ratios for fluorescence turn-on of $\mathbf{1}^{+}$ with 500 equivalents of chloride across a concentration range of 0.36 to 0.05 mM of $\mathbf{1}^{+}$.

REFERENCES CITED

CHAPTER I

1. Meyer, E. A.; Castellano, R. K.; Diederich, F. *Angew. Chem., Int. Ed.* **2003**, *42*, 1210–1250.

2. Hayashi, N.; Higuchi, H.; Ninomiya, K. *Top. Heterocycl. Chem.* **2009**, *18*, 1–5.

3. Frontera, A.; Quiñonero, D.; Deyà, P. M. *WIREs Comput. Mol. Sci.* **2011**, *1*, 440–459.

4. Gokel, G. W.; De Wall, S. L.; Meadows, E. S. *Eur. J. Org. Chem.* **2000**, 2967–2978.

5. Zacharias, N.; Dougherty, D. A. *Trends Pharmacol. Sci.* **2002**, *23*, 281–287.

6. Shi, Z.; Olson, C. A.; Bell, A. J., Jr.; Kallenbach, N. R. *Biopolymers* **2001**, *60*, 366–380.

7. Dougherty, D. A. *Acc. Chem. Res.* **2013**, *46*, 885–893.

8. Gamez, P.; Mooibroek, T. J.; Teat, S. J.; Reedijk, J. *Acc. Chem. Res.* **2007**, *40*, 435–444.

9. Schottel, B. L.; Chifotides, H. T.; Dunbar, K. R. *Chem. Soc. Rev.* **2008**, *37*, 68–83.

10. Meisenheimer, J. *Justus Liebigs Ann. Chem.* **1902**, *323*, 205–246.

11. Buncel, E.; Norris, A. R.; Russell, K. E. Q. Rev. Chem. Soc. 1968, 22, 123–146.

12. Bernstein, J. *Cryst. Growth Des.* **2013**, *13*, 961–964.

13. Schwalbe, C. H. *Crystallogr. Rev.* **2012**, *18*, 191–206.

14. Donohue, J. *J. Phys. Chem.* **1952**, *56*, 502–506.

15. Gordy, W. *J. Am. Chem. Soc.* **1938**, *60*, 605–612.

16. Sutor, J. R. *Nature* **1962**, *195*, 68–69.

17. Sutor, J. R. *J. Chem. Soc.* **1963**, 1105–1110.

18. Coppens, P. A. *Acta Cryst.* **1964**, *17*, 573–578.

19. Donohue, J. Selected Topics in Hydrogen Bonding. In *Structural Chemistry and Molecular Biology*; Rich, A.; Davidson, N., Eds.; Freeman: San Francisco, CA, 1968; pp 443–465.

20. Laing, M.; Somerville, P.; Piacenze, L. P. L. *Acta Crystallogr.* **1977**, *B33*, 2464–2471.

21. Taylor, R.; Kennard, O. *J. Am. Chem. Soc.* **1982**, *104*, 5063–5070.

22. Scheiner, S. *Phys. Chem. Chem. Phys.* **2011**. *13*, 13860–13872.

23. Cai, J.; Sessler, J. L. *Chem. Soc. Rev.* **2014**, DOI: 10.1039/C4CS00115J.

24. Chowdhury, S.; Kebarle, P. *J. Chem. Phys.* **1986**, *85*, 4989–4994.

25. Hiraoka, K.; Mizuse, S.; Yamabe, S. *J. Phys. Chem.* **1987**, *91*, 5294–5297.

26. Mascal, M.; Armstrong, A.; Bartberger, M. D. *J. Am. Chem. Soc.* **2002**, *124*, 6247–6276.

27. Quinoñero, D.; Garau, C.; Frontera, A.; Ballester, P.; Costa, A.; Deyà, P. M. *Chem. Phys. Lett.* **2002**, *359*, 486–492.

28. Quinoñero, D.; Garau, C.; Rotger, C.; Frontera, A.; Ballester, P.; Costa, A.; Deyà, P. M. *Angew. Chem., Int. Ed.* **2002**, *41*, 3389–3392.

29. Alkorta, I.; Rozas, I.; Elguero, J. *J. Am. Chem. Soc.* **2002**, *124*, 8593–8598.

30. Hay, B. P.; Bryantsev, V. S. *Chem. Commun.* **2008**, 2417–2428.

31. Berryman, O. B.; Johnson, D. W. *Chem. Commun.* **2009**, 3143–3153.

32. Frontera, A.; Gamez, P.; Mascal, M.; Mooibroek, T. J.; Reedijk, J. *Angew. Chem., Int. Ed.* **2011**, *50*, 9564–9583.

33. Kim, D.; Tarakeshwar, P.; Kim, K. S. *J. Phys. Chem. A* **2004**, *108*, 1250–1258.

34. Quiñonero, D.; Garau, C.; Rotger, C.; Frontera, A.; Ballester, P.; Costa, A.; Deyà, P. M. *Angew. Chem., Int. Ed.* **2002**, *41*, 3389–3392.

35. Wheeler, S.E.; Houk, K.N. *J. Phys. Chem. A* **2010**, *114*, 8658–8664.

36. Gamez, P.; Mooibroek, T. J.; Teat, S. J.; Reedijk, J. *Acc. Chem. Res.* **2007**, *40*, 435–444.

37. Rebek, J.; Askew, B.; Ballester, P.; Buhr, C.; Jones, S.; Nemeth, D.; Williams, K. *J. Am. Chem. Soc.* **1987**, *109*, 5033–5035.

38. Gil-Ramírez, G.; Escudero-Adán, E. C.; Benet-Buchholz, J.; Ballester, P. *Angew. Chem.* **2008**, *120*, 4182–4186; *Angew. Chem., Int. Ed.* **2008**, *47*, 4114–4118.

39. Wang, D.-X.; Zheng, Q.-Y.; Wang, Q.-Q.; Wang, M.-X. *Angew. Chem., Int. Ed.* **2008**, *47*, 7485–7488.

40. Chifotides, H. T.; Schottel, B. L.; Dunbar, K. R. *Angew. Chem., Int. Ed.* **2010**, *49*, 7202–7207.

41. Dawson, R. E.; Hennig, A.; Weimann, D. P.; Emery, D.; Ravikumar, V.; Montenegro, J.; Takeuchi, T.; Gabutti, S.; Mayor, M.; Mareda, J.; Schalley, C.A.; Matile, S. *Nat. Chem.* **2010**, *2*, 533–538.

42. Vargas Jentzsch, A.; Emery, D.; Mareda, J.; Metrangolo, P.; Resnati, G.; Matile, S. *Angew. Chem., Int. Ed.* **2011**, *50*, 11675–11678.

43. Berryman, O. B.; Hof, F.; Hynes, M. J.; Johnson, D. W. *Chem. Commun.* **2006**, 506–508.

44. Berryman, O. B.; Bryantsev, V. S.; Stay, D. P.; Johnson, D. W.; Hay, B. P. *J. Am. Chem. Soc.* **2007**, *129*, 48–58.

45. Berryman, O. B.; Sather, A. C.; Hay, B. P.; Meisner, J. S.; Johnson, D. W. *J. Am. Chem. Soc.* **2008**, *130*, 10895–10897.

46. Estarellas, C.; Frontera, A.; Quinonero, D.; Deyà, P. M. *Angew. Chem., Int. Ed.* **2011**, *50*, 415–418.

47. Robertazzi, A.; Krull, F.; Knapp, E.-W.; Gamez, P. *CrystEngComm.* **2011**, *13*, 3293–3300.

48. Krieger, I. V.; Freundlich, J. S.; Dawandi, V. B.; Roberts, J. P.; Sun, Q.; Owen, J. L.; Fraile, M. T.; Huss, S. I.; Lavandera, J. L.; Ioerger, T. R.; Sacchettini, J. C. *Chem. Biol.* **2012**, *19*, 1556–1567.

49. Philip, V.; Harris, J.; Adams, R.; Nguyen, D.; Spiers, J.; Baudry, J.; Howell, E. E.; Hinde, R. J. *Biochemistry* **2011**, *50*, 2939–2950.

50. Bauzá, A.; Quiñonero, D.; Deyà, P. M.; Frontera, A. *Chem. Eur. J.* **2014**, *20*, 6985–6990.

51. Vargas Jentzsch, A.; Hennig, A.; Mareda, J.; Matile, S. *Acc. Chem. Res.* **2013**, *46*, 2791–2800.

52. Adriaenssens, L.; Estarellas, C.; Vargas Jentzsch, A.; Belmonte, M. M.; Matile, S.; Ballester, P. *J. Am. Chem. Soc.* **2013**, *135*, 8324–8330.

53. He, Q.; Han, Y.; Wang, Y.; Huang, Z.-T.; Wang, D.-X. *Chem. Eur. J.* **2014**, *20*, 7486–7491.

54. Guha, S.; Goodson, F. S.; Corson, L. J.; Saha, S. *J. Am. Chem. Soc.* **2012**, *134*, 13679–13691.

55. Aragay, G.; Frontera, A.; Llovera, V.; Vidal-Gancedo, J.; Ballester, P. *J. Am. Chem. Soc.* **2013**, *135*, 2620–2627.

56. Zhao, Y.; Domoto, Y.; Orentas, E.; Beuchat, C.; Emery, D.; Mareda, J.; Sakai, N.; Matile, S. *Angew. Chem., Int. Ed.* **2013**, *52*, 9940–9943.

57. Zhao, Y.; Beuchat, C.; Domoto, Y.; Gajewy, J.; Wilson, A.; Mareda, J.; Sakai, N.; Matile, S. *J. Am. Chem. Soc.* **2014**, *136*, 2101–2111.

58. Chifotides, H. T.; Giles, I. D.; Dunbar, K. R. *J. Am. Chem. Soc.* **2013**, *135*, 3039–3055.

59. Mitra, A.; Clark, R. J.; Hubley, C. T.; Saha, S. *Supramol. Chem.* **2014**, *26*, 296–301.

60. Chang, K. -C.; Minami, T.; Koutnik, P.; Savechenkov, P. Y.; Liu, Y.; Anzenbacher, P., Jr. *J. Am. Chem. Soc.* **2014**, *136*, 1520–1525.

61. Wang, D.-X.; Wang, M.-X. *J. Am. Chem. Soc.* **2013**, *135*, 892–897.

62. Garau, C.; Frontera, A.; Quinoñero, D.; Ballester, P.; Costa, A.; Deyà, P. M. *Chem. Phys. Lett.* **2004**, *392*, 85–89.

63. Garau, C.; Frontera, A.; Quinoñero, D.; Ballester, P.; Costa, A.; Deyà, P. M. *J. Phys. Chem. A* **2004**, *108*, 9423–9427.

64. Arranz, P.; Bianchi, A.; Cuesta, R.; Giorgi, C.; Godino, M. L.; Gutiérrez, M. D.; López, R.; Santiago, A. *Inorg. Chem.* **2010**, *49*, 9321–9332; *Inorg. Chem.* **2012**, *51*, 4883–4883.

65. Arranz-Mascarós, P.; Bazzicalupi, C.; Bianchi, A.; Giorgi, C.; Godino-Salido, M.-L.; Gutiérrez-Valero, M.-D.; López-Garzón, R.; Savastano, M. *J. Am. Chem. Soc.* **2013**, *135*, 102–105.

66. Ballester, P. *Acc. Chem. Res.* **2013**, *46*, 874–884.

67. Adriaenssens, L.; Gil-Ramírez, G.; Frontera, A.; Quiñonero, D.; Escudero-Adán, E. C.; Ballester, P. *J. Am. Chem. Soc.* **2014**, *136*, 3208–3218.

68. Arranz-Mascarós, P.; Bazzicalupi, C.; Bianchi, A.; Giorgi, C.; Gutiérrez-Valero, M.-D.; López-Garzón, R.; Godino-Salido, M.-L.; Valtancoli, B. *Chem. Commun.* **2011**, *47*, 2814–2816.

69. Arranz-Mascarós, P.; Bazzicalupi, C.; Bianchi, A.; Giorgi, C.; Godino-Salido, M.-L.; Gutiérrez-Valero, M.-D.; López-Garzón, R.; Valtancoli, B. *New J. Chem.* **2011**, *35*, 1883–1891.

70. Bryantsev, V. S.; Hay, B. P. *J. Am. Chem. Soc.* **2005**, *127*, 8282–8283.

71. Bryantsev, V. S.; Hay, B. P. *Org. Lett.* **2005**, *7*, 5031–5034.

72. Yoon, D.-W.; Hwang, H.; Lee, C.-H. *Angew. Chem., Int. Ed.* **2002**, *41*, 1757–1759.

73. Lee, C.-H.; Na, H.-K.; Yoon, D.-W.; Won, D.-H.; Cho, W.-S.; Lynch, V. M.; Shevchuk, S. V.; Sessler, J. L. *J. Am. Chem. Soc.* **2003**, *125*, 7301–7306.

74. Lee, C.-H.; Miyaji, H.; Yoon, D.-W.; Sessler, J. L. *Chem. Commun.* **2008**, 24–34.

75. Yoon, D.-W.; Gross, D. E.; Lynch, V. M.; Sessler, J. L.; Hay, B. P.; Lee, C.-H. *Angew. Chem., Int. Ed.* **2008**, *47*, 5038–5042.

76. Li, Y.; Flood, A. H. *Angew. Chem., Int. Ed.* **2008**, *47*, 2649–2652.

77. Lee, S.; Chen, C.-H.; Flood, A. H. *Nature Chem.* **2013**, *5*, 704–710.

78. Carroll, C. N.; Berryman, O. B.; Johnson, C. A.; Zakharov, L. N.; Haley, M. M.; Johnson, D. W. *Chem. Commun.* **2009**, 2520–2522.

79. Carroll, C. N.; Coombs, B. A.; McClintock, S. P.; Johnson, C. A.; Berryman, O. B.; Johnson, D. W.; Haley, M. M. *Chem. Commun.* **2011**, *47*, 5539–55341.

80. Carroll, C. N.; Naleway, J. J.; Haley, M. M.; Johnson, D. W. *Chem. Soc. Rev.* **2010**, *39*, 3875–3888.

81. Engle, J. M. "Fluorescent Anion Sensors Based on the 2,6-Bis-(2-Anilinoethynyl) Pyridine Scaffold" (Doctoral Dissertation) **2013**, University of Oregon, U. S. A.

82. Engle, J. M.; Carroll, C. N.; Johnson, D. W.; Haley, M. M. *Chem. Sci.* **2012**, 1105–1110.

83. Tresca, B. W.; Zakharov, L. N.; Carroll, C. N.; Johnson, D. W.; Haley, M. M. *Chem. Commun.* **2013**, *49*, 7240–7242.

CHAPTER II

1. Kang, S.O.; Llinares, J.M.; Day, V.W.; Bowman-James, K. *Chem. Soc. Rev.* **2010**, *39*, 3980–4003.

2. Bisson, A.P.; Lynch, V.M.; Monahan, M.K.C.; A nslyn, E.V. *Angew. Chem., Int. Ed. Engl.* **1997**, *36*, 2340–2342.

3. Mascal, M.; Armstrong, A.; Bartberger, M. D. *J. Am. Chem. Soc.* **2002**, *124*, 6274–6276.

4. Mooibroek, T. J.; Gamez, P. *Inorg. Chim. Acta* **2007**, *360*, 381–404.

5. Kim, D.; Tarakeshwar, P.; Kim, K. S. *J. Phys. Chem. A* **2004**, *108*, 1250–1258.

6. Wang, D.-X.; Zheng, Q.-Y.; Wang, Q.-Q.; Wang, M.-X. *Angew. Chem., Int. Ed.* **2008**, *47*, 7485–7488.

7. Zuo, C.-S.; Quan, J.-M.; Wu, Y.-D. *Org. Lett.* **2007**, *9*, 4219–4222.

8. Demeshko, S.; Dechert, S.; Meyer, F. *J. Am. Chem. Soc.* **2004**, *126*, 4508–4509.

9. Frontera, A.; Saczewski, F.; Gdaniec, M.; Dziemidowicz-Borys, E.; Kurland, A.; Deyà, P. M.; Quiñonero, D.; Garau, C. *Chem. Eur. J.* **2005**, *11*, 6560–6567.

10. Wang, D.-X.; Zheng, Q.-Y.; Wang, Q.-Q.; Wang, M.-X. *Angew. Chem., Int. Ed.* **2008**, *47*, 7485–7488.

11. Wang, D.-X.; Wang, M. -X. *J. Am. Chem. Soc.* **2013**, *135*, 892–897.

12. He, Q.; Han, Y.; Wang, Y.; Huang, Z.-T.; Wang, D. -X. *Chem. Eur. J.* **2014**, *20*, 7486–7491.

13. Alkorta, I.; Rozas, I.; Elguero, J. *J. Am. Chem. Soc.* **2002**, *124*, 8593–8598.

14. Berryman, O. B.; Hof, F.; Hynes, M. J.; Johnson, D. W. *Chem. Commun.* **2006**, 506–508.

15. Albrecht, M.; Müller, M.; Mergel, O.; Rissanen, K.; Valkonen, A. *Chem. Eur. J.* **2010**, *16*, 5062–5069.

16. Li, X.; Chin, D.N.; Whitesides, G.M. *J. Org. Chem.* **1996**, *61*, 1779–1786.

17. Kang, S.O.; Day, V.W.; Bowman-James, K. *Org. Lett.* **2008**, *10*, 2677–2680.

18. Vargas Jentzsch, A.; Emery, D.; Mareda, J.; Metrangolo, P.; Resnati, G.; Matile, S. *Angew. Chem., Int. Ed.* **2011**, *50*, 11675–11678.

19. Giese, M.; Albrecht, M.; Krappitz, T.; Peters, M.; Gossen, V.; Raabe, G.; Valkonen, A.; Rissanen, K. *Chem. Commun.* **2012**, *48*, 9983–9985.

20. Adriaenssens, L.; Gil-Ramírez, G.; Frontera, A.; Quiñonero, D.; Escudero-Adán, E. C.; Ballester, P. *J. Am. Chem. Soc.* **2014**, *136*, 3208–3218.

21. Maeda, H.; Osuka, A.; Furuta, H. *J. Incl. Phenom. Macro.* **2004**, *49*, 33–36.

22. Bretschneider, A.; Andrada, D. M.; Dechert, S.; Meyer, S.; Mata, R. A.; Meyer, F. *Chem. Eur. J.* **2013**, *19*, 16988–17000.

23. Giese, M.; Albrecht, M.; Repenko, T.; Sackmann, J.; Valkonen, A.; Rissanen, K. *Eur. J. Org. Chem.* **2014**, 2435–2442.

CHAPTER III

1. United Nations Water Cooperation, *Water Quality Factsheet*, **2013**, http://www.unwater.org/fileadmin/user_upload/watercooperation2013/doc/Factsheets/water_quality.pdf.

2. Işiklan, M.; Saeed, M. A.; Pramanik, A.; Wong, B. M.; Fronczek, F. R.; Hossain, M. A. *Cryst. Growth Des.* **2011**, *11*, 959–963.

3. Brooks, S. J.; Gale, P. A.; Light, M. E. *Chem. Commun.* **2006**, 4344–4346.

4. Santacroce, P. V.; Okunola, O. A.; Zavalij, P. Y.; Davis, J. T. *Chem. Commun.* **2006**, 3246–3248.

5. Tongraung, P.; Chantarasiri, N.; Tuntulani, T. *Tetrahedron Lett.* **2003**, *44*, 29–32.

6. Herges, R.; Dikmans, A.; Jana, U.; Köhler, F.; Jones, P. G.; Dix, I.; Fricke, T.; König, B. *Eur. J. Org. Chem.* **2002**, 3004–3014.

7. Hettche, F.; Beiss, P.; Hoffmann, R. W. *Chem. Eur. J.* **2002**, *8*, 4946–4956.

8. Bisson, A. P.; Lynch, V. M.; Monahan, M. -K. C.; Anslyn, E. V. *Angew. Chem.* **1997**, *109*, 2435–2437; *Angew. Chem., Int. Ed. Engl.* **1997**, *36*, 2340–2342.

9. Makuc, D.; Albrecht, M.; Plavec, J.; Rissanen, K.; Valkonen, A.; Schalley, C. A. *Eur. J. Org. Chem.* **2009**, 4854–4866;

10. Sessler, J. L.; An, D.; Cho, W.-S.; Lynch, V.; Marquez, M. *Chem. Eur. J.* **2005**, *11*, 2001–2011.

11. Burns, D. H.; Calderon-Kawasaki, K.; Kularatne, S. *J. Org. Chem.* **2005**, *70*, 2803–2807.

12. Clare, J. P.; Ayling, A. J.; Joos, J.-B.; Sisson, A. L.; Magro, G.; Pérez-Payán, M. N.; Lambert, T. N.; Shukla, R.; Smith, B. D.; Davis, A. P. *J. Am. Chem. Soc.* **2005**, *127*, 10739–10746.

13. Hudeček, O.; Budka, J.; Dvořáková, H.; Cuřínová, P.; Císařová, I.; Lhoták, P. *New J. Chem.* **2013**, *37*, 220–227.

14. Young, P. G.; Jolliffe, K. A. *Org. Biomol. Chem.* **2012**, *10*, 2664–2672.

15. Juwarker, H.; Lenhardt, J. M.; Castillo, J. C.; Zhao, E.; Krishnamurthy, S.; Jamiolkowski, R. M.; Kim, K.-H.; Craig, S. L. *J. Org. Chem.* **2009**, *74*, 8924–8934.

16. Byrne, P.; Turner, D. R.; Lloyd, G. O.; Clarke, N.; Steed, J. W. *Cryst. Growth Des.* **2008**, *8*, 3335–3344.

17. Chang, K.-J.; Moon, D.; Lah, M. S.; Jeong, K.-S. *Angew. Chem.* **2005**, *117*, 8140–8143; *Angew. Chem., Int. Ed.* **2005**, *44*, 7926–7929.

18. Choi, K.; Hamilton, A. D. *J. Am. Chem. Soc.* **2003**, *125*, 10241–10249.

19. Choi, K.; Hamilton, A. D. *J. Am. Chem. Soc.* **2001**, *123*, 2456–2457.

20. Dawson, R. E.; Hennig, A.; Weimann, D. P.; Emery, D.; Ravikumar, V.; Montenegro, J.; Takeuchi, T.; Gabutti, S.; Mayor, M.; Mareda, J.; Schalley, C. A.; Matile, S. *Nat. Chem.* **2010**, *2*, 533–538.

21. Vargas Jentzsch, A.; Emery, D.; Mareda, J.; Metrangolo, P.; Resnati, G.; Matile, S. *Angew. Chem.* **2011**, *123*, 12772–12776; *Angew. Chem., Int. Ed.* **2011**, *50*, 11675–11678.

22. Gil-Ramírez, G.; Escudero-Adán, E. C.; Benet-Buchholz, J.; Ballester, P. *Angew. Chem.* **2008**, *120*, 4182–4186; *Angew. Chem., Int. Ed.* **2008**, *47*, 4114–4118.

23. Adriaenssens, L.; Estarellas, C.; Jentzsch, A. V.; Belmonte, M. M.; Matile, S.; Ballester, P. *J. Am. Chem. Soc.* **2013**, *135*, 8324–8330.

24. Engle, J. M.; Carroll, C. N.; Johnson, D. W.; Haley, M. M. *Chem. Sci.* **2012**, *3*, 1105–1110.

25. Carroll, C. N.; Coombs, B. A.; McClintock, S. P.; Johnson II, C. A.; Berryman, O. B.; Johnson, D. W.; Haley, M. M. *Chem. Commun.* **2011**, *47*, 5539–5541.

26. Carroll, C. N.; Naleway, J. J.; Haley, M. M.; Johnson, D. W. *Chem. Soc. Rev.* **2010**, *39*, 3875–3888;

27. Carroll, C. N.; Berryman, O. B.; Johnson, C. A.; Zakharov, L. N.; Haley, M. M.; Johnson, D. W. *Chem. Commun.* **2009**, 2520–2522.

28. Hay, B. P.; Gutowski, M.; Dixon, D. A.; Garza, J.; Vargas, R.; Moyer, B. A. *J. Am. Chem. Soc.* **2004**, *126*, 7925–7934.

29. Hay, B. P.; Dixon, D. A.; Bryan, J. C.; Moyer, B. A. *J. Am. Chem. Soc.* **2002**, *124*, 182–183.

30. Hennrich, G.; Echavarren, A. M. *Tetrahedron Lett.* **2004**, *45*, 1147–1149.

31. Wan, W. B.; Haley, M. M. *J. Org. Chem.* **2001**, *66*, 3893–3901.

32. Chaikovskii, V. K.; Filimonov, V. D.; Funk, A. A.; Skorokhodov, V. I.; Ogorodnikov, V. D. *Russ. J. Org. Chem.* **2007**, *43*, 1291–1296.

33. Vatsadze, S. Z.; Titanyuk, I. D.; Chernikov, A. V.; Zyk, N. V. *Russ. Chem. Bull., Int. Ed.* **2004**, *53*, 471–473.

34. Thordarson, P. *Chem. Soc. Rev.* **2011**, *40*, 1305–1323.

35. Chu, W.-J.; Yang, Y.; Chen, C.-F. *Org. Lett.* **2010**, *12*, 3156–3159.

36. Tresca, B. W.; Zakharov, L. N.; Carroll, C. N.; Johnson, D. W.; Haley, M. M. *Chem. Commun.* **2013**, *49*, 7240–7242.

CHAPTER IV

1. Engle, J. M.; Carroll, C. N.; Johnson, D. W.; Haley, M. M. *Chem. Sci.* **2012**, *3*, 1105–1110.

2. Carroll, C. N.; Berryman, O. B.; Johnson II, C. A.; Zakharov, L. N.; Haley, M. M.; Johnson, D. W. *Chem. Commun.* **2009**, 2520–2522.

3. Carroll, C. N.; Coombs, B. A.; McClintock, S. P.; Johnson II, C. A.; Berryman, O. B.; Johnson, D. W.; Haley, M. M. *Chem. Commun.* **2011**, *47*, 5539–5541.

4. Berryman, O. B.; Johnson II, C. A.; Zakharov, L. N.; Haley, M. M.; Johnson, D. W. *Angew. Chem., Int. Ed.* **2008**, *47*, 117–120.

5. United Nations Water Cooperation, *Water Quality Factsheet*, **2013**, http://www.unwater.org/fileadmin/user_upload/watercooperation2013/doc/Factsheets/water_quality.pdf.

6. Zhang, T.; Wu, Q.; Sun, H. W.; Rao, J.; Kannan, K. *Environ. Sci. Technol.* **2010**, *44*, 6947-6953.

7. O'Hara, M. J.; Burge, S. R., Grate, J. W. *Anal. Chem.* **2009**, *81*, 1068–1078.

8. Watt, M. M.; Zakharov, L. N.; Haley, M. M.; Johnson, D. W. *Angew. Chem., Int. Ed.* **2013**, *52*, 10275–10280.

9. Thordarson, P. *Chem. Soc. Rev.* **2011**, *40*, 1305–1323.

10. Hay, B. P.; Firman, T. K.; Moyer, B. A. *J. Am. Chem. Soc.* **2005**, *127*, 1810–1819.

CHAPTER V

1. Gunnlaugsson, T.; Glynn, M.; Tocci, G. M.; Kruger, P. E.; Pfeffer, F. M. *Coord. Chem. Rev.* **2006**, *250*, 3094–3117.

2. Beer, P. D.; Gale, P. A. *Angew. Chem. Int. Ed.* **2001**, *40*, 486–516.

3. Bianchi, A.; Bowman-James, K.; García-Espana, E. *Supramolecular Chemistry of Anions*, Wiley-VCH: New York, 1997.

4. Hong, Y.; Lam, J. W. Y.; Tang, B. Z. *Chem. Soc. Rev.* **2011**, *40*, 5361–5388.

5. Würthner, F.; Kaiser, T. E.; Saha-Möller, C. R. *Angew. Chem., Int. Ed.* **2011**, *50*, 3376–3410.

6. Ding, D.; Li, K.; Liu, B.; Tang, B. Z. *Acc. Chem. Res.* **2013**, *46*, 2441–2453.

7. Peng, L.; Wang, M.; Zhang, G.; Zhang, D.; Zhu, D. *Org. Lett.* **2009**, *11*, 1943–1946.

8. Wang, J.-X.; Chen, Q.; Bian, N.; Yang, F.; Sun, J.; Qi, A. -D.; Yan, C. -G.; Han, B. -H.; *Org. Biomol. Chem.* **2011**, *9*, 2219–2226.

9. Liu, Y.; Wang, Z.; Zhang, G.; Zhang, W.; Zhang, D.; Jiang, X. *Analyst* **2012**, *137*, 4654–4657.

10. Liu, Y.; Tang, Y.; Barashkov, N. N.; Irgibaeva, I. S.; Lam, J. W. Y.; Hu, R.; Birimzhanova, D.; Yu, Y.; Tang, B. Z. *J. Am. Chem. Soc.* **2010**, *132*, 13951–13953.

11. Li, D.; Liu, J.; Kwok, R. T. K.; Liang, Z.; Tang, B. Z.; Yu, J. *Chem. Commun.* **2012**, *48*, 7167–7169.

12. Engle, J. M.; Carroll, C. N.; Johnson, D. W.; Haley, M. M. *Chem. Sci.* **2012**, *3*, 1105–1110.

13. Carroll, C. N.; Berryman, O. B.; Johnson II, C. A.; Zakharov, L. N.; Haley, M. M.; Johnson, D. W. *Chem. Commun.* **2009**, 2520–2522.

14. Carroll, C. N.; Coombs, B. A.; McClintock, S. P.; Johnson II, C. A.; Berryman, O. B.; Johnson, D. W.; Haley, M. M. *Chem. Commun.* **2011**, *47*, 5539–5541.

15. Berryman, O. B.; Johnson II, C. A.; Zakharov, L. N.; Haley, M. M.; Johnson, D. W. *Angew. Chem., Int. Ed.* **2008**, *47*, 117–120.

16. Verkman, A. S.; Galietta, L. J. V. *Nat. Rev. Drug Discov.* **2009**, *8*, 153–171.

17. Chen, T.-Y.; Hwang, T.-C. Physiol Rev 2008, 88, 351–387.

18. Jentsch, T. J. *Crit. Rev. Biochem. Mol. Biol.* **2008**, *43*, 3–36.

19. Illsley, N. P.; Verkman, A. S. *Biochemistry* **1987**, *26*, 1215–1219.

20. Verkman, A. S. *Am. J. Physiol. - Cell Ph.* **1990**, *259*, C375–C388.

21. Sonawane, N. D.; Thiagarajah, J. R.; Verkman, A. S. *J. Biol. Chem.* **2002**, *277*, 5506–5513.

22. Wachter, R. M.; Remington, S. J. *Curr. Biol.* **1999**, *9*, R628–R629.

23. Jayaraman, S.; Haggie, P.; Wachter, R. M.; Remington, S. J.; Verkman, A. S. *J. Biol. Chem.* **2000**, *275*, 6047–6050.

24. Geddes, C. D. *Meas. Sci. Technol.* **2001**, *12*, R53–R88.

25. Wang, H.; Liu, L.; Wang, Y.; Peng, C.; Zhang, J.; Zhu, Q. *Tetrahedron Lett.*, **2009**, *50*, 6841–6843.

26. Thordarson, P. *Chem. Soc. Rev.* **2011**, *40*, 1305–1323.

27. Engle, J. M; Lakshminarayanan, P. S.; Carroll, C. N.; Zakharov, L. N.; Haley, M. M.; Johnson, D. W. *Cryst. Growth Des.* **2011**, *11*, 5144–5152.

28. Tresca, B. W.; Zakharov, L. N.; Carroll, C. N.; Johnson, D. W.; Haley, M. M. *Chem. Commun.* **2013**, *49*, 7240–7242.

29. Gavette, J. V.; Mills, N. S.; Zakharov, L. N.; Johnson II, C. A.; Johnson, D. W.; Haley, M. M. *Angew. Chem., Int. Ed.* **2013**, *52*, 10270–10274.

30. Gonzalez-Islas, C.; Chub, N.; Wenner, P. *J. Neurophysiol.* **2009**, *101*, 507–518.

31. Heimlich, G. Cidlowski, J. A. *J. Biol. Chem.* **2006**, *281*, 2232–2241.

32. Treharne, K. J.; Crawford, R. M.; Mehta, A. *Exp. Physiol.* **2006**, *91*, 131–139.

CHAPTER VI

1. Berryman, O. B.; Hof, F.; Hynes, M. J.; Johnson, D. W. *Chem. Commun.* **2006**, 506–508.

APPENDIX A

1. Schier, A.; Schmidbauer, H. *Organometallics* **2008**, *27*, 2361–2395.

2. Zukerman-Schpector, J.; Otero-de-la-Roza, A.; Lauña, V.; Tiekink, E. R. T. *Chem. Commun.* **2011**, *47*, 7608–7610.

3. Auer, A. A.; Mansfeld, D.; Nolde, C.; Schneider, W.; Schurmann, M.; Mehring, M. *Organometallics* **2009**, *28*, 5405–5411.

4. Vickaryous, W. J.; Herges, R.; Johnson, D. W. *Angew. Chem., Int. Ed.* **2004**, *43*, 5831– 5833.

5. Vickaryous, W. J.; Rather Healy, E.; Berryman, O. B.; Johnson, D. W. *Inorg. Chem.* **2005**, *44*, 9247–9252.

6. CAChe, version 5.0; Fujitsu, Ltd.: Kawasaki, Japan, 2000–2001.

7. Cangelosi, V. M.; Sather, A. C.; Zakharov, Z. N.; Berryman, O. B.; Johnson, D. W. *Inorg. Chem.* **2007**, *46*, 9278–9284.

8. Cangelosi, V. M.; Zakharov, L. N.; Fontenot, S. A.; Pitt, M. A.; Johnson, D. W. *Dalton Trans.* **2008**, 3447–3453.

9. Cangelosi, V. M.; Zakharov, L. N.; Crossland, J. L.; Franklin, B. C.; Johnson, D. W. *Cryst. Growth Des.* **2010**, *10*, 1471–1473.

10. Lindquist, N. R.; Carter, T. G.; Cangelosi, V. M.; Zakharov, L. N.; Johnson, D. W. *Chem. Commun.* **2010**, *46*, 3505–3507.

11. Pitt, M. A.; Zakharov, L. N.; Vanka, K.; Thompson, W. H.; Laird, B. B.; Johnson, D. W. *Chem. Commun.* **2008**, 1–3.

12. Cangelosi, V. M.; Pitt, M. A.; Vickaryous, W. J.; Allen, C. A.; Zakharov, L. N.; Johnson, D. W. *Cryst. Growth Des.* **2010**, *10*, 3531–3536.

13. Vickaryous, W. J.; Zakharov, L. N.; Johnson, D. W. *Main Group Chem.* **2006**, *5*, 51–59.

14. Cangelosi, V. M.; Zakharov, L. N.; Johnson, D. W. *Angew. Chem., Int. Ed.* **2010**, *49*, 1248– 1251.

15. Ma, J. C.; Dougherty, D. A. *Chem. Rev.* **1997**, *97*, 1303–1324.

16. Gokel, G. W. *Chem. Commun.* **2003**, 2847–2852.

17. Meyer, E. A.; Castellano, R. K.; Diederich, F. *Angew. Chem., Int. Ed.* **2003**, *42*, 1210–1250.

18. Burford, N.; Clyburne, J. A. C.; Bakshi, P. K.; Cameron, T. S. *J. Am. Chem. Soc.* **1993**, *115*, 8829–8830.

19. Cangelosi, V. M.; Carter, T. G.; Crossland, J. L.; Zakharov, L. N.; Johnson, D. W. *Inorg. Chem.* **2010**, *49*, 9985–9992.

20. Fontenot, S. A.; Cangelosi, V. M.; Pitt, M. A. W.; Sather, A. C.; Zakharov, L. N.; Berryman, O. B.; Johnson, D. W. *Dalton Trans.* **2011**, *40*, 12125–12131.

21. Zampella, G.; Neupane, K. P.; De Gioia, L.; Pecoraro, V. L. *Chem. Eur. J.* **2012**, *18*, 2040–2050.

APPENDIX C

1. Sheldrick, G. M. Bruker/Siemens Area Detector Absorption Correction Program, Bruker AXS, Madison, WI, 1998.

2. SHELXTL-6.10 "Program for Structure Solution, Refinement and Presentation" BRUKER AXS Inc., 5465 East Cheryl Parkway, Madison, WI 53711-5373 USA.